Addendum Cover Page

Complete only applicable items.

QA: QA

1. Total Pages: 344

2. Addendum to (Title):

Simulation of Net Infiltration for Present-Day and Potential Future Climates

3. DI (including Revision and Addendum No.):

MDL-NBS-HS-000023 REV01 AD01

	Printed Name	Signature	Date
4. Originator	Joshua S. Stein	Joshua S. Stein	1/28/2008
5. Independent Technical Reviewer	Kenneth Rehfeldt	Kenneth Rehfeldt	1/28/2008
6. Checker	Charles Haukwa	[signature]	1/28/2008
7. QCS / Lead Lab QA Reviewer	Peter Persoff	[signature]	01/28/2008
8. Responsible Manager / Lead	Ming Zhu	[signature]	1/28/08
9. Responsible Manager	M. Kathryn Knowles	[signature]	1/28/08

10. Remarks

Change History

11. Revision and Addendum No.	12. Description of Change
REV 01 AD01	This addendum addresses comments received from the DOE on July 7, 2007. It also addresses self-identified editorial corrections. This addendum also addresses conditions adverse to quality documented in CRs 10731, 10772, 10777, 10783, 10788, 11192, 11360, 11459, 11554, and 11620. A new section (7.2.4[a]) was added to Section 7[a] to address CR 10783 comments related to soil depth data collected by the Center for Nuclear Waste Regulatory Analyses (CNWRA). These data are compared to the YMP data used to establish statistical parameters for Soil Depth Class 4. Additional text and a figure were added to new Section 7.2.1.2.4[a] to compare MASSIF results to infiltration estimates provided in a recent CNWRA report.

ACKNOWLEDGEMENTS

Dan Levitt is the primary contributor to this addendum and originally acted as the originator for most of its development. Joshua Stein took over as document originator late in the process.

INTENTIONALLY LEFT BLANK

CONTENTS

Page

ACKNOWLEDGEMENTS iii

ACRONYMS AND ABBREVIATIONS xix

1[a]. PURPOSE 1-1
1.1[a]. INTENDED USE 1-4
1.2[a]. LIMITATIONS 1-6
1.3[a]. SCOPE OF THE DOCUMENT 1-8
1.4[a]. DEVIATIONS FROM THE TECHNICAL WORK PLAN 1-8

2[a]. QUALITY ASSURANCE 2-1

3[a]. USE OF SOFTWARE 3-1

4[a]. INPUTS 4-1
4.1[a]. DIRECT INPUT 4-1
4.2[a]. CRITERIA 4-1
4.3[a]. CODES, STANDARDS, AND REGULATIONS 4-1

5[a]. ASSUMPTIONS 5-1
5.1[a]. CERTAIN COMPONENTS OF THE WATER BALANCE MODEL CAN BE NEGLECTED FOR MODELING NET INFILTRATION AT YUCCA MOUNTAIN 5-1
5.2[a]. FAO-56 METHODS FOR DEVELOPING BASAL TRANSPIRATION COEFFICIENTS ARE APPROPRIATE FOR DESERT ENVIRONMENT 5-3
5.3[a]. ASSUMPTIONS RELATED TO SIMULATING YUCCA MOUNTAIN VEGETATION USING LANDSAT THEMATIC MAPPER DATA 5-3
5.4[a]. PHYSICAL PROPERTIES ARE ASSUMED TO REMAIN CONSTANT 5-3
5.5[a]. MISCELLANEOUS ASSUMPTIONS AND APPROXIMATIONS 5-3

6[a]. MODEL DEVELOPMENT 6-1
6.1[a]. FEATURES, EVENTS, PROCESSES 6-1
6.2[a]. INFILTRATION PROCESSES 6-1
6.2.1[a]. Processes Controlling Net Infiltration 6-1
6.2.2[a]. Modeling Processes Controlling Net Infiltration 6-7
6.2.3[a]. Criteria for Selection of Net Infiltration Model Components 6-7
6.2.4[a]. Alternative Models Considered 6-7
6.3[a]. DESCRIPTION OF THE CONCEPTUAL MODEL – MASS ACCOUNTING SYSTEM FOR SOIL INFILTRATION AND FLOW (MASSIF) 6-7
6.4[a]. MATHEMATICAL DESCRIPTION OF THE MODEL 6-7
6.4.1[a]. Precipitation (P) 6-7
6.4.2[a]. Mathematical Representation of Water Transport and Storage 6-7
6.4.3[a]. Surface Runoff and Run-on (Roff and Ron) 6-7

CONTENTS (Continued)

Page

6.4.4[a]. Mathematical Representation of Evapotranspiration 6-8
6.4.4.1[a]. Basal Transpiration, Soil Evaporation Coefficients, and Canopy Coefficient 6-8
6.4.4.2[a]. Depletions and Water Stress Coefficients 6-8
6.4.4.3[a]. ET Calculation 6-8
6.4.5[a]. Mathematical Representation of Reference Evapotranspiration on Flat and Sloped Surfaces 6-8
6.4.5.1[a]. Data Required for Daily Calculation of ET_0 6-8
6.4.5.2[a]. Use of the FAO Penman-Monteith Equation with a Limited Set of Weather Data 6-8
6.4.5.3[a]. Effect of Surface Elevation, Orientation, and Slope on ET_0 6-8
6.5[a]. ANALYSIS OF YUCCA MOUNTAIN NET INFILTRATION 6-8
6.5.1[a]. Weather Parameters for Anticipated Climate Episodes 6-8
6.5.1.1[a]. Climate Episodes 6-8
6.5.1.2[a]. Parameterization of Precipitation and Temperature Records 6-10
6.5.1.3[a]. Weather-File Parameters for the Remainder of the Present-Day Climate 6-10
6.5.1.4[a]. Weather-File Parameters for the Monsoon Climate 6-13
6.5.1.5[a]. Weather-File Parameters for the Glacial Transition Climate 6-13
6.5.1.6[a]. Generation of MASSIF Weather-File Input from Climate Parameters 6-13
6.5.1.7[a]. Other Climate Parameters 6-14
6.5.2[a]. Geologic and Geographic Inputs 6-20
6.5.2.1[a]. Geographic Inputs 6-21
6.5.2.2[a]. Soil Classification 6-29
6.5.2.3[a]. Soil Properties 6-34
6.5.2.4[a]. Soil Depth 6-34
6.5.2.5[a]. Bedrock Classification 6-47
6.5.2.6[a]. Bedrock Saturated Conductivity 6-51
6.5.3[a]. Vegetation Parameters 6-51
6.5.3.1[a]. Potential Vegetation for Monsoon and Glacial Transition Climates 6-51
6.5.3.2[a]. Maximum Rooting Depth 6-54
6.5.3.3[a]. Plant Height 6-54
6.5.3.4[a]. Method for Estimating Basal Transpiration Coefficients for the Infiltration Modeling Domain 6-55
6.5.3.5[a]. NDVI' Look-up Table and PVR Parameter Development 6-55
6.5.3.6[a]. Determination of K_{cb} from Ground Cover Measurements Made at Ecological Study Plots 6-58
6.5.3.7[a]. Correlating K_{cb} Profiles with NDVI' 6-58

CONTENTS (Continued)

Page

6.5.4[a]. Additional Parameter Development 6-58
6.5.5[a]. Parameter Uncertainty Screening 6-58
6.5.6[a]. Calculation Procedure 6-58
6.5.7[a]. Results of Net Infiltration Calculations 6-58
6.5.7.1[a]. Present-Day Simulation Results 6-59
6.5.7.2[a]. Monsoon Simulation Results 6-66
6.5.7.3[a]. Glacial Transition Simulation Results 6-73
6.5.7.4[a]. Summary of Weighted Water Fluxes for Each Climate 6-80
6.5.7.5[a]. Factors Influencing Temporal Variability in Net Infiltration 6-80
6.5.7.6[a]. Factors Influencing Spatial Variability in Net Infiltration 6-80
6.5.7.7[a]. Illustration of Daily Water Balance Patterns 6-83
6.5.7.8[a]. Summary and Discussion of Net Infiltration Results for Present-Day and Future Climates 6-87
6.5.7.9[a]. Comparison of Results from Each LHS Replicate 6-88
6.6[a]. INFILTRATION PREDICTION UNCERTAINTIES 6-89
6.6.1[a]. Uncertainty in Potential Recharge Averaged over the Unsaturated Zone Model Domain 6-90
6.6.1.1[a]. Uncertainty in Potential Recharge over the Unsaturated Zone Model Domain during the Present-Day Climate 6-91
6.6.1.2[a]. Uncertainty in Potential Recharge over the Unsaturated Zone Model Domain during the Monsoon Climate 6-94
6.6.1.3[a]. Potential Recharge over the Unsaturated Zone Model Domain during the Glacial Transition Climate 6-96
6.6.2[a]. Uncertainty in Local Net Infiltration 6-99
6.6.3[a]. Sources and Magnitude of Model Uncertainty 6-99
6.7[a]. SENSITIVITY ANALYSIS 6-101
6.8[a]. NOMENCLATURE USED IN SECTION 6 EQUATIONS 6-101

7[a]. VALIDATION 7-1
7.1[a]. CONFIDENCE BUILDING DURING MODEL DEVELOPMENT 7-1
7.1.1[a]. Precipitation 7-1
7.1.1.1[a]. Comparison of Seasonal Precipitation Patterns 7-1
7.1.1.2[a]. Comparison of Mean Annual Precipitation (MAP) 7-6
7.1.1.3[a]. Present-Day Precipitation Comparison 7-6
7.1.1.4[a]. Monsoon Precipitation Comparison 7-6
7.1.1.5[a]. Glacial Transition Precipitation Comparison 7-6
7.1.2[a]. Evapotranspiration and Storage 7-6
7.1.2.1[a]. Lysimeter Simulations at the Nevada Test Site 7-6

CONTENTS (Continued)

Page

7.1.2.2[a]. Lysimeter Simulations at the Reynolds Creek Experimental Watershed 7-14
7.1.3[a]. Run-on/Runoff 7-20
7.1.3.1[a]. Runoff and Net Infiltration Comparison 7-22
7.1.3.2[a]. Soil Conductivity Variation Illustration for Entire Net Infiltration Modeling Domain 7-22
7.1.4[a]. Extended Parameter Sensitivity Study (Large LHS) 7-29
7.1.5[a]. Summary of Confidence Building during Model Development 7-29
7.2[a]. POST-DEVELOPMENT MODEL VALIDATION 7-29
7.2.1[a]. Corroboration of Model Results with Data and Relevant Observations 7-29
7.2.1.1[a]. Corroboration of Model Results with Field Data 7-29
7.2.1.2[a]. Comparison of Infiltration Estimates with Other Models and Data from Comparable Environments 7-37
7.2.2[a]. Corroboration of MASSIF Infiltration Model Using Alternative Model Approach 7-59
7.2.3[a]. Corroboration of Model Results with Infiltration and Percolation Estimates from 1997 Expert Elicitation Panel 7-68
7.2.4[a]. Corroboration of Soil Depth Class 4 Data using Data Collected by the CNWRA 7-69
7.3[a]. VALIDATION AND CORROBORATION SUMMARY 7-74

8[a]. CONCLUSIONS 8-1
8.1[a]. SUMMARY AND FINDINGS 8-1
8.1.1[a]. Data Tracking Numbers for Data Generated in This Report 8-3
8.2[a]. MODEL UNCERTAINTY AND LIMITATIONS 8-9
8.3[a]. YUCCA MOUNTAIN REVIEW PLAN CRITERIA ASSESSMENT 8-9

9[a]. INPUTS AND REFERENCES 9-1
9.1[a]. DOCUMENTS CITED 9-1
9.2[a]. CODES, STANDARDS, REGULATIONS, AND PROCEDURES 9-18
9.3[a]. SOURCE DATA, LISTED BY DATA TRACKING NUMBER 9-18
9.4[a]. DEVELOPED DATA, LISTED BY DATA TRACKING NUMBER 9-20
9.5[a]. SOFTWARE CODES 9-21

APPENDIX A[a] OUTSIDE SOURCES QUALIFIED FOR INTENDED USE A-1

APPENDIX B[a] GEOSPATIAL DATABASE B-1

APPENDIX C[a] CALCULATION OF ET_0 (REFERENCE EVAPOTRANSPIRATION) AS A FUNCTION OF SLOPE AND AZIMUTH C-1

CONTENTS (Continued)

Page

APPENDIX D[a] METHODS FOR DERIVING TRANSPIRATION COEFFICIENTS FOR VEGETATION AT YUCCA MOUNTAIN D-1

APPENDIX E[a] QUANTIFYING AND SIMULATING YUCCA MOUNTAIN VEGETATION RESPONSE E-1

APPENDIX F[a] DEVELOPMENT OF STOCHASTIC PRECIPITATION AND OTHER CLIMATE INPUT FILES F-1

APPENDIX G[a] DESCRIPTION OF THE MASSIF ROUTINES G-1

APPENDIX H[a] SENSITIVITY ANALYSIS OF MEAN ANNUAL INFILTRATION H-1

APPENDIX I[a] TREATMENT OF UNCERTAINTIES I-1

APPENDIX J[a] SUPPORTING INFORMATION ON VALIDATION OF EVAPOTRANSPIRATION USING SOIL WATER STORAGE MEASUREMENTS IN WEIGHING LYSIMETERS J-1

APPENDIX K[a] SUPPORTING INFORMATION ON CORROBORATION OF INFILTRATION USING AN ALTERNATIVE MODEL APPROACH K-1

APPENDIX L[a] PRELIMINARY RESULTS AND OUTPUTS L-1

INTENTIONALLY LEFT BLANK

FIGURES

Page

6.2.1-1[a]. Processes Controlling Net Infiltration 6-2
6.5.1.7-1[a]. Number of Hourly Intervals of Precipitation Plotted against the Daily Amount of Precipitation for the Present Weather Stations BSC1, BSC2, BSC3, and BSC6 6-17
6.5.1.7-2[a]. Number of Hourly Intervals of Precipitation Plotted against the Daily Amount of Precipitation for the Upper Monsoon Weather Stations of Hobbs, NM, and Nogales, AZ 6-18
6.5.1.7-3[a]. Number of Hourly Intervals of Precipitation Plotted against the Daily Amount of Precipitation for the Lower Glacial Transition Weather Station of Delta, UT 6-18
6.5.1.7-4[a]. Number of Hourly Intervals of Precipitation Plotted against the Daily Amount of Precipitation for the Upper Glacial Transition Weather Station of Spokane, WA 6-19
6.5.2.1-1[a]. Infiltration Modeling Boundaries 6-23
6.5.2.1-2[a]. Yucca Mountain Watersheds (Basins) 6-24
6.5.2.1-3[a]. Elevation over the Model Area 6-26
6.5.2.1-4[a]. Slope over the Model Area 6-27
6.5.2.1-5[a]. Azimuths for Model Area 6-28
6.5.2.2-1[a]. Map Showing Distribution of Soil Types Over the Infiltration Domain 6-31
6.5.2.2-2[a]. Map Showing Distribution of Alternative Soil Groupings over the Infiltration Domain 6-33
6.5.2.4-1[a]. Distribution of Soil Depth Classes over the Infiltration Domain 6-35
6.5.2.4-2[a]. Normal Probability Plot for 35 Observations of Soil Depth in Soil Depth Class 4 Region 6-40
6.5.2.4-3[a]. CDFs for 35 Observations (red dots), Least-square Fitted Lognormal Distribution (blue line), and Probability Plot Fitted Lognormal Distribution (orange line) in Log-scale for Soil Depth (X-axis) 6-41
6.5.2.4-4[a]. CDF of Estimated Distribution of 1,000 Soil Depth Values Using Six Soil Depth Ranges from the Sanchez Notebook 6-43
6.5.2.4-5[a]. Probability Plot for Estimated Distribution Based on Sanchez Notebook 6-44
6.5.2.4-6[a]. CDFs for Estimated Distribution (red dots), Least-Square Fitted Lognormal Distribution (blue line), and Probability Plot Fitter Lognormal Distribution (orange line) 6-44
6.5.2.5-1[a]. Distribution of Infiltration Hydrogeologic Units across the Model Area 6-49
6.5.3.5-1[a]. Temporal Curves Developed by the Weighting Functions in Table E-4 6-57
6.5.7.1-1[a]. Present-Day Mean Annual Precipitation CDF 6-59
6.5.7.1-2[a]. Present-Day, 10th Percentile Mean Annual Net Infiltration Map (Replicate R2, Realization 10) 6-62
6.5.7.1-3[a]. Present-Day, 30th Percentile Mean Annual Net Infiltration Map (Replicate R2, Realization 2) 6-63
6.5.7.1-4[a]. Present-Day, 50th Percentile Mean Annual Net Infiltration Map (Replicate R2, Realization 8) 6-64

FIGURES (Continued)

Page

6.5.7.1-5[a]. Present-Day, 90th Percentile Mean Annual Net Infiltration Map (Replicate R2, Realization 14) 6-65
6.5.7.1-6[a]. Cumulative Distribution Function (CDF) of Present-Day Spatially Averaged Mean Annual Net Infiltration over the Infiltration Domain 6-66
6.5.7.2-1[a]. Monsoon Mean Annual Precipitation CDF 6-67
6.5.7.2-2[a]. Monsoon, 10th Percentile Mean Annual Net Infiltration Map (Replicate R1, Realization 17) 6-69
6.5.7.2-3[a]. Monsoon, 30th Percentile Mean Annual Net Infiltration Map (Replicate R2, Realization 10) 6-70
6.5.7.2-4[a]. Monsoon, 50th Percentile Net Infiltration Map (Replicate R1, Realization 2) 6-71
6.5.7.2-5[a]. Monsoon, 90th Percentile Net Infiltration Map (Replicate R1, Realization 7) 6-72
6.5.7.2-6[a]. Cumulative Distribution Function (CDF) of Monsoon Net Infiltration Averaged over the Infiltration Domain 6-73
6.5.7.3-1[a]. Glacial Transition Mean Annual Precipitation CDF 6-74
6.5.7.3-2[a]. Glacial Transition, 10th Percentile Mean Annual Net Infiltration Map (Replicate R2, Realization 6) 6-76
6.5.7.3-3[a]. Glacial Transition, 30th Percentile Mean Annual Net Infiltration Map (Replicate R2, Realization 10) 6-77
6.5.7.3-4[a]. Glacial Transition, 50th Percentile Mean Annual Net Infiltration Map (Replicate R1, Realization 18) 6-78
6.5.7.3-5[a]. Glacial Transition, 90th Percentile Mean Annual Net Infiltration Map (Replicate R2, Realization 1) 6-79
6.5.7.3-6[a]. Cumulative Distribution Function (CDF) of Glacial Transition Spatially Averaged Mean Annual Net Infiltration over the Infiltration Domain 6-80
6.5.7.7-1[a]. Daily Weather Inputs for the Simulated Year 6-84
6.5.7.7-2[a]. Daily Values of K_{cb} and Canopy Fraction (f_c) for the Simulated Year 6-84
6.5.7.7-3[a]. Daily Water Fluxes (Evaporation, Transpiration, and Reference ET) for the Simulated Year 6-85
6.5.7.7-4[a]. Daily Soil Water Levels for the Simulated Year 6-86
6.5.7.7-5[a]. Daily Run-on and Runoff for the Simulated Year 6-87
6.5.7.7-6[a]. Daily Net Infiltration for the Simulated Year 6-87

7.1.1.1-1[a]. Average Monthly Precipitation Comparison Between Observed Records and 1,000-yr Generation for Yucca Mountain Site 2: (a) Using Second Order (one-harmonic truncated) Fourier Series and (b) Using Third Order (one and two harmonics) Truncated Fourier Series 7-2
7.1.1.1-2[a]. Average Monthly Precipitation Comparison Between Observed Records and 1,000-yr Generation for Site A12: (a) Using Second Order (one-harmonic truncated) Fourier Series and (b) Using Third Order (one and two harmonics) Truncated Fourier Series 7-2

FIGURES (Continued)

Page

7.1.1.1-3[a]. Average Monthly Precipitation Comparison Between Observed Records and 1,000-yr Generation for Hobbs (NM): (a) Using Second Order (one-harmonic truncated) Fourier Series and (b) Using Third Order (one and two harmonics) Truncated Fourier Series 7-3

7.1.1.1-4[a]. Average Monthly Precipitation Comparison Between Observed Records and 1,000-yr Generation for Nogales (AZ): (a) Using Second Order (one-harmonic truncated) Fourier Series and (b) Using Third Order (one and two harmonics) Truncated Fourier Series 7-3

7.1.1.1-5[a]. Average Monthly Precipitation Comparison Between Observed Records and 1,000-yr Generation for Spokane (WA): (a) Using Second Order (one-harmonic truncated) Fourier Series and (b) Using Third Order (one and two harmonics) Truncated Fourier Series 7-4

7.1.1.1-6[a]. Average Monthly Precipitation Comparison Between Observed Records and 1,000-yr Generation for Delta (UT): (a) Using Second Order (one-harmonic truncated) Fourier Series and (b) Using Third Order (one and two harmonics) Truncated Fourier Series 7-5

7.1.2.1-1[a]. NTS Weighing Lysimeter Schematic 7-7

7.1.2.1-2[a]. Observed Daily Water Storage and Precipitation at the NTS Lysimeter Site 7-8

7.1.2.1-3[a]. Simulation of Soil Water Storage in the NTS Lysimeters 7-10

7.1.2.1-4[a]. Comparison between the Measured K_{cb} and NDVI Values and Calculated Vegetated Lysimeter K_{cb} Values for the Different Water Years 7-13

7.1.2.2-1[a]. Total Soil Water Storage Calculated Using Daily Change-in-storage from LSCW and Integrated Water Content from Neutron Probe Measurements 7-16

7.1.2.2-2[a]. Simulation of Soil Water Storage in RCEW Lysimeter 7-18

7.1.2.2-3[a]. 1978 Average Monthly Rates of Actual Evapotranspiration at RCEW 7-19

7.1.2.2-4[a]. 1979 Average Monthly Rates of Actual Evapotranspiration at RCEW 7-19

7.1.3-1[a]. Map View of Watersheds and Locations of Various Field Data 7-21

7.1.3.2-1[a]. Present-Day, 10th Percentile Net Infiltration Map (Soil Conductivity Variation) (Replicate R2, Realization 10) 7-25

7.1.3.2-2[a]. Present-Day, 30th Percentile Net Infiltration Map (Soil Conductivity Variation) (Replicate R2, Realization 2) 7-26

7.1.3.2-3[a]. Present-Day, 50th Percentile Net Infiltration Map (Soil Conductivity Variation) (Replicate R2, Realization 8) 7-27

7.1.3.2-4[a]. Present-Day, 90th Percentile Net Infiltration Map (Soil Conductivity Variation) (Replicate R2, Realization 14) 7-28

7.2.1.1-2[a]. Comparison of Net Infiltration Calculated from Neutron Logging Data versus MASSIF Net Infiltration for Winter 1995 7-37

7.2.1.2-1[a]. Comparison of MASSIF Net Infiltration Results for Three Climates with Several Models 7-39

7.2.1.2-2[a]. Comparison of Recharge Estimates for Nevada Hydrographic Areas/Subareas with MASSIF Estimates of Net Infiltration at Yucca Mountain 7-52

FIGURES (Continued)

Page

7.2.1.2-4[a]. Comparison of Recharge Estimates for Columbia Plateau with MASSIF Estimates of Net Infiltration at Yucca Mountain 7-55
7.2.1.2-5[a]. Comparison of MASSIF, Center for Nuclear Waste Regulatory Analyses, and NRC Net Infiltration (and Percolation) Fluxes. 7-58
7.2.2-1[a]. Conceptual Model Used in the Alternative Model Corroboration Analysis..... 7-60
7.2.2-2[a]. Atmospheric Boundary Conditions Used in MASSIF and HYDRUS-1D 7-61
7.2.2-3a[a]. Soil Water Storage and Cumulative Infiltration for Model 1 7-63
7.2.2-3b[a]. Soil Water Storage and Cumulative Infiltration for Model 2 7-64
7.2.2-3c[a]. Soil Water Storage and Cumulative Infiltration for Model 3 7-64
7.2.2-3d[a]. Soil Water Storage and Cumulative Infiltration for Model 4 7-65
7.2.2-4[a]. Annual Water Balance Components for Alternative Model Comparison 7-66
7.2.3-1[a]. MASSIF Net Infiltration Results for Present-Day Climate for the 2002 Repository Footprint Compared with Percolation Fluxes at the Repository Horizon from the 1997 Expert Elicitation Panel..... 7-69
7.2.4-1[a]. Extent of Soil Depth Class 4 With 35 Soil Sampling Locations Used In ANL-NBS-HS-000077 REV01 to Characterize Soil Depth Class 4, and 56 Soil Sampling Locations Recorded by the CNWRA 7-71
7.2.4-2[a]. Distribution of Soil Depths from YMP and CNWRA Observations..... 7-73

8-1[a]. Data Flow for the MASSIF Net Infiltration Model 8-5

B-1[a]. Infiltration Modeling Boundaries B-2
B-2[a]. Elevation across Project Area B-7
B-3[a]. Full Terrain Processing ArcToolbox Steps.....B-9
B-4[a]. Slope across Project Area B-11
B-5[a]. Azimuth across Project Area B-12
B-6[a]. Results of Three-Stage Watershed Delineation and Final Basin Combination.....B-15
B-7[a]. Bedrock Zones across Project Area as described in Section 6.5.2 .....B-18
B-8[a]. Soil Depth Zones across Project Area as described in Section 6.5.2.....B-19
B-9[a]. Road Soil Class (Red pixels in left frame) Removed within Project Area and Replaced with Appropriate Soil Class (right frame).....B-20
B-10[a]. Soil Type Zones across Project Area as described in Section 6.5.2 .....B-21
B-11[a]. PVR Values across Project Area as described in Appendix E.....B-22
B-12[a]. Downstream Cell ID Adjustment Values B-23
B-13[a]. Stream Gauges: Original and Spatial Database Locations B-24
B-15[a]. Locations of MASSIF Model Watersheds, UZ Boundary, and the Repository Footprint B-26

D-3[a]. Generalized Crop Coefficient Curve D-2

F-1[a]. Model versus Measured Temperatures for Wet Days, Beowawe, Nevada.....F-3
F-2[a]. Model versus Measured Temperatures for Dry Days, Beowawe, Nevada F-4

TABLES

Page

4-1[a]. Direct Input Data 4-1

6.1-1[a]. FEPs Addressed in This Model Report 6-1
6.5.1.1-1[a]. Meteorological Stations Selected to Represent Future Climate States at Yucca Mountain 6-10
6.5.1.7-1[a]. Nominal Values and Uncertainties for Snow Parameters 6-16
6.5.1.7-2[a]. Weather Stations Used for Precipitation Duration Analyses 6-16
6.5.1.7-3[a]. Precipitation Duration Linear Regression Results 6-19
6.5.1.7-4[a]. Precipitation Duration Parameter for Each Climate 6-19
6.5.2.1-1[a]. Number of Grid Cells within Various Boundaries in the Yucca Mountain Region 6-25
6.5.2.2-1[a]. Base Case Soil Units 6-30
6.5.2.2-2[a]. Soil Type Cell Counts for the UZ Grid and Infiltration Model Domain 6-34
6.5.2.4-1[a]. Soil Depth Class Cell Counts for the UZ and Infiltration Model Domains 6-36
6.5.2.4-2[a]. Summary of Recommended Distributions for Soil Depth 6-36
6.5.2.4-3[a]. Summary of Recommended Distributions for Effective Soil Depths ($depth_{soil}$) 6-38
6.5.2.4-4[a]. Summary of Soil Depth Ranges Defined Based on Alex Sanchez Observations 6-42
6.5.2.4-5[a]. Estimation of Geometric Mean and Confidence Interval (by adding or subtracting one standard error) 6-45
6.5.2.4-6[a]. Estimation of Arithmetic Mean and Confidence Bounds (by adding or subtracting one standard error) 6-46
6.5.2.5-1[a]. Bedrock Cell Counts for the UZ Grid and Infiltration Model Domain 6-50
6.5.3.1-1[a]. Monthly Temperature and Precipitation for Upper-Bound Monsoon (Nogales, Arizona, and Hobbs, New Mexico) and Present-Day (Desert Rock) Climates 6-52
6.5.3.1-2[a]. Monthly Temperature and Precipitation for the Glacial Transition Climate 6-53
6.5.3.5-1[a]. Landsat TM Data Used for Characterization of Yucca Mountain Vegetation 6-56
6.5.7.1-1[a]. Mean Annual Precipitation Statistics for the 40 Realizations Used to Represent Present-Day Climate for Net Infiltration Calculations 6-60
6.5.7.1-2[a]. Spatially Averaged Mean Annual Net Infiltration [mm/yr] Statistics for Present-Day Simulations 6-60
6.5.7.1-3[a]. Realizations Identified for Selected Percentiles of Present-Day Spatially Averaged Mean Annual Net Infiltration 6-61
6.5.7.2-1[a]. Mean Annual Precipitation Statistics for the 40 Realizations used to Represent Monsoon Climate for Net Infiltration Calculations 6-67
6.5.7.2-2[a]. Spatially Averaged Mean Annual Net Infiltration [mm/yr] Statistics for Monsoon Simulations 6-68
6.5.7.2-3[a]. Realizations Identified for Selected Percentiles of Monsoon Spatially Averaged Mean Annual Net Infiltration 6-68

TABLES (Continued)

Page

6.5.7.3-1[a]. Mean Annual Precipitation Statistics for the 40 Realizations Used to Represent Glacial Transition Climate for Net Infiltration Calculations 6-74
6.5.7.3-2[a]. Spatially Averaged Mean Annual Net Infiltration Statistics for Glacial Transition Simulations 6-75
6.5.7.3-3[a]. Realizations Identified for Selected Percentiles of Glacial Transition Spatially Averaged Mean Annual Net Infiltration 6-75
6.5.7.6-1[a]. Percent of Total Net Infiltration (and standard deviation) That Occurs in Each Soil Depth Class for Present-Day Climate Simulations (Entire Net Infiltration Modeling Domain) 6-81
6.5.7.6-2[a]. Percent of Total Net Infiltration (and standard deviation) That Occurs in Each Soil Group for Present-Day Climate Simulations (Entire Net Infiltration Modeling Domain) 6-81
6.5.7.6-3[a]. Percent of Total Net Infiltration (and standard deviation) That Occurs in Each Rock Type for Present-Day Climate Simulations (Entire Net Infiltration Modeling Domain) 6-82
6.5.7.7-1[a]. Properties of the Grid Cell Selected for Illustration of Daily Water Balance Patterns 6-83
6.5.7.8-1[a]. Summary Net Infiltration Statistics for the Three Climates 6-88
6.5.7.9-1[a]. Differences in Net Infiltration Statistics between Replicates 6-89
6.6.1-1[a]. Parameters of Lognormal Distributions Representing the Contributions of Parameter Uncertainty to Uncertainties in Potential Recharge, Averaged over the UZ Model Grid 6-91
6.6.1.1-1[a]. Values of Potential Recharge over the UZ Flow Model Area as Calculated for the Present-Day Climate, Sorted 6-92
6.6.1.1-2[a]. W test for Lognormal Uncertainty Distribution for Potential Recharge over the UZ Flow Model Area during the Present-Day Climate 6-93
6.6.1.2-1[a]. Values of Potential Recharge over the UZ Flow Model Area as Calculated for the Monsoon Climate, Sorted 6-95
6.6.1.2-2[a]. W Test for Lognormal Uncertainty Distribution for Potential Recharge over the UZ Flow Model Area during the Monsoon Climate 6-95
6.6.1.3-1[a]. Values of Potential Recharge over the Unsaturated Zone Model Domain as Calculated for the Glacial Transition Climate, Sorted 6-97
6.6.1.3-2[a]. W Test for Lognormal Uncertainty Distribution for Potential Recharge over the Unsaturated Zone Model Domain during the Glacial Transition Climate 6-98

7.1.3.2-1[a]. Comparison of Mean Net Infiltration Results of the Soil Conductivity Variation Simulations with Results of the Uncertainty Analysis 7-23
7.1.3.2-2[a]. Comparison of Percent of the Total Net Infiltration Occurring in Each Soil Group between the Soil Conductivity Variation Simulations and the Results of the Uncertainty Analysis 7-24
7.2.1.1-1[a]. Summary of MASSIF Results for South Ramp Infiltration Simulations 7-31
7.2.1.2-1[a]. Maxey-Eakin Recharge Estimates for Selected Nevada Hydrographic Areas/Subareas 7-40

TABLES (Continued)

Page

7.2.1.2-2[a]. Chloride Mass Balance Recharge Estimates for Selected Nevada Hydrographic Areas/Subareas [a] 7-47
7.2.1.2-3[a]. Water Budget Model Recharge Estimates for Selected Nevada Hydrographic Areas/Subareas [a] 7-48
7.2.1.2-4[a]. Deuterium Mixing Model Recharge Estimates for Selected Nevada Hydrographic Areas/Sub-Areas [a] 7-49
7.2.1.2-5[a]. Recharge to 3-Springs Basin, Central Nevada [a] 7-50
7.2.1.2-6[a]. Modified Maxey-Eakin Recharge Estimates for 16 Nevada Hydrographic Areas [a] 7-50
7.2.1.2-9[a]. Recharge Estimates for Zones on the Columbia Plateau 7-53
7.2.1.2-10[a]. Estimated Recharge Rates at the Hanford Site for Combinations of Soil Type and Vegetation/Land Use 7-56
7.2.2-1[a]. Summary of the Water Balance Results 7-67
7.2.4-1[a]. Comparison of Summary of Distributions for CNWRA and YMP Soil Depth Data 7-72
7.3-1[a]. Validation Output Data Tracking Numbers 7-75

8-1[a]. Output Data Sets Generated in the Development and Application of the Net Infiltration Model 8-3

B-1[a]. Elevation Change Documented as a Result of the *Fill* Process B-10
B-6[a]. Boundary Files Watershed Catchments B-28

E-1[a]. Landsat TM Data Used for Characterization of Yucca Mountain E-1
E-Uncertainty−3[a]. Reflectance Statistics of Pixel Values within the Model Boundary, Landsat TM5 4/11/1998 ..... E-1

F-1[a]. Fourier Parameters for p_{00} and p_{10} at Stations Representing the Present-Day Climate F-5
F-2[a]. Fourier Parameters for λ and m at Stations Representing the Present-Day Climate F-5
F-2a[a]. Mean Annual Precipitation at Site and Regional Stations Compared with Values Implied by Fourier Coefficients F-5
F-3[a]. Lapse Rates for Parameters of the Present-Day Climate F-7
F-4[a]. Parameters for p00 and p10 at Stations Representing the Present-Day Climate Adjusted to an Elevation of 1,524 m F-8
F-5[a]. Parameters for λ and m at Stations Representing the Present-Day Climate Adjusted to an Elevation of 1,524 m F-9
F-6[a]. Wet Day Fraction and Mean Annual Precipitation Implied by Parameters Adjusted to an Elevation of 1,524 m F-9
F-7[a]. Fourier Parameters for Wet Day Temperatures at Stations Representing the Present-Day Climate F-10
F-8[a]. Fourier Parameters for Dry Day Temperatures at Stations Representing the Present-Day Climate F-10

TABLES (Continued)

Page

F-9[a]. Zero-Order Temperature Parameters for Stations Representing the Present-Day Adjusted to an Elevation of 1,524 m..... F-11

ACRONYMS AND ABBREVIATIONS

BSC	Bechtel SAIC Company
CDF	cumulative distribution functions
cm	centimeter
CNWRA	Center for Nuclear Waste Regulatory Analyses
CR	Condition Report
DEM	digital elevation model
DIRS	Document Input Reference System
DOE	U.S. Department of Energy
DOY	day of the year
DTN	data tracking number
EPA	U.S. Environmental Protection Agency
ESF	Exploratory Studies Facility
ET	evapotranspiration
ET_0	reference evapotranspiration
FAO	Food and Agricultural Organization of the United Nations
FAO-56	Food and Agricultural Organization of the United Nations [FAO] Irrigation and Drainage Paper 56
f_c	fraction covered
FEP	feature, event, or process
GIS	geographic information system
GTC	Glacial Transition Climate
IBP	International Biological Program
LA	*Larrea-Ambrosia*
LHS	Latin Hypercube Sampling
LN m	lognormal mean
LSCW	Lower Sheep Creek West
m	meter
MAP	mean annual precipitation
MASSIF	Mass Accounting System for Soil Infiltration and Flow
MC	Monsoon Climate
mm	millimeter
MPa	megapascal
NDVI	Normalized Difference Vegetation Index
NDVI'	NDVI corrected for the Yucca Mountain environment
NED	national elevation dataset
NRC	U.S. Nuclear Regulatory Commission
NTS	Nevada Test Site

ACRONYMS AND ABBREVIATIONS (Continued)

NWRC	Northwest Watershed Research Center
PVR	potential vegetation response
QA	Quality Assurance
RCEW	Reynolds Creek Experimental Watershed
SRTM	Shuttle Radar Topography Mission
STN	software tracking number
SZ	saturated zone
TSPA	total system performance assessment
TWP	technical work plan
USDA	U.S. Department of Agriculture
USGS	United States Geological Survey
UTM	Universal Transverse Mercator
UZ	unsaturated zone
WY	water year
YM	Yucca Mountain
YMP	Yucca Mountain Project
YMRP	*Yucca Mountain Review Plan, Final Report*

1[a]. PURPOSE

The purpose of this addendum is to address conditions adverse to quality documented in 10 Condition Reports (CRs): 10731, 10772, 10777, 10783, 10788, 11192, 11360, 11459, 11554, and 11620. With the exception of CR 10788, these CRs only affect the parent report of this addendum.

Each section in the parent report, including unchanged sections, is mirrored in this addendum by a section with the same number with "[a]" added. Unchanged sections are indicated by the statement "No change." Changed sections completely replace their counterparts in the parent report, unless indicated otherwise. References to sections, figures, or tables without "[a]" refer to the parent report.

This addendum addresses four technical issues that were documented in CR 10783 identified by the U.S. Department of Energy (DOE) by adding new text and analyses to Section 7[a]. Three of the four issues are related to soil depth data. The fourth requires additional discussion to justify the exclusion of neutron logging data from model validation. A new section (7.2.4[a]) was added to Section 7[a] to address CR 10783 comments related to soil depth data collected by the CNWRA and documented in a letter to J. Guttmann by Fedors (2007 [DIRS 182469]). These data are compared to the YMP data used to establish statistical parameters for Soil Depth Class 4. Output DTN: SN0708T0502206.048, which contains the comparisons of CNWRA soil depth data to YMP soil depth data, has been developed for this addendum. This Output DTN also includes the calculations discussed in Appendix B of *Data Analysis for Infiltration Modeling: Technical Evaluation of Previous Soil Depth Estimation Methods and Development of Alternate Parameter Values* (BSC 2006 [DIRS 178819]). All eight issues identified in CR 10783, and responses to those issues follow:

- Reduce Uncertainty and Biased Spatial Variability of Soil Depth Classification 4

  Section 7.2.4[a] of this addendum includes a discussion of the impact of using lognormal versus uniform (and log-uniform) distributions for the soil depth datasets used to develop the range of shallow soil depth (Soil Depth Class 4). It also includes a comparison of Yucca Mountain Project (YMP) and Center for Nuclear Waste Regulatory Analyses (CNWRA) soil-depth datasets, and a discussion of potential spatial bias in sampling locations. In addition, some text in Section 6.5.2.4[a] was revised to clarify shallow soil depth data ranges and distributions.

- Reevaluate Definition and Range of Field Capacity

  The net infiltration model (MASSIF) documented in this addendum and the parent report uses a field capacity water content value that corresponds to water potential between -0.1 and -1/3 bars, which is consistent with literature on the subject. If a value higher (wetter) than -0.1 bars, perhaps as high as -0.04 bars, as suggested in CR 10783, is more appropriate for Yucca Mountain soils, then the range used adds conservatism to model results by over-estimating net infiltration.

- Consider Improving Data Spatial Variability for Soils, Hill Slopes and Ridges, and Hydraulic Properties

The acquisition of additional site-specific data was not necessary because the ranges used are bounding. The incorporation of other available data sets was not done due to the lack of transparency required for Yucca Mountain qualified datasets.

- List Assumptions that Bias Infiltration Calculations Toward Overestimation

The goal is to ensure net infiltration is not underestimated, and to use realistic parameter values and ranges. The only assumption that explicitly biases net infiltration estimates toward overestimation is the assumption that there is no removal of water from bedrock by evapotranspiration (Assumption 6 in Table 5-1 of the parent report).

- Consider Including Large Precipitation Events in Future Climates

Large precipitation events for future climates were included. Forty-year precipitation records from analog sites were not used as direct model input. Rather, 1,000-year stochastically generated precipitation records that included very large precipitation events were used as direct model input (see Section 6.5.1 and Appendix F of the parent report).

- Add Discussion of "Representativeness" as Data Quality Criterion [and include text to justify the exclusion of neutron probe data]

This type of discussion is not within the scope of this report. Additional text was added to Section 7.2.1.1.3[a] to justify the exclusion of neutron logging data from model validation.

- Consider Other Available Data Sets and Justify Pedo-Transfer Method

Soil depth data collected by the CNWRA was used for corroboration in this addendum in Section 7.2.4[a]. The pedotransfer approach is described in detail in *Data Analysis for Infiltration Modeling: Development of Soil Units and Associated Hydraulic Parameter Values* (BSC 2006 [DIRS 176335]), and is qualified for use in this model as output of that analysis (BSC 2006 [DIRS 176335]). Additional unqualified data sets, such as those for soil depth listed in Appendix A of *Data Analysis for Infiltration Modeling: Technical Evaluation of Previous Soil Depth Estimation Methods and Development of Alternate Parameter Values* (BSC 2006 [DIRS 178819]) cannot necessarily be readily qualified for use as suggested in CR 10783, and the YMP has chosen to use the qualified data that are available. As CR 10783 notes, some field measurements for saturated hydraulic conductivity values are available, but these measurements were conducted for only a few locations; therefore they have limited value and are not used here. In addition, there are no hydraulic properties other than saturated hydraulic conductivity associated with these measurements.

- Add Discussion of Model Element Checking to Report

The recommendation is to add a more complete description of the checking of various elements of MASSIF to the text of this report. This was not done because the information is available in records and including it directly in the report would not provide any additional clarity and is not required by procedure.

This addendum also addresses typographical and other minor editorial corrections identified in comments received from the DOE on July 7, 2007, following the completion of REV 01 of the parent report in May 2007. Additional changes include the following:

- Section 7.2.4[a] is a new section not included in the parent report (to address CR 10783);
- Section 7.2.1.1.3[a] includes additional text to justify the exclusion of the neutron logging data for model validation (to address CR 10783);
- Significant edits were made to Section 7.1.2.2[a] compared to Section 7.1.2.2 in the parent report (to address CR 10731);
- Clarifying edits were made to Section 7.2.1.2.3[a] compared to Section 7.2.1.2.3 in the parent report as a result of one of the DOE comments;
- Significant changes were made to Appendix A (to address CR 10788);
- Changes were made to Figures 6.2-1[a], 6.5.7.7-5[a], 6.5.7.7-6[a], 7.1.2.2-3[a], 7.1.2.2-4[a], and 7.2.1.2-4[a]; and finally,
- Additional text and a new figure were added to a new Section 7.2.1.2.4[a] to compare MASSIF results to a new report published by the CNWRA (Stothoff and Walter, 2007 [DIRS 183834]).

CR 10772 is addressed with corrections to Table 4-1[a]. CRs 5698 and 6334 were incorrectly identified as closed in the parent report (as identified in CR 10777); however, they have since been closed. CR 10777 is also addressed by referring to CRs that have been addressed in this addendum as "eligible for closure" rather than closed. CR 11192 is addressed by correcting the citation of "DOE 2007 [DIRS 180680]," in Section 9.1[a]. Previously, the citation had been given as "Howell and Runkle (2007)," but that was an unverified reference.

This addendum also addresses two CRs related to the UZ flow model domain and repository footprint that are used in the parent report. The UZ flow model and repository footprints are shown in numerous figures in the parent report, and statistics such as average annual net infiltration through these footprints are calculated and presented in numerous tables in the parent report. CR 11360 documented an error in the conversion of coordinates used for the UZ flow model domain. CR 11459 documented that the 2002 version of the repository footprint was used in the parent report, but that a newer repository footprint has been developed. For CR 11360, the UZ flow model domain shown in numerous figures and the calculations of infiltration (and other water balance parameters) shown in numerous tables have been corrected in this addendum. In addition, DTN: SN0612FTPRNUZB.002 has been superseded with DTN: SN0711FTPRNUZB.003 and the MASSIF Output DTN: SN0701T0502206.037 has been

revised with the corrected data (Output DTN: SN0701T0502206.037, REV002). With regard to CR 11459, notes have been added to all figures showing the repository footprint stating, "Repository footprint shown for illustrative purposes only", and notes have been added to all tables with statistics for the repository footprint indicating that the 2002 repository footprint was used. Calculations comparing net infiltration using the 2002 and 2007 repository footprints are included in the revised Output DTN: SN0701T0502206.037, in order to provide the necessary information to close CR 11459, but these comparisons are not discussed in this addendum further. The statistics of infiltration (and other water balance parameters) for the UZ flow model and repository footprints are not used by any downstream report or model, so the error documented in CR 11360 and the notification of a newer 2007 repository footprint in CR 11459 have no effect on the total system performance assessment for License Application (TSPA-LA). Therefore, CRs 11360 and 11459 are eligible for closure.

This addendum addresses CR 11554 by documenting the supersession of DTN: SN0601ALANDSAT.001 [DIRS 177239]. This file was found to be corrupted in the Technical Data Management Systems (TDMS). The corrupted file was replaced with an uncorrupted file as DTN: SN0712ALANDSAT.002 [DIRS 184297] that supersedes DTN: SN0601ALANDSAT.001 [DIRS 177239].

Finally, this addendum addresses CR 11620 by completely replacing Section 7.2.1.2.1 with an updated data analysis and associated tables and figure. CR 11620 is eligible for closure with these changes. As part of this update, validation output DTN: SN0704T0502206.047 has been superseded by validation output DTN: SN0801T0502206.049.

1.1[a]. INTENDED USE

This model report documents the development and validation of a conceptual, mathematical, and numerical model for predicting net infiltration of water into the unsaturated zone. The model applies a simple water mass-balance approach to the near surface layer that is influenced by evapotranspiration. It uses a simplified representation of downward water flow whereby water moves from the top soil layer downward by sequentially filling each layer to "field capacity" before draining to the layer below. Water is removed from the "root zone" by evapotranspiration, which is represented using an empirical model based on reference evapotranspiration, transpiration coefficients, and moisture content in the root zone. Water is redistributed as surface runoff when the soil cannot accept all the available water at the surface. Precipitation is stochastically simulated on a daily timestep based on observed weather records.

This report also documents the use of the model for predicting the range and patterns of net infiltration at the Yucca Mountain site for the next 10,000 years. *Future Climate Analysis* (BSC 2004 [DIRS 170002], Section 7.1) forecasts three distinct climates during the next 10,000 years at Yucca Mountain. The present-day climate is predicted to persist for the next 400 to 600 years, followed by a warmer and much wetter monsoon climate lasting from 900 to 1,400 years. Following the monsoon climate, a cooler and wetter glacial-transition climate is expected. The work in this report provides an estimate of the net infiltration up to 10,000 years into the future for the Yucca Mountain Site.

Additional provisions in 10 CFR 63.341 [DIRS 176544] require the U.S. Department of Energy (DOE) to assess the peak dose that would occur after 10,000 years. The U.S. Nuclear Regulatory Commission (NRC) released proposed rules (70 FR 53313 [DIRS 178394]) that DOE represent the effects of climate change after 10,000 years by assuming that deep percolation rates vary between 13 to 64 mm/yr. Predictions of peak dose after 10,000 years are expected to utilize the deep percolation rates as proposed by the NRC.

The specific purpose of the model documented in this report is to provide a spatial representation, including epistemic and aleatory uncertainty, of the predicted mean annual net infiltration at the Yucca Mountain site during each climate. The resulting maps of mean annual net infiltration provide input directly to the updated versions of the following model reports:

- *UZ Flow Models and Submodels* (SNL 2007 [DIRS 175177])
- *Calibrated Unsaturated Zone Properties* (SNL 2007 [DIRS 179545]).

Information from this model report indirectly feeds total system performance assessment (TSPA) through its connection with the identified downstream products. This model is not intended to be a direct input to TSPA.

Daily precipitation provides water for potential infiltration. The infiltration model simulates processes occurring in and on the soil, including return of water vapor to the atmosphere by evaporation and plant transpiration (evapotranspiration), flow along the ground surface (runoff/run-on), and infiltration into the bedrock below the soil.

Revision 01 of the infiltration model report (and this addendum) were developed in accordance with *Technical Work Plan for: Infiltration Model Assessment, Revision, and Analyses of Downstream Impacts* (BSC 2006 [DIRS 177492], Section 1.1.4). The purpose of the revision is to increase confidence in the results by improving the traceability, transparency, and reproducibility of the model development, the selection of inputs for calculations, and the determination of net infiltration maps and fluxes. To those ends, this revision includes the following changes:

- A Mathcad calculation, MASSIF (Mass Accounting System for Soil Infiltration and Flow), replaces the INFIL software (INFIL V. 2.0.2001, STN: 10307-2.0-00 [DIRS 139422]; INFIL V. A_2.a1. 2001, STN: 10253-A_2.a1-00 [DIRS 147608]) used in the previous revision of this report (BSC 2004 [DIRS 170007]), while the underlying conceptual models for MASSIF and INFIL remains similar. The reasons for replacing the INFIL software and completely revising the previous revision of this report are explained in a DOE report (DOE 2007 [DIRS 180680], Sections 5.2 and 5.3).

- This revision includes an uncertainty analysis, replacing and expanding work included in *Analysis of Infiltration Uncertainty* (BSC 2003 [DIRS 165991]).

- Instead of taking input directly from multi-decade precipitation records, those records provide the basis for the development of stochastic parameters. Precipitation inputs are selected from 1,000-year stochastic simulations, assuring that the full range of annual precipitation uncertainty is considered, including years with heavy precipitation. Ten representative years are selected from the 1,000-year simulations for each climate state.

- An evapotranspiration submodel, based on guidelines published by the Food and Agriculture Organization (FAO) of the United Nations in Irrigation and Drainage Paper 56 (FAO-56), replaces the submodel that was used in INFIL. The guidelines are based on a combination FAO Penman-Monteith model (Allen et al. 1998 [DIRS 157311], Preface).

- All previous inputs to the infiltration calculations have been revised or requalified.

1.2[a]. LIMITATIONS

This section presents a list of limitations associated with the net infiltration model estimates presented in this report. These limitations arise from a number of sources, including limited knowledge of the system, simplifications invoked to represent the system, and general uncertainties.

The estimates of mean annual net infiltration at the soil–bedrock interface are made without consideration of how the properties of the rock at deeper locations vary with depth. Instead of net infiltration, some authors call this quantity "deep drainage" or "potential recharge." *UZ Flow Models and Submodels* (SNL 2007 [DIRS 175177]) describes the method for calculating replenishment of the aquifer from the surface, "recharge," taking into consideration the potential recharge as well as the complex, three-dimensional hydrogeologic structure and properties of the fractured bedrock and other considerations.

One consideration is the possibility that a significant fraction of the water that enters bedrock is lost to evaporation in the Tiva Canyon welded tuff (TCw). Such a water loss has been suggested by researchers looking at the stable oxygen isotopic chemistry of secondary calcite deposited in the TCw (Whelan et al. 2002 [DIRS 160442], pp. 743 to 744; Figure 8). This study suggests that evaporation losses from the unsaturated zone (UZ) may extend to the top of the Paintbrush nonwelded unit (PTn), which means that evaporative losses from the UZ may extend as deep as 100 m below the surface (Whelan et al. 2002 [DIRS 160442], Figure 8). The net infiltration model domain described in this report extends only from the surface to the soil–bedrock interface, and the net infiltration flux includes all water that moves downward across this interface. The current UZ flow model (SNL 2007 [DIRS 175177]) does not explicitly allow water to evaporate from the UZ domain below the soil-bedrock interface. Therefore, evaporation from the TCw is not explicitly captured by either of these models. However, the resulting UZ flow fields predicted by the UZ flow model (SNL 2007 [DIRS 175177]) are weighted by comparing UZ model results to sub-surface thermal and chemical data observed in the UZ domain. These datasets generally indicate that percolation rates below the TCw are lower than the net infiltration predicted above the TCw. Thus, the UZ model assigns higher weights to the lower range of the net infiltration distribution and therefore may indirectly account for water loss in the TCw.

The model documented in this report is valid only for the Yucca Mountain site and for the climates specified in *Future Climate Analysis* (BSC 2004 [DIRS 170002], Section 7.1). For each climate, the model produces maps of average annual infiltration as a function of location, with no time dependence. These output maps cover the variability and range of uncertainty in average annual net infiltration over the modeling domain.

Infiltration predictions are limited by the uncertainty in future weather patterns. Although a substantial body of literature supports the use of stochastic precipitation models, there are no records to support extrapolation of historical weather records from the last few decades to 1,000 years. Each available and relatively complete precipitation record, whether from the Yucca Mountain site, from a nearby weather station, or from a site representative of a future climate, covers no more than about 60 years. The methods used to represent future climate conditions for this model are described in Section 6.5.1 and Appendix F.

Infiltration predictions are also limited by uncertainties in the hydrologic properties of the soil and upper zone of the fractured bedrock that covers the 125-km^2 infiltration modeling domain. These uncertainties arise primarily from several sources. The first is the use of a pedotransfer function to estimate soil hydrologic properties from measured grain size distributions. This work is documented and the resulting soil properties are qualified for use in *Data Analysis for Infiltration Modeling: Development of Soil Units and Associated Hydraulic Parameter Values* (BSC 2006 [DIRS 176335]). The pedotransfer approach introduces uncertainty due to the fact that the Hanford soil property database represents soils in a location and depositional environment that is different from Yucca Mountain (Hanford, WA). Another source of uncertainty is in the saturated conductivity of the bedrock at the soil–bedrock interface. This parameter set is based on work documented in *Data Analysis for Infiltration Modeling: Bedrock Saturated Hydraulic Conductivity Calculation* (BSC 2006 [DIRS 176355]). The saturated conductivity values and uncertainty are based on measurements of fracture apertures, fracture densities, saturated conductivities of bedrock matrix and fracture filling material, and a model of conductivity based on the combination of these measurements. For each bedrock type, the lower end of the conductivity uncertainty range assumes completely filled fractures, and the upper end of the conductivity uncertainty range assumes a small open fracture component in each of the filled fractures. When multiple bedrock types are included in the uncertainty analysis, the extent of fracture filling can vary independently between rock types (see Sections 6.5.2.5[a] and 6.5.2.6). However, a limitation of this approach is that heterogeneity within a bedrock type is not represented. Because this approach is based on indirect measurements of saturated conductivity, there is a potential for significant model uncertainty in the results of the conductivity estimates.

Uncertainty in the soil depth representing the zone of shallow soils is significant. The upscaled value of soil depth for the shallow soil depth class varies by a factor of 5 (see Section 6.5.2.4[a]). Such variation is the result of the fact that very few qualified measurements of soil depth were available upon which to base a model of soil depth across the site. As shallow soil depth is shown to be the most significant physical parameter influencing mean net infiltration, the uncertainty in this parameter represents an important limitation on the accuracy of the mean net infiltration over the site.

Despite the intent of estimating the spatial distribution of mean annual net infiltration across the model domain, the accuracy of net infiltration estimates at any one location is limited by uncertainties in soil, bedrock, and vegetation properties at that location. As described briefly above, there are few direct measurements of soil and rock properties at Yucca Mountain. In order to run the model, it was necessary to define these properties for every 30 × 30-m grid cell in the infiltration modeling domain. The approach taken was to upscale and group the few available measurements and estimates for properties. This approach assumes that small scale variations in soil and rock properties are not as significant as variations that occur between different soil and rock types. This assumption is valid as long as small scale spatial variations in net infiltration are not important for downstream users. An example of this limitation is the answer to the question of whether net infiltration at Yucca Mountain is focused beneath stream channels. The results of the uncertainty analysis described in Section 6.5.7[a] indicate that little to no net infiltration occurs beneath stream channels where soil is especially thick. However, in Sections 7.1.3.1 and 7.1.3.2[a], it is shown that this particular result is very sensitive to the spatial distribution of soil conductivity. Since there is very little direct information about such a spatial distribution, there is considerable and significant uncertainty in the spatial distribution of net infiltration results. Furthermore, because soil and bedrock properties are represented as uniform over a spatial area assumed to define a given soil or rock type, the actual spatial variability of net infiltration is likely underestimated by the model. In addition, other processes that might effect the spatial distribution of net infiltration on a local scale (e.g., interflow) are assumed to be insignificant and are not included in the model (Section 5).

Finally, it should be stressed that the approach used to estimate water flow and storage within the rootzone is a simplification of the actual physical processes that control flow in this environment. The use of the "field capacity" concept acts as a flow switch allowing downward water flow at a rate equal to the saturated hydraulic conductivity when the average water content in a layer equals or exceeds "field capacity," and allowing no flow to occur when average water content in a layer is less than "field capacity." In reality, water will flow within the vadose zone in response to gradients in total soil-water potential, which is the sum of various components such as elevation, matric, pressure, temperature, and osmotic potentials. This approximation is discussed more fully in Sections 5 and 6.4.

1.3[a]. SCOPE OF THE DOCUMENT

No change.

1.4[a]. DEVIATIONS FROM THE TECHNICAL WORK PLAN

No change.

2[a]. QUALITY ASSURANCE

No change.

INTENTIONALLY LEFT BLANK

3[a]. USE OF SOFTWARE

No change.

INTENTIONALLY LEFT BLANK

4[a]. INPUTS

4.1[a]. DIRECT INPUT

No additional direct references are used in this addendum. All direct references used in this addendum or its parent report are listed in Table 4-1 of the parent report. Specific locations where direct inputs are used in this addendum may be found by referring to the DIRS report for this addendum. Table 4-1[a] addresses CR 10772 by correcting two entries in Table 4-1 of the parent report. These two entries are the result of typographical errors and they do not impact any model results. Table 4-1[a] also includes a change showing DTN: SN0712ALANDSAT.002 [DIRS 184297] which supersedes DTN: SN0601ALANDSAT.001 [DIRS 177239] (which was found to be corrupted as documented in CR 11554). In addition, Table 4-1[a] includes a change showing that output DTN: SN0711FTPRNUZB.003 supersedes DTN: SN0612FTPRNUZB.002 (as a result of CR 11360). All other text in Section 4 and references in Table 4-1 in the parent report remain unchanged.

Table 4-1[a]. Direct Input Data

Input Data Type	Input Data Description	Location in This Model Report	Source
Soil maps	Soil depth class and type boundaries	Sections 6.5.2.2[a], 6.5.2.4[a], Appendix B; Output DTNs: SN0606T0502206.011, SN0701SPALAYER.002	DTN: MO0608SPASDFIM.006 [DIRS 178082]
Bedrock map	Bedrock boundaries	Sections 6.5.2.2[a], 6.5.2.4[a], 6.5.2.5[a], Appendix B; Output DTNs: SN0606T0502206.011, SN0701SPALAYER.002	DTN: MO0603SPAGRIDD.003 [DIRS 177121], file: *IHU_map_file2.txt*
LandSat images	Satellite imagery	Output DTNs: SN0608NDVIAUXD.001, SN0608NDVILSTM.001	DTN: SN0712ALANDSAT.002 [DIRS 184297] which supersedes DTN: SN0601ALANDSAT.001 [DIRS 177239]
UZ model boundary and repository footprint	Identification of grid cells inside and outside boundaries	Appendix B[a]; Output DTN: SN0711FTPRNUZB.003	DTN: LB0208HYDSTRAT.001 [DIRS 174491]

4.2[a]. CRITERIA

No change.

4.3[a]. CODES, STANDARDS, AND REGULATIONS

No change.

INTENTIONALLY LEFT BLANK

5[a]. ASSUMPTIONS

SCI-PRO-006, *Models*, defines an assumption as:

> A statement or proposition that is taken to be true or representative in the absence of direct confirming data or evidence, or those estimations, approximations, limitations, simplifications, and/or decisions made during model development (such as when expanding the range of variables to achieve conservatism).

The assumptions included in this section are only those made in the absence of direct or confirming data. In Section 6, there are many "modeling decisions" that were made that might be thought of as assumptions. These are listed in Table 5-1 at the end of Section 5 of the parent document.

5.1[a]. CERTAIN COMPONENTS OF THE WATER BALANCE MODEL CAN BE NEGLECTED FOR MODELING NET INFILTRATION AT YUCCA MOUNTAIN

The water balance equation used in this model of net infiltration includes the most important terms in the water balance and neglects terms that are reasonably assumed to be negligible. The model includes precipitation (rain and snow), evapotranspiration (ET), net infiltration, snowmelt, sublimation of snow, run-on, and runoff. The terms that are assumed to be negligible and are thus not represented in the model include: interception, interflow, storage of water on surface (either in puddles or in stream channels), subsurface vapor flow, and dew deposition.

- Interception is the process whereby a fraction of the total precipitation is stored on and eventually evaporated from the surface of plants without reaching the ground. In densely vegetated regions interception is a significant process; however, in arid regions with sparse vegetation, this process is assumed to be negligible.

- Interflow (sometimes called "storm seepage") is lateral flow of liquid water in the unsaturated zone that can occur during and following precipitation events. This flow is driven by a lateral head gradient component, which is typically the result of a sloping land surface. Such flows are neglected in the current model for the following reasons. First, most of the model domain is characterized by relatively low slopes. For example, the median slope for the model domain is approximately 10 degrees from horizontal and 90% of the domain has a slope less than 25 degrees. The lower the slope the less the lateral head gradient. Second, bulk bedrock conductivity values tend to be significantly higher than the conductivities in the overlying soil and, therefore, once water reaches the soil–bedrock interface, it would tend to enter bedrock instead of flowing laterally along the interface. Soil layering (anisotropic conductivity), if present, might increase the likelihood of interflow. However, steep slopes tend to be associated with shallow soils, where soil layering is unlikely to be important. Even if significant interflow does occur in certain areas, it is not likely to flow over several grid cells because of the shallow soils and high bedrock conductivity. Observations also support this assumption. For example, if significant interflow were occurring at the site, one would expect that stream flows would continue for several days following large precipitation events, seeps would

form at the toes of slopes, and mass wasting would occur when thin soils on steep slopes became saturated. None of these indicators of significant interflow characterize the site.

- Storage of water on the surface can occur in the form of puddles and/or as stream channel storage. Small ephemeral puddles do form on areas of bare bedrock after precipitation events, but only about 0.3% of the domain consists of bare bedrock (431 cells out of 139,092 cells; see Table 6.5.2.4-1). Stream flows do not tend to persist significantly beyond the precipitation period as discussed in the validation section (Section 7.1.3). For these reasons, surface water storage is assumed negligible and is excluded from the water balance.

- Subsurface vapor flow is driven by a gradient in matric potential in the subsurface. Relatively significant gradients in matric potential have been measured in semiarid regions with deep soil profiles (Walvoord et al. 2002 [DIRS 178108]; Scanlon et al. 2003 [DIRS 178109]). The presence of these gradients indicates upward vapor flow (Walvoord 2002 [DIRS 178108]); however, the fluxes inferred are of very low magnitude compared with the fluxes associated with episodic liquid water infiltration events that characterize shallow soil regions. Results of the simplified water mass balance approach described in this report suggest that little to no net infiltration occurs beneath thick soils and, therefore, including subsurface vapor flow in deep soil areas would not significantly change these results. In contrast, most of the net infiltration occurs beneath shallow soils, and little is known about the relative magnitude of subsurface vapor flow in these regions. For this reason, this process is assumed to be negligible and is excluded from the water balance.

- Deposition of water as dew is not considered in the modeling. It is assumed that this deposition mechanism is small relative to precipitation and therefore any contribution to net infiltration will be negligible. Dew deposition may be an important source of water to native vegetation, especially during especially dry periods, but its effect on net infiltration is not considered to be important.

- The approach used to estimate water flow and storage within the root zone is a simplification of the actual physical processes that control flow in this environment. The use of the "field capacity" concept acts as a flow switch allowing downward water flow at a rate equal to the saturated hydraulic conductivity when the average water content in a layer equals or exceeds "field capacity" and allowing no flow to occur when average water content in a layer is less than field capacity. In reality, water will flow within the vadose zone in response to gradients in total soil-water potential, which is the sum of various components such as elevation, matric, pressure, temperature, and osmotic potentials. The approach used here assumes that these components can be adequately represented with a unit head gradient when field capacity is equaled or exceeded and with a head gradient of zero when water content is less than field capacity. For this application, the value of field capacity is defined as the water content range between values of suction pressure equal to −0.33 and −0.1 bars. As explained in Sections 6.2.2 and 6.5.2.3, this range of values is considered an approximation for the uncertainty in this property. Osmotic potential is usually a very minor contributor to the total potential

unless pore-water concentration gradients are very high, which is not supported by observations at Yucca Mountain.

5.2[a]. FAO-56 METHODS FOR DEVELOPING BASAL TRANSPIRATION COEFFICIENTS ARE APPROPRIATE FOR DESERT ENVIRONMENT

No change.

5.3[a]. ASSUMPTIONS RELATED TO SIMULATING YUCCA MOUNTAIN VEGETATION USING LANDSAT THEMATIC MAPPER DATA

No change.

5.4[a]. PHYSICAL PROPERTIES ARE ASSUMED TO REMAIN CONSTANT

No change.

5.5[a]. MISCELLANEOUS ASSUMPTIONS AND APPROXIMATIONS

No change.

INTENTIONALLY LEFT BLANK

6[a]. MODEL DEVELOPMENT

No change.

6.1[a]. FEATURES, EVENTS, PROCESSES

Table 6.1-1[a] contains a list of 10 FEPs taken from *FY 2007 LA FEP List and Screening* (DTN: MO0706SPAFEPLA.001 [DIRS 181613]). The selected FEPs are those that are associated with the subject matter discussed in the present report. The cross-reference for each FEP to the relevant section(s) of this report is also given in Table 6.1-1[a].

Table 6.1-1[a]. FEPs Addressed in This Model Report

FEP Number	FEP Name	Relevant Sections
1.2.02.01.0A	Fractures	6.5.2
1.3.01.00.0A	Climate change	6.5.1, Appendix F
1.4.01.01.0A	Climate modification increases recharge	6.5.1, Appendix F
2.2.03.01.0A	Stratigraphy	6.5.2
2.2.03.02.0A	Rock properties of host rock and other units	6.5.2
2.2.07.02.0A	Unsaturated groundwater flow in the Geosphere	6.2, 6.3, 6.4
2.3.01.00.0A	Topography and morphology	6.5.2, Appendix B
2.3.11.01.0A	Precipitation	6.5.1, Appendix F
2.3.11.02.0A	Surface runoff and evapotranspiration	6.2, 6.3, 6.4
2.3.11.03.0A	Infiltration and recharge	Entire

NOTE: Relevant sections include the appro priate subsections in this addendum (e.g., 6.5.2.1[a]).

6.2[a]. INFILTRATION PROCESSES

No change.

6.2.1[a]. Processes Controlling Net Infiltration

Near-surface hydrologic processes are generally described in the context of the hydrologic cycle, which describes the pathways and reservoirs through which water moves near and on the surface of the earth. The hydrologic reservoirs consist of the atmosphere, biomass, soil, surface water (streams, lakes, puddles, etc.), snow, pore water in the bedrock overlying the water table, and groundwater. Water moves between these reservoirs via a set of natural processes, including precipitation, infiltration, soil-water movement and retention (e.g., drainage and interflow), evaporation, transpiration, runoff, and net infiltration (Figure 6.2.1-1[a]).

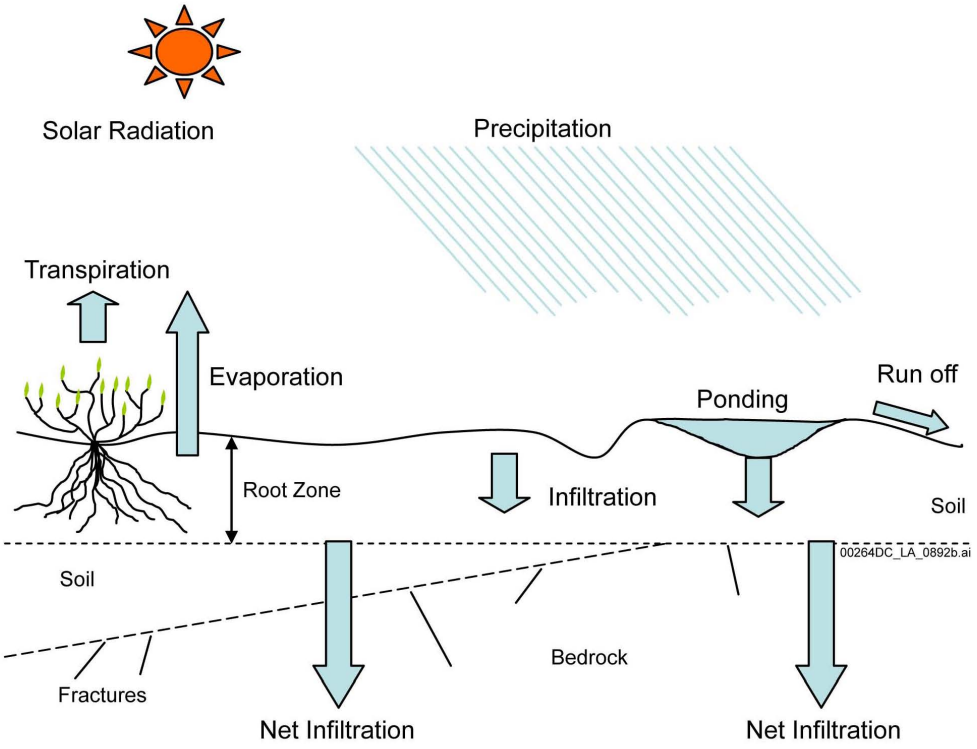

Source: For illustration purposes only.

NOTE: Figure not to scale.

Figure 6.2.1-1[a]. Processes Controlling Net Infiltration

The term "infiltration" refers to the volume flux of water through the soil–atmosphere interface, while the term "net infiltration" refers to the volume flux of water below the shallow zone where most evaporation and transpiration occurs. In this report, "mean annual net infiltration" refers to the temporally averaged net infiltration at a given location, and "spatially averaged net infiltration" refers to the average of mean net infiltration over a specific area, such as the 125 km^2 infiltration modeling domain used for representing the region around Yucca Mountain.

The depth to which evaporation and transpiration are significant processes is often referred to as the active zone to reflect the dynamic nature of the processes in this zone. The active zone often coincides with or may extend beyond the root zone. The amount of water in the active zone varies substantially over time; below this depth, the water content changes are attenuated. In general, when thin soils predominate, the active zone is confined to the soil layer on top of the rock, and net infiltration is defined as the amount of water that moves from the surface layer of soil into the underlying rock. Others have used such terms as "recharge," "drainage," and "deep percolation" to describe net infiltration. These terms imply that water moving below the active zone will eventually recharge phreatic aquifers at depth. While this may occur in humid environments, in arid and semiarid environments with very deep vadose zones, all water moving below the active zone may not recharge the aquifer since lateral and upward flow within the deep vadose zone can occur (Scanlon et al. 1997 [DIRS 142228], p. 463).

In arid and semiarid regions such as the desert basins of the southwestern United States, the processes controlling net infiltration are highly variable in both time and space, and the dominant mechanisms may vary throughout the basin. Net recharge to underlying groundwater in desert basins is often considered to be the sum of several distinct dominant processes occurring in different regions of the basin. Important regions include mountain block, mountain front, and ephemeral stream channels and interdrainage areas of the basin floor.

Mountain block regions are characterized by very thin soils covering fractured bedrock. Areas with thin soils have less total water storage capacity and, therefore, have a greater potential for high net infiltration as compared with deeper soil regions. Precipitation tends to be higher here than in other regions but is highly variable in time and space. The source of precipitation (i.e., snowmelt versus convective storms) can be important. Runoff may be very large in areas of high relief or other areas during storms. Evapotranspiration is often limited because vegetation is sparse. Difficulties in studying infiltration in this region (i.e., installing and maintaining gauging stations or other instrumentation) mean that very little quantitative information is available on mountain block net infiltration.

Soils in the mountain front region are typically thicker than those of mountain blocks, and relief is not as high. As with mountain block regions, the type of precipitation can be important. Runoff can also be important, and net infiltration in the mountain front region is very often focused beneath losing streams. Vegetation is also often focused around these streams, so evapotranspiration can be important.

Infiltration processes on basin floors have been studied more thoroughly than mountain block or mountain front regions. Basin floors typically receive less precipitation than surrounding mountains; however, they make up the majority of land surface and as such may receive the majority of rain that falls within the basin. In contrast with mountain block and mountain front regions, basin floors are often characterized by deep vadose zones; although in the case of Yucca Mountain, the vadose zone is thinner under the basin floor than under the mountain. In general, limited infiltrability of soils, intense convective storms, and high evapotranspiration rates tend to limit net recharge in interdrainage areas of the basin floor. Ephemeral channels and surface water bodies, however, are often the locus of focused net infiltration.

A common approach for conceptualizing net infiltration (I) is by means of a near-surface water balance equation:

$$I = P + RO - \Delta W - E - T \qquad \text{(Eq. 6.2.1-1[a])}$$

where

- P = Net precipitation
- RO = Surface water run-on/runoff
- ΔW = Change in water storage in the active zone
- E = Evaporation
- T = Transpiration.

Net precipitation is the supply of water to the soil surface in the form of rain and snowmelt, minus evaporation of liquid water stored on the surface and sublimation of snowpack. Infiltration across the soil atmosphere boundary is the sum of the net precipitation and run-on minus runoff.

Key processes of the near-surface water balance that affect net infiltration are described subsequently.

Net precipitation

In the general case, for net infiltration to occur at a location, water must be delivered to the ground surface as net precipitation and/or run-on (surface flow). Run-on is water that has moved on the surface from adjacent areas. Precipitation may be in the form of liquid water (rain) or a solid (snow), which later melts to supply liquid water to the soil surface. Precipitation can be described by the type (e.g., rain or snow), the amount (typically in depth units, e.g., mm) and duration of precipitation event. The intensity is the average precipitation rate (amount divided by duration). Snow has the added characteristic of water depth equivalent, averaging 10% water by volume. Some precipitation is temporarily stored on the surface and returned to the atmosphere before it infiltrates or runs off, including evaporation of water intercepted by vegetation and/or accumulated in surface depressions and sublimation of snowpack. Evaporation of surface water and sublimation of snowpack will depend principally upon climatic conditions.

Subsurface water movement and retention

Water movement in near-surface soil can be described by a flux law of the form:

$$\text{Flux} = \text{gradient} \times \text{conductivity}$$

The applicable gradient for this flux law is that of the soil water potential. The soil water potential is most often comprises two principal terms: the gravitation potential and the pressure potential. For unsaturated systems, the pressure potential is a negative quantity and is often referred to as matric potential or by its positive-termed value, suction potential. The gradient attributable to gravity always acts downward, whereas the matric potential gradient can be in any direction. Consequently, the net soil-water potential gradient and the resulting water movement can be in any direction (e.g., upward, downward, or laterally); the net soil water potential can also be zero corresponding to equilibrium conditions and no water movement. The hydraulic conductivity is the property that describes the ability of the soil to transmit liquid water and decreases nonlinearly with decreasing water content in an unsaturated soil, as capillary forces become relatively more important.

Infiltration

Water delivered to the soil surface from rain, snowmelt, or run-on from adjacent areas will infiltrate the soil at a rate that depends on soil properties, transient soil-water content, and water potential conditions. The infiltration rate is defined as the volume flux of water (mm^3/mm^2-yr) flowing into the soil profile per unit area of soil surface. The infiltration rate (or flux) resulting from water at atmospheric pressure being made freely available at the soil surface is referred to as the soil's infiltrability (Hillel 2004 [DIRS 178856], p. 260). Infiltrability varies with time and

is a function of the initial wetness and water potential, as well as soil texture, soil structure, and the layering of the soil profile. The rate of infiltration relative to the rate at which water is supplied to the surface will determine the amount that accumulates and/or runs off: water applied to the soil surface at a rate that exceeds the infiltrability of the soil will pond at the surface and/or runoff; water applied to the soil surface at a rate less than the infiltrability will all infiltrate into the soil.

In general, infiltrability is highest in the early stages of infiltration and decreases with time, eventually approaching a constant rate. The decrease in infiltrability with time is usually due to the decrease in water potential gradients in the soil profile as infiltration proceeds. In some cases, however, the decreasing infiltrability may be caused by deterioration of the soil structure, formation of a surface crust, small particles migrating into and blocking soil pores, or entrapment of air bubbles.

Water movement after infiltration

When the natural processes that supply water to the soil surface (rain, snowmelt, run-on) stop operating and free water on the surface disappears, the infiltration process ceases. Depending on net soil water potential gradient, water in the soil can move downward, upward, remain stationary (retained), or move laterally (interflow).

Interflow can occur as a result of vertical heterogeneity in soil conductivity (e.g., vertical layering), conductivity differences along the soil–bedrock interface, and as a result of a lateral head gradient (e.g., from a sloping land surface).

Often after substantial infiltration, water will continue to move downward under unsaturated conditions, increasing the wetness of successively deeper layers. This type of flow is often referred to as redistribution. The relatively dry deeper soil draws water from the upper soil that has been wetted, redistributing water between the zones. The relative size of the two zones is a function of the initial wetting depth. Redistribution is a dynamic process that depends upon the relative dryness of the lower zone, the initial wetting depth, and the time-varying hydraulic properties of the conducting soil. The initial redistribution rate can be very high when driven by steep matric potential gradients (i.e., if the initial wetting depth is small and the underlying layer is very dry). When matric potential gradients are small (for example when the initial wetting depth is large and the lower zone is relatively wet), the initial redistribution rate is lower.

Whatever the initial rate, soil moisture redistribution will tend to decrease with time because the water potential gradient decreases and the hydraulic conductivity of the wetter layer decreases with decreasing moisture content. Often, water movement within a soil profile will slow sufficiently after an infiltration event to such an extent that the amount of water in the soil profile remains nearly constant, at least temporarily. Early observations of this tendency led to the concept of field capacity. It was noted that the rate of water content change during redistribution decreases with time and often becomes negligible after a few days. The water content at which internal drainage becomes negligible is taken as the definition of field capacity of a soil (Hillel 2004 [DIRS 178856], p. 310).

Upward soil water movement will occur when the net soil water potential gradient is upward. This situation can arise when the near-surface soil dries in response to evapotranspiration and the resulting upward matric potential gradient overcomes the gradient due to gravity. Upward soil water movement is limited to a large extent by the very low hydraulic conductivity of relatively dry soils. Some upward water movement may be in the form of water vapor movement.

Soil water retention

The amount of water in a soil layer or profile within the active zone will change with time in response to water that enters or leaves the system from downward or upward water movement and/or evapotranspiration. The amount of soil water retained is a function of its moisture characteristic curve, which is the relationship between the soil water potential and the water content. Moisture characteristic curves are different for soils of different characteristics (e.g., texture); two adjacent soil layers at equilibrium (i.e., same water potential) have different water contents if their moisture characteristic curves are different. Moisture characteristic curves are also hysteretic as the amount of soil water retained depends on whether the soil is being wetted or dried.

Surface Water Runoff

Whenever the water delivery rate (precipitation + run-on) exceeds the soil's infiltrability, water accumulates on the soil surface. This free water is often referred to as surface water excess. Some water can be stored on vegetation surfaces as well. Because the soil surface is not flat and smooth, the surface water excess collects in depressions, forming puddles (ponding). If ponding exceeds the surface water storage capacity of the depressions, surface runoff commences.

Runoff comprises a wide variety of flow patterns. At one extreme is thin, sheet-like runoff called overland flow. Overland flow is often the primary type of surface runoff from small natural areas or areas having little topographic relief. As runoff accelerates and gains in erosive power, it eventually forms channels. Further erosion can deepen these channels, and individual channels may eventually converge, forming dendritic networks characteristic of stream flow.

Evapotranspiration

Water within the soil profile can be removed from the soil profile by direct evaporation or through extraction and transpiration by plants. Direct evaporation is the dominant mechanism of water transfer from the soil to the atmosphere when the soil surface is bare, while transpiration may dominate for vegetated soil surfaces. However, since the processes of evaporation and transpiration are often difficult to discern separately, they are commonly lumped into a single process called evapotranspiration (ET). Evapotranspiration is dependent on a variety of biotic and abiotic factors including vegetation characteristics (e.g., root density), climatic conditions (e.g., solar radiation), and soil properties (e.g., hydraulic conductivity function).

Direct evaporation from the soil occurs when three conditions persist: (1) presence of a sustained supply of thermal energy to change water from liquid to gas phase (latent heat), (2) presence of a water vapor pressure gradient at the soil–atmosphere surface, and (3) presence of a continuous supply of water from or through the soil.

Transpiration, loss of water from the plant to the atmosphere, is largely a passive response to the atmospheric environment. Terrestrial plant growth requires CO_2 for photosynthesis, which diffuses through open stomata on plant leaf surfaces to intercellular spaces inside the leaf. Concurrently, water vapor diffuses out of the leaf, from wet cell membranes through stomatal pores to the much dryer atmosphere (transpiration). Some of the water extracted from the soil by plant roots is used in photosynthesis and other essential metabolic processes. However, 95% to 99% of the water that passes through a plant is lost to the atmosphere through transpiration (Nobel 1983 [DIRS 160500], p. 506). Transpiration requires energy to convert water within the vegetation to water vapor, and also requires a water vapor gradient between the vegetation and the atmosphere. The supply of water for transpiration is dependent on the water uptake from the soil and transport within the vegetation. As the adjacent soil dries, water uptake by the vegetation slows. As the rate of water uptake decreases, the vegetation becomes water stressed and eventually will be unable to extract any water from the soil. The amount of water in the soil at this point is referred to as the wilting point and depends on both soil and vegetation characteristics.

6.2.2[a]. Modeling Processes Controlling Net Infiltration

No change.

6.2.3[a]. Criteria for Selection of Net Infiltration Model Components

No change.

6.2.4[a]. Alternative Models Considered

No change.

6.3[a]. DESCRIPTION OF THE CONCEPTUAL MODEL – MASS ACCOUNTING SYSTEM FOR SOIL INFILTRATION AND FLOW (MASSIF)

No change.

6.4[a]. MATHEMATICAL DESCRIPTION OF THE MODEL

6.4.1[a]. Precipitation (P)

No change.

6.4.2[a]. Mathematical Representation of Water Transport and Storage

No change.

6.4.3[a]. Surface Runoff and Run-on (Roff and Ron)

No change.

6.4.4[a]. Mathematical Representation of Evapotranspiration

6.4.4.1[a]. Basal Transpiration, Soil Evaporation Coefficients, and Canopy Coefficient

No change.

6.4.4.2[a]. Depletions and Water Stress Coefficients

No change.

6.4.4.3[a]. ET Calculation

No change.

6.4.5[a]. Mathematical Representation of Reference Evapotranspiration on Flat and Sloped Surfaces

No change.

6.4.5.1[a]. Data Required for Daily Calculation of ET_0

No change except to the title of this section.

6.4.5.2[a]. Use of the FAO Penman-Monteith Equation with a Limited Set of Weather Data

No change.

6.4.5.3[a]. Effect of Surface Elevation, Orientation, and Slope on ET_0

No change.

6.5[a]. ANALYSIS OF YUCCA MOUNTAIN NET INFILTRATION

No change.

6.5.1[a]. Weather Parameters for Anticipated Climate Episodes

No change.

6.5.1.1[a]. Climate Episodes

Future Climate Analysis (BSC 2004 [DIRS 170002) estimated climatic variables for the next 10,000 years by forecasting the timing and nature of climate change at Yucca Mountain. That analysis assumed that climate is cyclical, so past climates provide insight into potential future climates, and further assumed that a relation exists between the characteristics of past climates and the sequence of those climates in the 400,000-year earth-orbital cycle (BSC 2004 [DIRS 170002], Section 5). Each cycle, consisting of 400,000-year periods and four approximately 100,000-year subcycles, is a series of glacial and interglacial couplets.

Radiometric and isotopic analyses of calcite deposits at Devils Hole corroborate that past climate is cyclical and linked to earth-orbital forcing functions (BSC 2004 [DIRS 170002], Sections 6.3 and 6.4). *Future Climate Analysis* uses the microfossil record from cores drilled at Owens Lake, California, to reconstruct a climate history for the last long orbital cycle, calibrated to an elevation equivalent to the top of Yucca Mountain (BSC 2004 [DIRS 170002], Section 6.5). Based on these paleoclimate records and the cyclical nature of climate, *Future Climate Analysis* provides climate estimates for the next 10,000 years.

Nevertheless, forecasting long-term future climates is highly speculative and rarely attempted (BSC 2004 [DIRS 170002], Section 1). The uncertainty in such forecasts is aleatoric. That is, it arises from natural randomness and cannot be reduced through further testing and data collection; it can only be characterized. This analysis of net infiltration places emphasis on capturing the full range of the aleatoric uncertainty.

Future Climate Analysis (BSC 2004 [DIRS 170002], Section 6.6, Table 6-1) predicts three climate episodes during the next 10,000 years at Yucca Mountain. The Present-Day climate is part of the interglacial climatic interval, reflective of a warm and arid climatic condition. The Present-Day climate is predicted to persist for another 400 to 600 years. Following the Present-Day climate will be a warmer and wetter monsoonal climatic condition. The Monsoon climate will persist for approximately 900 to 1,400 years. Between the Monsoon climate and the next glacial climate interval is a transition period labeled the Glacial Transition climate. The Glacial Transition climate will be cooler and wetter than the relatively brief monsoonal period, persisting for the remainder of the 10,000-year regulatory period (BSC 2004 [DIRS 170002], Section 7).

There is variability within each climate state (Present-Day, Monsoon, and Glacial Transition) akin to the larger earth-orbital climatic cycle but of shorter frequency and smaller amplitudes. The seasonal cycles are related to the earth's orbit and the tropical and polar air masses. For all three future climates, temperature and precipitation variability in the western region of the conterminous United States is dominated by the interplay, expansion, and contraction of tropical and polar air masses, driven seasonally by the earth's solar orbit. The northern edge of the tropical air masses, the Subtropical Highs, are characterized by hot, dry, high-pressure and descending air. The southern edge of the polar air masses, called the Polar Lows, are typically low-pressure, consist of rising air that creates cool, wet, high precipitation and low evaporation climate (BSC 2004 [DIRS 170002], Section 6.2). A "mixing zone" exists between the tropical and polar air masses. This mixing zone in the northern hemisphere is called the westerlies. As the westerlies pass over large water bodies, moisture is picked up. When the moisture-laden westerlies cross over from water to land masses, moisture is released. In the western United States, the westerlies coming from the Pacific Ocean provide moisture to the western half of the United States. The Yucca Mountain region lies within a major rain shadow created and sustained by the Sierra Nevada Mountains and the Transverse Range. Consequently, as the westerlies move eastward from the Pacific Ocean inland, moisture-laden air is released west of the Yucca Mountain region. It is the interplay between these large air masses, which affect the expansion and contraction of the rain shadow, coupled with regional topology that dominates the annual cyclical weather in the Yucca Mountain region.

DTN: GS000308315121.003 [DIRS 151139] lists representative meteorological stations for each of the three anticipated climate episodes. These are reproduced in Table 6.5.1.1-1[a]. Section 6.5.1.2 below explains how the precipitation and temperature record at a meteorological station is represented by a set of 24 parameters. For each of the three anticipated climate episodes, Sections 6.5.1.3[a], 6.5.1.4, and 6.5.1.5 describe the development of nominal values and uncertainty ranges for the weather parameters, including twelve more parameters for wind speed. A MASSIF calculation requires an input weather file containing daily precipitation, temperature extremes, and wind speed. Section 6.5.1.6[a] describes the development of the weather input file using specific values for each of the 36 precipitation, temperature, and wind speed parameters. Section 6.5.1.7[a] discusses additional weather parameters, those that are not included in the weather input file.

Table 6.5.1.1-1[a]. Meteorological Stations Selected to Represent Future Climate States at Yucca Mountain

Climate State	Duration	Representative Meteorological Stations	Locations of Meteorological Stations	
Present-Day	400 to 600 years	Site and regional meteorological stations	Yucca Mountain region	
Monsoon	900 to 1,400 years	Average Upper Bound: Nogales, Arizona Hobbs, New Mexico	North Latitude 31° 21’ 32° 42’	West Longitude 110° 55’ 103° 08’
		Average Lower Bound: Site and regional meteorological stations	Yucca Mountain region	
Glacial Transition	8,000 to 8,700 years	Average Upper Bound: Spokane, Washington Rosalia, Washington St. John, Washington	North Latitude 47° 38’ 47° 14’ 47° 06’	West Longitude 117° 32’ 117° 22’ 117° 35’
		Average Lower Bound: Beowawe, Nevada Delta, Utah	North Latitude 40° 35’ 25” 39° 20’ 22”	West Longitude 116° 28’ 29” 112° 35’ 45”

Source: DTN: GS000308315121.003 [DIRS 151139].

6.5.1.2[a]. Parameterization of Precipitation and Temperature Records

No change.

6.5.1.3[a]. Weather-File Parameters for the Remainder of the Present-Day Climate

The present-day-like climate interval is an interval of time when summers are warm to hot. Snowpack at high elevation is typically low to moderate because the polar front does not remain fixed at a southerly position during the winter and as such does not set up a storm wave train that moves Pacific moisture over the Sierra Nevada Mountains. The wettest years, which represent the upper-bound moisture regimes during Present-Day climate, will typically be years when Pacific airflow focuses Pacific moisture toward southern Nevada, such as the El Nino climates that have been common during the last couple of decades. Dry years, which represent the lower-bound moisture regimes during Present-Day climate, will be those years with minimal winter precipitation, typically years when the polar front remains largely north of the region and summer precipitation is dominated by subtropical high activity, but not to the degree necessary to a monsoon-type climate (BSC 2004 [DIRS 170002], pp. 6-46 to 6-47).

Tables F-1[a] and F-2[a] provide the results of parameterization of precipitation records for ten local and regional meteorological stations. These include five Yucca Mountain stations, four Nevada Test Site (NTS) stations, and one National Climatic Data Center (NCDC) station, Amargosa Farms.

The NCDC normal precipitation provides corroboration for the Fourier coefficients for Amargosa Farms (NOAA 2002 [DIRS 178676], pp. 3 and 12). The NCDC normal precipitation for 1971 through 2000 is 100 mm, where missing data have been replaced using a weighting function derived from other station data and data from neighboring stations, and the peak precipitation months are February and March.

Table F-3[a] shows that the mean annual precipitation (MAP) calculated for Amargosa Farms from the zero-order Fourier coefficients (Equation F-42) is 119 mm, using the 26 years for which the records are complete, 1968, 1969, 1979 to 2000, 2002, and 2003. The phases of −1.17 radians and −2.61 radians for the Markov probabilities (Table F-4[a]) correspond to maximum wet-day probabilities in February through April, using Equation 6.5.1.2-2. The phase of +2.34 radians for the precipitation amount (Table F-5[a]) corresponds to peak storm size in January.

Tables F-7[a] and F-8[a] contain the results of parameterization of temperature records at four Yucca Mountain meteorological stations.

Appendix F also describes the use of temperature and precipitation lapse rates to adjust each station's parameters to an elevation equivalent to the top of Yucca Mountain (5,000 ft or 1,524 m). *Handbook of Hydrology* (Maidment 1993 [DIRS 125317], p. 3.3) provides a dry adiabatic temperature lapse rate of 0.01°C/m, with an implied uncertainty of ±0.005°C/m. In reality, a simple relationship does not exist to relate temperature and elevation at a given site. Rather, there are many complex factors which control local temperatures (e.g., ground conditions, wind patterns, slope and azimuth, etc.). This analysis assumes the use of the dry adiabatic temperature lapse rate is a reasonable approximation to the local terrestrial temperature lapse rate in areas such as Yucca Mountain, where terrain is not steep and conditions are generally windy enough to cause airflow over (rather than around) the terrain and dry enough that condensation is insignificant (Smith 2004 [DIRS 179904] pp. 193 to 222). Section 7.1.4 shows this assumption does not introduce a significant bias in estimates of net infiltration, and therefore this simplification is adequate for its intended use. This value has two applications:

1. In the development of Present-Day climate weather inputs, to adjust the zero-order temperature parameters to an elevation of 1,524 m.

2. In the MASSIF model, for all climates, to adjust the input temperatures from an elevation of 1,524 m to the elevation of each cell, regardless of climate.

Appendix F uses the parameters for the ten stations to develop a lapse rate for each zero-order precipitation parameter of the Present-Day climate. These lapse rates provide the basis for adjustment of the zero-order parameters to and elevation of 1,524 m. That is, the frequencies of wet days and the wet-day precipitation amounts include adjustment for elevation.

Using an approximation (Equation F-42), Appendix F estimates the MAP for each of the ten stations. These values lead to a lapse rate for MAP of 6.3 ± 0.7%/100 m (Table F-3[a]). The MASSIF model uses this lapse rate to adjust input precipitation from an elevation of 1,524 m to the elevation of each cell. In effect, the model makes the assumption that the lower frequency of precipitation at lower elevations may be adequately represented by having the same wet days as at 1,524 m, but providing an extra reduction in the amount of precipitation.

For each selected station, Table F-6[a] lists the probability of a wet day and the MAP, calculated in accordance with the following formulas (Appendix F, Equations F-41 and F-42):

- Mean probability that a day is wet: $\frac{1-a_{00}}{1-a_{00}+a_{10}}$
- MAP: $365\frac{1-a_{00}}{1-a_{00}+a_{10}}a_{\lambda}$.

The adjusted values for MAP for each station range from 170 to 250 mm.

The potential range of MAP is corroborated by other data. For example, Thompson et al. (1999 [DIRS 109462]) interpolated Present-Day climate estimates to an elevation of 1,524 m. On the basis of U.S. Weather Service "normal" values, based on three decades of records, without detailed coverage near Yucca Mountain, the estimated MAP was 125 mm. However, a baseline derived from 10 years of NTS data yielded an estimated MAP of 189 mm (Thompson et al. 1999 [DIRS 109462], Table 4). Neither of these estimates used measurements taken at the Yucca Mountain site; however, both values are within the range of the combined parameter uncertainties.

Also, the National Oceanic and Atmospheric Administration provides historic climatic data by divisions, with Yucca Mountain located on the boundary between Nevada Division 3 to the north and Nevada Division 4 on the south. Thompson et al. (1999 [DIRS 109462]) found that one-year precipitation totals in Division 3, generally at higher elevation, ranged from about 75 mm to one value as high as 360 mm for the period of record (about 100 years). Division 4 areas, which are at lower elevation, had a range of one-year precipitation from less than 50 mm to one value as high as 325 mm for the period of record (Thompson et al. 1999 [DIRS 109462], p. 30, Figure 16). The range of MAP from the combined parameter uncertainties is well within the range of these one-year extremes.

The wind speed at two meters above ground is summarized for a meteorological station as an average for each month of the year. Therefore, there are 12 wind-speed parameters, $u_2(m)$, for m from 1 to 12. Appendix F, Section F3.1, describes the method used to calculate a monthly wind speed averaged over four Yucca Mountain meteorological stations.

Table F-22 lists the nominal value and uncertainty for each parameter of the weather input file for the Present-Day climate. The approximate uncertainty distribution for each zero-order precipitation parameter is a uniform distribution. The extremes of the distribution are the minimum and the maximum values among those obtained by analysis of the ten stations,

extended by one standard error. These values also appear in Tables F-4[a] and F-5[a]. The nominal value is the mid-point between these extremes.

For each of the eight first-order precipitation parameters, the nominal value is the mean of the values for the 10 meteorological stations. The approximate uncertainty distribution is usually a normal distribution, established by the mean and standard deviation for the 10 stations. The one exception is $b_{10,1}$, which is only two standard deviations above zero, so that a uniform distribution, defined by the extreme values from the 10 stations, is a more representative distribution of this non-negative parameter. The values for the phase parameters are consistent with peak precipitation in the winter.

All of the temperature parameters have uncertainty distributions that are uniform, with a range determined by the minimum and maximum values for the four sites, as given in Tables F-8[a], F-9[a] and F-10. Each nominal value is at the center of its range. For determining temperature parameters, fewer weather stations were deemed necessary than for determining precipitation parameters because temperature is less directly related to net infiltration than precipitation and because the factors that effect temperature, such as ground conditions (color, vegetation) at sites far from Yucca Mountain may not be representative of conditions at Yucca Mountain. The wind speed averages have normal distributions, based on the mean and standard error calculated in Output DTN: SN0610T0502206.030.

The amount of runoff from a precipitation event is influenced by the intensity of the precipitation. The daily totals do not indicate the duration of an event within a day. Therefore, the duration of precipitation is one of the climate parameters required for simulating infiltration.

6.5.1.4[a]. Weather-File Parameters for the Monsoon Climate

No change.

6.5.1.5[a]. Weather-File Parameters for the Glacial Transition Climate

No change.

6.5.1.6[a]. Generation of MASSIF Weather-File Input from Climate Parameters

One of the inputs to MASSIF is a weather file with data for each day consisting of the amount of precipitation, the minimum and maximum temperatures, and the average wind speed at two meters above the ground.

For a given set of weather parameters, a stochastic algorithm develops a 1,000-yr sample of daily precipitation by sampling from a lognormal distribution. For wet days, the amount of precipitation, P, is determined from a random number $R \in (0,1)$ and the cumulative probability distribution; that is:

$$\int_0^{P(y,d)} \frac{e^{-[\ln x - m(d)]^2/2[s(d)]^2}}{xs(d)\sqrt{2\pi}} dx = R \qquad \text{(Eq. 6.5.1.6-1[a])}$$

where $s(d) = \sqrt{2[\ln \lambda(d) - m(d)]}$.

The domain for Yucca Mountain infiltration covers approximately 50 square miles. An infiltration calculation produces a map of daily infiltration through each of 143,000 grid cells, averaged over a sample of years.

Therefore, it is not practical to calculate daily infiltration through each area for 1,000 years. This difficulty is addressed by taking a sample of the simulated years, including several years with high precipitation. Each sample year is weighted by its relative probability in calculating the map of average annual infiltration. This approach assures that the effects of extreme events are recognized, but given appropriate weight in the analysis.

Input to the infiltration model is a subsample of the 1,000-yr sample. From the full sample sorted by total precipitation for the year, the subsample includes 1,000-yr, 300-yr, 100-yr, 30-yr, and 10-yr events, with a few additional years to represent the drier portion of the probability distribution. Each year in the subsample carries a weight proportional to probability; for example, the 1,000-yr event has a weight of 0.001. Appendix F contains the details of the procedures.

Daily temperature extremes and mean wind speeds are added to the weather input file as described in Appendix F.

6.5.1.7[a]. Other Climate Parameters

Maximum Daily Precipitation

The lognormal fit to wet-day precipitation amount does not fit the probability of extreme events very well. Although the assigned probability for extremely heavy precipitation is very small, it appears to be higher than the data. Therefore, MASSIF accepts an input that limits the total precipitation for one day. The value chosen is the largest observed rainfall in the USA during a 24-hour period over a 26-km^2 area, 983 mm (Maidment 1993 [DIRS 125317], p. 3.36, Table 3.10.2).

Snowmelt Coefficient

MASSIF employs a temperature-index snowmelt equation from *Handbook of Hydrology* (Maidment 1993 [DIRS 125317], p. 7.24) for calculating daily snowmelt for days with snow accumulation. Maidment (1993 [DIRS 125317], p. 7.24, Table 7.3.7) provides temperature-index expressions for calculating daily snowmelt for various regions of North America. The closest site to Yucca Mountain is Sierra Nevada, California. This site has latitude similar to that of Yucca Mountain and is therefore the most appropriate site to use in this table. The general form of the temperature-index snowmelt equation is:

$$M = SM \times T \qquad \text{(Eq. 6.5.1.7-1[a])}$$

where *SM* is the snowmelt coefficient in mm/day/°C (for days with mean daily air temperature greater than 0°C), *M* is snowmelt in mm/day and *T* is daily mean air temperature (°C). The snowmelt coefficients for the Sierra Nevada, California, are 1.78 and 1.92 for April and May, respectively (Maidment 1993 [DIRS 125317], p. 7.24).

There is large inherent uncertainty in this parameter. Maidment (1993 [DIRS 125317], Table 7.3.7, p. 7.24) reports values for the snowmelt coefficient (*SM*) ranging from 0.58 (for the Boreal forest) to 5.7 (for Southern Ontario). The greater the amount of forest cover, the lower the value of *SM*, suggesting that more snowmelt is slowed by the presence of tree shade. A mean value of 2 was selected for the MASSIF model, which is slightly higher than the Sierra Nevada values. A range of 1 to 3 (with a uniform distribution) is assumed to represent snowmelt conditions at Yucca Mountain during the Glacial Transition climate. This value was used for all climates because there is not significant snow during the Present-Day and Monsoon climates.

Sublimation Coefficient

Estimates of sublimation (or ablation) of snowpack vary widely. Hood et al. (1999 [DIRS 177996], p. 1,782) discuss a 1975 study in which sublimation was responsible for 80% of the ablation of fresh snow and 60% of the ablation of older snow during springtime conditions in the White Mountains of California. Hood et al. (1999 [DIRS 177996], p. 1,782) also discuss a 1959 study in which sublimation was only 2% to 3% of total ablation over the snow season at the Central Sierra Snow Laboratory in California.

Hood et al. (1999 [DIRS 177996], p. 1,782) also discuss more recent studies (e.g., Kattelmann and Elder 1991 [DIRS 177998]) that estimated sublimation from snow to be 18% of total precipitation over two water years for Emerald Lake Basin in the Sierra Nevada, and Berg (1986 [DIRS 177995]), who reported sublimation losses from blowing show to be between 30% to 51% of precipitation for the two year period 1973 to 1975. Hood et al. (1999 [DIRS 177996], p. 1,794) report sublimation from their own study to be 15%.

Based on the annual sublimation data reported by Hood et al. (1999 [DIRS 177996], p. 1,794), a nominal value of 10% was selected for Yucca Mountain. This value is lower than those estimated for the Sierra Nevada; however, this is justified because the snow pack is expected to persist for shorter periods of time at Yucca Mountain in the future than it does in the Sierra Nevada in the present climate. To incorporate uncertainty, a range of 0% to 20% (with a uniform distribution) is considered to represent annual snow sublimation amounts at Yucca Mountain during the Glacial Transition climate. This range is corroborated by the other studies discussed above. This value was used for all climates because there is not expected to be significant snow during the Present-Day and Monsoon climates.

The sublimation coefficient is multiplied by daily precipitation for days when the mean daily air temperature is less than 0°C, and that amount is removed from the precipitation total in the form of snow sublimation. The effect of this calculation is to partition 10% of daily precipitation on days when the mean daily temperature is less than 0°C into sublimation and thereby remove this water from the water balance.

Table 6.5.1.7-1[a] summarizes the snow parameters.

Table 6.5.1.7-1[a]. Nominal Values and Uncertainties for Snow Parameters

Parameter Name	Parameter Symbol	Nominal Value	Uncertainty Range	Uncertainty Distribution
Snowmelt (SM)	$C_{snowmelt}$	2.0	1.0 to 3.0	Uniform
Sublimation (SUB)	$C_{sublime}$	0.1	0.0 to 0.2	Uniform

Sources: Snowmelt coefficient estimates from Maidment 1993 [DIRS 125317], p. 7.24. Sublimation estimates from Hood et al. 1999 [DIRS 177996], p. 1,794.

Precipitation Duration

The precipitation duration is a highly variable parameter in the desert environments, so that the selection of the parameter values to be used in the MASSIF calculations needs a special justification. For each climate, this analysis develops a function that relates the precipitation duration to the amount of rain that falls on a given day. Because of limited data availability, only data from certain weather stations representing each climate were analyzed. Four sets of analyses were done to characterize precipitation duration parameters for each climate. Output DTN: SN0610T0502206.031 contains MathCAD applications in which the analyses are performed.

Table 6.5.1.7-2[a] lists the weather stations used for the four precipitation duration analyses.

Table 6.5.1.7-2[a]. Weather Stations Used for Precipitation Duration Analyses

Precipitation Duration Analysis	Weather Stations	Source DTN
Present-Day	BSC Stations 1, 2, 3, 6	SN0608WEATHER1.005 [DIRS 177912]
Monsoon (upper)	Hobbs, NM, and Nogales, AZ	MO0605SEPHOURL.000 [DIRS 177237]
Glacial Transition (lower)	Delta, UT	MO0605SEPHOURL.000 [DIRS 177237]
Glacial Transition (upper)	Spokane, WA	MO0605SEPHOURL.000 [DIRS 177237]

For each analysis listed in Table 6.5.1.7-2[a], the daily precipitation amount (*Amt*) and the number of hourly intervals (*Int*) in which precipitation was measured at each of the weather stations were calculated for every day of the year. Days with zero precipitation (number of hourly intervals equals zero) were filtered out. The remaining dataset was plotted (Figures 6.5.1.7-1[a] to 6.5.1.7-4[a]) and fit to a linear model:

$$Int = a + b * Amt \qquad \text{(Eq. 6.5.1.7-2[a])}$$

where a is the y-intercept and b is the slope.

The standard error on b was estimated as:

$$SE_b = \frac{mean\left\{\left[\frac{Int_i - a}{Amt_i} - b\right]^2\right\}}{n} \qquad \text{(Eq. 6.5.1.7-3[a])}$$

where n is the number of data, and i is the data index from 1 to n.

For the MASSIF calculation, which uses a daily time step, an assumption is made that daily precipitation occurs as a single event rather than multiple shorter events separated by dry periods during the day. Given this assumption and for a given precipitation day, the number of hourly intervals is, on average, equal to one hour greater than the actual precipitation duration for that day. This is because, for a given precipitation event, the actual start and end times within the hourly intervals that bound these start and end times are equally likely to occur during the first half as they are the last half of the intervals. For example, given it rains for 0.5 hours, there is a 0.5 probability that the rain event occurred in one hourly interval and a 0.5 probability that it occurred in two hourly intervals. The mean number of intervals is 1.5, which is one hour more than the actual duration of the rainfall. This one hour offset can be shown to apply for any given duration event. Table 6.5.1.7-3[a] lists the results of the linear regressions as the slope and intercept-1. The intercept-1 represents the minimum precipitation duration considered in the model. Table 6.5.1.7-4[a] lists the nominal values and distributions for these parameters for each climate.

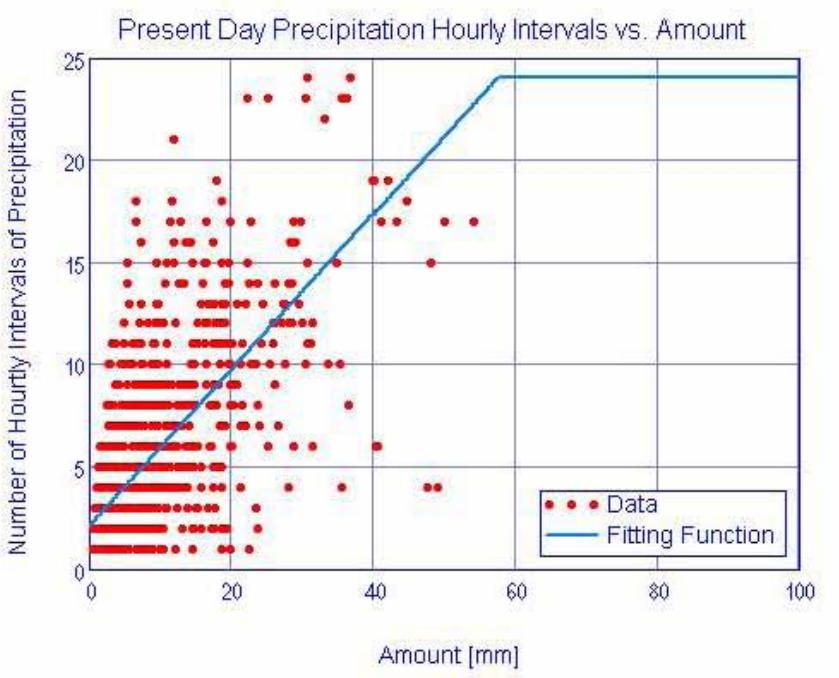

Figure 6.5.1.7-1[a]. Number of Hourly Intervals of Precipitation Plotted against the Daily Amount of Precipitation for the Present Weather Stations BSC1, BSC2, BSC3, and BSC6

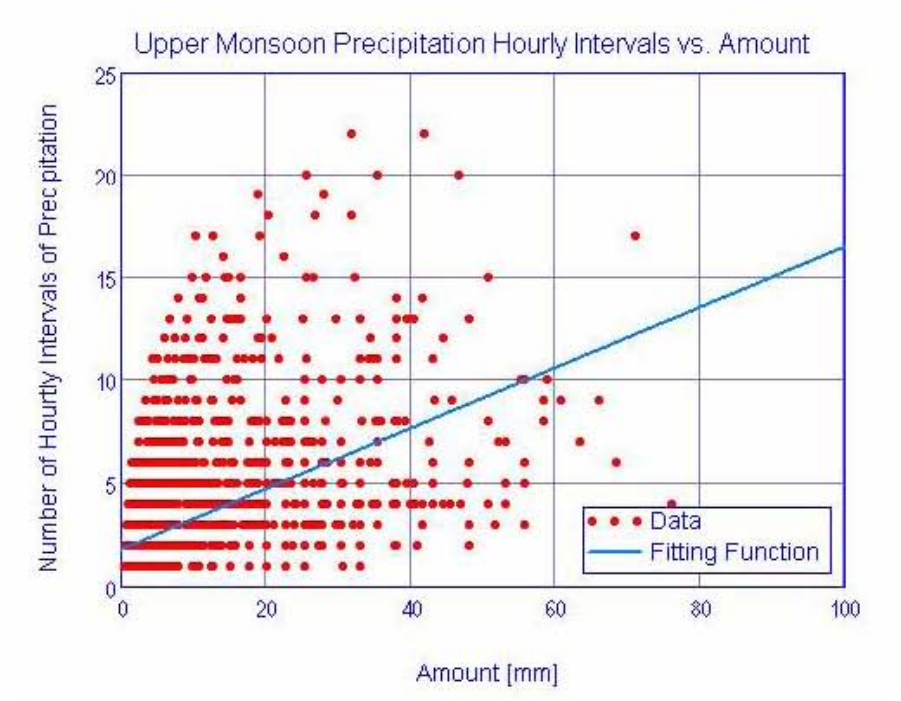

Source: Output DTN: SN0610T0502206.031.

Figure 6.5.1.7-2[a]. Number of Hourly Intervals of Precipitation Plotted against the Daily Amount of Precipitation for the Upper Monsoon Weather Stations of Hobbs, NM, and Nogales, AZ

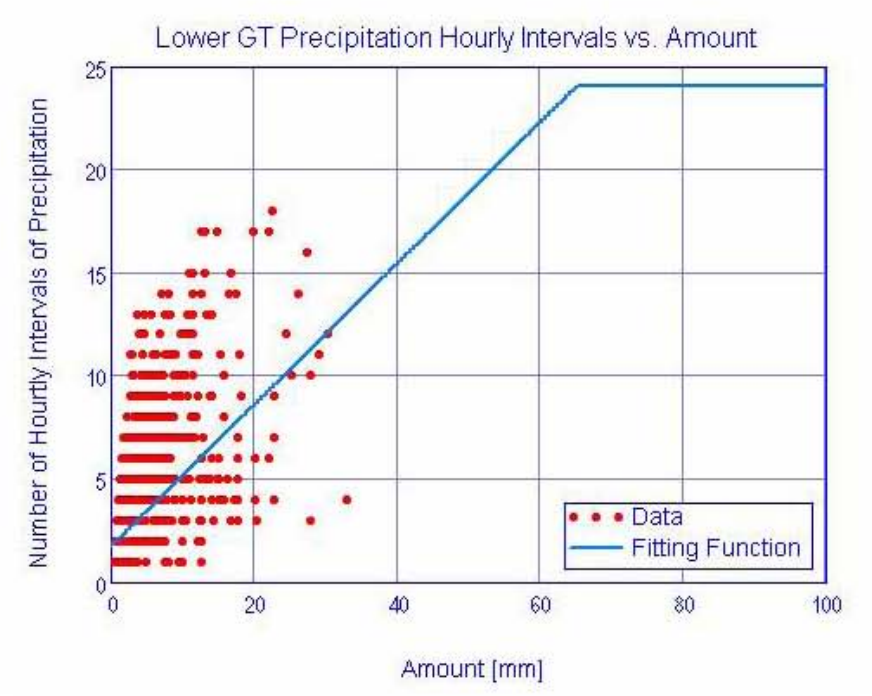

Source: Output DTN: SN0610T0502206.031.

Figure 6.5.1.7-3[a]. Number of Hourly Intervals of Precipitation Plotted against the Daily Amount of Precipitation for the Lower Glacial Transition Weather Station of Delta, UT

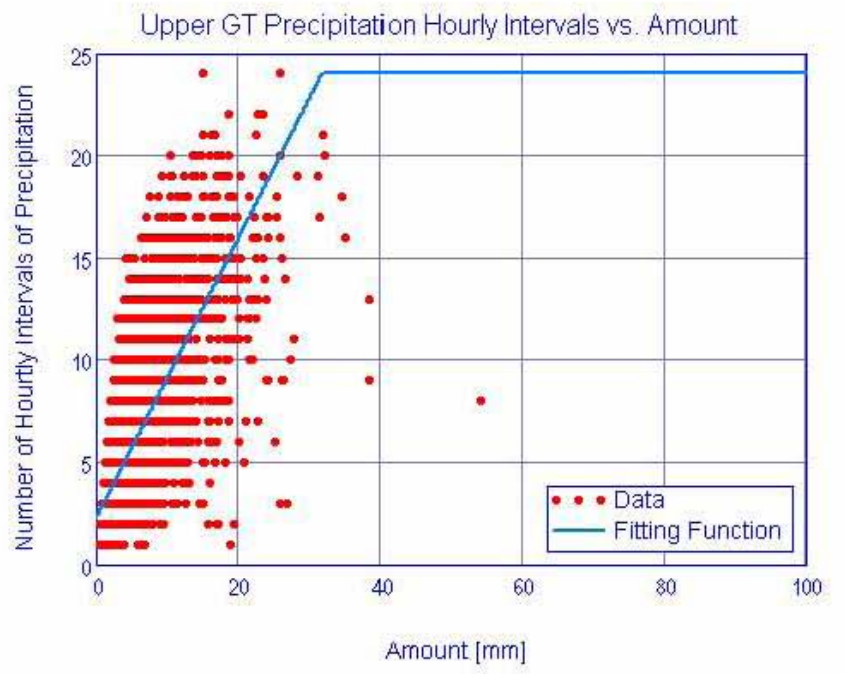

Source: Output DTN: SN0610T0502206.031.

Figure 6.5.1.7-4[a]. Number of Hourly Intervals of Precipit ation Plotted against the Daily Amount of Precipitation for the Upper Glacial Transition Weather Station of Spokane, WA

Table 6.5.1.7-3[a]. Precipitation Duration Linear Regression Results

Precipitation Duration Analysis	Slope	Std Err on Slope	Minimum Precipitation Duration (Intercept-1)
Present-Day	0.38	0.05	1.07
Monsoon (upper)	0.15	0.01	0.76
Glacial Transition (lower)	0.34	0.02	0.70
Glacial Transition (upper)	0.68	0.03	1.22

Source: Output DTN: SN0610T0502206.031, *Precipitation Duration Parameter Values and Distributions.xls*.

Table 6.5.1.7-4[a]. Precipitation Duration Parameter for Each Climate

Climate	Nominal Slope	Distribution (Slope)	Std Err on Slope	Minimum Precipitation Duration (Intercept-1)
Present-Day	0.38	Normal (mean = 0.38, SD = 0.05)	0.05	1.07
Monsoon	0.28 [a]	Uniform (0.14 – 0.43) [d]	0.08 [c]	0.91
Glacial Transition	0.52 [b]	Uniform (0.32 – 0.71) [d]	0.11 [c]	0.96

Source: Output DTN: SN0610T0502206.031, *Precipitation Duration Parameter Values and Distributions.xls.*

[a] Mean of Present-Day and Monsoon upper slope values (mean of values presented in Table 6.5.1.7-3[a] is 0.27 due to rounding in that table).

[b] Mean of Glacial Transition lower and upper slope values (mean of values presented in Table 6.5.1.7-3[a] is 0.51 due to rounding in that table).

[c] Standard deviation calculated using square root of Equation I-9.

[d] Upper and lower ends of uniform distribution are extended by one standard error.

6.5.2[a]. Geologic and Geographic Inputs

Geologic inputs to MASSIF include parameters for Yucca Mountain soils and bedrock, and spatial distributions for soil types, soil depth classes, and bedrock types over the modeling domain. Geographic inputs include data used to define cell coordinates, elevations, slope, azimuth, watershed delineations, and other site characteristics. This section presents a summary of the methods used to determine each of the geologic and geographic inputs and presents the nominal values and uncertainty ranges for all the geospatial parameters. Geographic inputs are described in Section 6.5.2.1[a]. Soil classification is presented in Section 6.5.2.2[a] followed by soil properties and soil depth in Sections 6.5.2.3 and 6.5.2.4[a], respectively. Bedrock classification and bedrock properties are presented in Sections 6.5.2.5[a] and 6.5.2.6, respectively.

The geologic and geographic parameters used by MASSIF were organized into a 'geospatial' database. Development of the geospatial database is presented in Appendix B. The database is used to identify spatially varying parameters for each cell within the modeling domain. The database includes the following:

- Cell ID
- UTM Easting (m)
- UTM Northing (m)
- Latitude (deg)
- Longitude (deg)
- Elevation (m)
- Downstream Cell ID – identifies the cell ID for the cell adjacent to and downstream of each cell, or specifies that there are no downstream cells
- Slope (deg)
- Azimuth (deg)
- Soil Depth Zone
- Soil Type
- Bedrock Type
- Potential Vegetative Response.

For the calculations described in this report, geospatial parameters are handled in two different ways. The values of some parameters are specified in the geospatial database such that they vary independently from cell to cell. Examples of parameters that vary from cell to cell include

elevation and potential vegetation response (PVR). For the remaining geospatial parameters, such as bedrock hydraulic conductivity or soil properties, the geospatial database contains an index that identifies groups of grid cells representing regions where particular properties are assigned uniform values. The value of the parameter is defined to be uniform over all locations with the same index. The following geospatial parameters are assigned to such grid cell groups or regions:

- Soil depth class (5 classes)
- Soil depth
- Soil type (8 types)
- Saturated hydraulic conductivity (K_{sat_soil})
- Saturated water content (θ_s)
- Field Capacity (θ_{FC})
- Permanent Wilting Point (θ_{WP})
- Water Holding Capacity (calculated from θ_{FC} and θ_{WP})
- Bedrock type (38 types)
- Saturated hydraulic conductivity (K_{sat_rock}).

Geospatial parameters represent the effective properties of 30 × 30-m grid cells, or in the case of parameters assigned to grid cell groups, these parameters represent the effective properties of much larger regions of the modeling domain. For this reason, the probability distributions of the effective or "upscaled" values of geospatial parameters will vary from the underlying spatial distributions of these parameters, which are derived from individual measurements made on a smaller scale. The region boundaries for each of the parameters were established independently of the estimation of spatial distributions of properties. Therefore, the spatial distributions are interpreted as applying to the entire region within the given boundaries, regardless of the original rationale for setting the boundaries.

Uncertainty in geologic inputs is reported with the nominal values in Sections 6.5.2.2[a], 6.5.2.3, 6.5.2.4[a], 6.5.2.5[a], and 6.5.2.6. For this infiltration analysis, uncertainty in parameters is propagated through the calculation if the parameter of interest meets the criteria established for the uncertainty analysis described in Appendix I.

6.5.2.1[a]. Geographic Inputs

Geographic inputs to MASSIF generally include data that describe the physical location and layout of each cell. Material properties associated with the soil, bedrock, or vegetation characteristics of each cell are treated separately in Sections 6.5.2.2[a], 6.5.2.3, 6.5.2.4[a], 6.5.2.5[a], and 6.5.2.6 of this addendum and parent report. Geographic inputs include:

- UTM Easting (m)
- UTM Northing (m)
- Latitude (deg)
- Longitude (deg)

- Elevation (m)
- Downstream Cell ID – identifies the cell ID for the cell adjacent to and downstream of each cell, or specifies that there are no downstream cells
- Slope (deg)
- Azimuth (deg).

The geographic inputs were organized into a Geographic Information System (GIS) developed for the MASSIF model and described in Appendix B. The spatial inputs elevation, azimuth, and slope are used for calculations of runoff and temperature and precipitation adjustments for elevation, and are important for developing other parameters relating to evapotranspiration.

The Shuttle Radar Topography Mission (SRTM) data were selected as the best source for topography data for infiltration modeling based on criteria described in Appendix B. The SRTM data were obtained from the U.S. Geological Survey (USGS) Earth Resources Observation and Science (EROS) Data Center (DTN: SN0601SRTMDTED.001 [DIRS 177242]).

The MASSIF infiltration model domain includes the area that drains Yucca Mountain above the UZ flow model area. Eleven separate drainages (or watersheds) were delineated; three larger basins drain the east face of the ridge and eight smaller basins drain the west face. The largest drainage in the north part of the domain (Yucca Wash) has been artificially cut off on its northern edge because of a lack of detailed information about soil and bedrock properties in this region. The implication of this cutoff is an assumption that any run-on from the parts of the drainage that are not included can be neglected for the purpose of estimating net infiltration inside this drainage. The delineation of watershed boundaries is presented in Appendix B.

The watersheds were delimited using elevation and slope to define surface water flow direction to a single outlet. The boundaries of the eleven watersheds also delineated the overall infiltration model boundary within the larger project boundary. Figure 6.5.2.1-1[a] shows the watershed boundaries, which lie within the larger project boundary area. The larger rectangular project boundary encompasses 226.34 km^2. The infiltration model boundary, composed of the combination of these eleven watersheds, encompasses 120.61 km^2. The eleven watersheds make up the individual model components that are used to calculate net infiltration. The individual watersheds are highlighted in Figure 6.5.2.1-2[a]. The region identified as the "UZ boundary" in Figure 6.5.2.1-1[a] (and many other figures) refers to the UZ flow model area boundary. This area is larger than the "repository footprint," which is also shown in Figure 6.5.2.1-1[a], and other figures. The UZ flow model area is of particular interest in the present analysis because areas outside this region, though important to the infiltration model, are not used in downstream models (SNL 2007 [DIRS 175177] and SNL 2007 [DIRS 179545]). For this reason, grid cells within the UZ flow model area are given special consideration in terms of identifying which parameters to include in a model of net infiltration uncertainty for Yucca Mountain. The number of cells in each region is shown in Table 6.5.2.1-1[a].

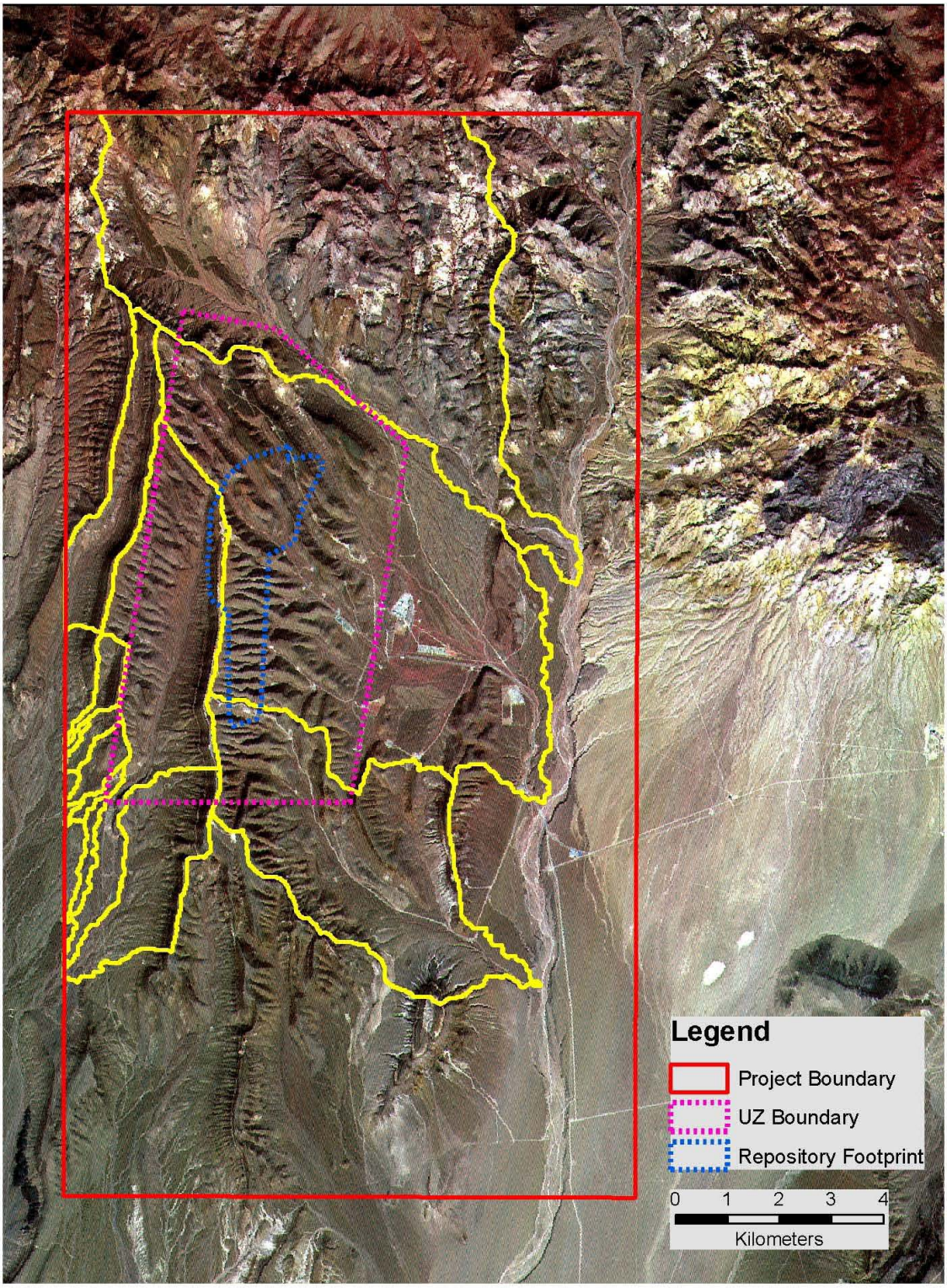

Source: Output DTNs: Project boundary from SN0608NDVIAUXD.001; UZ and Repository boundaries from SN0711FTPRNUZB.003; Watershed boundaries from SN0701SPALAYER.002; Satellite image from DTN: MO0705ASTRIMNT.000 [DIRS 181287] is shown for illustrative purposes only.

NOTE: Yellow lines indicate watershed boundaries. Repository footprint shown for illustrative purposes only.

Figure 6.5.2.1-1[a]. Infiltration Modeling Boundaries

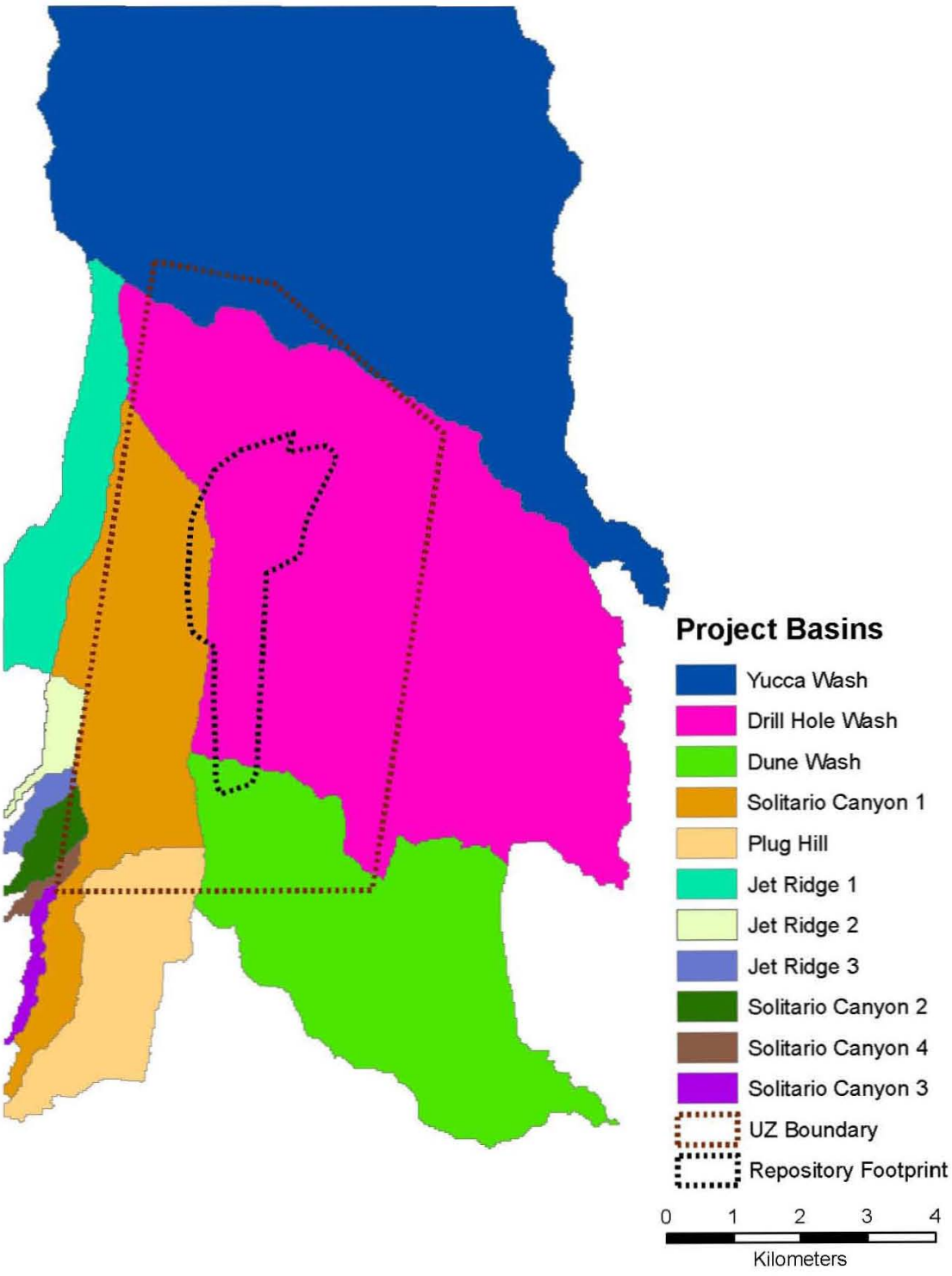

Source: Output DTNs: SN0701SPALAYER.002 and SN0711FTPRNUZB.003.

NOTE: Repository footprint shown for illustrative purposes only.

Figure 6.5.2.1-2[a]. Yucca Mountain Watersheds (Basins)

Table 6.5.2.1-1[a]. Number of Grid Cells within Various Boundaries in the Yucca Mountain Region

Boundary	Total Number of Cells
Project Boundary[a]	253,597
Infiltration Model Boundary (defined by eleven watersheds)[b]	139,092
UZ Flow Model Area Domain [c]	44,232
Repository Footprint [d]	6,322

[a] Output DTN: SN0608ASSEMBLY.001.
[b] Output DTN: SN0608DRAINDYM.001.
[c] LB0208HYDSTRAT.001 [DIRS 174491].
[d] LB0208HYDSTRAT.001 [DIRS 174491].

NOTE: Boundaries presented in this table correspond to the boundaries shown in Figure 6.5.2.1-1[a].

As described in Appendix B, a three-stage watershed delineation process was required to generate the fewest number of watersheds that would completely cover the UZ flow model area. Each watershed is a separate component of the MASSIF model, so fewer drainages result in fewer processing steps. However, the size of the drainages was dictated by two factors: the topography of the region and the UZ model domain. The surface area of each watershed varied widely, a result of the three nearly identical delineation stages needed to generate the eleven drainage basins that cover Yucca Mountain: three large, three moderate, and five small basins. During each stage, a specific threshold variable was set that would determine the size of the resulting drainages. Thus, each stage was responsible for generating either the large, medium, or small drainage basins. Variable basin sizes were necessary because the MASSIF model needed to trace potential infiltration from all locations directly over the UZ model domain down the mountain slopes to each basin pour point (the bottom-most part of the basin).

Elevation data from SRTM required processing for use in the geospatial database, as the SRTM cell size and map coordinate projections did not correspond to those needed for the infiltration model. Once cell size and projection were revised, the elevation data could then serve as the base data layer from which multiple derivative data layers could be created. These additional layers provided information, such as slope and aspect, which are required by the MASSIF infiltration model.

The raw form of the SRTM data layer was processed using Research Systems, Inc. (RSI) Environment for Visualizing Images (ENVI; ENVI + IDL, Version 4.2: STN: 11204-4.2-00) image processing software. The SRTM data were divided as a subset within the project boundary, converted to 30-m pixels and re-projected to accommodate the requirements of the MASSIF model. Elevations across the modeling domain are presented in Figure 6.5.2.1-3[a].

The elevation data were also used to create additional layers within the GIS including the slope and azimuth over the model area. The surface slope of each grid cell was calculated using the *slope* function in ArcGIS, which uses the elevations at eight neighboring cells. Slope was defined from 0° (horizontal) to 90° (vertical). Slopes over the infiltration modeling domain ranged between 0° and 49° (rounded to the nearest degree). A map of slopes over the modeling area is presented in Figure 6.5.2.1-4[a].

The azimuth layer was created using the *azimuth* function in ArcGIS, which estimates the compass direction of a vector normal to the surface of each grid cell. This parameter is used for

calculations involving the direction of incoming solar radiation. Azimuths were defined between 0° and 360° (rounded to the nearest degree). East is at 90°, South is at 180°, and West is at 270°. A map of azimuths over the modeling area is presented in Figure 6.5.2.1-5[a].

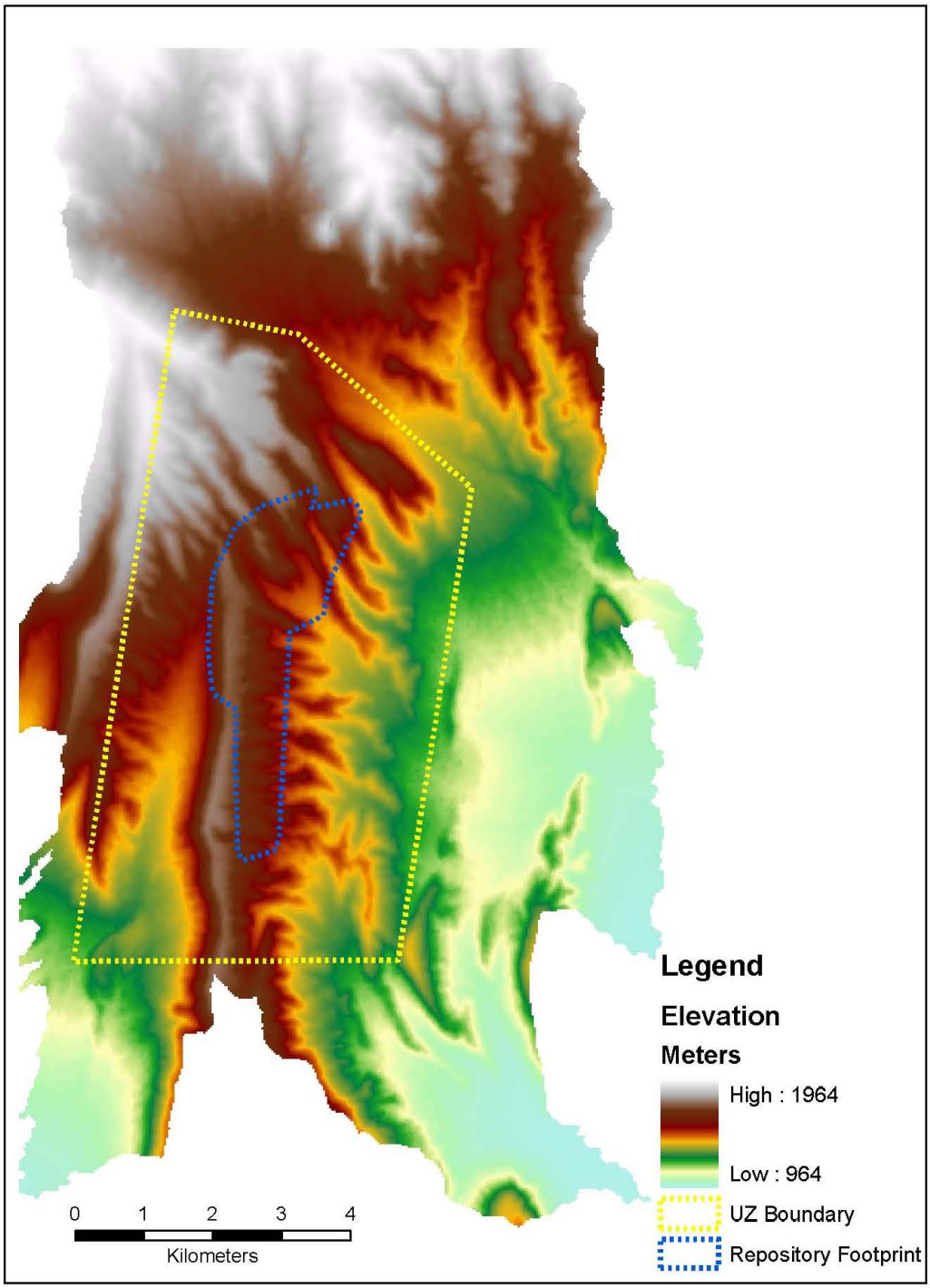

Source: Output DTNs: SN0701SPALAYER.002 and SN0711FTPRNUZB.003.

NOTE: Repository footprint shown for illustrative purposes only.

Figure 6.5.2.1-3[a]. Elevation over the Model Area

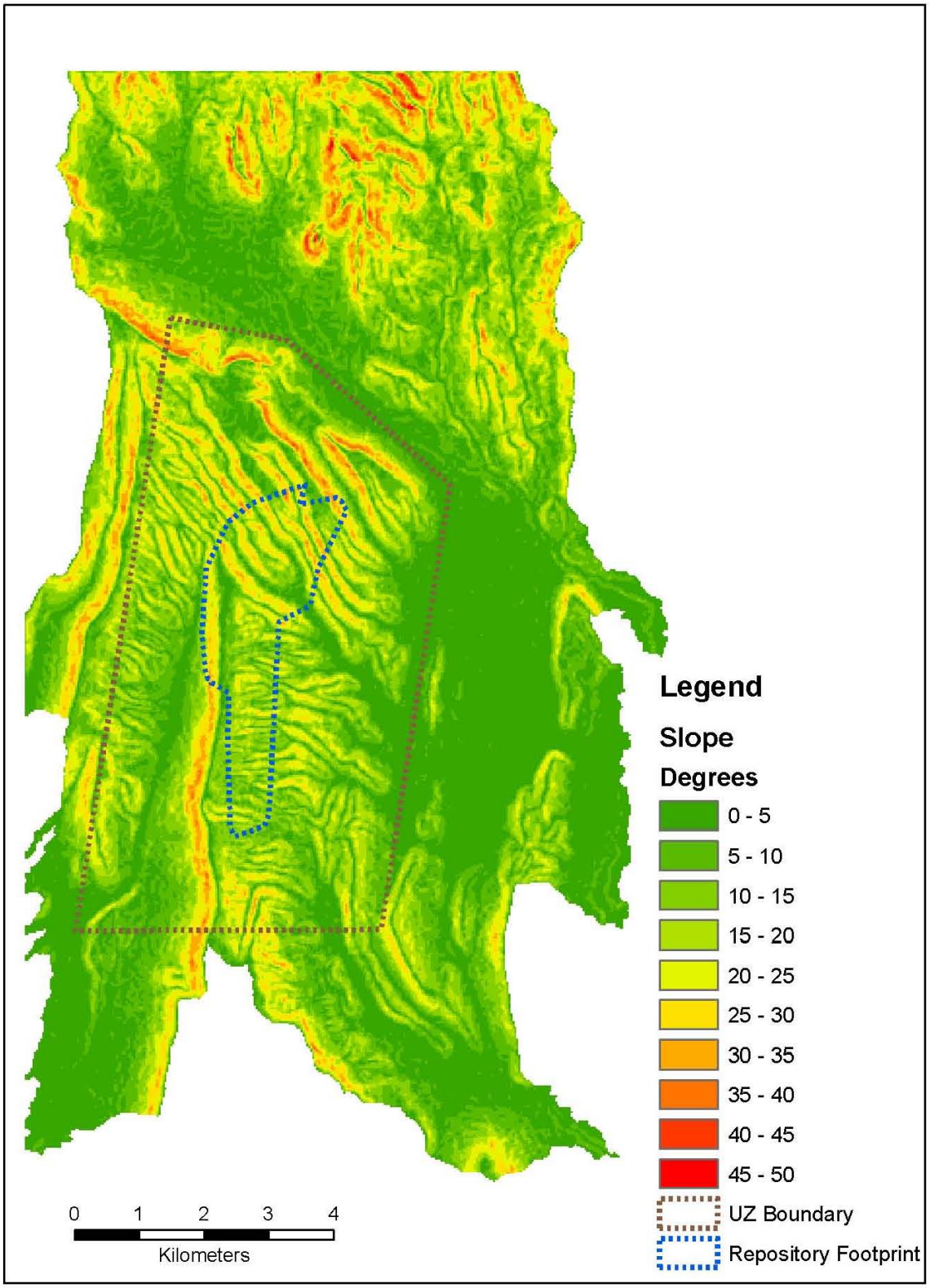

Source: Output DTNs: SN0701SPALAYER.002 and SN0711FTPRNUZB.003.

NOTE: Repository footprint shown for illustrative purposes only.

Figure 6.5.2.1-4[a]. Slope over the Model Area

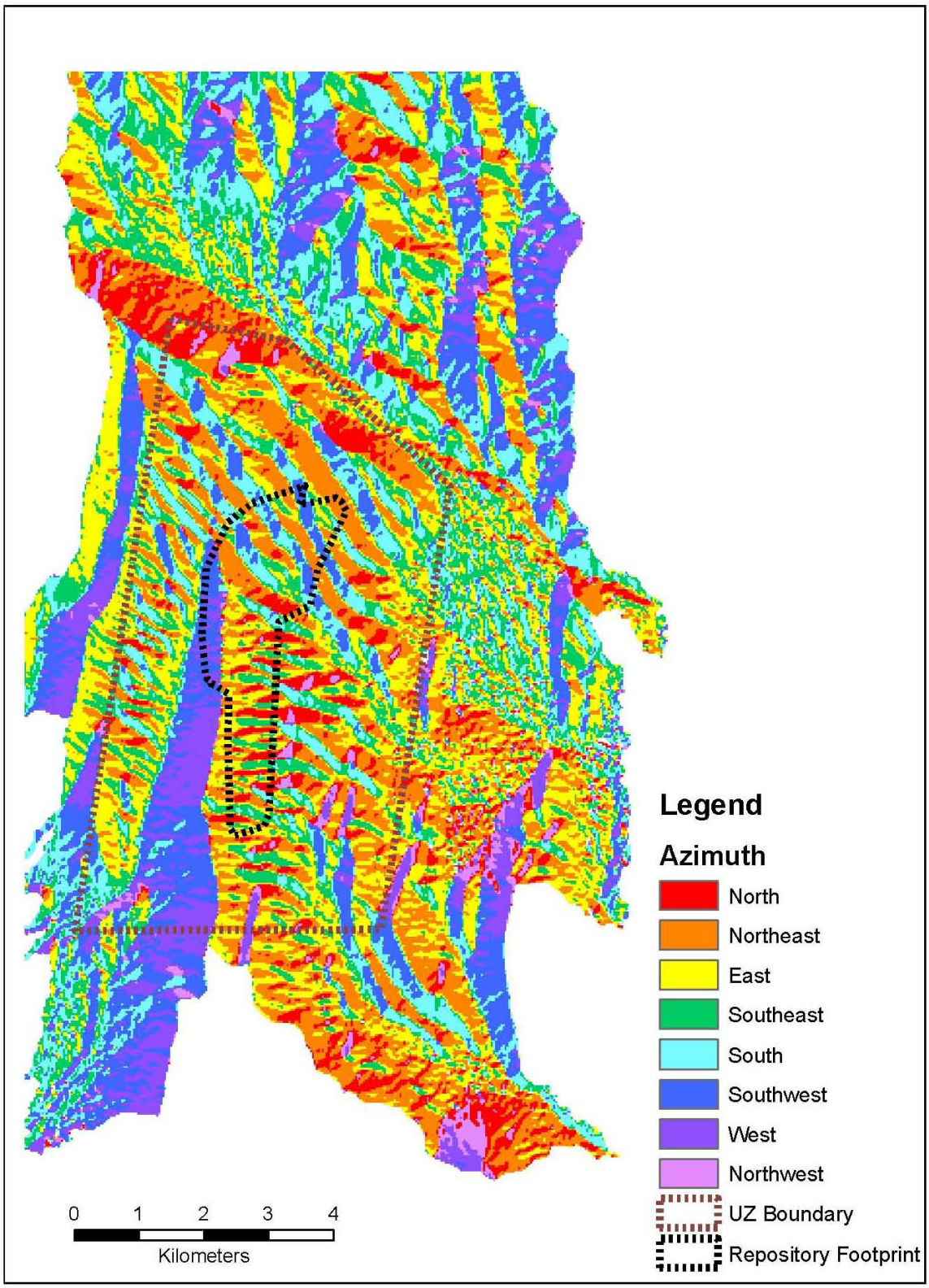

Source: Output DTNs: SN0701SPALAYER.002 and SN0711FTPRNUZB.003.

NOTE: Repository footprint shown for illustrative purposes only.

Figure 6.5.2.1-5[a]. Azimuths for Model Area

Uncertainties in geographic inputs may arise from uncertainties in the underlying SRTM data, as well as processes used to calculate parameters from that data (i.e., slope and azimuth calculations, watershed delineation). To minimize errors caused by transforming grids between coordinate systems and projections, the grid cell locations and elevations for the infiltration modeling domain were based on the locations of the SRTM grid cells. Uncertainties in the SRTM data were analyzed by Rodriguez et al. (2005 [DIRS 177738]) and are discussed in Appendix B. The absolute geolocation error for SRTM data in North America is 12.6 m for a 90% confidence interval. The absolute elevation error for SRTM data in North America is 7 m for a 90% confidence interval.

6.5.2.2[a]. Soil Classification

Yucca Mountain soil classifications and associated hydraulic properties are developed in *Data Analysis for Infiltration Modeling: Development of Soil Units and Associated Hydraulic Parameter Values* (BSC 2006 [DIRS 176335], Section 6.3). That report documents the development of site-specific soil units, hydraulic parameter values for soil units, and associated statistics and uncertainties for Yucca Mountain soils. Soil classifications and mapping based on analyses performed by the USGS in 1996 were evaluated for technical adequacy for use in infiltration modeling. The initial USGS soil classifications were developed from a map of surficial deposits that characterized soil types based primarily on extent of soil development, geomorphic character, and topographic position. These features provide relative ages of deposits (BSC 2006 [DIRS 176335], Section 6.2.1). The original 40 map units were combined into 10 soil units. The group of 10 soil units, referred to as the "base-case" units, is based on depositional character and relative age. The analysis (BSC 2006 [DIRS 176335], Section 6.2.3) concludes that the soil classifications developed by the USGS are appropriate for use in infiltration modeling.

The USGS classifications were also corroborated based on two other soil surveys that were completed for portions of the Yucca Mountain infiltration model area. In a 1989 soil survey, the distribution of four soil units was shown for Yucca Mountain (Resource Concepts 1989 [DIRS 103450], Figure 2). In 2004, a soil survey for the southwestern portion of Nye County was published (USDA 2004 [DIRS 173916]). The Busted Butte quadrangle of the 2004 survey (USDA 2004 [DIRS 173916]) covers the southwest portion of Yucca Mountain, which is administered by the Bureau of Land Management. The 2004 soil survey did not map the two-thirds of the Yucca Mountain infiltration model area that is administered by Nellis Air Force Base or the area that has been set aside for the Nevada Test Site. The mapping of soil units in the 1989 and 2004 soil surveys were compared with the USGS mapping of soil units (BSC 2006 [DIRS 176335], Section 6.2.4). The approach used by these two alternative soil surveys is equivalent to that used by the USGS in that the soils are identified by USDA taxonomic nomenclature and are subdivided by characteristics such as depth to bedrock, the presence or lack thereof of a duripan with depth, or observable pedogenic products. Overall, the 1989 soil survey (Resources Concepts 1989 [DIRS 103450]) and the 2004 soil survey (USDA 2004 [DIRS 173916]) corroborate the Yucca Mountain soil mapping used for input to an infiltration model with regard to approach and definition of units.

Table 6.5.2.2-1[a] shows the 10 soil classifications that represent the base case evaluated in *Data Analysis for Infiltration Modeling: Development of Soil Units and Associated Hydraulic Parameter Values* (BSC 2006 [DIRS 176335], Section 6.2). These soil types are described in detail in that report (BSC 2006 [DIRS 176335], Section 6.2.3.2) based on their taxonomic classifications.

Table 6.5.2.2-1[a]. Base Case Soil Units

Soil Unit	Type of Deposit [a]	Soil Taxonomic Name[a]	Number of 30 × 30-m Cells [b]	Map Area (%) [b]
1	Fluvial	Typic Argidurids	19,900	7.8
2	Fluvial	Typic Haplocalcids	44,065	17.4
3	Fluvial	Typic Haplocambids	33,115	13.1
4	Fluvial	Typic Torriorthents	4,630	1.8
5	Colluvium	Lithic Haplocambids	116,813	46.1
6	Eolian	Typic Torripsamments	12,205	4.8
7	Colluvium	Lithic Hapla	3,154	1.2
8	Bedrock	Rock	795	0.3
9	Colluvium	Typic Calciargids	16,441	6.5
10	Disturbed	Disturbed Ground	2,479	1.0

[a] BSC 2006 [DIRS 176335], Table 6-2.
[b] BSC 2006 [DIRS 176335], Table 6-3, based on a region surrounding the infiltration domain with 253,597 cells.

The distribution of soil types over the infiltration model domain is shown in Figure 6.5.2.2-1[a]. It should be noted that Soil Unit 8 is used to describe regions of bare bedrock and thus does not have any soil properties associated with it. Similarly, Soil Unit 10, which represents only 1% of the map area, is used to identify regions of disturbed soil such as roads and parking areas. For the purpose of modeling infiltration, cells with Soil Unit 10 were replaced with the soil unit surrounding each of these grid cells. Soil Unit 10 is replaced throughout the domain because areas with disturbed soil are not expected to exist on Yucca Mountain over the time scale of interest in this analysis (10,000 years). Nearby soils best represent the soil characteristics of regions that have been disturbed.

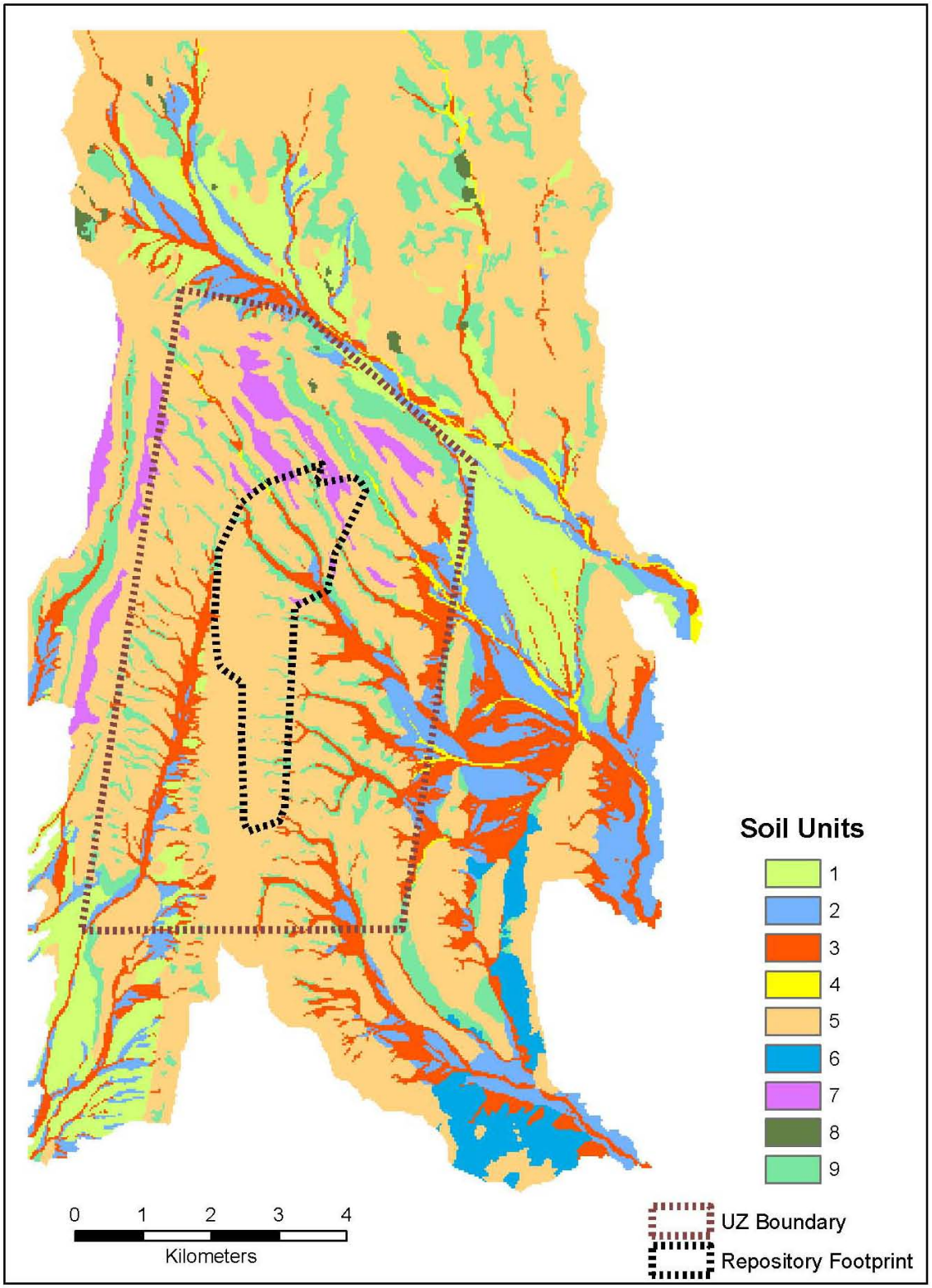

Source: Output DTNs: SN0701SPALAYER.002 and SN0711FTPRNUZB.003.

NOTE: Repository footprint shown for illustrative purposes only.

Figure 6.5.2.2-1[a]. Map Showing Distribution of Soil Types Over the Infiltration Domain

An alternative soil classification system is presented in *Data Analysis for Infiltration Modeling: Development of Soil Units and Associated Hydraulic Parameter Values* (BSC 2006 [DIRS 176335], Section 6.2.5). The alternative soil grouping consists of four soil groups, which are combinations of the eight base case soil units. The four alternative soil groups are: Soil Group 1, Soil Group 2/6, Soil Group 3/4, and Soil Group 5/7/9. The alternative grouping was developed because several of the base case soil units had similar properties but a very limited number of samples upon which to base the hydrologic properties for each unit. By combining soil units into fewer groups, based on depositional character (e.g., combining the 8 base case soil units into 4 groups), the sample size for each group was increased, thus providing a better basis for performing statistical analysis on the data sets without loss of relevant information or the characterization of uncertainty. Several of the base case soil units had such sparse data that it was not possible to characterize the spatial variability and uncertainty in the hydrologic properties. Figure 6.5.2.2-2[a] shows the distribution of the alternative soil groups over the infiltration modeling area.

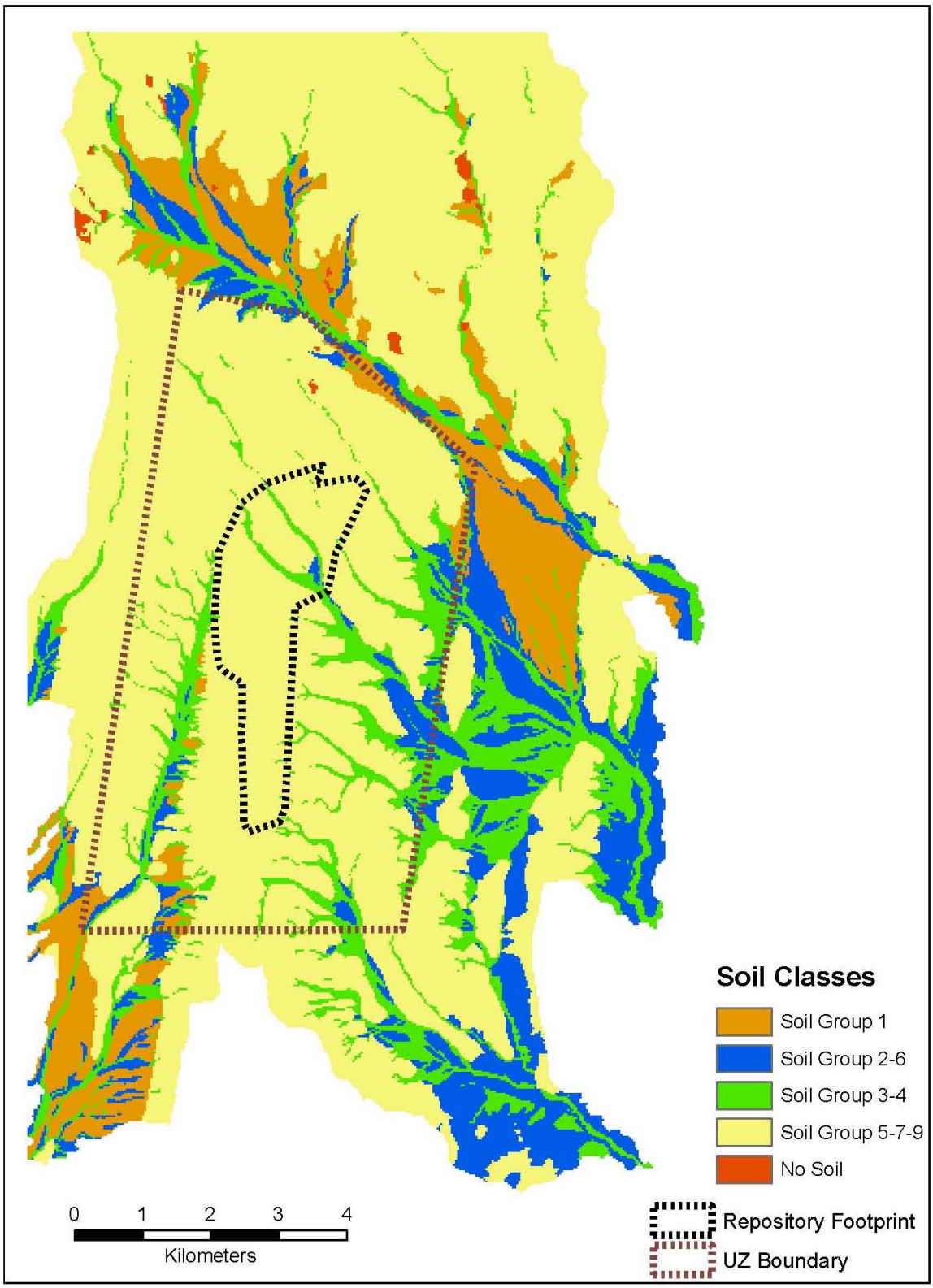

Source: Output DTNs: SN0701SPALAYER.002 and SN0711FTPRNUZB.003.

NOTE: Repository footprint shown for illustrative purposes only.

Figure 6.5.2.2-2[a]. Map Showing Distribution of Alternative Soil Groupings over the Infiltration Domain

This infiltration analysis uses properties derived for the alternative soil grouping; however, the original base case soil unit identifiers are maintained. The base case soil units are the inputs provided in the geospatial database (see Appendix B). In order to use the properties derived for the alternative soil grouping, the appropriate properties are applied to the base case soil units (i.e., Soil Units 2 and 6 have the same properties). Table 6.5.2.2-2[a] shows how much of the UZ grid and total model domain each soil unit occupies.

Table 6.5.2.2-2[a]. Soil Type Cell Counts for the UZ Grid and Infiltration Model Domain

Soil Unit	Total Cells (UZ Grid)	Percent (UZ Grid)	Total Cells	Percent (Total)
1	1,107	3	13,860	10
2	1,834	4	12,114	9
3	5,122	12	16,514	12
4	280	1	1,346	1
5	28,988	66	75,591	54
6	0	0	3,103	2
7	1,841	4	3,050	2
8	22	<1	431	<1
9	5,038	11	13,083	9
Total Cells	**44,232**		**139,092**	

Source: These values were obtained using database applications with data from Output DTNs: SN0606T0502206.011 (soil type code for each cell) and UZ boundary from SN0711FTPRNUZB.003.

6.5.2.3[a]. Soil Properties

No change.

6.5.2.4[a]. Soil Depth

Data Analysis for Infiltration Modeling: Technical Evaluation of Previous Soil Depth Estimation Methods and Development of Alternate Parameter Values (BSC 2006 [DIRS 178819], Section 6.2) evaluates soil depths at Yucca Mountain based on an approach that uses qualified data from boreholes, field surficial deposits mapping, and the geologic framework model (BSC 2004 [DIRS 170029], Figure 6-10). The evaluation divides the infiltration model area into five soil depth classes. Each soil depth class region is associated with a spatial distribution of soil depth and recommendations on the treatment of soil depth for infiltration modeling. Due to the limited number of qualified measurements of soil depth within each soil depth class, it was decided that an upscaled, effective uniform value of soil depth would be used for each net infiltration realization. Note that the word "uniform" is used throughout this report to describe how certain geospatial parameters are defined to be uniform over all locations having the same geospatial property, or how a parameter is upscaled as an effective uniform value to represent parameter uncertainty. The word "uniform" is also used to describe a distribution type.

A map of the soil depth classes over the infiltration model domain is given in Figure 6.5.2.4-1[a]. The percentage of the infiltration domain as well as the percentage of the UZ model domain occupied by each soil depth class is given in Table 6.5.2.4-1[a].

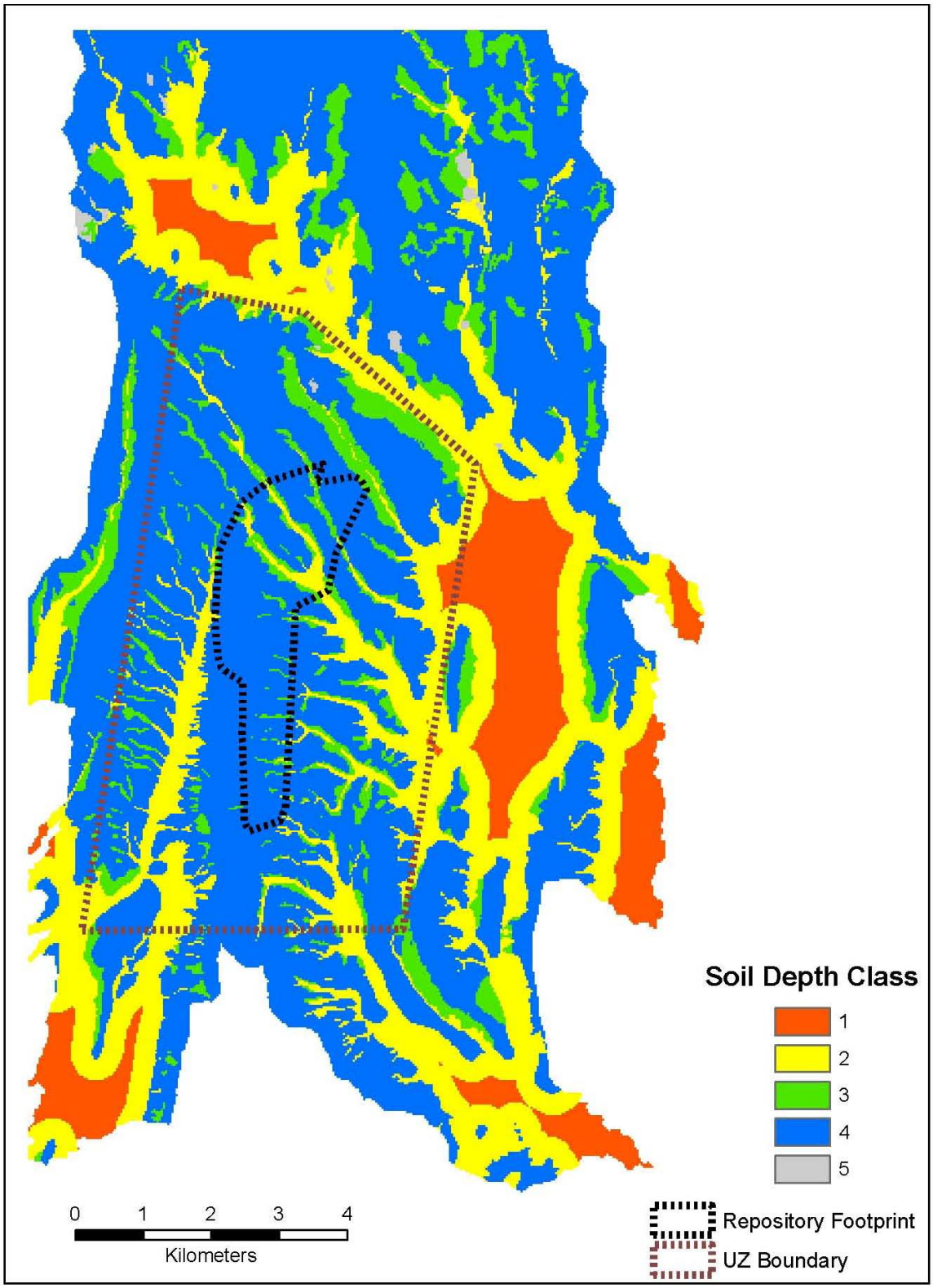

Source: Output DTNs: SN0701SPALAYER.002 and SN0711FTPRNUZB.003.

NOTE: Repository footprint shown for illustrative purposes only.

Figure 6.5.2.4-1[a]. Distribution of Soil Depth Classes over the Infiltration Domain

Table 6.5.2.4-1[a]. Soil Depth Class Cell Counts for the UZ and Infiltration Model Domains

Soil Depth Class	UZ Domain Total Cells	Percent (UZ Domain)	Infiltration Domain Total Cells	Percent (Infiltration Domain)
1	196	<1	12,343	9
2	8,074	18	34,479	25
3	5,069	11	13,116	9
4	30,871	70	78,723	57
5	22	<1	431	<1
Total cells	**44,232**		**139,092**	

Source: These values were obtained using database applications with input from DTNS: MO0608SPASDFIM.006 [DIRS 178082] (revised *soil depth file.txt*) and MO0603SPAGRIDD.003 [DIRS 177121].

Soil depth spatial distributions were developed in *Data Analysis for Infiltration Modeling: Technical Evaluation of Previous Soil Depth Estimation Methods and Development of Alternate Parameter Values* (BSC 2006 [DIRS 178819], Section 6.2.2). A discussion is presented in that report to provide recommendations on the spatial distribution of soil depth for each of the soil depth classes, and estimates of the population mean along with confidence intervals. A summary of the recommended soil depth spatial distributions for each depth class is presented in Table 6.5.2.4-2[a].

Table 6.5.2.4-2[a]. Summary of Recommended Distributions for Soil Depth

Soil Depth Class Designator	1	2	3	4	5
Soil Depth Class	**Very Deep Soils**	**Moderately Deep Soils**	**Intermediate Depth Soils**	**Shallow Soils**	**Exposed Bedrock**
Sample Distribution Type	Uniform	Left-Truncated Normal (truncated at 0.5 m)	Lognormal	Lognormal	Single Value
Sample Mean	N/A	16.47 (m)	3.26 (m)	0.45 (m)	N/A
Sample Mean of the Natural Logarithm	N/A	N/A	0.61 (LN m) (1.84 m)	−1.29 (LN m) (0.27 m)	N/A
Sample Standard Deviation	N/A	14.61 (m)	4.71 (m)	0.67 (m)	N/A
Sample Standard Deviation of the Natural Logarithm	—	—	1.07 (LN m)	0.88 (LN m)	
Sample Standard Error	N/A	1.84	1.22	0.11	N/A
Sample Median (also Estimated Population Median)	95 m	12.19 (m)	2.07 (m)	0.25 (m)	N/A
Sample Minimum Value (m)	40 (m)	0.5	N/A	N/A	0
Sample Maximum Value (m)	150 (m)	64	N/A	N/A	0
Number of Data Points	4	63	15	35	N/A

Table 6.5.2.4-2[a]. Summary of Recommended Distributions for Soil Depth (Continued)

Soil Depth Class Designator	1	2	3	4	5
Soil Depth Class	Very Deep Soils	Moderately Deep Soils	Intermediate Depth Soils	Shallow Soils	Exposed Bedrock
Estimated Population Mean	95 (m)	16.47 (m)	3.25 (m)	0.40 (m)	0
Confidence Interval for Population Mean at 80% Limit	—	14.09 to 18.86 (m)	2.21 to 5.73 (m)	0.33 to 0.52 (m)	N/A
Confidence Interval for Population Mean at 90% Limit	—	13.40 to 19.54 (m)	2.00 to 7.11 (m)	0.31 to 0.57 (m)	N/A
Confidence Interval for Population Median at 80% Limit	N/A	N/A	1.27 to 2.67 (m)	0.23 to 0.33 (m)	N/A
Confidence Interval for Population Median at 90% Limit	N/A	N/A	1.13 to 2.99 (m)	0.21 to 0.35 (m)	NA

Source: BSC 2006 [DIRS 178819], Table 6-10.

NOTE: The calculations of these statistical parameters are descri bed in Appendix B of BSC 2006 [DIRS 178819]. These calculations are also included in Output DTN: SN0708T0502206.048.

LN = natural logarithm; N/A = not applicable.

The soil depth class spatial distributions discussed in *Data Analysis for Infiltration Modeling: Technical Evaluation of Previous Soil Depth Estimation Methods and Development of Alternate Parameter Values* (BSC 2006 [DIRS 178819], Section 6.2) and displayed in Table 6.5.2.4-2[a] are subject to several types of uncertainty. Sources of uncertainty include (BSC 2006 [DIRS 178819], Section 6.2.2):

- Natural variability in soil depth that occurs at all scales in the infiltration modeling domain.
- Measurement errors made when determining soil depths at sampling localities.
- Uncertainty resulting from the difficulty in determining the soil–bedrock interface, especially in a borehole. This interface may be difficult to define when it is characterized by rubble or broken and fractured bedrock.
- Uncertainty in the statistical estimation of population parameters derived from a sample consisting of only a few observations from the population.

A summary of the characteristics of each depth class, including recommended distributions for the effective soil depth to be used in the infiltration modeling, which are based on an analysis of the uncertainty in the parameters, is provided in *Data Analysis for Infiltration Modeling: Technical Evaluation of Previous Soil Depth Estimation Methods and Development of Alternate Parameter Values* (BSC 2006 [DIRS 178819], Section 6.2.3) and quoted below for all soil depth classes except soil depth class 4, which is treated in more detail in the next section. The

distributions used to represent the effective soil depth for these classes in this analysis are listed in Table 6.5.2.4-3[a].

Table 6.5.2.4-3[a]. Summary of Recommended Distributions for Effective Soil Depths ($depth_{soil}$)

Soil Depth Class	Lower Bound Soil Depth (m)	Upper Bound Soil Depth (m)	Nominal Value Soil Depth (m)	Distribution	Comments
1	N/A	N/A	95	Constant	Estimated population mean
2	N/A	N/A	16.47	Constant	Estimated population mean
3	N/A	N/A	3.26	Constant	Sample mean
4	0.1	0.5	0.25	Uniform	See Section 6.5.2.4.1[a]
5	N/A	N/A	0	Constant	—

Effective Soil Depth for Soil Depth Class 1 ($depth_{soil(1)}$)

This depth class represents very thick soils, described by a uniform distribution with lower and upper bound values of 40 and 150 m, respectively. Because this class represents depths much deeper than the rooting depth (below which water is not removed by the infiltration model), using a representative value equal to the mean for the class of 95 m is appropriate. Because soil depths in this class are large and infiltration is expected to be small, the specific value chosen within this range is unlikely to cause a significant change to predicted infiltration.

Effective Soil Depth for Soil Depth Class 2 ($depth_{soil(2)}$)

This depth class represents moderately deep soils that range in depth from 0.5 to about 50 m. This class is intended to include the value where soil depth is sufficient to limit infiltration of water to the soil–bedrock contact, except in some channels, because the soils have sufficient storage capacity to retain precipitation in the root zone where it is subject to evapotranspiration. It is expected that infiltration in the soil depth class 2 areas is most likely to occur where soil thickness is small. Consequently, the appropriate bulk parameter value will lie closer to the small soil thickness portion of the distribution, rather than near the large soil thickness values.

Effective Soil Depth for Soil Depth Class 3 ($depth_{soil(3)}$)

This depth class represents areas of thicker foot-slope soils that occur intermittently in the area. The data are represented by a lognormal distribution with an estimated population mean soil depth of 3.25 m and a sample median of 2.07 m, which is also the estimated population median; only one value is larger than 5.18 m (BSC 2006 [DIRS 178819], Figure 6-15 and Table 6-7). As seen in Figure 6.5.2.4-1[a], depth class 3 is most often found between soils of depth class 2 (moderately deep) and depth class 4 (shallow), acting as a transition from deeper to shallower soils. The depth in soil depth class 3 will be small where it contacts soil depth class 4 but increases where it contacts deeper depth classes, primarily soil depth class 2. The majority of infiltration through soil depth class 3 will occur where the depth is small. The appropriate effective uniform depth for soil depth class 3 is a value that allows for the same total infiltration, through all of soil depth class 3, as occurs through the spatially variable material that exists in nature. Estimating a uniform value for this depth class is especially challenging. There are very few measurements for this depth class (15 measurements, four of which indicate that there is no

soil). Many of these measurements may represent disturbed regions where drilling pads were constructed and, thus, may not represent actual soil depth. Although it is common to choose the median of a lognormal distribution as a measure of central tendency, the potential underestimate previously noted suggests that the sample mean is a better measure of central tendency in this case. The 90% confidence interval about the mean ranges from 2 to 7 m; the lower bound of this range is approximately the median.

Effective Soil Depth for Soil Depth Class 5 ($depth_{soil(5)}$)

This class represents exposed bedrock in the area that does not have soil cover. Therefore, all cells in this class should be assigned a zero soil depth value.

6.5.2.4.1[a]. Effective Soil Depth Distribution for Soil Depth Class 4

Estimating the distribution of effective soil depth for this soil depth class is especially important because of the significant sensitivity of net infiltration to shallow soil depth and the large relative proportion of the modeling domain covered by this soil depth class. These two reasons prompted a more detailed analysis of shallow soil depth uncertainty than provided in *Data Analysis for Infiltration Modeling: Technical Evaluation of Previous Soil Depth Estimation Methods and Development of Alternate Parameter Values* (BSC 2006 [DIRS 178819], Section 6.2.2).

One upscaled value of soil depth is used to represent the spatial variability in soil depth class 4 for each realization. The estimation of uncertainty in this upscaled depth is calculated from a two-step process. The first step consists of determining a spatial distribution for soil depth class 4. The second step is to determine which statistic in this distribution is an adequate upscaled soil depth (in the sense that it will lead to a reasonable estimate of spatially averaged infiltration).

Estimation of the Spatial Distribution of Soil Depth

In *Data Analysis for Infiltration Modeling: Technical Evaluation of Previous Soil Depth Estimation Methods and Development of Alternate Parameter Values* (BSC 2006 [DIRS 178819], Section 6.2.2), the spatial distribution of soil depth is represented by a lognormal distribution, estimated using probability plot fitting. This distribution is based on 35 individual measurements over an area of approximately 71 km^2. That report (BSC 2006 [DIRS 178819], Section 6.2.2) assigned each observation a distinct quantile value even when duplicate values of soil depth were measured at different locations. Duplicate soil depth values should reflect the same quantile. Therefore, in this analysis the distribution fitting has been redone (although the probability plot fitting described below leads to nearly the same result). Two methods are applied for estimating parameters that define the lognormal distribution from the 35 observations: probability plotting and least-squares fitting. The updated fitting of these 35 observations is made in Output DTN: SN0612T0502206.039.

The first method of estimating the underlying lognormal distribution is based on a probability plot where the vertical axis represents the ordered values, while the horizontal axis represents the standard normal order distances. If the distribution is close to normal, then the points are linearly distributed on the plot. The mean and standard deviation of the distribution corresponds to the Y-intercept and slope of a linear regression model, respectively.

The resulting probability plot is shown in Figure 6.5.2.4-2[a]. The estimates for the mean and standard deviation are −1.295 and 0.93, respectively.

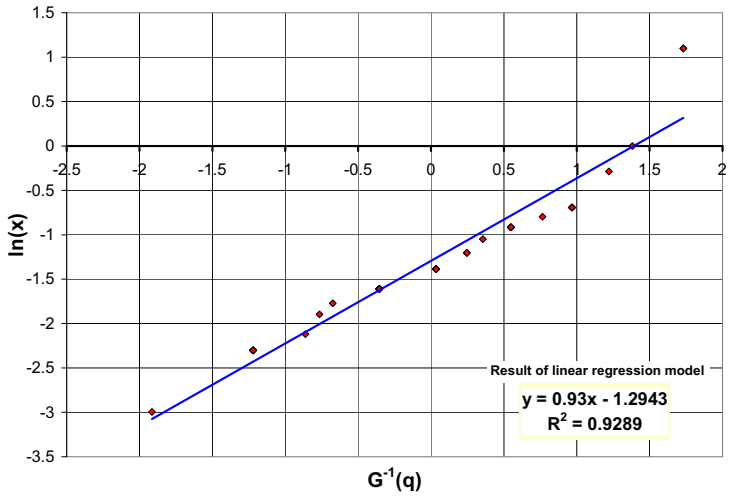

Source: Output DTN: SN0612T0502206.039, *LN_fitting_upper_bound_V2.0_12_2006.xls*. Data from DTN: GS011208312212.004 [DIRS 176317], Table S02086_001.

NOTE: Only 15 observations are displayed, as duplicates are assigned with an average quantile value.

Figure 6.5.2.4-2[a]. Normal Probability Plot for 35 Observations of Soil Depth in Soil Depth Class 4 Region

The second method consists in fitting a lognormal distribution, such that the sum of the squared differences between the quantiles of the observed values and the quantiles of such values in the lognormal distribution is minimized.

The cumulative distribution functions (CDFs) of both lognormal fitted distributions compared with observed values are displayed in Figure 6.5.2.4-3[a], showing good agreement between the data and both fitting methods.

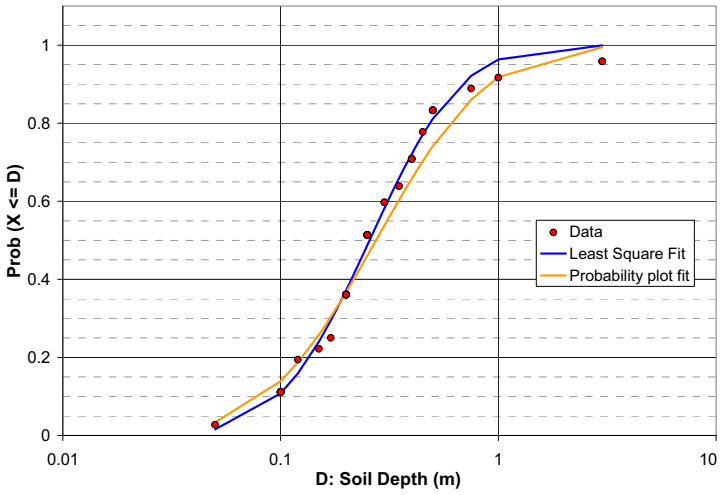

Source: Output DTN: SN0612T0502206.039, *LN_fitting_upper_bound_V2.0_12_2006.xls*. Data from DTN: GS011208312212.004 [DIRS 176317], Table S02086_001. Values with "Deposit Unit" designations of "Tpc" and "stone st" are interpreted to belong to soil depth class 4 (BSC 2006 [DIRS 178819], p. 6-27).

Figure 6.5.2.4-3[a]. CDFs for 35 Observations (red dots), Least-square Fitted Lognormal Distribution (blue line), and Probability Plot Fitted Lognormal Distribution (orange line) in Log-scale for Soil Depth (X-axis)

However, it is unclear how well the 35 observations represent the actual spatial distribution of this soil depth class. There may be a bias toward deeper soils since none of the 35 observations include soil depth of 0 m, while observations of patches of bare rock have been made in the area covering soil depth class 4 during field trips to the site.

For this reason, a second source of information was used to create a second spatial distribution of shallow soil depth (Sanchez 2006 [DIRS 176569], pp. 62 to 68). This scientific notebook contains observations made in several places at Yucca Mountain. Most of the observations are for shallow soil and should correspond to regions of soil depth class 4. The observations from the scientific notebook (and page numbers in the scientific notebook) are listed below:

Observations:

Page 62: (NRG-3 pad) Soil Depth from 0.3 to 0.5 m
Page 63: (Close up view NRG-3 pad) captured above – not considered
Page 64: (bleach bone ridge) half of the image is covered with rock (0 m) – the remaining part is with soil from 0.1 to 0.3 m
Page 65: (bleach bone ridge) same measurement as p. 64 – not considered
Page 66: (Above SD-9 pad) Soil Depth from 0 to 0.09 m
Page 67: (Yucca Crest) Soil range from 0 to 0.3 m
Page 67: (bleach bone ridge) consistent with p. 64 – not considered
Page 68: (tonsil ridge top) no soil – 0 m
Page 68: (tonsil ridge side-slope) thin soil 0.1 m
Page 68: (tonsil ridge foot-slope) up to 3 m – range from 0.1 to 3 m.

Out of these ten observations, three were not considered (as indicated above) as they concerned already included regions. One observation was split in two (p. 64) because two different patterns are seen in the photograph (one with soil and one with no soil). As a result, the new distribution was defined with eight ranges. Each range has been weighted equally (a weight of 1/8). The resulting ranges are listed in Table 6.5.2.4-4[a].

Table 6.5.2.4-4[a]. Summary of Soil Depth Ranges Defined Based on Alex Sanchez Observations

Reference	Location Description	Minimum (m)	Maximum (m)	Weight	Page
A	NRG-3 pad	0.3	0.5	0.125	62
(not considered)	NRG-3 pad (closeup)	—	0.3	—	63
B	Bleach Bone Ridge (no soil)	0	—	0.125	64
C	Bleach Bone Ridge (soil)	0.1	0.3	0.125	64
(not considered)	Bleach Bone Ridge	0.1	0.3	—	65
D	SD-9 pad	0	0.09	0.125	66
E	Yucca Crest (natural)	0	0.3	0.125	67
(not considered)	Bleach Bone Ridge	0.2	0.2	—	67
F	Tonsil Ridge (Top)	0	0	0.125	68
G	Tonsil Ridge (Side)	0.1	0.1	0.125	68
H	Tonsil Ridge (Foot)	0.1	3	0.125	68

Source: Output DTN: SN0612T0502206.039, *Lower_Bound_distribution_V4.0_12_05_2006.xls*. Data from Sanchez 2006 [DIRS 176569].

All but one range (Reference H in Table 6.5.2.4-4[a]) were represented with a uniform distribution due to a lack of information about these observations of soil depth. The soil depth range for the Tonsil Ridge Foot (Reference H) is significantly larger than for the other observations. Therefore, it is reasonable to increase the likelihood of values closer to the lower bound (i.e., 0.1 m), so a loguniform distribution was used instead of a uniform distribution. This approach is consistent with what was observed in the previous set of data (BSC 2006 [DIRS 178819]), for which two values are equal to 3.0 m, but no observations have been made between 1.0 and 3.0 m.

Two of the ranges included a component of bare rock (no soil) and result in lower bound values of zero (for which logarithm is not defined). To be able to work with log-transformed data, the distribution is defined starting with the 0.25 quantile (as a quarter of the distribution is equal to 0), and the remaining observations are associated with an equal weight of 1/6. This is consistent with the previously defined weight, as a weight of 1/6 for 3/4 of the distribution corresponds to a total weight of 1/8.

To represent the piecewise distribution, a series of two random numbers was generated; the first was used to randomly select one of the six predefined bins, and the second was used to sample a soil depth from within the selected bin. This Monte Carlo approach was repeated 1,000 times to create a distribution. The resulting distribution is displayed in Figure 6.5.2.4-4[a].

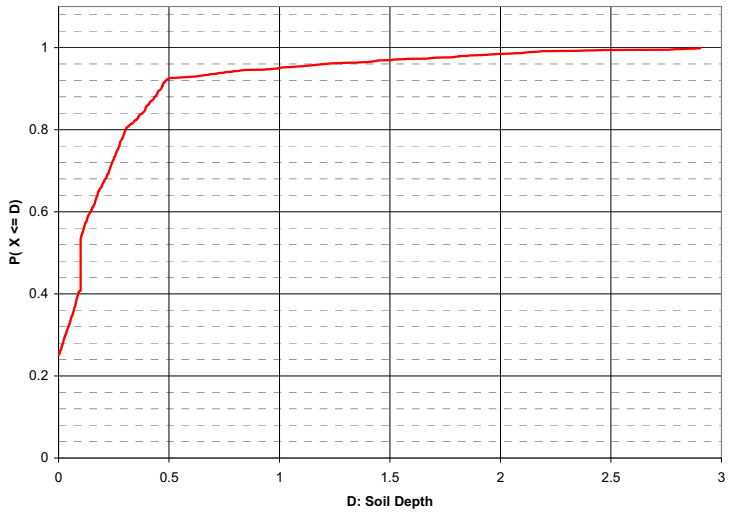

Source: Output DTN: SN0612T0502206.039, *Lower_Bound_distribution_V4.0_12_05_2006.xls*. Original data from Sanchez 2006 [DIRS 176569].

Figure 6.5.2.4-4[a]. CDF of Estimated Distribution of 1,000 Soil Depth Values Using Six Soil Depth Ranges from the Sanchez Notebook

The two fitting methods described above (probability plotting and least squares) were applied to the soil depth ranges obtained from Sanchez 2006 [DIRS 176569]. However, because 25% of the distribution is equal to 0 m and a lognormal distribution is not defined for values of zero, each of these fitting methods had to be modified. Two approaches were considered for modifying the fitting methods:

- In the first approach, it is assumed that the information available is known only for values greater than zero and that nonzero values represent only 75% of the distribution. This assumption allows calculation of the arithmetic and geometric means of the fitted lognormal distributions directly, but it does not necessarily result in a good fit.

- In the second approach, it is assumed that the distribution is bimodal. Like the first approach, the fitting is done with nonzero values; however, they are considered to represent the whole distribution. The final estimates of the arithmetic and geometric means are corrected to include 25% of zero values. This approach leads to a better fit but makes the estimation of the geometric mean more difficult.

The normal probability plot is displayed in Figure 6.5.2.4-5[a], for both approaches. Not considering the first quarter of the distribution (first approach) leads to an asymmetry in the plot on the left (as the X-axis goes from about −0.6 to 3.2). The fit is linear except near the edges. If nonzero values are assumed to represent the whole distribution (second approach; right frame), the fit is better even near the edges.

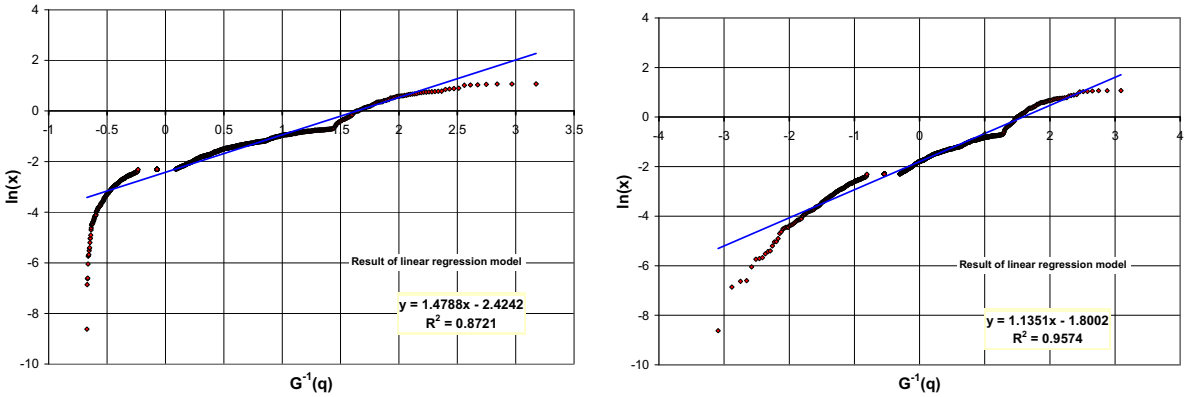

Source: Plots are produced in Output DTN: SN0612T0502206.039, *LN_fitting_lower_bound_V2.0_12_01_2006.xls*. The plot on the left is generated by setting the cell C2 on sheet "Calculations" to a value of 0.25. The plot on the right is generated when this cell is set to a value of zero. Original data from Sanchez 2006 [DIRS 176569].

NOTE: In the left frame, the nonzero values are considered to represent 3/4 of the distribution. In the right frame, the nonzero values represent the whole distribution.

Figure 6.5.2.4-5[a]. Probability Plot for Estimated Distribution Based on Sanchez Notebook

A least square fitting approach (based on quantile values) has been applied to generate a second distribution using both approaches (Figure 6.5.2.4-6[a]).

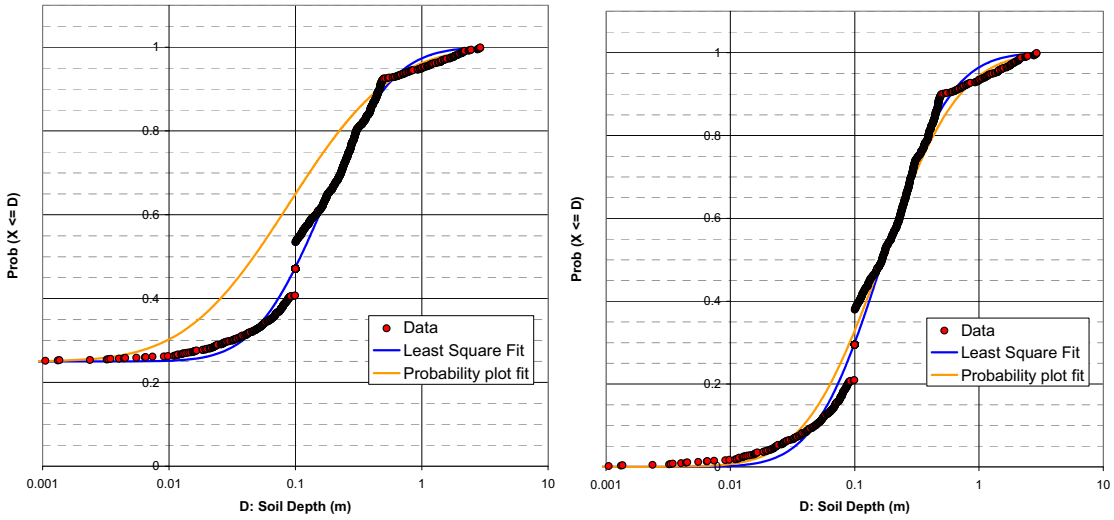

Source: Plots are produced in Output DTN: SN0612T0502206.039, *LN_fitting_lower_bound_V2.0_12_01_2006.xls*. The plot on the left is generated by setting the cell C2 on sheet "Calculations" to a value of 0.25. The plot on the right is generated when this cell is set to a value of zero. Original data from Sanchez 2006 [DIRS 176569].

NOTE: In the left frame, the nonzero values are considered to represent 3/4 of the distribution. In the right frame, the nonzero values represent the whole distribution.

Figure 6.5.2.4-6[a]. CDFs for Estimated Distribution (red dots), Least-Square Fitted Lognormal Distribution (blue line), and Probability Plot Fitter Lognormal Distribution (orange line)

Regardless of the approach, the least-square fitting method results in a good fit for low values of soil depth (0 to 50 cm) but cannot capture the distribution behavior for deeper soils.

The probability plot fitting method does not fit the distribution for shallow soil using the first approach, but the fit for deeper soil is better. The second approach results in a reasonably good fit for shallow soil and better fit for deeper soil than the least square method.

Estimation of Upscaled Distribution of Soil Depth for Soil Depth Class 4

Because of nonlinearities between soil depth and average net infiltration, it is difficult to determine which statistic would best represent an effective uniform value of soil depth that would lead to an accurate estimate of spatially averaged net infiltration.

In hydrologic modeling, flow parameters such as permeability (typically represented with a lognormal spatial distribution) are generally upscaled to the geometric mean, and storage parameters such as porosity (typically represented with a normal spatial distribution) are typically upscaled to the arithmetic mean. Soil depth follows a lognormal spatial distribution but is a storage-type parameter. Therefore, it is hypothesized that the upscaled value should lie between the geometric and arithmetic means.

Both arithmetic and geometric means have been estimated for the fitted lognormal distributions as well as their standard errors (where standard error for geometric mean is based on the standard deviation of log-transformed data). A confidence interval has been estimated by adding or subtracting one standard error to the quantity of interest. The results are displayed below for geometric mean (Table 6.5.2.4-5[a]) and arithmetic mean (Table 6.5.2.4-6[a]). Confidence intervals are rounded to the first significant digit because an examination of the underlying observations seems to suggest that soil depths were generally measured or estimated to the nearest 5 cm, especially for deeper soils. Furthermore, because it can be difficult to identify the exact location of the soil–bedrock interface, it is assumed that the accuracy of the observations is only good to about 5 cm and certainly not to as little as 1 cm. For the first distribution (i.e., based on 35 observations) and for the second distribution using the first approach (i.e., considering nonzero values represents 75% of the distribution), the calculation of arithmetic and geometric means is straightforward. For the second approach on the second data set (scientific notebook (Sanchez 2006 [DIRS 176569])), the estimate of both means has to be corrected to incorporate the second part of the bimodal distribution with values of zero soil depth.

Table 6.5.2.4-5[a]. Estimation of Geometric Mean and Confidence Interval (by adding or subtracting one standard error)

	Estimation (log space)	Standard Error (log space)	Lower Bound (linear space)	Upper Bound (linear space)
First distribution – Probability plot fitting	−1.29	0.16	0.2	0.3
First distribution – Least Square fitting	−1.36	0.13	0.2	0.3
Second distribution (1st approach) – Probability plot fitting	−2.38	0.05	0.1	0.1
Second distribution (1st approach) – Least Square fitting	−1.71	0.04	0.2	0.2

Table 6.5.2.4-5[a]. Estimation of Geometric Mean and Confidence Interval (by adding or subtracting one standard error) (Continued)

	Estimation (log space)	Standard Error (log space)	Lower Bound (linear space)	Upper Bound (linear space)
Second distribution – (2nd approach) – Probability plot fitting	−1.80	0.04	0.1[a]	0.1[a]
Second distribution – (2nd approach) – Least Square fitting	−1.78	0.03	0.1[a]	0.1[a]

NOTE: [a] Lower and upper confidence bounds (CB) are first estimated in log scale using mean and standard deviation, and then corrected using the formula 0.75 × CB+0.25 × ln(0.01) – results are then calculated using an exponential function.

Table 6.5.2.4-6[a]. Estimation of Arithmetic Mean and Confidence Bounds (by adding or subtracting one standard error)

	Estimation	Standard Error	Lower Bound	Upper Bound
First distribution – Probability plot fitting	0.42	0.08	0.3	0.5
First distribution – Least Square fitting	0.34	0.05	0.3	0.4
Second distribution (1st approach) – Probability plot fitting	0.39	0.05	0.3	0.4
Second distribution (1st approach) – Least Square fitting	0.34	0.02	0.3	0.4
Second distribution – (2nd approach) – Probability plot fitting	0.31	0.02	0.2[a]	0.2[a]
Second distribution – (2nd approach) – Least Square fitting	0.27	0.01	0.2[a]	0.2[a]

NOTE: [a] Lower and upper confidence bounds (CB) are first estimated using mean and standard deviation and then corrected using the formula 0.75 × CB+0.25 × 0.

The correction is applied directly on the lower and upper confidence bounds, as it is not possible to directly estimate the updated standard deviation.

The estimate of arithmetic mean is done by simply summing, for each bound, 75% of the previous value, to 25% of a value of 0.

The estimate of geometric mean is more difficult. Indeed, if any of the values of the distribution are equal to zero, the geometric mean is equal to zero. Thus, the inclusion of zero values will lead to a useless estimate. One solution to this problem is to associate a very small (constant) value to represent the fraction of the spatial distribution with zero soil depth. Of course, as the geometric mean is equivalent to an arithmetic mean calculated on log-transformed data, taking a value too small will lead again to a very low value of the geometric mean. Therefore, it was assumed that the presence of 1 cm of soil is essentially equivalent to there being no soil in regards to the resulting net infiltration. The geometric mean was then estimated using log-transformed data, estimating the mean and its confidence bounds, summing 75% of these bounds with 25% of the logarithm of 0.01 m (approximately −4.6), and exponentiating the results to convert to a linear scale. Higher values of soil depth, from 2 to 9 cm, have been tested to represent the fraction of bare rock and to estimate the sensitivity of confidence bounds to the selected values. With a 10-cm accuracy, all values lead to the same confidence interval.

The minimum value estimate is equal to 0.1 m (bounds for geometric mean using probability plot fitting method on second data set using first approach and geometric mean on second data set using second approach). The maximum is equal to 0.5 m (upper bound of arithmetic mean using probability-plot fitting method on first dataset). Because there is no reason to favor any of these values (or any intermediate value), a uniform distribution for soil depths between 0.1 m and 0.5 m was selected to represent the uncertainty in the upscaled quantity used to represent effective uniform value of soil depth class 4.

To summarize, a lognormal distribution was selected for the first soil depth dataset (DTN: GS011208312212.004 [DIRS 176317]). The second dataset (Sanchez 2006 [DIRS 176569]) was used to generate a synthetic dataset of 1,000 soil depth values. Uniform distributions were selected for 5 of the 6 soil depth ranges, and a log-uniform for the 6th soil depth range given in the scientific notebook (Sanchez 2006 [DIRS 176569]). Several different statistical analyses were applied to the synthetic dataset to find a representative lower bound, using a lognormal distribution. The final selected range was 0.1 to 0.5 m, with a uniform distribution. This distribution represents an effective upscaled uniform soil depth to capture a large uncertainty in soil depth class 4, and it is not a range representing the spatial variability of soil depth class 4 (which would have a range of 0 to 3 m).

6.5.2.5[a]. Bedrock Classification

An infiltration hydrogeologic unit (IHU) system was developed consisting of bedrock types (IHUs) that have differing hydrogeologic properties with special emphasis on hydraulic conductivity (BSC 2006 [DIRS 176355], Section 6.2). The IHUs are defined on the basis of lithostratigraphic contacts in boreholes (BSC 2004 [DIRS 170029]). The correlation of lithostratigraphic units and IHUs enables the extrapolation of the IHUs to exposures at the ground surface where most of the correlated lithostratigraphic units have been documented on the following geologic maps:

- Preliminary Geologic Map of Yucca Mountain, Nye County, Nevada, with Geologic Sections (Scott and Bonk 1984 [DIRS 104181])
- Bedrock Geologic Map of the Central Block Area, Yucca Mountain, Nye County, Nevada (Day et al. 1998 [DIRS 101557])
- Digital Geologic Map of the Nevada Test Site and Vicinity, Nye, Lincoln and Clark Counties, Nevada, and Inyo County, California, Revision 4; Digital Aeromagnetic Map of the Nevada Test Site and Vicinity, Nye, Lincoln, and Clark Counties, Nevada, and Inyo County, California; and Digital Isostatic Gravity Map of the Nevada Test Site and Vicinity, Nye, Lincoln, and Clark Counties, Nevada, and Inyo County, California (Slate et al. 2000 [DIRS 150228]).

For map units that do not have any correlative IHUs, proxy IHUs have been proposed that are based on similarities in lithostratigraphic characteristics. These correlations of IHUs to lithostratigraphic units to map units are the basis for the new bedrock hydraulic conductivity map (Figure 6.5.2.5-1[a]).

The infiltration model uses an input file containing 253,597 records of data with each record corresponding to a 30 × 30-m grid cell in the model area. The model area includes the entire Busted Butte 7.5 min quadrangle and the southern half of the Topopah Spring NW 7.5 min quadrangle. Because bedrock hydrologic properties are assigned on the basis of lithology, bedrock geologic units were assigned to each grid cell. This was accomplished with a digital manipulation of existing geologic mapping data covering the area (BSC 2006 [DIRS 176355], Section 6.2.2).

In DTN: MO0603SPAGRIDD.003 [DIRS 177121] (*IHU_map_file2.txt*), each comma delimited record includes fields representing x- and y-coordinates for the center of the associated 30 × 30-m cell. The lithologic mapping unit corresponding to the center-cell coordinates was determined from the source polygon coverages using both ARCINFO and EarthVision (BSC 2006 [DIRS 176355], Section 6.2). The source files use a number code to designate stratigraphic units in the digital coverage files. The stratigraphic unit identified is shown at the point at the center of the cell in the "Geology" field of DTN: MO0603SPAGRIDD.003 [DIRS 177121].

The use of the center point of a grid cell to determine lithology can result in a generalization of the bedrock geology from that shown on the source maps. Cells that contain contacts between two or more units have been generalized to the unit found at the center of the cell. This means that thin units may occasionally be under- or over-represented in the file or that contacts may be displaced by up to 15 m. Given that the infiltration model contains over 250,000 cells, this level of generalization is considered acceptable for the purposes of the infiltration model when the natural variation within each lithologic unit and the uncertainties regarding the properties assigned to each unit are considered.

The three source maps (DTNs: GS971208314221.003 [DIRS 107128], *cb6k.ps*; MO0003COV00095.000 [DIRS 146848], *scotbons.e00*; and MO0603GSCGEOMP.000 [DIRS 176585], *ofr-99-0554-e00.tar*) each show significant areas covered by deep Quaternary alluvium (BSC 2006 [DIRS 176355], Figures 6-3, 6-4, and 6-5). Since the infiltration model needs the bedrock types underlying this alluvium to calculate infiltration into the bedrock from any water that percolates through the alluvium and reaches the bedrock contact, the GFM (DTN: MO0012MWDGFM02.002 [DIRS 153777]) was queried, and all cells within the GFM range that were classified as alluvial type were identified according to their underlying bedrock type (BSC 2006 [DIRS 176355], Section 6.2.2). Areas on the north, east, and south edges of the model area are not covered by the GFM and are still shown as alluvium (IHUs 490 and 491) in Figure 6.5.2.5-1[a]. For infiltration modeling, the bedrock conductivity report (BSC 2006 [DIRS 176355], Section 7) recommends that the saturated hydraulic conductivity value for IHU 405 be used as the bedrock saturated hydraulic conductivity value for those areas mapped as IHUs 490 and 491 in DTN: MO0603SPAGRIDD.003 [DIRS 177121].

Table 6.5.2.5-1[a] shows the bedrock cell counts for each bedrock type in the UZ model area as well as the infiltration model domain. Note that the infiltration calculation model domain (containing 139,092 cells) is smaller than the region mention above (containing 253,597 cells) because the infiltration model uses watersheds within that domain as its boundaries. As can be seen in Table 6.5.2.5-1[a], bedrock types 405 and 406 are the most prominent in the UZ modeling domain, each occupying more than 15% of the total area.

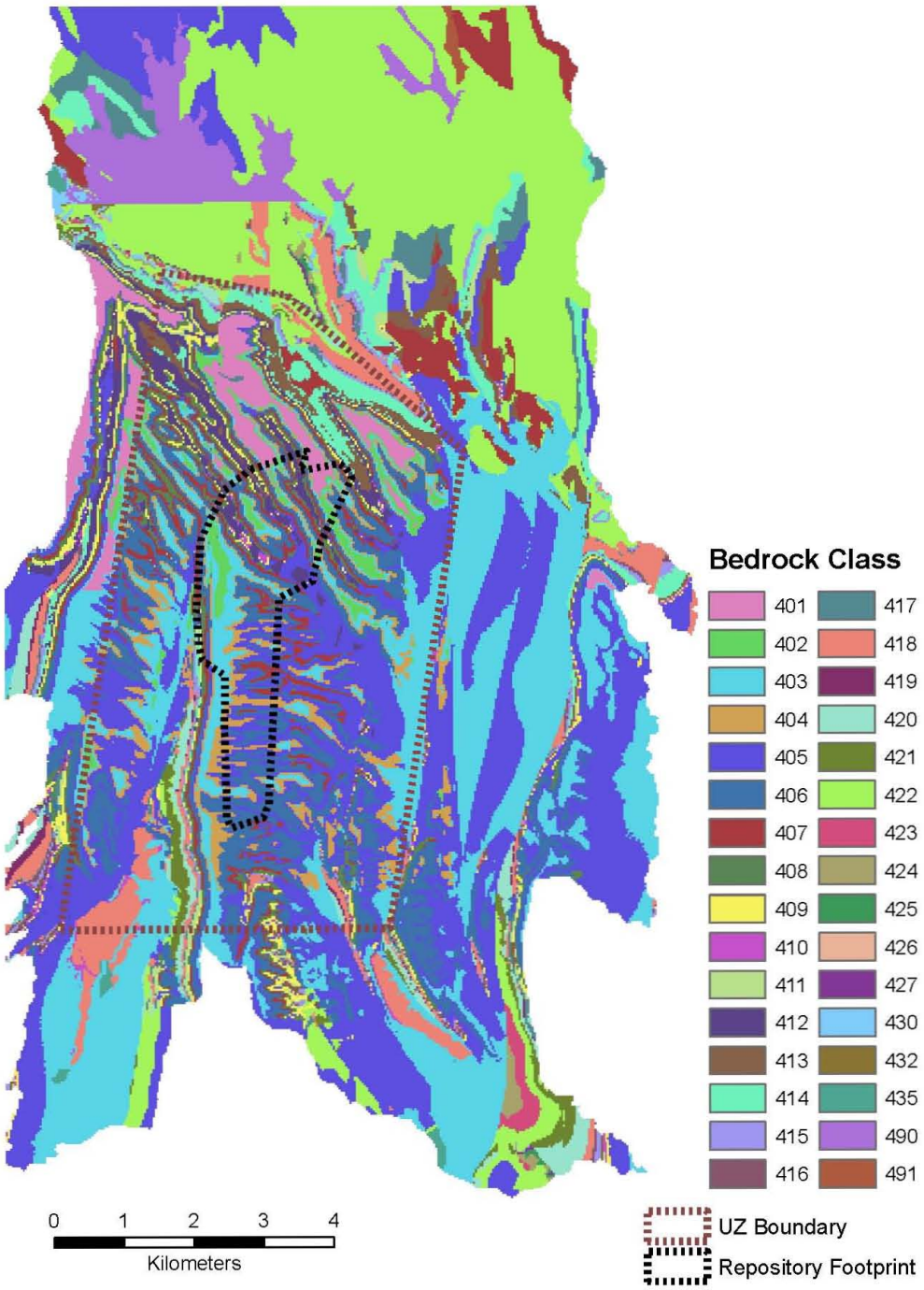

Source: DTN: MO0603SPAGRIDD.003 [DIRS 177121].

Output DTNs: SN0701SPALAYER.002 and SN0711FTPRNUZB.003.

NOTE: Repository footprint shown for illustrative purposes only.

Figure 6.5.2.5-1[a]. Distribution of Infiltration Hydrogeologic Units across the Model Area

Table 6.5.2.5-1[a]. Bedrock Cell Counts for the UZ Grid and Infiltration Model Domain

Bedrock IHU	UZ Domain Total Cells	Percent (UZ Domain)	Infiltration Domain Total Cells	Percent (Infiltration Domain)
401	1,731	4	2,974	2
402	1,445	3	1,651	1
403	6,367	14	24,672	18
404	3,567	8	3,921	3
405	9,905	22	30,953	22
406	8,537	19	11,819	8
407	2,645	6	5,701	4
408	1,588	4	2,562	2
409	753	2	1,827	1
410	146	<1	483	<1
411	141	<1	1,058	1
412	1,750	4	2,620	2
413	1,022	2	2,608	2
414	1,348	3	3,974	3
415	308	1	1,106	1
416	51	<1	373	<1
417	174	<1	2,222	2
418	1,302	3	4,702	3
419	41	<1	296	<1
420	509	1	1,742	1
421	371	1	1,044	1
422	461	1	24,427	18
423	25	<1	483	<1
424	31	<1	432	<1
425	11	<1	124	<1
426	1	<1	20	<1
427	0	0	85	<1
428	0	0	0	0
429	0	0	0	0
430	2	<1	234	<1
431	0	0	0	0
432	0	0	30	0
433	0	0	0	0
434	0	0	0	0
435	0	0	257	<1
436	0	0	0	0
437	0	0	0	0

Table 6.5.2.5-1[a]. Bedrock Cell Counts for the UZ Grid and Infiltration Model Domain (Continued)

Bedrock IHU	UZ Domain Total Cells	Percent (UZ Domain)	Infiltration Domain Total Cells	Percent (Infiltration Domain)
438	0	0	0	0
490	0	0	4,513	3
491	0	0	179	<1
Total cells	**44,232**		**139,092**	

Source: These values were obtained using database applications with data from Output DTNs: SN0606T0502206.011 (bedrock IHU for each cell) and UZ boundary from SN0711FTPRNUZB.003.

6.5.2.6[a]. Bedrock Saturated Conductivity

No change.

6.5.3[a]. Vegetation Parameters

No change.

6.5.3.1[a]. Potential Vegetation for Monsoon and Glacial Transition Climates

To develop distributions for plant height and rooting depth for Monsoon and Glacial Transition climates it was necessary to consider what taxa might reasonably be expected to occur at Yucca Mountain. The species composition of future vegetation communities at Yucca Mountain is a complex issue. It is recognized that multiple possibilities for vegetation assemblages exist and outcomes are dependent on several factors including climate, disturbance, and species-specific ability to adapt or migrate. The potential for certain plant taxa to occur was evaluated by considering several factors including predicted future-climate rainfall and temperature patterns, natural vegetation associated with the climate at analogue meteorological station locations, historical vegetation change in response to climate change, species tolerance ranges and requirements, and current species composition of plant communities at Yucca Mountain. It is important to note that edaphic factors and topography at Yucca Mountain differ from those of natural vegetation stands associated with analogue meteorological station locations. Therefore, species were not selected as potential components of future vegetation simply on the basis that they are likely to occur in natural vegetation stands associated with the analogue meteorological stations.

6.5.3.1.1[a]. Monsoon Climate and Vegetation at Analogue Sites

The Monsoon climate state is predicted to last around 900 to 1,400 years, with temperature and precipitation patterns in the lower bound similar to current conditions at Yucca Mountain (BSC 2004 [DIRS 170002], pp. 6-44 to 6-45, Table 6-1). Temperature and precipitation patterns during the upper bound Monsoon climate are predicted to be similar to those in Hobbs, New Mexico, and Nogales, Arizona (BSC 2004 [DIRS 170002], pp. 6-44 to 6-45, Table 6-1). The main difference between the Present-Day climate and upper-bound Monsoon climate that would affect species composition of plant communities at Yucca Mountain is a substantial increase in summer precipitation. Average monthly minimum and maximum air temperatures

are predicted to be slightly lower for the upper-bound Monsoon climate state compared to the Present-Day climate (Table 6.5.3.1-1[a]).

Table 6.5.3.1-1[a]. Monthly Temperature and Precipitation for Upper-Bound Monsoon (Nogales, Arizona, and Hobbs, New Mexico) and Present-Day (Desert Rock) Climates

	Nogales, Arizona[a] (1971 to 2000)				Hobbs, New Mexico[b] (1914 to 2001)				Desert Rock, Nevada[b,c] (1984 to 2000)			
	Temperature[d] (°C)			Pcp[e] (mm)	Temperature[d] (°C)			Pcp[e] (mm)	Temperature[d] (°C)			Pcp[e] (mm)
Month	Mean	Max	Min		Mean[f]	Max	Min		Mean	Max	Min	
Jan.	7.5	17.7	−2.7	33.3	—	13.6	−2.3	11.4	6.6	12.7	0.4	23.6
Feb.	9.2	19.5	−1.2	27.7	—	16.6	0.0	11.2	9.1	15.5	2.7	22.1
March	11.5	21.8	1.1	25.4	—	20.5	2.9	13.0	12.1	19.1	5.1	15.0
April	14.7	25.7	3.6	12.4	—	25.3	7.8	20.3	16.3	23.8	8.7	8.9
May	18.7	30.1	7.3	8.1	—	29.7	12.9	52.8	20.8	28.5	13.2	7.1
June	23.9	35.4	12.4	13.7	—	33.7	17.4	48.0	25.9	34.1	17.8	1.8
July	26.1	34. 6	17.5	108.5	—	34.3	19.2	53.8	29.0	36.8	21.2	18.3
August	25.3	33.4	17.2	107.7	—	33.3	18.6	60.7	28.4	36.1	20.8	16.0
Sept.	22.8	32.3	13.2	42.7	—	29.9	15.2	66.8	23.9	31.8	16.1	8.4
Oct.	17.1	27.8	6.4	46.7	—	25.1	9.1	39.9	17.9	25.6	10.2	9.1
Nov.	11.2	22.0	0.3	19.8	—	18.4	2.6	14.7	10.1	16.9	3.2	11.2
Dec.	7.8	18.1	−2.4	37.3	—	14.4	−1.4	14.2	6.2	12.7	−0.2	14.2

[a] Western Regional Climate Center 2003 [DIRS 162307].
[b] Western Regional Climate Center 2002 [DIRS 165987].
[c] Desert Rock, located in Mercury, Nevada, is used here to represent climate at Yucca Mountain.
[d] Temperature was converted from °F to °C (°C = [°F−32]/1.8).
[e] Precipitation was converted from inches to millimeters (mm = inches * 25.4).
[f] Mean temperature was not available for Hobbs, New Mexico.

Using the monthly climate summaries for Nogales and Hobbs (Table 6.5.3.1-1[a]), approximately 66% to 80% of total annual precipitation (average = 460 mm) falls between May and October when average monthly maximum temperatures range from 25°C to 34°C. Average minimum winter temperatures (November to February) range from −2.3°C to 2.8°C. These climate conditions support both high Sonoran (Nogales) and northern Chihuahuan (Hobbs) desert vegetation.

Much of the Sonoran Desert is subtropical and typically supports a diverse mix of trees, shrubs, and cacti represented by the genera *Cercidium* (paloverde), *Olneya* (desert ironweed), *Prosopis* (mesquite), *Larrea* (creosotebush), *Carnegiea* (saguaro), and *Lophocereus* (senita cactus), with distinct winter and summer floras (Smith et al. 1997 [DIRS 103636], p. 23). This diversity is due to a variety of factors including a mixture of soil types in the region, virtual absence of frost, and a bimodal pattern of yearly rainfall. However, low elevation bajadas and valley floors dominated by *Larrea – Ambrosia* desert scrub are typical of northern and western regions with vegetation similar to that found at Yucca Mountain. Nogales lies near the mid-eastern boundary of the Sonoran Desert.

Much of the Chihuahuan desert region has calcareous soils derived from limestone beds. Vegetation is often dominated by grasses and frost-tolerant plants such as yuccas and agaves. Grasslands generally dominate valley basins (Smith et al. 1997 [DIRS 103636], p. 24). Upper bajadas with deep soils are often dominated by desert scrub or arborescent woodland (Smith et al. 1997 [DIRS 103636], p. 24). Important perennial grass genera in the Chihuahuan Desert include Bouteloua (grama), Erioneuron (woollygrass), Muhlenbergia (muhly), Scleropogon (burrograss), Pleuraphis (galleta grass), and Sporobolis (dropseed). Desert scrub vegetation in northern reaches of the Chihuahuan Desert is dominated by Larrea and Prosopis with Flourensia (tarbush), Ephedra (jointfir), and Yucca as codominants. Hobbs, New Mexico, is near the northeastern boundaries of the Chihuahuan desert.

6.5.3.1.2[a]. Glacial Transition Climate and Historical Vegetation Change

The Glacial Transition climate state is predicted to follow the Monsoon climate and last about 8,700 years. This climate state is characterized by cool wet winters and warm dry summers, with precipitation and temperature patterns similar to those in eastern Washington (BSC 2004 [DIRS 170002], pp. 6-44 to 6-45, Table 6-1). Data from analogue climate stations at St. John, Rosalia, and Spokane, Washington, indicate that total annual precipitation at Yucca Mountain during the Glacial Transition climate state will be about 460 mm, with about 60% falling between November and March (Table 6.5.3.1-2[a]). Average minimum temperatures are below freezing during this time period. Cold desert shrub and shrub steppe vegetation typical of that found in the Great Basin extends into the eastern Washington area (Smith et al. 1997 [DIRS 103636], p. 6) where the analogue climate stations are located.

Table 6.5.3.1-2[a]. Monthly Temperature and Precipitation for the Glacial Transition Climate

	Rosalia, Washington [a] (1948 to 2000)				Spokane, Washington [a] (1889 to 2000)			
	Temperature[b] (°C)			Pcp[c] (mm)	Temperature[b] (°C)			Pcp[c] (mm)
Month	Mean	Max	Min		Mean	Max	Min	
January	−2.1	1.3	−5.6	57.4	−2.7	0.5	−5.9	50.5
February	0.8	4.7	−3.1	41.4	0.1	3.9	−3.8	39.9
March	3.8	8.8	−1.1	40.1	4.1	9.0	−0.8	35.1
April	7.7	13.9	1.5	34.5	8.6	14.6	2.5	28.2
May	11.7	18.6	4.9	39.4	12.9	19.4	6.5	35.3
June	15.2	22.4	7.9	34.8	16.7	23.4	10.1	30.7
July	18.9	27.7	10.2	16.3	21.0	28.8	13.2	14.2
August	18.9	27.8	10.1	18.0	20.3	28.1	12.5	15.7
September	14.6	22.9	6.2	21.3	15.2	22.4	8.1	20.6
October	8.6	15.7	1.6	35.1	9.1	15.1	3.1	30.0
November	2.5	6.6	−1.7	56.6	2.4	6.0	−1.2	53.3
December	−1.2	2.1	−4.6	60.5	−1.4	1.5	−4.3	55.6

[a] Western Regional Climate Center 2002 [DIRS 165987].
[b] Temperature was converted from °F to °C (°C = [°F−32]/1.8).
[c] Precipitation was converted from inches to millimeters (mm = inches * 25.4).

Paleobotanical evidence from fossilized plant material preserved in packrat (*Neotoma* spp.) middens and fossil pollen preserved in lake and cave deposits have been used to reconstruct historical climate and floral composition of the four major deserts of western North America (Smith et al. 1997 [DIRS 103636], pp. 25 to 27). Packrat middens provide the primary source of evidence for historical vegetation in the Mojave Desert. The flora of the Mojave Desert during the late Wisconsin (21,000 to 11,000 years before present (B.P.)), early Holocene (11,000 to 8,000 years B.P.), and middle Holocene (8,000 to 4,000 years B.P.) are relevant to this analysis.

During the period 23,000 to 11,000 years B.P., juniper-dominated pygmy conifer woodlands (north of 36°N latitude) existed at lower elevations that are currently occupied by desert scrub vegetation (Smith et al. 1997 [DIRS 103636], p. 26). Desert taxa persisted in these woodlands as components of under-stories and south slopes. It was estimated that these woodlands were prevalent at elevations ranging from 600 m to 1,200 m below current distributions. Currently on the Nevada Test Site, open pygmy conifer woodlands occur at elevations above 1,830 m throughout the central and northwestern mountains and mesas (Wills and Ostler 2001 [DIRS 177624], p. 35). These woodlands are dominated by *Pinus monophylla* at higher elevations and *Juniperus osteosperma* at lower elevations (e.g., northwestern part of Pahute Mesa). *Artemisia* spp. are codominants in both woodlands (Wills and Ostler 2001 [DIRS 177624], p. 35). Thus, during this period, these woodlands would have existed at elevations starting at 630 to 1,230 m on the Nevada Test Site, well within the elevations of the infiltration model domain for Yucca Mountain.

During the terminal Wisconsin and early Holocene (12,000 to 8,000 years B.P.), summer precipitation increased in most of the Sonoran and Chihuahuan deserts due to monsoonal moisture patterns (Smith et al. 1997 [DIRS 103636], p. 27). However, this moisture did not reach the Mojave and western Sonoran Deserts, which had begun conversion to desert shrublands. During this time period coniferous woodlands still dominated most of the Sonoran and Chihuahuan deserts. *Larrea - Ambrosia* desert scrub of the Mojave and western Sonoran Deserts was in place by the middle Holocene (8,000 years B.P.). Elevational and geographic changes in species distributions have occurred over the past 8,000 years in response to climatic variation, but there has been little change in general floristic composition in the Mojave since the middle Holocene (Smith et al. 1997 [DIRS 103636], p. 28).

6.5.3.1.3[a]. Potential Vegetation for Future Climate States at Yucca Mountain

No change.

6.5.3.2[a]. Maximum Rooting Depth

No change.

6.5.3.3[a]. Plant Height

No change.

6.5.3.4[a]. Method for Estimating Basal Transpiration Coefficients for the Infiltration Modeling Domain

No change.

6.5.3.5[a]. NDVI' Look-up Table and PVR Parameter Development

No change.

6.5.3.5.1[a]. Direct Inputs

Direct inputs used to develop the NDVI' look-up table and the values of PVR are:

- Landsat TM (thematic mapper) images of the infiltration model domain (DTN: SN0712ALANDSAT.002 [DIRS 184297])
- Precipitation for WYs 1990, 1991, 1993 (Output DTN: MO0607SEPTOTAL.003), 1998, 2000, and 2001 (Output DTN: MO0602SPAPRECP.000)
- Geospatial data including input to PVR, slope and azimuth of model grid cells, ESP location coordinates, etc.

Digital Ortho Quarter Quad (DOQQ)	DTN: SN0601DOQQYM98.001 [DIRS 177240]
Shuttle Radar Topography	DTN: SN0601SRTMDTED.001 [DIRS 177242]
Ground Control Points	DTN: MO0512COV05112.000 [DIRS 177249]
	DTN: MO9906GPS98410.000 [DIRS 109059]
ESP Location Coordinates	DTN: MO9901ESPYMNYE.000 [DIRS 177247]

6.5.3.5.2[a]. Development of NDVI' Look-up Table

Selected scenes from a 20-year archive of Landsat TM were chosen as the basis for characterizing large-scale Yucca Mountain vegetation patterns. Table 6.5.3.5-1[a] lists the images chosen for three representative water years (dry [2002], moderate [2001], and wet [1998]).

Table 6.5.3.5-1[a]. Landsat TM Data Used for Characterization of Yucca Mountain Vegetation

WY1998		WY2001		WY2002	
Filename	Sensor	Filename	Sensor	Filename	Sensor
t519971102	TM5	t520001009	TM5	t720011207	TM7
t519980121	TM5	t520010129	TM5	t720020124	TM7
t519980310	TM5	t520010318	TM5	t720020225	TM7
t519980411	TM5	t520010419	TM5	t720020329	TM7
t519980427	TM5	t520010505	TM5	t720020414	TM7
t519980529	TM5	t520010606	TM5	t720020430	TM7
t519980630	TM5	t520010724	TM5	t720020516	TM7
t519980716	TM5	t520011012	TM5	t720020601	TM7
t519980817	TM5	t720001220	TM7	t720020617	TM7
		t720010326	TM7	t720020719	TM7
		t720010630	TM7	t720020804	TM7
		t720010817	TM7		
		t720011004	TM7		

Source: DTN: SN0712ALANDSAT.002 [DIRS 184297].

NOTE: Filenames list satellite, year, month, and day.

Two Landsat satellites were available for the periods of interest, TM5 and TM7 (Section E2.1). The basic processing steps are summarized as follows:

1. Reflectance data from the scenes listed in Table 6.5.3.5-1[a] were used to calculate NDVI from Equation 6.5.3.4-1 for each pixel of each scene. Pixel size of TM data is approximately 28 × 28 m.

2. NDVI was then corrected for atmospheric differences between scenes and the images were geocorrected using a set of ground control points (DTN: MO0512COV05112.000 [DIRS 177249]) (Sections E2.2 and E2.3). Geocorrection ensures that pixels on each image overlie each other so that differences in pixels between scenes can be identified.

3. The NDVI values were scaled to calculate $NDVI_{offset}$, which is calculated as:

$$NDVI_{offset} = NDVI - NDVI_0 \qquad \text{(Eq. 6.5.3.5-1[a])}$$

   where NDVI is the atmospheric and geocorrected NDVI and $NDVI_0$ is the NDVI expected in areas with no vegetation (Section E2.4).

4. A positive NDVI signal arising from desert varnish that was present on many exposed rocks in the area was subtracted to get NDVI' for time steps throughout the growing season for the three water years. NDVI' represents a clean and coherent vegetation signal from the TM data To remove the effect of rock varnish, $NDVI_{offset}$ values from the lowest vegetation period of the driest year were subtracted from the other scenes (Section E2.6):

$$NDVI'_i = NDVI_{offset-i} - NDVI_{offset-min-i} \quad \text{(Eq. 6.5.3.5-2[a])}$$

where *i* refers to the i^{th} pixel and *min* refers to NDVI expression during a very dry year when vegetation response would be near zero.

The effects of slope and azimuth on NDVI' values over time for WY1998 were determined by extracting NDVI' from two subregions of pixels with either north- or south-facing slopes (Section E3.2). The NDVI' values from these subregions (Section E3.2) were fit with smooth curves and extended to other subregions of slope and azimuth by geometric interpolation (Figure 6.5.3.5-1[a]). These curves represent NDVI' values for WY1998 and are referred to as "base" NDVI'.

Base NDVI' values for each day of the water year defined for 13 unique classes of slope and azimuth were organized into a table for use as direct input to the infiltration model (Section E3, Table E-4; Output DTN: SN0606T0502206.012, *Daily_NDVI_Estimation.xls*). Each of the model grid cells was assigned a slope-azimuth class (Section E3). Based on the slope-azimuth class, the model assigns the corresponding base NDVI' for the WYDOY from Table E-4 to each grid cell.

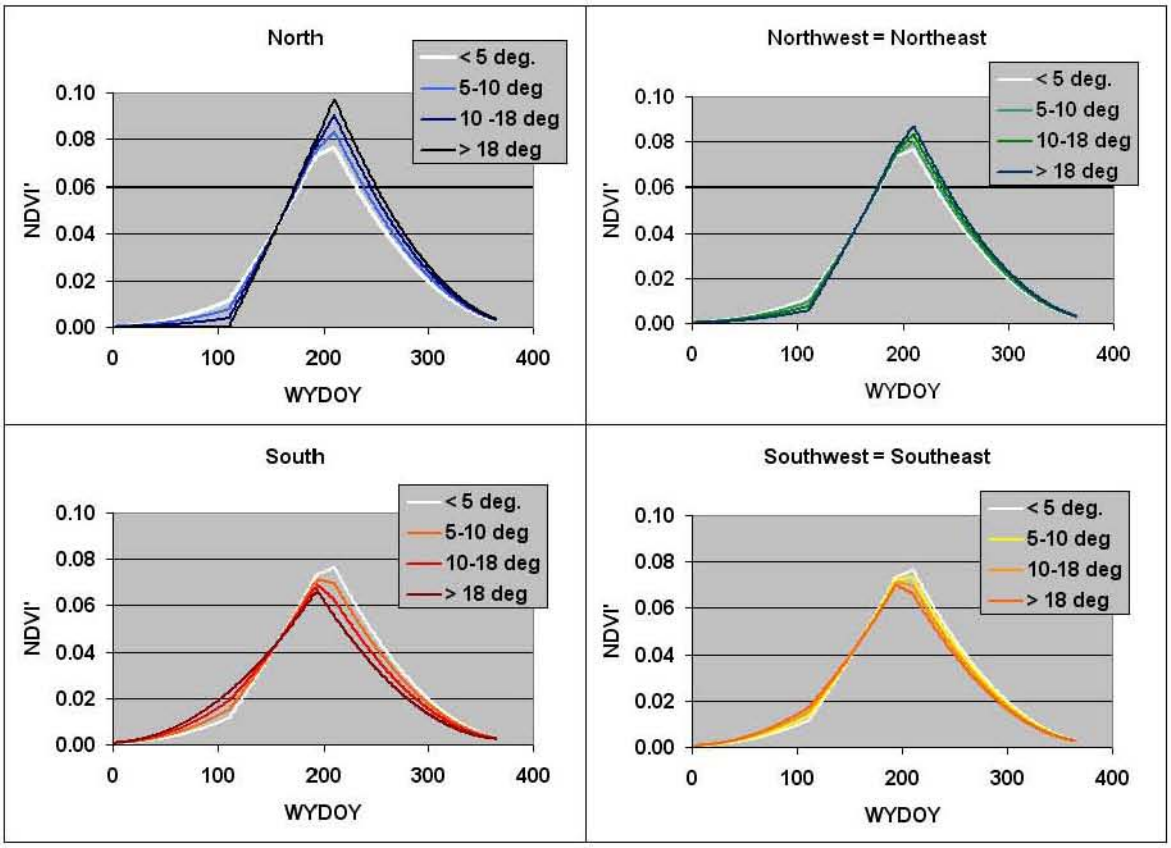

Source: Output DTN: SN0606T0502206.012, *Daily_NDVI_Estimation.xls*.

NOTE: There are 13 unique combinations of curves. The curve representing level ground (<5°) and E and W slopes is reproduced (white) in each graph.

Figure 6.5.3.5-1[a]. Temporal Curves Developed by the Weighting Functions in Table E-4

6.5.3.5.3[a]. Development of the Potential Vegetation Response for Each Grid Cell in the Model Domain

No change.

6.5.3.6[a]. Determination of K_{cb} from Ground Cover Measurements Made at Ecological Study Plots

No change.

6.5.3.7[a]. Correlating K_{cb} Profiles with NDVI'

No change.

6.5.4[a]. Additional Parameter Development

No change.

6.5.5[a]. Parameter Uncertainty Screening

No change.

6.5.6[a]. Calculation Procedure

No change.

6.5.7[a]. Results of Net Infiltration Calculations

The results of the net infiltration calculation performed for the 125 km^2 infiltration modeling domain around Yucca Mountain are presented in this section. The calculations described in this section are included in Output DTN: SN0701T0502206.037. *UZ Flow Models and Submodels* (SNL 2007 [DIRS 175177]) and *Calibrated Unsaturated Zone Properties* (SNL 2007 [DIRS 179545]) use preliminary sets of results that were generated during the preparation of initial drafts of this report and are slightly different than the qualified output DTNs described in this section. These preliminary output DTNs are discussed in Appendix L. The output DTNs with net infiltration results for each climate that are considered qualified in this report include Output DTNs: SN0701T0502206.034 (Present-Day), SN0701T0502206.036 (Monsoon), and SN0701T0502206.035 (Glacial Transition).

As discussed in Sections 6.5.5 and 6.5.6, for each climate, two Latin Hypercube Sampling (LHS) replicates of 20 realizations each were run to estimate the uncertainty and stability of model results. The differences between the two replicates for each climate are an indication of the additional uncertainty caused by the small sample size of 20 realizations. The results of both replicates are combined for the main uncertainty analysis.

Sections 6.5.7.1[a] to 6.5.7.3[a] present an overview of precipitation and net infiltration results for each of the future climates considered (Present-Day, Monsoon, and Glacial Transition). These results include: (1) presentation of the precipitation variability between realizations,

(2) comparisons of average values of net infiltration over various domains, and (3) a presentation of net infiltration maps representing the 10th, 30th, 50th, and 90th percentiles. Section 6.5.7.4 compares the magnitudes of the various water balance components for each climate and for runs made with an alternative set of initial soil moisture content initial conditions. Section 6.5.7.5 discusses factors that influence the temporal variability in net infiltration. Section 6.5.7.6 discusses factors that influence the spatial variability in net infiltration during the Present-Day climate. Section 6.5.7.7[a] illustrates daily conditions in a single grid cell in Pagany Wash to demonstrate some of the key features of the model. Section 6.5.7.8[a] summarizes the results of the uncertainty analysis.

Plots of daily precipitation and temperature used for each realization can be found in Output DTN: SN0701T0502206.037 in the individual Mathcad files in which the realizations are run.

6.5.7.1[a]. Present-Day Simulation Results

6.5.7.1.1[a]. Present-Day Precipitation Results

The mean annual precipitation (MAP) (averaged over all grid cells) used for the 40 realizations representing Present-Day climate is summarized in Figure 6.5.7.1-1[a] and Table 6.5.7.1-1[a]. The parameters used to represent Present-Day climate are described in Section 6.5.1 and Appendix F.

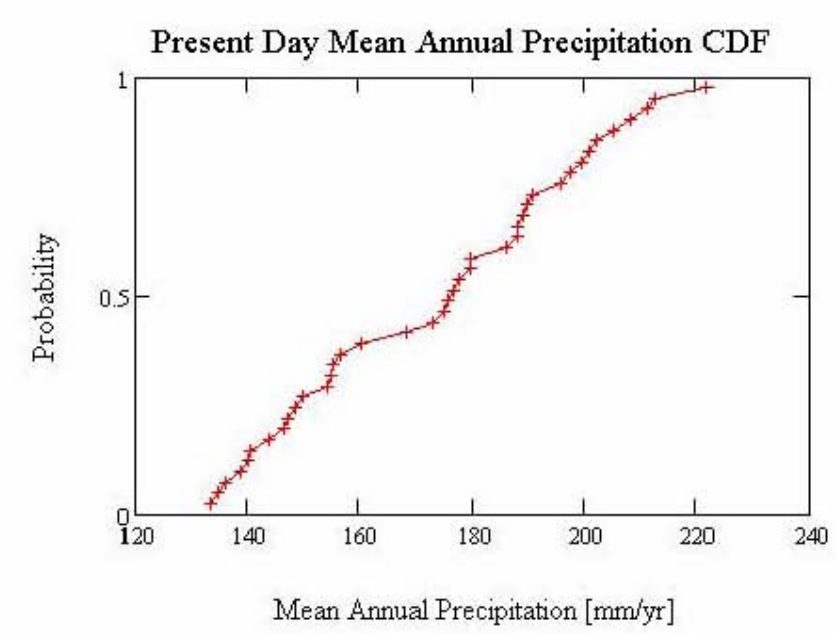

Source: Output DTN: SN0701T0502206.037, file: \Welcome to Massif\Massif\Present Day Uncertainty\Post Processing*PD_Combined_Replicates.xmcd*.

NOTE: A total of 40 realizations (2 LHS replicates) defin e the distribution. MAP values represent the spatially averaged precipitation over the entire domain. These values represent precipitation at the spatially averaged elevation (1,328 meters above seal level).

Figure 6.5.7.1-1[a]. Present-Day Mean Annual Precipitation CDF

Table 6.5.7.1-1[a]. Mean Annual Precipitation Statistics for the 40 Realizations Used to Represent Present-Day Climate for Net Infiltration Calculations

Present-Day Precipitation	R1 (mm/yr)	R2 (mm/yr)	R1 and R2 (mm/yr)
Minimum (mm/yr)	134.9	133.6	133.6
Mean (mm/yr)	173.4	173.7	173.6
Median (mm/yr)	176.3	176.4	176.3
Maximum (mm/yr)	222.0	212.7	222.0
Standard Deviation (mm/yr)	26.2	25.3	25.4

Source: Output DTN: SN0701T0502206.037, file: \Welcome to Massif\Massif\Present Day Uncertainty\Post Processing*PD_Combined_Replicates.xmcd*.

6.5.7.1.2[a]. Present-Day Net Infiltration Uncertainty Analysis Results

As described in Sections 6.5.5 and 6.5.6, two replicates (R1 and R2) of 20 realizations each were run for Present-Day climate mean annual net infiltration estimation. Table 6.5.7.1-2[a] compares mean annual net infiltration statistics for these realizations. Table 6.5.7.1-3[a] identifies the maps that represent the 10th, 30th, 50th, and 90th percentiles of mean annual net infiltration over the entire model domain. Figures 6.5.7.1-2[a] to 6.5.7.1-5[a] show maps of mean annual net infiltration for these four maps. Figure 6.5.7.1-6[a] presents a CDF of spatially averaged mean annual net infiltration over the full modeling domain for the Present-Day climate results.

Table 6.5.7.1-2[a]. Spatially Averaged Mean Annual Net Infiltration [mm/yr] Statistics for Present-Day Simulations

Present-Day Climate	Domain	R1 (mm/yr)	R2 (mm/yr)	R1 and R2 (mm/yr)
Minimum [mm/yr]	Infiltration modeling domain (125 km^2)	2.0	3.1	2.0
	UZ modeling domain (39.8 km^2)	1.4	2.1	1.4
	Repository footprint (5.7 km^2)[a]	1.5	1.9	1.5
Mean [mm/yr]	Infiltration modeling domain (125 km^2)	13.4	15.2	14.3
	UZ modeling domain (39.8 km^2)	14.0	15.7	14.9
	Repository footprint (5.7 km^2) [a]	16.7	18.6	17.6
Median [mm/yr]	Infiltration modeling domain (125 km^2)	11.4	13.7	12.9
	UZ modeling domain (39.8 km^2)	12.0	12.7	12.3
	Repository footprint (5.7 km^2) [a]	14.9	14.0	14.5
Maximum [mm/yr]	Infiltration modeling domain (125 km^2)	28.8	35.4	35.4
	UZ modeling domain (39.8 km^2)	32.2	40.3	40.3
	Repository footprint (5.7 km^2) [a]	38.6	48.2	48.2
Standard Deviation [mm/yr]	Infiltration modeling domain (125 km^2)	8.3	9.5	8.8
	UZ modeling domain (39.8 km^2)	9.5	11.2	10.3
	Repository footprint (5.7 km^2) [a]	11.5	13.6	12.5

Source: Output DTN: SN0701T0502206.037, file: \Welcome to Massif\Massif\Present Day Uncertainty\Post Processing*PD_Combined_Replicates.xmcd*.

[a] 2002 repository footprint used (DTN: LB0208HYDSTRAT.001 [DIRS 174491]).

Table 6.5.7.1-3[a]. Realizations Identified for Selected Percentiles of Present-Day Spatially Averaged Mean Annual Net Infiltration

Percentile	Replicate	Realization	Net Infiltration (mm/yr)	Mean Annual Precipitation (mm/yr)
10th	R2	10	3.9	144.1
30th	R2	2	7.3	160.6
50th	R2	8	13.0	189.3
90th	R2	14	26.7	212.7

Source: Output DTN: SN0701T0502206.037, file: \Welcome to Massif\Massif\Present Day Uncertainty\Post Processing*PD_Combined_Replicates.xmcd*.

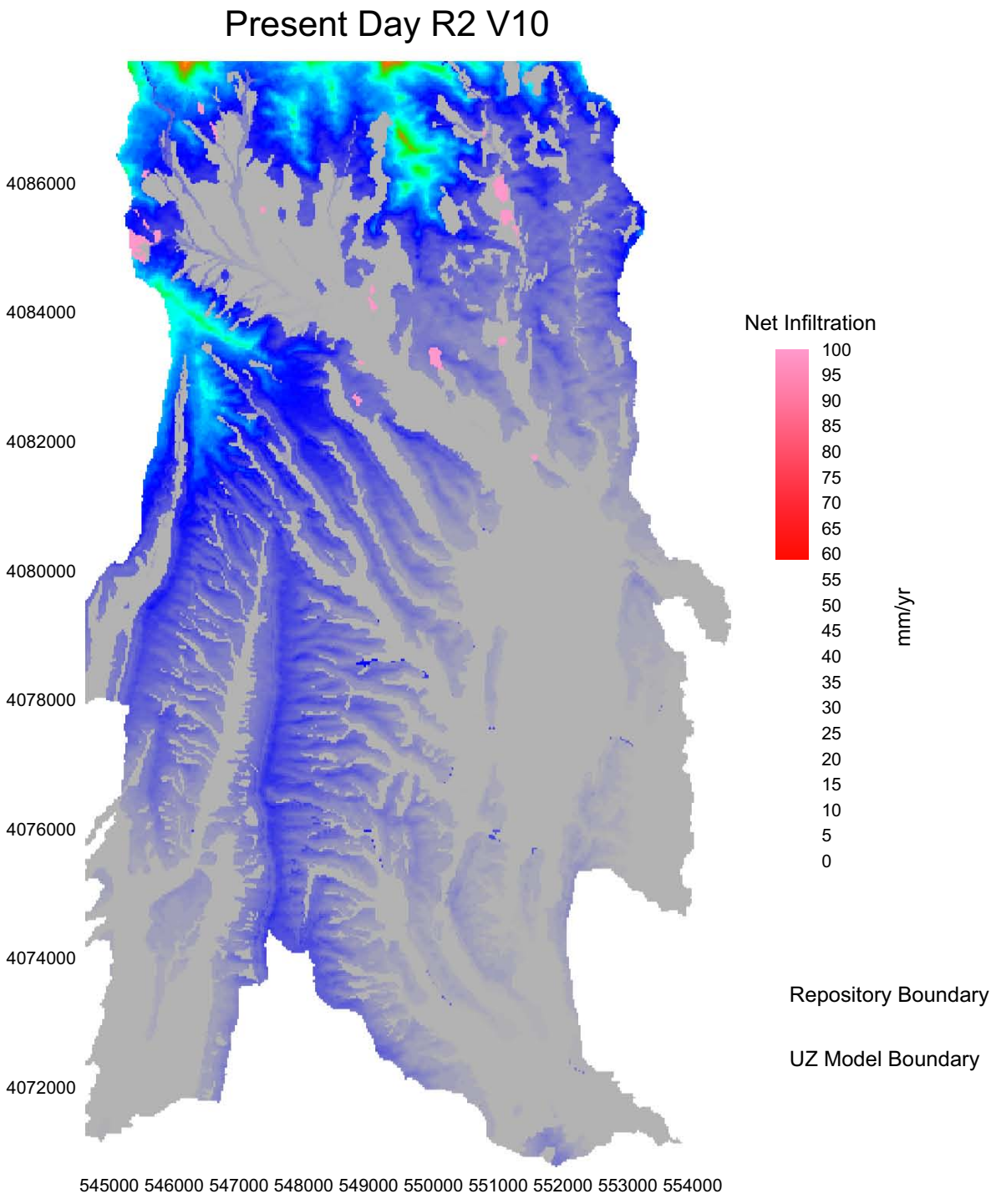

Coordinates are in meters; UTM NAD 27, Zone 11

Source: Output DTNs: SN0701T0502206.034 (Mean Annual Net Infiltration Results); SN0711FTPRNUZB.003 (UZ Model and Repository Boundaries).

NOTE: Repository footprint shown for illustrative purposes only.

Figure 6.5.7.1-2[a]. Present-Day, 10th Percentile Mean Annual Net Infiltration Map (Replicate R2, Realization 10)

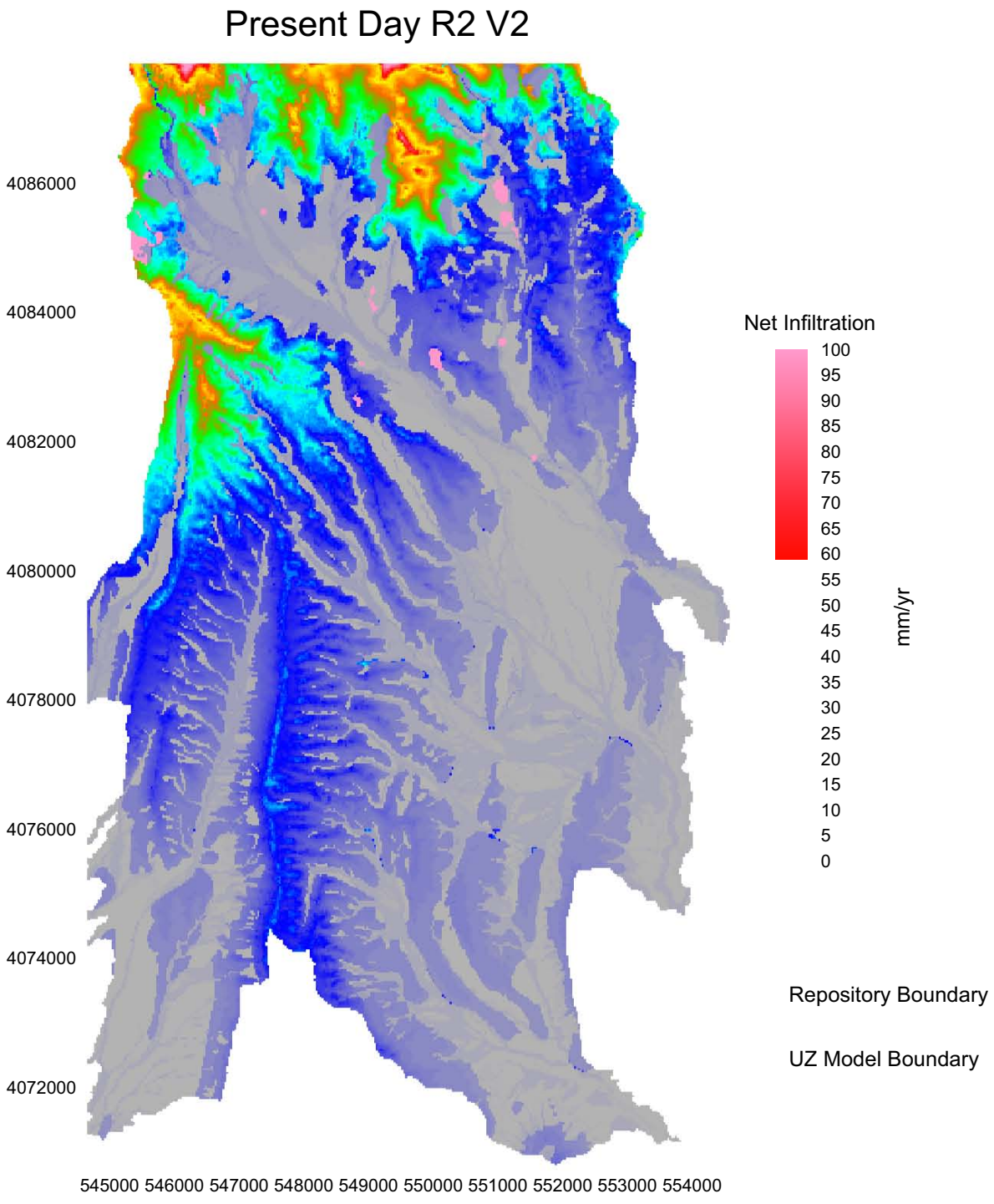

Coordinates are in meters; UTM NAD 27, Zone 11

Source: Output DTNs: SN0701T0502206.034 (Mean Annual Net Infiltration Results); SN0711FTPRNUZB.003 (UZ Model and Repository Boundaries).

NOTE: Repository footprint shown for illustrative purposes only.

Figure 6.5.7.1-3[a]. Present-Day, 30th Percentile Mean Annual Net Infiltration Map (Replicate R2, Realization 2)

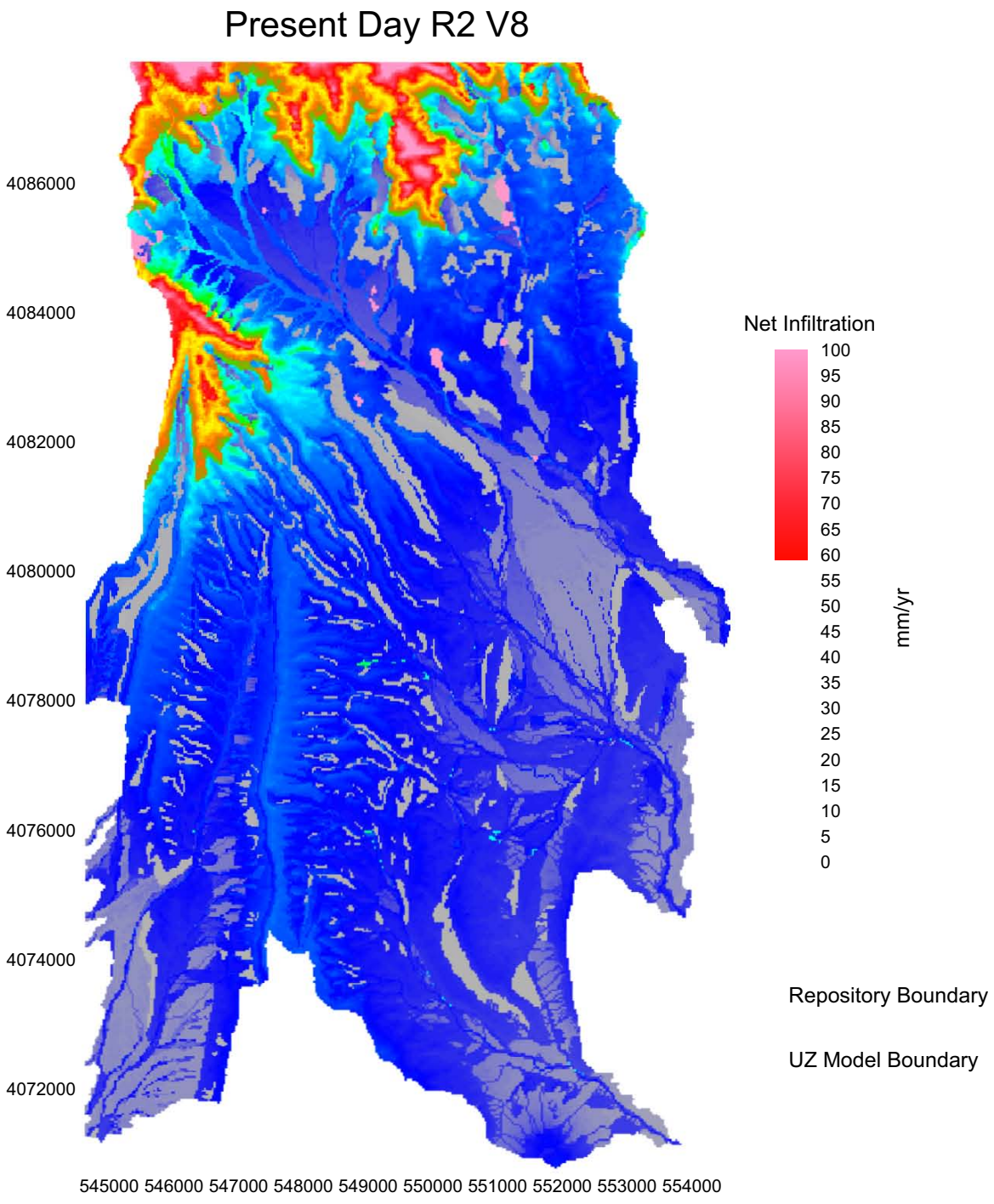

Coordinates are in meters; UTM NAD 27, Zone 11

Source: Output DTNs: SN0701T0502206.034 (Mean Annual Net Infiltration Results); SN0711FTPRNUZB.003 (UZ Model and Repository Boundaries).

NOTE: Repository footprint shown for illustrative purposes only.

Figure 6.5.7.1-4[a]. Present-Day, 50th Percentile Mean Annual Net Infiltration Map (Replicate R2, Realization 8)

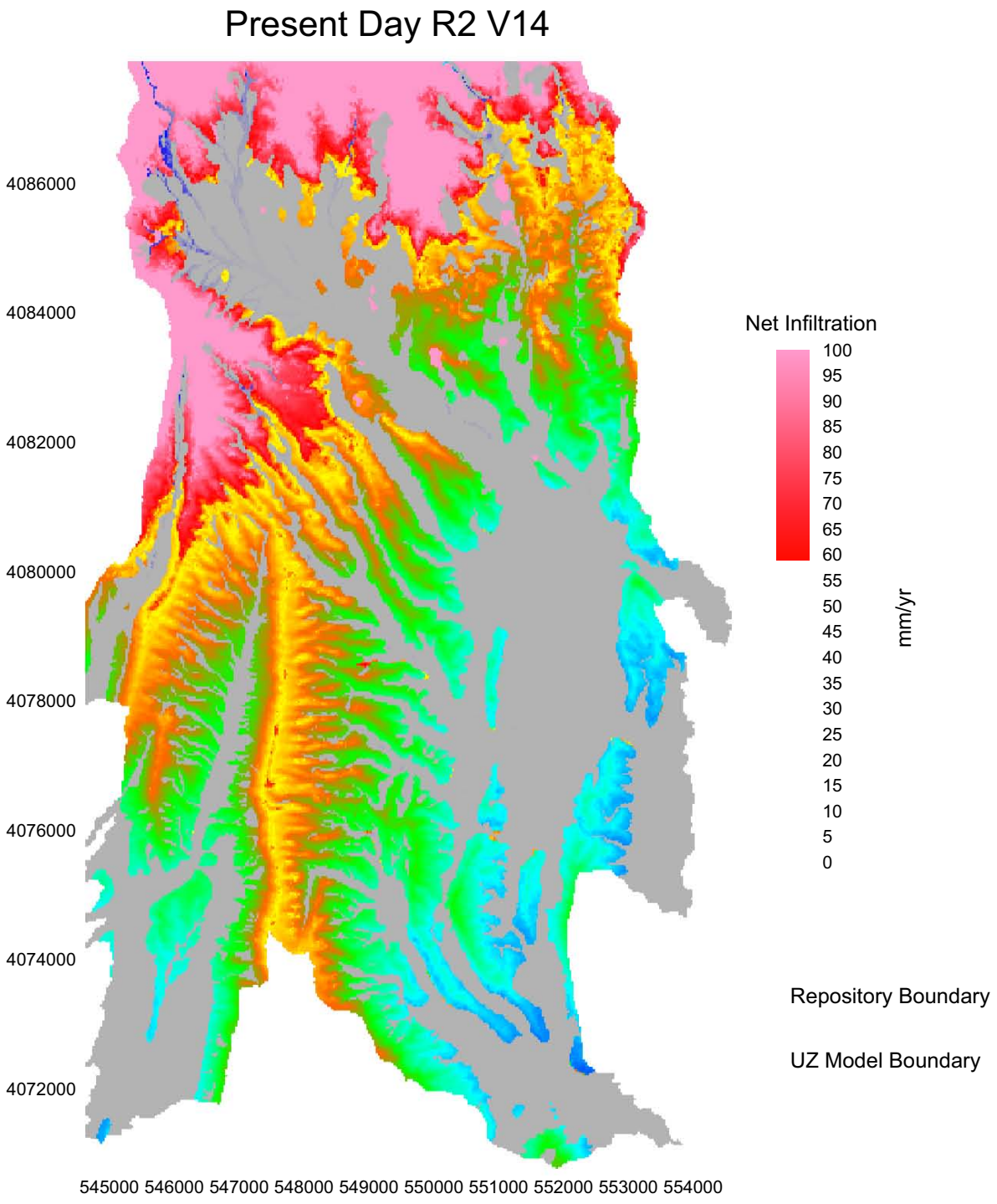

Coordinates are in meters; UTM NAD 27, Zone 11

Source: Output DTN: SN0701T0502206.034 (Mean Annual Net Infiltration Results); SN0711FTPRNUZB.003 (UZ Model and Repository Boundaries).

NOTE: Repository footprint shown for illustrative purposes only.

Figure 6.5.7.1-5[a]. Present-Day, 90th Percentile Mean Annual Net Infiltration Map (Replicate R2, Realization 14)

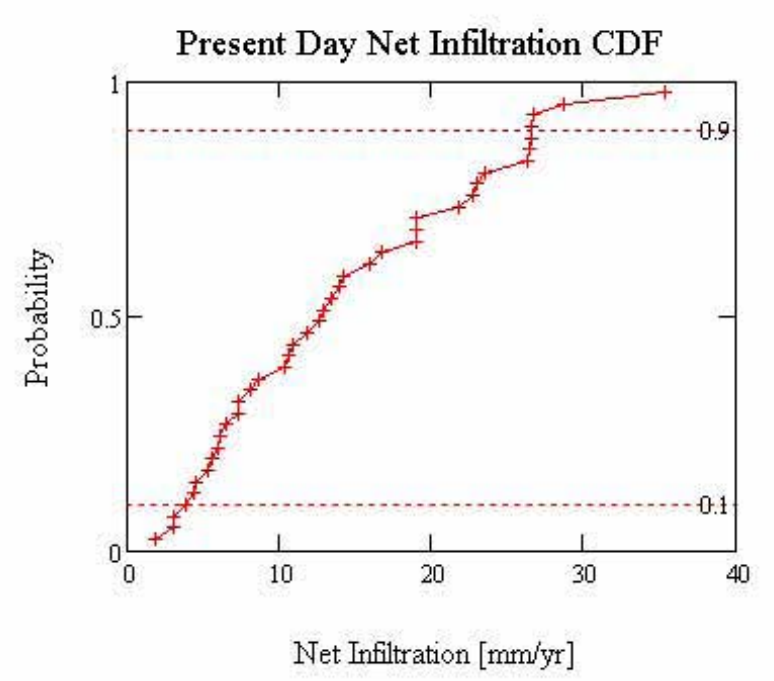

Source: Output DTN: SN0701T0502206.037, file: \Welcome to Massif\Massif\Present Day Uncertainty\Post Processing*PD_Combined_Replicates.xmcd*.

NOTE: A total of 40 realizations (2 LHS replicates) define the distribution.

Figure 6.5.7.1-6[a]. Cumulative Distribution Function (CDF) of Present-Day Spatially Averaged Mean Annual Net Infiltration over the Infiltration Domain

6.5.7.2[a]. Monsoon Simulation Results

6.5.7.2.1[a]. Monsoon Precipitation Results

The mean annual precipitation (MAP) (averaged over all grid cells) used for the 40 realizations representing Monsoon climate is summarized in Figure 6.5.7.2-1[a] and Table 6.5.7.2-1[a] below. The parameters used to represent the Monsoon climate are described in Section 6.5.1 and Appendix F.

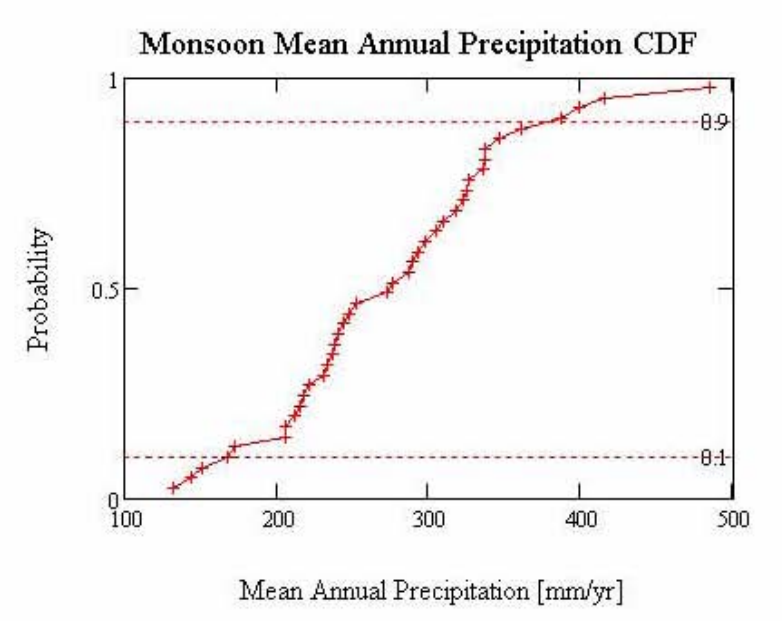

Source: Output DTN: SN0701T0502206.037, file: \Welcome to Massif\Massif\Monsoon Uncertainty\Post Processing*MO_Combined_Replicates.xmcd*.

NOTE: A total of 40 realizations (2 LHS replicates) defin e the distribution. MAP values represent the spatially averaged precipitation over the entire domain. These values represent precipitation at the spatially averaged elevation (1,328 meters above seal level).

Figure 6.5.7.2-1[a]. Monsoon Mean Annual Precipitation CDF

Table 6.5.7.2-1[a]. Mean Annual Precipitation Statistics for the 40 Realizations used to Represent Monsoon Climate for Net Infiltration Calculations

Monsoon Precipitation	R1 (mm/yr)	R2 (mm/yr)	R1 and R2 (mm/yr)
Minimum (mm/yr)	132.1	144.0	132.1
Mean (mm/yr)	272.7	277.8	275.2
Median (mm/yr)	262.7	279.8	274.8
Maximum (mm/yr)	399.7	484.7	484.7
Standard Deviation (mm/yr)	71.9	85.5	78.0

Source: Output DTN: SN0701T0502206.037, file: \Welcome to Massif\Massif\Monsoon Uncertainty\Post Processing*MO_Combined_Replicates.xmcd*.

6.5.7.2.2[a]. Monsoon Net Infiltration Uncertainty Analysis Results

As described in Sections 6.5.5 and 6.5.6, two replicates (R1 and R2) of 20 realizations each were run for the Monsoon climate net infiltration estimation. Table 6.5.7.2-2[a] compares spatially averaged mean annual net infiltration statistics for these realizations. Table 6.5.7.2-3[a] identifies the maps that represent the 10th, 30th, 50th, and 90th percentiles of spatially averaged mean annual net infiltration over the entire model domain. Figures 6.5.7.2-2[a] to 6.5.7.2-5[a] show maps of mean annual net infiltration for these four realizations. Figure 6.5.7.2-6[a] presents a CDF of spatially averaged mean annual net infiltration over the full domain for the Monsoon climate results.

Table 6.5.7.2-2[a]. Spatially Averaged Mean Annual Net Infiltration [mm/yr] Statistics for Monsoon Simulations

Monsoon Climate	Domain	R1 (mm/yr)	R2 (mm/yr)	R1 and R2 (mm/yr)
Minimum [mm/yr]	Infiltration modeling domain (125 km^2)	3.0	2.4	2.4
	UZ modeling domain (39.8 km^2)	1.9	1.2	1.2
	Repository footprint (5.7 km^2)[a]	2.0	1.2	1.2
Mean [mm/yr]	Infiltration modeling domain (125 km^2)	23.5	27.6	25.5
	UZ modeling domain (39.8 km^2)	25.4	29.8	27.6
	Repository footprint (5.7 km^2) [a]	30.5	35.3	32.9
Median [mm/yr]	Infiltration modeling domain (125 km^2)	23.3	20.4	22.8
	UZ modeling domain (39.8 km^2)	24.7	22.4	23.8
	Repository footprint (5.7 km^2) [a]	29.3	27.1	28.4
Maximum [mm/yr]	Infiltration modeling domain (125 km^2)	52.6	83.4	83.4
	UZ modeling domain (39.8 km^2)	61.3	85.4	85.4
	Repository footprint (5.7 km^2) [a]	74.5	95.3	95.3
Standard Deviation [mm/yr]	Infiltration modeling domain (125 km^2)	14.9	21.1	18.2
	UZ modeling domain (39.8 km^2)	17.1	22.8	20.0
	Repository footprint (5.7 km^2) [a]	20.4	26.2	23.3

Source: Output DTN: SN0701T0502206.037, file: \Welcome to Massif\Massif\Monsoon Uncertainty\Post Processing*MO_Combined_Replicates.xmcd*.

[a] 2002 repository footprint used (DTN: LB0208HYDSTRAT.001 [DIRS 174491]).

Table 6.5.7.2-3[a]. Realizations Identified for Selected Percentiles of Monsoon Spatially Averaged Mean Annual Net Infiltration

Percentile	Replicate	Realization	Net Infiltration [mm/yr]	Mean Annual Precipitation [mm/yr]
10th	R1	17	6.3	206.5
30th	R2	10	14.4	150.7
50th	R1	2	22.9	240.8
90th	R1	7	52.6	310.2

Source: Output DTN: SN0701T0502206.037, file: \Welcome to Massif\Massif\Monsoon Uncertainty\Post Processing*MO_Combined_Replicates.xmcd*.

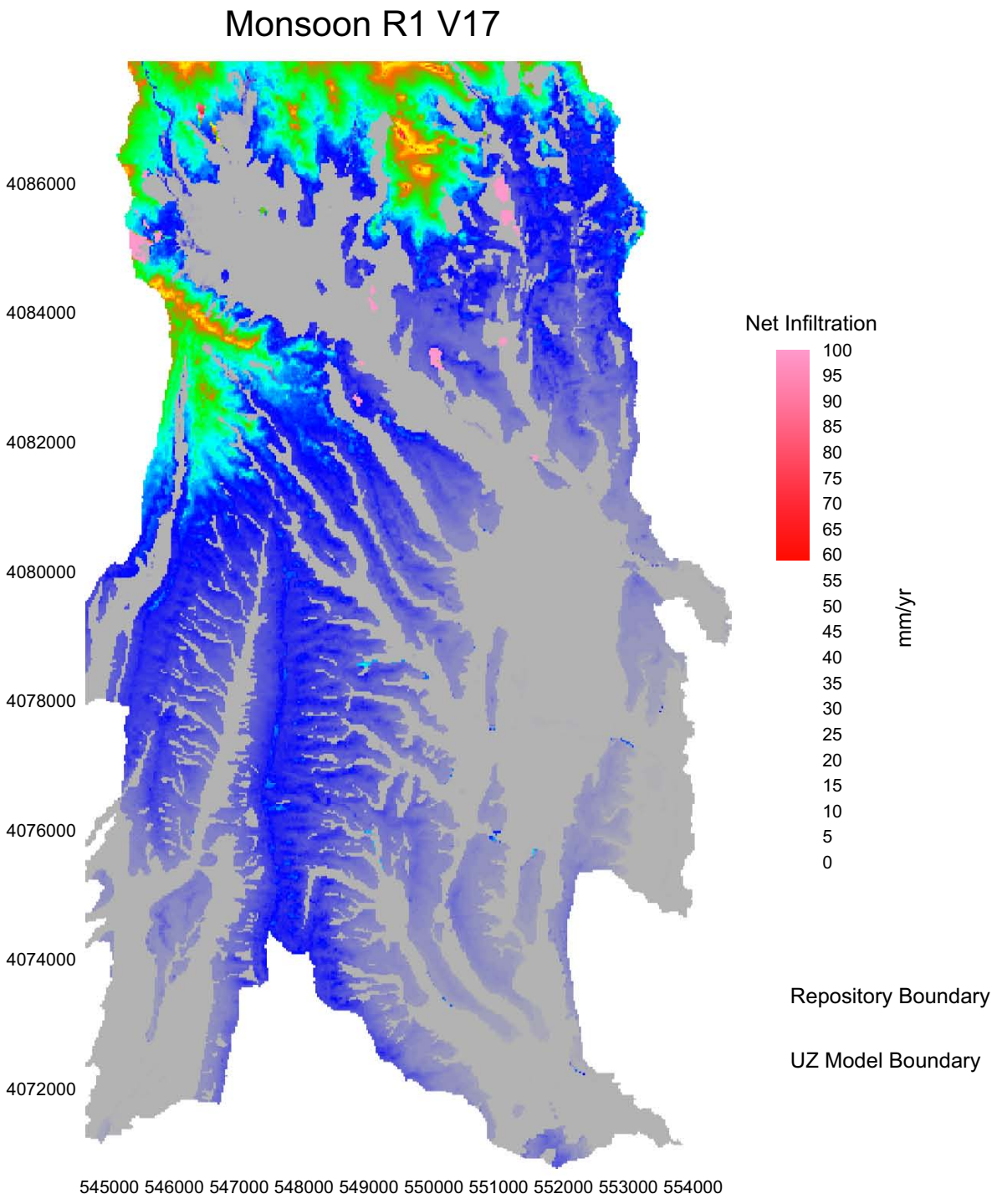

Coordinates are in meters; UTM NAD 27, Zone 11

Source: Output DTNs: SN0701T0502206.036 (Mean Annual Net Infiltration Results); SN0711FTPRNUZB.003 (UZ Model and Repository Boundaries).

NOTE: Repository footprint shown for illustrative purposes only.

Figure 6.5.7.2-2[a]. Monsoon, 10th Percentile Mean Annual Net Infiltration Map (Replicate R1, Realization 17)

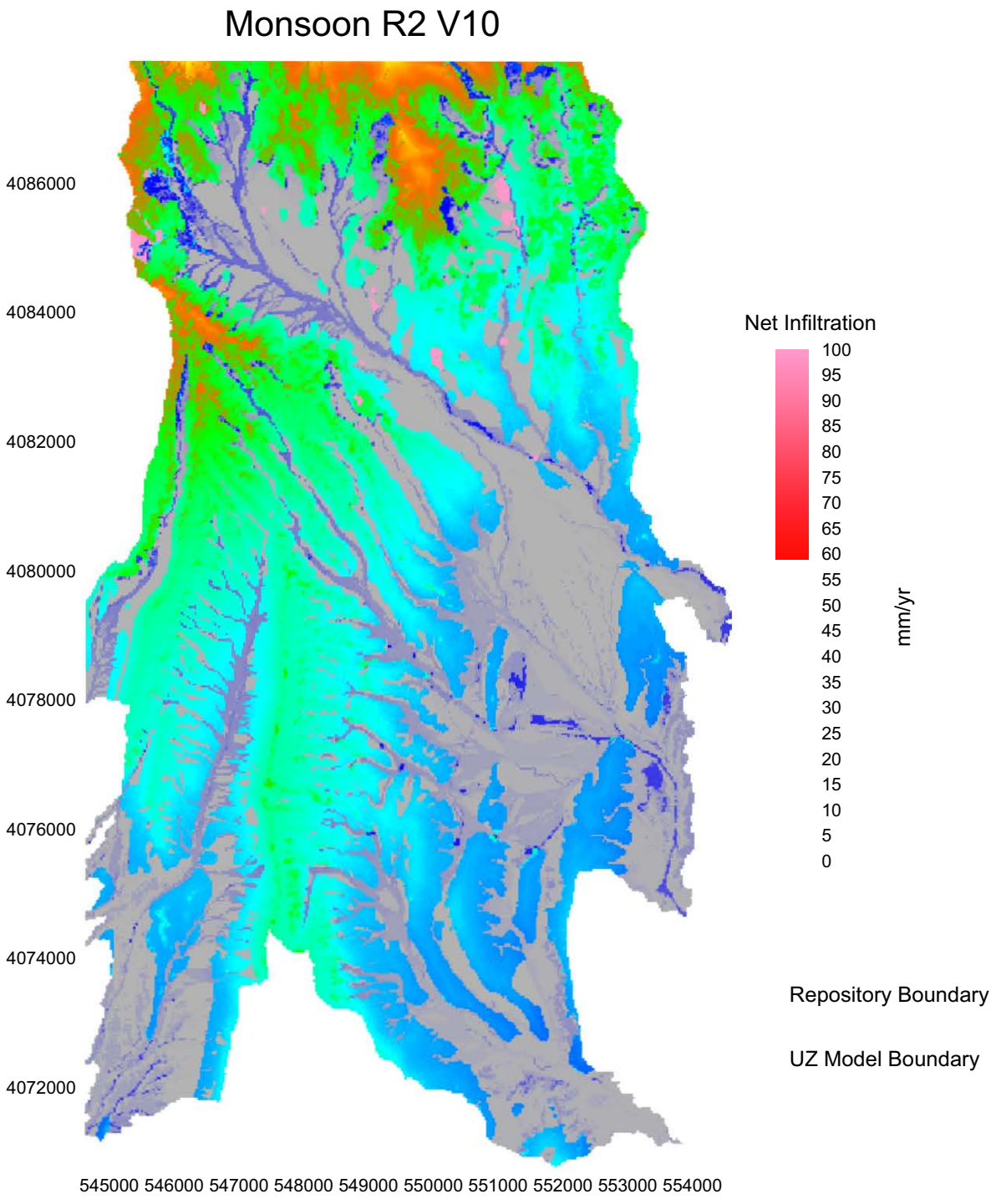

Coordinates are in meters; UTM NAD 27, Zone 11

Source: Output DTNs: SN0701T0502206.036 (Mean Annual Net Infiltration Results); SN0711FTPRNUZB.003 (UZ Model and Repository Boundaries).

NOTE: Repository footprint shown for illustrative purposes only.

Figure 6.5.7.2-3[a]. Monsoon, 30th Percentile Mean Annual Net Infiltration Map (Replicate R2, Realization 10)

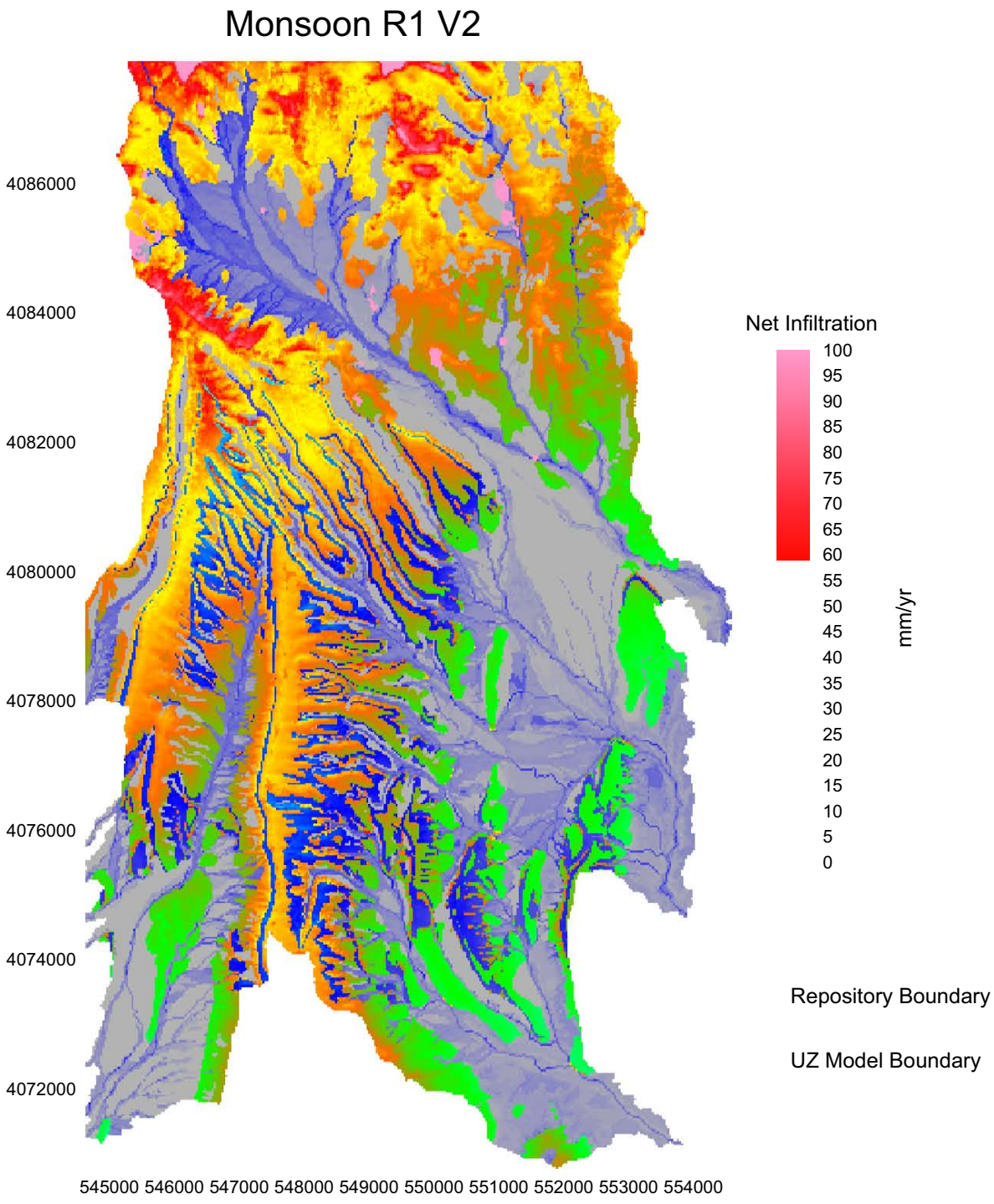

Coordinates are in meters; UTM NAD 27, Zone 11

Source: Output DTNs: SN0701T0502206.036 (Mean Annual Net Infiltration Results); and SN0711FTPRNUZB.003 (UZ Model and Repository Boundaries).

NOTE: Repository footprint shown for illustrative purposes only.

Figure 6.5.7.2-4[a]. Monsoon, 50th Percentile Net Infiltration Map (Replicate R1, Realization 2)

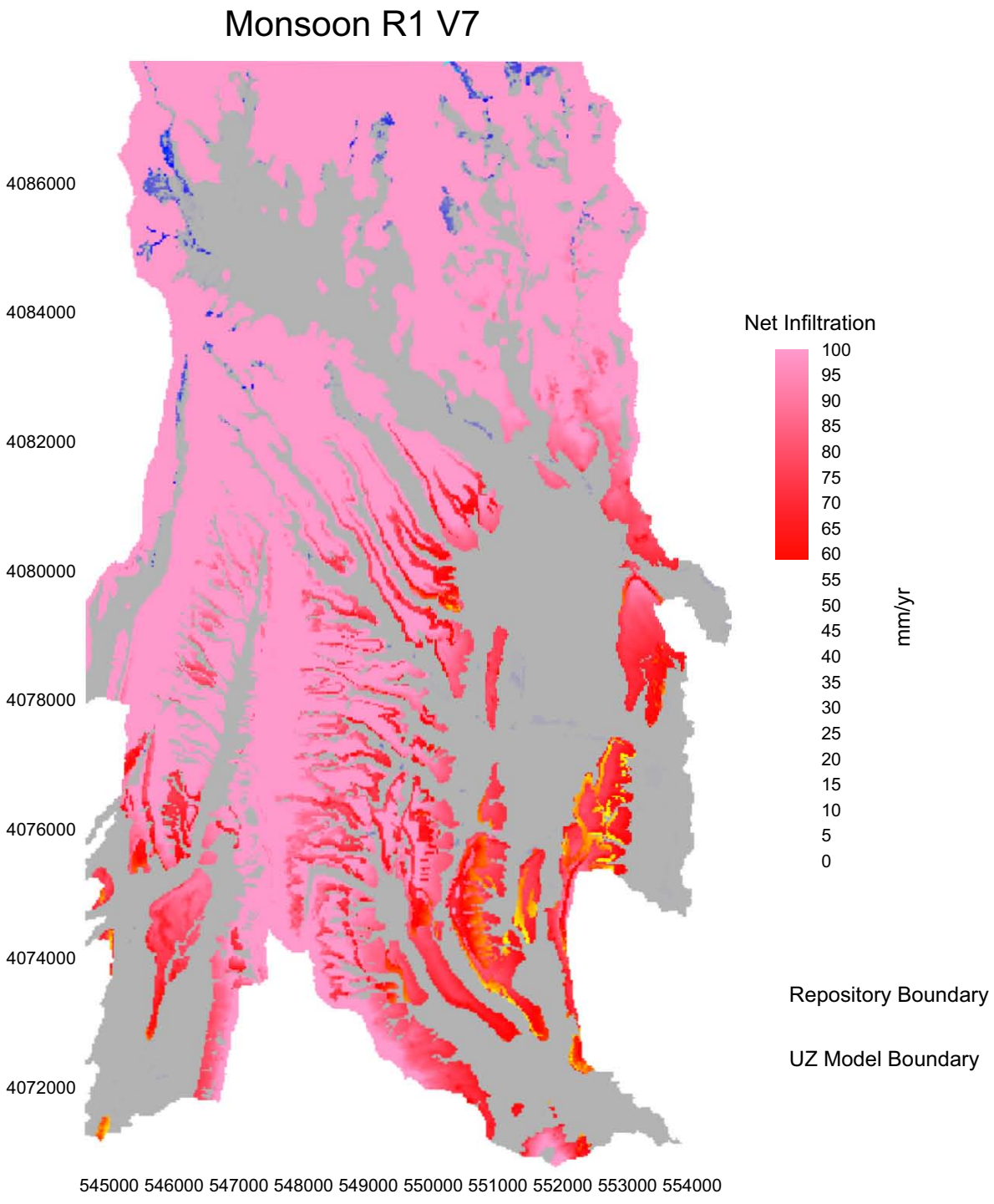

Coordinates are in meters; UTM NAD 27, Zone 11

Source: Output DTN: SN0701T0502206.036 (Mean Annual Net Infiltration Results); and SN0711FTPRNUZB.003 (UZ Model and Repository Boundaries).

NOTE: Repository footprint shown for illustrative purposes only.

Figure 6.5.7.2-5[a]. Monsoon, 90th Percentile Net Infiltration Map (Replicate R1, Realization 7)

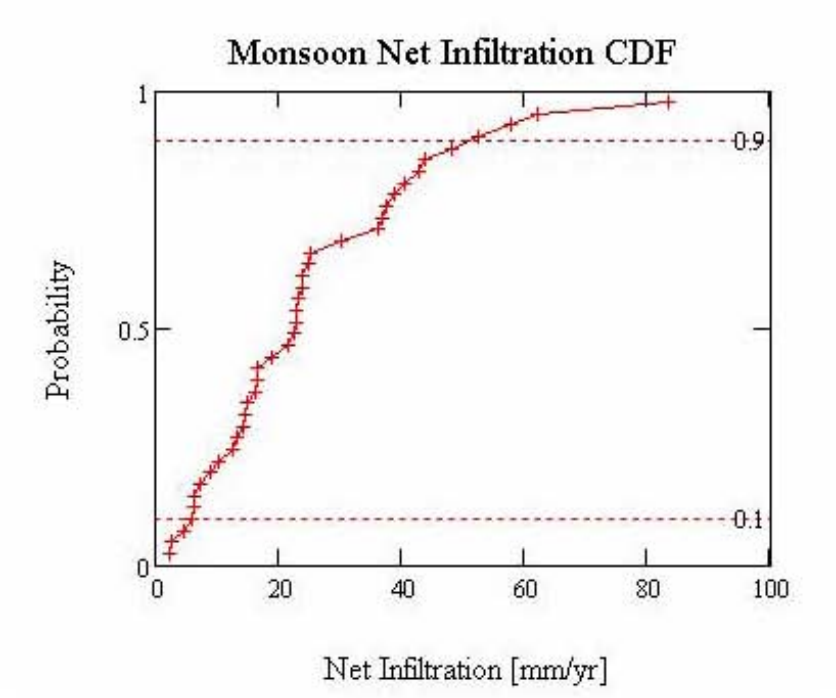

Source: Output DTN: SN0701T0502206.037, file: \Welcome to Massif\Massif\Monsoon Uncertainty\Post Processing*MO_Combined_Replicates.xmcd*.

NOTE: A total of 40 realizations (2 LHS replicates) define the distribution.

Figure 6.5.7.2-6[a]. Cumulative Distribution Function (CDF) of Monsoon Net Infiltration Averaged over the Infiltration Domain

6.5.7.3[a]. Glacial Transition Simulation Results

6.5.7.3.1[a]. Glacial Transition Precipitation Results

The mean annual precipitation (MAP) (averaged over all grid cells) used for the 40 realizations representing glacial transition climate is summarized in Figure 6.5.7.3-1[a] and Table 6.5.7.3-1[a]. The parameters used to represent glacial transition climate are described in Section 6.5.1 and Appendix F. The range of precipitation summarized in Table 6.5.7.3-1[a] is less than the range of precipitation summarized in Table 6.5.7.2-1[a] for the monsoon climate. Therefore, the monsoon climate can have greater precipitation than the glacial-transition climate.

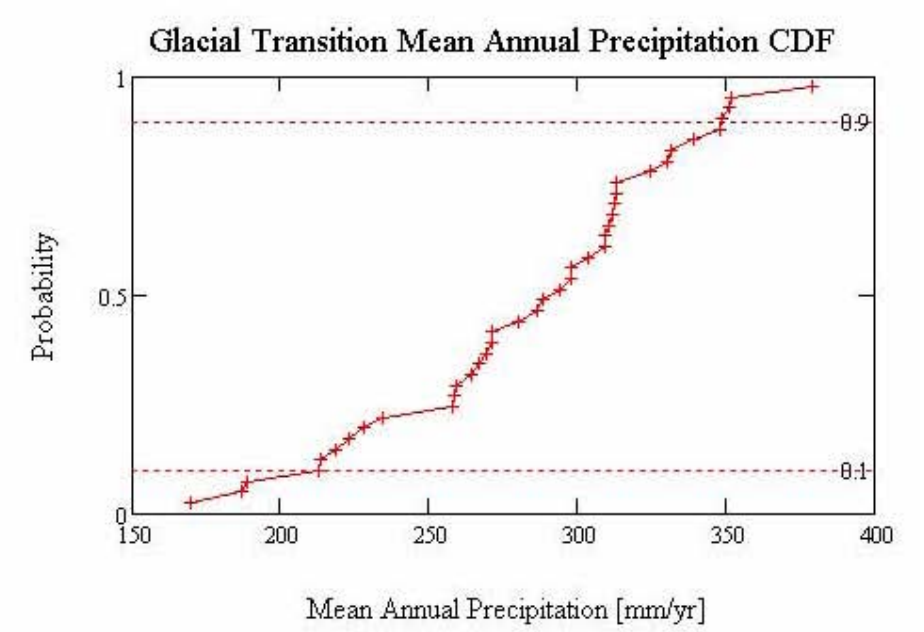

Source: Output DTN: SN0701T0502206.037, file: \Welcome to Massif\Massif\Glacial Uncertainty\Post Processing*GT_Combined_Replicates.xmcd*.

NOTE: A total of 40 realizations (2 LHS replicates) defin e the distribution. MAP values represent the spatially averaged precipitation over the entire domain. These values represent precipitation at the spatially averaged elevation (1,328 meters above seal level).

Figure 6.5.7.3-1[a]. Glacial Transition Mean Annual Precipitation CDF

Table 6.5.7.3-1[a]. Mean Annual Precipitation Statistics for the 40 Realizations Used to Represent Glacial Transition Climate for Net Infiltration Calculations

Glacial Transition Precipitation	R1 (mm/yr)	R2 (mm/yr)	R1 and R2 (mm/yr)
Minimum (mm/yr)	169.8	187.0	169.8
Mean (mm/yr)	282.2	284.6	283.4
Median (mm/yr)	296.5	290.3	291.5
Maximum (mm/yr)	351.9	379.3	379.3
Standard Deviation (mm/yr)	53.5	49.0	50.6

Source: Output DTN: SN0701T0502206.037, file: \Welcome to Massif\Massif\Glacial Uncertainty\Post Processing*MO_Combined_Replicates.xmcd*.

6.5.7.3.2[a]. Glacial Transition Infiltration Uncertainty Analysis Results

Two replicates (R1 and R2) of 20 realizations each were run for the Glacial Transition climate net infiltration estimation. Table 6.5.7.3-2[a] compares spatially averaged mean annual net infiltration statistics for these realizations. Table 6.5.7.3-3[a] identifies the maps that represent the 10th, 30th, 50th, and 90th, percentiles of spatially averaged mean annual net infiltration over the entire model domain. Figures 6.5.7.3-2[a] to 6.5.7.3-5[a] show maps of mean annual net infiltration for these percentiles. Figure 6.5.7.2-6[a] presents a CDF of spatially averaged mean annual net infiltration over the full domain for the Glacial Transition climate results.

Table 6.5.7.3-2[a]. Spatially Averaged Mean Annual Net Infiltration Statistics for Glacial Transition Simulations

Glacial Transition Climate	Domain	R1 (mm/yr)	R2 (mm/yr)	R1 and R2 (mm/yr)
Minimum [mm/yr]	Infiltration modeling domain (125 km^2)	6.6	13.2	6.6
	UZ modeling domain (39.8 km^2)	4.2	8.0	4.2
	Repository footprint (5.7 km^2)[a]	4.0	8.5	4.0
Mean [mm/yr]	Infiltration modeling domain (125 km^2)	30.8	29.2	30.0
	UZ modeling domain (39.8 km^2)	29.7	27.8	28.8
	Repository footprint (5.7 km^2) [a]	39.9	37.5	38.7
Median [mm/yr]	Infiltration modeling domain (125 km^2)	28.5	28.1	28.5
	UZ modeling domain (39.8 km^2)	28.0	25.4	27.5
	Repository footprint (5.7 km^2) [a]	38.6	35.9	38.6
Maximum [mm/yr]	Infiltration modeling domain (125 km^2)	64.7	56.2	64.7
	UZ modeling domain (39.8 km^2)	70.9	61.0	70.9
	Repository footprint (5.7 km^2) [a]	97.3	81.7	97.3
Standard Deviation [mm/yr]	Infiltration modeling domain (125 km^2)	14.3	12.1	13.1
	UZ modeling domain (39.8 km^2)	16.5	14.2	15.2
	Repository footprint (5.7 km^2) [a]	23.3	19.5	21.2

Source: Output DTN: SN0701T0502206.037, file: \Welcome to Massif\Massif\Glacial Uncertainty\Post Processing*GT_Combined_Replicates.xmcd*.

[a] 2002 repository footprint used (DTN: LB0208HYDSTRAT.001 [DIRS 174491]).

Table 6.5.7.3-3[a]. Realizations Identified for Selected Percentiles of Glacial Transition Spatially Averaged Mean Annual Net Infiltration

Percentile	Replicate	Realization	Net Infiltration (mm/yr)	Mean Annual Precipitation (mm/yr)
10th	R2	6	13.2	271.7
30th	R2	10	22.8	264.8
50th	R1	18	28.6	223.1
90th	R2	1	47.0	286.6

Source: Output DTN: SN0701T0502206.037, file: \Welcome to Massif\Massif\Glacial Uncertainty\Post Processing*GT_Combined_Replicates.xmcd*.

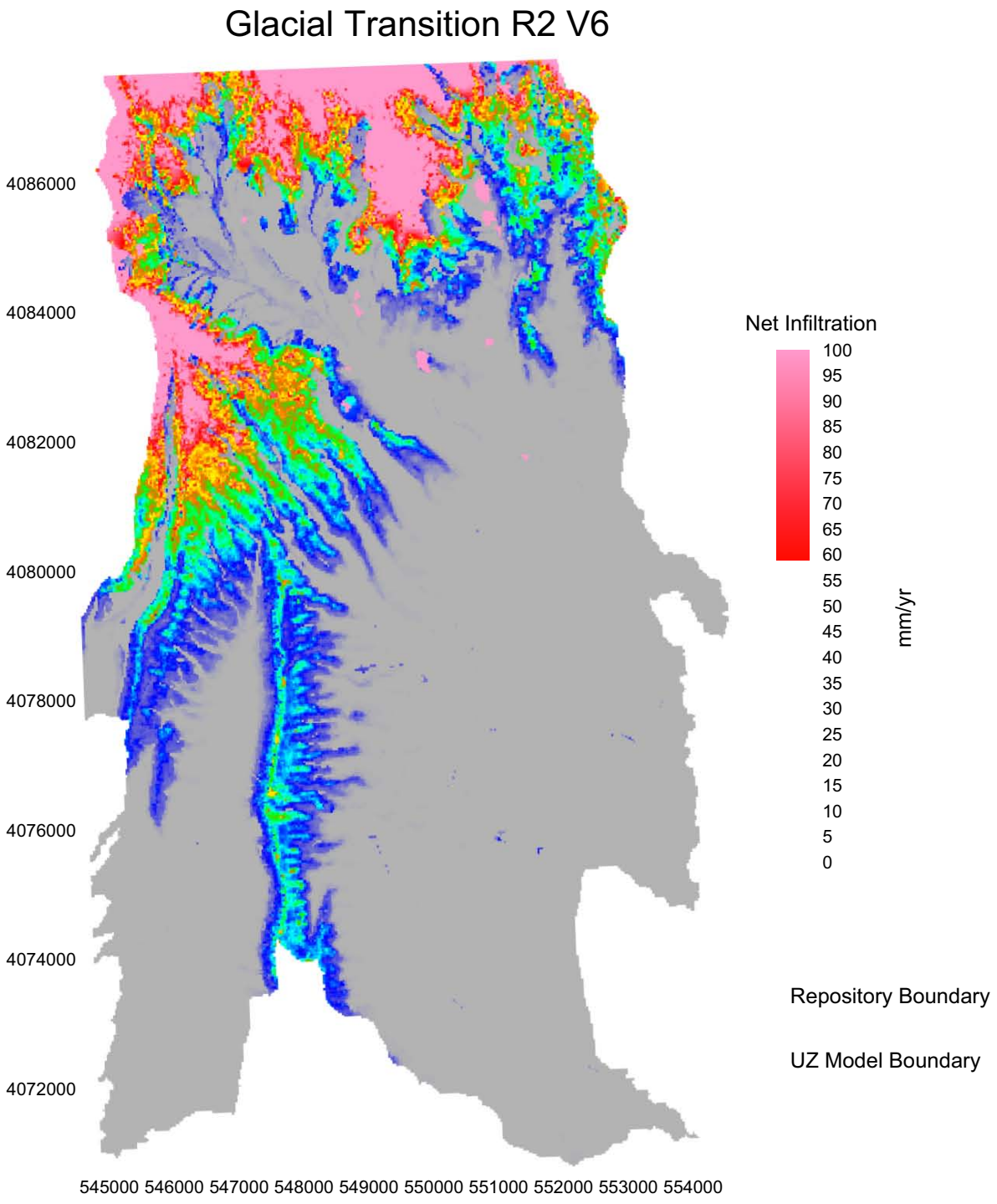

Coordinates are in meters; UTM NAD 27, Zone 11

Source: Output DTNs: SN0701T0502206.035 (Mean Annual Net Infiltration Results) and SN0711FTPRNUZB.003 UZ (Model and Repository Boundaries).

NOTE: Repository footprint shown for illustrative purposes only.

Figure 6.5.7.3-2[a]. Glacial Transition, 10th Percentile Mean Annual Net Infiltration Map (Replicate R2, Realization 6)

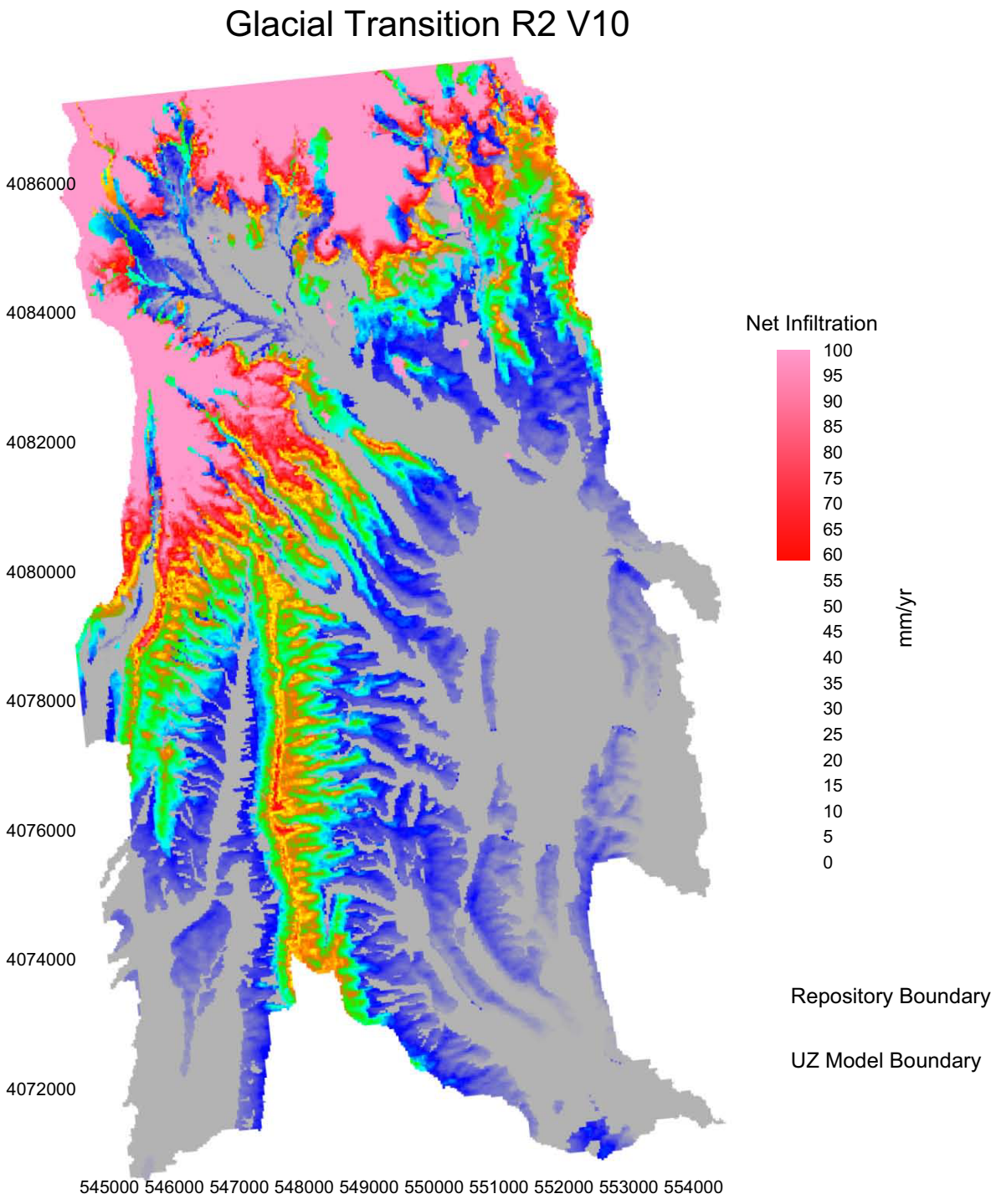

Coordinates are in meters; UTM NAD 27, Zone 11

Source: Output DTNs: SN0701T0502206.035 (Mean Annual Net Infiltration Results) and SN0711FTPRNUZB.003 UZ (Model and Repository Boundaries).

NOTE: Repository footprint shown for illustrative purposes only.

Figure 6.5.7.3-3[a]. Glacial Transition, 30th Percentile Mean Annual Net Infiltration Map (Replicate R2, Realization 10)

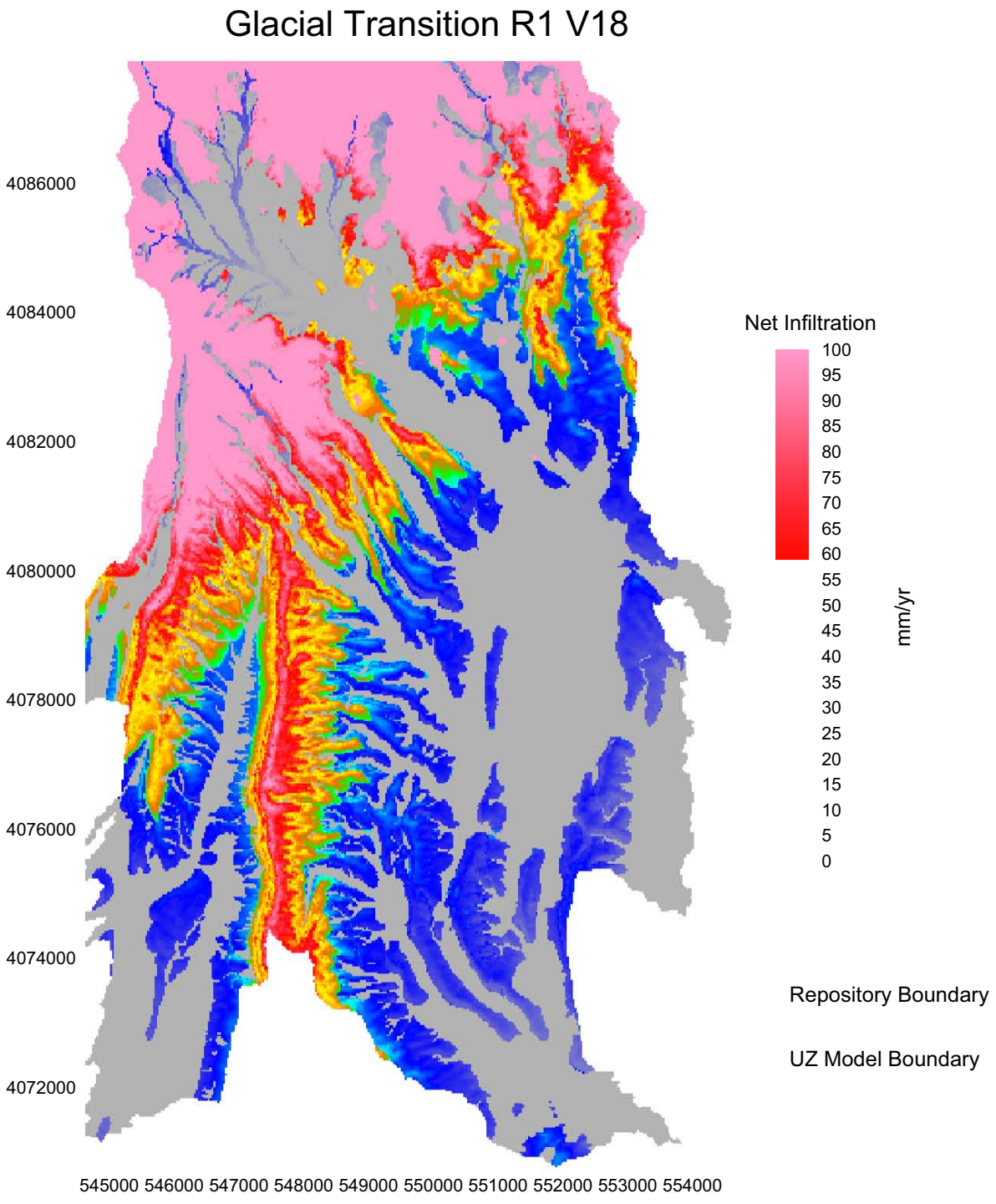

Coordinates are in meters; UTM NAD 27, Zone 11

Source: Output DTNs: SN0701T0502206.035 (Mean Annual Net Infiltration Results) and SN0711FTPRNUZB.003 UZ (Model and Repository Boundaries).

NOTE: Repository footprint shown for illustrative purposes only.

Figure 6.5.7.3-4[a]. Glacial Transition, 50th Percentile Mean Annual Net Infiltration Map (Replicate R1, Realization 18)

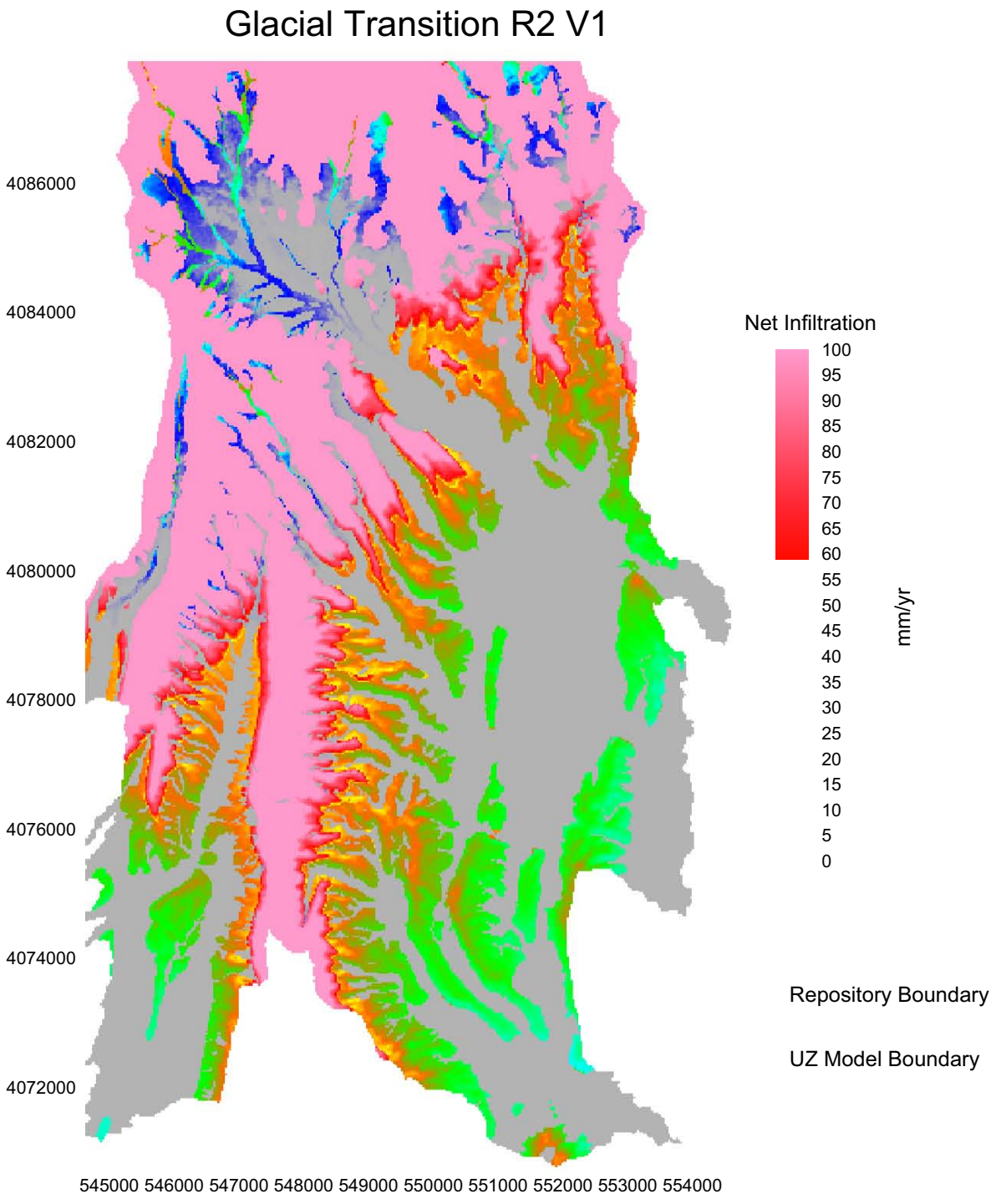

Source: Output DTNs: SN0701T0502206.035 (Mean Annual Net Infiltration Results) and SN0711FTPRNUZB.003 UZ (Model and Repository Boundaries).

NOTE: Repository footprint shown for illustrative purposes only.

Figure 6.5.7.3-5[a]. Glacial Transition, 90th Percentile Mean Annual Net Infiltration Map (Replicate R2, Realization 1)

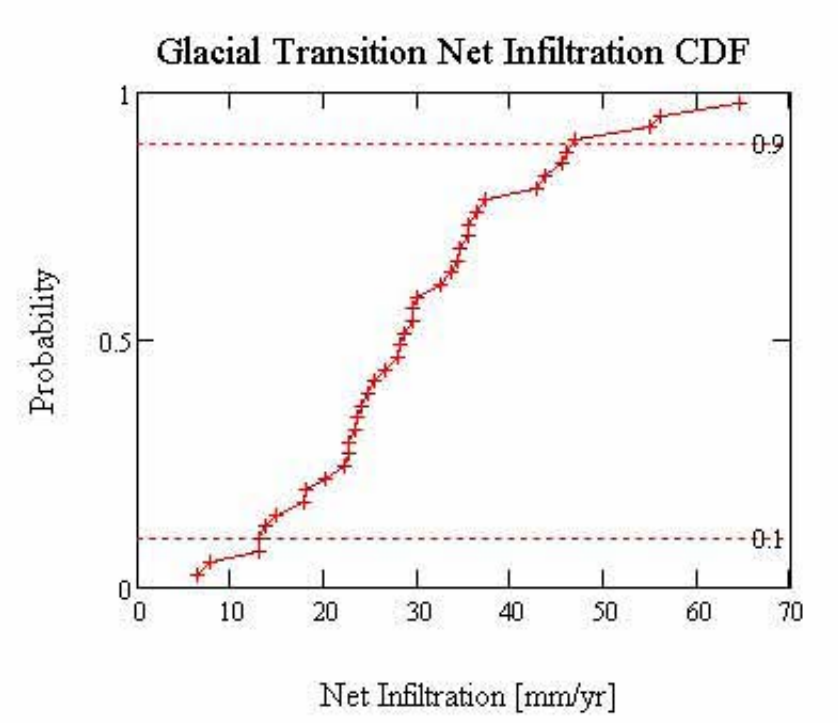

Source: Output DTN: SN0701T0502206.037, file: \Welcome to Massif\Massif\Glacial Uncertainty\Post Processing*GT_Combined_Replicates.xmcd*.

NOTE: A total of 40 realizations (2 LHS replicates) define the distribution.

Figure 6.5.7.3-6[a]. Cumulative Distribution Function (CDF) of Glacial Transition Spatially Averaged Mean Annual Net Infiltration over the Infiltration Domain

6.5.7.4[a]. Summary of Weighted Water Fluxes for Each Climate

No change.

6.5.7.5[a]. Factors Influencing Temporal Variability in Net Infiltration

No change.

6.5.7.6[a]. Factors Influencing Spatial Variability in Net Infiltration

No change.

6.5.7.6.1[a]. Influence of Soil Depth

Soil depth is one of the most significant factors controlling local net infiltration (see Section 6.7 and Appendix H). Unfortunately, soil depth in each of the model grid cells is largely not known with any degree of accuracy (see BSC 2006 [DIRS 178819] for details). Instead, the domain has been divided into five soil depth classes where soil depth decreases with increasing class number (described in Section 6.5.2). Soil depth distributions are developed in Section 6.5.2.4[a] and the actual sampled soil depths for soil depth class 4 for each realization are listed in Section 6.5.5. Table 6.5.7.6-1[a] lists the percent of the total infiltration that occurs in each soil depth class

region for replicate R1 of the Present-Day climate net infiltration results. It is clear that areas with shallow soils (soil depth class 4) and areas with no soil (class 5) dominate the total predicted net infiltration over the full domain.

Table 6.5.7.6-1[a]. Percent of Total Net Infiltration (and standard deviation) That Occurs in Each Soil Depth Class for Present-Day Climate Simulations (Entire Net Infiltration Modeling Domain)

Soil Depth Class	Percent of Total Infiltration [a]	Standard Deviation (%)	Percent of UZ Model Domain	Percent of Infiltration Model Domain
1	0.50	0.92	<1	9
2	2.30	3.85	18	25
3	0.52	0.97	11	9
4	90.53	7.15	70	57
5	6.15	4.69	<1	<1

Source: Output DTN: SN0701T0502206.037, file: \Welcome to Massif\Massif\Present Day Uncertainty\Post Processing*PD_Combined_Replicates.xmcd*.

[a] Total infiltration is the average net infiltration over the entire 125-km^2 modeling domain over epistemic uncertainty.

6.5.7.6.2[a]. Influence of Soil Group

Soil properties also influence spatial variations in net infiltration. Table 6.5.7.6-2[a] lists the percent of the total infiltration that occurs in the regions a specific soil type group for the Present-Day climate simulations. Five soil type groups are used to represent spatial variations in soil properties (includes a group representing cells with bare bedrock). Soil group 5/7/9 covers approximately 65% of the infiltration domain but accounts for about 91% of the total infiltration. Areas with bare rock cover only 0.3% of the infiltration domain but account for more than 6% of the total infiltration.

Table 6.5.7.6-2[a]. Percent of Total Net Infiltration (and standard deviation) That Occurs in Each Soil Group for Present-Day Climate Simulations (Entire Net Infiltration Modeling Domain)

Soil Group	Percent of Total Infiltration [a]	Standard Deviation (%)	Percent of UZ Model Domain	Percent of Infiltration Model Domain
1	0.48	0.94	3	10
2/6	0.66	1.27	4	11
3/4	1.78	2.65	13	13
5/7/9	90.93	6.68	81	65
Bare Rock	6.15	4.69	<1	<1

Source: Output DTN: SN0701T0502206.037, file: \Welcome to Massif\Massif\Present Day Uncertainty\Post Processing*PD_Combined_Replicates.xmcd*.

[a] Total infiltration is the average net infiltration over the entire 125-km^2 modeling domain over epistemic uncertainty.

6.5.7.6.3[a]. Influence of Rock Type

The hydraulic conductivity of the underlying bedrock may influence the spatial variability of net infiltration. Table 6.5.7.6-3[a] lists the percent of the total infiltration that occurs in the regions

underlain by a specific rock type for the Present-Day climate simulations. Nominal hydraulic conductivity values used for each rock type are explained in Section 6.5.2, and sampled values are listed in Section 6.5.5 for each climate-replicate combination. 30% of the total infiltration occurs in cells underlain by rock type 422, which accounts for 18% of the entire infiltration domain.

Table 6.5.7.6-3[a]. Percent of Total Net Infiltration (and standard deviation) That Occurs in Each Rock Type for Present-Day Climate Simulations (Entire Net Infiltration Modeling Domain)

Rock Type	Percent of Total Infiltration [a]	Standard Deviation (%)	Percent of UZ Model Domain	Percent of Infiltration Model Domain
401	5.25	0.53	4	2
402	1.94	0.23	3	1
403	7.72	1.52	14	18
404	3.55	0.72	8	3
405	15.09	2.18	22	22
406	8.25	2.16	19	8
407	6.25	0.61	6	4
408	2.90	0.27	4	2
409	1.70	0.07	2	1
410	0.10	0.04	<1	<1
411	1.39	0.36	<1	1
412	2.09	0.20	4	2
413	1.40	0.08	2	2
414	2.88	0.10	3	3
415	0.55	0.07	1	1
416	0.08	0.04	<1	<1
417	2.43	0.17	<1	2
418	1.32	0.43	3	3
419	0.01	0.03	<1	<1
420	0.49	0.10	1	1
421	0.43	0.08	1	1
422	30.16	2.53	1	18
423	0.11	0.03	<1	<1
424	0.19	0.07	<1	<1
425	0.01	0.03	<1	<1
426	0.01	0.03	<1	<1
427	0.00	0.00	0	<1
430	1.81	1.13	<1	<1
432	0.01	0.03	0	<1
435	0.20	0.02	0	<1
490	1.28	0.66	0	3
491	0.32	0.07	0	<1

Source: Output DTN: SN0701T0502206.037, file: \Welcome to Massif\Massif\Present Day Uncertainty\Post Processing*PD_Combined_Replicates.xmcd*.

[a] Total infiltration is the average net infiltration over the entire 125 km^2 modeling domain over epistemic uncertainty.

6.5.7.7[a]. Illustration of Daily Water Balance Patterns

As an illustration of the daily behavior of the MASSIF model, a single grid cell, located in the upper part of Pagany Wash watershed, was selected for monitoring during a one-year simulation. The purpose of this illustration is to help provide a sense of the intricate calculations that are performed in the MASSIF model of net infiltration. In theory, such detailed data could be obtained for every grid cell for every simulated day. However, the number of grid cells in a watershed and computer memory resources limit the number of cells that can be monitored for a given run.

The parameter set selected was from the Present-Day Replicate 2, Realization V08, which is the 50th percentile net infiltration Present-Day simulation. The year chosen was Year 2 (probability of occurrence = 0.003) from the stochastically generated weather file for the realization. The sampled parameter values for this realization are shown in Table 6.5.5.1-4. The geospatial characteristics of this grid cell are listed in Table 6.5.7.7-1[a].

Table 6.5.7.7-1[a]. Properties of the Grid Cell Selected for Illustration of Daily Water Balance Patterns

Parameter	Value
Easting (m)	548,261
Northing (m)	4,081,803
Elevation (m)	1,515
Slope (deg)	21
Azimuth (deg)	86
Soil Depth Class	4
Soil Type	5
Bedrock Type	403
PVR	0.5261

Source: Output DTN: SN0701T0502206, file: \Welcome to Massif\Massif\Present Day Uncertainty\Examples*Monitor Cell Characteristics.xls*.

There are a number of daily variables that can be monitored for a given grid cell. The figures below plot a selection of these variables for simulated year for the grid cell identified above. Figure 6.5.7.7-1[a] plots daily values of minimum and maximum temperatures and precipitation. The effect of precipitation on temperature in the model is evident in the plot as temperature depressions on days with rain. Such depressions result in reductions in the solar radiation and reference ET. Note that the temperature and precipitation values are lapse-corrected to the elevation of the monitored cell.

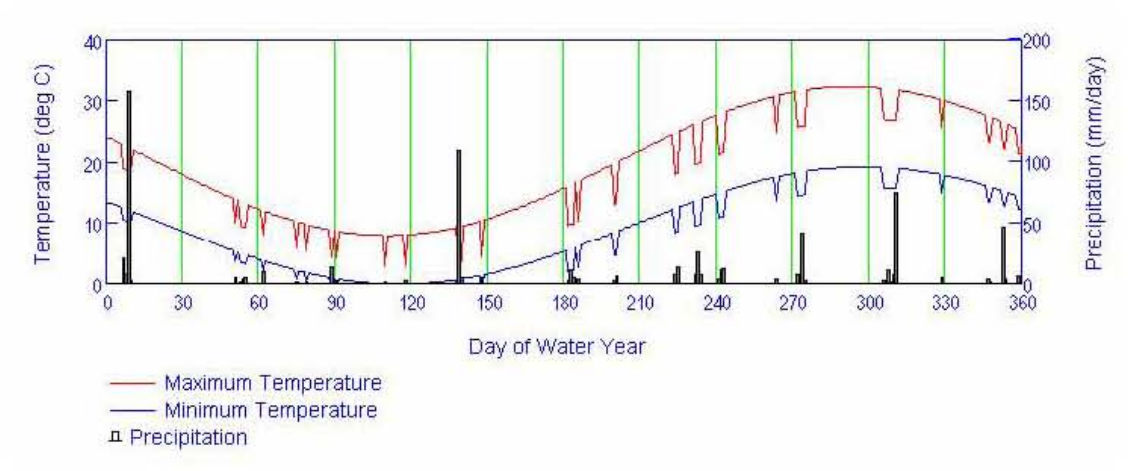

Source: Output DTN: SN0701T0502206, file: \Welcome to Massif\Massif\Present Day Uncertainty\Examples*Present Day R2 V08_example.xmcd*.

Figure 6.5.7.7-1[a]. Daily Weather Inputs for the Simulated Year

Figure 6.5.7.7-2[a] shows how values of K_{cb} and the canopy coefficient (f_c) vary for this cell over the water year. These values are independent of the daily precipitation; however, the total annual precipitation for the water year, slope, azimuth, and PVR are used in the calculation of K_{cb} (Section 6.5.3).

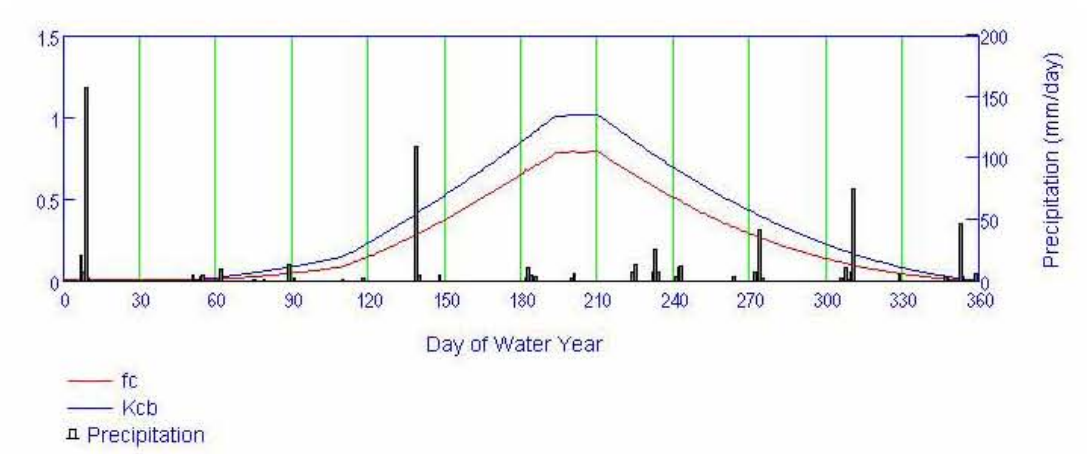

Source: Output DTN: SN0701T0502206, file: \Welcome to Massif\Massif\Present Day Uncertainty\Examples*Present Day R2 V08_example.xmcd*.

Figure 6.5.7.7-2[a]. Daily Values of K_{cb} and Canopy Fraction (f_c) for the Simulated Year

Figure 6.5.7.7-3[a] shows the reference ET along with the daily water losses of evaporation and transpiration. Several features of the model are evident in these results. For example, both evaporation and transpiration are proportional to reference ET. In addition, transpiration is also proportional to K_{cb}.

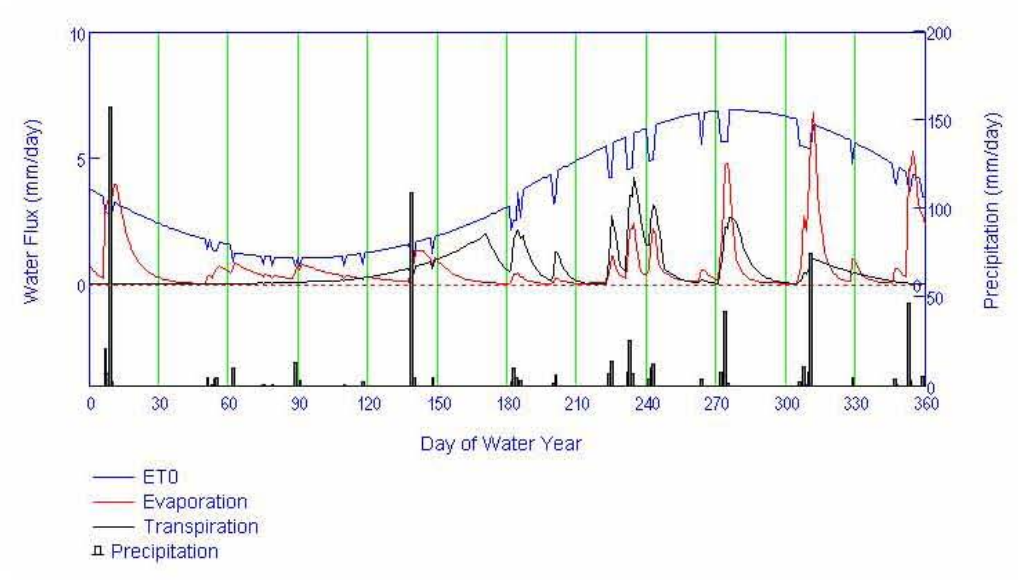

Source: Output DTN: SN0701T0502206, file: \Welcome to Massif\Massif\Present Day Uncertainty\Examples*Present Day R2 V08_example.xmcd.*

Figure 6.5.7.7-3[a]. Daily Water Fluxes (Evaporation, Transpiration, and Reference ET) for the Simulated Year

Figure 6.5.7.7-4[a] shows the water levels in each of the four nodes in the water balance calculation. Water levels 1 and 2 are for the surface evaporation layer of thickness Z_e. Water level 3 is for layer 2 (layer below evaporation layer). In this case, layer 2 thickness is equal to soil depth minus Z_e. In this example, the thickness of node 4 is equal to zero, because soil depth is less than the maximum rooting depth. The plots illustrates that for small precipitation events, water levels can increase in the surface layer (nodes 1 and 2), while continuing to decrease in the underlying layer (for example see day 60). When precipitation is greater, enough water is added to the surface layer to exceed its field capacity and thus water levels increase in the next lower layer (for example, see day 135). Also note the difference in the rate of water level decrease between days 1 and 135 as opposed to the rate between days 135 and 200. The increased rate of water level decrease corresponds to periods of higher reference ET and vegetation vigor (K_{cb}).

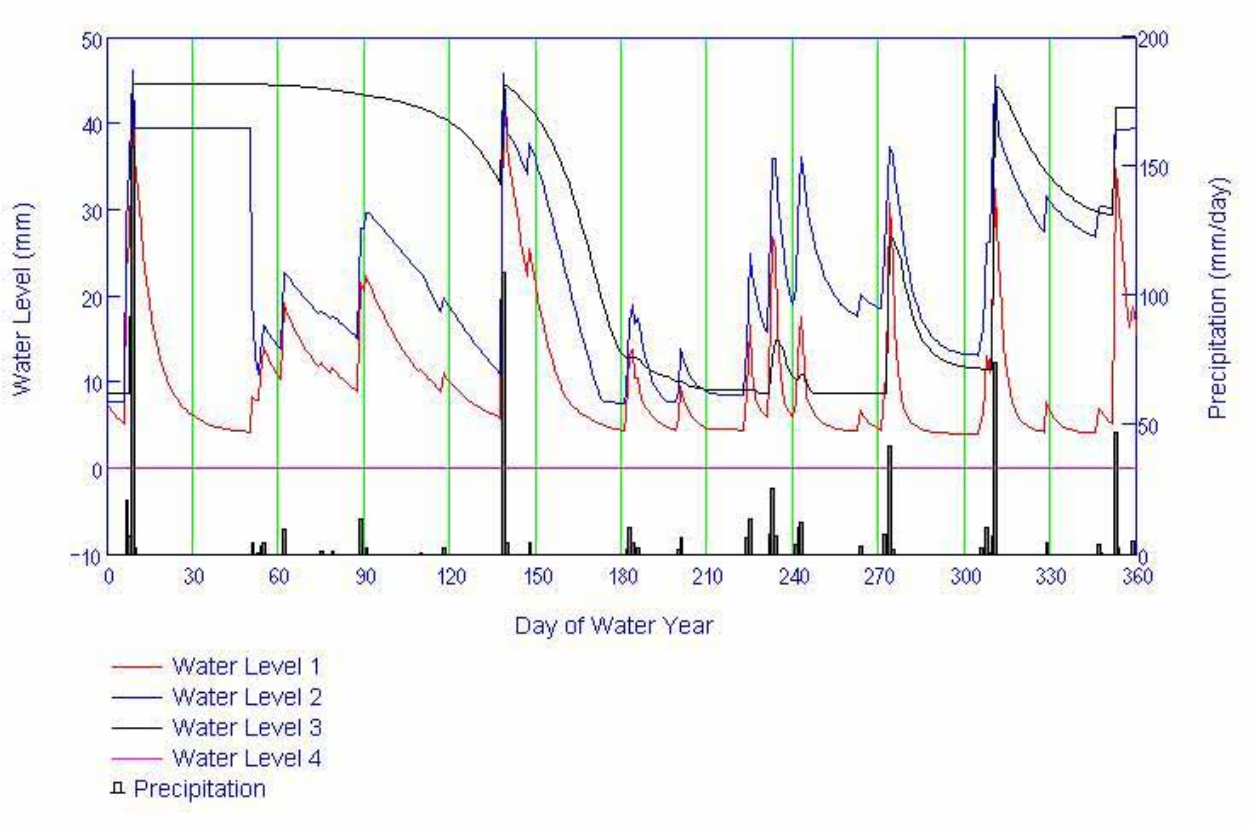

Source: Output DTN: SN0701T0502206, file: \Welcome to Massif\Massif\Present Day Uncertainty\Examples*Present Day R2 V08_example.xmcd.*

Figure 6.5.7.7-4[a]. Daily Soil Water Levels for the Simulated Year

Figure 6.5.7.7-5[a] shows a plot of daily run-on flowing into the cell and daily runoff flowing out of the cell. In this example, such runoff events only occurred two times during the year, both during particularly large precipitation events.

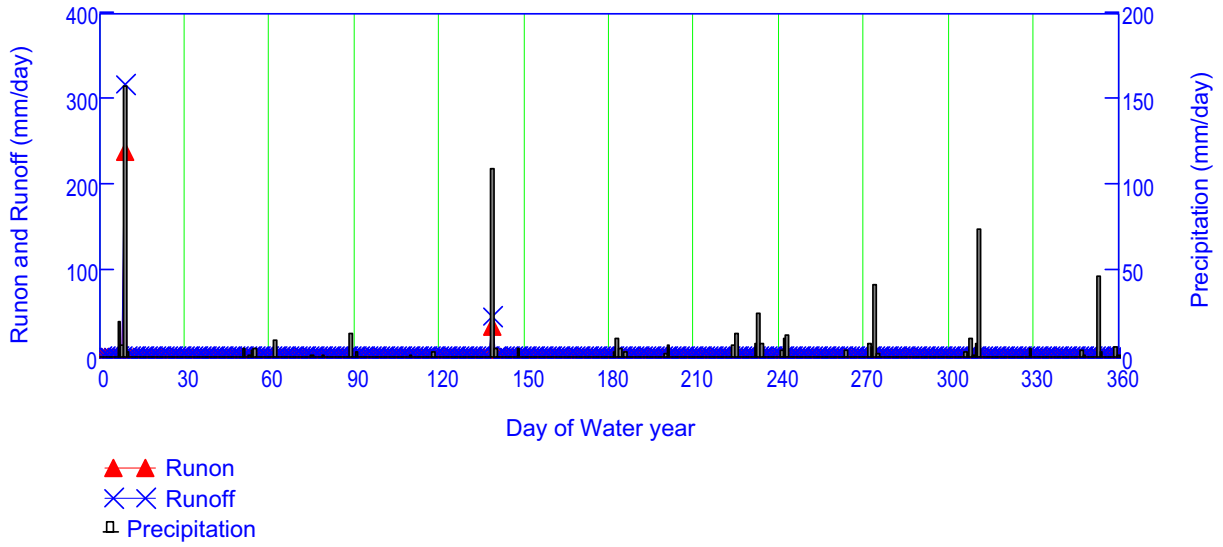

Source: Output DTN: SN0701T0502206, file: \Welcome to Massif\Massif\Present Day Uncertainty\Examples*Present Day R2 V08_example.xmcd*.

Figure 6.5.7.7-5[a]. Daily Run-on and Runoff for the Simulated Year

Figure 6.5.7.7-6[a] shows daily net infiltration during the year. In this example, net infiltration occurred during three periods each lasting two days.

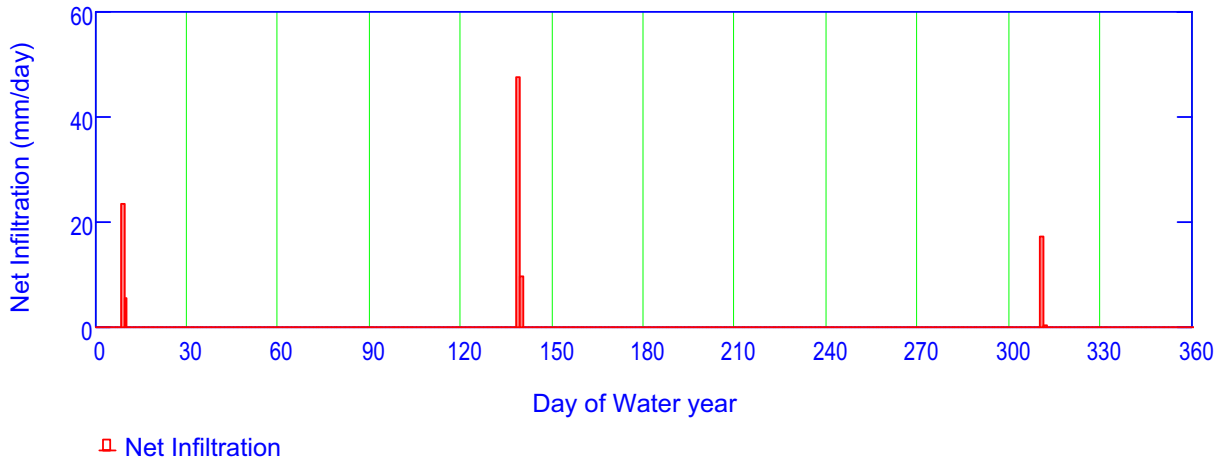

Source: Output DTN: SN0701T0502206, file: \Welcome to Massif\Massif\Present Day Uncertainty\Examples*Present Day R2 V08_example.xmcd*.

Figure 6.5.7.7-6[a]. Daily Net Infiltration for the Simulated Year

6.5.7.8[a]. Summary and Discussion of Net Infiltration Results for Present-Day and Future Climates

Table 6.5.7.8-1[a] summarizes the net infiltration statistics averaged over several spatial domains for all realizations and for all three climates. Predicted net infiltration generally is lowest for the Present-Day climate and increases in the Monsoon and Glacial Transition climates. However,

net infiltration predictions for the Monsoon climate appear to be more uncertain (span a greater range) than predictions for the Glacial Transition climate. This is the result of there being a greater amount of uncertainty in the expected precipitation in the Monsoon than for the Glacial Transition climate.

Table 6.5.7.8-1[a]. Summary Net Infiltration Statistics for the Three Climates

	Domain	PD	MO	GT
Minimum [mm/yr]	Infiltration modeling domain (125 km^2)	2.0	2.4	6.6
	UZ modeling domain (39.8 km^2)	1.4	1.2	4.2
	Repository footprint (5.7 km^2)[a]	1.5	1.2	4.0
Mean [mm/yr]	Infiltration modeling domain (125 km^2)	14.3	25.5	30.0
	UZ modeling domain (39.8 km^2)	14.9	27.6	28.8
	Repository footprint (5.7 km^2) [a]	17.6	32.9	38.7
Median [mm/yr]	Infiltration modeling domain (125 km^2)	12.9	22.8	28.5
	UZ modeling domain (39.8 km^2)	12.3	23.8	27.5
	Repository footprint (5.7 km^2) [a]	14.5	28.4	38.6
Maximum [mm/yr]	Infiltration modeling domain (125 km^2)	35.4	83.4	64.7
	UZ modeling domain (39.8 km^2)	40.3	85.4	70.9
	Repository footprint (5.7 km^2) [a]	48.2	95.3	97.3
Standard Deviation [mm/yr]	Infiltration modeling domain (125 km^2)	8.8	18.2	13.1
	UZ modeling domain (39.8 km^2)	10.3	20.0	15.2
	Repository footprint (5.7 km^2) [a]	12.5	23.3	21.2

Source: Output DTN: SN0701T0502206.037, file: \Welcome to Massif\Massif\Post Processing All Climates*Summary Net Infiltration All Climates.xls*.

[a] 2002 repository footprint used (DTN: LB0208HYDSTRAT.001 [DIRS 174491]).

PD = Present-Day, MO = Monsoon, GT = Glacial Transition.

One significant result of these simulations is the fact that most of the simulated net infiltration appears to occur in the regions with shallow soils rather than in the stream channels. This result raises some important questions about the predicted spatial distribution of net infiltration produced by the model. Section 7.1.3.2[a] presents some alternate simulations based on inferences made at Pagany Wash that result in significant infiltration in the stream channels. These alternate simulations allow soil conductivity to vary from the uncertainty distributions qualified in this report in Section 6.5.2, and therefore do not represent qualified net infiltration results. More field work would have to be performed in order to evaluate the accuracy of the spatial distribution of net infiltration in the current maps. There is greater confidence in the spatial averaged net infiltration values produced by this analysis.

6.5.7.9[a]. Comparison of Results from Each LHS Replicate

An examination of Tables 6.5.7.1-2[a], 6.5.7.2-2[a], and 6.5.7.3-2[a] shows that the results from each of the two replicates run for each climate can vary considerably at the tails of the distribution but are more similar when comparing the mean and median. Because of random variation in any stochastic analysis, it is expected that there can be significant variation in the minimum and maximum values between the two replicate distributions. A more-robust statistic to compare replicates is the first, second, and third quartiles (25th, 50th, 75th percentiles). The

absolute differences between the two replicates for these quartiles in the infiltration modeling domain range from 0.0 (Present-Day, 25%) to 4.8 mm (Monsoon, 25%).

An estimate of the error on the mean net infiltration is given by the standard error on the mean (standard deviation divided by the square root of the number of samples). Standard deviations for each climate and spatial domain are listed in Tables 6.5.7.1-2[a], 6.5.7.2-2[a], and 6.5.7.3-2[a]. The average standard errors on the mean for the infiltration modeling domain are listed in the last row of Table 6.5.7.9-1[a]. It would not be surprising if the differences in the quartiles, closer to the tails of the distribution, were somewhat greater than the standard error on the mean. But, as is shown in Table 6.5.7.9-1[a], the maximum standard error for the 25th, 50th, and 75th percentile values is only 1.2, 0.8, and 1.3 mm/yr greater than the mean standard error on the mean for the three climates (Present-Day, Monsoon, and Glacial Transition), respectively.

The conclusion drawn from these comparisons is that there is an inherent uncertainty in the resulting net infiltration estimates made in this analysis, which is due to the small sample size. The uncertainty on the mean net infiltration over the infiltration modeling domain is estimated by the standard error on the mean, which varies from 2.0 to 4.0 mm/yr, depending on climate. This uncertainty is certainly similar to the difference between the two replicates compared at the 25th, 50th, and 75th percentiles. This result provides confidence that the results of the combined replicates are representative of the actual distribution given the uncertainty estimated by the standard error on the mean. This uncertainty would be reduced by running more LHS realizations; however, the accuracy of the model predictions will not be improved upon because this accuracy is also limited by other sources of uncertainty (e.g., model uncertainty).

Table 6.5.7.9-1[a]. Differences in Net Infiltration Statistics between Replicates

ABS(R1-R2)	Domain	PD	MO	GT
25th Percentile (mm/yr)	Infiltration modeling domain (125 km^2)	***0.0***	***4.8***	***4.3***
	UZ modeling domain (39.8 km^2)	0.0	5.6	2.1
	Repository footprint (5.7 km^2) [a]	0.4	6.9	1.9
50th Percentile (mm/yr)	Infiltration modeling domain (125 km^2)	***2.2***	***2.9***	***0.4***
	UZ modeling domain (39.8 km^2)	0.6	2.3	2.7
	Repository footprint (5.7 km^2) [a]	0.9	2.2	2.7
75th Percentile (mm/yr)	Infiltration modeling domain (125 km^2)	***3.2***	***1.7***	***2.0***
	UZ modeling domain (39.8 km^2)	3.6	2.3	2.2
	Repository footprint (5.7 km^2) [a]	4.4	2.4	3.1
Mean Standard Error on Mean	Infiltration modeling domain (125 km^2)	***2.0***	***4.0***	***3.0***

Source: Output DTN: SN0701T0502206.037, file: \Welcome to Massif\Massif\Post Processing*Summary Net Infiltration All Climates.xls*.

[a] 2002 repository footprint used (DTN: LB0208HYDSTRAT.001 [DIRS 174491]).

NOTE: PD = Present-Day; MO = Monsoon; GT = Glacial-Transition.

6.6[a]. INFILTRATION PREDICTION UNCERTAINTIES

No change.

6.6.1[a]. Uncertainty in Potential Recharge Averaged over the Unsaturated Zone Model Domain

Section 6.5 reports the results of 120 calculations (2 replicates of 20 realizations for each of three climates). For each of the three climates, there are twenty calculations, called realizations, for which certain input parameters are varied in accordance with their uncertainty for that climate. This section develops summaries of the results.

Each of the 120 calculations reported in Section 6.5 provides three values for potential recharge, one for each of the following surface areas:

- Repository footprint
- The UZ flow model domain
- Entire surface treated by the MASSIF calculations.

Each value represents a space-time average over the area of interest and over the duration of the particular climate. A set of realizations for a particular climate provides three approximate uncertainty distributions, one for each of the space-time averages. This section models the uncertainty distributions of average potential recharge over the UZ model domain for each of the three climates. The UZ model domain represents the region expected to influence percolation of moisture from the surface to the vicinity of the repository.

Because the potential recharge must have positive values, a normal distribution cannot represent the uncertainty in potential recharge. Instead, this section models each uncertainty distribution as a lognormal distribution. The probability density for a lognormal distribution is (Gilbert 1987 [DIRS 163705], p. 152, Equation 12.1):

$$f(x) = \frac{1}{xS\sqrt{2\pi}} \exp\left[-\frac{1}{2S^2} (\ln x - M)^2 \right] \qquad \text{(Eq. 6.6.1-1[a])}$$

where M and S^2 are the true mean and variance of the random variable ln x, exp(M) is the median value of the random variable x, and M is the median value of the random variable ln x.

This section applies the W test to the logarithm of potential recharge over the UZ model grid. Testing the logarithm provides information about whether the uncertainty in potential recharge may be represented as a lognormal distribution.

This section combines both replicates for each climate and makes the approximation that the sample vectors represent random points in the parameter space. This permits the use of the W test for normality (Gilbert 1987 [DIRS 163705], Section 12.3.1). The null hypothesis for the W test is that the logarithms have a normal distribution. For a sample of size 40, the null hypothesis is rejected at the 0.02 significance level if W is less than 0.929 (Gilbert 1987 [DIRS 163705], Table A7). That is, the probability of W being less than 0.929 for a population of size 40 is less than 0.02.

If the hypothesis is not rejected, then:

- The experimental mean of ln x is an unbiased estimator of M (Gilbert 1987 [DIRS 163705], p. 27, Equation 4.3). The median value of x is exp(M).
- The experimental standard deviation of ln x is an unbiased estimator of S (ANSI/NCSL Z540-2-1997 [DIRS 157394], pp. 33, Section B.2.17, Note 1).
- The mean of x is exp(M+S^2/2) (Gilbert 1987 [DIRS 163705], p. 156, Table 12.1). (The mean of a lognormal distribution is always larger than the median.)

The following sections analyze the calculated amounts of potential recharge, averaged over the UZ model grid. To facilitate traceability, all values are rounded as shown in the tables before being used for subsequent calculations. The analyses show that the hypothesis of a lognormal distribution is not rejected for any of the three climates. Table 6.6.1-1[a] summarizes the parameters of the lognormal distributions. Because the uncertainty distribution is not symmetric, the table includes an uncertainty factor, defined to be exp(S). The uncertainty factor is (1) the ratio of the value "one sigma" above the median, exp(M+S), to the median and (2) the ratio of the median to the value one sigma below the median, exp(M−S).

The uncertainty in potential recharge over the UZ model grid is approximately a factor of two for the Present-Day climate or the Monsoon climate. For the Glacial Transition climate, the uncertainty factor is 1.6. Much of the uncertainty stems from uncertainty in parameters that are independent of climate. Section 6.7 discusses the relative contributions of the parameter uncertainties.

Table 6.6.1-1[a]. Parameters of Lognormal Distributions Representing the Contributions of Parameter Uncertainty to Uncertainties in Potential Recharge, Averaged over the UZ Model Grid

Climate	M [(a)]	S [(b)]	Median (e^M) (mm/yr)	Uncertainty Factor (e^S)	Mean of Distribution exp(M+S^2/2) (mm/yr)
Present-Day	2.4	0.9	12	2	17
Monsoon	3.0	0.9	24	2	30
Glacial Transition	3.2	0.6	28	1.6	29

[(a)] Mean of ln(I_{avg}) from Tables 6.6.1.1-1[a], 6.6.1.2-1[a], and 6.6.1.3-1[a].
[(b)] Standard deviation of ln(I_{avg}) from Tables 6.6.1.1-1[a], 6.6.1.2-1[a], and 6.6.1.3-1[a].

6.6.1.1[a]. Uncertainty in Potential Recharge over the Unsaturated Zone Model Domain during the Present-Day Climate

Table 6.6.1.1-1[a] presents the results of both replicates for the Present-Day climate, sorted by potential recharge over the UZ flow model area. The table also shows the logarithms of the results, as well as the mean and standard deviation of each column.

Table 6.6.1.1-2[a] develops the W test for the logarithm of net infiltration. The value of W is 0.939, so that the hypothesis that the distribution is lognormal is not rejected at the 0.02 significance level. For the Present-Day climate, therefore, the uncertainty in potential recharge may be represented by a lognormal distribution. The parameters of the lognormal distribution are $M = 2.4$ and $S = 0.9$.

The median value of potential recharge is 12 mm/yr. The value of S is equivalent to an uncertainty of a factor of 2 in potential recharge over the UZ flow model area. The mean value of the lognormal distribution is 17 mm/yr, close to the value of 15 mm/yr, which is the mean of the calculated values of potential recharge. The agreement between these two values corroborates that the lognormal distribution models the distribution of calculated results.

Table 6.6.1.1-1[a]. Values of Potential Recharge over the UZ Flow Model Area as Calculated for the Present-Day Climate, Sorted

Replicate [a]	Vector [b]	I_{avg} (mm/yr) [c]	ln(I_{avg}) [d]		Replicate [a]	Vector [b]	I_{avg} (mm/yr) [c]	ln(I_{avg}) [d]
R1	4	1.4	0.34		R2	15	13.2	2.58
R2	4	2.1	0.74		R1	2	14.0	2.64
R1	10	2.4	0.88		R1	18	14.6	2.68
R2	10	3.3	1.19		R2	19	16.3	2.79
R2	18	3.3	1.19		R2	3	19.3	2.96
R1	7	3.6	1.28		R1	12	19.9	2.99
R2	17	3.8	1.34		R1	9	20.4	3.02
R2	1	5.3	1.67		R2	13	20.6	3.03
R1	1	5.4	1.69		R2	7	24.0	3.18
R1	17	5.4	1.69		R1	14	24.7	3.21
R1	11	5.8	1.76		R1	6	24.9	3.21
R2	2	5.9	1.77		R1	15	25.3	3.23
R1	8	6.7	1.90		R2	14	28.3	3.34
R1	20	8.1	2.09		R2	20	28.6	3.35
R2	5	8.5	2.14		R2	12	28.9	3.36
R2	6	10.2	2.32		R1	19	29.6	3.39
R2	8	10.8	2.38		R2	9	29.7	3.39
R1	3	11.2	2.42		R1	5	32.2	3.47
R1	16	11.7	2.46		R2	16	40.3	3.70
R2	11	12.1	2.49			Mean[e]	15	2.4
R1	13	12.4	2.52		Standard Deviation[e]		10	0.9

Source: Output DTN: SN0701T0502206.037, files: \Welcome to Massif\Massif\Present Day Uncertainty\Post Processing\Intermediate Output Files*PD_Mean_Infiltration_R1.txt* and \Welcome to Massif\Massif\Present Day Uncertainty\Post Processing\Intermediate Output Files*PD_Mean_Infiltration_R2.txt*.

[a] Identifies source file in Output DTN: SN0701T0502206.037.
[b] Identifies data line in source file.
[c] Rounded to nearest 0.1 mm before further calculation.
[d] Rounded to nearest 0.01.
[e] Standard deviation rounded to two significant digits if first digit is one, otherwise to one significant digit. Mean rounded consistent with standard deviation.

Table 6.6.1.1-2[a]. W test for Lognormal Uncertainty Distribution for Potential Recharge over the UZ Flow Model Area during the Present-Day Climate

i [(a)]	$x_i = \ln(I_{avg})$ [(b)]	$x_i - x_{mean}$	a_i [(c)]	x_{41-i}	$a_i (x_{41-i} - x_i)$
1	0.34	-2.05	0.3964	3.70	1.332
2	0.74	-1.65	0.2737	3.47	0.747
3	0.88	-1.51	0.2368	3.39	0.594
4	1.19	-1.20	0.2098	3.39	0.462
5	1.19	-1.20	0.1878	3.36	0.408
6	1.28	-1.11	0.1691	3.35	0.350
7	1.34	-1.05	0.1526	3.34	0.305
8	1.67	-0.72	0.1376	3.23	0.215
9	1.69	-0.70	0.1237	3.21	0.188
10	1.69	-0.70	0.1108	3.21	0.168
11	1.76	-0.63	0.0986	3.18	0.140
12	1.77	-0.62	0.087	3.03	0.110
13	1.90	-0.49	0.0759	3.02	0.085
14	2.09	-0.30	0.0651	2.99	0.059
15	2.14	-0.25	0.0546	2.96	0.045
16	2.32	-0.07	0.0444	2.79	0.021
17	2.38	-0.01	0.0343	2.68	0.010
18	2.42	0.03	0.0244	2.64	0.005
19	2.46	0.07	0.0146	2.58	0.002
20	2.49	0.10	0.0049	2.52	0.000
21	2.52	0.13		sum	5.245
22	2.58	0.19		$W=sum^2/d$	0.940
23	2.64	0.25			
24	2.68	0.29			
25	2.79	0.40			
26	2.96	0.57			
27	2.99	0.60			
28	3.02	0.63			
29	3.03	0.64			
30	3.18	0.79			
31	3.21	0.82			
32	3.21	0.82			
33	3.23	0.84			
34	3.34	0.95			
35	3.35	0.96			
36	3.36	0.97			
37	3.39	1.00			
38	3.39	1.00			
39	3.47	1.08			
40	3.70	1.31			
x_{mean}	2.39	29.28	$d=sum(x_i - x_{mean})^2$		

[(a)] Index number after sorting.
[(b)] From Table 6.6.1.1-1[a].
[(c)] Gilbert 1987 [DIRS 163705], Table A6.

6.6.1.2[a]. Uncertainty in Potential Recharge over the Unsaturated Zone Model Domain during the Monsoon Climate

Table 6.6.1.2-1[a] presents the results of both replicates for the monsoon climate, sorted by potential recharge over the UZ flow model area. The table also shows the logarithms of the results, as well as the mean and standard deviation of each column.

Table 6.6.1.2-2[a] develops the W test for the logarithm of net infiltration. The value of W is 0.930, so that the hypothesis that the distribution is lognormal is not rejected at the 0.02 significance level. For the monsoon climate, therefore, the uncertainty in potential recharge may be represented by a lognormal distribution. The parameters of the lognormal distribution are $M = 3.0$ and $S = 0.9$. The median value of potential recharge is 24 mm/yr. The value of S is equivalent to an uncertainty of a factor of 2 in potential recharge over the UZ flow model area. The mean value of the lognormal distribution is 30 mm/yr, close to the value of 28 mm/yr, which is the mean of the calculated values of potential recharge. The agreement between these two values corroborates that the lognormal distribution models the distribution of calculated results.

Table 6.6.1.2-1[a]. Values of Potential Recharge over the UZ Flow Model Area as Calculated for the Monsoon Climate, Sorted

Replicate[a]	Vector[b]	I_{avg} (mm/yr)[c]	ln(I_{avg})[d]		Replicate[a]	Vector[b]	I_{avg} (mm/yr)[c]	ln(I_{avg})[d]
R2	20	1.2	0.18		R2	9	24.6	3.20
R1	18	1.9	0.64		R1	1	24.8	3.21
R1	20	4.5	1.50		R2	11	25.6	3.24
R1	17	5.3	1.67		R1	9	26.5	3.28
R1	3	6.4	1.86		R1	15	27.7	3.32
R2	6	6.8	1.92		R2	15	29.6	3.39
R2	4	7.5	2.01		R1	6	36.0	3.58
R1	10	9.1	2.21		R1	19	37.9	3.63
R1	11	10.5	2.35		R2	17	38.7	3.66
R1	5	13.7	2.62		R1	14	40.4	3.70
R2	14	14.4	2.67		R2	12	44.3	3.79
R2	5	14.9	2.70		R1	16	44.6	3.80
R2	10	15.8	2.76		R1	4	44.9	3.80
R1	12	16.9	2.83		R1	8	48.9	3.89
R2	18	17.8	2.88		R2	16	55.9	4.02
R2	8	17.9	2.88		R2	1	56.3	4.03
R2	13	19.0	2.94		R1	7	61.3	4.12
R2	2	21.7	3.08		R2	19	74.6	4.31
R1	13	23.0	3.14		R2	3	85.4	4.45
R2	7	23.1	3.14			Mean[e]	28	3.0
R1	2	24.5	3.20		Standard Deviation[e]		20	0.9

Source: Output DTN: SN0701T0502206.037, files: \Welcome to Massif\Massif\Monsoon Uncertainty\Post Processing\Intermediate Output Files*MO_Mean_Infiltration_R1.txt* and \Welcome to Massif\Massif\Monsoon Uncertainty\Post Processing\Intermediate Output Files*MO_Mean_Infiltration_R2.txt*.

[a] Identifies source file in Output DTN: SN0701T0502206.037.
[b] Identifies data line in source file.
[c] Rounded to nearest 0.1 mm before further calculation.
[d] Rounded to nearest 0.01.
[e] Standard deviation rounded to two significant digits if first digit is one, otherwise to one significant digit. Mean rounded consistent with standard deviation.

Table 6.6.1.2-2[a]. W Test for Lognormal Uncertainty Distribution for Potential Recharge over the UZ Flow Model Area during the Monsoon Climate

i [(a)]	$x_i = \ln(I_{avg})$ [(b)]	$x_i - x_{mean}$	a_i [(c)]	x_{41-i}	$a_i (x_{41-i} - x_i)$
1	0.18	-2.81	0.3964	4.45	1.693
2	0.64	-2.35	0.2737	4.31	1.004
3	1.50	-1.49	0.2368	4.12	0.620
4	1.67	-1.32	0.2098	4.03	0.495
5	1.86	-1.13	0.1878	4.02	0.406
6	1.92	-1.07	0.1691	3.89	0.333

Table 6.6.1.2-2[a]. W Test for Lognormal Uncertainty Distribution for Potential Recharge over the UZ Flow Model Area during the Monsoon Climate (Continued)

i [(a)]	$x_i = \ln(I_{avg})$ [(b)]	$x_i - x_{mean}$	a_i [(c)]	x_{41-i}	$a_i (x_{41-i} - x_i)$
7	2.01	-0.98	0.1526	3.80	0.273
8	2.21	-0.78	0.1376	3.80	0.219
9	2.35	-0.64	0.1237	3.79	0.178
10	2.62	-0.37	0.1108	3.70	0.120
11	2.67	-0.32	0.0986	3.66	0.098
12	2.70	-0.29	0.087	3.63	0.081
13	2.76	-0.23	0.0759	3.58	0.062
14	2.83	-0.16	0.0651	3.39	0.036
15	2.88	-0.11	0.0546	3.32	0.024
16	2.88	-0.11	0.0444	3.28	0.018
17	2.94	-0.05	0.0343	3.24	0.010
18	3.08	0.09	0.0244	3.21	0.003
19	3.14	0.15	0.0146	3.20	0.001
20	3.14	0.15	0.0049	3.20	0.000
21	3.20	0.21		sum	5.675
22	3.20	0.21		$W=sum^2/d$	0.931
23	3.21	0.22			
24	3.24	0.25			
25	3.28	0.29			
26	3.32	0.33			
27	3.39	0.40			
28	3.58	0.59			
29	3.63	0.64			
30	3.66	0.67			
31	3.70	0.71			
32	3.79	0.80			
33	3.80	0.81			
34	3.80	0.81			
35	3.89	0.90			
36	4.02	1.03			
37	4.03	1.04			
38	4.12	1.13			
39	4.31	1.32			
40	4.45	1.46			
x_{mean}	2.99	34.58	$d=sum(x_i - x_{mean})^2$		

(a) Index number after sorting.
(b) From Table 6.6.1.2-1[a].
(c) Gilbert 1987 [DIRS 163705], Table A6.

6.6.1.3[a]. Potential Recharge over the Unsaturated Zone Model Domain during the Glacial Transition Climate

Table 6.6.1.3-1[a] presents the results of both replicates for the glacial transition climate, sorted by potential recharge over the unsaturated zone model domain. The table also shows the logarithms of the results, as well as the mean and standard deviation of each column.

Table 6.6.1.3-2[a] develops the W test for the logarithm of net infiltration. The value of W is 0.943, so that the hypothesis that the distribution is lognormal is not rejected at the 0.02 significance level. For the glacial transition climate, therefore, the uncertainty in potential recharge may be represented by a lognormal distribution. The parameters of the lognormal distribution are $M = 3.2$ and $S = 0.6$.

The median value of potential recharge is 28 mm/yr. The value of S is equivalent to an uncertainty of a factor of 1.6 in potential recharge over the unsaturated zone model domain. The mean value of the lognormal distribution is 29 mm/yr, which is the same as the mean of the calculated values of potential recharge. The agreement between these two values corroborates that the lognormal distribution models the distribution of calculated results.

Table 6.6.1.3-1[a]. Values of Potential Recharge over the Unsaturated Zone Model Domain as Calculated for the Glacial Transition Climate, Sorted

Replicate [a]	Vector [b]	I_{avg} (mm/yr) [c]	ln(I_{avg}) [d]		Replicate [a]	Vector [b]	I_{avg} (mm/yr) [c]	ln(I_{avg}) [d]
R1	7	4.2	1.44		R1	1	28.1	3.34
R1	4	5.7	1.74		R2	12	28.6	3.35
R2	6	8.0	2.08		R1	18	28.9	3.36
R1	9	9.6	2.26		R1	10	32.5	3.48
R2	11	10.8	2.38		R2	18	32.8	3.49
R2	15	10.9	2.39		R2	20	32.9	3.49
R2	16	15.9	2.77		R1	19	33.0	3.50
R2	5	17.4	2.86		R2	8	33.1	3.50
R2	13	18.4	2.91		R2	3	33.6	3.51
R1	15	18.9	2.94		R1	14	34.7	3.55
R1	6	19.4	2.97		R1	2	36.5	3.60
R2	14	19.6	2.98		R2	2	43.1	3.76
R2	10	20.3	3.01		R1	12	45.7	3.82
R1	3	20.6	3.03		R2	7	46.4	3.84
R2	4	21.9	3.09		R1	5	48.8	3.89
R1	17	22.3	3.10		R2	1	51.0	3.93
R1	11	23.0	3.14		R1	13	56.7	4.04
R2	17	23.8	3.17		R2	19	61.0	4.11
R1	16	26.2	3.27		R1	8	70.9	4.26
R2	9	27.1	3.30			Mean [e]	29	3.2
R1	20	28.0	3.33			Standard Deviation [e]	15	0.6

Source: Output DTN: SN0701T0502206.037, files: \Welcome to Massif\Massif\Glacial Uncertainty\Post Processing\Intermediate Output Files*GT_Mean_Infiltration_R1.txt* and \Welcome to Massif\Massif\Glacial Uncertainty\Post Processing\Intermediate Output Files*GT_Mean_Infiltration_R2.txt*.

[a] Identifies source file in Output DTN: SN0701T0502206.037.
[b] Identifies data line in source file.
[c] Rounded to nearest 0.1 mm before further calculation.
[d] Rounded to nearest 0.01.
[e] Standard deviation rounded to two significant digits if first digit is one, otherwise to one significant digit. Mean rounded consistent with standard deviation.

Table 6.6.1.3-2[a]. W Test for Lognormal Uncertainty Distribution for Potential Recharge over the Unsaturated Zone Model Domain during the Glacial Transition Climate

i [(a)]	$x_i = \ln(I_{avg})$ [(b)]	$x_i - x_{mean}$	a_i [(c)]	x_{41-i}	$a_i (x_{41-i} - x_i)$
1	1.44	-1.76	0.3964	4.26	1.118
2	1.74	-1.46	0.2737	4.11	0.649
3	2.08	-1.12	0.2368	4.04	0.464
4	2.26	-0.94	0.2098	3.93	0.350
5	2.38	-0.82	0.1878	3.89	0.284
6	2.39	-0.81	0.1691	3.84	0.245
7	2.77	-0.43	0.1526	3.82	0.160
8	2.86	-0.34	0.1376	3.76	0.124
9	2.91	-0.29	0.1237	3.60	0.085
10	2.94	-0.26	0.1108	3.55	0.068
11	2.97	-0.23	0.0986	3.51	0.053
12	2.98	-0.22	0.087	3.50	0.045
13	3.01	-0.19	0.0759	3.50	0.037
14	3.03	-0.17	0.0651	3.49	0.030
15	3.09	-0.11	0.0546	3.49	0.022
16	3.10	-0.10	0.0444	3.48	0.017
17	3.14	-0.06	0.0343	3.36	0.008
18	3.17	-0.03	0.0244	3.35	0.004
19	3.27	0.07	0.0146	3.34	0.001
20	3.30	0.10	0.0049	3.33	0.000
21	3.33	0.13		sum	3.764
22	3.34	0.14		$W=sum^2/d$	0.943
23	3.35	0.15			
24	3.36	0.16			
25	3.48	0.28			
26	3.49	0.29			
27	3.49	0.29			
28	3.50	0.30			
29	3.50	0.30			
30	3.51	0.31			
31	3.55	0.35			
32	3.60	0.40			
33	3.76	0.56			
34	3.82	0.62			
35	3.84	0.64			
36	3.89	0.69			
37	3.93	0.73			

Table 6.6.1.3-2[a]. W Test for Lognormal Uncertainty Distribution for Potential Recharge over the Unsaturated Zone Model Domain during the Glacial Transition Climate (Continued)

i [(a)]	$x_i = \ln(I_{avg})$ [(b)]	$x_i - x_{mean}$	a_i [(c)]	x_{41-i}	$a_i (x_{41-i} - x_i)$
38	4.04	0.84			
39	4.11	0.91			
40	4.26	1.06			
x_{mean}	3.20	15.02	$d=\text{sum}(x_i - x_{mean})^2$		

Sources: [(a)] Index number after sorting.
[(b)] From Table 6.6.1.3-1[a].
[(c)] Gilbert 1987 [DIRS 163705], Table A6.

6.6.2[a]. Uncertainty in Local Net Infiltration

No change.

6.6.3[a]. Sources and Magnitude of Model Uncertainty

Model uncertainty represents a limitation of any model to accurately represent the physical processes being considered. Models are simplified representations of reality and, as such, introduce inherent errors in estimated quantities due to the simplifications and abstractions necessary for formulating the model. In addition to the limitations in model predictions due to model uncertainty, parameter uncertainty introduces additional uncertainty. Measurement theory provides a useful analogy to compare model and parameter uncertainties. Model uncertainty is similar to measurement accuracy, while parameter uncertainty is similar to measurement precision. Both sources of uncertainty contribute to the final uncertainty in a model prediction or measurement quantity.

In the analysis of net infiltration at Yucca Mountain, both sources of uncertainty are important and must be estimated. Most of the effort has been focused on evaluating and quantifying parameter uncertainty. As discussed in Sections 6.6.1[a] and 6.6.2, parameter uncertainty represents approximately a factor of 2 uncertainty in the mean net infiltration averaged over the unsaturated zone model domain and a factor of approximately 6 in the uncertainty in local net infiltration predicted in areas with shallow soils.

Sources of model uncertainty in this study include: (1) the accuracy of the coupled NDVI/FAO-56 approach for estimating evapotranspiration at the site, (2) the accuracy of the layered field capacity approach for representing subsurface water flow, (3) the accuracy of the assumption that evapotranspiration from bedrock is negligible, and (4) the accuracy of the distributed runoff model used to represent surface water flow.

The uncertainty associated with the ET submodel is evaluated by comparing ET measurements using lysimeter data to simulated results using MASSIF (Section 7.1.2). These comparisons indicate that the model performs well in the context of parameter uncertainty, especially for estimates of cumulative annual ET.

The present study was unable to explicitly test the accuracy of the field capacity approach for representing subsurface water flow against field data from the Yucca Mountain site. However, a

comparison was made against HYDRUS 1-D (a comparable model that represents subsurface water flow using Richards' equation) in Section 7.2.2[a]. This comparison demonstrates that while the field capacity approach may not represent the transient nature of this flow accurately, it does an adequate job of representing the cumulative net infiltration over the year.

The assumption that ET from the bedrock is negligible is highly uncertain and is dependent upon knowledge of the bedrock properties and applicable physics of potential processes for water removal from bedrock overlain by soil. Certain neutron logs that extend into bedrock show that water removal does occur at certain locations (BSC 2004 [DIRS 170007], p. 6-16), however these results are not at all consistent when all the logs are examined. Therefore, the implication of this assumption is that it will tend to overestimate net infiltration model predictions, but it is not clear by how much and where these overestimates occur.

Finally, comparisons of runoff predictions with stream gauge observations (Section 7.1.3) provide confidence that the model uncertainty related to the runoff submodel is not a significant source of uncertainty for mean net infiltration over the a large area (e.g., unsaturated zone model domain); however, this process may contribute significantly to uncertainty in local net infiltration (Sections 7.1.3.1 and 7.1.3.2[a]).

The challenge of estimating net infiltration model uncertainty is exacerbated by the difficulty of directly measuring net infiltration in this and similar environments. Instead, model uncertainty is usually inferred by comparing the results of the various submodels (e.g., ET, runoff, etc.) to available field data as described above. However, such comparisons do not directly evaluate the model uncertainty in net infiltration estimates. Another approach is to assume that the regional estimates of net infiltration presented in Section 7.2 are representative of net infiltration conditions expected for the unsaturated zone model domain at Yucca Mountain. If this assumption is valid, then model uncertainty could be estimated by comparing MASSIF model predictions with estimates of net infiltration and recharge from these other sites. The comparison presented in Figure 7.2.1.2-2 suggests that model uncertainty is comparable in magnitude to parameter uncertainty. However, it is not clear that the assumption that regional sites are comparable with the unsaturated zone model domain is entirely valid. The unsaturated zone model domain is characterized by uplands with very shallow soils and may host a different net infiltration regime than is more typical of the other hydrographic basins represented in Section 7.2. One indication that this assumption may not be valid is in the comparison of the net infiltration predictions with net infiltration inferred from an analysis of the 95 neutron boreholes at the Yucca Mountain site (Figure 7.2.1.1-2[a]). This figure clearly shows that nearly all of the net infiltration estimates derived from the neutron logging analyses are higher than the values predicted by the MASSIF model. If the spatial distribution of neutron borehole locations is representative of the unsaturated zone modeling domain and the net infiltration estimates from the analysis of the neutron logs is representative of conditions away from the boreholes, this would suggest that the MASSIF model may underestimate actual net infiltration for this area by a factor of 3 (Figure 7.2.1.1-2[a]). It is not clear, however, that either of these criteria is met, and therefore it is not clear how these data can help to estimate model uncertainty. Given these challenges, and the comparisons that have been made, it is difficult to quantify model uncertainty. Available comparisons suggest that model uncertainty may be of a comparable magnitude to parameter uncertainty. Given the complexity of modeling net infiltration over such a large and heterogeneous domain, such uncertainty is not unprecedented.

6.7[a]. SENSITIVITY ANALYSIS

No change.

6.8[a]. NOMENCLATURE USED IN SECTION 6 EQUATIONS

No change.

INTENTIONALLY LEFT BLANK

7[a]. VALIDATION

No change.

7.1[a]. CONFIDENCE BUILDING DURING MODEL DEVELOPMENT

No change.

7.1.1[a]. Precipitation

No change.

7.1.1.1[a]. Comparison of Seasonal Precipitation Patterns

This section presents a comparison of monthly average precipitation measured at selected weather stations with monthly average precipitation from the 1,000-yr stochastically-generated precipitation records for selected weather sites using the truncated Fourier series (one-harmonic). In addition, to provide a basis for comparison, the 1,000-yr generated precipitation record for a two-harmonic truncated Fourier series is also presented. Adding another harmonic will always improve the fitting; however, it also results in more parameters that need to be estimated. In addition, since each climate representation is based on weather records from several stations (rather than one) and these stations differ considerably in their precipitation seasonality, there is no meaningful way to combine parameters for the two-harmonic Fourier series such that they represent the suite of precipitation records from all stations. For this reason a single harmonic representation was used for representing precipitation patterns for each climate. Two sites for each of the three climate states predicted to occur at Yucca Mountain (Present-Day, Monsoon, and Glacial Transition climates) during the next 10,000 years are shown. The sites for the Present-Day climate are Yucca Mountain weather station Site 2 and NTS Station A12; for the Monsoon climate, Hobbs, NM and Nogales, AZ; and for the Glacial Transition climate, Spokane, WA and Delta, UT.

Figure 7.1.1.1-1(a)[a] shows a comparison of recorded average monthly precipitation from the Yucca Mountain Site 2 weather station versus average monthly precipitation of 1,000-yr generation using a one-harmonic truncated Fourier series. Figure 7.1.1.1-1(b)[a] shows the same comparison using a two-harmonic truncated Fourier series. In this example, the two-harmonic estimate does little to improve the fit. This is because the annual precipitation pattern is characterized by a single wet and dry period rather than a two wet and dry periods during the year.

The comparison of NTS Station A12 average monthly precipitation record versus the 1,000-yr generated precipitation using a one-harmonic truncated Fourier series is shown in Figure 7.1.1.1-2(a)[a]. The one-harmonic here captures the general trend of the precipitation but not as well as in the Site 2 case. The reason is that NTS Station A12 experiences a four-season trend variation that cannot be captured with only one harmonic. The two harmonic brings significant improvement in allowing the capture of four seasons. Therefore, the two-harmonic does a better job of more closely fitting the NTS Station A12 data.

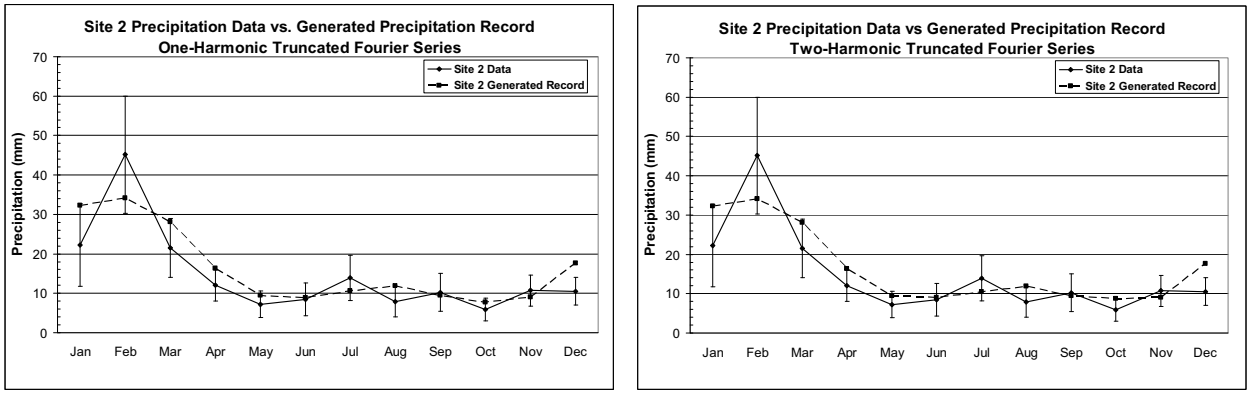

(a) (b)

Source: Validation Output DTN: SN0701T0502206.045.

Figure 7.1.1.1-1[a]. Average Monthly Precipitation Comparison Between Observed Records and 1,000-yr Generation for Yucca Mountain Site 2: (a) Using Second Order (one-harmonic truncated) Fourier Series and (b) Using Third Order (one and two harmonics) Truncated Fourier Series

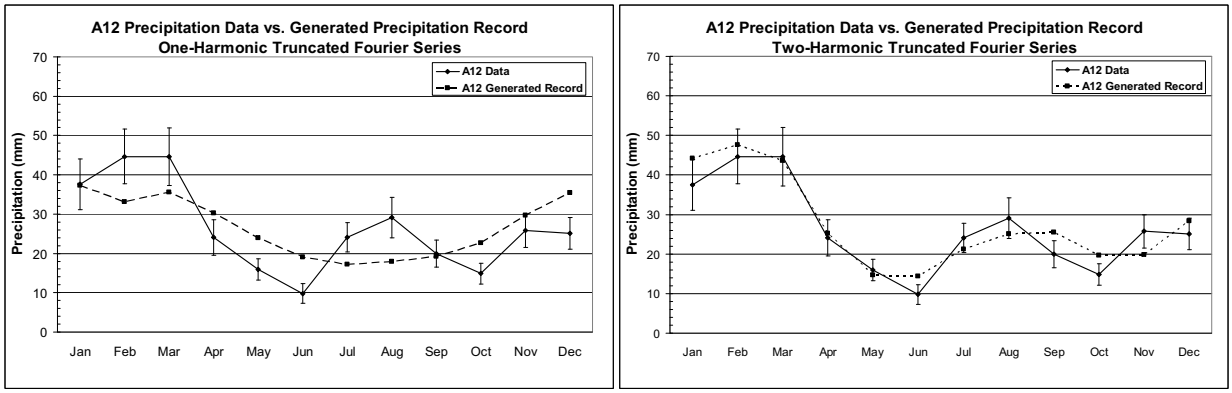

(a) (b)

Source: Validation Output DTN: SN0701T0502206.045.

Figure 7.1.1.1-2[a]. Average Monthly Precipitation Comparison Between Observed Records and 1,000-yr Generation for Site A12: (a) Using Second Order (one-harmonic truncated) Fourier Series and (b) Using Third Order (one and two harmonics) Truncated Fourier Series

Monthly precipitation comparison for the upper-bound Monsoon analogue site of Hobbs, NM is shown in Figure 7.1.1.1-3[a]. In this case, recorded data shows a two-seasons behavior; a one-harmonic curve fits this behavior very well, as Figure 7.1.1.1-3(a)[a] shows. Applying a two harmonic correction does not improve the fit significantly (Figure 7.1.1.1-3(b)[a]).

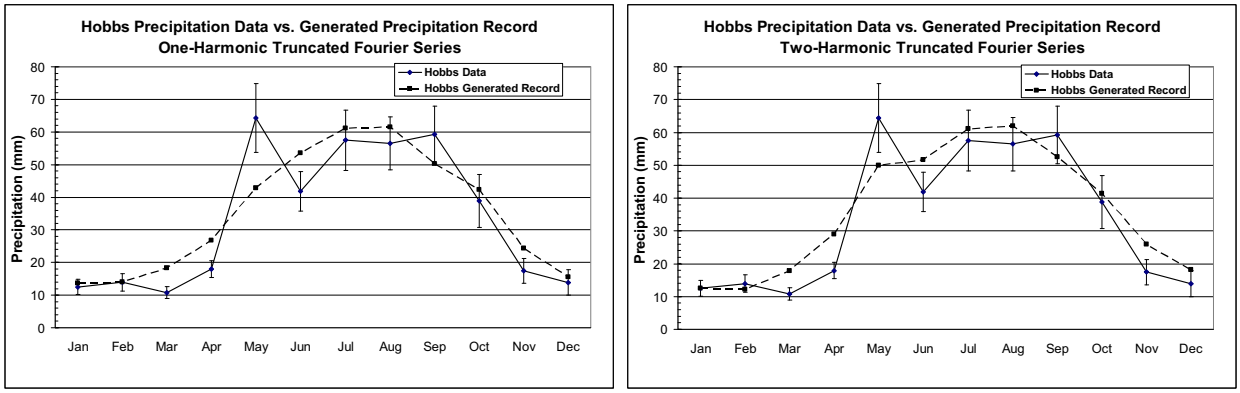

(a) (b)

Source: Validation Output DTN: SN0701T0502206.045.

Figure 7.1.1.1-3[a]. Average Monthly Precipitation Comparison Between Observed Records and 1,000-yr Generation for Hobbs (NM): (a) Using Second Order (one-harmonic truncated) Fourier Series and (b) Using Third Order (one and two harmonics) Truncated Fourier Series

Figure 7.1.1.1-4[a] shows the data for the upper-bound Monsoon analogue site of Nogales, AZ. This Monsoon analogue site has a more pronounced monsoon pattern that strongly spikes in July and August. The monthly average precipitation based on 1,000-yr generated record using the one-harmonic truncated Fourier series does not provide a close match to the actual data. The limit is again due to the use of only one harmonic to represent a nonsinusoidal function. Adding a two-harmonic correction provides a significant improvement. It is important, however, to point out that Nogales site parameters are not directly used in our model but are first aggregated with the other representative site Hobbs, NM, which is matched quite well with a one-harmonic model.

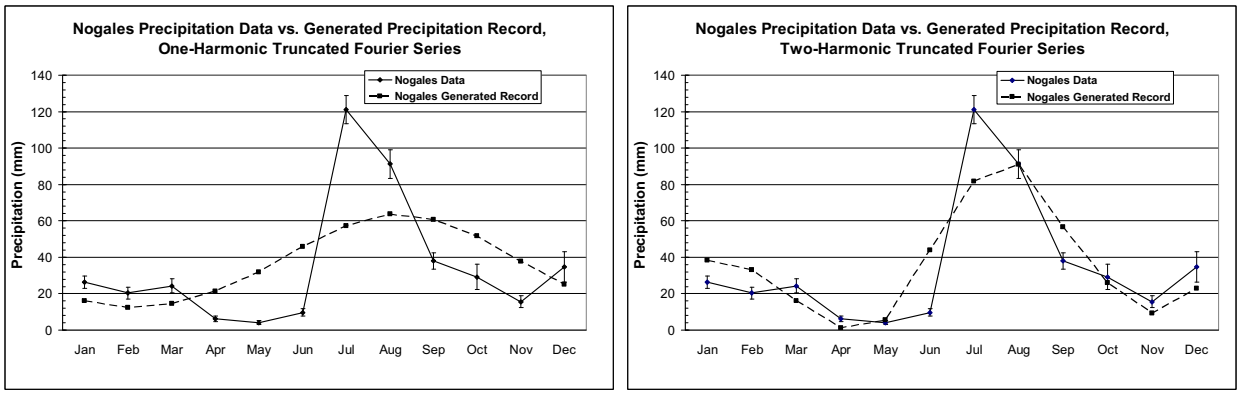

(a) (b)

Source: Validation Output DTN: SN0701T0502206.045.

Figure 7.1.1.1-4[a]. Average Monthly Precipitation Comparison Between Observed Records and 1,000-yr Generation for Nogales (AZ): (a) Using Second Order (one-harmonic truncated) Fourier Series and (b) Using Third Order (one and two harmonics) Truncated Fourier Series

The comparison of site data for average monthly precipitation records at Spokane, WA (one of the upper-bound Glacial Transition analogue sites) versus the average monthly precipitation estimated from 1,000-yr generated precipitation using one and two-harmonic truncated Fourier series is shown in Figure 7.1.1.1-5[a]. The one-harmonic (a) fits the site data very well. The two-harmonic (b) correction provides a slightly improved fit.

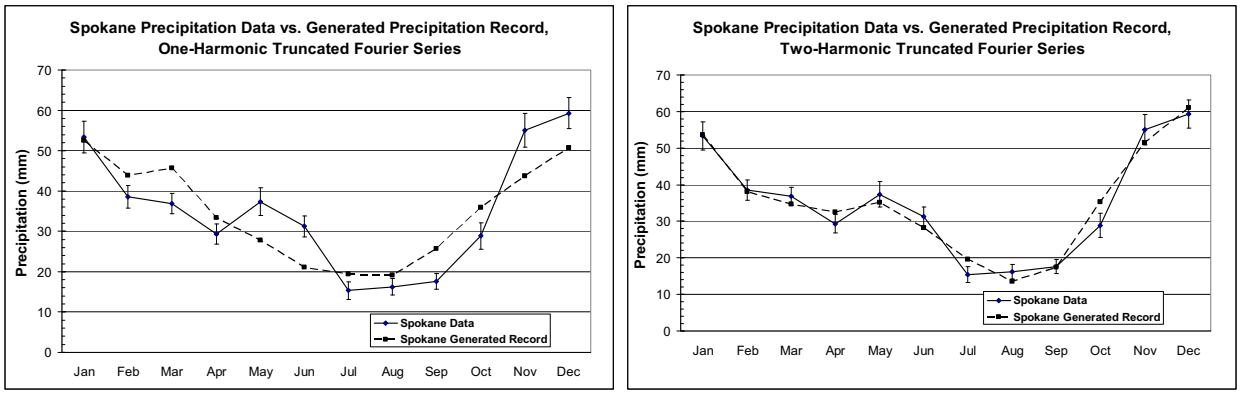

(a) (b)

Source: Validation Output DTN: SN0701T0502206.045.

Figure 7.1.1.1-5[a]. Average Monthly Precipitation Comparison Between Observed Records and 1,000-yr Generation for Spokane (WA): (a) Using Second Order (one-harmonic truncated) Fourier Series and (b) Using Third Order (one and two harmonics) Truncated Fourier Series

The average monthly precipitation record at Delta, UT (lower-bound Glacial Transition analogue site) is shown in Figure 7.1.1.1-6[a]. Delta experiences a four-season variation with respect to precipitation, similar to the pattern at NTS Station A12 (Figure 7.1.1.1-2[a]). The monthly precipitation based on only one harmonic does not provide a good fit, and only a two-harmonic correction allows a good representation of monthly variation. As discussed for Nogales data, it is important to note that the parameters are aggregated with parameters fitted to other sites (e.g. Spokane), for which the one-harmonic fit is very good.

Adding another term to the Fourier series will always give a better fit, as this additional term accounts for the residual between the Fourier series and the actual data. For half of the selected sites, precipitation records show a two-seasons variation over the year (on average), and a one-harmonic truncated Fourier series fits the data well. The second harmonic correction gives significant improvement when the selected site presents distinct four-season variations (Figures 7.1.1.1-2[a] and 7.1.1.1-6[a]) or a strong gradient of differences for a period (Figure 7.1.1.1-5[a]).

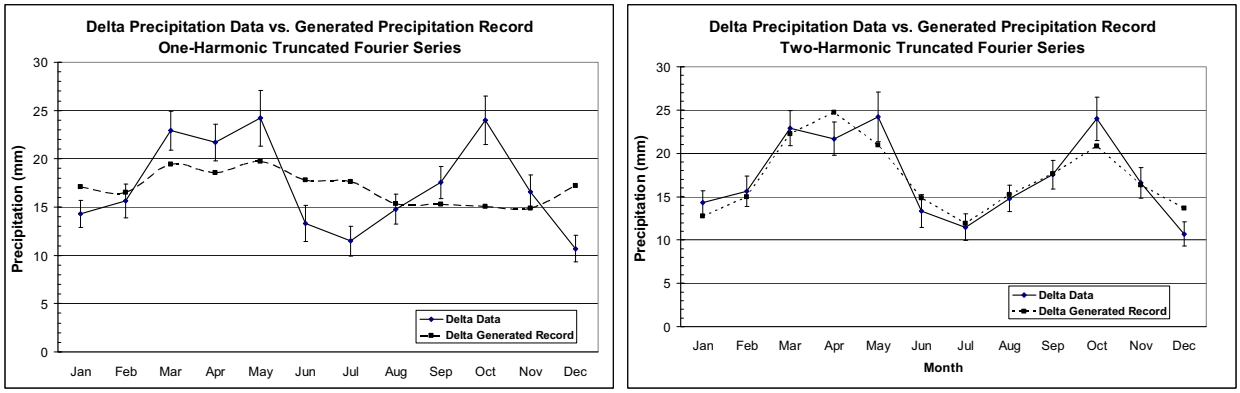

(a) (b)

Source: Validation Output DTN: SN0701T0502206.045.

Figure 7.1.1.1-6[a]. Average Monthly Precipitation Comparison Between Observed Records and 1,000-yr Generation for Delta (UT): (a) Using Second Order (one-harmonic truncated) Fourier Series and (b) Using Third Order (one and two harmonics) Truncated Fourier Series

There is a cost of adding an additional harmonic to improve these fits. Four quantities are considered in our Markov Chain Monte Carlo model: p_{00} (probability that current day is dry knowing that previous day is dry), p_{10} (probability that current day is dry knowing that previous day is wet), λ (expected infiltration for a wet day) and m (median infiltration for a wet day). A new harmonic adds two parameters (an amplitude parameter b_i and a phase parameter θ_i) for each of the quantities, so eight new parameters are added. Several sites are used to represent the uncertainty on annual precipitation for each climate (10 for Present-Day climate, the same 10 plus two more for Monsoon climate, and five for Glacial Transition climate). The representation of uncertainty consists of aggregating each of these parameters. The value of attempting to aggregate the eight parameters representing the second harmonic is outweighed by the ambiguous and nonphysical meaning of the additional parameters. An attempt to add such complexity is considered to be unwarranted.

Moreover, each parameter has a physical meaning up to the first harmonic:

- a represents the average value of the quantity over the whole year (Appendix F, Section F1.1.2)
- b_1 represents the amplitude of (seasonal) variation of the quantity during the year
- θ_1 is the phase shift. In other words, it controls the date when the maximum value is obtained during the year.

The second harmonic parameters do not have a direct physical meaning because they represent a correction on the residual.

Therefore, it was decided to limit the representation of daily precipitation over the year with a 2nd order Fourier series (the average and one harmonic). The estimate reasonably represents the variation of daily precipitation over the year.

7.1.1.2[a]. Comparison of Mean Annual Precipitation (MAP)

No change.

7.1.1.3[a]. Present-Day Precipitation Comparison

No change.

7.1.1.4[a]. Monsoon Precipitation Comparison

No change.

7.1.1.5[a]. Glacial Transition Precipitation Comparison

No change.

7.1.2[a]. Evapotranspiration and Storage

No change.

7.1.2.1[a]. Lysimeter Simulations at the Nevada Test Site

Two weighing lysimeters were installed in Area 5 Radioactive Waste Management Site of the NTS in 1994 to conduct water balance studies. The lysimeters are located in northern Frenchman Flat (northern part of Mojave Desert). The lysimeter coordinates are: 36° 51' 9.13" (latitude) and 115° 56' 56.06" (longitude), and the lysimeter site elevation is 976 m (Scanlon et al. 2005 [DIRS 175977]).

There are a number of studies where the NTS lysimeter data were used for various water balance analyses, including calibration of flow models. The results of these studies are reported by Desotell et al. (2006 [DIRS 176858]), Scanlon et al. (2005 [DIRS 175977]), Levitt et al. (1999 [DIRS 177521]), and Levitt et al. (1996 [DIRS 163183]).

The long-term mean annual precipitation in this area reported by Desotell et al. (2006 [DIRS 176858]) is 125 mm. The mean annual precipitation calculated using the lysimeter data is 125.5 mm (Di Sanza 2006 [DIRS 178797]; Output DTN: SN0701T0502206.037, file *NTSLysimeter.xls*), which is close to the long-term average. The mean annual temperature during the period of observation was 15.7°C (Output DTN: SN0701T0502206.037, file: \Welcome to Massif\Massif\Validation Analyses\Lysimeter*NTSLysimeter.xls*). In only 1.3% of the observation time was the mean daily temperature below 0°C. The average daily wind speed during the period of observation was 2.8 m/s (see Appendix J for details).

One lysimeter is vegetated with the creosote bush, four-wing salt bush, and annual grasses at the approximate density of the surrounding landscape (Desotell et al. 2006 [DIRS 176858]). Another lysimeter is maintained under the bare soil conditions. Each lysimeter is a 2-m- by 4-m- by 2-m-deep steel tank filled with native alluvium at a bulk density of about 1.5 kg/m^3 (Scanlon et al. 2005 [DIRS 175977]). The alluvium was classified as a well- to poorly graded sand with silt and gravel (Unified Soil Classification System) with approximately 70% sand, 20% gravel,

and 10% fines. A schematic of one lysimeter is shown in Figure 7.1.2.1-1[a] (from Figure 7 in supporting information to Scanlon et al. 2005 [DIRS 175977]).

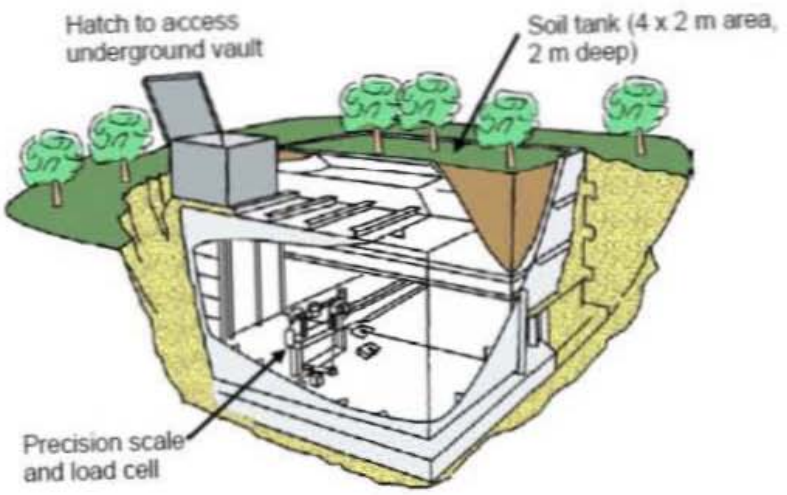

NOTE: Reproduced from Figure 7 in supporting information to Scanlon et al. 2005 [DIRS 175977].

Figure 7.1.2.1-1[a]. NTS Weighing Lysimeter Schematic

Eighteen core samples were collected throughout the lysimeter depth profile in 10-cm increments. The measured soil hydraulic properties are reported by Desotell et al. (2006 [DIRS 176858]) and include:

- Saturated hydraulic conductivity (geometric mean): 14 cm/hr
- Residual moisture content: 0.04 m^3/m^3
- Porosity: 0.357 m^3/m^3
- van Genuchten parameter alpha: 0.0328 cm^{-1}
- van Genuchten parameter n: 1.57.

Based on these parameters, the field capacity is 0.117 m^3/m^3 (calculated using pressure of −1/3 bar), and wilting point is 0.044 m^3/m^3 (calculated using pressure of −60 bars). Since a higher pressure may be more appropriate for the coarse grained textured soils (up to −1/10 bars) than the pressure of −1/3 bars (medium textured soils), the bare soil lysimeter storage data were analyzed during periods with heavy precipitation over a few or more consecutive days. The largest storage value was 277.3 mm. This corresponds to the moisture content of 0.139 m^3/m^3 and a pressure of −2/10 bars. This is consistent with the pressure range of −1/3 bars to −1/10 bars at which field capacity is calculated.

The lysimeter storage observations are available for the period of time from March 3, 1994 until December 31, 2004 from Di Sanza (2006 [DIRS 178797]). However, the vegetated lysimeter was irrigated for about 6 months to establish the vegetation cover and the irrigation rates are not available, and it took about 1.5 years for the transplanted vegetation to equilibrate with moisture conditions in the lysimeter box. Consequently, the period of observations for the vegetated lysimeter was considered from October 1, 1995 until December 31, 2004. The MASSIF model can be run only for a whole number of the water years. To satisfy this requirement, the bare soil

lysimeter observations used began on October 1, 1994. Figure 7.1.2.1-2[a] shows the observation data and precipitation data for the NTS lysimeter site.

Analysis of precipitation data (see Appendix J for details) showed that 5% (bare soil lysimeter) to 10% (vegetated lysimeter) of observations have daily increases in storage that exceed daily precipitation. The maximum difference between the storage increase and precipitation was about 4 mm. Most of these observations are related to the high intensity precipitation events. Rain gauges are subject to under-measurement caused by (1) splash out of drops, (2) blow-by of drops due to venturi effects, and (3) evaporation of intercepted drops along the sides of the collector (Sevruk 1992 [DIRS 177480]). Consequently, some of the differences between precipitation data and lysimeter gains may have been caused by under-measurement by the precipitation gauge. The inaccuracy in precipitation measurements could be at least 4 mm. Since the ET is calculated as the difference between precipitation and storage, the 4-mm error in precipitation measurement will result in the corresponding error in the ET estimate.

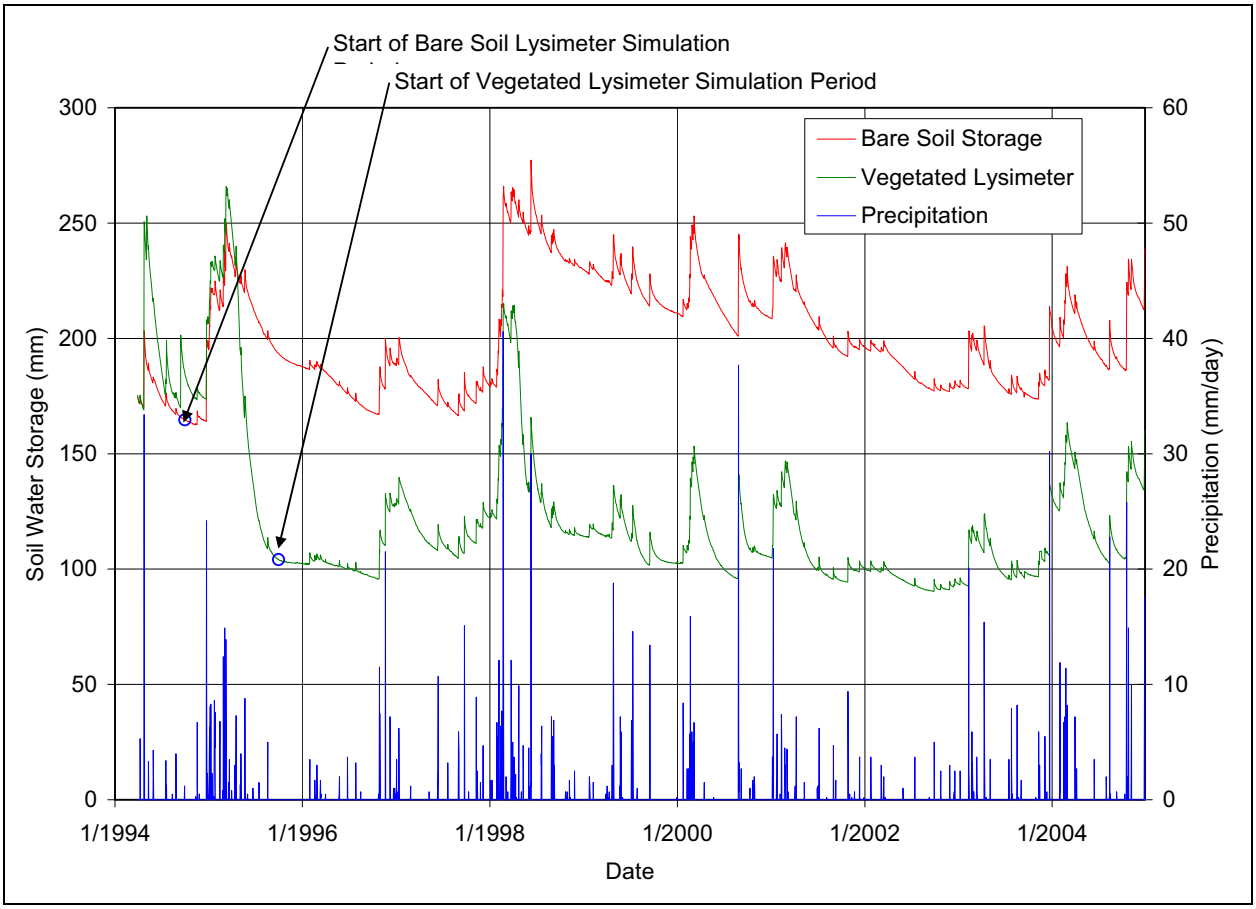

Source: Di Sanza 2006 [DIRS 178797]; compiled in Output DTN: SN0701T0502206.037, file: \Welcome to Massif\Massif\Validation Analyses\Lysimeter*NTSLysimeter.xls*.

Figure 7.1.2.1-2[a]. Observed Daily Water Storage and Precipitation at the NTS Lysimeter Site

The MASSIF input parameters for the lysimeter simulations were defined in accordance with NTS site-specific information, when available. For certain parameters, NTS site-specific data were not available and parameter values were estimated using an inverse modeling approach

described below and in Appendix J. The following MASSIF parameters cannot be specified based on the data available for the NTS lysimeter site:

- Diffusive evaporation parameter, K_{c_min}
- Canopy fraction, f_c
- C_{kcb} coefficient representing the slope of the NDVI-K_{cb} regression line (see Appendix E for details).

The values of these three parameters were estimated by minimizing the difference between the observed and calculated storages in both lysimeters. The following objective function $F1_{obj}$ was used in the conjugate gradient minimization procedure in MathCAD.

$$F1_{obj}(K_{c\_min}, f_c, C_{kcb}) = [\sum(BS^{obs}_i - BS^{cal}_i)^2 + \sum(V^{obs}_j - V^{cal}j)^2]/(N_{bs}+N_v) \qquad \text{(Eq. 7.1.2.1-2[a])}$$

$$I = 1, N_{bs} \text{ and } j = 1, N_v$$

where BS^{obs}_i and BS^{cal}_i are observed and calculated bare soil lysimeter storage during the simulation day i; V^{obs}_j and $V^{cal}j$ are observed and calculated vegetated lysimeter storage during the simulation day j; N_{bs} is the number of days in the bare soil lysimeter data set; and N_v is the number of days in the vegetated lysimeter data set. As it was explained above, the bare soil lysimeter data set is from 10/01/1994 to 12/31/2004 (N_{bs} = 3,745), and the vegetated lysimeter data set is from 10/01/1995 to 12/31/2004 (N_v= 3380).

In calculating bare soil lysimeter storage, the transpiration parameters p (depletion factor for computing readily available water), C_{kcb}, and f_c were set to zero to represent bare soil conditions. In calculating vegetated lysimeter storage, parameter p was set to 0.65 (Sections 6.3.3 and 6.3.4) and C_{kcb} and f_c were the objective function parameters as defined by Equation 7.1.2.1-2[a].

The results of the minimization are:

- K_{c_min} = 0.0135
- f_c = 0.26
- C_{kcb} = 2.4
- $F1_{obj}$ = 137.92 mm^2.

Based on the obtained objective function value, the overall goodness of fit is 11.74 mm for both lysimeters. The estimated parameter values were used to calculate the root mean square errors for each lysimeter. The calculated mean root square errors are 11.63 and 11.87 mm (or about 9% of the mean annual precipitation) for the bare soil and vegetated lysimeters, respectively. Taking into account that the possible inaccuracy in storage measurements is at least 4 mm, the obtained goodness of fit is reasonable for both lysimeters. These root mean square errors are comparable to the ones reported by Desotell et al. (2006 [DIRS 176858]). The NTS lysimeters were modeled by Desotell et al. 2006 [DIRS 176858]) with UNSAT-H (Fayer 2000 [DIRS 177499]), which is a soil physics based code similar to HYDRUS-1D (Sections 6.2.4.1, and 7.2.2[a]) in its capability to model variably-saturated flow, except it allows for simulating vapor phase. Mean root square errors reported are 12 mm (bare soil) and 4 mm (vegetated). However, to obtain this fit, the

potential evaporation was reduced by 50% during the wintertime. No adjustment to reference ET was done in MASSIF calculations to improve the curve fitting.

The only interval with a noticeable difference between observed and calculated storages is during February through April of 1998. This corresponds to a series of large precipitation events that resulted in a significant increase in storage in both lysimeters (Figure 7.1.2.1-2[a]). The calculated increase in storages is about 40 mm smaller than was observed (Figure 7.1.2.1-3[a]). The UNSAT-H curves (Desotell et al. 2006 DIRS 176858], Figures 3 and 4) also do not reproduce the observed increase.

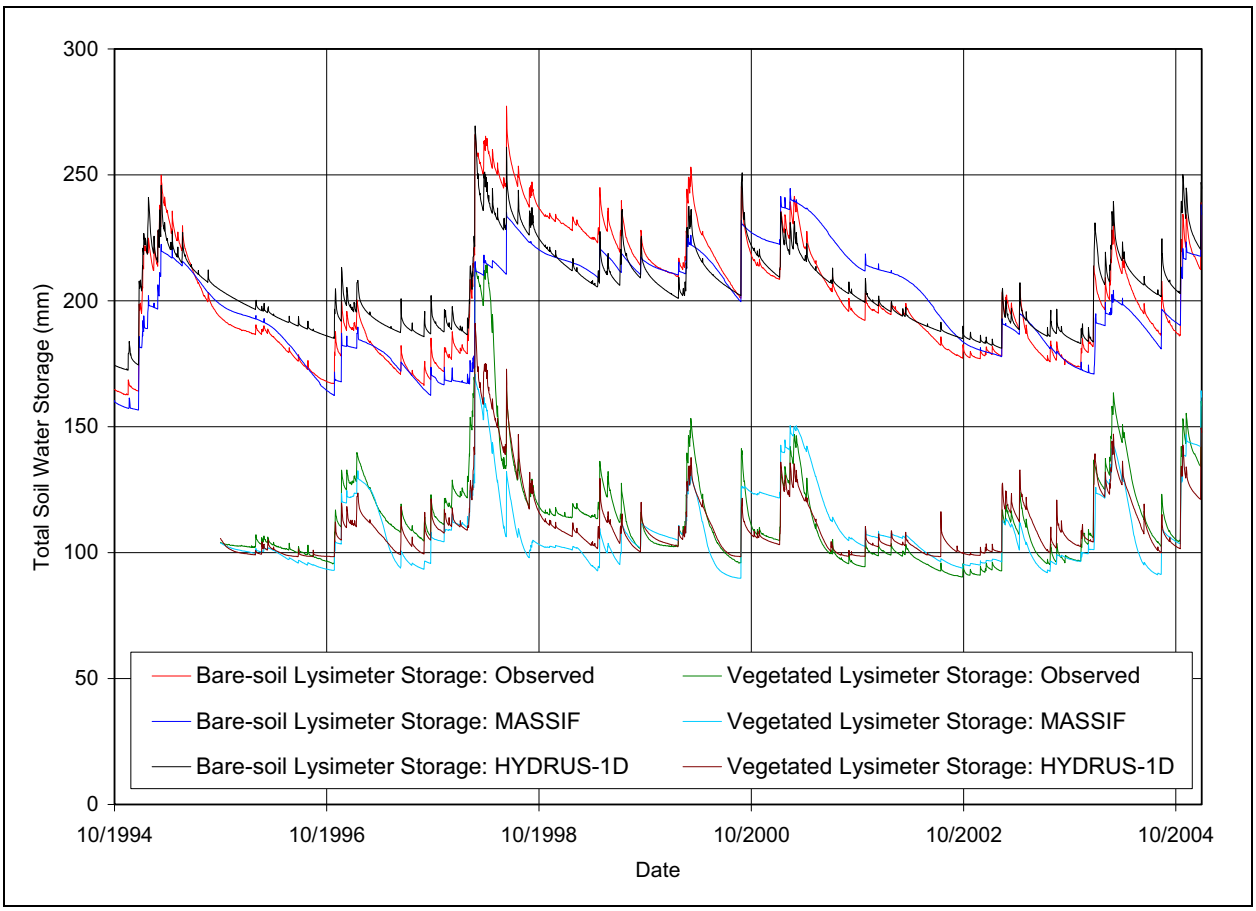

Source: Di Sanza 2006 [DIRS 178797] (lysimeter data); Validation Output DTN: SN0607T0502206.016 (Hydrus-1D data); Output DTN: SN0701T0502206.037, file: \Welcome to Massif\Massif\Validation Analyses\Lysimeter*NTSLysimeter.xls*.

Figure 7.1.2.1-3[a]. Simulation of Soil Water Storage in the NTS Lysimeters

Some differences between the observed and calculated storages are also seen when soil water storage decreases from spring to fall. The observed storages tend to decrease more rapidly than the simulations. Desotell et al. (2006 DIRS 176858]), attributes this to the dynamic response of the plant growth that is not simulated by the model. However, the same tendency is observed in the bare soil lysimeter as well. Also, the difference between the decreasing portions of the storage curves are more pronounced in the case of the bare soil lysimeter. This may indicate evaporation at depth in the lysimeter that is a phenomenon of the lysimeter but not of the natural

conditions. This can be caused by heat transfer along lysimeter walls from the surface and through lysimeter walls from the subterranean lysimeter chamber. This phenomenon is described by Howell et al. (1991 DIRS 177190]) in relation to the steel container weighing lysimeters. Other aspects of this phenomenon are given by Campbell et al. (1991 DIRS 177100]) and Kirkham et al. (1991 DIRS 177191]). However, the effects of this phenomenon cannot be bounded quantitatively in the absence of the soil profile temperature data. In contrast, it is possible that the lysimeter geometry is limiting rather than enhancing evaporation by preventing the slow upward evaporative flow of water from depths greater than the lysimeter depth.

The bare soil and vegetated lysimeter storages were also simulated with HYDRUS-1D. The same mean properties of the soil and climate data were used in the calculations (see Appendix J for details). The results of these simulations are shown in Figure 7.1.2.1-3[a]. The mean root square errors obtained with HYDRUS-1D are 10.6 mm and 9.2 mm for bare soil and vegetated lysimeters, respectively. The same tendencies as described above in the differences between the calculated and observed storages can be noted. The mean root square errors between the storages calculated by HYDRUS-1D and MASSIF are 10.9 mm and 9.0 mm for the bare soil and vegetated lysimeters, respectively. This falls within the same range as the mean root square errors described above. The runoff and infiltration calculated by HYDRUS-1D were equal to zero (or negligibly small) during the entire period of observation in both lysimeters as well.

An important component of ET is transpiration. The transpiration in MASSIF is modeled using the basal crop coefficient (K_{cb}) concept (Allen et al. 1998 [DIRS 157311]). As described in Sections 6.3.3 and 6.3.4 and Appendix E, the daily K_{cb} values are calculated from daily *NDVI'* values using the following formula (Equation 7.1.2.1-3[a]):

$$K_{cb}=(C^{0}_{kcb}+C_{kcb} \times NDVI') \times P_i/P_{1998} \times PVR \qquad \text{(Eq. 7.1.2.1-3[a])}$$

where C^{0}_{kcb} and C_{kcb} are intercept and slope of the regression line approximating the K_{cb} data plotted against the *NDVI'* data (Appendix E); P_i is the total annual precipitation for the year in consideration; P_{1998} is the total annual precipitation in 1998 equal to 378 mm (representing the wet year); and *PVR* is the potential vegetation response. C^{0}_{kcb} and C_{kcb} were developed based on the K_{cb} and *NDVI'* values measured at the site. For the Present-Day climate, nominal values for these parameters are −0.05 and 9.7, respectively (Section 6.5.3.7). The daily *NDVI'* values used in MASSIF are tabulated for each day of the year and different combinations of the slopes and azimuths (see Appendix D for details). The base *NDVI'* values are used for the slopes less than 5º, and no azimuth correction is required for such slopes.

Regression coefficients C^{0}_{kcb} and C_{kcb} were set equal to 0 for the bare soil lysimeter. C_{kcb} was a parameter of the vegetated lysimeter in the optimization scheme described above. C^{0}_{kcb} is very small and was set to 0 for vegetated lysimeter as well. No information was available on the lysimeter site-specific *PVR* value, which is the MASSIF input parameter. The *PVR* was set equal to 1. The optimization scheme estimates the value of the lumped transpiration parameter equal to $C_{kcb} \times PVR$. Thus, the actual values of *PVR* can be set to any arbitrary values without affecting the estimation of the lumped parameter. The estimation of this lumped parameter is achieved by adjusting $C_{kcb,}$ as a result of the manner in which the MASSIF calculation is implemented.

Shown in Figure 7.1.2.1-4[a] are daily K_{cb} and *NDVI'* values for the wet, average, and dry water years. These are the actual values measured at the Yucca Mountain site that include the water stress impacts caused by dry soil (see Appendix D for details on these data). The water stress impacts are maximal for the dry year and minimal for the wet year. The water years representing wet, average, and dry years are 1993, 1991, and 1990, respectively. The K_{cb} data used are for these 3 years. The *NDVI'* data (taken in 1998, 2001, and 2002) were corrected (Appendix E) to represent the same years. The *NDVI'* data were scaled using a nominal regression slope of 9.7 (the details on how this slope was calculated are provided in Section 6.5.3.7), so they can be directly compared to the K_{cb} data.

The values based on the Yucca Mountain site-specific measurements are compared to the values calculated by MASSIF using Equation 7.1.2.1-3[a] above. The daily *NDVI'* values in this equation are base *NDVI'* values from the look-up table in MASSIF. P_{1998} is 378 mm. The precipitation (P_i) at the lysimeter site in 1998 (wet year), 2001 (average year), and 2002 (dry year) was 256, 122, and 31 mm, respectively. The *PVR* was set equal to 1, and C_{kcb} estimated from the optimization scheme is 2.4. The daily K_{cb} values calculated by MASSIF are shown in Figure 7.1.2.1-4[a] as "vegetated lysimeter K_{cb}" (the calculations are in the worksheet "NDVI" in *NTSLysimeter.xls* file located in folder \NTS in Validation Output DTN: SN0607T0502206.016. They are in good agreement with the *NDVI'* values measured for the *Larrea-Ambrosia* (*LA*) association. This is the predominant association for the lower elevations and bajadas of the Yucca Mountain site (Appendix D). *LA* association includes (Appendix J) the following dominant species: *Ambrosia dumosa*, *Larrea tridentata* (creosotebush), *Menodora spinescens* (spiny menodora), and *Lycium pallidum*. The similar species are present at the vegetated lysimeter site (Scanlon et al. 2005 [DIRS 175977]).

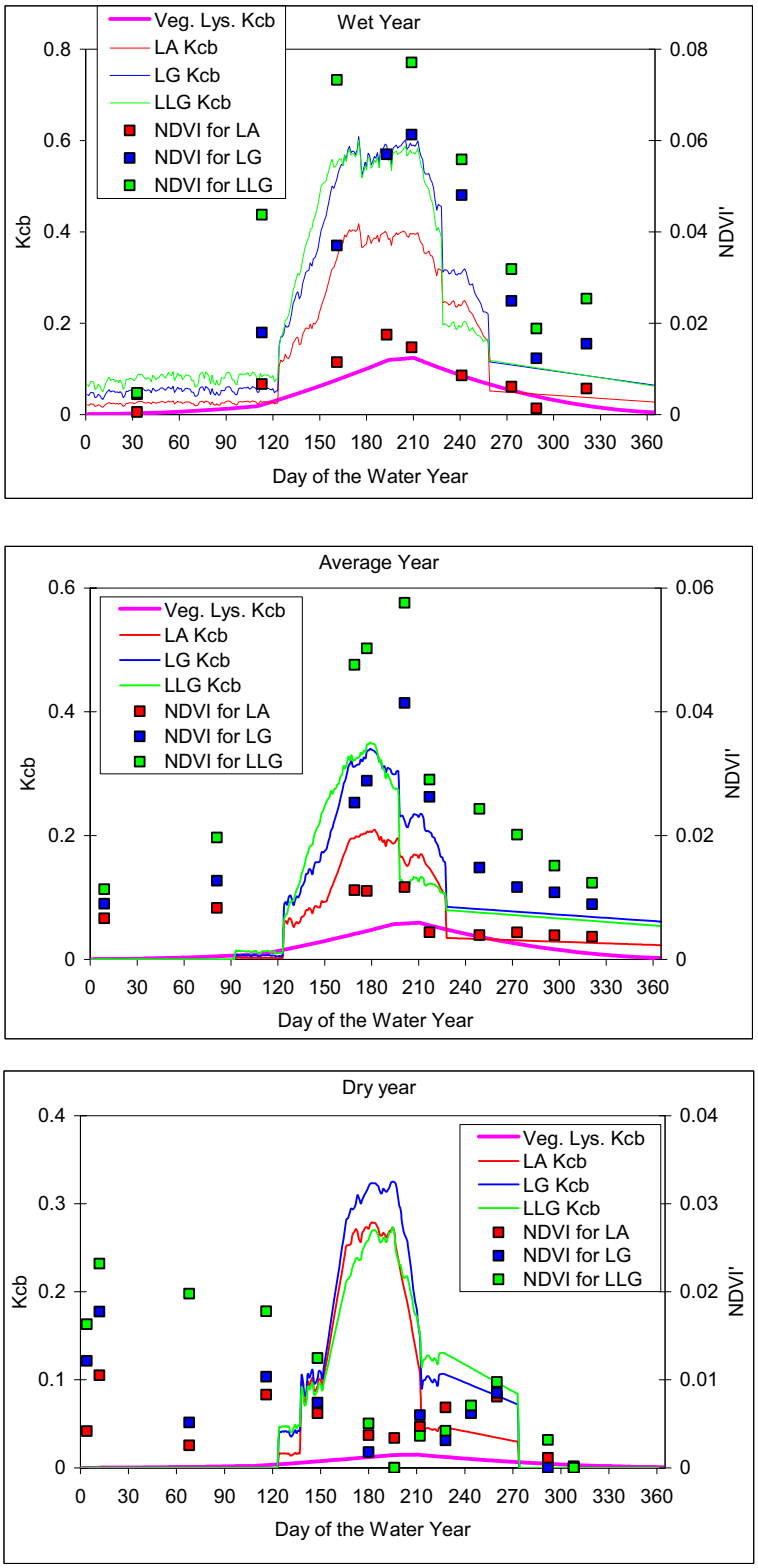

Source: Validation Output DTN: SN0607T0502206.016, file: NTS*NTSLysimeter.xls*.

Figure 7.1.2.1-4[a]. Comparison between the Measured K_{cb} and NDVI Values and Calculated Vegetated Lysimeter K_{cb} Values for the Different Water Years

Another parameter related to the vegetated lysimeter is the vegetation (canopy) fraction parameter f_c. It was assumed that f_c is constant for the entire period of simulation. As estimated in Appendix D, the vegetation fractions of *LA* association are 0.21, 0.11, and 0.15 for the wet, dry, and average years, respectively. The estimated f_c is 0.26 is close to the value for the wet year. The parameter K_{c_min} estimated value (0.0135) is within the ranges of K_{c_min} measured for *LA* association as described in Appendix D (0 for dry and average and 0.016 for the wet water years).

Summary of Lysimeter Simulations at NTS:

- The simplified water balance approach incorporated in MASSIF allows for adequate simulation of water storage and ET in both bare soil and vegetated NTS lysimeters.
- The ET parameters such as K_{cb}, K_{c_min}, and f_c estimated for the bare soil and vegetated lysimeters using MASSIF are in good agreement with the experimental data obtained for the plant association similar to the one present at the lysimeter site.
- The MASSIF results are comparable to the results obtained with physics-based models such as UNSAT-H (Desotell et al. 2006 [DIRS 176858]).
- MASSIF's ability to reproduce the lysimeter water storage over 10 years (bare soil) and 9 years (vegetated) confirms that the most important processes are represented correctly.
- The same tendencies in the differences between the observed storage and storage calculated with other models were also found using MASSIF. These tendencies are consistent with the ones described in the other studies related to the NTS lysimeters (e.g., Desotell et al. 2006 [DIRS 176858]). These differences may indicate evaporation at depth in the lysimeters that is a phenomenon of the lysimeter but not of the natural conditions.

7.1.2.2[a]. Lysimeter Simulations at the Reynolds Creek Experimental Watershed

The Reynolds Creek Experimental Watershed (RCEW) data were collected by the U.S. Department of Agriculture (USDA) Northwest Watershed Research Center (NWRC), in Boise, Idaho. The data are available from *ftp.nwrc.ars.usda.gov*. The data used in this analysis were obtained directly from USDA NWRC. The information included in the CD provided by the USDA NWRC can be found in DTN: SN0608T0502206.020 [DIRS 179875]. There are a series of articles published in the Water Resources Research Journal, vol. 37, No. 11 in November 2001 summarizing research goals and the data collection efforts at the RCEW. The series includes Seyfried et al. (2001 [DIRS 177515], 2001 [DIRS 177501], 2001 [DIRS 177505], 2001 [DIRS 177506]), Marks (2001 [DIRS 177512]), Marks et al. (2001 [DIRS 177504]), Slaughter et al. (2001 [DIRS 177354]), Pierson et al. (2001 [DIRS 177503]), Hanson et al. (2001 [DIRS 177509]), and Hanson (2001 [DIRS 177508]).

RCEW occupies 239 km^2 in the Owyhee Mountain region located in the southwestern Idaho, 80 km southwest of Boise (Hanson et al. 2001 [DIRS 177509]). Two sets of soil lysimeters were installed at RCEW. The lysimeter used in this analysis is located at the Lower Sheep Creek climate station, lysimeter Lower Sheep Creek West (LSCW). The details are presented in Appendix J.

The mean precipitation at the lysimeter site is 349 mm (Wight et al. 1986 [DIRS 177104]), and the mean annual temperature is 7.4°C (Wight et al. 1990 [DIRS 177113]). About 21% of precipitation comes in the form of snow. These are wetter and cooler conditions than in Spokane (mean precipitation 325 mm and mean annual temperature 8.5°C) an analogue site representing the upper bound of the glacial transition climate.

The LSCW lysimeter is located at: 43° 08' 24.088" latitude, and 116° 43' 57.732" longitude, and the elevation is 1,656 m (DTN: SN0608T0502206.020 [DIRS 179875]). The lysimeter diameter is 1.47 m and depth is 1.22 m. The lysimeter contains native undisturbed soil. The upper 0.1 m is loam. It is underlain by a 0.48-m-thick argillic horizon with up to 50% clay. The remaining cross section is sandy loam. The soil samples were taken at the neutron tubes 127707, 127807, and 127907 located within the lysimeter or next to it. Nine soil horizons were characterized down to the depth of 1.83 m. The soil layer is underlain by the basalt bedrock (Wight et al. 1986 [DIRS 177104]). The soil property average values weighted by the horizon thickness within the 1.22-m lysimeter depth are as follows (see Appendix J for details):

- Porosity is 0.47 m^3/m^3
- Field capacity corresponds to a water content of 0.33 m^3/m^3 at the pressure of −1/3 bar
- Wilting point corresponds to a water content of 0.19 m^3/m^3 at the pressure of −15 bars (no measurements at −60 bars are available).

The vegetation at the lysimeter site is dominated by low sagebrush which grows to a height of about 0.3 m and is accompanied by perennial bunchgrasses and forbs (Seyfried et al. (2001 [DIRS 177515]). The lysimeter site contained a mature shrub along with the naturally associated plants with the slightly higher vegetation density than the surrounding landscape.

The climate data include precipitation and temperatures collected at the climate station 12 × 07 located next to the lysimeter site. The period of time from October 1, 1977 through September 30, 1984 was selected based on the availability of the soil storage data. The observation data used in this simulation are changes in water storage values during no snow season measured in the lysimeter from April 1978 through September 1984. The changes in storage were converted to the total soil water storage values using initial storage calculated for the point in time when the moisture within the profile was measured in the neutron tubes (see Appendix J for details). These data are shown in Figure 7.1.2.2-1[a].

The lysimeter calibration is described by Seyfried et al. (2001 [DIRS 177515]). As concluded in this publication, the lysimeter observations have the precision of ±8 mm.

The MASSIF input parameters for the lysimeter simulations were defined in accordance with the site-specific information. The modeling set up is described in Appendix J. The following MASSIF parameters were estimated from the optimization scheme described below:

- Diffusive evaporation parameter, K_{c_min}
- Canopy fraction, f_c
- Coefficient representing the slope of the $NDVI'$-K_{cb} regression line, C_{kcb}
- Field capacity, θ_f.

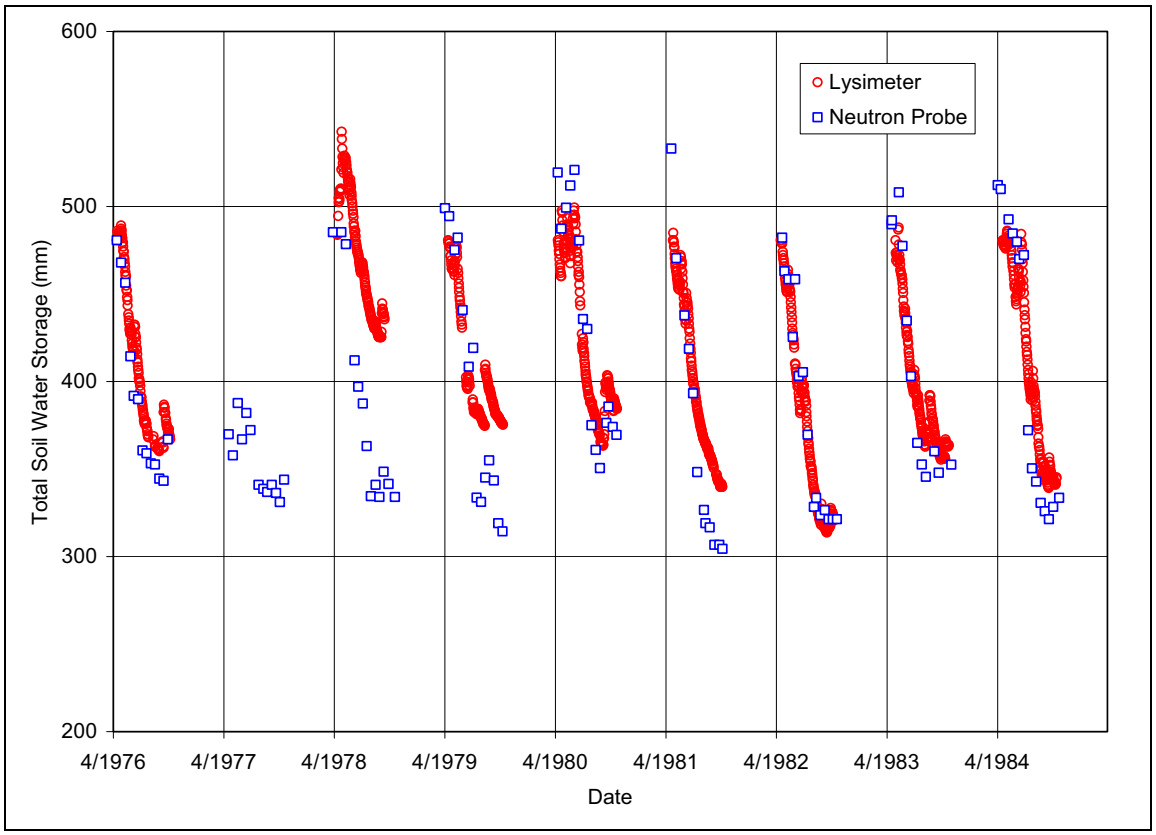

Source: Validation Output DTN: SN0607T0502206.016, *RCEWLysimeter.xls*.

Figure 7.1.2.2-1[a]. Total Soil Water Storage Calculated Using Daily Change-in-storage from LSCW and Integrated Water Content from Neutron Probe Measurements

The values of these four parameters were estimated by minimizing the difference between the observed and calculated soil water storage. The following objective function $F3_{obj}$ was used in the conjugate gradient minimization procedure in MathCAD:

$$F3_{obj}(K_{c\_min}, f_c, C_{kcb}, \theta_f) = [\sum(S^{obs}_i - S^{cal}_i)^2]/N \qquad \text{(Eq. 7.1.2-4[a])}$$

where S^{obs}_i and S^{cal}_i are observed and calculated lysimeter storage during the simulation day i on which the observation data is available, and N is the number of observations (N=1179). The lysimeter data were not recorded every day.

The results of the minimization and subsequent manual adjustment are:

- $K_{c\_min} = 0.0$
- $f_c = 0.7$
- $C_{kcb} = 13.685$
- $\theta_f = 0.415$
- $F1_{obj} = 1037.81$.

Based on the obtained objective function value, the overall goodness of fit is 32.22 mm (9.5% of the mean annual precipitation). The goodness of fit is very similar to the one obtained for the NTS site, which is about 9% of the mean annual precipitation. Considering that the measurement precision is ±8 mm, this is a reasonably good fit. The results of minimization are shown in Figure 7.1.2.2-2[a]. The storage calculated based on the neutron probe measurements of moisture content within the soil profile is shown in Figure 7.1.2.2-2[a] in addition to the soil water storage measured in the lysimeter (see Appendix J for details). The storage calculated with MASSIF is well within the boundaries of the observed values.

The lysimeter site was designed to exclude run-on and runoff. The intent was also to exclude or minimize deep percolation. Very little drainage has probably occurred from the lysimeter bottom, but the timing of these small events is not known (Seyfried et al. 2001 [DIRS 177515]). Runoff and run-on calculated by MASSIF was zero. The mean annual infiltration calculated by MASSIF is 7 mm, which is 2% of the mean annual precipitation (349 mm). The actual site-specific infiltration is unknown. However, the infiltration for the rangeland in this area is considered to be around 4% (Wight et al. 1986 [DIRS 177104]). MASSIF-calculated infiltration is consistent with this estimate and the site conceptual model (little drainage). Since infiltration, if any, constitutes a very small portion of the overall water balance, it should not affect the estimates of the other water balance constituents, such as ET.

The RCEW lysimeter storage was also simulated with HYDRUS-1D. The same mean properties of the soil and climate data were used in the calculations (see Appendix J for details). The results of these simulations are shown in Figure 7.1.2.2-2[a]. The mean root square error obtained with HYDRUS-1D is 42.3 mm (12% of the mean annual precipitation). The same tendencies as described above in the differences between the calculated and observed storages can be noted. The mean root square error between the storages calculated by HYDRUS-1D and MASSIF is 33.57 mm. The runoff calculated by HYDRUS-1D is zero during all period of observation. The mean annual infiltration is 3 mm (0.9% of precipitation), which is close to the value calculated by MASSIF.

The monthly averages of daily actual ET calculated by MASSIF for 1978 and 1979 were compared to the data presented by Wight et al. (1986 [DIRS 177104], Table 2). This is demonstrated in Figures 7.1.2.2-3[a] and 7.1.2.2-4[a]. The calculated and measured ET values are in reasonably good agreement. The sum of the monthly averages of daily actual ET for the six months in 1978 calculated by MASSIF and presented by Wight et al. (1986 [DIRS 177104], Table 2) are 10.48 and 9.84 mm, respectively. The sum of the mean monthly averages of daily ET for the six months in 1979 calculated by MASSIF and presented by Wight et al. (1986 [DIRS 177104], Table 2) are 7.48 and 8.70 mm, respectively.

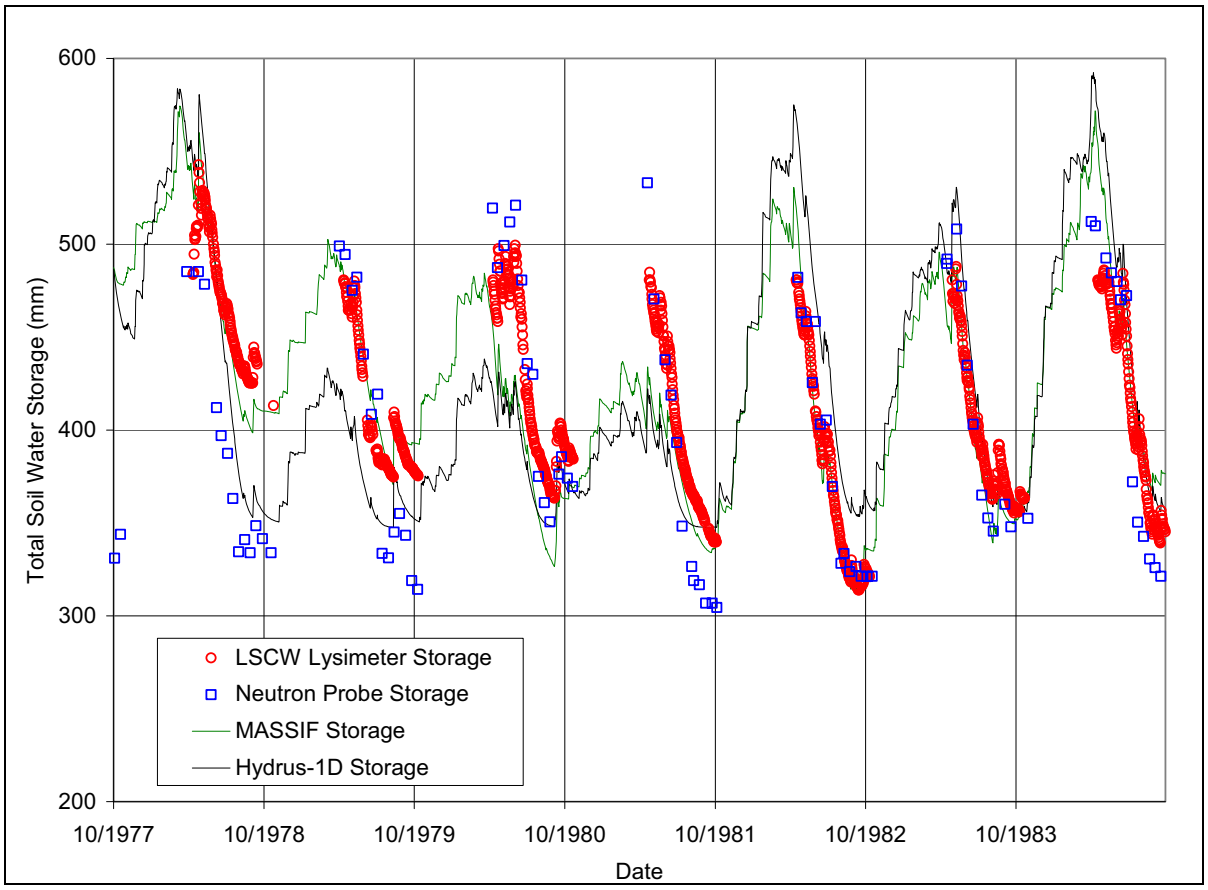

Source: DTN: SN0608T0502206.020 [DIRS 179875] (lysimeter and neutron probe data); Validation Output DTN: SN0607T0502206.016 (HYDRUS-1D data); Output DTN: SN0701T0502206.037, file: \Welcome to Massif\Massif\Validation Analyses\Lysimeter*RCEWLysimeter.xls*.

Figure 7.1.2.2-2[a]. Simulation of Soil Water Storage in RCEW Lysimeter

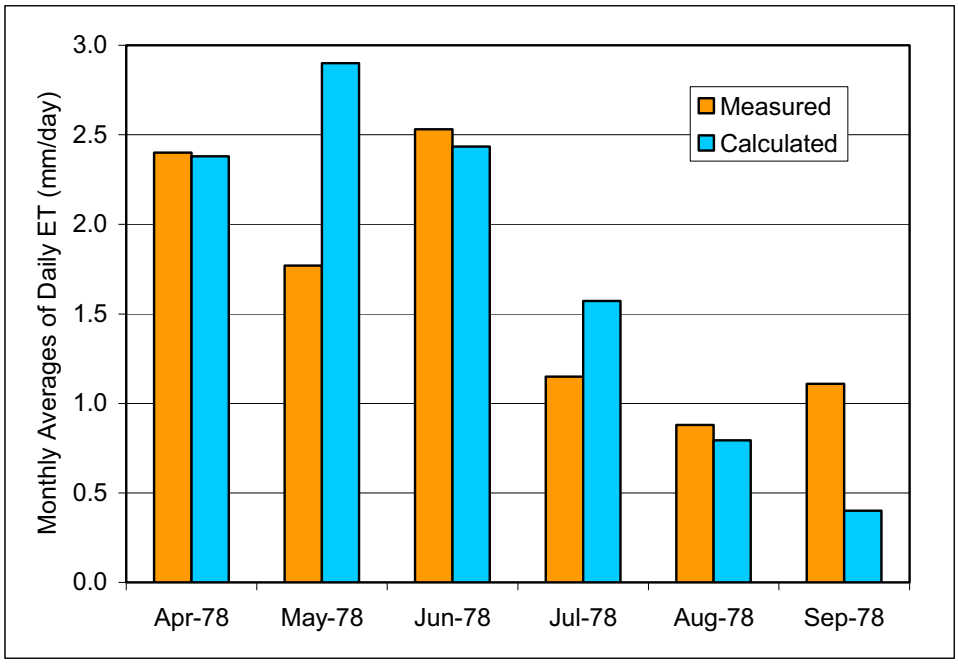

Source: Output DTN: SN0701T0502206.037, file: \Welcome to Massif\Massif\Validation Analyses\Lysimeter*Reynolds Creek.xmcd*, p. 15, Embedded Excel file, sheet1.

Figure 7.1.2.2-3[a]. 1978 Average Monthly Rates of Actual Evapotranspiration at RCEW

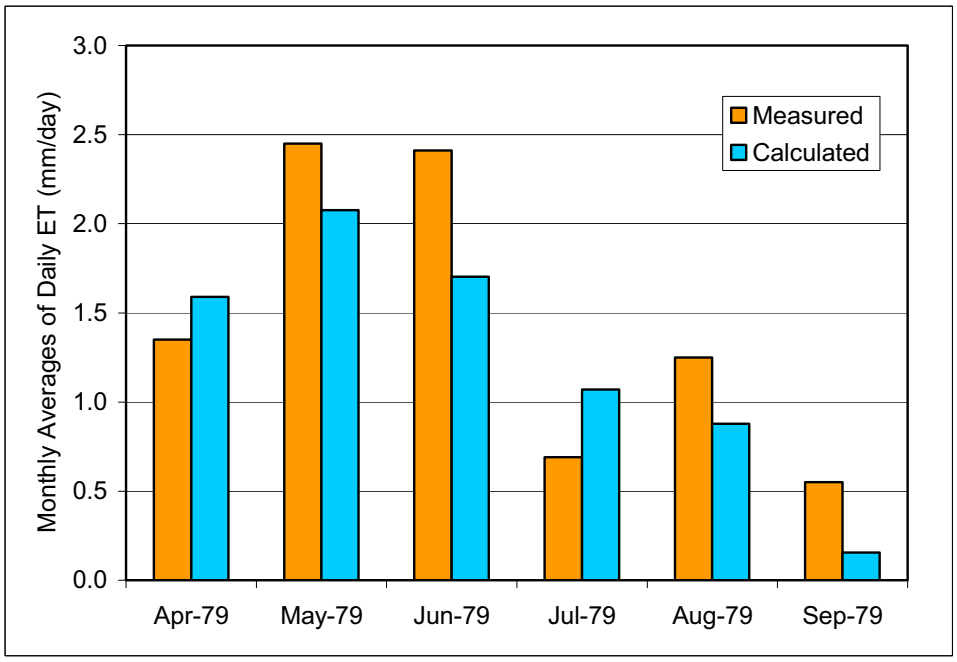

Source: Output DTN: SN0701T0502206.037, file: \Welcome to Massif\Massif\Validation Analyses\Lysimeter\ *Reynolds Creek.xmcd*, page 15, Embedded Excel file, sheet 1.

Figure 7.1.2.2-4[a]. 1979 Average Monthly Rates of Actual Evapotranspiration at RCEW

The field capacity estimated from the lysimeter modeling is 0.415. This falls into the range of the site-specific field capacity values of 0.28 to 0.42 obtained for the different soil horizons (Appendix J). The maximum measured lysimeter storage was 542.7 mm. This corresponds to the field capacity of 0.44. The actual soil profile is heterogeneous and the effective soil properties of the equivalent homogeneous profile are not known. The effective soil properties may be different from the weighted average values. In this case (effective field capacity is equal to the clay and clay loam field capacity), the amount of water that can be stored in the clay and clay loam layers controls the lysimeter storage.

The estimated K_{c_min} value is 0. This is consistent with the conceptual model of ET (Sections 6.3.3 and 6.3.4).

There are no daily K_{cb} data at the site. The mean K_{cb} value at the site for the growing season estimated for the site by Wight et al. (1990 [DIRS 177113]) is 0.85 (standard deviation is 0.06). The mean K_{cb} during the growing period over the seven years of observations (1978 through 1984) calculated using estimated C_{kcb} = 13.685 is 0.77. This is consistent with the estimate by Wight et al. (1990 [DIRS 177113]).

The vegetation cover f_c estimated for the site is 0.7. The estimate of the mean vegetation cover including live plants and litter at the site over the 11 years of observations provided by Wight et al. (1986 [DIRS 177104]) is 50% or 0.5.

Summary of Lysimeter Simulations at RCEW:

- The MASSIF water balance approach was capable of reproducing the changes in storage over the seven years of observations at the RCEW lysimeter site. This site is considerably different from the NTS site. The climate is wetter and cooler with 21% of precipitation being snow, and the soils are finer with the smaller permeability and significantly higher field capacity and wilting point. The vegetation cover is twice as dense, and the plants species are different.

- The soil properties, ET parameters, and infiltration estimated using MASSIF for the RCEW lysimeter fall within the site-specific ranges obtained from the literature.

- The MASSIF and HYDRUS-1D results are fairly consistent. The same tendencies in differences between the observed and calculated storages were obtained with MASSIF and HYDRUS-1D.

- The infiltration predicted by MASSIF is in good agreement with the infiltration predicted by HYDRUS-1D.

- The MASSIF ability to adequately model RCEW lysimeter site confirms that the physical processes incorporated in MASSIF are applicable to a wide range of condition. Present-day and future climates can thus be accurately represented.

7.1.3[a]. Run-on/Runoff

No change with the exception of a source DTN change and a NOTE added to Figure 7.1.3.1[a].

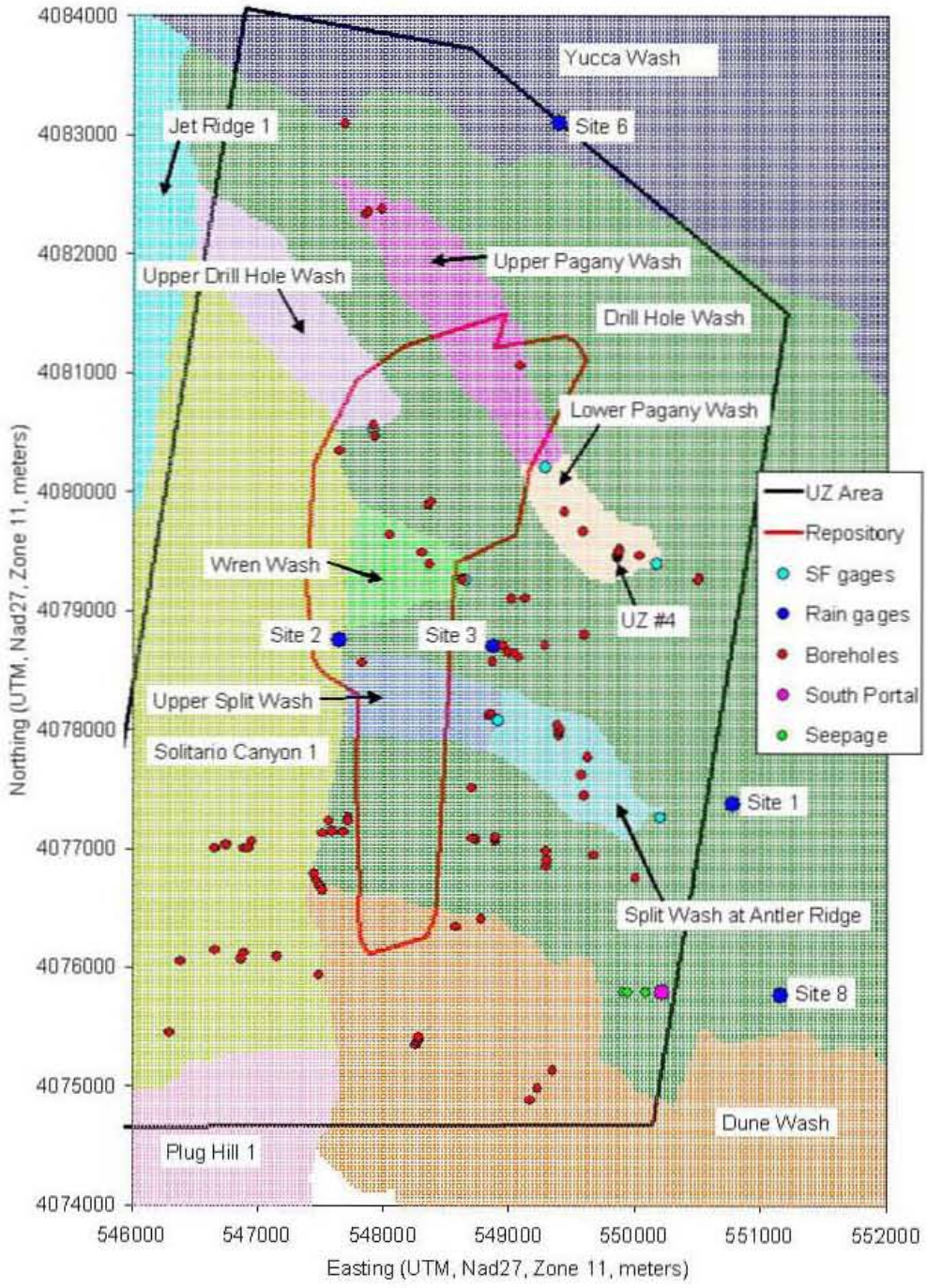

Sources: Output DTNs: SN0606T0502206.011 (Watersheds coordinates); SN0711FTPRNUZB.003 (UZ flow model and Repository areas). Inputs: MO0601GSCSPINF.000 [DIRS 177236] (Locations of streamflow gauges); MO9906GPS98410.000 [DIRS 109059] (Locations of neutron logging boreholes); MO9906GPS98410.000 [DIRS 109059] (Location of UZ #4). Finsterle and Seol 2006 [DIRS 177754], p. 1 (Locations of seepage); CRWMS M&O 1997 [DIRS 100117], Table 2-1 (Locations of rain gauges); BSC 2003 [DIRS 165572], p. 15 (Location of south portal).

NOTE: SF gauges = Streamflow gauges; UZ Area = UZ flow model area; Repository = Repository footprint. Repository footprint shown for illustrative purposes only.

Figure 7.1.3-1[a]. Map View of Watersheds and Locations of Various Field Data

7.1.3.1[a]. Runoff and Net Infiltration Comparison

No change.

7.1.3.2[a]. Soil Conductivity Variation Illustration for Entire Net Infiltration Modeling Domain

When calculating runoff at monitored streamflow gauge sites, a variation scenario was simulated for Pagany Wash watershed in which the soil conductivity of the dominant soil type representing stream channels (soil type 3) was increased by an order of magnitude while the conductivity of the other soil types was decreased by a constant factor. This scenario was investigated because of the LeCain borehole data on infiltration (Section 7.2.1.1.2[a]). A conclusion of this scenario was to point out that the spatial distribution of soil conductivity plays an important role in determining the spatial distribution of net infiltration.

To explore the implications of the Pagany Wash study on the larger modeled domain, the four representative realizations (10th, 30th, 50th, and 90th) from the Present-Day simulations were run using an alternate soil conductivity assignment, as defined by the Pagany Wash example. Specifically, the four realizations identified in Table 6.5.7.1-3[a] were run with the following modifications: 1) the conductivity of soil types 3 and 4 were set to 7×10^{-6} m/s, 2) the rock conductivities were set uniformly to 10^{-3} m/s, and 3) the conductivity of the soil types other than 3 and 4 were reduced by a factor of 0.44. Soil types 3 and 4 were selected because, in general, these soil types are associated with the main stream channels (see Figure 6.5.2.2-2[a]). These alternate runs are meant only as an example of how such differences could affect the final infiltration results. The choice of the specific soil conductivities is based on Pagany Wash simulations and data from a single high precipitation year, and this choice is probably not representative of the rest of the domain. Nevertheless, these results illustrate aspects of model sensitivity that are not explored in the sensitivity studies that look at spatial averages of net infiltration.

Figures 7.1.3.2-1[a] to 7.1.3.2-4[a] show net infiltration maps for the alternate soil conductivity realizations: 10th, 30th, 50th, 90th, respectively. These maps can be compared to Figures 6.5.7.1-2[a] to 6.5.7.1-5[a] to see how this change affects the patterns of net infiltration. One obvious difference is that the stream channels show up clearly on the infiltration maps representing the alternate soil conductivity scenario.

To quantitatively summarize these comparisons, two tables are presented below. Table 7.1.3.2-1[a] compares mean net infiltration over three different domains (net infiltration model domain, UZ model domain, and the repository footprint) for each realization. In addition, the runoff fraction is compared and the total weighted precipitation for each realization is listed. The tabulated results suggest that mean net infiltration over these regions and the total runoff leaving the domain are not significantly altered by this variation in soil conductivity.

Table 7.1.3.2-2[a] compares the percent of the total infiltration that occurs in each soil group. It is here that a significant difference can be seen from the original base-case results. In the base-case realizations, between 76% and 97% of the total net infiltration occurred in areas covered with soil types 5, 7, or 9. In the alternate soil conductivity (Variation) runs, this

percentage range fell to 34% to 70%. The fraction of the total infiltration in soil types 3 and 4, increased from a range of 0.2% to 11% to a range of 20% to 55%. The lesson learned from these results is that it is impossible to determine from the available characterization data exactly where the bulk of the net infiltration occurs. Furthermore, the results suggest that the predicted mean net infiltration over relatively large areas (e.g., UZ model domain and repository footprint) is fairly stable. It is the spatial distribution of net infiltration that is especially sensitive to the spatial distribution of soil properties.

Table 7.1.3.2-1[a]. Comparison of Mean Net Infiltration Results of the Soil Conductivity Variation Simulations with Results of the Uncertainty Analysis

Present-Day Climate				
Percentile	10th	30th	50th	90th
Replicate	R2	R2	R2	R2
Realization	10	2	8	14
Entire Domain Infiltration (mm/yr)	3.9	7.3	13.0	26.7
Entire Domain Variation Infiltration (mm/yr)	4.1	7.7	15.9	27.2
UZ Infiltration (mm/yr)	3.3	5.9	10.8	28.3
UZ Variation Infiltration (mm/yr)	3.5	5.9	13.4	27.3
Repository Infiltration (mm/yr)[a]	3.9	6.5	10.9	34.4
Repository Variation Infiltration (mm/yr)[a]	3.9	4.9	9.5	28.3
Runoff Fraction (%)	0.9	1.8	3.8	1.3
Runoff Fraction Variation (%)	0.8	1.6	3.2	1.1
Mean Annual Precipitation (mm/yr)	144.1	160.6	189.3	212.7

Source: Output DTN: SN0701T0502206.037, file: \Welcome to Massif\Massif\Post Processing All Climates*PD Soil Conductivity Variation Study.xls*.

[a] 2002 repository footprint used (DTN: LB0208HYDSTRAT.001 [DIRS 174491]).

Table 7.1.3.2-2[a]. Comparison of Percent of the Total Net Infiltration Occurring in Each Soil Group between the Soil Conductivity Variation Simulations and the Results of the Uncertainty Analysis

Present-Day Climate				
Percentile	10th	30th	50th	90th
Replicate	R2	R2	R2	R2
Realization	10	2	8	14
Soil Group 1 (%)	0.2	0.7	3.5	0.0
Soil Group 1 Variation (%)	0.0	0.1	0.6	0.0
Soil Groups 2/6 (%)	0.4	1.0	5.2	0.0
Soil Groups 2/6 Variation (%)	0.0	0.1	0.7	0.0
Soil Groups 3/4 (%)	1.4	2.3	10.6	0.2
Soil Groups 3/4 Variation (%)	19.7	35.4	55.1	24.9
Soil Groups 5/7/9 (%)	85.7	88.6	76.0	97.1
Soil Groups 5/7/9 Variation (%)	66.6	54.6	34.4	69.9
Soil Group 8 (%)	12.3	7.3	4.7	2.7
Soil Group 8 Variation (%)	13.7	9.8	9.2	5.2

Source: Output DTN: SN0701T0502206.037, file: \Welcome to Massif\Massif\Post Processing All Climates*PD Soil Conductivity Variation Study.xls.*

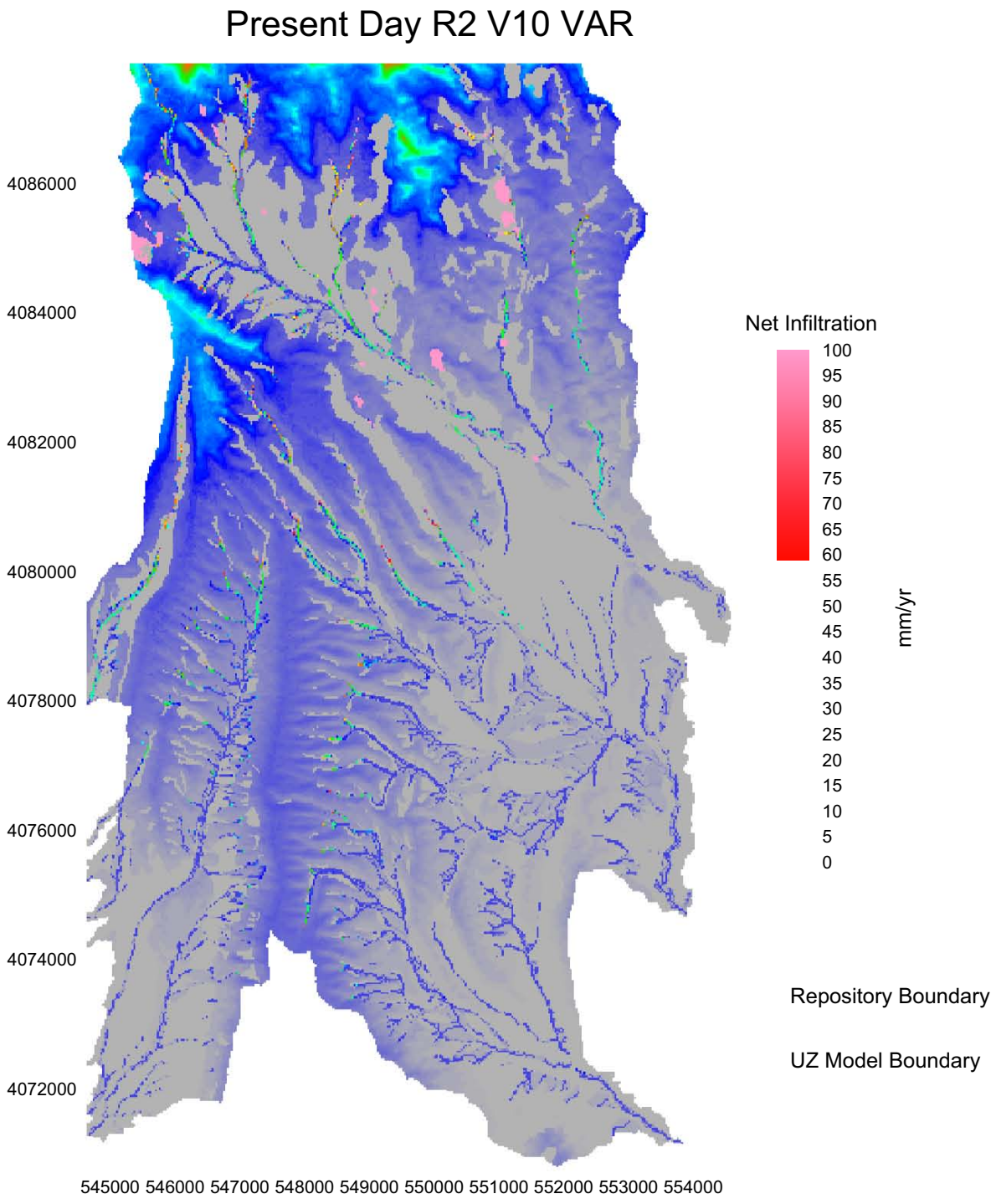

Coordinates are in meters; UTM NAD 27, Zone 11

Source: Output DTN: SN0701T0502206.037, file: \Welcome to Massif\Massif\Present Day Uncertainty\Infiltration Map Variations*Present Day R2 V10.xmcd* (net infiltration results from soil conductivity variation study); Output DTN: SN0711FTPRNUZB.003 (UZ model and repository boundaries).

NOTE: Repository footprint shown for illustrative purposes only.

Figure 7.1.3.2-1[a]. Present-Day, 10th Percentile Net Infiltration Map (Soil Conductivity Variation) (Replicate R2, Realization 10)

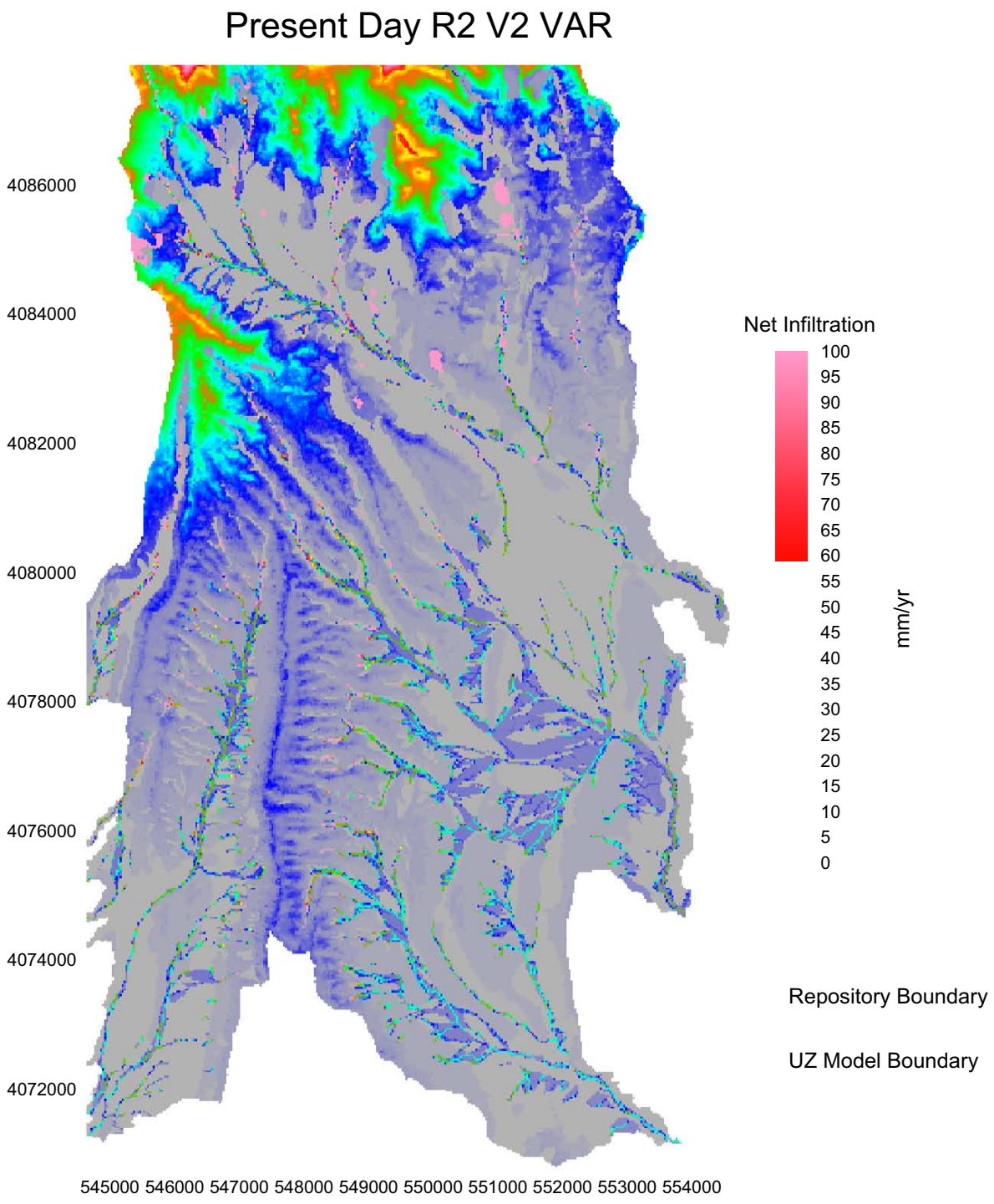

Coordinates are in meters; UTM NAD 27, Zone 11

Source: Output DTN: SN0701T0502206.037, file: \Welcome to Massif\Massif\Present Day Uncertainty\Infiltration Map Variations*Present Day R2 V02.xmcd* (net infiltration results from soil conductivity variation study); Output DTN: SN0711FTPRNUZB.003 (UZ model and repository boundaries).

NOTE: Repository footprint shown for illustrative purposes only.

Figure 7.1.3.2-2[a]. Present-Day, 30th Percentile Net Infiltration Map (Soil Conductivity Variation) (Replicate R2, Realization 2)

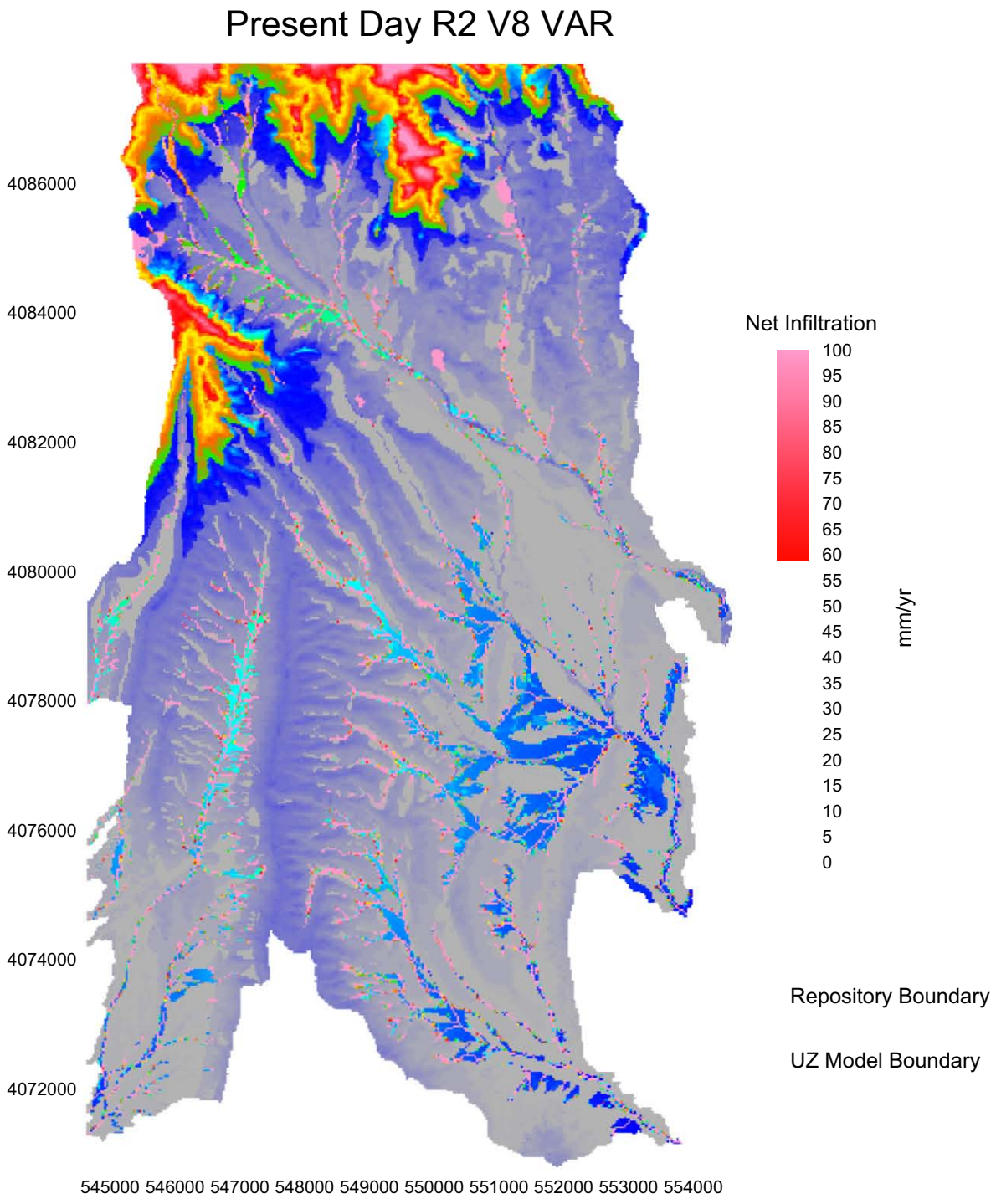

Coordinates are in meters; UTM NAD 27, Zone 11

Source: Output DTN: SN0701T0502206.037, file: \Welcome to Massif\Massif\Present Day Uncertainty\Infiltration Map Variations*Present Day R2 V08.xmcd* (net infiltration results from soil conductivity variation study); Output DTN: SN0711FTPRNUZB.003 (UZ model and repository boundaries).

NOTE: Repository footprint shown for illustrative purposes only.

Figure 7.1.3.2-3[a]. Present-Day, 50th Percentile Net Infiltration Map (Soil Conductivity Variation) (Replicate R2, Realization 8)

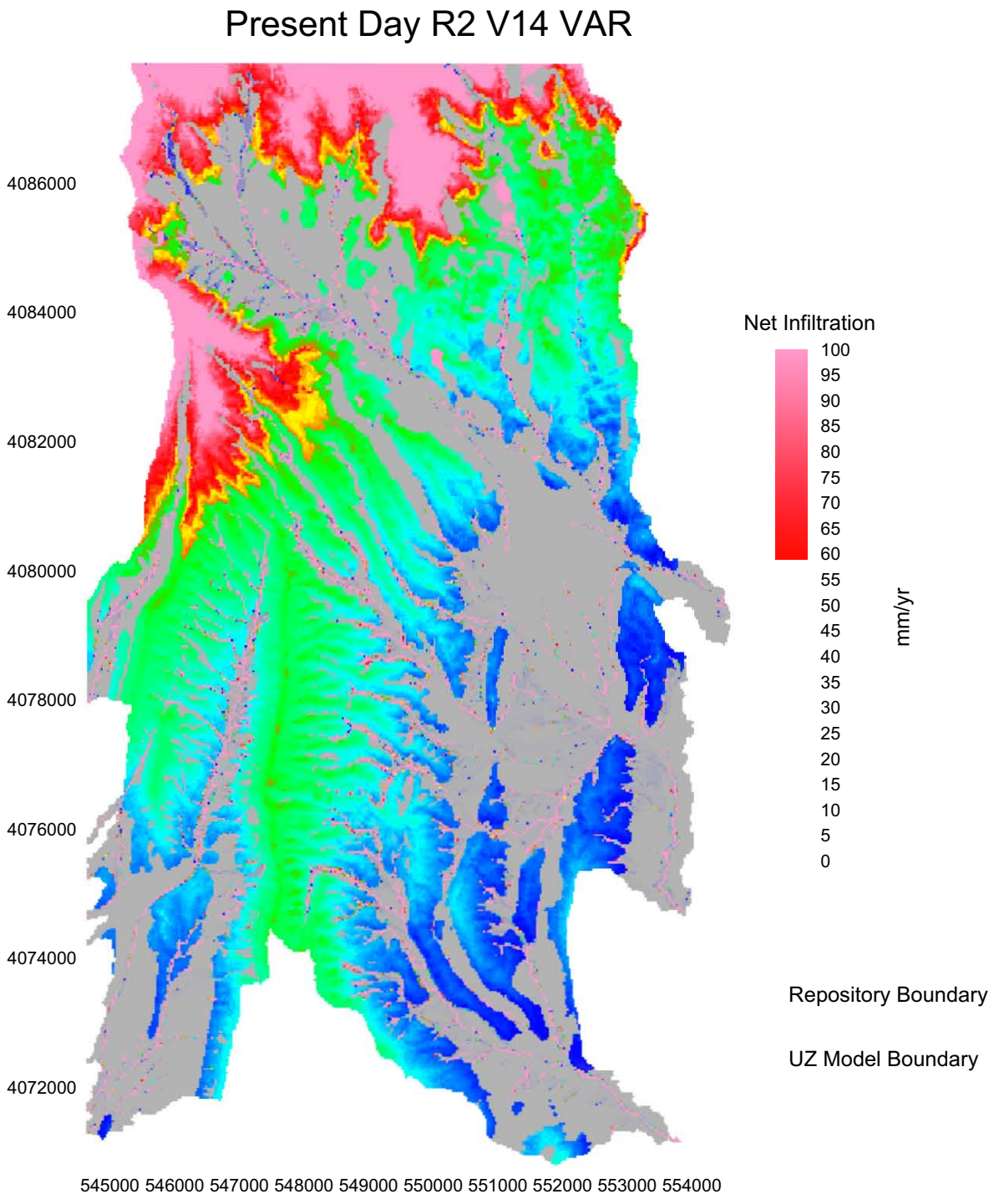

Source: Output DTN: SN0701T0502206.037, file: \Welcome to Massif\Massif\Present Day Uncertainty\Infiltration Map Variations*Present Day R2 V14.xmcd* (net infiltration results from soil conductivity variation study); Output DTN: SN0711FTPRNUZB.003 (UZ model and repository boundaries).

NOTE: Repository footprint shown for illustrative purposes only.

Figure 7.1.3.2-4[a]. Present-Day, 90th Percentile Net Infiltration Map (Soil Conductivity Variation) (Replicate R2, Realization 14)

7.1.4[a]. Extended Parameter Sensitivity Study (Large LHS)

No change.

7.1.5[a]. Summary of Confidence Building during Model Development

No change.

7.2[a]. POST-DEVELOPMENT MODEL VALIDATION

Post-development model validation includes several methods listed in paragraph 6.3.2) of SCI-PRO-006. The methods used to validate the infiltration model include (1) corroboration of model results with data (e.g., field data, analogue studies) not previously used to develop or calibrate the model and (2) corroboration of model results with other alternative mathematical model results. In addition, post-development model validation includes one method given in paragraph 6.3.2b) of SCI-PRO-006, technical review by an external agency, and documented by the external agency. This review is the 1997 expert elicitation panel on unsaturated zone (UZ) flow model issues (CRWMS M&O 1997 [DIRS 100335]). Although this review was conducted 10 years ago, and the panel reviewed an entirely different infiltration model from that presented in this report, the conceptual models employed by the infiltration models are quite similar, and the conclusions of the expert elicitation project (CRWMS M&O 1997 [DIRS 100335]) remain generally relevant in 2007.

Section 7.2.1 describes corroboration of the model results with data, Section 7.2.2[a] presents corroboration of the model results with alternative models, and Section 7.2.3 summarizes the conclusions and infiltration estimates from the 1997 expert elicitation panel on UZ flow model issues (CRWMS M&O 1997 [DIRS 100335]). Section 7.2.4[a] discusses soil depth data collected by the CNWRA compared to soil depth data collected by the USGS that is part of the basis for the soil depth ranges used with MASSIF.

7.2.1[a]. Corroboration of Model Results with Data and Relevant Observations

No change.

7.2.1.1[a]. Corroboration of Model Results with Field Data

No change.

7.2.1.1.1[a]. Comparison of Model Predictions of Infiltration with Seepage Observations and Simulations above the South Ramp in 2005

During the 5-month period between October 2004 and February 2005, 324 mm (12.75 in) of precipitation fell in the Yucca Mountain area. On February 28, 2005, YMP personnel working in the South Ramp of the ESF observed wet spots on the main drift crown, ribs, and invert. This field observation is considered the first unambiguous evidence of seepage under ambient conditions. Based on several assumptions, it was estimated that 13% of a 5.1-m-long drift section experienced seepage (Finsterle and Seol 2006 [DIRS 177754]).

Finsterle and Seol (2006 [DIRS 177754]) applied a Monte Carlo simulation using *Seepage Model for PA Including Drift Collapse* (BSC 2004 [DIRS 167652]) to simulate the seepage fraction to resolve whether or not the observed seepage was an unexpected condition. Percolation flux was assumed to be equivalent to net infiltration flux, which was assumed to be on the order of 10% of precipitation, whose rate ranged from 393 to 1,309 mm/yr for November 2004, and February 2005, respectively. These precipitation rates are considerably higher than the long-term average value of 188.5 mm/yr reported by Finsterle and Seol (2006 [DIRS 177754], Table 1). Using probability distributions for fracture and capillary parameters and for net infiltration flux, it was estimated that seepage would occur along about 37% of the ESF South Ramp, compared with the observation that about 13% of the length exhibited wet spots. Therefore, these simulations confirm that the seepage observations in 2005 were not an unexpected condition, given the precipitation during this 5-month period (Finsterle and Seol 2006 [DIRS 177754], p. 17).

This section describes how MASSIF was used to corroborate the net infiltration fluxes assumed by Finsterle and Seol (2006 [DIRS 177754]). Although MASSIF results cannot be directly compared with quantitative field measurements of seepage, MASSIF infiltration can be compared to the ranges used by Finsterle and Seol (2006 [DIRS 177754]) in their seepage simulations. If MASSIF results are consistent with their infiltration ranges used to predict seepage, then this calculation provides additional model validation.

Monitor cells were identified at the ground surface directly above the areas identified as having seepage in the south ramp of the ESF. Precipitation and air temperature data for WY2004 and WY2005 were acquired for site 8, located about 1.2 km east of the seepage observations. Since wind speed data were not collected at site 8, wind speed data from site 1 were used instead. Site 1 weather station has an elevation of only 12 m higher than the site 8 station (CRWMS M&O 1997 [DIRS 100117], Table 2-1). MASSIF was used to calculate the average net infiltration for WY2005, with particular focus on monthly rates in November 2004 through February 2005.

MASSIF was run for WY 2004 and WY 2005 (October 1, 2003 through September 2005). The sources for the weather data used in the simulation follow:

2003 weather data:

- Maximum and minimum air temperature and precipitation data from site 8: DTN: MO0503SEPMMD03.001 [DIRS 176097]
- Wind speed data from site 1: DTN: SN0608WEATHER1.005 [DIRS 177912].

2004 weather data:

- Maximum and minimum air temperature and precipitation data from site 8: DTN: MO0607SEPMMD04.001 [DIRS 178311]
- Wind speed data from site 1: DTN: SN0608WEATHER1.005 [DIRS 177912].

2005 weather data:

- Maximum and minimum air temperature and precipitation data from site 8 and wind speed data from site 1: DTN: MO0708METMND05.001 [DIRS 182647].

The 2005 site 8 precipitation dataset from DTN: MO0708METMND05.001 [DIRS 182647] is not complete. Missing data information was used for a storage gauge (DTN: MO0605SEPSGP05.000 [DIRS 178663]). The timing of the missing data is taken from Site 1: DTN: MO0708METMND05.001 [DIRS 182647]. Excel file *Site 8 Pcp vs Site 1 Pcp.xls* in Output DTN: SN0701T0502206.037 details how site 1 hourly data were scaled with a factor of 1.41 to replace site 8 missing data.

Monitor cells were identified at the ground surface directly above the locations within the South Ramp of the ESF where seepage was observed in 2005. Three primary wet areas were identified in the ESF between stations 75+62 and 75+82, Stations 75+92 and 76+07, and Stations 77+48 to 77+53 (Finsterle and Seol 2006 [DIRS 177754], p. 1). These locations were converted into UTM coordinates using reference points and documented in Excel file *seepage locations.xls* located in the South Ramp Infiltration folder within the MASSIF model Output DTN: SN0701T0502206.037. Mathcad file *Locate cells above SR Seepage.xmcd* was used to locate the monitor cell IDs for these UTM coordinates. These three areas of observed seepage are directly beneath three monitor cells in the Drill Hole Wash watershed. Refer to Figure 7.1.3-1[a] for a map view of the infiltration watersheds, and the location of the South Portal and the grid cells below which seepage was observed. This figure also includes locations of other field data that are discussed later in Chapter 7.

MASSIF predicted net infiltration totals of 133, 130, and 113 mm for the three monitor cells for WY2005. This is equivalent to 31.4%, 30.7%, and 27.3% of precipitation for the three monitor cells. On a monthly basis, the infiltration/precipitation ratio ranged from 0.0 to 0.54. Refer to Table 7.2.1.1-1[a] for the results of the MASSIF simulations of infiltration above the South Ramp. These values are compared to the monthly values used in *Preliminary Evaluation of Seepage Observations from the ESF South Ramp Using the Drift Seepage Abstraction Model* (Finsterle and Seol 2006 [DIRS 177754]).

Table 7.2.1.1-1[a]. Summary of MASSIF Results for South Ramp Infiltration Simulations

		Precipitation (mm/yr)			
Month	Year	Finsterle & Seol 2006	MASSIF Cell1	MASSIF Cell2	MASSIF Cell3
October	2004	814.0	861.5	856.8	839.5
November	2004	393.0	419.2	416.9	408.5
December	2004	575.0	564.4	561.4	550.0
January	2005	865.0	894.5	889.6	871.7
February	2005	1,309.0	1,317.0	1,309.8	1,283.4

Table 7.2.1.1-1[a]. Summary of MASSIF Results for South Ramp Infiltration Simulations (Continued)

Month	Year	Infiltration (mm/yr)			
		Finsterle & Seol 2006 LBNL	MASSIF Cell1	MASSIF Cell2	MASSIF Cell3
October	2004	81.4	143.3	136.0	107.9
November	2004	39.3	108.7	103.2	86.3
December	2004	57.5	242.7	238.9	210.4
January	2005	86.5	391.3	377.8	329.7
February	2005	130.9	714.7	698.4	619.9

Source: Output DTN: SN0701T0502206.037, file: \Welcome to Massif\Massif\Validation Analyses\South Ramp Seepage*South Ramp Results.xls*.

The results of this MASSIF calculation demonstrate that the estimate of net infiltration used as a boundary condition to predict seepage in the South Ramp by Finsterle and Seol (2006 [DIRS 177754]) was reasonable and in fact, considerably lower than the monthly infiltration predicted by MASSIF. Based on the Finsterle and Seol (2006 [DIRS 177754]) assumption and conclusions and the MASSIF results in this section, observations of seepage in the South Ramp in 2005 were not unexpected.

However, the results of this MASSIF calculation beg the question of why wasn't more seepage observed in the south ramp if the seepage model predicted seepage along 37% of south ramp when seepage along about 13% of the south ramp was observed, and MASSIF predicts more infiltration than the boundary condition used by Finsterle and Seol (2006 [DIRS 177754]). One explanation is that Finsterle and Seol (2006 [DIRS 177754]) did not account for any delay of infiltration between the bottom of the root zone, and the ceiling of the south ramp, or for any change in storage or lateral flow in this zone that has a thickness ranging from 70 to 40 m. This range in thickness is calculated in *Seepage Locations.xls* in the MASSIF calculation (Output DTN: SN0701T0502206.037). In addition, the seepage model did not account for evaporation effects in the ESF, which would have reduced their estimate of observed seepage in the ESF ceiling. These additional considerations would support the conclusion that the MASSIF results, the seepage model results, and the observed seepage in the ESF are not inconsistent.

7.2.1.1.2[a]. Comparison of Model Predictions with Pagany Wash Infiltration Data from 1998

MASSIF was used to simulate infiltration at a monitor cell that contains the location of borehole UE-25 UZ #4 (also referred to as UZ #4). This is an instrumented borehole in Pagany Wash. The winter of 1997 to 1998 was an El Nino winter and, therefore, was considerably wetter than average winters. The total precipitation recorded at Site 3 for WY1998 was 402.6 mm (DTN: SN0608WEATHER1.005 [DIRS 177912]). In the spring of 1998, 183.4 mm of precipitation was recorded during 14 out of 23 days between February 2 and 24 (DTN: SN0608WEATHER1.005 [DIRS 177912]), and approximately 35,000 m^3 of runoff was recorded at the lower Pagany Wash streamflow gauge (Table 7.1.3-1) during this 23-day period in February 1998 (DTN: GS960908312121.001 [DIRS 107375]). LeCain et al. (2002 [DIRS 158511]) describe infiltration data collected at this borehole during the spring of 1998. Borehole UZ #4 is located in the alluvial deposits of Pagany Wash, a stream-carved, dry channel. This borehole was instrumented with temperature, pressure, and water potential sensors in

July 1995, to gain insight into infiltration through the alluvial deposits of the usually dry stream channels (LeCain et al. 2002 [DIRS 158511]). Figure 7.1.3-1[a] shows a map view of the infiltration watersheds and the location of Pagany Wash and UZ #4.

LeCain et al. (2002 [DIRS 158511]) describe two methods for estimating infiltration in Pagany Wash based on data collected at UZ #4. The first is an analytical method in which the infiltration flux is calculated from soil saturated conductivity, porosity, and velocity of a wetting front observed to pass from a depth of 3.0 m to 6.1 m. The second method uses a numerical model to estimate infiltration flux given temperature data measured in UZ #4. The first method produced a total of 1.13 m of infiltrated water while the second method produced a total of 1 to 2 m, for the time period described.

First, MASSIF was used with nominal input values to simulate infiltration at the monitor cell containing borehole UZ#4. Infiltration for WY1998 at UZ #4 was calculated to be 11.8 mm using precipitation data from the Site 6 station, and 28.3 mm using precipitation data from the Site 3 station. Second, soil and rock hydraulic conductivities (K_{sats}) for the grid cell containing borehole UZ #4 were adjusted to test the sensitivity of infiltration to K_{sat}, and to demonstrate that modeled infiltration can match the measured infiltration reported by LeCain et al. (2002 [DIRS 158511]) with adjustments to K_{sat}s. Soil K_{sat} was increased by about one order of magnitude to a value of 7×10^{-6} m/s, and rock K_{sat} was increased to a value of 10^{-3} m/s so that it would not be a limiting factor on infiltration. The analytical method used by LeCain et al. (2002 [DIRS 158511]) to calculate infiltration flux from 3.0 to 6.1 m does not include rock hydraulic conductivity, so rock hydraulic conductivity should not be a limiting factor for a comparison with MASSIF. MASSIF calculated a total net infiltration for WY1998 at the grid cell containing UZ #4 of 414 mm and 375 mm for Site 3 and Site 6 stations, respectively. When soil K_{sat}s were increased to 10^{-5} m/s, infiltration increased to 597 and 548 mm, for Sites 3 and 6 precipitation, respectively. These MASSIF calculations can be found in the Pagany Wash Borehole folder in the Validation Analyses folder in the MASSIF calculation (Output DTN: SN0701T0502206.037, file: \Welcome to Massif\Massif\Validation Analyses\Pagany Wash Borehole*Pagany Wash Results.xls*.).

In the analytical method described by LeCain et al. (2002 [DIRS 158511]), if the value of soil porosity is changed from 0.31 to 0.157 m^3/m^3, which is the porosity assigned to the soil type in this grid cell, then the percolation flux would change from 1,130 to 573 mm (Output DTN: SN0701T0502206.037, file *PW infiltration analytical calculation.xmcd*). This is very close to the net infiltration flux calculated by MASSIF when soil and rock K_{sat}s are adjusted.

This comparison of percolation flux between MASSIF and an analytical method reported by LeCain et al. (2002 [DIRS 158511]) shows that MASSIF calculated approximately the same amount of infiltration at UZ #4, if soil K_{sat} for that grid cell is increased by ~1.5 orders of magnitude, and if rock hydraulic conductivity for that grid cell is increased so that it is not a limiting factor. Although this increase in soil K_{sat} is outside of the standard error range in soil K_{sat} for soil type 3 (K_{sat} range = 9.5 to 6.2×10^{-7} m/s) reported in *Data Analysis for Infiltration Modeling: Development of Soil Units and Associated Hydraulic Parameter Values* (BSC 2006 [DIRS 176335], Table 6-7), it is within the range of maximum and minimum values (1.7×10^{-7} to 1.7×10^{-5} m/s), and this adjusted soil K_{sat} may be more appropriate for the soil near the grid cell containing UZ #4 on Yucca Mountain. The soil K_{sat} values (BSC 2006 [DIRS 176335],

Table 6-7) are not directly measured, but are developed from Yucca Mountain textural data using pedotransfer functions (BSC 2006 [DIRS 176335], Section 6.4.5). Therefore, they are appropriate and defensible for large-scale assessments of infiltration at Yucca Mountain. However, they are likely to be inaccurate for comparison to borehole-scale infiltration estimates as has been seen in this validation calculation.

Although not referenced in *Data Analysis for Infiltration Modeling: Development of Soil Units and Associated Hydraulic Parameter Values* (BSC 2006 [DIRS 176335]), Hofmann et al. (2000 [DIRS 153709]) report measurements of soil saturated hydraulic conductivity at two locations at Yucca Mountain. These locations included a measurement in Pagany Wash near borehole UE-25 UZN #14 and a measurement on a stable terrace adjacent to Fortymile Wash at borehole UE-25 UZN #85, both using a prototype-automated-infiltrometer. They measured a saturated hydraulic conductivity of 17.79 cm/hr (4.94×10^{-5} m/s) for the location in Pagany Wash and 1.78 cm/hr (4.94×10^{-6} m/s) for the terrace location (Hofmann et al. 2000 [DIRS 153709], Table 4). The measurement in Pagany Wash corroborates the adjustments to soil conductivity required to match infiltration inferred at UZ #4.

7.2.1.1.3[a]. Discussion of Soil Moisture Data

Discussion of Neutron Logging Data

Neutron logging data were collected from mid-1989 through September 1995 at 99 boreholes. Ninety-five of the 99 boreholes are located within the current infiltration model domain. Refer to Figure 7.1.3-1[a] for a map view of the infiltration watersheds and the locations of the 95 neutron logging boreholes. All 95 boreholes are located within four watersheds; one borehole is located within Yucca Wash while the remaining 94 boreholes are located within Drill Hole Wash, Dune Wash, or Solitario Canyon 1 watersheds. Details of the neutron logging program and datasets can be found in *Technical Evaluation and Review of Results, Technical Procedures, and Methods Related to the Collection of Moisture Monitoring Data Using Neutron Probes in Shallow Boreholes* (BSC 2006 [DIRS 177083]), and in *Shallow Infiltration Processes at Yucca Mountain, Nevada—Neutron Logging Data 1984-93* (Flint and Flint 1995 [DIRS 100394]). All neutron logging data are located in DTN: MO0601SEPNEULG.002 [DIRS 184298].

An uncertainty analysis of this dataset concluded that water content values from the neutron logging are accurate to approximately ±6% absolute water content within a 95% confidence interval (BSC 2006 [DIRS 177083], Section 5.3.2). Given a typical water content value of 20%, this uncertainty translates to a 30% relative error in the measured value. However, the precision of the measurement is higher (less than 2% relative difference), which suggests that estimates of changes in water content are more certain. This increased certainty is limited by the fact that precision errors associated with each log are additive when considering changes in water content over time.

The manner in which neutron logging data have been used has changed over time on the Yucca Mountain Project. Neutron logging data were used to calibrate the 1996 USGS net infiltration model (Flint et al. 1996 [DIRS 100147], p. 84), however data-model comparisons are only shown for two of the 99 boreholes and the calibration method used and the results obtained are not adequately documented. Streamflow data (and no neutron logging data) were used to

calibrate the 2000 USGS net infiltration model (USGS 2001 [DIRS 160355], Section 6.8). The 2004 revision of the 2000 USGS net infiltration model (BSC 2004 [DIRS 170007]) only used neutron logging data for model validation.

This dataset was deemed to be of limited use for validation (or calibration) of the 2007 SNL net infiltration model for several reasons. First, the errors associated with water content derived from these measurements make direct comparison with simulated water contents problematic, especially since conditions at each borehole (such as soil depth and properties) are likely to differ from the average values assigned to the soil depth class and soil group assigned to the cell. Second, the field capacity modeling approach is a "lumped" approach and is therefore not intended to be used to match moisture profiles with depth in the soil. Third, flux estimates using the change in water content over an interval require an estimate of the root-zone depth, which is likely to vary for each location. Despite this limitation, fluxes were estimated assuming a constant root-zone depth and compared with net infiltration calculated over the same time interval. The following comparisons between measured and modeled infiltration provides justification for its exclusion from model validation.

Neutron logging measures the number of reflected (thermalized) neutrons at depth intervals in a region surrounding a borehole. The count of neutrons is also affected by the integrated properties of the material (e.g., density, mineral composition, etc.) and in relatively homogeneous materials has successfully been used to estimate water content. Several researchers have estimated net infiltration fluxes from neutron logging data collected at time intervals during which water content profiles were changing (e.g., Looney and Falta 2000 [DIRS 154273], p. 457 and McElroy 1993 [DIRS 177910], p. 13). However, many assumptions are required to estimate net infiltration flux from these measurements. Net infiltration flux can be estimated from the change in water content ($d\theta v$ in m^3/m^3), with time, multiplied by a given depth interval ($d\theta v \times dz$), and then summing these changes, for depths below the root zone (Looney and Falta 2000 [DIRS 154273], p. 457; McElroy 1993 [DIRS 177910], p. 13). Net infiltration flux can also be calculated as the change in integrated water content below the root zone, between two time periods. This method was implemented with Mathcad in *Borehole Processing Nominal.xmcd* located in the "Neutron Logging Boreholes" folder in the "Validation Analyses" folder within the MASSIF calculation (Output DTN: SN0701T0502206.037), for the time period spanning the greatest increase in borehole water content between about January 1 and mid-March 1995. Other time periods were examined during the period of record. During most of the neutron logging record there was zero or sporadic infiltration flux calculated from the changes in water content measured at neutron logging boreholes. The root zone was assumed to be 1.6 m below the ground surface for soil depths of 1.6 m or greater, and the root zone was set equivalent to soil depth for soil depths less than 1.6 m.

The use of these methods for calculating flux in fractured rock from water content data has not been widely used, and limitations in the approach, as well as limitations within the dataset, should be acknowledged. For example, this approach assumes one-dimensional piston flow, with no lateral flow at the soil–bedrock interface. The MASSIF model assumes that lateral flow can be neglected for estimating a water balance for a 30- × 30-m grid cell (Section 5). However, this assumption may not be appropriate for measurements occurring on the scale of a borehole, since the active fracture spacing in the bedrock is likely to be greater than the region measured by the neutron probe. In addition, single calibrations, independent of media, were developed for

each neutron probe, and were applied to all the neutron measurements made in various media (e.g., soil, "rotten" tuff near the soil–bedrock interface, or intact tuff). Refer to *Technical Evaluation and Review of Results, Technical Procedures, and Methods Related to the Collection of Moisture Monitoring Data Using Neutron Probes in Shallow Boreholes* (BSC 2006 [DIRS 177083]) for details of the neutron probe calibrations. Since calibrations provide the means of interpreting water contents, the consequence of using a single calibration for different media is that there may be systematic errors in water contents for media not used in the calibration. In addition, as a result of the drilling methods, preferential pathways for water flow along the annulus space between the borehole casing and the geologic media may have been inadvertently created, and formerly solid rock may have been extensively fractured.

Despite the limitations of the dataset, and the assumptions inherent in calculating infiltration from changes in water content, this six-year dataset represents the only YMP site-specific dataset that measured wetting front movement, depths of infiltration, and indirectly, net infiltration flux, over a large area of the infiltration model area, and over a period with wet years and dry years. Therefore, it is worthwhile to compare MASSIF predictions of infiltration at the grid cells containing the neutron logging boreholes, with the infiltration calculated from neutron logging data. Figure 7.2.1.1-2[a] shows such a comparison for a period of infiltration spanning the wet winter of 1995, using three precipitation stations with MASSIF. As the figure shows, the comparison is not good. Even the comparison of the averaged infiltration for all boreholes was not good (71 mm for MASSIF using Site 6 precipitation versus 200 mm from neutron logging data). This figure is included to demonstrate that the neutron logging data are not reliable for calculating infiltration flux due to the possible drilling-induced preferential pathways through bedrock, which explains why these data could not be used for model calibration. This conclusion is supported by the lack of any corroborating data to support the high infiltration fluxes at the neutron logging boreholes. In fact, all other types of data and analyses used to quantify net infiltration at Yucca Mountain are generally lower than the mean net infiltration calculated using MASSIF for present-day climate, and the MASSIF results are a factor of 3 lower than flux calculated from neutron logging data (for the time period discussed above).

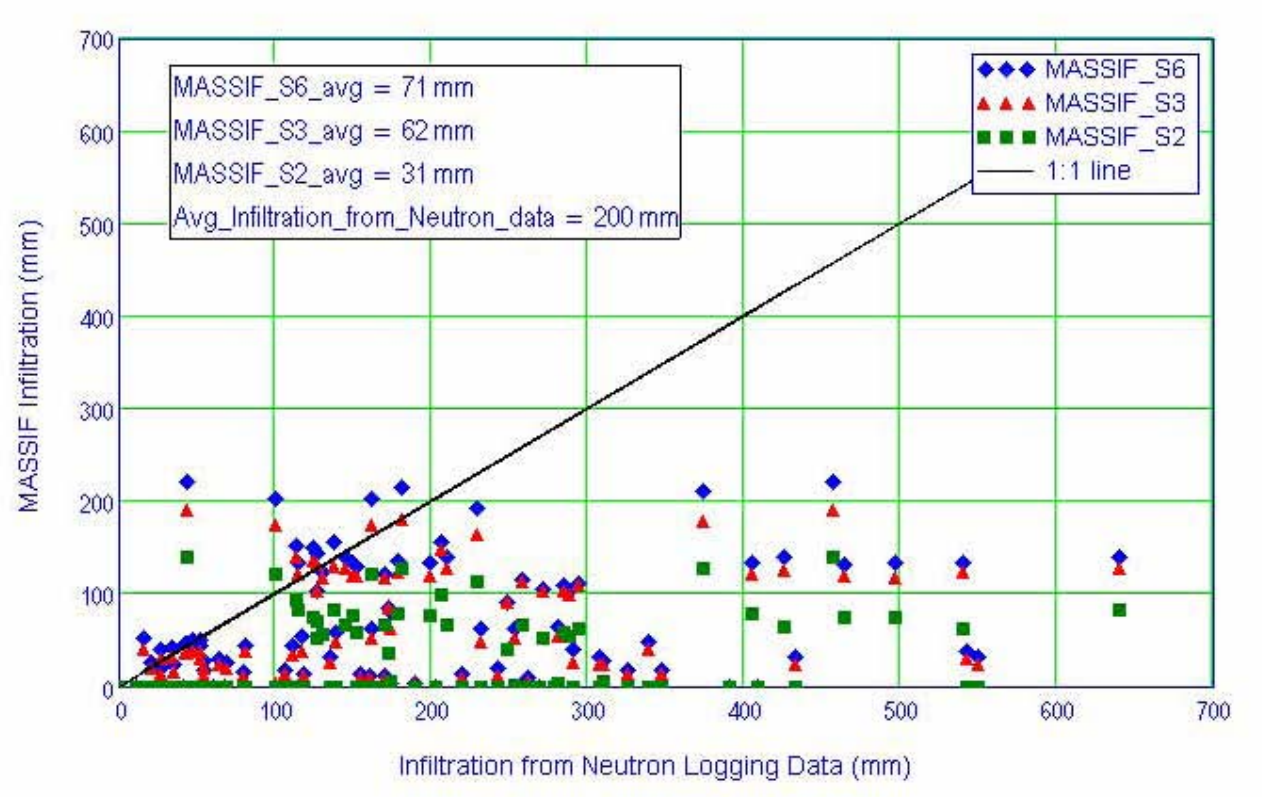

Source: Neutron logging data from DTN: MO0601SEPNEULG.002 [DIRS 184298]; Output DTN: SN0701T0502206.037, file: \Welcome to Massif\Massif\Validation Analyses\Neutron Logging Boreholes*Borehole_Processing_Nominal.xmcd*.

Figure 7.2.1.1-2[a]. Comparison of Net Infiltration Calculated from Neutron Logging Data versus MASSIF Net Infiltration for Winter 1995

Discussion of Heat Dissipation Probe Data

Heat dissipation probe data, which measures water potential at different depths in the soil, are available for at least one location at Yucca Mountain (DTN: GS960908312211.004 [DIRS 146872]). Water potential data can be converted into water content data and then compared to model results using MASSIF, if the water retention properties of the soils are known. These data were not analyzed for additional model validation due to the problems with data traceability and the availability of site-specific soil property data needed to convert water potential to water content.

7.2.1.2[a]. Comparison of Infiltration Estimates with Other Models and Data from Comparable Environments

In this section, MASSIF results for Present-Day, Monsoon, and Glacial Transition climates (Output DTNs: SN0701T0502206.034, SN0701T0502206.036, and SN0701T0502206.035, respectively) are compared to infiltration and/or recharge estimates from other models and data from comparable environments. These environments include other locations in Nevada (Section 7.2.1.2.1), the southwestern United States (Section 7.2.1.2.2), and the western United States (Section 7.2.1.2.3[a]). Estimates from locations in the southwestern U.S. are

approximately analogous to the predicted recharge expected for the monsoon climate, based on the selection of analogue climate sites in *Future Climate Analysis* (BSC 2004 [DIRS 170002], Table 6-1). And estimates from locations in the western United States are approximately analogous to the predicted recharge expected for the glacial-transition climate, based on the selection of analogue climate sites in *Future Climate Analysis* (BSC 2004 [DIRS 170002], Table 6-1). Recharge and infiltration estimates for the Hanford site are briefly discussed in Section 7.2.1.2.3[a], although this site is quite dry and more analogous to Yucca Mountain under the Present-Day climate than the Glacial-Transition climate.

MASSIF results for Present-Day, Monsoon, and Glacial Transition climates (Output DTNs: SN0701T0502206.034, SN0701T0502206.036, and SN0701T0502206.035, respectively) are compared to several published models of infiltration and/or recharge versus precipitation and shown in Figure 7.2.1.2-1[a]. The publication dates of these models span nearly 60 years and Figure 7.2.1.2-1[a] demonstrates the similarity of these models, despite the advances made in hydrologic sciences in the past 60 years. The step function of the Maxey-Eakin model (Maxey and Eakin 1950 [DIRS 100598], p. 40) is shown primarily for its historical significance as a well-recognized recharge model. Figure 7.2.1.2-1[a] shows a modified Maxey-Eakin model (Nichols 2000 [DIRS 178863], page C35), a Maxey-Eakin model fit developed by Wilson and Guan (2004 [DIRS 172585], Equation 12), and MASSIF results compared to a model developed by Maurer and Berger (1997 [DIRS 177370], Equation 9) for west-central Nevada. The Maurer and Berger (1997 [DIRS 177370]) model predicts water yield based on precipitation in which water yield is defined as subsurface flow plus surface runoff, so it is not directly comparable to other models. Figure 7.2.1.2-1[a] also shows MASSIF results compared to a recent model developed by Faybishenko (2007 [DIRS 178766], Equation 16) for Yucca Mountain using analogue meteorological data, and a fit to a dataset referred to as Davisson and Rose (Faybishenko 2007 [DIRS 178766], Figure 10). MASSIF results for three climate states are above the general trend of most of these models. However, the acceptance criteria established in the TWP (BSC 2006 [DIRS 177492]) are met because these empirical models fall within range of uncertainty of the MASSIF calculations.

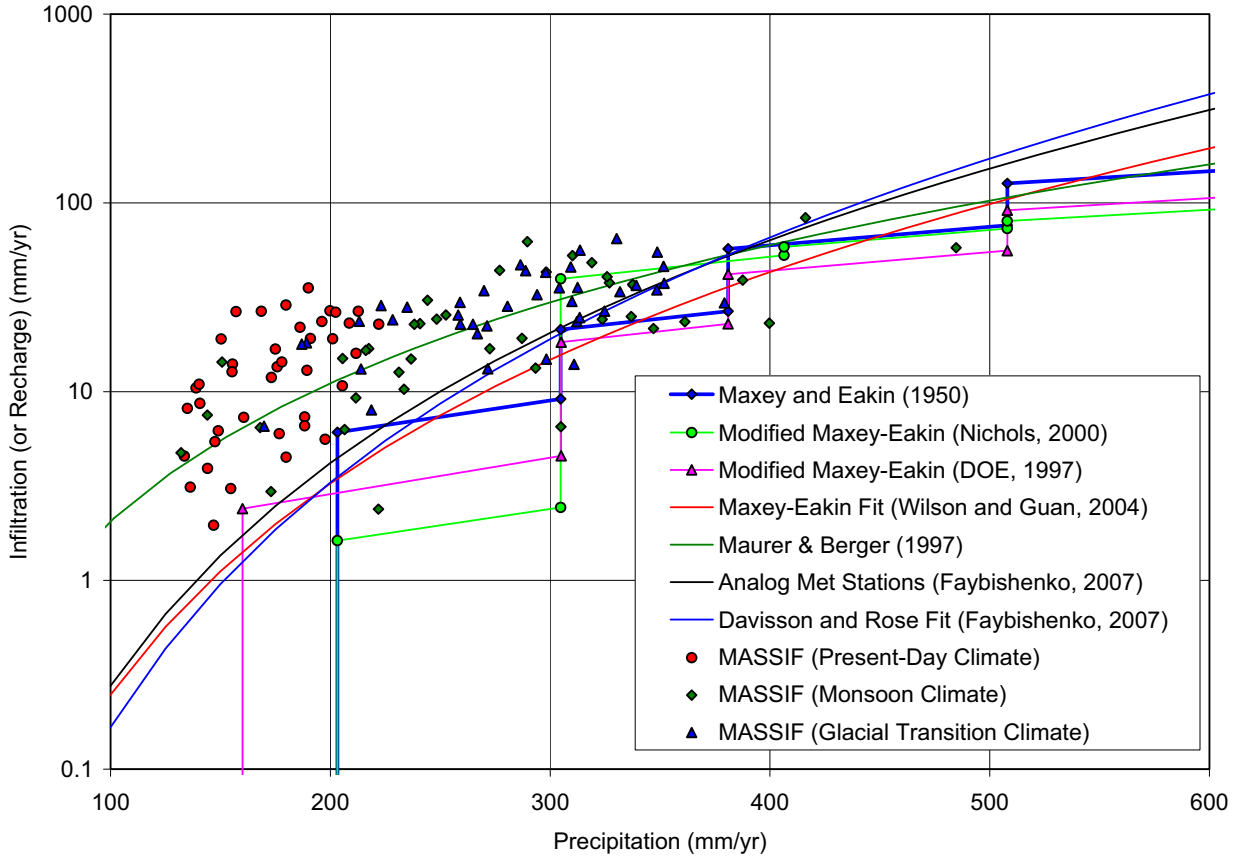

Source: Output DTNs: SN0701T0502206.034, SN0701T0502206.036, and SN0701T0502206.035; Validation Output DTN: SN0801T0502206.049.

NOTE: Vertical lines that extend to the horizontal axis associated with the Maxey-Eakin and Modified Maxey-Eakin models represent the precipitation amounts below which the models predict zero recharge.

Figure 7.2.1.2-1[a]. Comparison of MASSIF Net Infiltration Results for Three Climates with Several Models

7.2.1.2.1[a]. Infiltration Estimates for Other Locations in Nevada

This entire section has been updated from the parent document for this addendum. The update was necessary because of issues raised in CR 11620, which identified inconsistencies in the calculations described in this section of the parent report. This update corrects these inconsistencies so that CR 11620 is eligible for closure.

The Nevada Division of Water Resources, Department of Conservation and Natural Resources and the U.S. Geological Survey have divided Nevada into 14 Hydrographic Regions or basins, which are used to compile information on water resources. These regions are further subdivided into 232 Hydrographic Areas (256 Hydrographic Areas and Sub-areas, combined) for more detailed study. A variety of technical publications have reported recharge estimates for Nevada Hydrographic Areas. Noteworthy examples include two series of publications by the Nevada Department of Conservation and Natural Resources: (1) the Groundwater Resources Reconnaissance Series; and (2) the Water-Resources Bulletins. In some cases, multiple recharge

estimates using different methods, inputs and assumptions are available for the same area/subarea.

Most of the recharge estimates that are available are based on application of the Maxey-Eakin method (Maxey and Eakin 1950 [DIRS 100598], p. 40). Because the focus of these reports is on quantifying how much water is available for groundwater development, these reports provide estimates of the total annual volume of recharge in acre-ft/yr rather than estimating a recharge rate in mm/yr. To generate the recharge estimate, the authors first estimate total annual precipitation for various precipitation zones. Total precipitation in each zone is equal to the area of the zone multiplied by the average annual precipitation rate within that zone. For example precipitation in the zone "15-20 inches" is represented by 1.46 ft of precipitation. Within this zone, the Maxey-Eakin method assumes that 15% of this precipitation volume is available for recharge to the aquifer. By calculating the total precipitation and recharge volume in each zone and summing up the results, a basin-wide estimate of precipitation and recharge can be calculated. One complicating factor is that the Maxey-Eakin method assumes that no recharge occurs in areas with less than 8 inches of annual precipitation. In some cases, the precipitation calculated for a basin does not include areas that receive less than 8 inches of precipitation. Neglecting this precipitation volume has no consequence for the estimate of recharge volume since the neglected areas are assumed to contribute no recharge, but these areas are important when the goal is to estimate precipitation and recharge rates over the entire basin. When total precipitation volume for the areas receiving less than 8 inches of annual precipitation is not estimated in the report, we have assumed that the precipitation in these areas is equal to 0.5 ft, which is consistent with many of the reports that include precipitation estimates for the entire basin. It should be noted that the Maxey Eakin method is very approximate and estimates based on this method are characterized by considerable uncertainties. No effort has been made to quantify these uncertainties in this report. Table 7.2.1.2-1[a] lists recharge estimates from application of the Maxey-Eakin method. The basin areas, precipitation and recharge estimates originate from a large collection of reports and the values are typically rounded according to individual author preference.

Table 7.2.1.2-1[a]. Maxey-Eakin Recharge Estimates for Selected Nevada Hydrographic Areas/Subareas

Number [a]	Name	Area (acres)	Precipitation		Recharge		DIRS Sources for Basin Size and Precipitation
			(acre-ft/yr)	(mm/yr)	(acre-ft/yr)	(mm/yr)	
1	Pueblo Valley	70,100	57,000	248	2,000	8.7	184734
2	Continental Lake Valley	348,100	284,000	249	11,000	9.6	184734
3	Gridley Lake Valley	110,100	97,900	271	4,500	12.5	184734
4	Virgin Valley	280,000	230,000	250	7,000	7.6	184734
6	Guano Valley	237,200	206,000	265	7,500	9.6	184707
8	Massacre Lake Valley	116,400	97,000	254	3,500	9.2	184707
9	Long Valley	340,600	241,000	216	6,000	5.4	184707
11	Coleman Valley	32,400	28,000	263	1,000	9.4	184707
12	Mosquito Valley	19,600	16,000	249	700	10.9	184707
14	Surprise Valley	41,900	37,500	273	1,500	10.9	184707
15	Boulder Valley	63,600	54,000	259	2,000	9.6	184707

Table 7.2.1.2-1[a]. Maxey-Eakin Recharge Estimates for Selected Nevada Hydrographic Areas/Subareas (Continued)

Number [a]	Name	Area (acres)	Precipitation		Recharge		DIRS Sources for Basin Size and Precipitation
			(acre-ft/yr)	(mm/yr)	(acre-ft/yr)	(mm/yr)	
16	Duck Lake Valley	355,000	282,000	242	9,000	7.7	184709
17	Pilgrim Flat	6,360	7,000	335	500	24.0	184725
18	Painters Flat	35,650	31,000	265	1,300	11.1	184725
19	Dry Valley	27,120	14,000	157	200	2.2	184725
20	Sano Valley	7,600	3,100	124	<10	0.1	184725
21	Smoke Creek Desert	716,500	440,000	187	13,000	5.5	184725
22	San Emidio Desert	197,000	100,000	155	2,100	3.2	184725
24	Hualapai Flat	115,000	85,000	225	4,000	10.6	184705
25	High Rock Lake Valley	525,000	435,000	253	13,000	7.5	184712
27	Summit Lake Valley	34,800	42,700	374	4,200	36.8	184712
28	Black Rock Desert	202,600	205,200	309	13,000	19.6	184712
29	Pine Forest Valley	342,300	260,000	232	10,000	8.9	184696
30	Kings River Valley	265,000	222,000	255	15,000	17.3	184760
31	Desert Valley	670,000	300,000	136	5,000	2.3	184739
33	Quinn River Valley	1,300,000	1,200,000	281	74,000	17.4	184751
34	East Little Owyhee River Area	453,000	357,000	240	2,700	1.8	184726
35	South Fork Owyhee River Area	1,006,000	1,004,000	304	28,000	8.5	184726
36	Independence Valley	320,000	441,000	420	20,000	19.1	184726
37	Owyhee River Area	331,000	458,000	422	17,000	15.7	184726
38	Bruneau River Area	326,000	497,000	465	26,000	24.3	184726
39	Jarbidge River Area	174,000	334,000	585	32,000	56.1	184726
40	Salmon Falls Creek Area	771,000	1,021,000	404	44,000	17.4	184726
41	Goose Creek Area	204,000	198,000	296	6,700	10.0	184726
46	South Fork Area	66,000	98,000	453	4,000	18.5	184721
47	Huntington Valley	505,000	554,000	334	14,000	8.4	184721
48	Dixie Creek-Tenmile Creek Area	249,000	235,000	288	13,000	15.9	184721
50	Susie Creek Area	140,000	150,000	327	9,700	21.1	184752
51	Maggie Creek Area	260,000	280,000	328	23,000	27.0	184752
52	Marys Creek Area	38,000	35,000	281	2,100	16.8	184752
53	Pine Valley	638,000	654,220	313	46,000	22.0	184693
55	Carico Lake Valley	243,000	160,000	201	4,300	5.4	184722
56	Upper Reese River Valley	762,000	702,000	281	37,000	14.8	184717
57	Antelope Valley (Region 4)	290,000	261,200	275	11,000	11.6	184711
61	Boulder Flat	360,000	290,000	246	14,000	11.9	184752
62	Rock Creek Valley	290,000	260,000	273	13,000	13.7	184752
63	Willow Creek Valley	270,000	280,000	316	20,000	22.6	184752
67	Little Humboldt Valley	453,000	400,000	269	21,000	14.1	184755
68	Hardscrabble Area	113,000	120,000	324	9,000	24.3	184755
69	Paradise Valley	381,000	250,000	200	10,000	8.0	184755
71	Grass Valley	332,800	250,000	229	12,000	11.0	184740
72	Imlay Area	480,000	310,300	197	4,000	2.5	184699
74	White Plains	101,000	51,000	154	100	0.3	184735

Table 7.2.1.2-1[a]. Maxey-Eakin Recharge Estimates for Selected Nevada Hydrographic Areas/Subareas (Continued)

Number [a]	Name	Area (acres)	Precipitation		Recharge		DIRS Sources for Basin Size and Precipitation
			(acre-ft/yr)	(mm/yr)	(acre-ft/yr)	(mm/yr)	
75	Bradys Hot Springs Area	114,000	59,000	158	160	0.4	184746
76	Fernley Area	75,300	43,000	174	600	2.4	184747
77	Fireball Valley	37,800	21,000	169	200	1.6	184746
78	Granite Springs Valley	626,000	350,000	170	3,500	1.7	184746
79	Kumiva Valley	214,000	120,000	171	1,000	1.4	184746
80	Winnemucca Lake Valley	230,000	130,000	172	2,900	3.8	184747
81	Pyramid Lake Valley	320,000	320,000	305	6,600	6.3	184747
82	Dodge Flat	57,800	43,000	227	1,400	7.4	184747
83	Tracy Segment	188,000	150,000	243	6,000	9.7	184747
84	Warm Springs Valley	159,800	130,000	248	6,000	11.4	184724
85	Spanish Springs Valley	46,600	30,000	196	600	3.9	184747
86	Sun Valley	6,330	4,000	193	50	2.4	184747
87	Truckee Meadows	131,000	160,000	372	27,000	62.8	184747
88	Pleasant Valley	23,500	46,000	597	10,000	129.7	184747
89	Washoe Valley	49,600	87,000	535	15,000	92.2	184747
91	Truckee Canyon Segment	48,600	110,000	690	27,000	169.3	184747
92	Lemmon Valley	62,000	50,000	246	1,500	7.4	184723
95	Dry Lake Valley	52,200	44,000	257	2,400	14.0	184724
96	Newcomb Lake Valley	4,790	4,500	286	300	19.1	184724
97	Honey Lake Valley	150,000	86,000	175	15,000	30.5	184724
98	Skedaddle Creek Valley	26,820	20,000	227	600	6.8	184725
100	Cold Spring Valley	19,800	18,000	277	900	13.9	184724
101	Carson Desert	1,290,000	660,000	156	1,300	0.3	184735
102	Churchill Valley	314,000	170,000	165	1,300	1.3	184735
103	Dayton Valley	233,000	180,000	235	7,900	10.3	184735
104	Eagle Valley	45,400	58,000	389	8,700	58.4	184744
105	Carson Valley	270,000	275,000	310	25,000	28.2	184735
110	Walker Lake Valley	717,000	410,000	174	6,500	2.8	181394
111	Alkali Valley	43,300	36,000	253	1,400	9.9	180759
112	Mono Valley	18,400	16,000	265	700	11.6	180759
113	Huntoon Valley	68,600	43,000	191	800	3.6	180759
114	Teels Marsh Valley	201,000	120,000	182	1,300	2.0	180759
115	Adobe Valley	7,410	6,400	263	300	12.3	180759
116	Queen Valley	40,400	35,000	264	2,000	15.1	180759
117	Fish Lake Valley	647,000	465,000	219	33,000 [c]	15.5	184733
118	Columbus Salt Marsh Valley	242,000	100,000	126	700	0.9	180759
119	Rhodes Salt Marsh Valley	130,000	59,000	138	500	1.2	180759
120	Garfield Flat	61,400	34,000	169	300	1.5	180759
121	Soda Spring Valley	244,900	107,000	133	700	0.9	180759
122	Gabbs Valley	735,000	523,000	217	5,200	2.2	184701
123	Rawhide Flats	145,000	75,000	158	150	0.3	181394
130	Pleasant Valley	23,500	46,000	597	10,000	129.7	184747

Table 7.2.1.2-1[a]. Maxey-Eakin Recharge Estimates for Selected Nevada Hydrographic Areas/Subareas (Continued)

Number [a]	Name	Area (acres)	Precipitation		Recharge		DIRS Sources for Basin Size and Precipitation
			(acre-ft/yr)	(mm/yr)	(acre-ft/yr)	(mm/yr)	
133	Edwards Creek Valley	262,000	187,000	218	8,000	9.3	184715
134	Smith Creek Valley	359,000	276,000	234	12,000	10.2	184716
134	Smith Creek Valley	349,000 [b]	249,000 [b]	217	9,600 [b]	8.4	177727 and 184716
135	Ione Valley	309,000	230,000	227	8,000	7.9	184716
136	Monte Cristo Valley	178,000	94,000	161	500	0.9	180759
137	Big Smoky Valley	1,025,000	580,000	172	12,000	3.6	182756
138	Grass Valley	384,000	290,000	230	13,000	10.3	184722
139	Kobeh Valley	560,000	460,000	250	11,000	6.0	184741
140	Monitor Valley	677,000	510,000	230	21,300	9.6	184741
141	Ralston Valley	621,000	475,000	233	16,000	7.9	176818
142	Alkali Spring Valley	205,000	100,000	149	100	0.1	176849
143	Clayton Valley	332,000	180,000	165	1,500	1.4	176849
144	Lida Valley	342,000	170,000	152	500	0.4	176849
145	Stonewall Flat	219,000	110,000	153	100	0.1	176849
146	Sarcobatus Flat	542,000	190,000	107	1,200	0.7	106695
147	Gold Flat	435,000	250,000	175	3,800	2.7	102893
148	Cactus Flat	257,000	130,000	154	600	0.7	102893
149	Stone Cabin Valley	613,000	477,000	237	16,000	8.0	176818
151	Antelope Valley (Region 10)	292,000	190,000	198	4,100	4.3	184741
152	Stevens Basin	11,800	8,500	220	200	5.2	184741
153	Diamond Valley	455,000	378,000	253	16,000	10.7	148765
153	Diamond Valley	470,000	400,000	259	21,000	13.6	184721
154	Newark Valley	512,000	410,000	244	18,000	10.7	184690
155	Little Smoky Valley (Northern Part)	374,400	230,000	187	4,000	3.3	176950
156	Little Smoky Valley (Southern Part)	336,500	200,000	181	1,400	1.3	176950
157	Kawich Valley	230,000	150,000	199	3,500	4.6	102893
159	Yucca Flat	192,000	100,000	159	700	1.1	102893
160	Frenchman Flat	296,000	150,000	154	100	0.1	102893
161	Indian Springs Valley	418,000	270,000	197	10,000	7.3	102893
163	Mesquite Valley (NV & CA)	294,000	160,000	166	1,500	1.6	105354
164	Ivanpah Valley	438,000	230,000	160	1,500	1.0	105354
165	Jean Lake Valley	82,800	32,000	118	100	0.4	105354
167	Eldorado Valley	337,000	190,000	172	1,100	1.0	184720
169	Tikapoo Valley (Northern Part)	401,000	230,000	175	2,600	2.0	102893
169	Tikapoo Valley (Southern Part)	243,000	150,000	188	3,400	4.3	102893
170	Penoyer Valley	443,000	270,000	186	4,300	3.0	176848
171	Coal Valley	219,000	172,000	239	2,000	2.8	184710
172	Garden Valley	316,000	227,000	219	10,000	9.6	184710
173	Railroad Valley (N+S)	1,760,000	1,200,000	208	52,000	9.0	176848
175	Long Valley	416,000	344,000	252	10,000	7.3	184694

Table 7.2.1.2-1[a]. Maxey-Eakin Recharge Estimates for Selected Nevada Hydrographic Areas/Subareas (Continued)

Number [a]	Name	Area (acres)	Precipitation		Recharge		DIRS Sources for Basin Size and Precipitation
			(acre-ft/yr)	(mm/yr)	(acre-ft/yr)	(mm/yr)	
176	Ruby Valley	640,000	674,000	321	68,000	32.4	101237
177	Clover Valley	288,000	259,000	274	20,700	21.9	101237
180	Cave Valley	235,000	221,000	287	14,000	18.2	184708
181	Dry Lake Valley	575,400	244,000	129	5,000	2.6	148766
182	Delamar Valley	247,000	138,000	170	1,000	1.2	148766
185	Tippett Valley	223,000	160,000	219	6,900	9.4	184732
186	Antelope Valley, Northern Part (Region 10)	171,000	120,000	214	3,200	5.7	184732
187	Antelope Valley, Southern Part (Region 10)	82,100	58,000	215	1,500	5.6	184732
188	Independence Valley (Pequop Valley)	336,000	258,000	234	9,300	8.4	101237
189	Thousand Springs Valley	914,000	600,000	200	12,000	4.0	184727
191	Pilot Creek Valley	213,000	130,000	186	2,400	3.4	184732
192	Great Salt Lake Desert	327,000	200,000	186	4,800	4.5	184732
193	Deep Creek Valley (Nevada Part)	134,000	86,000	196	2,200	5.0	184732
195	Snake Valley	2,230,000	2,000,000	273	105,000	14.4	184743
197	Escalante Desert	71,000	76,000	326	2,300	9.9	184730
201	Spring Valley	184,000	178,000	295	10,000	16.6	176502
202	Patterson Valley	266,000	194,000	222	6,000	6.9	176502
206+210	Coyote and Kane Springs Valleys	605,500	312,000	157	2,600	1.3	184714
208	Pahroc Valley	328,000	188,000	175	2,200	2.0	176646
209	Pahranagat Valley	507,000	272,000	164	1,800	1.1	176646
211	Three Lakes Valley, Northern Part	192,000	110,000	175	2,000	3.2	102893
211	Three Lakes Valley, Southern Part	199,000	130,000	199	6,000	9.2	102893
212	Las Vegas Valley (W slope of sheep range only)	56,000	48,000	261	4,700	25.6	102893
213	Colorado River Valley	415,000	180,000	132	200	0.1	184720
214	Piute Valley	493,000	240,000	148	1,700	1.1	184720
215	Black Mountains Area	401,000	200,000	152	70	0.1	184729
216	Garnet Valley	107,000	58,000	165	400	1.1	184729
217	Hidden Valley	46,000	28,000	186	400	2.7	184729
218	California Wash	208,000	100,000	147	60	0.1	184729
220	Lower Moapa Valley	151,000	76,000	153	40	0.1	184729
221	Tule Desert	163,000	106,000	198	2,100	3.9	184730
222	Virgin River Valley	976,000	580,000	181	9,500	3.0	184730
223	Gold Butte Area	339,000	180,000	162	1,000	0.9	184729
224	Greasewood Area	72,700	43,000	180	600	2.5	184729
225	Mercury Valley	71,900	38,000	161	250	1.1	102893
226	Rock Valley	51,100	26,000	155	30	0.2	102893
228	Oasis Valley	278,000	150,000	164	1,000	1.1	102893
229	Crater Flat	116,000	61,000	160	220	0.6	102893
230	Amargosa Desert	1,675,000	875,000	159	1,500	0.3	103022

Table 7.2.1.2-1[a]. Maxey-Eakin Recharge Estimates for Selected Nevada Hydrographic Areas/Subareas (Continued)

Number [a]	Name	Area (acres)	Precipitation		Recharge		DIRS Sources for Basin Size and Precipitation
			(acre-ft/yr)	(mm/yr)	(acre-ft/yr)	(mm/yr)	
231	Grapevine Canyon	96,000	49,000	156	50	0.2	176849
232	Oriental Wash	118,000	58,000	150	300	0.8	176849

[a] A number of the 256 hydrographic basins are not listed because the data necessary to estimate recharge was not found (basin area, precipitation, etc)

[b] Basin area and annual precipitation volume calculated as the sum of values provided in the two references listed. For area above 7,000 ft in elevation, values (including total recharge) are given in Thomas et al. (1989 [DIRS 177727], pp. 15-16). For area below 7,000 ft in elevation values are from Evertt and Rush (1964 [DIRS 184716], Table 3, p. 10).

[c] Source indicates that recharge estimate may be high.

In addition to the Maxey-Eakin method, there are several other methods that have been applied to a number of the Nevada basins. These include: chloride mass balance, water balance modeling, and modeling of chemical tracers (e.g., deuterium). The application of these methods to basins in Nevada is summarized below.

Dettinger (1989 [DIRS 105384], Table 2) provides average chloride concentrations from 15 hydrographic areas/subareas in Nevada. In addition, Thomas et al. (1989 [DIRS 177727], pp. 15 and 16) provides a chloride concentration measured in the groundwater for Smith Creek Valley. These concentrations, along with estimates of total precipitation for the basins (sources listed in Table 7.2.1.2-2[a]) were used to calculate recharge volumes for these basins. Recharge rates were calculated by dividing recharge volumes by total basin area. This method differs somewhat from the method followed by Dettinger (1989 [DIRS 105384]), who assumed that parts of the basins with less than 12 inches of precipitation did not contribute to the chloride mass balance. In this way, the estimates provided by Dettinger are dependant upon Maxey-Eakin estimates. The problem with this assumption is that chloride present in the groundwater today may have been transported to the water table over thousands of years. This means that during wetter climates (such as during the last glacial period), the area over which recharge occurred was probably more extensive and therefore it is not reasonable to exclude these areas from contributing chloride to the groundwater, unless there is adequate soil data to quantify the amount of chloride stored in the soil and bedrock. Chloride and other tracer studies at the Nevada Test Site have confirmed that tracers (including chloride) are not in steady state and concentrations at depth may represent paleoclimate conditions (Tyler et al. 1996 [DIRS 108774]). In fact, the chloride mass balance estimates may represent lower bounds because modern precipitation is considerably less than rates during the last glacial maximum. In any case chloride mass balance estimates are associated with numerous uncertainties, which are not quantified in this report.

Avon and Durbin (1994 [DIRS 177200], Table 2) collected and evaluated basin-wide recharge estimates based on a water budget model for a number of Nevada hydrographic areas/subareas. Using basin areas and annual precipitation volumes, equivalent precipitation and recharge rates in mm/yr are calculated. Table 7.2.1.2-3[a]) presents these recharge estimates.

Avon and Durbin (1994 [DIRS 177200], Table 3) also present "model estimates" for 27 hydrographic areas/subareas. The "model estimates" were calculated using a variety of methods: (1) groundwater flow models; (2) a numerical infiltration model; (3) chloride mass balance; and (4) a deuterium-calibrated mixing-cell flow model. Table 7.2.1.2-4[a] lists six recharge estimates from the deuterium-calibrated mixing-cell flow model for basins with known area and precipitation. The other model estimates either are presented in other tables in this section or sufficient information about basin area or precipitation was not found.

Table 7.2.1.2-2[a]. Chloride Mass Balance Recharge Estimates for Selected Nevada Hydrographic Areas/Subareas [a]

Number [a]	Name [b]	Size (acres)	Precipitation		Recharge (CMB) [b]		DIRS Sources for Basin Size and Precipitation
			(acre-ft/yr)	(mm/yr)	(acre-ft/yr)	(mm/yr)	
16	Duck Lake Valley	355,000	282,000	242	10,743	9.2	184709
56	Upper Reese River	762,000	702,000	281	35,100	14.0	184717
92	Lemmon	62,000	50,000	246	2,667	13.1	184753
117	Fish Lake	647,000	465,000	219	48,947	23.1	184733
122	Gabbs	735,000	523,000	217	6,339	2.6	184701
134	Smith Creek Valley	349,000 [c]	249,000 [c]	217	22,636	19.8	177727 and 184716
153	Southern Diamond	275,800	240,000	265	10,787	11.9	184754
163	Mesquite Valley (NV & CA)	294,000	160,000	177	7,273	7.5	105354
170	Penoyer	443,000	270,000	186	9,818	6.8	176848
173	Railroad Valley (Northern)	1,380,000	960,000	212	43,636	9.6	176848
173	Railroad Valley (Southern)	381,000	240,000	192	9,143	7.3	176848
178	Northern Butte Valley	170,000	140,000	251	6,437	11.5	184728
178	Southern Butte Valley	465,000	420,000	275	27,097	17.8	184728
184	Spring	1,085,000	960,000	270	75,294	21.2	184718

[a] Hydrographic area number

[b] Basin and sub-basin names and chloride data (except Smith Creek Valley) are from Dettinger (1989 [DIRS 105384], Table 2, p. 69). Recharge calculated as the product of chloride concentration ratio and the total annual precipitation. Note that resulting recharge rates reported here are higher than reported in Dettinger (1989 [DIRS 105384], Table 2, p. 69) because precipitation over entire basin was used to calculate recharge, while Dettinger only used precipitation falling in areas receiving greater than 8 inches per year.

[c] Basin area and annual precipitation volume calculated as the sum of values provided in the two references listed. For area above 7,000 ft in elevation, values are given in Thomas et al. (1989 [DIRS 177727], pp. 15-16). For area below 7,000 ft in elevation values are from Evertt and Rush (1964 [DIRS 184716], Table 3, p. 10).

Table 7.2.1.2-3[a]. Water Budget Model Recharge Estimates for Selected Nevada Hydrographic Areas/Subareas [a]

Number [a]	Name	Size (acres)	Precipitation		Recharge		DIRS Sources for basin size and precipitation
			(acre-ft/yr)	(mm/yr)	(acre-ft/yr)	(mm/yr)	
16	Duck Lake Valley	355,000	282,000	242	7,000	6.0	184709
18	Painter Flat	35,650	31,000	265	1,200	10.3	184725
21	Smoke Creek Desert	716,500	440,000	187	18,620	7.9	184725
22	San Emidio Desert	197,000	100,000	155	3,200	5.0	184725
24	Hualapai Flat	115,000	85,000	225	6,700	17.8	184705
29	Pine Forest Valley	342,000	260,000	232	14,100	12.6	184696
53	Pine Valley	638,000	654,220	313	24,000	11.5	184693
55	Carico Lake Valley	243,000	160,000	201	4,500	5.6	184722
71	Grass Valley (entire)	384,000	290,000	230	16,800	13.3	184722
84	Warm Springs Valley	159,800	130,000	248	2,000	3.8	184724
92	Lemmon Valley	61,200	48,000	239	900	4.5	184724
95	Dry Valley	52,200	44,000	257	2,300	13.4	184724
96	Newcomb Lake Valley	4,790	4,500	286	130	8.3	184724
111A	Alkali Valley (Northern Part)	11,200	9,500	259	300	8.2	180759
113	Huntoon Valley	68,600	43,000	191	300	1.3	180759
114	Teels Marsh Valley	201,000	120,000	182	1,400	2.1	180759
117	Fish Lake Valley	647,000	465,000	219	27,000	12.7	184733
118	Columbus Salt Marsh Valley	242,000	100,000	126	3,800	4.8	180759
119	Rhodes Salt Marsh Valley	130,000	59,000	138	600	1.4	180759
121	Soda Springs Valley Eastern Part	160,000	72,000	137	700	1.3	180759
133	Edwards Creek Valley	262,000	187,000	218	7,600	8.8	184715
134	Smith Creek	359,000	276,000	234	7,000	5.9	184716
136	Monte Cristo Valley	178,000	94,000	161	400	0.7	180759
150	Little Fish Lake Valley	278,300	230,000	252	10,000	11.0	176950
153	Diamond Valley	470,000	400,000	259	21,000	13.6	184754
156	Hot Creek	658,000	390,000	181	6,100	2.8	176950
170	Penoyer Valley	443,000	270,000	186	3,800	2.6	176848

Table 7.2.1.2-3[a]. Water Budget Model Recharge Estimates for Selected Nevada Hydrographic Areas/Subareas [a] (Continued)

Number [a]	Name	Size (acres)	Precipitation		Recharge		DIRS Sources for Basin Size and Precipitation
			(acre-ft/yr)	(mm/yr)	(acre-ft/yr)	(mm/yr)	
178	Butte Valley (South + North)	635,000	560,000	269	20,700	9.9	184728
179	Steptoe Valley	1,265,000	1,200,000	289	70,000	16.9	184723
183	Lake Valley	354,000	293,000	252	11,500	9.9	184713
184	Spring Valley	1,085,000	960,000	270	74,000	20.8	184718

[a] Hydrographic area number.

Source: Recharge values are from Avon and Durbin (1994 [DIRS 177200], Table 2; "Water-Budget Discharge"). A number of the basins listed in this source are not included in this table because data necessary for the calculation was not found (e.g., basin area and/or precipitation volumes).

Table 7.2.1.2-4[a]. Deuterium Mixing Model Recharge Estimates for Selected Nevada Hydrographic Areas/Sub-Areas [a]

Number	Name	Size (acres)	Precipitation		Recharge [a]		DIRS Sources for Basin Size and Precipitation
			(acre-ft/yr)	(mm/yr)	(acre-ft/yr)	(mm/yr)	
175	Long Valley	416,000	344,000	252	5,000	3.7	184694
180	Cave Valley	235,000	221,000	287	12,000	15.6	184708
181	Dry Lake Valley	575,400	244,000	129	6,700	3.5	148766
182	Delamar Valley	247,000	138,000	170	1,800	2.2	148766
208	Pahroc Valley	328,000	188,000	175	2,000	1.9	176646
209	Pahranagat Valley	507,000	272,000	164	1,500	0.9	176646

[a] Source: Recharge values are from Avon and Durbin (1994 [DIRS 177200], Table 3. Only values from the "deuterium model" are listed here. The other recharge estimates are either included in other tables in this section (e.g., Table 7.2.1.2-2[a]) or data necessary to estimate recharge rate was not found (e.g., basin area and/or precipitation volumes).

Lichty and McKinley (1995 [DIRS 100589], Tables 1 and 15) investigated groundwater recharge rates for 3-Springs and East Stewart basins, two small basins in central Nevada. Two independent modeling approaches were used at each site: water budget and chloride mass balance methods. Their results are presented in Table 7.2.1.2-5[a]. The results for the East Stewart basin are included even though the precipitation in this basin is substantially higher than would be expected at Yucca Mountain, even for the glacial transition climate. One observes that for the 3-Springs basin, the chloride mass balance estimates are approximately three times higher than the water balance estimate.

Table 7.2.1.2-5[a]. Recharge to 3-Springs Basin, Central Nevada [a]

Basin	Area (km^2)	Precipitation (mm/yr)	Recharge (mm/yr)	
			WB [b]	CMB [b]
3-Springs	4.20	336.4	11.4	32.8
East Stewart	0.93	639.1	321.6	309.9

Source: Lichty and McKinley (1995 [DIRS 100589], Tables 1 and 15). Index-site extrapolation model estimates are given but not included here.

Nichols (2000 [DIRS 178863]) estimated basin-scale recharge rates for 16 hydrographic basins in Nevada. These estimates, which used a modified Maxey-Eakin approach, are listed in Table 7.2.1.2-6[a]. The basin areas used to calculate the annual precipitation in mm/yr are from Nichols (2000 [DIRS 178863], Table C19) and may differ from the areas of these basins presented in other tables in this report. The differences arise from the use of different maps and different analysis techniques that were used.

Table 7.2.1.2-6[a]. Modified Maxey-Eakin Recharge Estimates for 16 Nevada Hydrographic Areas [a]

Number	Name	Area (acres)	Precipitation		Recharge	
			(acre-ft/yr)	(mm/yr)	(acre-ft/yr)	(mm/yr)
150	Little Fish Lake Valley	276,482	236,430	261	9,628	10.6
154	Newark Valley	509,282	515,470	309	49,092	29.4
155	Little Smoky Valley	740,575	523,359	215	12,681	5.2
156	Hot Creek Valley	658,501	424,067	196	5,756	2.7
174	Jakes Valley	270,498	289,477	326	38,203	43.0
175	Long Valley	419,844	452,368	328	47,740	34.7
176	Ruby Valley	638,936	867,225	414	145,636	69.5
177	Clover Valley	292,115	363,327	379	58,802	61.4
178	Butte Valley	652,363	700,905	327	68,989	32.2
179	Steptoe Valley	1,245,618	1,344,191	329	131,469	32.2
184	Spring Valley	1,067,010	1,141,444	326	103,569	29.6
185	Tippett Valley	221,574	211,904	291	12,389	17.0
186	Antelope Valley	255,680	246,551	294	16,824	20.1
187	Goshute Valley	612,169	592,875	295	40,911	20.4
188	Independence Valley	360,670	394,415	333	50,065	42.3
173B	Railroad Valley/Northern Part	1,369,671	1,089,249	242	61,083	13.6

Source: Nichols 2000 [DIRS 178863], Chapter C. Basin areas and annual precipitation volumes differ from values reported for the Maxey-Eakin estimates. The values used here are from Nichols 2000 [DIRS 178863], Table C-19.

Figure 7.2.1.2-2[a] summarizes the basin-scale, net infiltration estimates listed in Tables 7.2.1.2-1[a] through 7.2.1.2-6[a] and plots these data with the MASSIF net infiltration results for three climates. The Maxey-Eakin model (1950 [DIRS 100598], p. 40) (represented as a stepped line on the figure) is also shown for reference. Note that the Maxey-Eakin model line does not match the individual basin-scale Maxey-Eakin model net infiltration estimates, shown as black crosses on the figure. This is because each of these precipitation and recharge estimates is an area-weighted mean value derived from subareas of the basin in which precipitation is estimated locally. For each of these subareas an associated recharge amount is determined using the percent recharge values from Maxey-Eakin (1950 [DIRS 100598] p. 40). Thus the total precipitation and total recharge values are area-weighted mean values and vary depending on the precipitation patterns across the basin, which largely depend on the basin's topographic character. There is fairly good agreement among the methods for relatively low precipitation, but estimates tend to diverge as precipitation increases. The hydrographic areas closest to Yucca Mountain fall at the low end of the recharge scale (less than 10 mm/yr) and correspond well with the MASSIF net infiltration estimates for the Present-Day climate at Yucca Mountain. The MASSIF net infiltration estimates for the monsoon and glacial transition climates are generally within the range for the wetter Nevada basins.

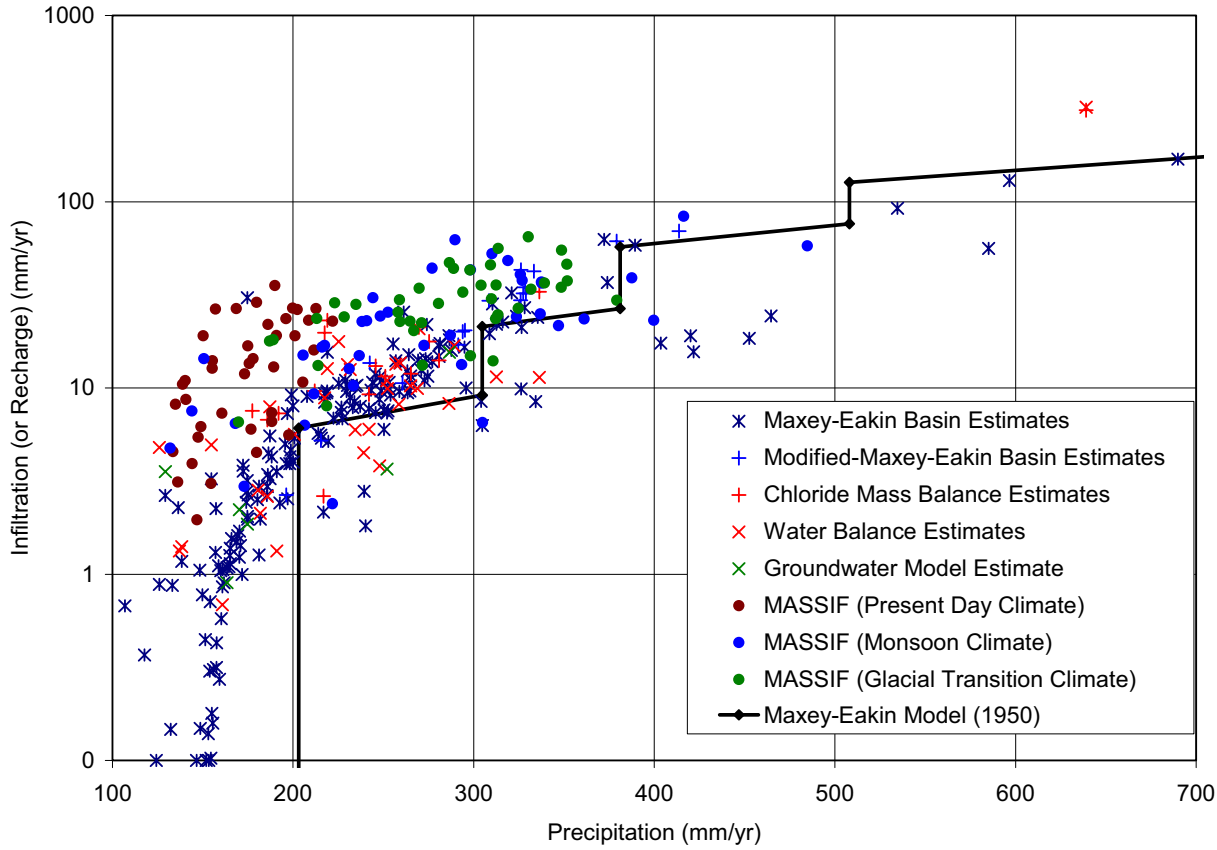

Source: Output DTNs: SN0701T0502206.034, SN0701T0502206.036, and SN0701T0502206.035, respectively (MASSIF results for Present-Day, Monsoon, and Glacial Transition climates). Data are from sources listed for Tables 7.2.1.2-1[a], 7.2.1.2-2[a], 7.2.1.2-3[a], 7.2.1.2-4[a], 7.2.1.2-5[a], and 7.2.1.2-6[a], which are also compiled in validation Output DTN: SN0801T0502206.049.

NOTE: Vertical line that extends to the horizontal axis associated with the Maxey-Eakin Model (1950) represents the precipitation amount below which the model predicts zero recharge.

Figure 7.2.1.2-2[a]. Comparison of Recharge Estimates for Nevada Hydrographic Areas/Subareas with MASSIF Estimates of Net Infiltration at Yucca Mountain

Note that because this section has been completely updated, Table 7.2.1.2-7 of the parent report has been deleted in this addendum. Therefore, Table 7.2.1.2-8 (in Section 7.2.1.2.2 of the parent report) follows Table 7.2.1.2-6[a] in this section.

7.2.1.2.2[a]. Infiltration Estimates for Other Locations in the Southwestern United States

No change.

7.2.1.2.3[a]. Infiltration Estimates for Other Locations the Western United States

Future Climate Analysis (BSC 2004 [DIRS 170002], Table 6-1) identifies several sites on the Columbia Plateau in Eastern Washington (Spokane, Rosalia, and St. John) as average upper bound glacial transition climate analogues. Data from the Columbia Plateau in Washington State are therefore useful because they provide inferences into potential precipitation and recharge at

Yucca Mountain during wetter climates. The Columbia Plateau's position in the rain shadow of the Cascade Mountains is also analogous to the Great Basin position behind the Sierra Nevada Mountains.

Model-derived estimates of average groundwater recharge to the Columbia Plateau regional aquifer system have been reported by Bauer and Vaccaro (1990 [DIRS 177726]). The deep-percolation model for estimating recharge used precipitation, temperature, streamflow, soils, land-use, and altitude data to calculate transpiration, soil evaporation, snow accumulation, snowmelt, sublimation, and evaporation of intercepted moisture. Estimated annual average precipitation, and recharge rates for the various zones included in the Columbia Plateau study are shown in Table 7.2.1.2-9[a]. The average annual precipitation for individual modeling zones ranges from approximately 168 to 956 mm/yr. The majority of these precipitation values are clustered within the range of the bottom half (0.02 to 0.49 probability) of the 40 realizations of precipitation results for the glacial-transition climate shown in Figure 6.5.7.3-1[a] (170 to 289 mm/yr). For these precipitation values, the recharge efficiency varies from about 0.1% to approximately 16%. The precipitation estimates that are within the upper half (0.51 to 0.98 probability) of the 40 realizations exhibit a recharge efficiency varying from approximately 9% to 46%. Bauer and Vaccaro (1990 [DIRS 177726]) estimates are compared with predicted Yucca Mountain net infiltration rates in Figure 7.2.1.2-4[a]. The Maxey-Eakin model is also shown in Figure 7.2.1.2-4[a] for reference.

Table 7.2.1.2-9[a]. Recharge Estimates for Zones on the Columbia Plateau

Zone	Average Annual Precipitation (in/yr)	Average Annual Recharge (in/yr)	Average Annual Precipitation (mm/yr)	Average Annual Recharge (mm/yr)	Efficiency (%)
1	7.29	0.43	185.2	10.9	5.9
2	8.91	1.25	226.3	31.8	14.0
3	9.34	1.37	237.2	34.8	14.7
4	6.61	0.38	167.9	9.7	5.7
5	8.77	1.18	222.8	30.0	13.5
6	8.64	0.66	219.5	16.8	7.6
7	8.26	1.31	209.8	33.3	15.9
8	6.95	0.3	176.5	7.6	4.3
9	7.64	0.43	194.1	10.9	5.6
10	7.93	0.45	201.4	11.4	5.7
11	7.76	0.44	197.1	11.2	5.7
12	7.41	0.15	188.2	3.8	2.0
13	8.19	0.47	208.0	11.9	5.7
14	7.95	0.23	201.9	5.8	2.9
15	6.98	0.13	177.3	3.3	1.9
16	8.31	0.39	211.1	9.9	4.7
17	8.09	0.26	205.5	6.6	3.2
18	12.05	1.3	306.1	33.0	10.8
19	10.09	0.83	256.3	21.1	8.2

Table 7.2.1.2-9[a]. Recharge Estimates for Zones on the Columbia Plateau (Continued)

Zone	Average Annual Precipitation (in/yr)	Average Annual Recharge (inch/yr)	Average Annual Precipitation (mm/yr)	Average Annual Recharge (mm/yr)	Efficiency (%)
20	9.19	0.87	233.4	22.1	9.5
21	17.27	5.39	438.7	136.9	31.2
22	22.75	10.52	577.9	267.2	46.2
23	22.32	6.01	566.9	152.7	26.9
24	9.64	0.57	244.9	14.5	5.9
25	10.33	1.36	262.4	34.5	13.2
26	12.61	2.3	320.3	58.4	18.2
27	12.54	1.68	318.5	42.7	13.4
28	10.05	1.16	255.3	29.5	11.5
29	21.8	3.51	553.7	89.2	16.1
30	10.09	1.42	256.3	36.1	14.1
31	8.69	0.73	220.7	18.5	8.4
32	7.78	0.58	197.6	14.7	7.5
33	11.12	2.74	282.4	69.6	24.6
34	10.24	1.04	260.1	26.4	10.2
35	8.94	0.24	227.1	6.1	2.7
36	10.26	1.17	260.6	29.7	11.4
37	24.3	10.65	617.2	270.5	43.8
38	8.24	0.13	209.3	3.3	1.6
39	22.42	4.13	569.5	104.9	18.4
40	8.15	0.57	207.0	14.5	7.0
41	8.04	0.82	204.2	20.8	10.2
42	9.12	0.84	231.6	21.3	9.2
43	9.04	0.01	229.6	0.3	0.1
44	8.61	0.44	218.7	11.2	5.1
45	18.28	3.3	464.3	83.8	18.1
46	21.06	6.79	534.9	172.5	32.2
47	16.49	1.53	418.8	38.9	9.3
48	20.96	2.98	532.4	75.7	14.2
49	12.93	1.45	328.4	36.8	11.2
50	37.65	15.06	956.3	382.5	40.0
51	11.35	0.29	288.3	7.4	2.6
52	11.34	0.9	288.0	22.9	7.9
53	8.93	0.84	226.8	21.3	9.4

Source: Bauer and Vaccaro 1990 [DIRS 177726], Table 5.

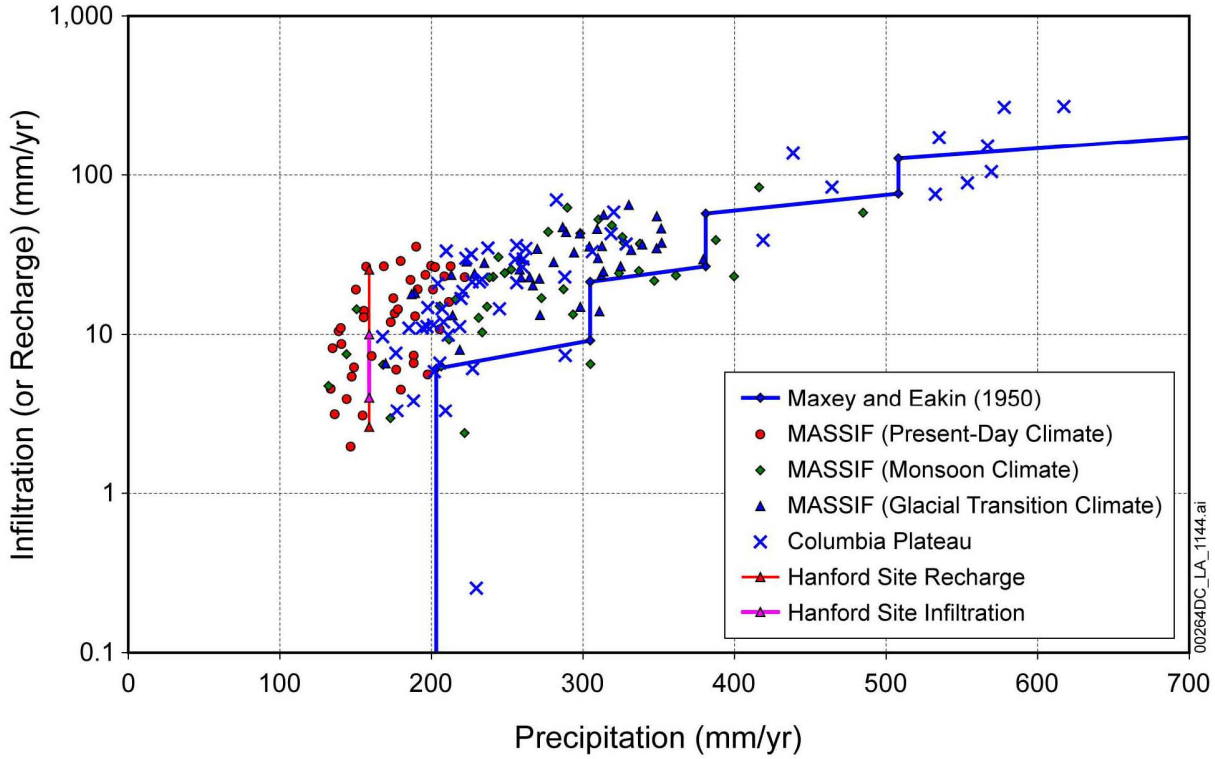

Source: Output DTNs: SN0701T0502206.034, SN0701T0502206.036, and SN0701T0502206.035, respectively (MASSIF results for Present-Day, Monsoon, and Glacial Transition climates). All other data from Validation Output DTN: SN0801T0502206.049.

NOTE: Vertical line that extends to the horizontal axis associated with the Maxey-Eakin model represents the precipitation amount below which the model predicts zero recharge.

Figure 7.2.1.2-4[a]. Comparison of Recharge Estimates for Columbia Plateau with MASSIF Estimates of Net Infiltration at Yucca Mountain

Fayer and Walters (1995 [DIRS 178191]) reported estimated recharge rates at the Hanford site in eastern Washington. They mapped soil type and vegetation/land use categories to measured or estimated recharge rates from a variety of sources (Table 7.2.1.2-10[a]). Estimation methods included lysimeter studies, chloride mass balance calculations, ^{36}Cl studies, and computer modeling. The long-term average recharge rates varied from 2.6 mm/yr for several soil and vegetation combinations to 25.4 mm for cheatgrass. The 30-yr average annual precipitation value of 159 mm/yr for 1951 to 1980 is from the report by Fayer and Walters (1995 [DIRS 178191], Figure A.3). Maher et al. (2003 [DIRS 178540]) reported vadose zone infiltration rates of 4 to 10 mm/yr at the Hanford site. Their estimate was based on strontium isotope ratios measured in pore water, acid extracts, and sediments of a 70-m-thick vadose zone core.

Although average annual precipitation at the Hanford site is closer to the Yucca Mountain Present-Day climate than the Glacial Transition climate, the range in recharge rates from the report by Fayer and Walters (1995 [DIRS 178191], Table 4.1), and the range in infiltration rates from the report by Maher et al. (2003 [DIRS 178540]) are shown plotted in Figure 7.2.1.2-4[a] because the Hanford site is located in eastern Washington.

Table 7.2.1.2-10[a]. Estimated Recharge Rates at the Hanford Site for Combinations of Soil Type and Vegetation/Land Use

Vegetation/Land Use		Recharge Rates (mm/yr)														
		Soil Types[a]														
Index	Description	Ri	Rp	He	Kf	Ba	E1	Ls	Eb	Ki	Wa	Sc	P	Qu	Rv	D
1	Shrub-steppe on slopes	3.4	8.6	2.6	2.6	2.6	2.6	3.4	2.6	3.4	3.4	3.4	3.4	3.4	8.6	8.6
2	Shrub-steppe on plain/uplands	3.4	8.6	2.6	2.6	2.6	2.6	3.4	2.6	3.4	3.4	3.4	3.4	3.4	8.6	8.6
3	Recovering shrub-steppe on plain/uplands	3.4	11.3	2.6	2.6	2.6	2.6	3.4	2.6	3.4	3.4	3.4	3.4	3.4	11.3	11.3
4	Bunchgrass on slopes	3.4	11.3	2.6	2.6	2.6	2.6	3.4	2.6	3.4	3.4	3.4	3.4	3.4	11.3	11.3
5	Hopsage/greasewood	3.4	8.6	2.6	2.6	2.6	2.6	3.4	2.6	3.4	3.4	3.4	3.4	3.4	8.6	8.6
6	Cheatgrass	4.8	25.4	3.4	3.4	2.6	4.9	4.8	4.9	4.8	4.8	4.8	4.8	4.8	25.4	25.4
7	Abandoned fields	4.8	25.4	3.4	3.4	2.6	4.9	4.8	4.9	4.8	4.8	4.8	4.8	4.8	25.4	25.4
10	Sand Dunes	55.4	55.4	55.4	55.4	55.4	55.4	55.4	55.4	55.4	55.4	55.4	55.4	55.4	55.4	55.4
11	Disturbed/Facilities	6.8	55.4	6.4	6.4	4.4	17.3	6.8	17.3	6.8	6.8	6.8	6.8	6.8	55.4	55.4
13	Basalt outcrops	86.7	86.7	86.7	86.7	86.7	86.7	127.1	86.7	86.7	86.7	86.7	86.7	86.7	86.7	86.7

Source: Fayer and Walters 1995 [DIRS 178191], Table 4.1.

[a] Ri = Ritzville silt loam, Rp = Rupert sand, He = Hezel sand, Kf = Koehler sand, Ba = Burbank loamy sand, El = Ephrata sandy loam, Ls = Lickskillet silt loam, Eb = Ephrata stony loam, Ki = Kiona silt loam, Wa = Warden silt loam, Sc = Scootney stoney silt loam, P = Pasco silt loam, Qu = Esquatzel silt loam, Rv = Riverwash, D = Dune sand.

7.2.1.2.4[a]. Infiltration Estimates from the CNWRA

A recent report by the CNWRA staff describes models that were developed and used to calculate the areal average net infiltration, temporally averaged over the next one million years (Stothoff and Walter, 2007 [DIRS 183834]). They also used these models to calculate areal average net infiltration, temporally averaged to represent the present-day climate. The areal averages are calculated for a 13 km^2 footprint box that overlaps the 5.7 km^2 repository footprint (Output DTN: SN0711FTPRNUZB.003). Therefore, comparisons of the CNWRA net infiltration results are not exactly comparable with net infiltration for the repository footprint calculated using MASSIF due to the differences in footprint areas.

Stothoff and Walter (2007 [DIRS 183834]) describe the Orbital-Cycle Climate for Yucca Mountain and Infiltration Tabulator for Yucca Mountain models used for their calculations of net infiltration. The CNWRA net infiltration results are shown in Figure 7.2.1.2-5[a] for present-day and million-year average net infiltration over the footprint box. Net infiltration results calculated using MASSIF for the repository footprint are also shown in this figure. In addition, the range of percolation flux proposed by the NRC (70 FR 53313 [DIRS 178394]) to represent deep percolation for the period after 10,000 years (13 to 64 mm/yr) is also shown in this figure. Figure 7.2.1.2-5[a] shows that MASSIF results for present-day are slightly higher than those calculated by Stothoff and Walter (2007 [DIRS 183834]), a result that is consistent with the comparison to other models shown in Figure 7.2.1.2-1[a]. Figure 7.2.1.2-5[a] also shows MASSIF results for monsoon and glacial-transition climates which are lower than the million-year range reported by Stothoff and Walter (2007 [DIRS 183834]). As shown in Figure 7.2.1.2-5[a], the recent results reported by Stothoff and Walter (2007 [DIRS 183834]) corroborate and bound the range of net infiltration results calculated using MASSIF.

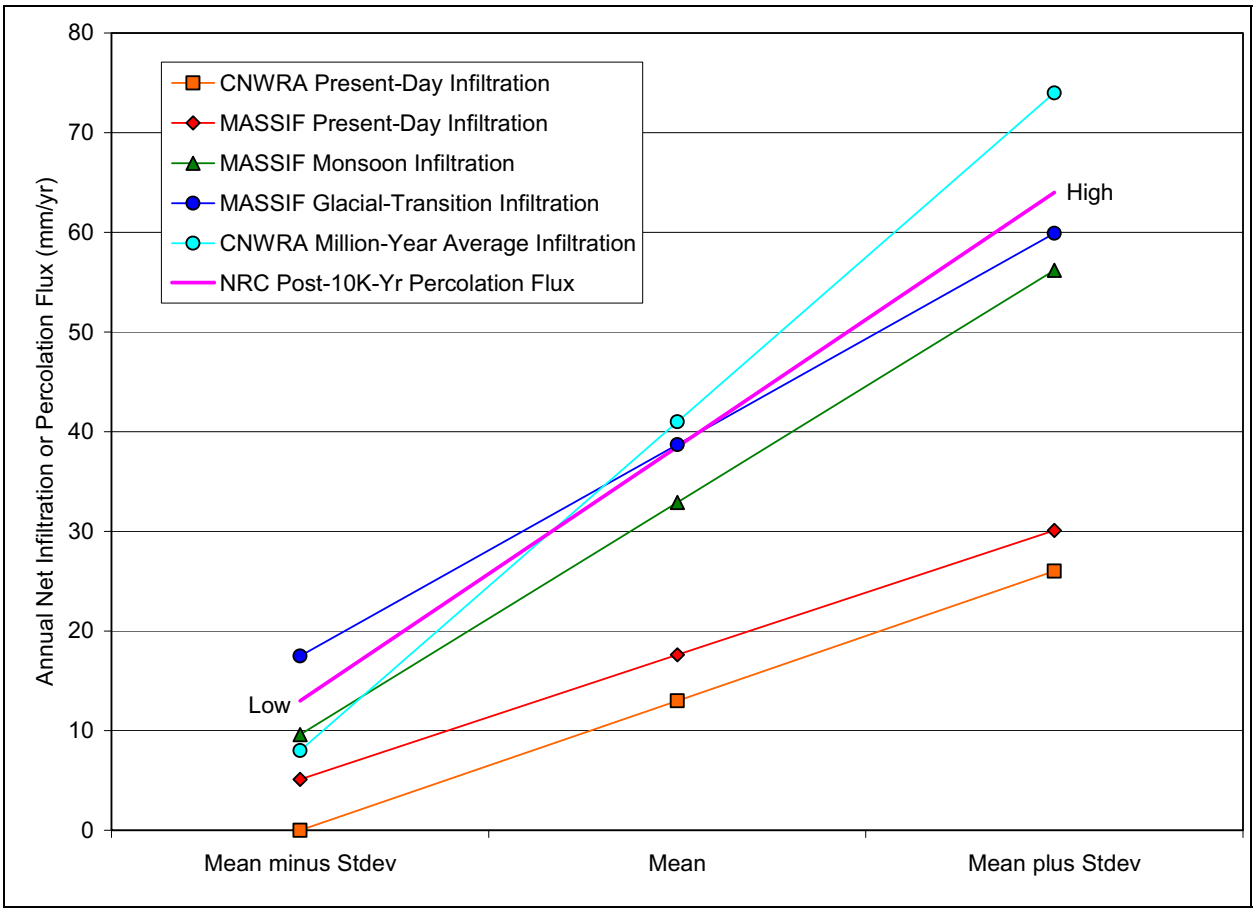

Sources: MASSIF results: Tables 6.5.7.1-2, 6.5.7.2-2, and 6.5.7.3-2 for repository footprint. CNWRA results: Stothoff and Walter (2007 [DIRS 183834], p. iii). NRC proposed post-10,000-year percolation flux: (70 FR 53313 [DIRS 178394]).

NOTE: The NRC proposed post-10,000-year percolation flux is shown as low and high values rather than using standard deviation.

Figure 7.2.1.2-5[a]. Comparison of MASSIF, Center for Nuclear Waste Regulatory Analyses, and NRC Net Infiltration (and Percolation) Fluxes.

7.2.2[a]. Corroboration of MASSIF Infiltration Model Using Alternative Model Approach

This section provides additional corroboration of the MASSIF infiltration model estimates. As discussed previously, there are no site-specific measurements of net infiltration that can be used for model validation. In this section, the model corroboration approach described in Step 6.2.1 of SCI-PRO-006 was used. The approach consists of corroborating model results with other model results obtained from the implementation of mathematical models. The alternative model considered is a one-dimensional unsaturated flow model based on Richards' equation. The computer code HYDRUS-1D (Šimùnek et al. 2005 [DIRS 178140]) was used to perform the simulations. Because HYDRUS-1D is unqualified software its use is limited (by SCI-PRO-006) to model corroboration and cannot be used to directly support model validation. The summary of this model corroboration activity is provided below. The details concerning modeling setup and supporting calculations are in Appendix K.

Four model scenarios were implemented with MASSIF and HYDRUS-1D in this corroboration analysis (Figure 7.2.2-1[a]). The four model scenarios represent one-dimensional homogeneous soil columns that are identical except for the depth of soil and roots in each column. The difference in the depths of the soil columns are as follows: Model 1 has a soil depth of 50 cm, Model 2 has a soil depth of 100 cm, Model 3 has a soil depth of 150 cm, and Model 4 has a soil depth of 200 cm. The plant rooting depth was assumed to be equal to the soil depth in each model scenario. The simulations were performed for one water year (365 days). These conceptual models were incorporated with MASSIF and HYDRUS-1D.

It was anticipated that significant infiltration would be generated in the case of Model 1 (thin soils) and negligible or zero infiltration would be generated in the case of the Model 4 (thick soils). This is consistent with the YMP site conceptual model according to which most infiltration occurs in the places where soils are thin or absent (bedrock outcrops). The corroboration can be considered successful if the cumulative infiltration estimates obtained with MASSIF and HYDRUS-1D are similar.

The same climate data were used as an atmospheric boundary condition in both MASSIF and HYDRUS-1D. The minimum and maximum daily temperatures, precipitation, and wind speed (wind speed is not used in HYDRUS-1D) for one water year were taken from *Weather Summary v2.1 for nominal of PD parameters.xls* located in *Present Day Precipitation* directory supplied with the MASSIF Package (Output DTN: SN0701T0502206.037). The climate data are for set 4 (representative year 952) with the probability of occurrence equal to 0.02. This set was selected because it has high total annual precipitation (471 mm) and consequently, may result in significant infiltration. This annual precipitation has 2% probability under the Present-Day climate at the YMP site.

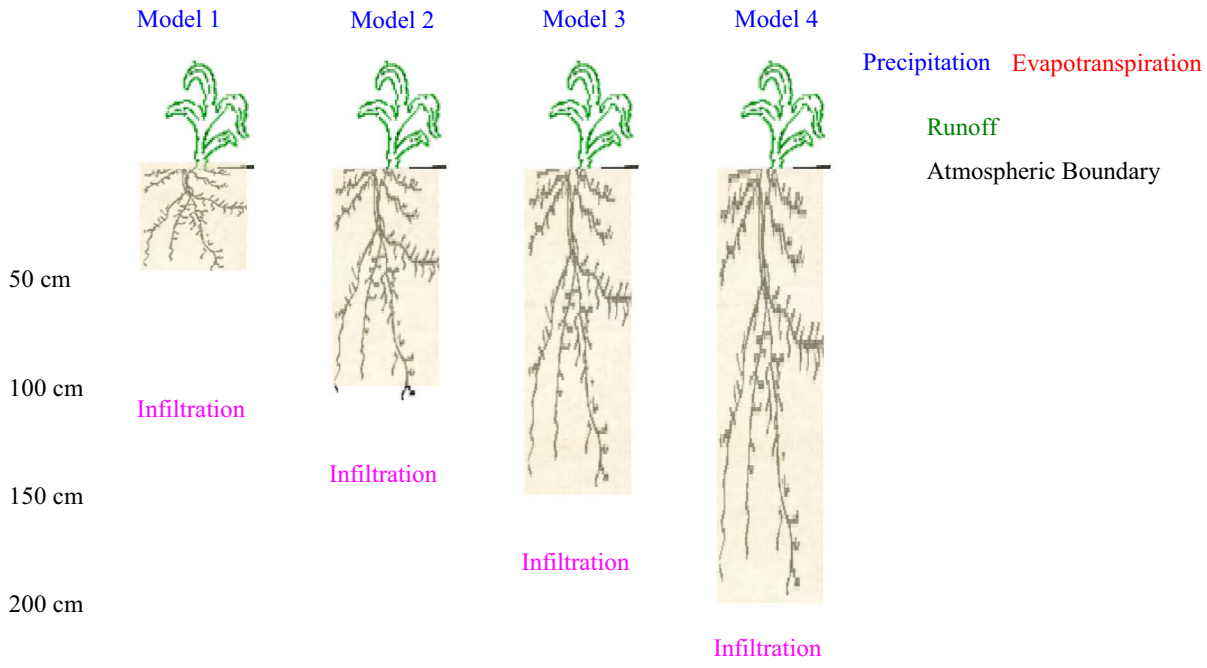

Figure 7.2.2-1[a]. Conceptual Model Used in the Alternative Model Corroboration Analysis

Another input required at the atmospheric boundary is the limiting ET. Slightly different approaches are used in MASSIF and HYDRUS-1D to estimate the limiting ET. MASSIF uses the reference ET concept (Sections 6.3.3 and 6.4.4). Reference ET is calculated internally using the climate data. The default MASSIF parameters for the Present-Day climate (such as first and last day of winter) were used in calculating reference ET. HYDRUS-1D uses the concept of the potential ET. The potential ET is calculated externally using Hargreaves formula (Jensen et al. 1997 [DIRS 177103]). The details are presented in Appendix K. The potential evaporation and potential transpiration have to be specified separately to run HYDRUS-1D. The potential transpiration was calculated as the product of the potential ET and vegetation cover. The vegetation cover was assigned a value of 0.25 for both models. This is a reasonable assumption for the vegetation cover at the site (Appendix D).

The atmospheric boundary conditions used in both codes are shown in Figure 7.2.2-2[a]. As can be seen from this figure, the reference ET tends to be a little higher than the potential ET. This might be due to the fact that the reference ET accounts for the daily wind speed and the mean annual wind speed is higher than 2 m/s, and a value of 2 m/s characterizes the standard condition when the wind correction is not needed.

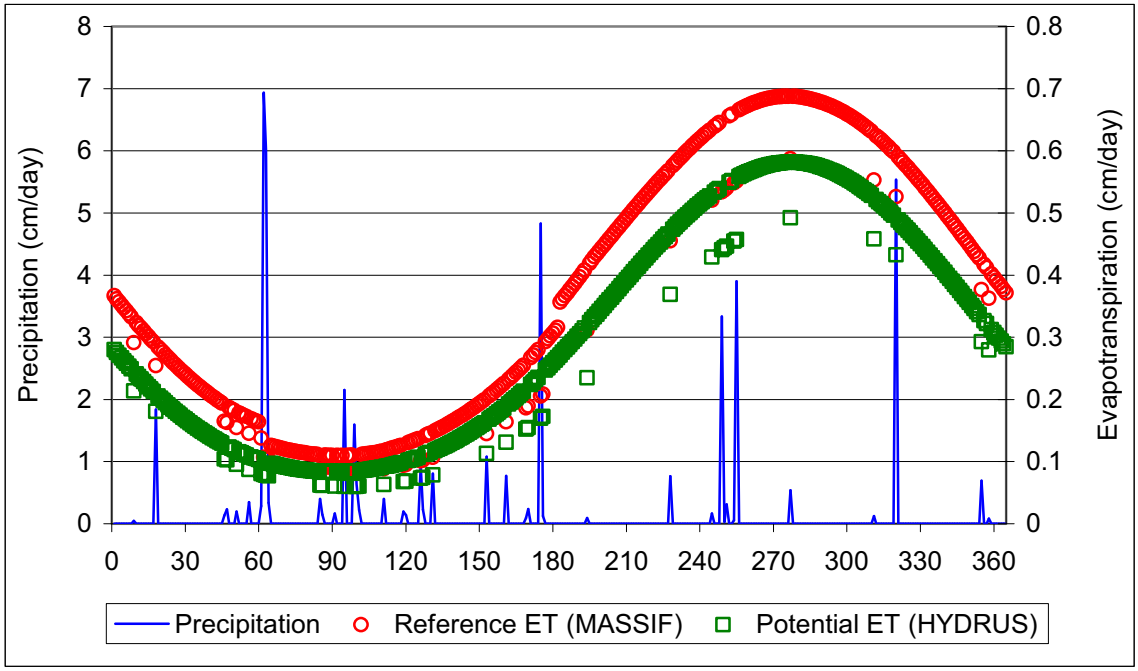

Sources: Output DTN: SN0701T0502206.037; Validation Output DTN: SN0609T0502206.022 (HYDRUS-1D data).

Figure 7.2.2-2[a]. Atmospheric Boundary Conditions Used in MASSIF and HYDRUS-1D

The lower boundary condition (the bottom of the soil profile) in MASSIF is incorporated through the bedrock layer. When the soil water holding capacity is exceeded, the bedrock drains the excess water at the rate equal to the bedrock saturated hydraulic conductivity. The lower boundary in HYDRUS-1D was defined as the seepage boundary. The seepage boundary condition assumes that a zero-flux boundary condition applies as long as the local pressure head at the bottom of the soil profile is negative. However, a zero pressure head will be used as soon as the bottom of the profile becomes saturated. This is conceptually close to, but not equivalent to the boundary condition in MASSIF. This boundary condition does not require the presence of the lower soil or bedrock layer. Thus, the bedrock properties are not used in HYDRUS-1D modeling.

Different concepts are used in MASSIF and in HYDRUS-1D to calculate actual transpiration. MASSIF uses the K_{cb} function concept (Sections 6.3.3 and 6.3.4), and HYDRUS-1D uses the water stress function concept. The water stress function plays a role similar to K_{cb} function—it decreases the potential transpiration. The major difference is that the water stress function reduces potential transpiration based on the pressure head (saturation) in the soil profile, and the K_{cb} function reduces potential transpiration based on the season of the year. Although the saturation is low during the dry season and high during the wet season, there is no direct translation from one function to another one.

The K_{cb} function is incorporated in MASSIF using two coefficients. The first coefficient (C_{kcb1}) represents the intercept and the second one (C_{kcb2}) represents the slope of the $K_{cb} - NDVI'$ linear regression line (Section 6.5.3). Both, C_{kcb1} and C_{kcb2} were set equal to MASSIF defaults for the Present-Day climate (−0.05 and 9.7, respectively).

The other transpiration and evaporation parameters in MASSIF were set equal to the following defaults for the Present-Day climate:

- Evaporation depth Z_e = 0.15 m
- Diffusive evaporation parameter K_{c_min} = 0
- Readily evaporable water parameter rew_1 = 6 mm
- Depletion factor parameter p = 0.65
- Plant height h_{plant} = 0.4 m.

There are no equivalents to these parameters in HYDRUS-1D. The actual ET in HYDRUS-1D is calculated based on the pressure and moisture within the soil profile.

The initial moisture conditions within the soil profile were set equal to 0.08 m^3/m^3 in MASSIF and HYDRUS-1D.

The soil properties used in MASSIF are soil porosity, saturated hydraulic conductivity, field capacity, and wilting point. The additional parameter required is the bedrock saturated hydraulic conductivity. The most common soil grouping within the YMP site is soil group 5/7/9 with the saturated hydraulic conductivity of 6.82×10^{-7} m/s. This group was selected for the analysis. The most common bedrock type selected for this analysis is bedrock type 405 with the saturated hydraulic conductivity of 1.1×10^{-6} m/s. Minimum and maximum bedrock conductivities of 7.37×10^{-7} m/s and 3.34×10^{-6} m/s were used to see if the MASSIF estimates of infiltration would be affected by the type of the bedrock underlying the soil layer. This range of conductivities for rock type 405 is different from the range of values reported in *Data Analysis for Infiltration Modeling: Bedrock Saturated Hydraulic Conductivity Calculation* (BSC 2006 [DIRS 176355], Table 6-11) and used in the MASSIF net infiltration calculations.

The field capacity in MASSIF is considered to lie between the water contents at –1/3 bars and –1/10 bars (Section 6.5.2.3). The wilting point is defined as the water content at –60 bars. The water contents at –1/3 bars, –1/10 bars, and –60 bars were calculated using porosity, residual water content, and van Genuchten parameters *alpha* and *n* selected for HYDRUS-1D runs as described below. The details of these calculations are provided in Appendix K, but it should be noted that the resulting soil properties are not the same as defined for soil group 5/7/9 (Section 6.5.2.3) because the purpose of assigning parameter values is to compare model results run with equivalent parameter inputs not to match Yucca Mountain soil data exactly. The resulting parameter values used in MASSIF are 0.173 m^3/m^3 (water content at –1/3 bars), 0.184 m^3/m^3 (water content at –1/10 bars), and 0.083 m^3/m^3 (water content at –60 bars). These parameters are close to the nominal properties of this soil group.

The soil parameters used in HYDRUS-1D are the parameters needed to define the moisture retention function and hydraulic conductivity–moisture relationship. The van Genuchten model in HYDRUS-1D was used to define these relationships. The input parameters are: residual water content, porosity, saturated hydraulic conductivity, and van Genuchten parameters *alpha* and *n*. The saturated hydraulic conductivity was set equal to the corresponding value in MASSIF. The van Genuchten parameter *alpha* and *n* were set equal to 0.002 cm^{-1} and 1.21. The residual water content and porosity were set equal to 0.022 and 0.19 m^3/m^3. Note that porosity is not used in MASSIF unless a significant runoff is generated (which should not be the

case for the conceptual models in consideration). As described above, these parameters result in the soil properties close to the nominal ones.

Four HYDRUS-1D models were developed using the initial and boundary conditions and modeling parameters described above. The inputs for these models are in Validation Output DTN: SN0609T0502206.021. The results of calculations are in Validation Output DTN: SN0609T0502206.022.

The MASSIF simulations were performed using an interface (*Alternative_Model.xmcd*) to MASSIF that was specifically designed for this purpose. This interface is provided as part of the MASSIF package (Output DTN: SN0701T0502206.037). The interface defines the MASSIF parameters described above, runs MASSIF calculations, and stores the results of the calculations. The interface calculates the soil water storage within the soil column, the daily cumulative infiltration, the total annual runoff, infiltration, and actual ET, and the change in storage. The interface reads the HYDRUS-1D results consisting of daily soil water storage and cumulative infiltration values. The interface displays the daily water storage and cumulative infiltration values calculated by MASSIF and HYDRUS-1D and calculates the mean root squared error between the MASSIF and HYDRUS-1D storage values to provide some basis for the comparison. The best match between the HYDRUS-1D and MASSIF results was obtained with the field capacity set equal to the water content at –1/10 bars (0.184 m^3/m^3).

The comparison between the water storage and cumulative infiltration calculated by MASSIF and HYDRUS-1D for the four models is presented in Figures 7.2.2-3 a[a] through d[a]).

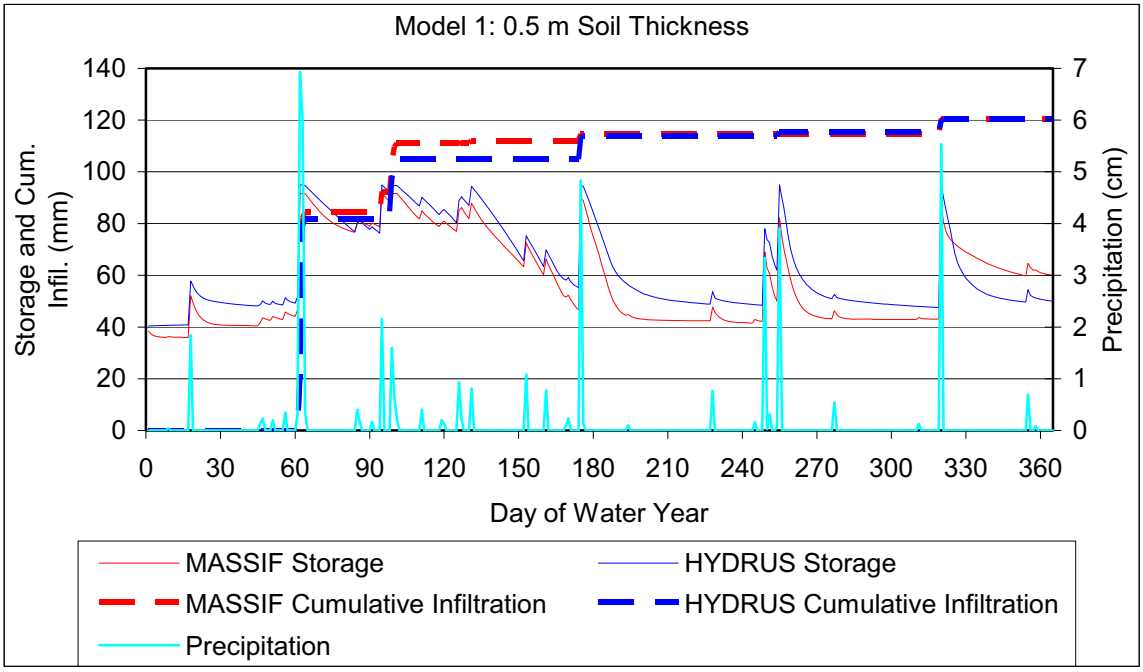

Source: Validation Output DTN: SN0609T0502206.022, *Alternative_Model_Outputs\Alternative_Model_Output.xls*.

Figure 7.2.2-3a[a]. Soil Water Storage and Cumulative Infiltration for Model 1

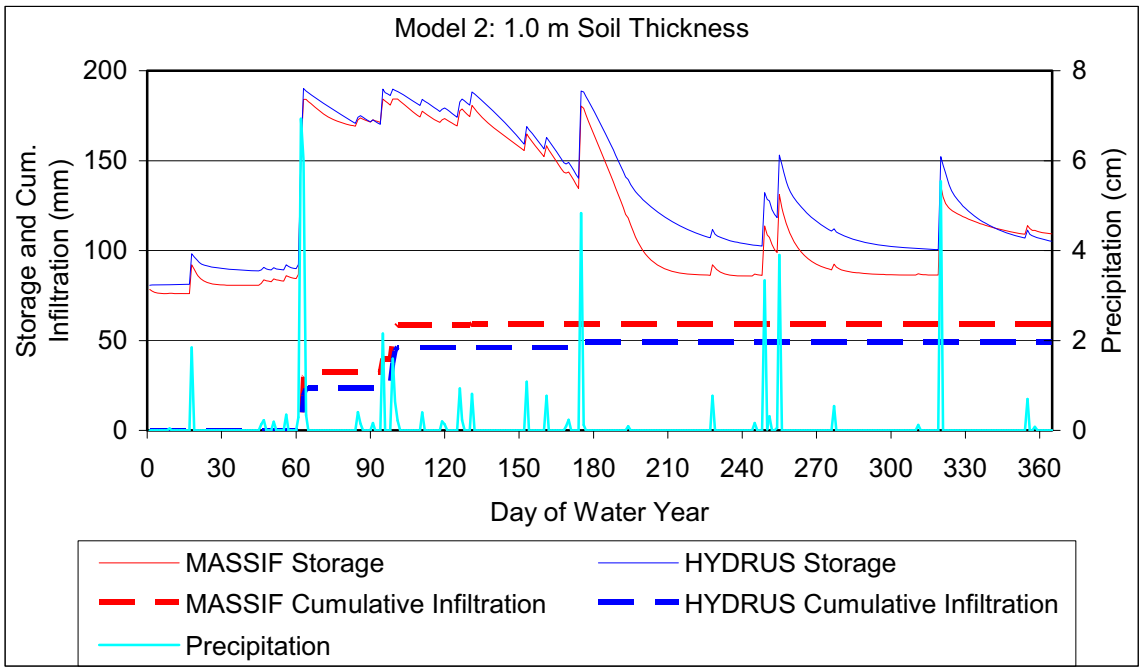

Source: Validation Output DTN: SN0609T0502206.022, *Alternative_Model_Outputs\Alternative_Model_Output.xls.*

Figure 7.2.2-3b[a]. Soil Water Storage and Cumulative Infiltration for Model 2

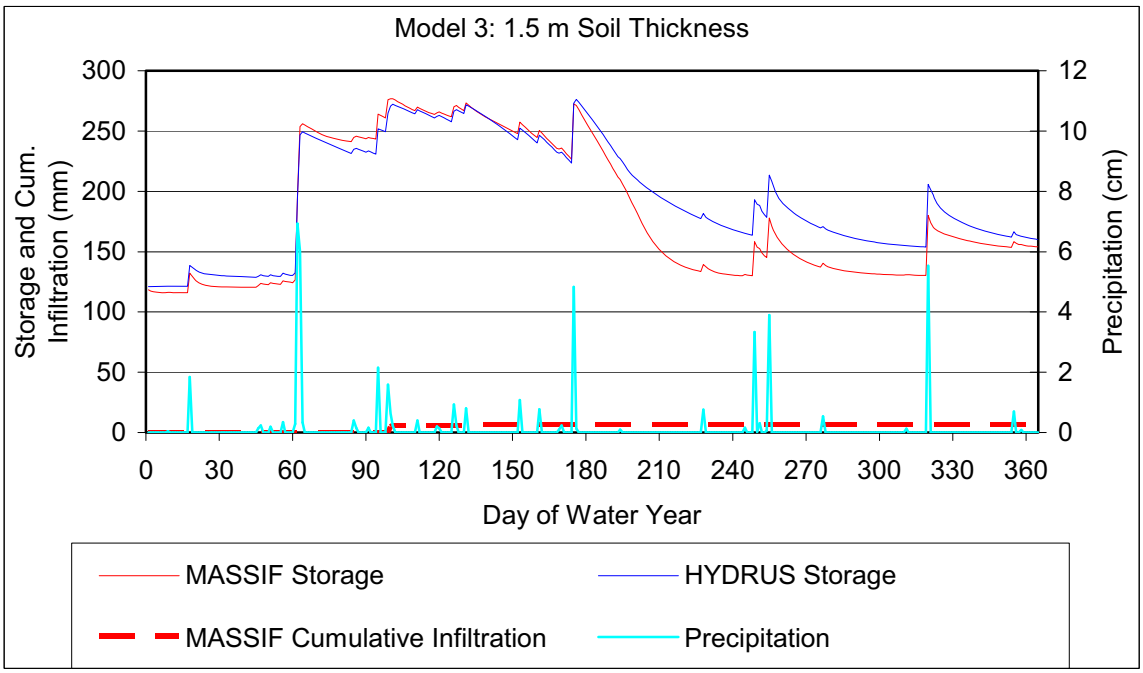

Source: Validation Output DTN: SN0609T0502206.022, *Alternative_Model_Outputs\Alternative_Model_Output.xls.*

Figure 7.2.2-3c[a]. Soil Water Storage and Cumulative Infiltration for Model 3

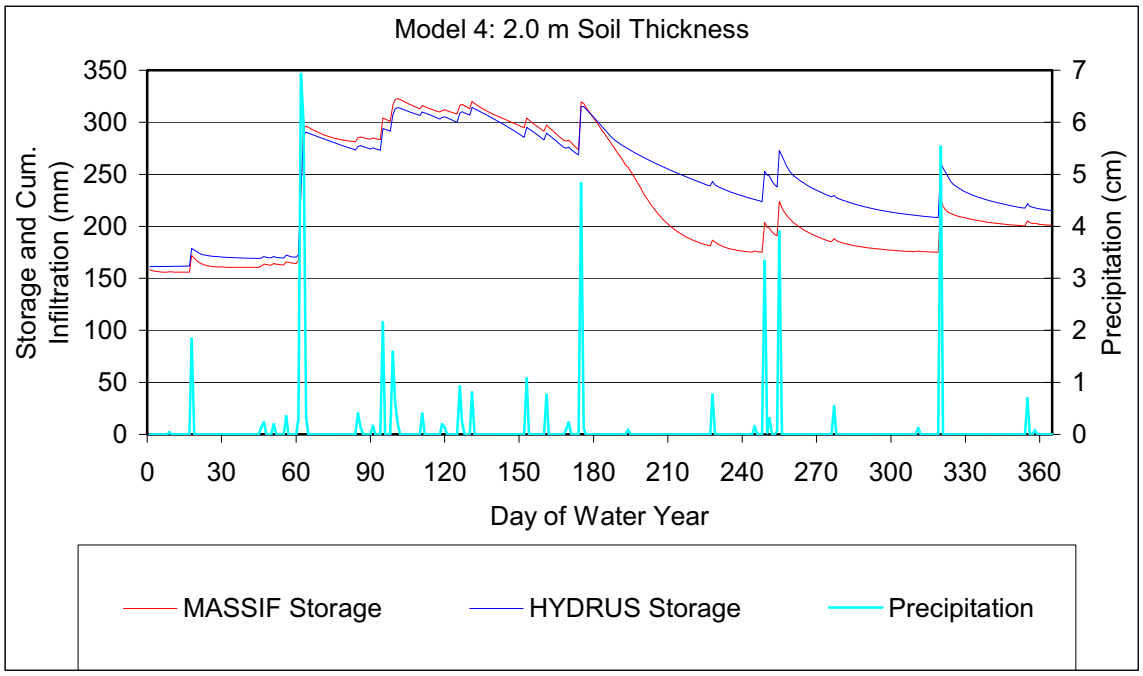

Source: Validation Output DTN: SN0609T0502206.022, *Alternative_Model_Outputs\Alternative_Model_Output.xls*.

Figure 7.2.2-3d[a]. Soil Water Storage and Cumulative Infiltration for Model 4

The comparison between the annual values of the water balance components is presented in Figures 7.2.2-4 a[a] through d[a]. The summary of these results is in Table 7.2.2-1[a].

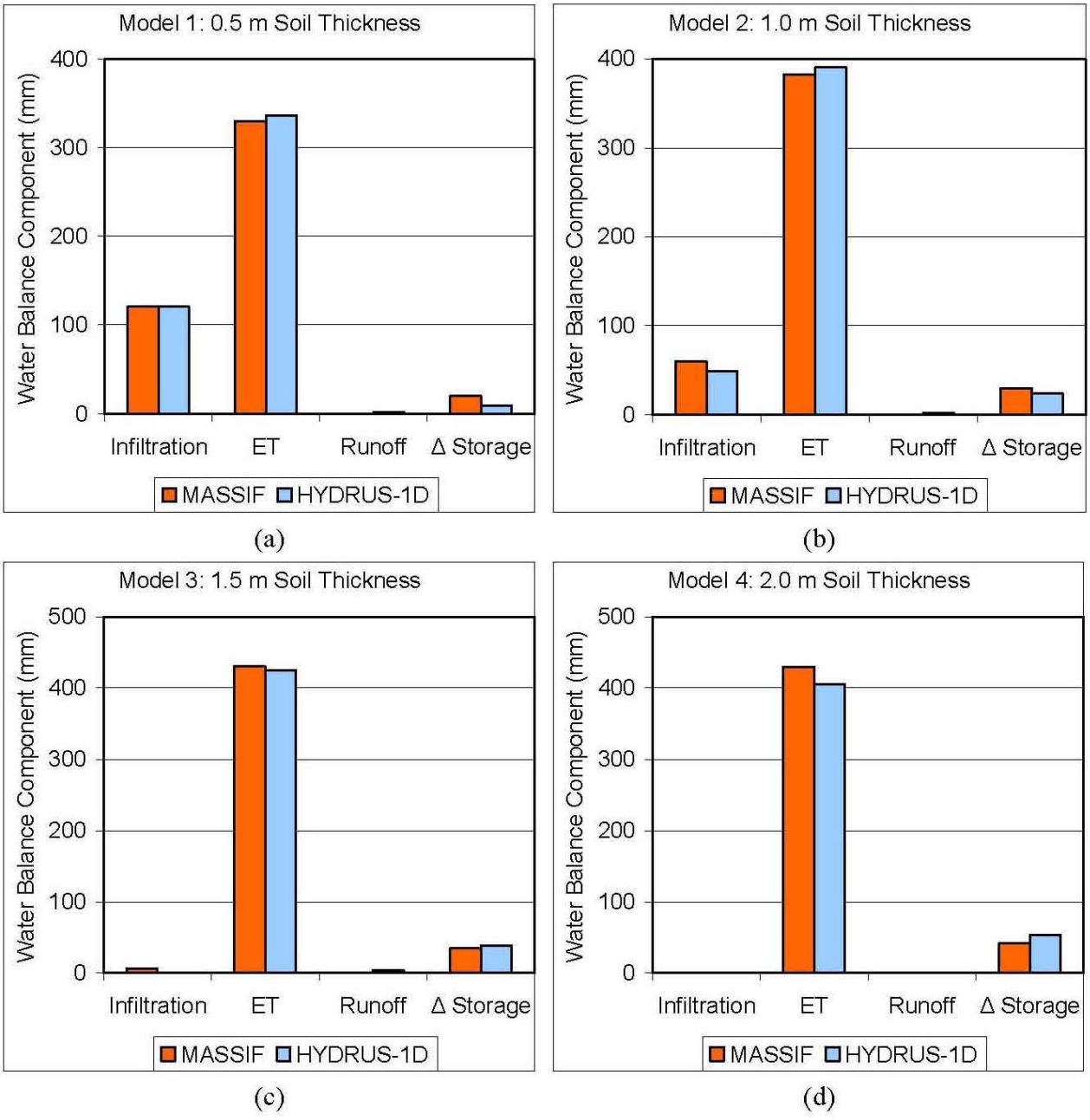

Source: Validation Output DTN: SN0609T0502206.022, *Alternative_Model_Outputs\Alternative_Model_Output.xls.*

Figure 7.2.2-4[a]. Annual Water Balance Components for Alternative Model Comparison

Table 7.2.2-1[a]. Summary of the Water Balance Results

		Annual Water Balance Constituents					
		Infiltration	Actual ET	Runoff	Change in Storage	Mean Root Squared Error	
Model	Code	mm	mm	mm	mm	mm	% Precipitation
Model 1	MASSIF	120.4	326.7	0.70	25.3	8.9	1.9
	HYDRUS-1D	120.5	336.8	2.5	9.6		
Model 2	MASSIF	63.9	377.8	0.70	30.8	17.1	3.6
	HYDRUS-1D	49.3	390.6	2.5	24.5		
Model 3	MASSIF	13.5	427.1	0.70	31.9	26.1	5.5
	HYDRUS-1D	0	425.1	3.7	39		
Model 4	MASSIF	0	437.5	0.70	35.0	33.4	7.1
	HYDRUS-1D	0	404.9	0.45	53.5		

Source: Validation Output DTN: SN0609T0502206.022, *Alternative_Model_Outputs\Alternative_Model_Output.xls*.

As anticipated, Model 1 produced the highest infiltration. MASSIF and HYDRUS-1D calculated high total annual infiltration (120.4 mm from MASSIF and 120.5 mm from HYDRUS-1D), which constitutes 25% of the annual precipitation. As seen from Figure 7.2.2-3a[a], even the timing of the infiltration events is the same. The first infiltration event occurs at the time of the highest precipitation event. The soil moisture increases significantly and the following smaller precipitation events result in another infiltration event since the soil holding capacity is close to the maximum. A few following infiltration events coincide with the high precipitation events. The mean root squared difference between the MASSIF and HYDRUS-1D daily storage values is 8.9 mm (or 1.9% of the annual precipitation). The actual ET and runoff are in close agreement as well (Table 7.2.2-1[a]).

The total annual infiltration calculated in Model 2 is 64 mm (MASSIF) and 49 mm (HYDRUS-1D). The timing of the infiltration events is the same. There are only two infiltration events in this case. The first infiltration event occurs at the time of the highest precipitation event. The second infiltration event occurs after a series of the smaller precipitation events during the period of time when the soil moisture content is high. The other high precipitation events do not result in infiltration as was in the case of Model 1 because the thicker soil was able to store all the moisture received. The mean root squared difference between the MASSIF and HYDRUS-1D daily storage values is 17.1 mm (or 3.6% of the annual precipitation). The actual ET and runoff are in close agreement (Table 7.2.2-1[a]).

In the case of Model 3, MASSIF predicted one small infiltration event (13.75 mm) during the period of high moisture content that follows the highest precipitation event. The infiltration calculated by HYDRUS-1D is zero. The infiltration predicted by MASSIF in this case is a very small part (2.9%) of the annual precipitation. The mean root squared difference between the MASSIF and HYDRUS-1D daily storage values is 26.1 mm (or 5.5% of the annual precipitation). The actual ET and runoff are in close agreement (Table 7.2.2-1[a]).

As anticipated, no infiltration occurs in the case of Model 4. MASSIF and HYDRUS-1D both predict zero infiltration. The mean root squared difference between the MASSIF and HYDRUS-1D daily storage values is 33.4 mm (or 7.1% of the annual precipitation). The actual ET and runoff are in close agreement (Table 7.2.2-1[a]).

The difference between MASSIF and HYDRUS-1D results is slightly larger in the case when field capacity is defined at the water content at –1/3 bars. However, the agreement between these results is still good.

All four models were run again with MASSIF, first using minimum and second using maximum values for the bedrock hydraulic conductivities. The estimates of all the balance constituents were identical to the cases when the hydraulic conductivity of the bedrock type 405 was used. This means that considering the seepage boundary condition in HYDRUS-1D (that does not require bedrock modeling) is appropriate. It also means that the conclusions made are not bedrock specific.

Conclusions:

- The simplified water balance approach used in MASSIF produces annual infiltration estimates that are very close to the estimates obtained with physics based model such as HYDRUS-1D.

- MASSIF is capable of reproducing the same timing of the infiltration events as HYDRUS-1D. This means that the important physical processes resulting in infiltration are adequately represented in MASSIF.

- The other water balance components such as annual actual ET and annual runoff are in good agreement with the HYDRUS-1D estimates as well.

- The mean root squared difference between the daily storage value calculated by MASSIF and HYDRUS-1D was in the range from 9 to 33 mm, which corresponds to 2% to 7% of the annual precipitation.

- Consequently, it can be concluded that corroboration of the MASSIF net infiltration model is successful. The corroboration criterion (close estimates of the cumulative infiltration calculated by MASSIF and HYDRUS-1D) was met.

7.2.3[a]. Corroboration of Model Results with Infiltration and Percolation Estimates from 1997 Expert Elicitation Panel

No change except the NOTE added to Figure 7.2.3-1[a].

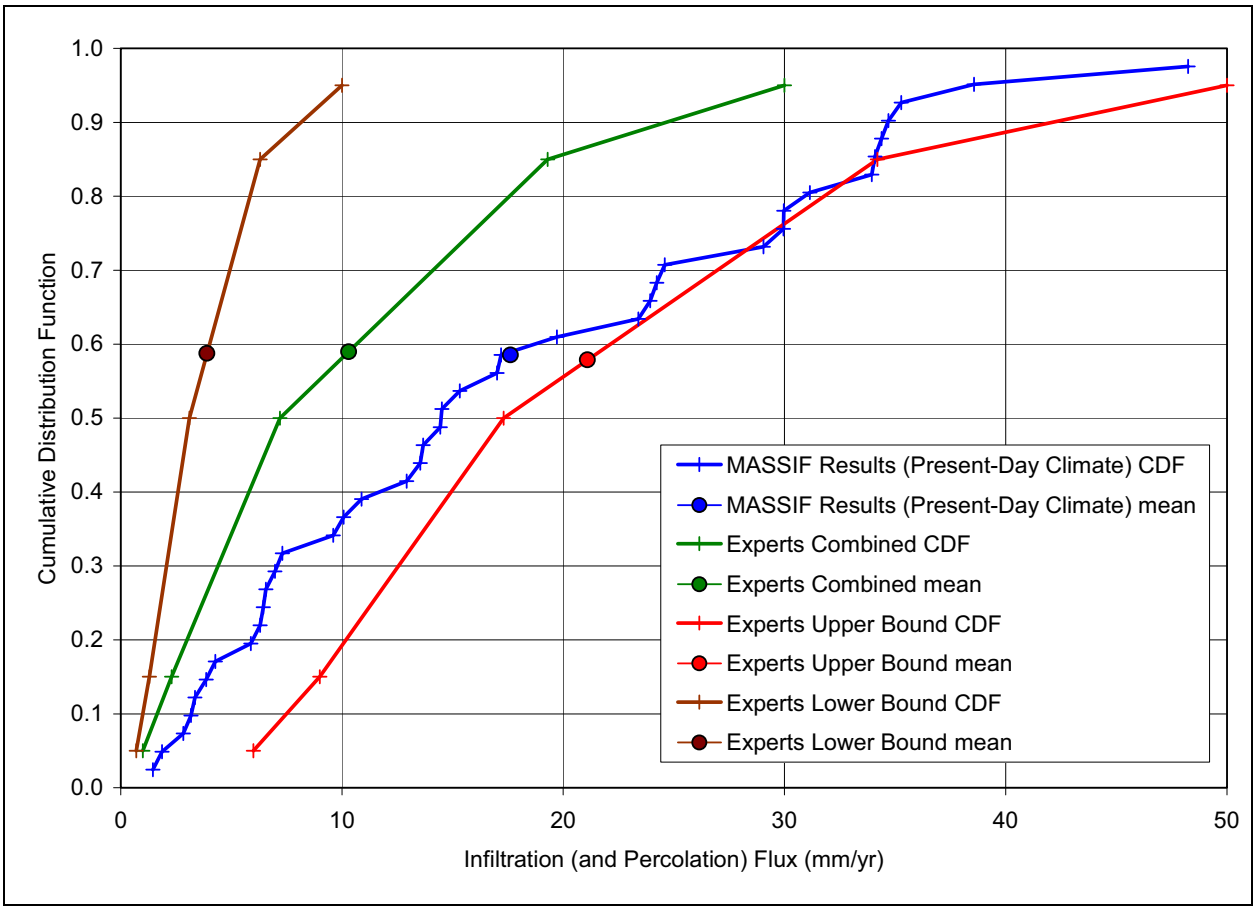

Source: Output DTN: SN0701T0502206.034 (MASSIF results for Present-Day climate); CRWMS M&O 1997 [DIRS 100335], Table 3-2 (Expert Elicitation Panel values).

NOTE: CDF values corresponding to mean values are interpolated. 2002 repository footprint used (DTN: LB0208HYDSTRAT.001 [DIRS 174491]).

Figure 7.2.3-1[a]. MASSIF Net Infiltration Results for Present-Day Climate for the 2002 Repository Footprint Compared with Percolation Fluxes at the Repository Horizon from the 1997 Expert Elicitation Panel

7.2.4[a]. Corroboration of Soil Depth Class 4 Data using Data Collected by the CNWRA

Section 6.5.2.4[a] describes how an upscaled, effective uniform value of soil depth was used in the MASSIF calculations. Soil depth class 4 represents the shallowest soils in the infiltration model domain and covers 71% of the unsaturated zone model domain, and 57% of the infiltration model domain (Table 6.5.2.4-1[a]). The spatial variability of soil depth class 4 was determined to have a lognormal distribution with a sample mean of 0.45 m, a geometric mean of 0.27 m, and a median of 0.25 m, based on the initial analysis of 35 soil samples discussed in *Data Analysis for Infiltration Modeling: Technical Evaluation of Previous Soil Depth Estimation Methods and Development of Alternate Parameter Values* (BSC 2006 [DIRS 178819], Table 6-10). Section 6.5.2.4.1 describes how a second source of information (Sanchez 2006 [DIRS 176569], pp. 62 to 68) was used to enhance the basis for the soil depth class 4 range, distribution type, and nominal value.

Soil depths were measured by the Center for Nuclear Waste Regulatory Analyses (CNWRA) staff and contractors during two site visits to Yucca Mountain, January 26 to 29, 1998, and May 13 to 18, 1998. Nine transects were completed. Spacing of locations of soil measurements along each transect varied from 10 to 50 m such that 5 to 10 locations were sampled along most transects. The soil at each measurement location was cleared off using shovel, trowel, and brushes over an area <1 m^2. Average (or representative) soil depth was visually estimated by qualitatively taking into account an area weighting of soil depths in the pit supported by measuring several locations with ruler or measuring tape. Maximum and minimum soil depths were recorded for many locations. Slope of the bedrock surface was also approximated. A total of 57 values of maximum soil depth were recorded; a total of 56 values of representative soil depth were recorded; and a total of 31 values of minimum soil depth were recorded (Fedors 2007 [DIRS 182469]). The locations for these soil depth measurements were not randomly selected and follow a pattern. Such a selection is known to introduce bias in estimating a distribution.

The purpose of this section is to compare the soil depth data and the sampling locations of the 56 values of representative soil depth collected by the CNWRA, to the original soil depth dataset consisting of 35 soil depth measurements and described in *Data Analysis for Infiltration Modeling: Technical Evaluation of Previous Soil Depth Estimation Methods and Development of Alternate Parameter Values* (BSC 2006 [DIRS 178819]) that was used to characterize shallow soil depth class 4 (herein referred to as YMP soil depth data). This comparison provides additional confidence that the soil depth data used in the infiltration calculations and uncertainty analysis are appropriate.

The locations of the CNWRA transects and the 35 YMP soil depths used to characterize soil depth class 4, as well as the extent of soil depth class 4 are shown in Figure 7.2.4-1[a]. Also refer to the Fedors (2007 [DIRS 182469], Figure 1) letter for locations of the CNWRA sampling locations. Figure 7.2.4-1[a] shows that the CNWRA sampling locations are further west than all but a few of the 35 YMP sample locations. This difference in sampling locations should be expected to result in the CNWRA samples having slightly shallower soil depths than the YMP samples because the CNWRA samples are closer to the mountain crest, and are likely to be located at higher elevation than the YMP samples. Although the 35 YMP soil samples were sampled over a much larger area (71 km^2) compared to the sampling area of the CNWRA soils, the comparison of these datasets indicate that there may possibly be a bias toward deeper soils in the YMP dataset than the CNWRA dataset. A bias toward deeper soils in the shallow soil depth class will, in general, result in a bias to less infiltration due to increased storage capacity.

Statistical analysis of the CNWRA and YMP samples indicates that the CNWRA samples are slightly shallower than the YMP samples, based on their mean, median, and geometric mean values. A summary of the statistical analysis is shown in Table 7.2.4-1[a]. The CNWRA dataset, like the YMP dataset, was found to have a lognormal distribution (Output DTN: SN0708T0502206.048, file, *CNWRA vs YMP Soil Depth Data.xls*, sheet, "log test"). A comparison of the distributions of maximum and representative CNWRA soil depths and YMP soil depths are shown in Figure 7.2.4-2[a]. These two datasets appear to be very similar based on their statistical summaries (Table 7.2.4-1[a]) and their distributions shown in Figure 7.2.4-2[a]. However, these two datasets should not necessarily be expected to be statistically the same given their difference in sampling locations. A Wilcoxon rank-sum test was conducted to compare these two datasets. Results of this test for similarity of distribution (and not similarity of mean)

indicate that the hypothesis of similarity of distributions can be rejected. These calculations are contained in Output DTN: SN0708T0502206.048; file: *T_test+rank-sum_test.xls*.

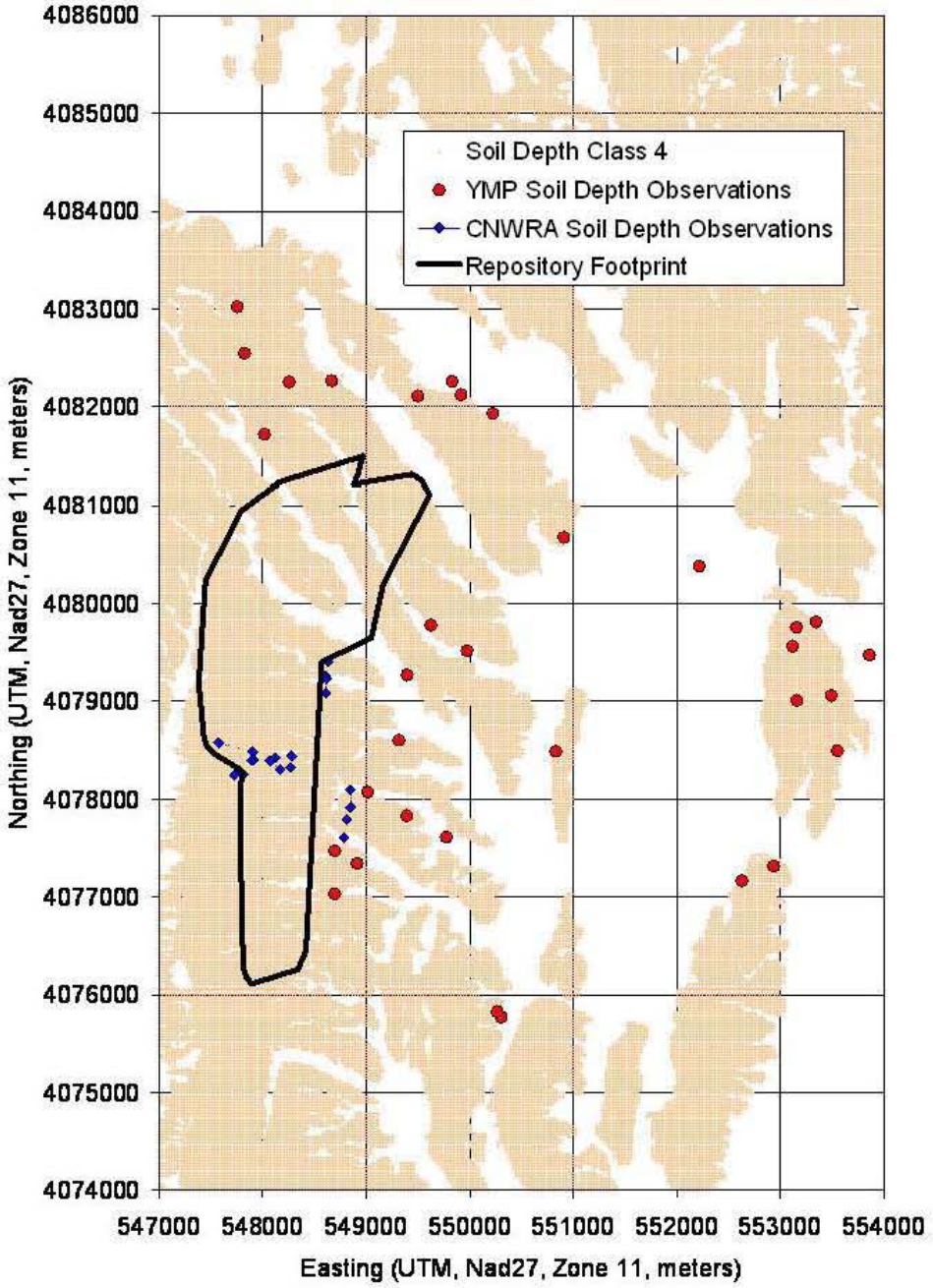

Source: Output DTN: SN0708T0502206.048, file: *Soil Sampling Locations (Map).xls*. Repository footprint is from Output DTN: SN0711FTPRNUZB.003.

NOTE: Repository footprint shown for illustrative purposes only.

Figure 7.2.4-1[a]. Extent of Soil Depth Class 4 With 35 Soil Sampling Locations Used In ANL-NBS-HS-000077 REV01 to Characterize Soil Depth Class 4, and 56 Soil Sampling Locations Recorded by the CNWRA

Table 7.2.4-1[a]. Comparison of Summary of Distributions for CNWRA and YMP Soil Depth Data

Soil Depth Description	YMP Shallow Soils (Depth Class 4)	CNWRA Representative Soil Depth	CNWRA Maximum Soil Depth
Sample Distribution Type	Lognormal	Lognormal	Lognormal
Sample Mean	0.45 (m)	0.26 (m)	0.33 (m)
Sample Mean of the Natural Logarithm	−1.29 (LN m) (0.27 m)	−1.55 (LN m) (0.21 m)	−1.26 (LN m) (0.28 m)
Sample Standard Deviation	0.67 (m)	0.16 (m)	0.17 (m)
Sample Standard Deviation of the Natural Logarithm	0.88 (LN m)	0.72 (LN m)	0.59 (LN m)
Sample Standard Error	0.11 (m)	0.02 (m)	0.02 (m)
Sample Median (also Estimated Population Median)	0.25 (m)	0.24 (m)	0.31 (m)
Sample Geometric Standard Error for the Median	1.16 (m)	1.10 (m)	1.08 (m)
Sample Minimum Value (m)	NA	NA	NA
Sample Maximum Value (m)	NA	NA	NA
Number of Data Points	35	56	57
Estimated Population Mean	0.40 (m)	0.27 (m)	0.34 (m)
Confidence Interval for Population Mean at 80% Limit	0.33 to 0.52 (m)	0.24 to 0.32 (m)	0.30 to 0.38 (m)
Confidence Interval for Population Mean at 90% Limit	0.31 to 0.57 (m)	0.23 to 0.33 (m)	0.29 to 0.39 (m)
Confidence Interval for Population Median at 80% Limit	0.23 to 0.33 (m)	0.19 to 0.24 (m)	0.25 to 0.31 (m)
Confidence Interval for Population Median at 90% Limit	0.21 to 0.35 (m)	0.18 to 0.25 (m)	0.25 to 0.32 (m)

Source: Output DTN: SN0708T0502206.048.

LN = natural logarithm; NA = not applicable.

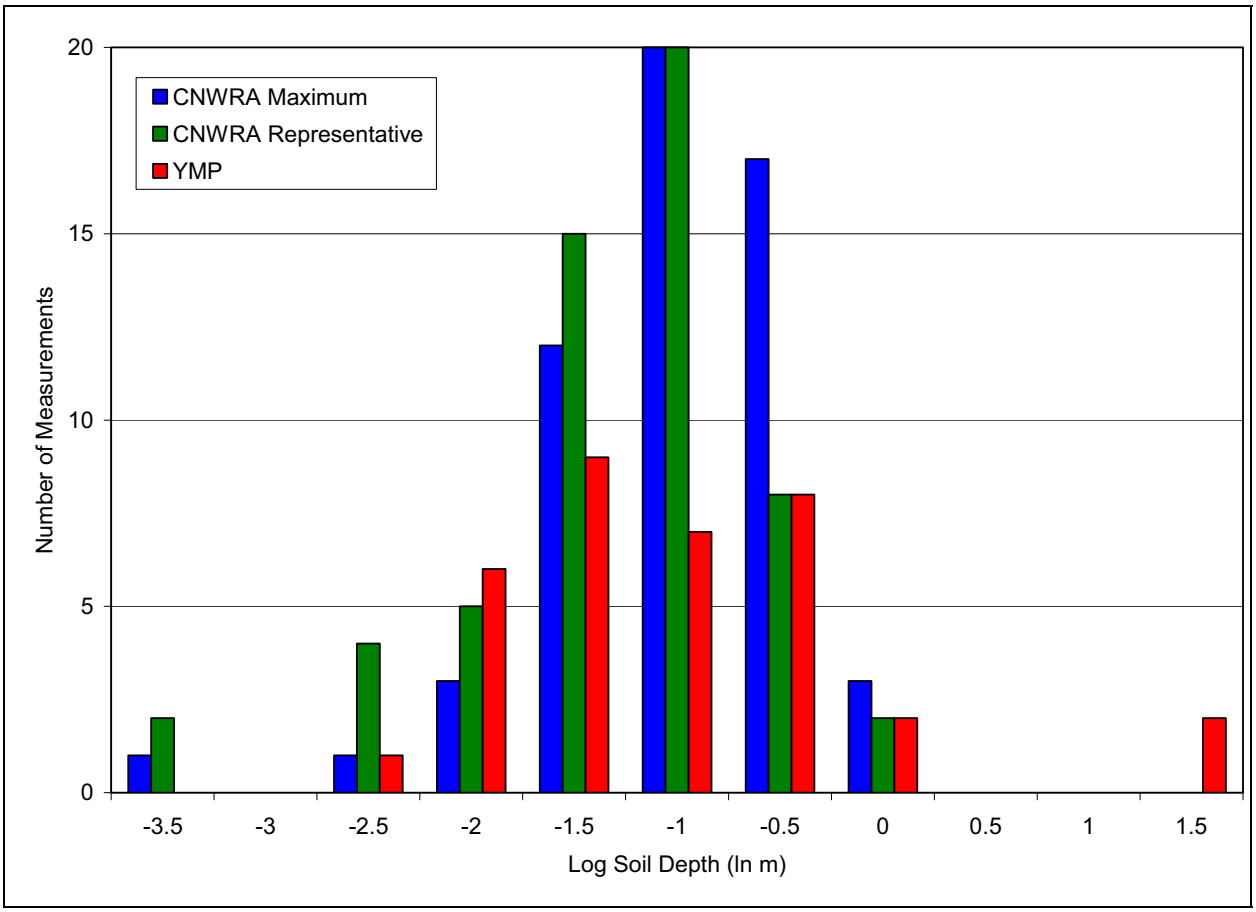

Source: Output DTN: SN0708T0502206.048, file: *CNWRA vs YMP Soil Depth Data.xls*.

Figure 7.2.4-2[a]. Distribution of Soil Depths from YMP and CNWRA Observations

Section 6.5.2.4.1[a] discusses why a uniform distribution was selected for the uncertainty analysis rather than a lognormal distribution. It is important to note that the uniform distribution and the range selected represent the uncertainty in an upscaled quantity and not the spatial variability at every point of the domain. If the spatial variability of soil depth class 4 was being modeled by MASSIF by taking a different value for soil depth class 4 at each corresponding cell in the domain, then a lognormal distribution would have been used. Since one value for soil depth class 4 is used for a given realization by MASSIF, this value cannot represent the spatial variability distribution. This upscaled value is expected to lie between the median and arithmetic mean, which is why a range of 0.1 to 0.5 m was selected (Section 6.5.2.4.1[a]). If a lognormal distribution was used with the full range of soil depth class 4 (0 to 3 m) for the LHS sampling of soil depth, then deeper soil depths would be sampled than using a uniform distribution for a range of soil depths between 0.1 and 0.5. The reason of using a uniform distribution for the ranges described above is that there is not enough information suggesting how to weight the values between the median and the mean. The impact of using a uniform rather than a lognormal distribution for the LHS sampling is likely to be counteracted by any potential bias in sampling deeper soils (compared to CNWRA samples) described previously.

The CNWRA dataset provides additional confidence in the range of soil depth values used for the shallow depth class 4 with MASSIF since this independent dataset closely overlaps the YMP dataset, especially given the heterogeneity of soil depth measurements at Yucca Mountain.

7.3[a]. VALIDATION AND CORROBORATION SUMMARY

Section 7.1 presented confidence building activities during model development. These activities included descriptions of MASSIF's abstraction of precipitation modeling using Fourier series parameters. MASSIF's ability to simulate ET and storage was demonstrated by comparing MASSIF output with lysimeter datasets from Area 5 at the Nevada Test Site, and Reynolds Creek, ID. These comparisons demonstrate that MASSIF can be applied to other sites to accurately predict water balance parameters such as ET. Section 7.1 also presented a comparison of MASSIF predictions of streamflow with measured streamflow data, and described the extended parameter sensitivity study (large LHS).

Section 7.2 presented post-development model validation activities. These activities included comparison of MASSIF predictions of infiltration with seepage estimates observed in the South ramp of the ESF in the winter of 2005. MASSIF predictions of infiltration were qualitatively compared to borehole-scale estimates of infiltration, and this comparison was used to illustrate that MASSIF predictions of infiltration for a given grid cell cannot be accurately compared to borehole-scale estimates of infiltration due to the lack of site-specific Yucca Mountain soils data including soil depth data, and soil hydraulic property data.

Section 7.2 also compares MASSIF predictions of infiltration for Present-Day, Monsoon, and Glacial Transition climates for 40 realizations for each climate, with infiltration estimates from published models and data for the Yucca Mountain area, the southwestern United States, and the western United States. The infiltration estimates from some southwestern sites is analogous to infiltration that could be expected during the monsoon climate state, and infiltration estimates from the Columbia River plateau sites is analogous to infiltration that could be expected during the glacial-transition climate state. These comparisons indicate that MASSIF predictions of infiltration for Present-Day, Monsoon, and Glacial Transition climates compare well to watershed-scale models and data for Nevada, and the southwestern and western United States.

Section 7.2 also describes an alternative model approach corroboration activity in which MASSIF results are compared to HYDRUS 1-D results for four different soil depths and using the same model inputs. These comparisons indicate that MASSIF and HYDRUS-1D give similar results. Finally, Section 7.2 summarizes some of the conclusions and infiltration and percolations estimates from the 1997 expert elicitation panel on the UZ flow model (CRWMS M&O 1997 [DIRS 100335]). The MASSIF predictions of infiltration for Present-Day climate were almost entirely within the range between the mean and upper bounds of percolation flux predicted by the 1997 expert panel (which assumed that percolation flux was approximately equivalent to infiltration). Section 7.2.4[a] compares soil depth data collected by the Center for Nuclear Waste Regulatory Analyses (CNWRA) to YMP soil depth data that is the basis for the shallow depth class (4) that is used with MASSIF.

The results of calculations of net infiltration have been validated by applying acceptance criteria based on an evaluation of the model's relative importance to the potential performance of the repository system. Validation requirements defined in *Technical Work Plan for: Infiltration Model Assessment, Revision, and Analyses of Downstream Impacts* (BSC 2006 [DIRS 177492], Section 2.2.1) have been fulfilled (with the exceptions described in Section 1.4), including corroboration of model results with experimental data, and corroboration with alternative models. Activities requirements for confidence building during model development have also been satisfied. The model development activities and post-development model validation activities described establish the scientific bases for the infiltration model. Based on this, the infiltration model used in this report is considered to be sufficiently accurate and adequate for the intended purpose.

Table 7.3-1[a] lists the Validation Output DTNs generated from model validation activities described in Section 7. These DTNs are not considered qualified product outputs.

Table 7.3-1[a]. Validation Output Data Tracking Numbers

Title	Product Output DTN
Comparison of the calculated precipitation record with site data	SN0701T0502206.045
Analysis of soil water storage in Nevada Test Site (NTS) and Reynolds Creek Experimental Watershed (RCEW) lysimeters	SN0607T0502206.016
Recharge estimates used to validate the MASSIF model of net infiltration at Yucca Mountain	SN0801T0502206.049
Alternative infiltration model inputs	SN0609T0502206.021
Alternative infiltration modeling results	SN0609T0502206.022
YMP and Center for Nuclear Waste Regulatory Analyses (CNWRA) Soil Depth Class 4 Statistics	SN0708T0502206.048

INTENTIONALLY LEFT BLANK

8[a]. CONCLUSIONS

8.1[a]. SUMMARY AND FINDINGS

The purpose of the model documented in this report is to provide a spatial representation, including uncertainty, of the predicted average annual net infiltration at the Yucca Mountain site for three future climates predicted to occur at the site over the next 10,000 years. The resulting maps of average annual net infiltration provide input directly to the updated versions of the following model reports:

- *UZ Flow Models and Submodels* (SNL 2007 [DIRS 175177])
- Calibrated Unsaturated Zone Properties (SNL 2007 [DIRS 179545]).

The net infiltration model, MASSIF, presented in this report is a mass balance calculation of the surface and near surface water budget. Water enters the system as precipitation, which is simulated from a stochastic model of daily precipitation based on historical weather records from proxy climate sites identified in *Future Climate Analysis* (BSC 2004 [DIRS 170002]. The MASSIF infiltration model simulates processes occurring at the soil layer, including: flow through and storage of water in the soil layer, return of water vapor to the atmosphere by evaporation and plant transpiration (evapotranspiration), flow along the surface (runoff/run-on), and infiltration into the bedrock below the soil. Processes not included in the model are listed in Section 5.1[a].

The model documented in this report calculates net infiltration at the soil–bedrock interface without consideration of the properties of the rock at deeper locations. Instead of net infiltration, some authors call this parameter "deep drainage" or "potential recharge." *UZ Flow Models and Submodels* (SNL 2007 [DIRS 175177]) describes the method for calculating replenishment of the aquifer from the surface (i.e., recharge), taking into consideration the potential recharge and the make-up and orientation of the geologic strata, as well as other considerations.

The model documented in this report is valid only for the Yucca Mountain site for 10,000 years and for the climates specified in *Future Climate Analysis* (BSC 2004 [DIRS 170002]), Section 7.1). For each climate, the model produces maps of average annual infiltration as a function of location, with no time dependence, although an examination of the nonaveraged results indicates that net infiltration in this environment is highly episodic (Section 6.5.7). *UZ Flow Models and Submodels* (SNL 2007 [DIRS 175177]) provides the justification for characterizing net infiltration with nonepisodic, time-averaged values. These output maps indicate the range of uncertainty in average annual steady-state net infiltration.

Infiltration predictions are limited by the uncertainty in future weather. Although a substantial body of literature supports the use of stochastic precipitation models, there are no records to validate our approach of extrapolation to 1,000 years. Each available precipitation record, whether from the Yucca Mountain site, from a nearby weather station, or from a site representative of a future climate, covers periods of time much less than 100 years.

This model report documents the development and validation of a model for net infiltration of precipitation at the Yucca Mountain site and completely replaces the previous revision of this

model report and model of average annual net infiltration (BSC 2004 [DIRS 170007]). While the underlying conceptual model remains similar to the previous model, this revision increases confidence in the results by improving the traceability, transparency, and reproducibility of both the model development and the selection of inputs for calculations.

The results of this modeling work are the generation of 40 maps of net infiltration for each of the three future climates considered for the next 10,000 years (Output DTNs: SN0701T0502206.034, SN0701T0502206.036, and SN0701T0502206.035). For a given climate each of these 40 maps provides an equally probable outcome of net infiltration over the modeling domain. The range of net infiltration values within the set of 40 maps provides a reasonable estimate of the uncertainty in magnitude of net infiltration. This uncertainty is estimated using the structured Monte Carlo technique of Latin Hypercube sampling (Sections 6.5.5 and 6.5.6). This method propagates uncertainty in a collection of input parameters to uncertainty in model outputs (net infiltration).

There are a number of ways that the results of this study could be used. First, for a given climate, the set of 40 maps could be ranked by net infiltration over some specified domain (e.g., full domain, UZ model domain, repository footprint) and predefined percentiles could be selected. Such a selection was done for the results in Section 6.5.7, where the 10th, 30th, 50th, and 90th percentiles are identified. A weight or probability of occurrence could be defined from the resulting empirical distribution. Second, the empirical distribution could be tested against a theoretical distribution (e.g., lognormal) and the representative maps could be defined from this "fitted" distribution. This was done in Section 6.6, where the results of each climate are compared and tested against lognormal distributions. Third, the results of this study can be used to estimate the nature and character of net infiltration at the site, including the timing and frequency of infiltration events and the relative importance of low-probability high-precipitation years. Finally, the results of the sensitivity study can be used to define performance confirmation goals and identify sensitive parameters that could be the focus of possible future field studies at the site; however, this is not deemed necessary.

The MASSIF model is validated using two of the methods available in SCI-PRO-006: (1) discussion of documented decisions and activities that are implemented during the model development process that build confidence and verify that a reasonable, credible, and technical approach using scientific and engineering principles was taken, and (2) post-development model validation employing one of several methods described in paragraph 6.3.2) of SCI-PRO-006. The first method is implemented by comparing certain model components (such as evapotranspiration, runoff, and precipitation) to field observations. The second method is to compare the results of the net infiltration calculations to independent regional measurements and estimates of net infiltration and recharge. Previous studies have used observations of steam flow measured at the site to calibrate models of net infiltration (BSC 2004 [DIRS 170007]). This methodology was considered invalid and not used in the present work. The reason for this lies in the fact that parameters that significantly influence surface run-off (e.g., soil hydraulic conductivity) in the model are not the same parameters that significantly influence net infiltration (e.g., soil depth and water holding capacity). As an alternative to model calibration, the MASSIF model was run with nominal input parameter values and compared to field observations of stream flow (Section 7.1.3), point estimates of net infiltration (Section 7.2.1), field observations from analogue sites (Sections 7.1.2 and 7.2.1), and infiltration model results from an alternative modeling approach (Section 7.2.2[a]). Comparisons made in this model validation indicate that

the MASSIF model performs well, especially considering the uncertainty present in the input parameters.

The results of the uncertainty analysis for net infiltration are summarized in Section 8.2[a].

8.1.1[a]. Data Tracking Numbers for Data Generated in This Report

This section is identical to Section 8.1.1 in the parent document except that Figure 8-1[a] has been updated and has a corrected figure caption. In addition, one output DTN has been superseded, and one new output DTN has been developed. These two DTNs are the only Table 8-1[a] entries. Refer to Table 8-1 in the parent report for all other output data sets.

Table 8-1[a]. Output Data Sets Generated in the Development and Application of the Net Infiltration Model

Description	Title	Product Output DTN
Developed input to the net infiltration model	Unsaturated Zone (UZ) Boundary and Repository Footprint	SN0711FTPRNUZB.003 (supersedes SN0612FTPRNUZB.002)
Shallow soil depth class statistics	YMP and Center for Nuclear Waste Regulatory Analyses (CNWRA) Soil Depth Class 4 Statistics	SN0708T0502206.048

INTENTIONALLY LEFT BLANK

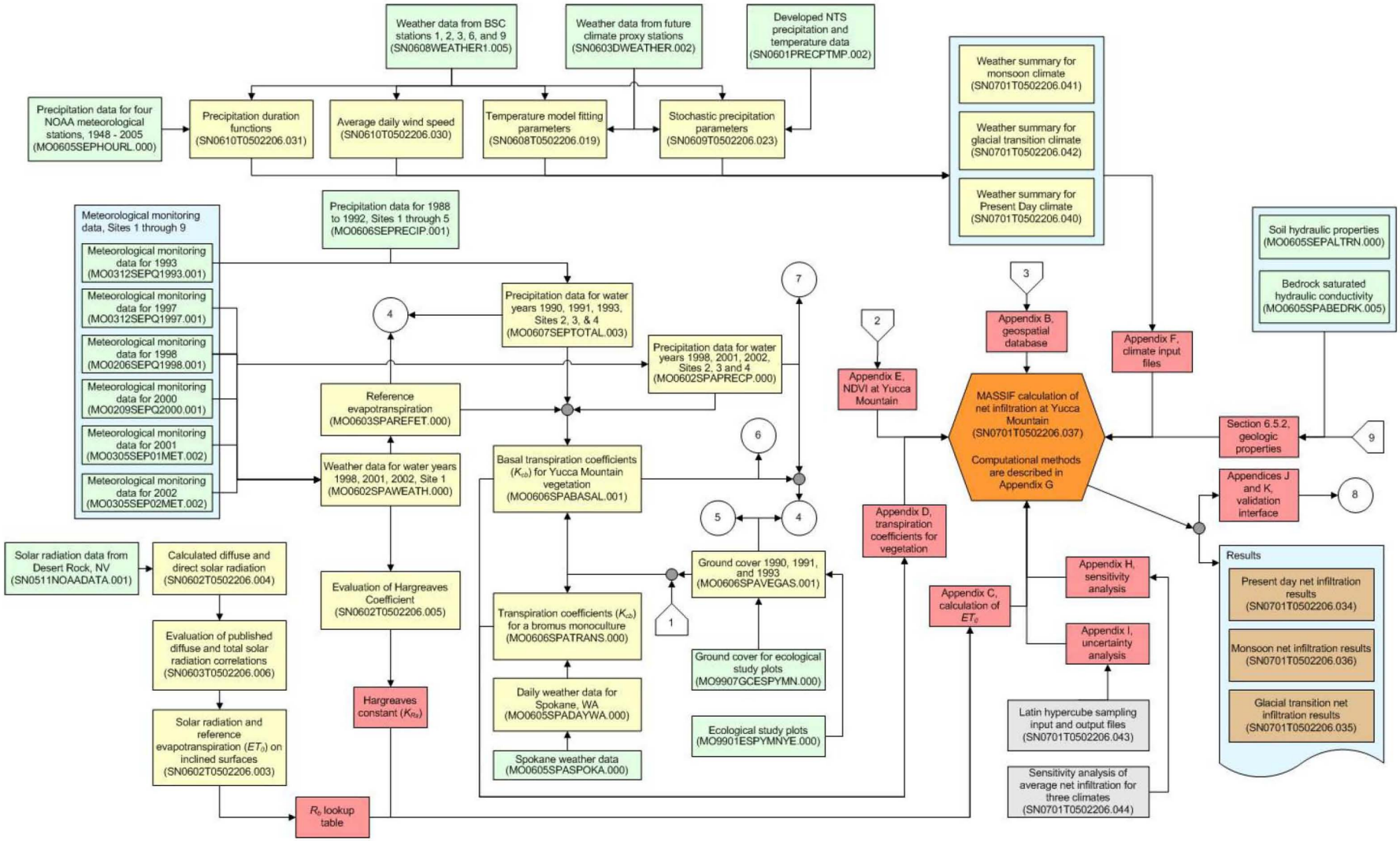

Figure 8-1[a]. Data Flow for the MASSIF Net Infiltration Model

INTENTIONALLY LEFT BLANK

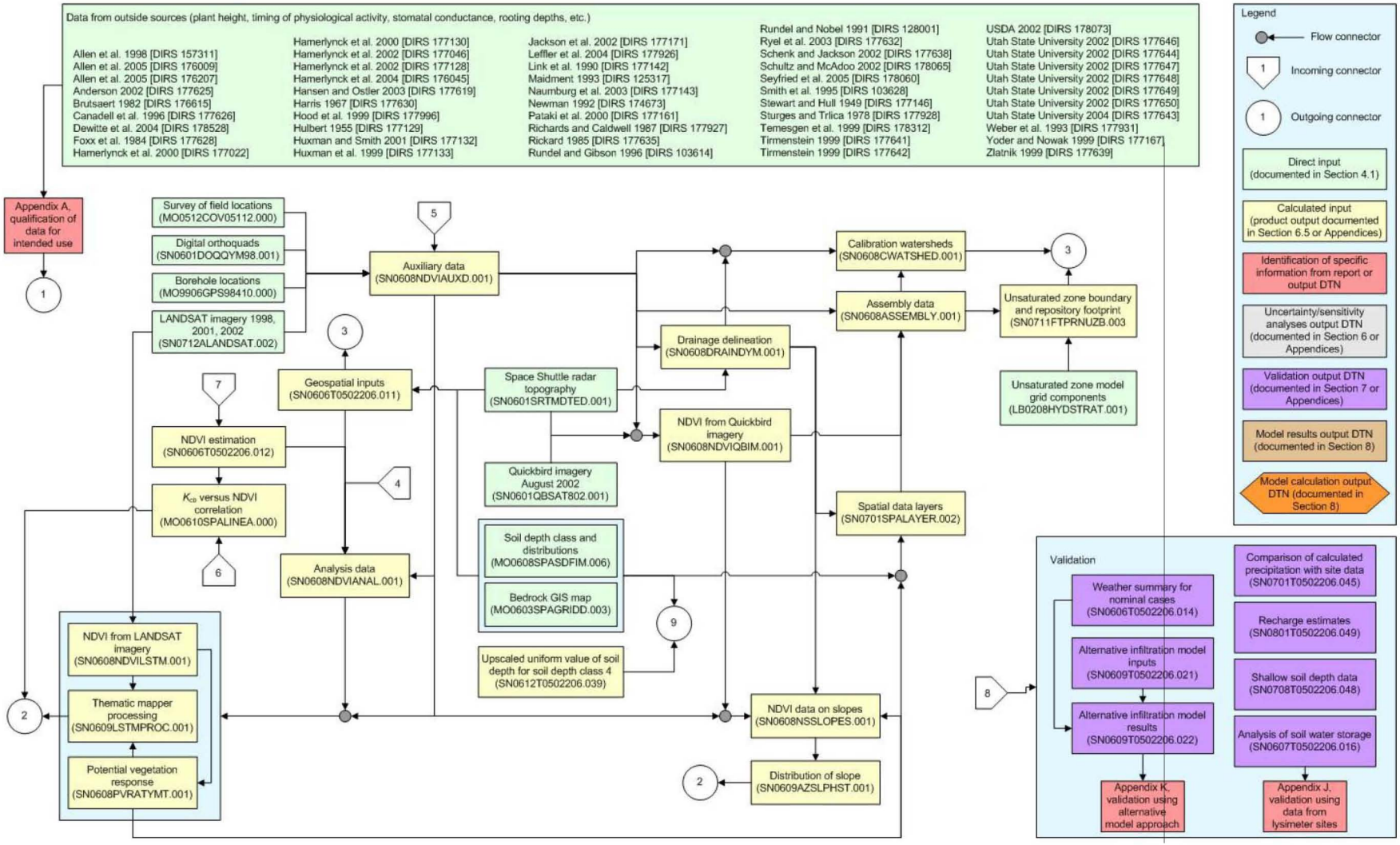

Figure 8-1[a]. Data Flow for the MASSIF Net Infiltration Model (Continued)

INTENTIONALLY LEFT BLANK

8.2[a]. MODEL UNCERTAINTY AND LIMITATIONS

The model documented in this report calculates average annual net infiltration at the soil–bedrock interface without consideration of the properties of the bedrock at deeper locations. All water that enters the bedrock is assumed to be net infiltration. Instead of net infiltration, some authors call this parameter "deep drainage" or "potential recharge." Such terminology acknowledges that other mechanisms exist to move or remove water from the bedrock below the root zone. *UZ Flow Models and Submodels* (SNL 2007 [DIRS 175177]) describes the method used for simulating water flow from the bottom of the root zone through the unsaturated zone to the underlying aquifer (i.e., recharge), taking into consideration the potential recharge and the make-up and orientation of the geologic strata, as well as other considerations.

The model documented in this report is valid only for the Yucca Mountain site over 10,000 years and for the climates specified in *Future Climate Analysis* (BSC 2004 [DIRS 170002], Section 7.1). For each climate, the model produces maps of average annual infiltration as a function of location, with no time dependence. These output maps indicate the range of uncertainty in average annual net infiltration.

Infiltration predictions are limited by the uncertainty in future weather, and this uncertainty is accounted for in this model. Although a substantial body of literature supports the use of stochastic precipitation models, there are no records to support extrapolation to 1,000 years. Each available precipitation record, whether from the Yucca Mountain site, from a nearby weather station, or from a site representative of a future climate, covers much less than 100 years.

Another significant uncertainty in the results of the net infiltration model is related to the spatial distribution of the net infiltration over the modeling domain. Sensitivity analyses presented in Sections 7.1.4 and 6.7 suggest that there may be insufficient characterization of soil properties (depth, holding capacity, and hydraulic conductivity) over the modeling domain to obtain accurate and detailed maps of net infiltration. Instead, results suggest that spatially averaged net infiltration estimates are more reliable than the resulting spatial distributions of net infiltration. This conclusion is supported by model validation comparisons of spatially averaged net infiltration model results with analogue site data from the region (Section 7.2).

8.3[a]. YUCCA MOUNTAIN REVIEW PLAN CRITERIA ASSESSMENT

The general requirements to be satisfied by the TSPA are stated in 10 CFR 63 [DIRS 176544]. The acceptance criteria that will be used by the U.S. Nuclear Regulatory Commission staff to determine whether the technical requirements have been met are identified in *Yucca Mountain Review Plan*, *Final Report* (YMRP) (NRC 2003 [DIRS 163274]).

The acceptance criteria identified in Section 2.2.1.3.5.3 of the YMRP (NRC 2003 [DIRS 163274]) that are applicable to this report are included in the discussions that follow along with a summary of where in this report each criterion is addressed.

Acceptance Criteria from Section 2.2.1.3.5.3, Climate and Infiltration

Acceptance Criterion 1: *System Description and Model Integration Are Adequate*

(1) The total system performance assessment adequately incorporates, or bounds, important design features, physical phenomena, and couplings, and uses consistent and appropriate assumptions throughout the climate and net infiltration abstraction process.

This model, which feeds the TSPA through the UZ flow model, explicitly includes the following natural features and physical phenomena and couplings that control the processes of net infiltration in the area above the planned Yucca Mountain repository: 1) terrain elevation and contours (Section 6.5.2 and Appendices B and C); 2) site specific estimates of vegetation as a function of mean annual precipitation (Section 6.5.3 and Appendix D); 3) change of climate through time using inputs from the future climates model report (Section 6.5.1); and 4) appropriate soil and bedrock permeability estimates as discussed in Section 6.5.2.

(2) The aspects of geology, hydrology, geochemistry, physical phenomena, and couplings, that may affect climate and net infiltration, are adequately considered. Conditions and assumptions in the abstraction of climate and net infiltration are readily identified and consistent with the body of data presented in the description.

This model includes the effects of geology by distinguishing soil and bedrock types present in the model domain (Sections 6.5.2.2[a] and 6.5.2.5[a]) and assigning properties to these units consistent with available data (Sections 6.5.2.3 and 6.5.2.6). In addition, soil depth is represented as distinct soil depth class regions in the model domain (Section 6.5.2.4[a]). The effects of local surface water hydrology (i.e., stream flow) are captured in the methods used to estimate surface runoff and run-on and watershed discharge (as summarized in Section 6.4.3) and controlled by the representation of elevation over the domain (Section 6.5.2.1[a] and Appendix B). Physical phenomena and couplings that are included in the modeling include: 1) elevation adjustments to precipitation and temperature (Sections 6.4.1 and 6.4.5.3); 2) adjustments to incoming daily solar radiation as a function of slope, azimuth, elevation, and day of year (Section 6.4.5.3); and 3) a detailed approach to estimating evapotranspiration as a function of reference evapotranspiration, site-specific vegetation characteristics, and soil water contents that all vary with time (Section 6.4.4).

(3) The abstraction of climate and net infiltration uses assumptions, technical bases, data, and models that are appropriate and consistent with other related U.S. Department of Energy abstractions. For example, the assumptions used for climate and net infiltration are consistent with the abstractions of flow paths in the unsaturated zone (UZ) and flow paths in the saturated zone (SZ) (Sections 2.2.1.3.6 and 2.2.1.3.8 of the Yucca Mountain Review Plan, respectively). The descriptions and technical bases provide transparent and traceable support for the abstraction of climate and net infiltration.

This model uses input data from the following DOE reports, all of which summarize YMP-relevant data:

1. ANL-NBS-GS-000008, *Future Climate Analysis* (BSC 2004 [DIRS 170002])

2. ANL-MGR-MD-000015, *Analysis for Infiltration Modeling: Extracted Weather Station Data Used to Represent Present Day and Potential Future Climate Conditions within the Vicinity of Yucca Mountain* (BSC 2006 [DIRS 177081])

3. TDR-NBS-HS-000019, *Technical Evaluation and Review of Results, Technical Procedures, and Methods Related to the Collection of Moisture Monitoring Data Using Neutron Probes in Shallow Boreholes* (BSC 2006 [DIRS 177083])

4. ANL-NBS-HS-000054, *Data Analysis for Infiltration Modeling: Bedrock Saturated Hydraulic Conductivity Calculation* (BSC 2006 [DIRS 176355])

5. ANL-NBS-HS-000077, *Data Analysis for Infiltration Modeling: Technical Evaluation of Previous Soil Depth Estimation Methods and Development of Alternate Parameter Values* (BSC 2006 [DIRS 178819])

6. ANL-NBS-HS-000055, *Data Analysis for Infiltration Modeling: Development of Soil Units and Associated Hydraulic Parameter Values* (BSC 2006 [DIRS 176335]).

The outputs (net infiltration maps) from this model are used as feeds to the unsaturated zone models to ensure continuity of repository system-wide modeling approach. Outputs from this model are indirectly coupled to the saturated zone through the coupling in the unsaturated zone. Output from this model is also indirectly coupled through the unsaturated zone flow fields (generated in the unsaturated zone models) to the predictions of in-drift temperature and humidity as described in *Multiscale Thermohydrologic Model* (SNL 2007 [DIRS 184433]).

(4) Sufficient data and technical bases to assess the degree to which FEPs have been included for this abstraction are provided.

Table 6.1-1[a] contains a list of 10 FEPs taken from *FY 2007 LA FEP List and Screening* (DTN: MO0706SPAFEPLA.001 [DIRS 181613]). The selected FEPs are those that are associated with the subject matter discussed in the present report. The cross-reference for each FEP to the relevant section(s) of this report is also given in Table 6.1-1[a].

(5) Adequate spatial and temporal variability of model parameters and boundary conditions are employed to model the different parts of the system.

Spatially varying parameters are listed in Section 6.5.2 and Appendix B. These parameters are distributed onto a grid comprised of 30 × 30-m grid cells. Spatial variations at a scale smaller than 30 × 30 m are not explicitly represented. Parameters associated with the terrain include elevation, slope, azimuth, and latitude for each 30 × 30-m grid cell. Elevation is used to divide the entire domain into 11 distinct watersheds (Appendix B). Each grid cell is assigned to a soil group, a bedrock type, and a soil depth group. The properties of these groups are represented with property sets that are uniform for all cells in the group. These properties include: bedrock

hydraulic conductivity, soil depth, soil properties (conductivity, field capacity, wilting point, and saturated water content). Values and uncertainties for these parameters are described in Section 6.5.2. Potential vegetation response (PVR) is a spatially varying parameter that indicates the potential for vegetation at a given location given sufficient precipitation. This variable was developed from satellite measurements made at the site during a set of three representative years. This parameter is discussed in Section 6.5.3 and Appendix E. In addition, elevation adjustments are made to daily values of precipitation and temperature (Sections 6.4.1 and 6.4.5.3).

(6) Average parameter estimates are used in process-level models over time and space scales that are appropriate for the model discretization.

The MASSIF model is built on parameter estimates to enable infiltration estimates that are tailored to the site-specific conditions, including climate, vegetation type and coverage, soil types, properties, and depths and bedrock permeability. Net infiltration estimates are developed for Present-Day, as well as future climates predicted for the next 10,000 years. The modeling domain for Yucca Mountain Project infiltration covers approximately 125 km^2 and is comprised of 139,092 30×30-m grid cells. Each of these grid cells must be assigned parameters of elevation, slope, azimuth, potential vegetation response, soil depth, soil properties, and bedrock conductivity. The large expanse of the model domain required that these parameters be grouped into spatial zones, most often contiguously, and average properties over each of the zones were assigned based on available data. The delineations of the various parameters are displayed in Figures B-6[a] through B-11[a].

(7) Projections of future climate change are based on evaluation of paleoclimate information over the past 500,000 years. For example, numerical climate models, if used for projection of future climate, are calibrated based on such paleoclimate data.

Future climate predictions are based in part on *Future Climate Analysis* (BSC 2004 [DIRS 170002], Section 7.1), which forecasts three distinct climate states during the next 10,000 years at Yucca Mountain based on an examination of paleoclimate information over the past 800,000 years. The Present-Day climate is estimated to persist for the next 400 to 600 years, followed by a warmer and much wetter Monsoon climate spanning 900 to 1,400 years, and then followed by a cooler and wetter Glacial Transition climate that is expected to last until and beyond the 10,000-yr mark. Climate conditions expected beyond 10,000 years are not explicitly stated in *Future Climate Analysis* (BSC 2004 [DIRS 170002]). Proxy sites representing upper and lower bounds for each of these climates are specified, and data from these sites has been compiled and analyzed. Relevant weather parameters (e.g., mean annual temperature and precipitation) have been derived from these data, and the parameters have been used to generate stochastic simulations of weather for each of the three climates. Weather inputs are discussed in *Analysis for Infiltration Modeling: Extracted Weather Station Data Used to Represent Present Day and Potential Future Climate Conditions within the Vicinity of Yucca Mountain* (BSC 2006 [DIRS 177081]). Parameter extraction methods and applications to generate stochastic future weather inputs are described in Section 6.5.1 and Appendix F.

(8) Guidance in NUREG–1297 and NUREG–1298 (Altman et al. 1988a,b [DIRS 103597 and 103750]), or other acceptable approaches for peer reviews and data qualification, is followed.

No peer reviews were conducted in support of this report. A summary of findings from an expert elicitation panel is discussed in Section 7.2.3. All direct input data used for estimates of net infiltration were qualified for use according to applicable procedures.

Acceptance Criterion 2: ***Data Are Sufficient for Model Justification***

(1) Climatological and hydrological values used in the license application (e.g., time of onset of climate change, mean annual temperature, mean annual precipitation, mean annual net infiltration, etc.) are adequately justified. Adequate descriptions of how the data were used, interpreted, and appropriately synthesized into the parameters are provided.

Future climates predictions are based in part on *Future Climate Analysis* which forecasts three distinct climates during the next 10,000 years at Yucca Mountain (BSC 2004 [DIRS 170002], Section 7.1). The Present-Day climate should persist for the next 400 to 600 years, followed by a warmer and much wetter Monsoon climate spanning 900 to 1,400 years, and then by a cooler and wetter Glacial Transition climate that is expected to last until and beyond the 10,000-yr mark. Proxy sites representing upper and lower bounds for each of these climates are specified, and data from these sites has been compiled and analyzed. Relevant weather parameters (e.g., mean annual temperature and precipitation) have been derived from these data, and the parameters have been used to generate stochastic simulations of weather for each of the three climates. Weather inputs are discussed in *Analysis for Infiltration Modeling: Extracted Weather Station Data Used to Represent Present Day and Potential Future Climate Conditions within the Vicinity of Yucca Mountain* (BSC 2006 [DIRS 177081]). Parameter extraction methods and applications to generate stochastic future weather inputs are described in Section 6.5.1 and Appendix F.

(2) Estimates of present-day net infiltration using mathematical models at appropriate time and space scales are reasonably verified with site-specific climatic, surface, and subsurface information.

Present-Day net infiltration estimates have been reasonably verified, as discussed in Section 7. The evapotranspiration model has been shown to accurately predict evapotranspiration from weighing lysimeters at a location on the Nevada Test Site located approximately 40 miles from the YMP (Section 7.1.2[a]). Runoff has been shown to be adequately predicted, as described in Section 7.1.3, where several runoff events were recorded at the YMP during two relatively wet years. The stochastic simulations of weather are shown to be a good representation of the weather observed at the proxy sites for each climate in Section 7.1.1.

(3) The effects of fracture properties, fracture distributions, matrix properties, heterogeneities, time-varying boundary conditions, evapotranspiration, depth of soil cover, and surface-water run off and run on are considered, such that net infiltration is not underestimated.

Bedrock fracture and matrix properties, distributions, and uncertainties are developed in *Data Analysis for Infiltration Modeling: Bedrock Saturated Hydraulic Conductivity Calculation* (BSC 2006 [DIRS 176355]), and inputs to the MASSIF model based on this report are summarized in Section 6.5.2. Uncertainty in bulk bedrock conductivity includes the possibility that some portion of the filled bedrock fractures contain open conduits, and therefore, the potential for net infiltration is not underestimated.

Parameter ranges and distributions used to develop evapotranspiration estimates are discussed in Sections 6.5.3 and 6.5.4, and Appendices D and E. Uncertainties in these parameters ensure that the full range of uncertainty in evapotranspiration is captured and not overestimated, and therefore, net infiltration is not underestimated.

Soil depth estimates, including uncertainty and spatial variability are developed in *Data Analysis for Infiltration Modeling: Technical Evaluation of Previous Soil Depth Estimation Methods and Development of Alternate Parameter Values* (BSC 2006 [DIRS 178819]) and are further summarized for the MASSIF model in Section 6.6. Assumptions are made (Section 5) that state that soil depth and properties can be considered to be constant for the next 10,000 years. The inclusion of uncertainties in soil depth provides confidence that net infiltration results and is not underestimated. This is because soil depth is one of the most important parameters controlling net infiltration over the modeling domain.

As part of model validation, comparisons are made between observations and model predictions of runoff. Within the uncertainty range of input variables, these comparisons are quite consistent (Section 7.1.3). Therefore, there is no reason to believe that net infiltration is underestimated.

All of the parameters that influence infiltration are briefly discussed in Appendix I where they are screened for inclusion in the uncertainty analysis. Appendix H describes sensitivity analyses and identifies parameters that have the greatest influence on net infiltration. The most influential parameters are included in the uncertainty analysis. The range of predicted net infiltration reasonably represents the uncertainty in a manner that precludes that net infiltration is underestimated.

(4) Sensitivity or uncertainty analyses are performed to assess data sufficiency and determine the possible need for additional data.

Sensitivity analyses have been conducted to determine the influence of various parameters over their expected ranges, which include uncertainty, and these analyses are developed in Section 6.7. Sufficient data exist to enable credible and bounding predictions of infiltration. These studies show that soil depth in depth class 4 (shallow soils) and water holding capacity of soil group 5/7/9 are the most important physical parameters in the MASSIF model. In addition, the uncertainty related to future precipitation patterns is another significant source of uncertainty. While further data are not needed to develop sufficiently accurate estimates of infiltration for TSPA, such data would serve to reduce the uncertainty in predicted infiltration ranges.

(5) Accepted and well-documented procedures are used to construct and calibrate numerical models.

The fundamental conceptual model is based on a mass-balance calculation where water enters a grid cell through precipitation (rain or snowmelt) and/or run-on and water leaves a cell through evapotranspiration, sublimation, runoff, and/or net infiltration. Mass balance implies that the sum of these fluxes equals zero. The mass balance approach is generally accepted and well documented. The primary subcomponents upon which MASSIF is built are described in Section 6 and include: 1) FAO-56 methods to estimate evapotranspiration, and 2) Darcy's Law in conjunction with the field capacity concept for estimating water movement and storage in the soil. Both of these procedures are well-accepted and well-documented approaches. The actual physics controlling run-on and runoff processes are not represented in the model. Instead, runoff is routed along flow networks through the model domain during the course of the day with the constraint of mass balance being enforced. The only calibration done is in the definition of the parameters used to convert satellite data quantifying vegetation (NDVI') to ground measurements of basal crop coefficients (K_{cb}) at ecological study plots. A linear regression accounting for measurement uncertainties was performed for this purpose. The methods used are accepted and well-documented. See Section 6.5.3 for details.

(6) Reasonably complete process-level conceptual and mathematical models are used in this model report. In particular: (a) mathematical models provided are consistent with conceptual models and site characteristics; and (b) the robustness of results from different mathematical models is compared.

The conceptual and mathematical models used in this report are complete in the sense that they represent the complete near surface hydrologic system at the YMP. Section 6 describes the conceptual model development process, the mathematical model, and the use of the model to estimate net infiltration at the YMP. The use of the FAO-56 procedures in conjunction with satellite and ground-based measurements of vegetation at the YMP site ensure that the ET component of the calculation is customized for the YMP site. The generation of stochastic precipitation records is also entirely based on weather data collected in the vicinity of the YMP site and at other locations that represent the predicted range of future climates.

An alternative mathematical model (HYDRUS 1-D) was run, and results were compared with similar runs of the MASSIF model for model corroboration. These comparisons are described in Section 7.2.2[a]. In addition, the MASSIF model was run with historical weather data for comparing model results with observations of ET, runoff, and net infiltration at various locations both on and off the YMP site (Section 7). In general these comparisons indicate that the MASSIF model is valid for its intended use.

Number 7 under Acceptance Criterion 2 was listed in the TWP (BSC 2006 [DIRS 177492]), but it is not included in this report because expert elicitation was not used to support model development.

Acceptance Criterion 3: ***Data Uncertainty Is Characterized and Propagated through the Model Abstraction***

(1) Models use parameter values, assumed ranges, probability distributions, and bounding assumptions that are technically defensible, reasonably account for uncertainties and variabilities, and do not result in an under-representation of the risk estimate.

Each of the parameters that potentially influence infiltration is briefly discussed in Appendix I where it is evaluated and screened for inclusion in the uncertainty analysis. Parameters are screened into the uncertainty analysis if their relative standard uncertainty (standard deviation) is above 15% or they represent the properties of materials that cover more than 15% of the unsaturated zone domain. Parameter uncertainty is propagated to net infiltration by way of a Monte Carlo analysis using Latin Hypercube Sampling (LHS) (Sections 6.5.5 and 6.5.6). The range of net infiltration is demonstrated to reasonably bound the estimates of infiltration in a manner to preclude under-representation of the risk estimate.

(2) The technical bases for the parameter values used in this abstraction are provided.

Each of the parameters that serve as input to the infiltration analysis have been technically evaluated and selected based on their appropriateness for use in calculating infiltration. Bedrock fracture and matrix properties and distributions are developed in *Data Analysis for Infiltration Modeling: Bedrock Saturated Hydraulic Conductivity Calculation* (BSC 2006 [DIRS 176355]) and inputs to the MASSIF model are summarized in Section 6.5.2.6, *Bedrock Saturated Conductivity*. Parameter ranges and distributions used to develop evapotranspiration estimates are discussed in Sections 6.5.3 and 6.5.4 and Appendix D. Soil depth estimates, including uncertainty and spatial variability are developed in *Data Analysis for Infiltration Modeling: Technical Evaluation of Previous Soil Depth Estimation Methods and Development of Alternate Parameter Values* (BSC 2006 [DIRS 178819]) and are further summarized for the MASSIF model in Section 6.5.2.4[a]. Soil hydraulic properties and associated uncertainties are developed in *Data Analysis for Infiltration Modeling: Development of Soil Units and Associated Hydraulic Parameter Values* (BSC 2006 [DIRS 176335]) and are further summarized for the MASSIF model in Section 6.5.2.3. Geographic parameters such as elevation and slope are presented in Appendix B, and summarized in Section 6.5.2.1[a]. All of the parameters that influence infiltration are briefly discussed in Appendix I, where they are screened for inclusion in the uncertainty analysis.

(3) Possible statistical correlations are established between parameters in this abstraction. An adequate technical basis or bounding argument is provided for neglected correlations.

Correlations between parameters have been considered to constrain the LHS sample of input parameters to physically realistic combinations. The sample size of each probabilistic analysis was limited to 20. Up to fifteen parameters were sampled to generate the inputs for each of the 20 realizations. For the physical parameters (parameter related to physical properties of materials), no technical basis justifying imposing correlations between parameters was identified. Therefore, no correlations were applied.

For some of the stochastic precipitation parameters, two strong correlations have been identified between parameters. The first one is an actual correlation between two parameters (e.g., the annual average of average daily precipitation amount and annual average of average daily log of precipitation amount). These parameters are strongly correlated, as they are estimated from the same data (records of daily precipitation). As the relation between the two parameters has been shown to be linear, correlation has been taken into account by sampling one of the two parameters and estimating the other with a linear regression model as discussed in Section 6.5.5 and Appendix I. The second correlation identified is associated with a set of assumptions present in *Future Climate Analysis* (BSC 2004 [DIRS 170002]). For instance, it is stated that Monsoon Climate will experience series of years either with small amounts of rain, mainly in winter, or with a larger amount of rain, mainly in summer (BSC 2004 [DIRS 170002]). Therefore, the annual variation of the precipitation parameters was adjusted to match either of the two cases. This weather pattern has been taken into account by sampling one of the parameters controlling seasonal variation and estimating the other parameters using linear regression models as discussed in Section 6.5.5 and Appendix I. The purpose of including these two correlations is to ensure that the parameter inputs represent a realistic combination of parameter values.

(4) The hydrologic effects of future climate change that may alter the rates and patterns of present-day net infiltration into the UZ are addressed. Such effects may include changes in soil depths, fracture-fill material, and types of vegetation.

The potential for future climates to affect various parameters is captured in inputs including stochastic weather parameters and vegetation parameters. The variation of stochastic weather parameters including temperature and stochastic precipitation parameters for future climates is discussed in Section 6.5.1 and Appendix F. The response in vegetation to the predicted climate change is provided in Section 6.5.3. The amount of vegetation is directly related to the annual precipitation which varies with climate. In addition, vegetation parameters (maximum rooting depth and plant height) are given climate specific and appropriate values and distributions. Field observations of bedrock fracture filling indicate that these fillings were stable during previous wet climate cycles, and therefore, these fillings are expected to remain stable for the regulatory period of the repository. Potential variation in soil depth as a result of future climate change is assumed to be negligible (Section 5.4).

Acceptance Criterion 4: ***Model Uncertainty Is Characterized and Propagated through the Model Abstraction***

(1) Alternate modeling approaches of FEPs, consistent with available data and current scientific understanding, are investigated. The results and limitation are appropriately considered in the abstraction.

Net infiltration results of an alternative conceptual and numerical model (HYDRUS-1D) are compared with the results of the MASSIF model in Section 7.2.2[a] and Appendix K. HYDRUS-1D is a model based on the Richards' equation and thus solves a different set of equations than MASSIF. The comparison demonstrated that while the models exhibit different transient net infiltration behaviors the results are very similar when summed over the year. Thus, since the purpose of the net infiltration calculation is to calculate a steady-state, long term average flux, both MASSIF and HYDRUS-1D provide comparable results, which corroborates the MASSIF model.

(2) The bounds of uncertainty created by process-level models are considered in this abstraction.

It is assumed in this analysis (Section 5) that net infiltration uncertainty caused by the selection of the model is not as significant as the uncertainty caused by the epistemic parameter uncertainty.

(3) Consideration of conceptual model uncertainty is consistent with available site characterization data, laboratory experiments, field measurements, natural analogue information and process-level modeling studies; and the treatment of conceptual model uncertainty does not result in an under-representation of the risk estimate.

The model uncertainties have been estimated by comparing model predictions to field observations and predictions of an alternative model (HYDRUS-1D). These comparisons are described in the model validation sections of the report (Section 7.2.2[a] and Appendices J and K).

Acceptance Criterion 5: ***Model Abstraction Output Is Supported by Objective Comparisons***

The first item under Acceptance Criterion 5 listed in the TWP (BSC 2006 [DIRS 177492]), is not included in this report because the output from this model is not a direct TSPA abstraction.

(2) Abstractions of process-level models may conservatively bound process-level predictions.

Net infiltration estimates presented in this report include the quantification of uncertainty which bounds these estimates. While it was not the intent of this analysis to provide a "conservative" estimate of net infiltration, the results of the analysis may be conservative (overestimate) due to the lack of certain site-specific data to constrain the results. For example, as identified in Section 1.2, it is assumed in this analysis that there is no significant water loss below the soil-rock interface. If, in fact, a significant amount of water is lost from within the rock, then the net infiltration estimates from this analysis provide an upper bound on net infiltration.

(3) Comparisons are provided of output of abstracted models of climate and net infiltration with output of sensitivity studies, detailed process-level models, natural analogs, and empirical observations, as appropriate.

Section 7 includes: (a) comparisons of model outputs of precipitation to observed patterns of precipitation at the Yucca Mountain site as well as at analogue meteorological sites used to represent future climate conditions (Section 7.1.1[a]), (b) comparisons of model predictions of evapotranspiration to lysimeter observations (Section 7.1.2[a]), (c) comparisons of simulated runoff to observations at Yucca Mountain monitoring stations (Section 7.1.3), (d) results of an extended sensitivity study examining the influence of parameter uncertainty on net infiltration uncertainty (Section 7.1.4), (e) comparison of net infiltration predictions with field estimates of net infiltration from the region (Section 7.2.1), (f) comparisons of net infiltration estimates with estimates calculated using an alternative, more detailed and mechanistic model (HYDRUS-1D) (Section 7.2.2[a]), and (g) comparisons of net infiltration model predictions with the estimates provided as part of an expert elicitation (Section 7.2.3).

Acceptance Criteria from Section 2.2.1.1.3

(3) Technical Basis for Barrier Capability is Adequately Presented

The near-surface hydrologic system is part of the natural barrier capability of the repository design. The net infiltration model contributes to the natural barrier system by simulating the precipitation of water to the land surface and calculating the fraction of that water that enters the unsaturated zone as deep percolation. The representation of precipitation processes is described in Section 6.5.1 and Appendix F. Evapotranspiration is discussed in Sections 6.5.3 and 6.5.4 and Appendices C, D, and E.

INTENTIONALLY LEFT BLANK

9[a]. INPUTS AND REFERENCES

The following is a list of the references cited in this document. Column 1 lists the Document Input Reference System number (DIRS). Column 2 lists the bibliographic citation.

9.1[a]. DOCUMENTS CITED

176568 Allen, R.G. 1997. "Self-Calibrating Method for Estimating Solar Radiation from Air Temperature." *Journal of Hydrologic Engineering, 2,* (2), 56-67. New York, New York: American Society of Civil Engineers. TIC: 258131.

157311 Allen, R.G.; Pereira, L.S.; Raes, D.; and Smith, M. 1998. *Crop Evapotranspiration, Guidelines for Computing Crop Water Requirements.* FAO Irrigation and Drainage Paper 56. Rome, Italy: Food and Agriculture Organization of the United Nations. TIC: 245062.

176009 Allen, R.G.; Pereira, L.S.; Smith, M.; Raes, D.; and Wright, J.L. 2005. "FAO-56 Dual Crop Coefficient Method for Estimating Evaporation from Soil and Application Extensions." *Journal of Irrigation and Drainage Engineering, 131,* (1), 2-13. Reston, Virginia: American Society of Civil Engineers. TIC: 257869.

176207 Allen, R.G.; Walter, I.A.; Elliott, R.L.; Howell, T.; Itenfisu, D.; and Jensen, M. 2005. *The ASCE Standardized Reference Evapotranspiration Equation.* Reston, Virginia: American Society of Civil Engineers. TIC: 257138.

103597 Altman, W.D.; Donnelly, J.P.; and Kennedy, J.E. 1988. *Peer Review for High-Level Nuclear Waste Repositories: Generic Technical Position.* NUREG-1297. Washington, D.C.: U.S. Nuclear Regulatory Commission. TIC: 200651.

177200 Avon, L. and Durbin, T.J. 1994. "Evaluation of the Maxey-Eakin Method for Estimating Recharge to Ground-Water Basins in Nevada." *Water Resources Bulletin, 30,* (1), 99-111. Herndon, Virginia: American Water Resources Association. TIC: 255352.

177726 Bauer, H.H. and Vaccaro, J.J. 1990. *Estimates of Ground-Water Recharge to the Columbia Plateau Regional Aquifer System, Washington, Oregon, and Idaho, for Predevelopment and Current Land-Use Conditions.* Water-Resources Investigations Report 88-4108. Denver, Colorado: U.S. Geological Survey. ACC: MOL.20061115.0001.

177995 Berg, N.H. 1986. "Blowing Snow at a Colorado Alpine Site: Measurements and Implications." *Arctic and Alpine Research, 18,* (2), 147-161. Boulder, Colorado: University of Colorado, Institute of Arctic and Alpine Research. TIC: 258763.

176615 Brutsaert, W. 1982. *Evaporation into the Atmosphere, Theory, History, and Applications.* Environmental Fluid Mechanics. Csanady, G.T., ed. Boston, Massachusetts: D. Reidel Publishing Company. TIC: 239388.

165991 BSC (Bechtel SAIC Company) 2003. *Analysis of Infiltration Uncertainty.* ANL-NBS-HS-000027 REV 01. Las Vegas, Nevada: Bechtel SAIC Company. ACC: DOC.20031030.0003.

165572 BSC 2003. *Underground Layout Configuration.* 800-P0C-MGR0-00100-000-00E. Las Vegas, Nevada: Bechtel SAIC Company. ACC: ENG.20031002.0007; ENG.20050817.0005.

170002 BSC 2004. *Future Climate Analysis.* ANL-NBS-GS-000008 REV 01. Las Vegas, Nevada: Bechtel SAIC Company. ACC: DOC.20040908.0005.

170029 BSC 2004. *Geologic Framework Model (GFM2000).* MDL-NBS-GS-000002 REV 02. Las Vegas, Nevada: Bechtel SAIC Company. ACC: DOC.20040827.0008.

167652 BSC 2004. *Seepage Model for PA Including Drift Collapse.* MDL-NBS-HS-000002 REV 03. Las Vegas, Nevada: Bechtel SAIC Company. ACC: DOC.20040922.0008; DOC.20051205.0001.

170007 BSC 2004. *Simulation of Net Infiltration for Present-Day and Potential Future Climates.* MDL-NBS-HS-000023 REV 00. Las Vegas, Nevada: Bechtel SAIC Company. ACC: DOC.20041109.0004.

176335 BSC 2006. *Data Analysis for Infiltration Modeling: Development of Soil Units and Associated Hydraulic Parameter Values.* ANL-NBS-HS-000055 REV 00. Las Vegas, Nevada: Bechtel SAIC Company. ACC: DOC.20060912.0006.

178819 BSC 2006. *Data Analysis for Infiltration Modeling: Technical Evaluation of Previous Soil Depth Estimation Methods and Development of Alternate Parameter Values.* ANL-NBS-HS-000077 REV 01. Las Vegas, Nevada: Bechtel SAIC Company. ACC: DOC.20060918.0009.

176355 BSC 2006. *Data Analysis for Infiltration Modeling: Bedrock Saturated Hydraulic Conductivity Calculation.* ANL-NBS-HS-000054 REV 00. Las Vegas, Nevada: Bechtel SAIC Company. ACC: DOC.20060710.0001.

177083 BSC 2006. *Technical Evaluation and Review of Results, Technical Procedures, and Methods Related to the Collection of Moisture Monitoring Data Using Neutron Probes in Shallow Boreholes.* TDR-NBS-HS-000019 REV 00. Las Vegas, Nevada: Bechtel SAIC Company. ACC: DOC.20060425.0005.

177492 BSC 2006. *Technical Work Plan for: Infiltration Model Assessment, Revision, and Analyses of Downstream Impacts.* TWP-NBS-HS-000012 REV 02. Las Vegas, Nevada: Bechtel SAIC Company. ACC: DOC.20060831.0006.

177100 Campbell, M.D.; Gee, G.W.; Kirkham, R.R.; Phillips, S.J.; and Wing, N.R. 1991. "Water Balance Lysimetry at a Nuclear Waste Site." *Lysimeters for Evapotranspiration and Environmental Measurements, Proceedings of the International Symposium on Lysimetry, Honolulu, Hawaii, July 23-25, 1991.* Allen, R.G.; Howell, T.A.; Pruitt, W.O.; Walter, I.A.; and Jensen, M.E., eds. Pages 125-132. New York, New York: American Society of Civil Engineers. TIC: 258304.

184740 Cohen, P. 1964. *A Brief Appraisal of the Ground-Water Resources of the Grass Valley Area, Humboldt and Pershing Counties, Nevada.* Ground-Water Resources - Reconnaissance Series Report 29. Carson City, Nevada: State of Nevada, Department of Conservation and Natural Resources. ACC: LLR.20080117.0027.

184711 Crosthwaite, E.G. 1963. *Ground-Water Appraisal of Antelope and Middle Reese River Valleys, Lander County, Nevada.* Ground-Water Resources - Reconnaissance Series Report 19. Carson City, Nevada: State of Nevada, Department of Conservation and Natural Resources. ACC: LLR.20080117.0020.

100117 CRWMS M&O 1997. *Engineering Design Climatology and Regional Meteorological Conditions Report.* B00000000-01717-5707-00066 REV 00. Las Vegas, Nevada: CRWMS M&O. ACC: MOL.19980304.0028.

100335 CRWMS M&O 1997. *Unsaturated Zone Flow Model Expert Elicitation Project.* Las Vegas, Nevada: CRWMS M&O. ACC: MOL.19971009.0582.

105031 CRWMS M&O 1999. *Final Report: Plant and Soil Related Processes Along a Natural Thermal Gradient at Yucca Mountain, Nevada.* B00000000-01717-5705-00109 REV 00. Las Vegas, Nevada: CRWMS M&O. ACC: MOL.19990513.0037.

101557 Day, W.C.; Potter, C.J.; Sweetkind, D.S.; Dickerson, R.P.; and San Juan, C.A. 1998. *Bedrock Geologic Map of the Central Block Area, Yucca Mountain, Nye County, Nevada.* Miscellaneous Investigations Series Map I-2601. Washington, D.C.: U.S. Geological Survey. ACC: MOL.19980611.0339.

176858 Desotell, L.T.; Hudson, D.B.; Yucel, V.; and Carilli, J.T. 2006. *Use of Long-Term Lysimeter Data in Support of Shallow Land Waste Disposal Cover Design.* DOE/NV11718--1148. Las Vegas, Nevada: U.S. Department of Energy, Nevada Site Office. ACC: MOL.20060413.0159.

105384 Dettinger, M.D. 1989. "Reconnaissance Estimates of Natural Recharge to Desert Basins in Nevada, U.S.A., by Using Chloride-Balance Calculations." *Journal of Hydrology, 106,* 55-78. Amsterdam, The Netherlands: Elsevier. TIC: 236967.

178797 Di Sanza, E.F. 2006. "Yucca Mountain Project (YMP) Request for Area 5 Weighing Lysimeter Data." Memorandum from E.F. Di Sanza (DOE/NVO) to E.T. Smistad (YMP), January 26, 2006, WMD:1671.JC, with attachments. ACC: MOL.20060510.0140.

180680 DOE (U.S. Department of Energy) 2007. *Root Cause Analysis Report in Response to Condition Report 5223 Regarding Emails Suggesting Noncompliance with Quality Assurance Requirements.* Las Vegas, Nevada: U.S. Department of Energy, Office of Civilian Radioactive Waste Management. ACC: LLR.20070504.0081.

184690 Eakin, T.E 1960. *Ground-Water Appraisal of Newark Valley, White Pine County, Nevada.* Ground-Water Resources- -Reconnaissance Series Report 1. Carson City, Nevada: State of Nevada Department of Conservation and Natural Resources. ACC: LLR.20080117.0008.

184694 Eakin, T.E. 1961. *Ground-Water Appraisal of Long Valley, White Pine and Elko Counties, Nevada.* Ground-Water Resources -- Reconnaissance Series Report 3. Carson City, Nevada: State of Nevada, Department of Conservation and Natural Resources. ACC: LLR.20080117.0010.

184693 Eakin, T.E. 1961. *Ground-Water Appraisal of Pine Valley Eureka and Elko Counties, Nevada.* Ground-Water Resources-–Reconnaissance Series Report 2. Carson City, Nevada: State of Nevada, Department of Conservation and Natural Resources. ACC: LLR.20080117.0009.

184708 Eakin, T.E. 1962. *Ground-Water Appraisal of Cave Valley in Lincoln and White Pines Counties, Nevada.* Ground-Water Resources - Reconnaissance Series Report 13. Carson City, Nevada: State of Nevada, Department of Conservation and Natural Resources. ACC: LLR.20080117.0016.

184701 Eakin, T.E. 1962. *Ground-Water Appraisal of Gabbs Valley, Mineral and Nye Counties, Nevada.* Ground-Water Resources - Reconnaissance Series Report 9. Carson City, Nevada: State of Nevada, Department of Conservation and Natural Resources. ACC: LLR.20080117.0014.

176818 Eakin, T.E. 1962. *Ground-Water Appraisal of Ralston and Stonecabin Valleys, Nye County, Nevada.* Ground-Water Resources - Reconnaissance Series Report 12. Carson City, Nevada: State of Nevada, Department of Conservation and Natural Resources. ACC: MOL.20060417.0024.

184699 Eakin, T.E. 1962. *Ground-Water Appraisal of the Imlay Area Humboldt River Basin, Pershing County, Nevada.* Ground-Water Resources - Reconnaissance Series Report 5. Carson City, Nevada: State of Nevada, Department of Conservation and Natural Resources. ACC: LLR.20080117.0012.

148766 Eakin, T.E. 1963. *Ground-Water Appraisal of Dry Lake and Delmar Valleys, Lincoln County, Nevada.* Ground-Water Resources – Reconnaissance Series Report 16. Carson City, Nevada: State of Nevada, Department of Conservation and Natural Resources. TIC: 208667.

184710 Eakin, T.E. 1963. *Ground-Water Appraisal of Garden and Coal Valleys, Lincoln and Nye Counties, Nevada.* Ground-Water Resources - Reconnaissance Series Report 18. Carson City, Nevada: State of Nevada, Department of Conservation and Natural Resources. ACC: LLR.20080117.0019.

176646 Eakin, T.E. 1963. *Ground-Water Appraisal of Pahranagat and Pahroc Valleys, Lincoln and Nye Counties, Nevada.* Ground-Water Resources - Reconnaissance Series Report 21. Carson City, Nevada: State of Nevada, Department of Conservation and Natural Resources. TIC: 230793.

184714 Eakin, T.E. 1964. *Ground-Water Appraisal of Coyote Spring and Kane Spring Valleys and Muddy River Springs Area, Lincoln and Clark Counties, Nevada.* Ground-Water Resources - Reconnaissance Series Report 25. Carson City, Nevada: State of Nevada, Department of Conservation and Natural Resources. ACC: LLR.20080117.0024.

148765 Eakin, T.E. 1962. *Ground-Water Appraisal of Diamond Valley, Eureka and Elko Counties, Nevada.* Reconnaissance Series Report 6. Carson City, Nevada: Nevada Department of Conservation and Natural Resources. TIC: 221367.

184723 Eakin, T.E.; Hughes, J.L.; and Moore, D.O. 1967. *Water-Resources Appraisal of Steptoe Valley, White Pine and Elko Counties, Nevada.* Water Resources - Reconnaissance Series Report 42. Carson City, Nevada: State of Nevada, Department of Conservation and Natural Resources. ACC: LLR.20080117.0036.

101237 Eakin, T.E.; Maxey, G.B.; Robinson, T.W.; Fredericks, J.C.; and Loeltz, O.J. 1951. *Contributions to the Hydrology of Eastern Nevada.* Water Resources Bulletin 12. Carson City, Nevada: State of Nevada, Office of the State Engineer. ACC: NNA.19870406.0382.

184717 Eakin, T.E.; Moore, D.O.; and Everett, D.E. 1965. *Water Resources Appraisal of the Upper Reese River Valley, Lander and Nye Counties, Nevada.* Water Resources - Reconnaissance Series Report 31. Carson City, Nevada: State of Nevada, Department of Conservation and Natural Resources. ACC: LLR.20080117.0029.

184715 Everett, D.E. 1964. *Ground-Water Appraisal of Edwards Creek Valley, Churchill County, Nevada.* Ground-Water Resources - Reconnaissance Series Report 26. Carson City, Nevada: State of Nevada, Department of Conservation and Natural Resources. ACC: LLR.20080117.0025.

184722 Everett, D.E. and Rush F.E. 1966. *A Brief Appraisal of the Water Resources of Grass and Carico Lake Valleys, Lander and Eureka Counties, Nevada.* Water Resources - Reconnaissance Series Report 37. Carson City, Nevada: State of Nevada, Department of Conservation and Natural Resources. ACC: LLR.20080117.0034.

184716 Everett, D.E. and Rush, F.E. 1964. *Ground-Water Appraisal of Smith Creek and Ione Valleys, Lander and Nye Counties, Nevada.* Ground-Water Resources - Reconnaissance Series Report 28. Carson City, Nevada: State of Nevada, Department of Conservation and Natural Resources. ACC: LLR.20080117.0026.

181394 Everett, D.E. and Rush, F.E. 1967. *A Brief Appraisal of the Water Resources of the Walker Lake Area, Mineral, Lyon, and Churchill Counties, Nevada.* Water Resources-Reconnaissance Series Report 40. Carson City, Nevada: Nevada Department of Conservation and Natural Resources. ACC: HQS.19880517.2129.

178766 Faybishenko, B. 2007. "Climatic Forecasting of Net Infiltration at Yucca Mountain Using Analogue Meterorological Data." *Vadose Zone Journal, 6,* 77-92. Madison, Wisconsin: Soil Science Society of America. TIC: 259076.

177499 Fayer, M.J. 2000. *UNSAT-H Version 3.0: Unsaturated Soil Water and Heat Flow Model, Theory, User Manual, and Examples.* PNNL-13249. Richland, Washington: Pacific Northwest National Laboratory. ACC: MOL.20060712.0224.

178191 Fayer, M.J. and Walters, T.B. 1995. *Estimated Recharge Rates at the Hanford Site.* PNL-10285. Richland, Washington: Pacific Northwest Laboratory. ACC: MOL.20061026.0075.

182469 Fedors, R. 2007. "Soil Depths Measured at Yucca Mountain During Site Visits in 1998." Letter from R. Fedors to J. Guttmann, January 9, 2007. ACC: LLR.20070815.0081.

177754 Finsterle, S. and Seol, Y. 2006. *Preliminary Evaluation of Seepage Observations from the ESF South Ramp Using the Drift Seepage Abstraction Model.* Albuquerque, New Mexico: Sandia National Laboratories. ACC: MOL.20060510.0330.

100147 Flint, A.L.; Hevesi, J.A.; and Flint, L.E. 1996. *Conceptual and Numerical Model of Infiltration for the Yucca Mountain Area, Nevada.* Milestone 3GUI623M. Denver, Colorado: U.S. Geological Survey. ACC: MOL.19970409.0087.

100394 Flint, L.E. and Flint, A.L. 1995. *Shallow Infiltration Processes at Yucca Mountain, Nevada—Neutron Logging Data 1984-93.* Water-Resources Investigations Report 95-4035. Denver, Colorado: U.S. Geological Survey. ACC: MOL.19960924.0577.

163705 Gilbert, R.O. 1987. *Statistical Methods for Environmental Pollution Monitoring.* New York, New York: John Wiley & Sons. TIC: 252619.

184728 Glancy, P.A. 1968. *Water-Resources Appraisal of Butte Valley, Elko and White Pine Counties, Nevada.* Water Resources - Reconnaissance Series Report 49. Carson City, Nevada: State of Nevada, Department of Conservation and Natural Resources. ACC: LLR.20080117.0041.

105354 Glancy, P.A. 1968. *Water-Resources Appraisal of Mesquite-Ivanpah Valley Area, Nevada and California.* Water Resources – Reconnaissance Series Report 46. Carson City, Nevada: State of Nevada, Department of Conservation and Natural Resources. ACC: NNA.19940520.0075.

184735 Glancy, P.A. and Katzer, T.L. 1976. *Water-Resources Appraisal of the Carson River Basin, Western Nevada.* Water Resources - Reconnaissance Series Report 59. Carson City, Nevada: State of Nevada, Department of Conservation and Natural Resources. ACC: LLR.20080117.0049.

184725 Glancy, P.A. and Rush, F.E. 1968. *Water-Resources Appraisal of Smoke Creek-San Emidio Desert Area Nevada and California.* Water Resources - Reconnaissance Series Report 44. Carson City, Nevada: State of Nevada, Department of Conservation and Natural Resources. ACC: LLR.20080117.0038.

184730 Glancy, P.A. and Van Denburgh, A.S. 1969. *Water-Resources Appraisal of the Lower Virgin River Valley Area, Nevada, Arizona, and Utah.* Water Resources - Reconnaissance Series Report 51. Carson City, Nevada: State of Nevada, Department of Conservation and Natural Resources. ACC: LLR.20080117.0043.

177508 Hanson, C.L. 2001. "Long-Term Precipitation Database, Reynolds Creek Experimental Watershed, Idaho, United States." *Water Resources Research, 37,* (11), 2831-2834. Washington, D.C.: American Geophysical Union. ACC: MOL.20060712.0230.

177509 Hanson, C.L.; Marks, D.; and Van Vactor, S.S. 2001. "Long-Term Climate Database, Reynolds Creek Experimental Watershed, Idaho, United States." *Water Resources Research, 37,* (11), 2839-2841. Washington, D.C.: American Geophysical Union. ACC: MOL.20060712.0231.

184746 Harrill, J.R. 1970. *Water-Resources Appraisal of the Granite Springs Valley Area, Pershing, Churchill, and Lyon Counties, Nevada.* Water Resources - Reconnaissance Series Report 55. Carson City, Nevada: State of Nevada, Department of Conservation and Natural Resources. ACC: LLR.20080117.0045.

184732 Harrill, J.R. 1971. *Water-Resources Appraisal of the Pilot Creek Valley Area, Elko and White Pine Counties, Nevada.* Water Resources - Reconnaissance Series Report 56. Carson City, Nevada: State of Nevada, Department of Conservation and Natural Resources. ACC: LLR.20080117.0046.

184753 Harrill, J.R. 1973. *Evaluation of the Water Resources of Lemmon Valley, Washoe County, Nevada, with Emphasis on Effects of Ground-Water Development to 1971.* Water Resources Bulletin No. 42. Carson City, Nevada: State of Nevada, Department of Conservation and Natural Resources. ACC: LLR.20080117.0006.

184754 Harrill, J.R. and Lamke, R.D. 1968. *Hydrologic Response to Irrigation Pumping in Diamond Valley, Eureka and Elko Counties, Nevada, 1950-1965.* Water Resources Bulletin No. 35. Carson City, Nevada: State of Nevada, Department of Conservation and Natural Resources. ACC: LLR.20080117.0004.

184755 Harrill, J.R. and Moore, D.O. 1970. *Effects of Ground-Water Development on the Water Regimen of Paradise Valley, Humboldt County, Nevada, 1948-68, and Hydrologic Reconnaissance of the Tributary Areas.* Water Resources Bulletin No. 39. Carson City, Nevada: State of Nevada, Department of Conservation and Natural Resources. ACC: LLR.20080117.0005.

178856 Hillel, D. 2004. *Introduction to Environmental Soil Physics.* New York, New York: Elsevier. TIC: 259102.

153709 Hofmann, L.L.; Guertal, W.R.; and Flint, A.L. 2000. *Development and Testing of Techniques to Obtain Infiltration Data for Unconsolidated Surficial Materials, Yucca Mountain Area, Nye County, Nevada.* Open-File Report 95-154. Denver, Colorado: U.S. Geological Survey. TIC: 249343.

177996 Hood, E.; Williams, M.; and Cline, D. 1999. "Sublimation from a Seasonal Snowpack at a Continental, Mid-Latitude Alpine Site." *Hydrological Processes, 13,* 1781-1797. New York, New York: John Wiley & Sons. TIC: 258621.

184743 Hood, J.W. and Rush, F.E. 1965. *Water-Resources Appraisal of the Snake Valley Area, Utah and Nevada.* Water Resources - Reconnaissance Series Report 34. Carson City, Nevada: State of Nevada, Department of Conservation and Natural Resources. ACC: LLR.20080117.0031.

177190 Howell, T.A.; Schneider, A.D.; and Jensen, M.E. 1991. "History of Lysimeter Design and Use for Evapotranspiration Measurements." *Lysimeters for Evapotranspiration and Environmental Measurements, Proceedings of the International Symposium on Lysimetry, Honolulu, Hawaii, July 23-25, 1991.* Allen, R.G.; Howell, T.A.; Pruitt, W.O.; Walter, I.A.; and Jensen, M.E., eds. Pages 1-9. New York, New York: American Society of Civil Engineers. TIC: 258304.

184751 Huxel, C.J., Jr.; Parkes, J.E.; and Everett, D.E. 1966. *Effects of Irrigation Development on the Water Supply of Quinn River Valley Area, Nevada and Oregon, 1950-1964.* Water Resources Bulletin No. 34. Carson City, Nevada: State of Nevada, Department of Conservation and Natural Resources. ACC: LLR.20080117.0003.

177103 Jensen, D.T.; Hargreaves, G.H.; Temesgen, B.; and Allen, R.G. 1997. "Computation of ETo Under Nonideal Conditions." *Journal of Irrigation and Drainage Engineering, 123,* (5), 394-400. Reston, Virginia: American Society of Civil Engineers. TIC: 258407.

177998 Kattelmann, R. and Elder, K. 1991. "Hydrologic Characteristics and Water Balance of an Alpine Basin in the Sierra Nevada." *Water Resources Research, 27,* (7), 1553-1562. Washington, D.C.: American Geophysical Union. TIC: 258622.

177191 Kirkham, R.R.; Rockhold, M.L.; Gee, G.W.; Fayer, M.J.; and Campbell, M.D. 1991. "Lysimeters: Data Acquisition and Analysis." *Lysimeters for Evapotranspiration and Environmental Measurements, Proceedings of the International Symposium on Lysimetry, Honolulu, Hawaii, July 23-25, 1991.* Allen, R.G.; Howell, T.A.; Pruitt, W.O.; Walter, I.A.; and Jensen, M.E., eds. Pages 362-370. New York, New York: American Society of Civil Engineers. TIC: 258304.

158511 LeCain, G.D.; Lu, N.; and Kurzmack, M. 2002. *Use of Temperature, Pressure, and Water Potential Data to Estimate Infiltration and Monitor Percolation in Pagany Wash Associated with the Winter of 1997–98 El Niño Precipitation, Yucca Mountain, Nevada.* Water Resources Investigations Report 02-4035. Denver, Colorado: U.S. Geological Survey. TIC: 252641.

163183 Levitt, D.G.; Lohrstorfer, C.F.; Sully, M.J.; and Ginanni, J.M. 1996. "An Arid Zone Lysimeter Facility for Performance Assessment and Closure Investigations at the Nevada Test Site." *HLW, LLW, Mixed Wastes and Environmental Restoration — Working Towards a Cleaner Environment, WM '96, Proceedings, February 25-29, 1996, Tucson, Arizona.* Tucson, Arizona: Laser Options. TIC: 254421.

177521 Levitt, D.G.; Sully, M.J.; Dozier, B.L.; and Lohrstorfer, C.F. 1999. "Determining the Performance of an Arid Zone Radioactive Waste Site Through Site Characterization, Modeling and Monitoring." *HLW, LLW, Mixed Wastes and Environmental Restoration — Working Towards a Cleaner Environment, WM'99, Proceedings, February 28-March 4, 1999, Tucson, Arizona.* Tucson, Arizona: WM Symposia. TIC: 250888.

100589 Lichty, R.W. and McKinley, P.W. 1995. *Estimates of Ground-Water Recharge Rates for Two Small Basins in Central Nevada.* Water-Resources Investigations Report 94-4104. Denver, Colorado: U.S. Geological Survey. ACC: MOL.19960924.0524.

154273 Looney, B.B. and Falta, R.W., eds. 2000. *Vadose Zone, Science and Technology Solutions.* Two volumes. Columbia, Ohio: Battelle Press. TIC: 249256.

178540 Maher, K.; DePaolo, D.J.; Conrad, M.E.; and Serne, R.J. 2003. "Vadose Zone Infiltration Rate at Hanford, Washington, Inferred from Sr Isotope Measurements." *Water Resources Research, 39,* (8), SBH 3-1-SBH 3-14. Washington, D.C.: American Geophysical Union. TIC: 259095.

125317 Maidment, D.R., ed. 1993. *Handbook of Hydrology.* New York, New York: McGraw-Hill. TIC: 236568.

106695 Malmberg, G.T. and Eakin, T.E. 1962. *Ground-Water Appraisal of Sarcobatus Flat and Oasis Valley, Nye and Esmeralda Counties, Nevada.* Ground-Water Resources – Reconnaissance Series Report 10. Carson City, Nevada: State of Nevada, Department of Conservation and Natural Resources. TIC: 208666.

184760 Malmberg, G.T. and Worts, G.F., Jr. 1966. *The Effects of Pumping on the Hydrology of Kings River Valley, Humboldt County, Nevada, 1957-1964.* Water Resources Bulletin No. 31. Carson City, Nevada: State of Nevada, Department of Conservation and Natural Resources. ACC: LLR.20080117.0002.

177512 Marks, D. 2001. "Introduction to Special Section: Reynolds Creek Experimental Watershed." *Water Resources Research, 37,* (11), 2817. Washington, D.C.: American Geophysical Union. ACC: MOL.20060712.0232.

177504 Marks, D.; Cooley, K.R.; Robertson, D.C.; and Winstral, A. 2001. "Long-Term Snow Database, Reynolds Creek Experimental Watershed, Idaho, United States." *Water Resources Research, 37,* (11), 2835-2838. Washington, D.C: American Geophysical Union. ACC: MOL.20060712.0227.

177370 Maurer, D.K. and Berger, D.L. 1997. *Subsurface Flow and Water Yield from Watersheds Tributary to Eagle Valley Hydrographic Area, West-Central Nevada.* Water-Resources Investigations Report 97-4191. Carson City, Nevada: U.S. Geological Survey. ACC: MOL.20060808.0017.

184752 Maurer, D.K.; Plume, R.W.; Thomas, J.M.; and Johnson, A.K. 1996. *Water Resources and Effects of Changes in Ground-Water Use Along the Carlin Trend, North-Central Nevada.* Water-Resources Investigations Report 96-4134. Carson City, Nevada: U.S. Geological Survey. ACC: LLR.20080117.0007.

100598 Maxey, G.B. and Eakin, T.E. 1950. *Ground Water in White River Valley, White Pine, Nye, and Lincoln Counties, Nevada.* Water Resources Bulletin No. 8. Carson City, Nevada: State of Nevada, Office of the State Engineer. TIC: 216819.

177910 McElroy, D.L. 1993. *Soil Moisture Monitoring Results at the Radioactive Waste Management Complex of the Idaho National Engineering Laboratory, FY-1993.* EGG-WM-11066. Idaho Falls, Idaho: EG&G Idaho, Idaho National Engineering Laboratory. ACC: MOL.20061016.0249.

184726 Moore, D.O. and Eakin, T.E. 1968. *Water-Resources Appraisal of the Snake River Basin in Nevada.* Water Resources - Reconnaissance Series Report 48. Carson City, Nevada: State of Nevada, Department of Conservation and Natural Resources. ACC: LLR.20080117.0040.

178863 Nichols, W.D. 2000. *Regional Ground-Water Evapotranspiration and Ground-Water Budgets, Great Basin, Nevada.* U.S. Geological Survey Professional Paper 1628. Reston, Virginia: U.S. Geological Survey. ACC: LLR.20070213.0076.

178676 NOAA (National Oceanic and Atmospheric Administration) 2002. *Monthly Station Normals of Temperature, Precipitation, and Heating and Cooling Degree Days 1971-2000, 26 Nevada.* Climatography of the United States No. 81. Asheville, North Carolina: National Oceanic and Atmospheric Administration. ACC: MOL.20070125.0053.

160500 Nobel, P.S. 1983. "Plants and Fluxes." *Biophysical Plant Physiology and Ecology.* Pages 461-523. New York, New York: W.H. Freeman and Company. TIC: 252952.

163274 NRC (U.S. Nuclear Regulatory Commission) 2003. *Yucca Mountain Review Plan, Final Report.* NUREG-1804, Rev. 2. Washington, D.C.: U.S. Nuclear Regulatory Commission, Office of Nuclear Material Safety and Safeguards. TIC: 254568.

177503 Pierson, F.B.; Slaughter, C.W.; and Cram, Z.K. 2001. "Long-Term Stream Discharge and Suspended-Sediment Database, Reynolds Creek Experimental Watershed, Idaho, United States." *Water Resources Research, 37,* (11), 2857-2861. Washington, D.C.: American Geophysical Union. ACC: MOL.20060712.0226.

103450 Resource Concepts 1989. *Soil Survey of Yucca Mountain Study Area, Nye County, Nevada.* NWPO EV 003-89. Carson City, Nevada: Resource Concepts. TIC: 206227.

177738 Rodríguez, E.; Morris, C.S.; Belz, J.E.; Chapin, E.C.; Martin, J.M.; Daffer, W.; and Hensley, S. 2005. *An Assessment of the SRTM Topographic Products.* D-31639. Pasadena, California: Jet Propulsion Laboratory. ACC: MOL.20061011.0062.

176849 Rush, F.E. 1968. *Water–Resources Appraisal of Clayton Valley–Stonewall Flat Area, Nevada and California.* Water Resources – Reconnaissance Series Report 45. Carson City, Nevada: State of Nevada, Department of Conservation and Natural Resources. TIC: 217156.

184729 Rush, F.E. 1968. *Water-Resources Appraisal of the Lower Moapa-Lake Mead Area, Clark County, Nevada.* Water Resources - Reconnaissance Series Report 50. Carson City, Nevada: State of Nevada, Department of Conservation and Natural Resources. ACC: LLR.20080117.0042.

184727 Rush, F.E. 1968. *Water-Resources Appraisal of Thousand Springs Valley, Elko County, Nevada.* Water Resources - Reconnaissance Series Report 47. Carson City, Nevada: State of Nevada, Department of Conservation and Natural Resources. ACC: LLR.20080117.0039.

176502 Rush, F.E. 1964. *Ground-Water Appraisal of the Meadow Valley Area, Lincoln and Clark Counties, Nevada.* Ground-Water Resources-Reconnaissance Series Report 27. Carson City, Nevada: State of Nevada, Department of Conservation and Natural Resources. TIC: 218944.

102893 Rush, F.E. 1971. *Regional Ground-Water Systems in the Nevada Test Site Area, Nye, Lincoln, and Clark Counties, Nevada.* Water Resources – Reconnaissance Series Report 54. Carson City, Nevada: State of Nevada, Department of Conservation and Natural Resources. ACC: HQS.19880517.1834.

184713 Rush, F.E. and Eakin, T.E. 1963. *Ground-Water Appraisal of Lake Valley in Lincoln and White Pine Counties, Nevada.* Ground-Water Resources - Reconnaissance Series Report 24. Carson City, Nevada: State of Nevada, Department of Conservation and Natural Resources. ACC: LLR.20080117.0023.

184741 Rush, F.E. and Everett, D.E 1964. *Ground-Water Appraisal of Monitor, Antelope, and Kobeh Valleys, Nevada.* Ground-Water Resources - Reconnaissance Series Report 30. Carson City, Nevada: State of Nevada, Department of Conservation and Natural Resources. ACC: LLR.20080117.0028.

176950 Rush, F.E. and Everett, D.E. 1966. *Water-Resources Appraisal of Little Fish Lake, Hot Creek, and Little Smoky Valleys, Nevada.* Water Resources -- Reconnaissance Series Report 38. Carson City, Nevada: State of Nevada, Department of Conservation and Natural Resources. ACC: MOL.20060524.0139.

184721 Rush, F.E. and Everett, D.E. 1966. *Water-Resources Appraisal of the Huntington Valley Area, Elko and White Pine Counties, Nevada.* Water Resources - Reconnaissance Series Report 35. Carson City, Nevada: State of Nevada, Department of Conservation and Natural Resources. ACC: LLR.20080117.0032.

184724 Rush, F.E. and Glancy, P.A. 1967. *Water-Resources Appraisal of the Warm Springs-Lemmon Valley Area, Washoe County, Nevada.* Water Resources - Reconnaissance Series Report 43. Carson City, Nevada: State of Nevada, Department of Conservation and Natural Resources. ACC: LLR.20080117.0037.

184720 Rush, F.E. and Huxel, C.J., Jr. 1966. *Ground-Water Appraisal of the Eldorado-Piute Valley Area, Nevada and California.* Water Resources - Reconnaissance Series Report 36. Carson City, Nevada: State of Nevada, Department of Conservation and Natural Resources. ACC: LLR.20080117.0033.

184733 Rush, F.E. and Katzer, T.L. 1973. *Water-Resources Appraisal of Fish Lake Valley, Nevada and California.* Water Resources - Reconnaissance Series Report 58. Carson City, Nevada: State of Nevada, Department of Conservation and Natural Resources. ACC: LLR.20080117.0048.

184718 Rush, F.E. and Kazmi, S.A.T. 1965. *Water Resources Appraisal of Spring Valley, White Pine and Lincoln Counties, Nevada.* Water Resources - Reconnaissance Series Report 33. Carson City, Nevada: State of Nevada, Department of Conservation and Natural Resources. ACC: LLR.20080117.0030.

182756 Rush, F.E. and Schroer, C.V. 1971. *Water Resources of Big Smokey Valley, Lander, Nye, and Esmeralda Counties, Nevada.* Water Resources Bulletin No. 41. Carson City, Nevada: State of Nevada, Department of Conservation and Natural Resources. ACC: MOL.20070831.0088.

176569 Sanchez, A. 2006. Conducting Confirmatory Field Observations for Special Infiltration Project [partial submittal]. Scientific Notebook SN-M&O-SCI-053-V1. Pages 1-83. ACC: MOL.20060306.0186.

178109 Scanlon, B.R.; Keese, K.; Reedy, R.C.; Simunek, J.; and Andraski, B.J. 2003. "Variations in Flow and Transport in Thick Desert Vadose Zones in Response to Paleoclimate Forcing (0-90 kyr): Field Measurements, Modeling, and Uncertainties." *Water Resources Research, 39,* (7), 3/1-3/6. Washington, D.C.: American Geophysical Union. TIC: 258648.

175977 Scanlon, B.R.; Levitt, D.G.; Reedy, R.C.; Keese, K.E.; and Sully, M.J. 2005. "Ecological Controls on Water-Cycle Response to Climate Variability in Deserts." *Proceedings of the National Academy of Sciences of the United States of America, 102,* (17), 6033-6038. Washington, D.C.: National Academy of Sciences of the USA. TIC: 257888.

142228 Scanlon, B.R.; Tyler, S.W.; and Wierenga, P.J. 1997. "Hydrologic Issues in Arid, Unsaturated Systems and Implications for Contaminant Transport." *Reviews of Geophysics, 35,* (4), 461-490. Washington, D.C.: American Geophysical Union. TIC: 246881.

104181 Scott, R.B. and Bonk, J. 1984. *Preliminary Geologic Map of Yucca Mountain, Nye County, Nevada, with Geologic Sections.* Open-File Report 84-494. Denver, Colorado: U.S. Geological Survey. ACC: HQS.19880517.1443.

177480 Sevruk, B. 1982. *Methods of Correction for Systematic Error in Point Precipitation Measurement for Operational Use.* Operational Hydrology Report No. 21. WMO - No. 589. Geneva, Switzerland: World Meteorological Organization. TIC: 258537.

177501 Seyfried, M.; Harris, R.; Marks, D.; and Jacob, B. 2001. "Geographic Database, Reynolds Creek Experimental Watershed, Idaho, United States." *Water Resources Research, 37,* (11), 2825-2829. Washington, D.C.: American Geophysical Union. ACC: MOL.20060712.0225.

177505 Seyfried, M.S.; Flerchinger, G.N.; Murdock, M.D.; Hanson, C.L.; and Van Vactor, S. 2001. "Long-Term Soil Temperature Database, Reynolds Creek Experimental Watershed, Idaho, United States." *Water Resources Research, 37,* (11), 2843-2846. Washington, D.C.: American Geophysical Union. ACC: MOL.20060712.0228.

177515 Seyfried, M.S.; Hanson, C.L.; Murdock, M.D.; and Van Vactor, S. 2001. "Long-Term Lysimeter Database, Reynolds Creek Experimental Watershed, Idaho, United States." *Water Resources Research, 37,* (11), 2853-2856. Washington, D.C.: American Geophysical Union. ACC: MOL.20060821.0215.

177506 Seyfried, M.S.; Murdock, M.D.; Hanson, C.L.; Flerchinger, G.N.; and Van Vactor, S. 2001. "Long-Term Soil Water Content Database, Reynolds Creek Experimental Watershed, Idaho, United States." *Water Resources Research, 37,* (11), 2847-2851. Washington, D.C.: American Geophysical Union. ACC: MOL.20060712.0229.

178140 Šimùnek, J.; van Genuchten, M.Th.; and Šejna, M. 2005. *The HYDRUS-1D Software Package for Simulating the One-Dimensional Movement of Water, Heat, and Multiple Solutes in Variably-Saturated Media.* Version 3.0. Riverside, California: University of California, Department of Environmental Sciences. ACC: MOL.20060828.0051.

184696 Sinclair, W.C. 1962. *Ground Water Resources of Pine Forest Valley, Humboldt County, Nevada.* Ground-Water Resources -- Reconnaissance Series Report 4. Carson City, Nevada: State of Nevada, Department of Conservation and Natural Resources. ACC: LLR.20080117.0011.

184739 Sinclair, W.C. 1962. *Ground-Water Resources of Desert Valley, Humboldt and Pershing Counties, Nevada.* Ground-Water Resources - Reconnaissance Series Report 7. Carson City, Nevada: State of Nevada, Department of Conservation and Natural Resources. ACC: LLR.20080117.0013.

184705 Sinclair, W.C. 1962. *Ground-Water Resources of Hualapai Flat Washoe, Pershing, and Humboldt Counties, Nevada.* Ground-Water Resources--Reconnaissance Series Report 11. Carson City, Nevada: State of Nevada, Department of Conservation and Natural Resources. ACC: LLR.20080117.0015.

184712 Sinclair, W.C. 1963. *Ground-Water Appraisal of the Black Rock Desert Area Northwestern Nevada.* Ground-Water Resources -- Reconnaissance Series Report 20. Carson City, Nevada: State of Nevada, Department of Conservation and Natural Resources. ACC: LLR.20080117.0021.

184734 Sinclair, W.C. 1963. *Ground-Water Appraisal of the Pueblo Valley-Continental Lake Region, Humboldt County, Nevada.* Ground-Water Resources - Reconnaissance Series Report 22. Carson City, Nevada: State of Nevada, Department of Conservation and Natural Resources. ACC: LLR.200080117.0022.

184709 Sinclair, W.C. and Malchow, R.L. 1963. *Ground-Water Appraisal of Duck Lake Valley, Washoe County, Nevada.* Ground-Water Resources - Reconnaissance Series Report 17. Carson City, Nevada: State of Nevada, Department of Conservation and Natural Resources. ACC: LLR.20080117.0018.

184707 Sinclair, W.C. and Malchow, R.L. 1963. *Ground-Water Appraisal of the Long Valley Massacre Lake Region, Washoe County, Nevada.* Ground-Water Resources - Reconnaissance Series Report 15. Carson City, Nevada: State of Nevada, Department of Conservation and Natural Resources. ACC: LLR.20080117.0017.

150228 Slate, J.L.; Berry, M.E.; Rowley, P.D.; Fridrich, C.J.; Morgan, K.S.; Workman, J.B.; Young, O.D.; Dixon, G.L.; Williams, V.S.; McKee, E.H.; Ponce, D.A.; Hildenbrand, T.G.; Swadley, W C; Lundstrom, S.C.; Ekren, E.B.; Warren, R.G.; Cole, J.C.; Fleck, R.J.; Lanphere, M.A.; Sawyer, D.A.; Minor, S.A.; Grunwald, D.J.; Laczniak, R.J.; Menges, C.M.; Yount, J.C.; Jayko, A.S.; Mankinen, E.A.; Davidson, J.G.; Morin, R.L.; and Blakely, R.J. 2000. *Digital Geologic Map of the Nevada Test Site and Vicinity, Nye, Lincoln and Clark Counties, Nevada, and Inyo County, California, Revision 4; Digital Aeromagnetic Map of the Nevada Test Site and Vicinity, Nye, Lincoln, and Clark Counties, Nevada, and Inyo County, California; and Digital Isostatic Gravity Map of the Nevada Test Site and Vicinity, Nye, Lincoln, and Clark Counties, Nevada, and Inyo County, California.* Open-File Report 99-554—A, —B, and —C. Denver, Colorado: U.S. Geological Survey. TIC: 248049; 251985; 251981.

177354 Slaughter, C.W.; Marks, D.; Flerchinger, G.N.; Van Vactor, S.S.; and Burgess, M. 2001. "Thirty-Five Years of Research Data Collection at the Reynolds Creek Experimental Watershed, Idaho, United States." *Water Resources Research, 37,* (11), 2819–2823. Washington, D.C.: American Geophysical Union. TIC: 258491.

177358 Smith, B. and Sandwell, D. 2003. "Accuracy and Resolution of Shuttle Radar Topography Mission Data." *Geophysical Research Letters, 30,* (9), 20-1-20-4. Washington, D.C.: American Geophysical Union. TIC: 258765.

179904 Smith, R.B. 2004. "Mountain Meteorology and Regional Climates." Chapter 9 of *Atmospheric Turbulence and Mesoscale Meteorology: Scientific Research Inspired by Doug Lilly.* Fedorovich, E.; Rotunno, R.; and Stevens, B., eds. Pages 193-222. New York, New York: Cambridge University Press. TIC: 259247.

103636 Smith, S.D.; Monson, R.K.; and Anderson, J.E. 1997. *Physiological Ecology of North American Desert Plants.* New York, New York: Springer-Verlag. TIC: 242260.

177081 SNL (Sandia National Laboratories) 2006. *Data Analysis for Infiltration Modeling: Extracted Weather Station Data Used to Represent Present-Day and Potential Future Climate Conditions in the Vicinity of Yucca Mountain.* ANL-MGR-MD-000015 REV 00. Las Vegas, Nevada: Sandia National Laboratories. ACC: DOC.20070109.0002.

179545 SNL 2007. *Calibrated Unsaturated Zone Properties.* ANL-NBS-HS-000058 REV 00. Las Vegas, Nevada: Sandia National Laboratories. ACC: DOC.20070530.0013.

175177 SNL 2007. *UZ Flow Models and Submodels.* MDL-NBS-HS-000006 REV 03. Las Vegas, Nevada: Sandia National Laboratories. ACC: DOC.20070907.0001.

184077 SNL 2008. *Data Qualification Report for the Qualification of the Preliminary Output from MDL-NBS-HS-000023, REV 01.* TDR-NBS-HS-000020 REV 00. Las Vegas, Nevada: Sandia National Laboratories. ACC: DOC.20080118.0006.

184433 SNL 2008. *Multiscale Thermohydrologic Model.* ANL-EBS-MD-000049 REV 03 AD 02. Las Vegas, Nevada: Sandia National Laboratories.

183834 Stothoff, S. and Walter, G. 2007. *Long-Term-Average Infiltration at Yucca Mountain, Nevada: Million-Year Estimates.* CNWRA 2007-003. San Antonio, Texas: Center for Nuclear Waste Regulatory Analyses. ACC: LLR.20071108.0001.

177727 Thomas, J.M.; Carlton, S.M.; and Hines, L.B. 1989. *Ground-Water Hydrology and Simulated Effects of Development in Smith Creek Valley, a Hydrologically Closed Basin in Lander County, Nevada.* U.S. Geological Survey Professional Paper 1409-E. Denver, Colorado: U.S. Geological Survey. ACC: MOL.20061115.0002.

109462 Thompson, R.S.; Anderson, K.H.; and Bartlein, P.J. 1999. *Atlas of Relations Between Climatic Parameters and Distributions of Important Trees and Shrubs in North America - Introduction and Conifers.* Professional Paper 1650-A. Washington, D.C.: U.S. Geological Survey. TIC: 245909.

108774 Tyler, S.W.; Chapman, J.B.; Conrad, S.H.; Hammermeister, D.P.; Blout, D.O.; Miller, J.J.; Sully, M.J.; and Ginanni, J.M. 1996. "Soil-Water Flux in the Southern Great Basin, United States: Temporal and Spatial Variations Over the Last 120,000 Years." *Water Resources Research, 32,* (6), 1481-1499. Washington, D.C.: American Geophysical Union. TIC: 235938.

173916 USDA (U.S. Department of Agriculture) 2004. *Soil Survey of Nye County, Nevada, Southwest Part.* Two parts. Washington, D.C.: U.S. Department of Agriculture. ACC: MOL.20050614.0146.

160355 USGS (U.S. Geological Survey) 2001. *Simulation of Net Infiltration for Modern and Potential Future Climates.* ANL-NBS-HS-000032 REV 00 ICN 02. Denver, Colorado: U.S. Geological Survey. ACC: MOL.20011119.0334.

180759 Van Denburgh, A.S. and Glancy, P.A 1970. *Water-Resources Appraisal of the Columbus Salt Marsh - Soda Spring Valley Area, Mineral and Esmeralda Counties, Nevada.* Water Resources - Reconnaissance Series Report 52. Carson City, Nevada: Nevada Department of Conservation and Natural Resources. TIC: 217168.

176848 Van Denburgh, A.S. and Rush, F.E. 1974. *Water–Resources Appraisal of Railroad and Penoyer Valleys, East–Central Nevada.* Water Resources – Reconnaissance Series Report 60. Carson City, Nevada: State of Nevada, Department of Conservation and Natural Resources. TIC: 217169.

184747 Van Denburgh, A.S.; Lamke, R.D.; and Hughes, J.L. 1973. *A Brief Water-Resources Appraisal of the Truckee River Basin, Western Nevada.* Water Resources - Reconnaissance Series Report 57. Carson City, Nevada: State of Nevada Department of Conservation and Natural Resources. ACC: LLR.20080117.0047.

103022 Walker, G.E. and Eakin, T.E. 1963. *Geology and Ground Water of Amargosa Desert, Nevada-California.* Ground-Water Resources – Reconnaissance Series Report 14. Carson City, Nevada: State of Nevada, Department of Conservation and Natural Resources. TIC: 208665.

178108 Walvoord, M.A.; Plummer, M.A.; Phillips, F.M.; and Wolfsberg, A.V. 2002. "Deep Arid System Hydrodynamics 1. Equilibrium States and Response Times in Thick Desert Vadose Zones." *Water Resources Research, 38,* (12), 44/1-44/15. Washington, D.C.: American Geophysical Union. TIC: 255212.

160442 Whelan, J.F.; Paces, J.B.; and Peterman, Z.E. 2002. "Physical and Stable-Isotope Evidence for Formation of Secondary Calcite and Silica in the Unsaturated Zone, Yucca Mountain, Nevada." *Applied Geochemistry, 17,* (6), 735-750. New York, New York: Elsevier. TIC: 253462.

177113 Wight, J.R. and Hanson, C.L. 1990. "Crop Coefficients for Rangeland." *Journal of Range Management, 43,* (6), 482-485. Denver, Colorado: Society for Range Management. TIC: 258409.

177104 Wight, J.R.; Hanson, C.L.; and Cooley, K.R. 1986. "Modeling Evapotranspiration from Sagebrush-Grass Rangeland." *Journal of Range Management, 39,* (1), 81-85. Denver, Colorado: Society for Range Management. TIC: 258408.

177624 Wills, C.A. and Ostler, W.K. 2001. *Ecology of the Nevada Test Site: An Annotated Bibliography.* DOE/NV/11718–594. Las Vegas, Nevada: U.S. Department of Energy, National Nuclear Security Administration. ACC: MOL.20060712.0222.

172585 Wilson, J.L. and Guan, H. 2004. "Mountain-Block Hydrology and Mountain-Front Recharge." In *Groundwater Recharge in a Desert Environment: The Southwestern United States,* Hogan, J.F.; Phillips, F.M.; and Scanlon, B.R., eds, *Water Science and Application 9.* Pages 113-137. Washington, D.C.: American Geophysical Union. TIC: 256760.

184744 Worts, G.F., Jr. and Malmberg, G.T. 1966. *Hydrologic Appraisal of Eagle Valley, Ormsby County, Nevada.* Water Resources - Reconnaissance Series Report 39. Carson City, Nevada: State of Nevada, Department of Conservation and Natural Resources. ACC: LLR.20080117.0035.

165987 WRCC (Western Regional Climate Center) 2002. *Western U.S. Historical Summaries by State Arizona, California, Idaho, Nevada, New Mexico, Oregon, Utah, and Washington.* Reno, Nevada: Western Regional Climate Center, Desert Research Institute. TIC: 253357.

162307 WRCC (Western Regional Climate Center) 2003. "Nogales 6N, Arizona, NCDC 1971-2000 Monthly Normals." Reno, Nevada: Desert Research Institute, Western Regional Climate Center. Accessed March 4, 2003. TIC: 253915. http://www.wrcc.dri.edu/cgi-bin/cliNORMNCDC2000.pl?aznoga.

9.2[a]. CODES, STANDARDS, REGULATIONS, AND PROCEDURES

176544 10 CFR 63. 2006. Energy: Disposal of High-Level Radioactive Wastes in a Geologic Repository at Yucca Mountain, Nevada. Internet Accessible.

178394 70 FR 53313. Implementation of a Dose Standard After 10,000 Years. Internet Accessible.

SCI-PRO-001, Rev. 5, ICN 0. *Qualification of Unqualified Data*. Washington, DC: U.S. Department of Energy, Office of Civilian Radioactive Waste Management. ACC: DOC.20071106.0020.

SCI-PRO-006, Rev. 7, ICN 0. *Models*. Washington, DC: U.S. Department of Energy, Office of Civilian Radioactive Waste Management. ACC: DOC.20080118.0004.

9.3[a]. SOURCE DATA, LISTED BY DATA TRACKING NUMBER

151139 GS000308315121.003. Meteorological Stations Selected to Represent Future Climate States at Yucca Mountain, Nevada. Submittal date: 03/14/2000.

176317 GS011208312212.004. SN-USGS-SCI-113 V1: Empirical Calculation of Soil Thickness Based on Field Measurements. Submittal date: 01/24/2002.

107375 GS960908312121.001. Surface-Water Discharge Data for the Yucca Mountain Area, Southern Nevada and Southern California, 1995 Water Year. Submittal date: 10/10/1996.

146872 GS960908312211.004. Heat Dissipation Probe Data: Bleach Bone Ridge 3/95 - 11/95. Submittal date: 09/19/1996.

107128 GS971208314221.003. Revised Bedrock Geologic Map of the Central Block Area, Yucca Mountain, Nevada. Submittal date: 12/30/1997.

174491 LB0208HYDSTRAT.001. 2002 UZ Model Grid Components. Submittal date: 08/26/2002.

146848 MO0003COV00095.000. Coverage: Scotbons. Submittal date: 03/01/2000.

153777 MO0012MWDGFM02.002. Geologic Framework Model (GFM2000). Submittal date: 12/18/2000.

176097 MO0503SEPMMD03.001. Meteorological Monitoring Data for 2003. Submittal date: 03/03/2005.

177249 MO0512COV05112.000. Special Infiltration Project - Survey of Field Observation Locations. Submittal date: 12/12/2005.

177236 MO0601GSCSPINF.000. Special Infiltration Project Position of Field Observation Locations of Ecological Study Plot Corners and Streamflow Gauges. Submittal date: 01/30/2006.

184298 MO0601SEPNEULG.002. Neutron Logging and Volumetric Water Content Data from Boreholes from May 3, 1989 to September 30, 1995. Submittal date: 01/23/2006.

176585 MO0603GSCGEOMP.000. Digital Geologic Map of Nevada Test Site and Vicinity, Nye, Lincoln, and Clark Counties, Nevada, and Inyo County, California. Submittal date: 03/09/2006.

177121 MO0603SPAGRIDD.003. Gridded Infiltration Model Input File Showing Infiltration Hydrogeologic Units. Submittal date: 03/06/2006.

177237 MO0605SEPHOURL.000. Hourly Precipitation Data for Four NOAA Meteorological Stations for the Years 1948 through 2005. Submittal date: 05/17/2006.

178663 MO0605SEPSGP05.000. Storage Gauge Precipitation 2005. Submittal date: 05/19/2006.

178311 MO0607SEPMMD04.001. Meteorological Monitoring Data for 2004. Submittal date: 07/18/2006.

178082 MO0608SPASDFIM.006. Soil Depth Input File for Use in Infiltration Modeling. Submittal date: 8/31/2006.

181287 MO0705ASTRIMNT.000. Aster Image Mosaic of the Greater Nevada Test Site Area. Submittal date: 05/30/2007.

181613 MO0706SPAFEPLA.001. FY 2007 LA FEP List and Screening. Submittal date: 06/20/2007.

182647 MO0708METMND05.001. Meteorological Monitoring Data for 2005. Submittal date: 08/22/2007.

177247 MO9901ESPYMNYE.000. Ecological Study Plots at Yucca Mountain, Nye County, Nevada. Submittal date: 01/04/1999.

109059 MO9906GPS98410.000. Yucca Mountain Project (YMP) Borehole Locations. Submittal date: 06/23/1999.

177239 SN0601ALANDSAT.001. Landsat Imagery of Yucca Mountain from January 1998 to August 2002. Submittal date: 02/07/2006.

177240 SN0601DOQQYM98.001. Digital Ortho Quarter Quad (DOQQ), Yucca Mountain 06/01/1998 - 08/18/1998. Submittal date: 01/24/2006.

176122 SN0601PRECPTMP.002. Developed Precipitation Data at NTS Sites from 1959-2004, and Precipitation and Temperature Data at Amargosa Farms-Garey from 1965-2005. Submittal date: 01/16/2006.

177242 SN0601SRTMDTED.001. Shuttle Radar Topography Mission (SRTM) Digital Terrain Elevation Data (DTED) of Yucca Mountain, February 2000. Submittal date: 01/23/2006.

179875 SN0608T0502206.020. Climate Data, Geospatial Information, and Soil Moisture and Property Data for Reynolds Creek Experimental Watershed (RCEW), Idaho. Submittal date: 08/21/2006.

177912 SN0608WEATHER1.005. Temperature, Precipitation, Wind Speed, Relative Humidity, Dew Point Temperatures, and Barometric Pressure Data Collected from 1993-2004 Measured at Yucca Mountain Weather Stations 1,2,3,6, and 9. Submittal date: 08/23/2006.

184297 SN0712ALANDSAT.002. Landsat Imagery of YUCCA Mountain from January 1998 to August 2002. Submittal date: 12/11/2007.

9.4[a]. DEVELOPED DATA, LISTED BY DATA TRACKING NUMBER

SN0606T0502206.011. Geospatial Inputs for Net Infiltration Model of Yucca Mountain. Submittal date: 05/31/2006.

SN0607T0502206.016. Analysis of Soil Water Storage in Nevada Test Site (NTS) and Reynolds Creek Experimental Watershed (RCEW) Lysimeters. Submittal date: 08/24/2006.

SN0608CWATSHED.001. Calibration Watersheds at Yucca Mountain Based on Pour Point Stream Gages. Submittal date: 08/15/2006.

SN0608NDVILSTM.001. Normalized Difference Vegetation Index (NDVI) Derived from Calibrated and Geocorrected LANDSAT TM Data at Yucca Mountain, 1997–2002. Submittal date: 08/15/2006.

SN0608T0502206.019. Temperature Model Fitting Parameters for Present-Day and Future Climate Proxy Sites. Submittal date: 08/16/2006.

SN0609T0502206.021. Alternative Infiltration Model Inputs. Submittal date: 09/18/2006.

SN0609T0502206.022. Alternative Infiltration Modeling Results. Submittal date: 09/18/2006.

SN0609T0502206.023. Precipitation Parameters Calculated using Fourier Analyses for Modern Interglacial and Future Climates. Submittal date: 09/07/2006.

SN0610T0502206.031. Precipitation Duration Functions for the Present-Day, Monsoon, and Glacial Transition Climates for Infiltration Modeling at Yucca Mountain, NV. Submittal date: 10/09/2006.

SN0612T0502206.039. Estimation of Uncertainty on Upscaled Uniform Value for Soil Depth Class 4. Submittal date: 12/06/2006.

SN0701SPALAYER.002. Spatial Data Layers at Yucca Mountain. Submittal date: 01/16/2007.

SN0701T0502206.034. Present-Day Net Infiltration Results, Rev 1. Submittal date: 01/11/2007.

SN0701T0502206.035. Glacial Transition Net Infiltration Results, Rev 1. Submittal date: 01/11/2007.

SN0701T0502206.036. Monsoon Net Infiltration Results, Rev 1. Submittal date: 01/11/2007.

SN0701T0502206.037. MASSIF Calculation of Net Infiltration at Yucca Mountain, Rev 2. Submittal date: 12/10/2007.

SN0701T0502206.045. Comparison of the Calculated Precipitation Record with Site Data. Submittal date: 01/23/2007.

SN0801T0502206.049. Recharge Estimates Used to Validate the Massif Model of Net Infiltration at Yucca Mountain. Submittal date: 01/25/2008.

SN0708T0502206.048. YMP and Center for Nuclear Waste Regulatory Analyses (CNWRA) Soil Depth Class 4 Statistics. Submittal date: 08/29/2007.

SN0711FTPRNUZB.003. Unsaturated Zone (UZ) Boundary and Repository Footprint. Submittal date: 11/05/2007.

9.5[a]. SOFTWARE CODES

139422 Software Code: INFIL V. 2.0. 2001. PC, Windows NT 4.0. STN: 10307-2.0-00.

147608 Software Code: Infil V. A_2.a1. 2001. DEC Alpha, VMS AXP V7.2-1. STN: 10253-A_2.a1-00.

INTENTIONALLY LEFT BLANK

APPENDIX A[a]
OUTSIDE SOURCES QUALIFIED FOR INTENDED USE

Sections A1[a], A2[a], and A3[a] have been revised to address the condition adverse to quality documented in CR 10788 related to inadequate documentation of qualification of external data sources. These three sections have been revised such that they are in accordance with SCI-PRO-006, Section 6.2.1.K. The primary procedure used to qualify the external data sources in these three sections is SCI-PRO-001. The primary method chosen to qualify the data is Method 5, Technical Assessment. This method was selected because it was determined that it is suitable to raise the confidence of the data to a level appropriate for the intended use. In most cases, the data collection procedures were unavailable for review or the proof of proper data acquisition was unavailable for review. In limited cases, Method 2, corroborating data, was also applied.

A1[a]. QUALIFICATION OF VEGETATION PARAMETERS FOR USE AS DIRECT INPUT

This section documents the demonstration that data for vegetation parameters are suitable for their intended use as inputs for calculating net infiltration at Yucca Mountain. Appropriate data sources were identified through literature searches for each of the vegetation parameter inputs. Because these data were not acquired or developed for the Yucca Mountain Project (YMP), the documentation of the qualification for intended use in this report is performed in accordance with SCI-PRO-006, Section 6.2.1.K. The primary procedure used to qualify the data listed below is SCI-PRO-001. The following vegetation parameter inputs are addressed:

- Plant height (Sections A1.1 to A1.3)
- Timing of phenological events (Section Al.1) and physiological activity (Section A1.2)
- Stomatal conductance (Section A1.4)
- Rooting depth (Sections A1.5 and A1.6).

Each of these parameters is described in greater detail in the associated subsequent sections. The primary method chosen to qualify the data is Method 5, Technical Assessment. This method was selected because it was determined that it is suitable to raise the confidence of the data to a level appropriate for the intended use. In most cases, the data collection procedures were unavailable for review or the proof of proper data acquisition was unavailable for review. In limited cases, Method 2, corroborating data, was also applied. This method was used when corroborating data were available and the inferences drawn to corroborate the unqualified data were clearly identified, justified, and documented. Data qualification attributes (SCI-PRO-001, Attachment 4) considered in the qualification process are: (1) qualification of personnel or organizations generating the data (also called reliability of data sources), (3) the extent to which the data demonstrate the properties of interest, and (10) extent and quality of corroborating data (used only in the cases where such data are available). The data qualification subject matter expert was Dr. Kaylie Rasmuson, a senior scientist with Bechtel SAIC Company, LLC (BSC) Environmental Compliance Department. She has a B.S. in ecology and a Ph.D. in biology with emphasis on plant ecophysiology from Idaho State University. Dr. Rasmuson has been involved in plant ecological research for over 15 years. The data evaluation criteria for qualification of the data for intended use in this document is affirmative documentation of the data qualification attributes, primarily attributes (1) and (3). No other organizations or subject matter experts were involved in the qualification process.

A1.1[a]. Plant Height and Timing of Phenological Events

No change.

A1.2[a]. Timing of Physiological Activity for Mojave Desert Vegetation

No change.

A1.3[a]. Plant Height for the Glacial Transition Climate

No change.

A1.4[a]. Stomatal Conductance

No change.

A1.5[a]. Rooting Depths for Present-Day and Monsoon Climates

No change.

A1.6[a]. Rooting Depths for the Glacial Transition Climate

No change.

A2[a]. QUALIFICATION OF EVAPOTRANSPIRATION DATA AND CALCULATION METHODS FOR USE AS DIRECT INPUT

This section documents the demonstration that data and calculation methods are suitable for their intended use as inputs for calculating evapotranspiration at Yucca Mountain. Because these data were not acquired or developed for the YMP, the documentation of the qualification for intended use in this report is performed in accordance with SCI-PRO-006, Section 6.2.1.K. The primary procedure used to qualify the data listed below is SCI-PRO-001. The following inputs are addressed:

- Surface Albedo (Section A2.1)
- Solar Radiation on Inclined Surfaces (Section A2.2)
- Evaporation Layer Depth (Section A2.3)
- Solar Constant (Section A2.4)
- Dew point temperature offset (Section A2.5).

Each of these parameters is described in greater detail in the associated subsequent sections. The primary method chosen to qualify the data is Method 5, Technical Assessment. This method was selected because it was determined that it is suitable to raise the confidence of the data to a level appropriate for the intended use. In most cases, the data collection procedures were unavailable for review or the proof of proper data acquisition was unavailable for review. Data qualification attributes (SCI-PRO-001, Attachment 4) considered in the qualification process are: (1) qualification of personnel or organizations generating the data (also called reliability of data sources), and (3) the extent to which the data demonstrate the properties of interest. The data

qualification subject matter expert was Dr. Richard Allen, a research professor at the University of Idaho. Dr. Allen is the first author of the FAO Irrigation and Drainage Paper No. 56 (Allen et al. 1998 [DIRS 157311]), a method for calculating evapotranspiration that is the basis for the MASSIF model. Dr. Allen has been involved in research related to evapotranspiration and crop water use for over 25 years, and he is considered to be a leading world expert in evapotranspiration. The data evaluation criteria for qualification of the data for intended use in this document is affirmative documentation of the data qualification attributes (1) and (3). No other organizations or subject matter experts were involved in the qualification process.

A2.1[a]. Surface Albedo Values

No change.

A2.2[a]. Solar Radiation on Inclined Surfaces

No change.

A2.3[a]. Evaporation Layer Depth

No change.

A2.4[a]. Solar Constant

No change.

A2.5[a]. Dew Point Temperature Offset

No change.

A3[a]. QUALIFICATION OF SUBLIMATION COEFFICIENT FOR USE AS DIRECT INPUT

The following information was used to evaluate whether the measurements of fraction of snowpack lost to sublimation reported by Hood et al**.** (1999 [DIRS 177996]) were suitable for use in development of the sublimation parameter (SUB). This source is used as direct input in Section 6.5.1.7[a]. Because these data were not acquired or developed for the Yucca Mountain Project (YMP), the documentation of the qualification for intended use in this report is performed in accordance with SCI-PRO-006, Section 6.2.1.K. The primary procedure used to qualify the data is SCI-PRO-001.

The fraction of snowpack lost to sublimation is used to represent the portion of precipitation that falls as snow that is returned to the atmosphere before it melts and becomes available as potential infiltration. The primary method chosen to qualify the data is Method 5, Technical Assessment. This method was selected because it was determined that it is suitable to raise the confidence of the data to a level appropriate for the intended use. The data collection procedures were unavailable for review or the proof of proper data acquisition was unavailable for review. Data qualification attributes (SCI-PRO-001, Attachment 4) considered in the qualification process are: (1) qualification of personnel or organizations generating the data (also called reliability of data

sources) and (3) the extent to which the data demonstrate the properties of interest. The data qualification subject matter expert was Dr. Daniel Levitt, a Technical Staff Member in the Earth and Environmental Sciences Division at Los Alamos National Laboratory. He has a B.S. in Geology from Colorado College, and M.S. and Ph.D. degrees in Soil Science with emphasis on evapotranspiration from the University of Arizona. Dr. Levitt has been involved in vadose zone applied research for over 20 years. The data evaluation criteria for qualification of the data for intended use in this document is affirmative documentation of the data qualification attributes (1) and (3). No other organizations were involved in the qualification process.

Extent to Which the Data Demonstrate Properties of Interest—Hood et al. (1999 [DIRS 177996]) report measured sublimation over a nine-month period and is therefore more reliable than previous studies which were based on data only from the snowmelt season.

Reliability of Data Source—The median value of 10% snow sublimation used in the infiltration model originates from studies cited by Hood et al. (1999 [DIRS 177996]). These studies include the author's own study in which they found snow sublimation to be about 15% of the total seasonal snow accumulation at Niwot Ridge in the Colorado Front Range. They also cite seasonal sublimation estimates of 18% and 20% for Sierra Nevada, California, reported in two other studies. Seasonal snow sublimation is extremely difficult to measure, and there is large inherent uncertainty in this parameter. Hood et al. (1999 [DIRS 177996]) can be considered to be experts in the field given their organizations and publication records. Their organizations include the Institute of Arctic and Alpine Research (INSTAAR) at University of Colorado, Boulder, and the National Operational Hydrologic Remote Sensing Center, which provides comprehensive snow observations, analyses, data sets and map products for the Nation. Eran Hood, Mark Williams, and Don Cline have all published numerous articles related to snow. Therefore, the information from this journal article is considered to be reliable and qualified for the intended use.

A4[a]. ESTABLISHED FACT INPUTS

No change.

APPENDIX B[a]
GEOSPATIAL DATABASE

B1[a]. INTRODUCTION

No change.

B2[a]. GEOGRAPHIC INFORMATION SYSTEM WATERSHED CHARACTERIZATION

The MASSIF infiltration model addresses the area that drains Yucca Mountain above the UZ flow model area. Eleven separate drainages (or watersheds) were identified; three larger watersheds drain the east face of the ridge and eight smaller watersheds drain the west face. Each watershed formed a component of the MASSIF model.

The watersheds were delimited using elevation and slope to define surface water flow direction to a single outlet (pour point). Defining the eleven watersheds also delineated the overall infiltration model boundary within the larger project boundary. The larger rectangular project boundary encompassed 226.34 km^2. The mix of eleven larger (up to 41.16 km^2) and smaller (down to 0.11 km^2) watersheds made up the individual model components that were used to calculate net infiltration. The infiltration model boundary, comprised of the combination of these eleven watersheds, encompassed 125.18 km^2. Figure B-1[a] shows the relationship between these three sets of boundaries. The following discussion details the tools and source data used to create these watershed delineations.

B2.1[a]. Software and Data Considerations

In a geographic information system (GIS), spatial attributes are stored in conjunction with descriptive attributes allowing tabular data to be displayed in reference to their position on the earth. Data can consist of points, lines, and polygon shapes with multiple attributes connected to each of these features, allowing a layering of data values. With the layered features, spatial relationships can be measured and complex models can be constructed. The capacity to combine separate data layers and run a model to extract additional data layers from existing layers is extremely important for the infiltration model database; therefore, a GIS is the perfect tool for the tasks required.

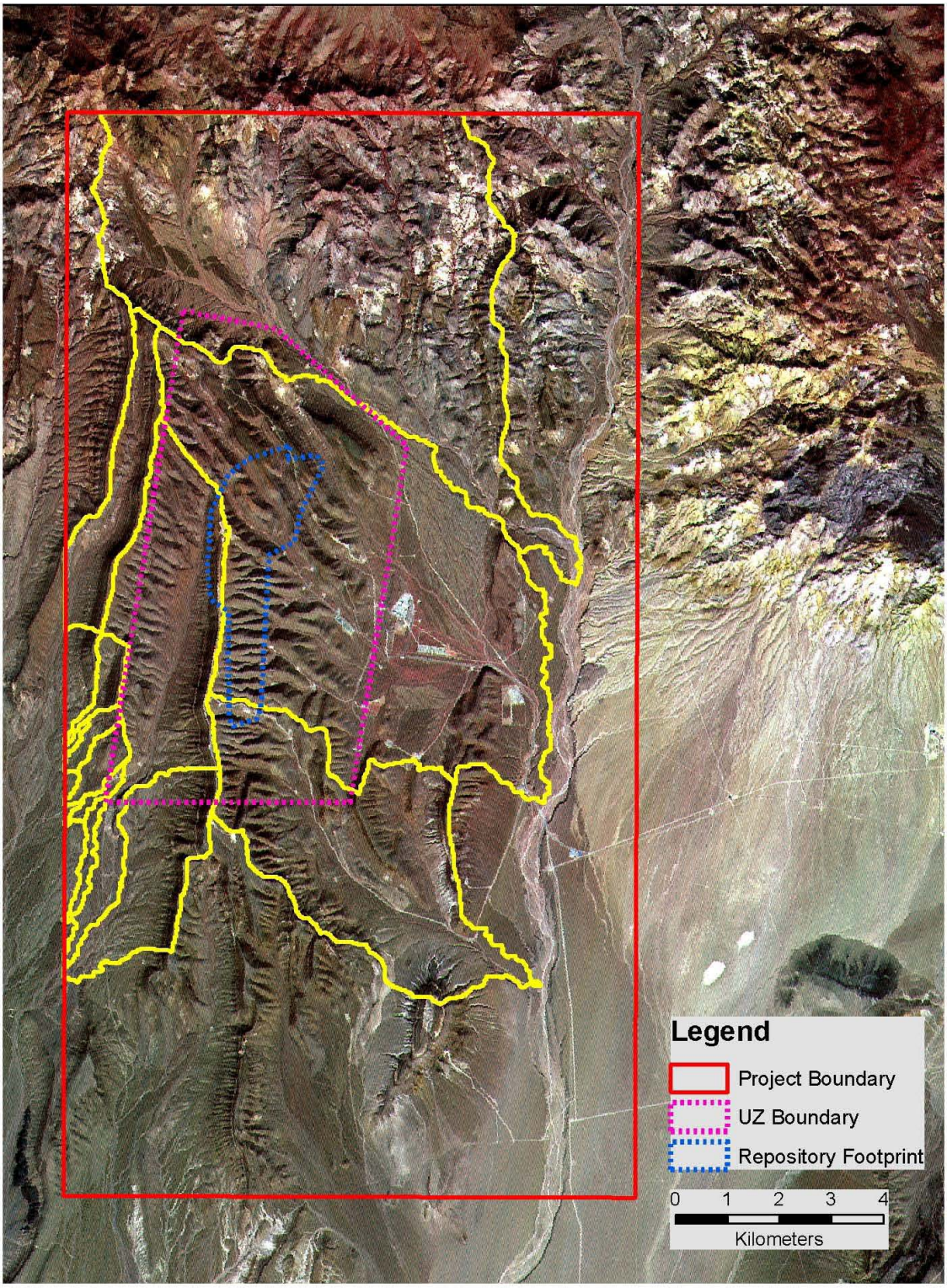

Sources: Output DTNs: Project boundary from SN0608NDVIAUXD.001; UZ and Repository boundaries from SN0711FTPRNUZB.003; Watershed boundaries from SN0701SPALAYER.002; Satellite image from DTN: MO0705ASTRIMNT.000 [DIRS 181287] is shown for illustrative purposes only.

NOTE: Yellow lines indicate watershed boundaries. Repository footprint shown for illustrative purposes only.

Figure B-1[a]. Infiltration Modeling Boundaries

The GIS used for these tasks is ArcGIS (ArcGIS Desktop Version 9.1 STN: 11205-9.1-00 [DIRS 176015]), from Environmental Systems Research Institute, the market leader in off-the-shelf GIS software. In addition, the spatial analyst extension increases the flexibility of ArcGIS to work with raster-based data. Using the model builder functionality of the ArcGIS ArcToolbox, a fully automated routine was established where base data and parameters can be loaded into the model to then have a series of watershed characterization tasks applied iteratively to derive a final watershed catchment grid. In addition, nearly all the data processing functions required to prepare the spatial inputs for MASSIF were conducted within the GIS database. The spatial database format also allowed data queries to be conducted prior to running MASSIF.

The most accurate topographic data available were chosen from a field of three data sets. Spatial data supply the measures of elevation, azimuth, and slope that play important roles for accessing parameters, including vegetation cover, runoff, and evapotranspiration (ET) that are active in the calculation of net infiltration in each model grid. Therefore, spatial accuracy is crucial for model accuracy.

The three candidate data sets for topographic data were U.S. Geological Service (USGS) digital elevation model (DEM), the USGS National Elevation Dataset (NED) and the Shuttle Radar Topography Mission (SRTM) data. All elevation data sets are created through a sampling technique using different methods and resolution. A set of single elevation values can never truly represent all the variability found in all represented grid cells no matter the data resolution be it 10 m or 30 m. With this knowledge, there is an understanding that the data may need some modification to effectively model certain aspects of the landscape.

DEM, and as a result NED, data is created from using existing contour maps and augmented with aerial photography. Much of this data consists of passively collected data, so even though the resolution may be quite high (up to 10-m square) actual measurements used to create the data are limited and most data values were created through interpolation.

USGS DEM data often are used to supply the topological information necessary to run basic watershed characterization models. A DEM is constructed as a 10-m or 30-m grid where the centroid of each grid cell is assigned an elevation based on its corresponding location on a topographic map. Because they are digitized from maps that represent earlier interpretation of topography, these data incorporate inherent flaws, especially in areas that experience significant elevation change over a short distance.

NED was compiled by the USGS to assemble the best available topographic data into a continuous elevation model for the entire country. This dataset typically employs the USGS 10-m DEM data, when available, that is nine times more detailed than the coarser 30-m data. For the YMP, the NED metadata indicated that 10-m data were available and incorporated into the dataset; however, these data still contain inherent limitations of accuracy because they were formulated by extrapolating elevation data from topographic maps.

SRTM is a more recent dataset that was collected through an interferometric synthetic-aperture radar system carried aboard a U.S. space shuttle mission during February 2000. These data are highly accurate because the active sensor collected a data value for each 30-m target, meaning no extrapolation was necessary. The data will still be limited by having a single value in a 30-m^2

grid cell represent all the possible variation in that cell, but this is the case with all three of the data sets spacing. One drawback with SRTM datasets are occasional problematic gaps due to radar shadow at low angles of incidence or signal interference from numerous vertical surfaces (i.e., signal bounces between tall buildings or forest tree trunks). These influences are not problematic for the remote treeless Yucca Mountain region, and the dataset showed none of these characteristics.

The availability of three adequate data sets raised the issue of which would best serve the model's needs. The 30-m DEM was eliminated because, with its 10-m resolution, the NED superseded the coarser DEM; however, the question remained whether to use NED or SRTM data. A raster subtraction method was employed to observe the differences between these datasets. The resulting grid showed a misalignment between the two data sets. Smith and Sandwell (2003 [DIRS 177358]) faced this question on a project in the Amazon and devised a selection method that compared SRTM, NED, and high-resolution aerial laser datasets. Their results showed the NED possessed an 11.87-m longitudinal and 10.58-m latitudinal shift versus the spatially accurate, high-resolution laser imagery. The laser data were used as the benchmark because a Laser Imagining Detection and Range (LIDAR) system is an active sensor, typically flown from an aircraft that has very fine resolution and can easily incorporate ground control points for accuracy. A comparable shift was not detected with the SRTM. On the basis of the Smith and Sandwell (2003 [DIRS 177358]) results, SRTM data were selected as the superior choice for the infiltration model. In addition, the SRTM data has been subjected an independent assessment of accuracy that is detailed below (Rodriguez et al. 2005 [DIRS 177738]). A similar investigation for the NED data set is planned, but has not been completed and users have to compile the errors present in each contributing DEM to access overall accuracy.

The SRTM data were obtained from the USGS Earth Resources Observation and Science Data Center (DTN: SN0601SRTMDTED.001 [DIRS 177242]).

Assessment of SRTM Accuracy

The NASA Shuttle Radar Topography Mission (SRTM) collected interferometric radar data that was used to generate a near global topography data product. This data underwent a ground-truth analysis to provide a detail measure of the different components of the error, their magnitudes, and spatial structure (Rodriguez et al. 2005 [DIRS 177738]).

The data was collected to meet the following performance requirements:

1. The linear vertical absolute height error shall be less than 16 m for 90% of the data
2. The linear vertical relative height error shall be less than 10 m for 90% of the data
3. The circular absolute geolocation error shall be less than 20 m for 90% of the data
4. The circular relative geolocation error shall be less than 15 m for 90% of the data.

The table shown below summarizes the SRTM performance observed by comparison against the available ground-truth data. The displayed measurements represent 90% errors in meters. It has been modified here to display just the North America results.

	N. America – Observed	Required
Absolute Geolocation Error	12.6	<16
Absolute Height Error	9.0	<10
Relative Height Error	7.0	<15

The study's authors found, "the analysis had shown that the SRTM error could be divided into very long wavelength (continental scale or larger) errors and short wavelength random errors. The ground-truth data were not appropriate for validating relative geolocation errors. It is expected that the main sources of geolocation errors are also long wavelength, so that the relative geolocation error will in general be smaller than the absolute geolocation error, since common errors will cancel. The absolute geolocation performance is better than that required for the relative geolocation, which provides indirect evidence that the relative geolocation requirement was also met" (Rodriguez et al. 2005 [DIRS 177738], page 9).

Smith and Sandwell (2003 [DIRS 177358]) further showed the small error involved in the geolocation measurements in the SRTM data. In all, the error falls within the breadth of a single model pixel. As to the height error, for this infiltration model a small error in actual measured height could potentially interfere in the delineation of a watershed by creating a pixel surrounded with higher elevation values, creating a 'sink' with no access for flowing water to exit the cell. A GIS step of filling such sinks and thus removing the error impact is discussed in Section B2.2[a], Processing the Elevation Data.

B2.2[a]. Processing the Elevation Data

The raw form of the SRTM data required processing for use in the spatial database, as the SRTM file format and map coordinate projection do not correspond to those needed for the infiltration model. Once format and projection were revised, the elevation data could then serve as the base data layer from which multiple derivative data layers could be created. These additional layers provided information, such as slope direction and steepness that is required by the MASSIF infiltration model.

The raw form of the SRTM data layer was processed using Research Systems, Inc. (RSI) Environment for Visualizing Images (ENVI; ENVI + IDL, Version 4.2: STN: 11204-4.2-00) image processing software. ENVI offers more options in choosing how to process raster data than ArcGIS software. All the data processing represented in Sections B2.2[a] and B2.3[a] are archived in 'Drainage Delineation at Yucca Mountain' (Output DTN: SN0608DRAINDYM.001). The SRTM data were divided as a subset within the project boundary, set to 30-m pixels and reprojected to UTM NAD 83 Zone 11. This conflicted with the MASSIF model requirement of UTM NAD 27 Zone 11 but would be reprojected in Section B-4[a], *Assembling the Spatial Database*, after concurrent image processing tasks detailed in Appendix E were completed. With the data resized and reprojected, the elevation data were saved as an ESRI grid file ready for watershed delineation. Figure B-2[a] highlights the elevation range from 964 m to 1,964 m across the YMP area.

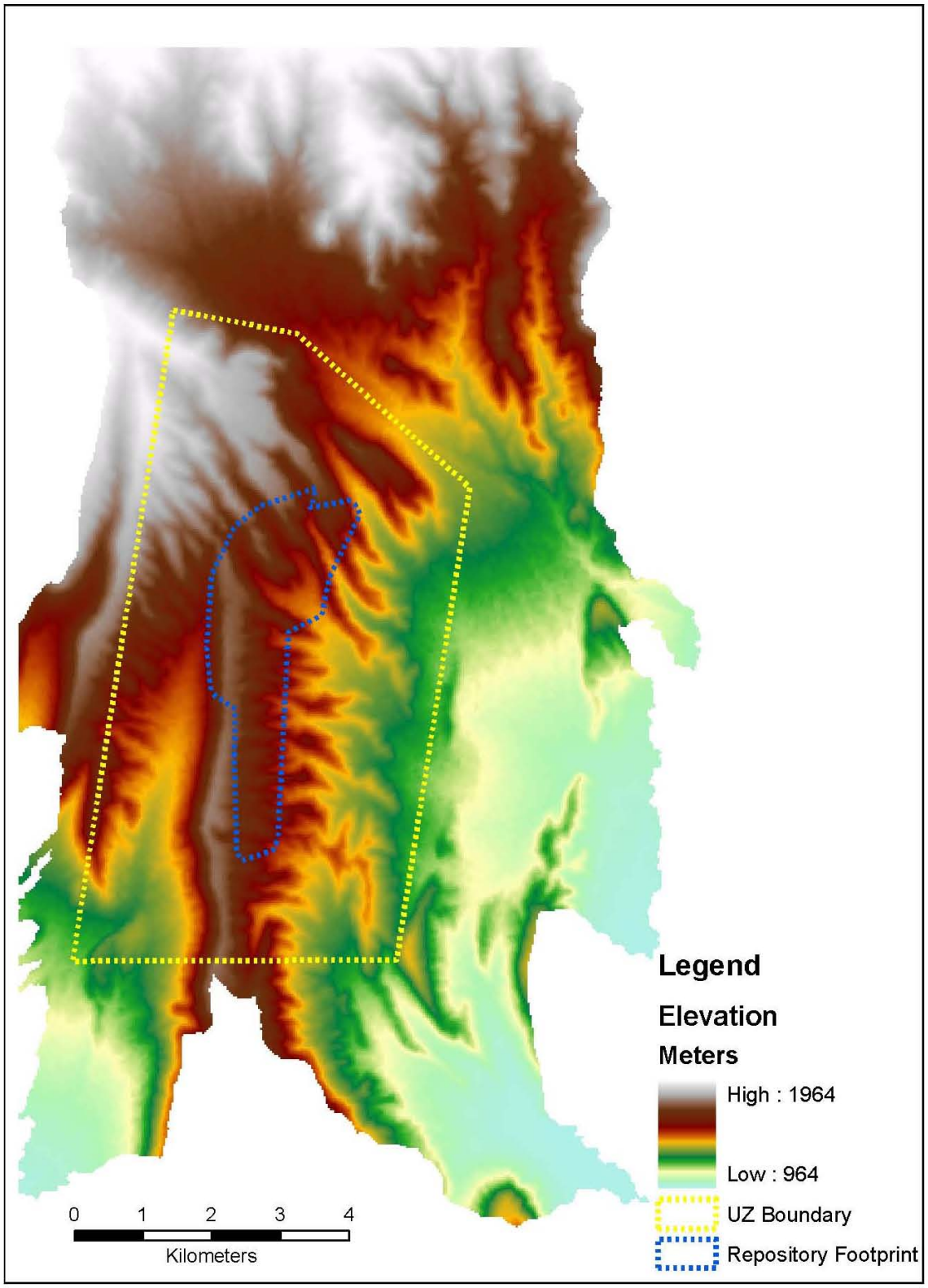

Source: Output DTNs: SN0701SPALAYER.002 and SN0711FTPRNUZB.003.

NOTE: Repository footprint shown for illustrative purposes only.

Figure B-2[a]. Elevation across Project Area

A three-stage watershed delineation process was required to generate the fewest number of watersheds that would cover the UZ flow model area. Each stage set a different water flow accumulation value (15,000, 1,000, and 200) which controlled the size of the resulting model watersheds. The MASSIF model runs each watershed separately, so a fewer number of drainages results in fewer modeling steps. Moreover, all watersheds must drain to single points on the edge of the YMP area, otherwise intermediate runoff values would need to be passed between drainages during the computation. Therefore, the size of the drainages was dictated by two factors: the topography of the region and the placement of the YMP boundary. The surface area of each watershed varied widely, a result of the three nearly identical delineation stages needed to generate the eleven drainage basins that cover Yucca Mountain: three large, three moderate, and five small basins. During each stage, a specific threshold variable was set that would determine the size of the resulting drainages. Thus each stage was responsible for generating either the large, medium, or small drainage basins. Variable basin sizes were necessary because the MASSIF model needed to trace potential infiltration from all locations directly over the repository footprint down the mountain slopes to each basin's pour point (the bottom-most part of the basin). The further the drainage travels, the greater is the size of the watershed; i.e., the more distant a pour point is from the headwaters, more space is provided for numerous smaller drainages to combine together and form larger, wider basin delineations. The YMP boundary, as defined, allowed the less steep eastern slopes to be followed out to distant pour points resulting in three large watersheds, but the steeper western basins were truncated by the close proximity of the YMP boundary. This limited the distance the drainages traveled before a pour point was assigned. Thus several small- and medium-sized watersheds were generated, as opposed to a few larger units had the YMP boundary allowed the drainages to travel further downslope. The results would be the same no matter how many watersheds were defined, as long as each grid unit within the UZ flow model area was assigned to a watershed within MASSIF.

The required size of the watersheds in each stage also limited how much of the UZ flow model area was covered. The first stage created a few large watersheds but did not cover areas where only smaller drainages could fit. Stage two created many more watersheds, but only three added additional coverage in areas previously missed in stage one. Stage three created many, very small drainages, but only five were required to fill the remaining coverage gap over the UZ flow model area. The final step was the process of fitting the eleven watersheds from the three-stage delineation process back together to create a single file representing the MASSIF model project area. Below are the details that completed this process.

The full Terrain Processing toolbox that ArcGIS utilized was a series of nine separate computations. The accompanying schematic, recreated (for legibility) from a screen-captured image while using the 'Full Terrain Processing' ArcToolbox, graphically displays the steps detailed here (Figure B-3[a]). The figure shows the GIS tasks used and output files created during watershed delineation. All the tasks contained in the Full Terrain Processing toolbox are available individually within the ArcGIS Spatial Analyst.

The *fill* function was the first process applied to the SRTM data. *Fill* located low points or 'sinks' in the data set where all the surrounding pixels were of higher values. These sinks were accurate elevation values at the center of a data collection grid. However, elevation variation within a specific 30-m grid cell might be high enough that the elevation at the center might not

represent an elevation suitable to allow a small potential drainage to pass through the grid cell from an upstream grid cell or into a downstream cell. These sinks are probably artifacts of the sampling technique used to create the elevation dataset, where 900 potential $1m^2$ elevation values are represented by a single value. Thus, these sinks are a consequence of simplifying the YMP area elevation to a specific set of grid-cell elevations, which neglect smaller scale features. There is really no geomorphic reason to expect significant sinks in the model domain because spillover from these sinks during heavy precipitation events would lead to erosion and the elimination of the sinks over time. Such features are more characteristic of karst terrain. If a pixel was identified as a sink, the *fill* function raised the elevation value in the pixel until a surrounding pixel is identified as having an equal or lower value, thus capable of accepting any potential accumulated surface flow that would have collected within the sink with no identified outlet cell in which to flow. The output 'filled SRTM' grid mirrored the original SRTM data with only small adjustments made to certain 'sink' pixels. Simple spatial subtraction between these two grids showed that most of the sinks occurred along drainage bottoms. Table B-1[a] shows how many pixels' elevation was modified by the *Fill* function over the YMP area, within the smaller delineated watersheds model area, and over the repository footprint, stressing just how slightly (1.06 %, 0.44%, and 0.11%) this vital step affected the data. *Fill* is a required process to convert the current elevation dataset into a usable form for hydrology modeling within ArcGIS, because an uninterrupted flow is critical as opposed to slightly modifying a representative grid cell elevation value.

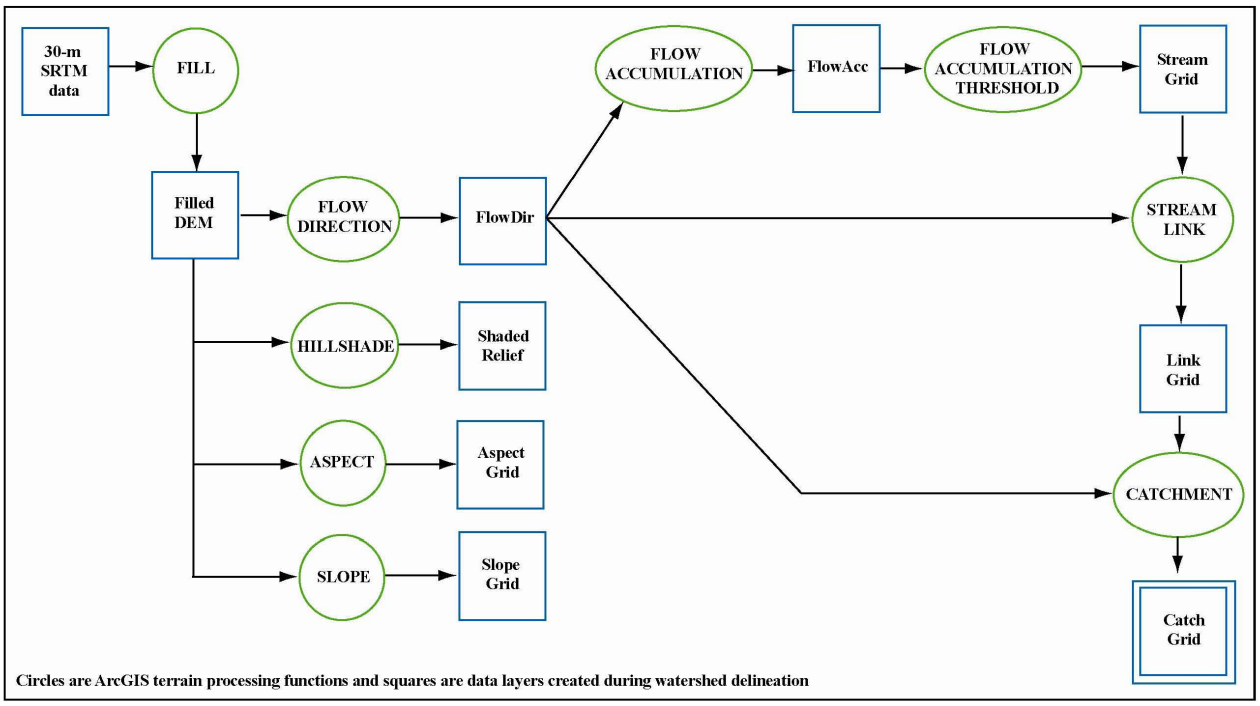

Figure B-3[a]. Full Terrain Processing ArcToolbox Steps

Table B-1[a]. Elevation Change Documented as a Result of the *Fill* Process

Elevation Change (m)	Number of Pixels in Project Area	Percentage of Project Area	Number of Pixels in Model Area	Percentage of Model Area	Number of Pixels in Footprint Area	Percentage of Footprint Area
0	250,807	98.90	138,521	99.59	6,357	99.86
1	2,340	0.92	467	0.34	6	0.09
2	389	0.15	87	0.06	2	0.03
3	54	0.02	13	0.01	1	0.02
4	5	< 0.01	2	< 0.01	0	< 0.01
9	1	< 0.01	1	< 0.01	0	< 0.01
16	1	< 0.01	1	< 0.01	0	< 0.01

Source DTN: SN0601SRTMDTED.001 [DIRS 177242]; Output DTN: SN0608DRAINDYM.001.

The resulting 'filled SRTM' layer provided the elevation data layer for the MASSIF model, but this layer was also used to create five additional datasets equally important to the model. Two of these extra layers, slope and azimuth, were stand-alone products; two more, catchment and flow accumulation, were used to organize the database but were not included in the final database; and the fifth, flow direction, required additional processing to convert it into a layer providing the downslope cell ID number. The filled elevation data, and all subsequent generated data layers used to create the MASSIF spatial database, are assembled together in Output DTN: SN0606T0502206.011.

The full suite of output created in the Full Terrain Processing ArcToolbox (Figure B-3[a]) was as follows. The *hillshade* function created a raster layer that resembled a three-dimensional representation of the YMP area by calculating light and shadow effects based on topography and a default sun angle of 315° and a 45° incident angle. The hillshade layer was only a visual aid in presenting the data layers and did not provide a direct input to the MASSIF model.

The elevation data were also used to create additional layers within the GIS including the slope and azimuth over the model area. The surface slope of each grid cell was calculated using the *slope* function in ArcGIS, which uses the elevations at eight neighboring cells. Slope is defined from 0° (horizontal) to 90° (vertical). Slopes over the infiltration modeling domain ranged between 0° and 49° (rounded to the nearest degree). A map of slopes over the modeling area is presented in Figure B-4[a].

The azimuth layer was created using the *azimuth* function in ArcGIS, which estimates the compass direction of a vector normal to the surface of each grid cell. This parameter is used for calculations involving the direction of incoming solar radiation. Azimuths were defined between 0° and 360° (rounded to the nearest degree) and proceeding clockwise, with 90° representing east. A map of azimuths over the modeling area is presented in Figure B-5[a].

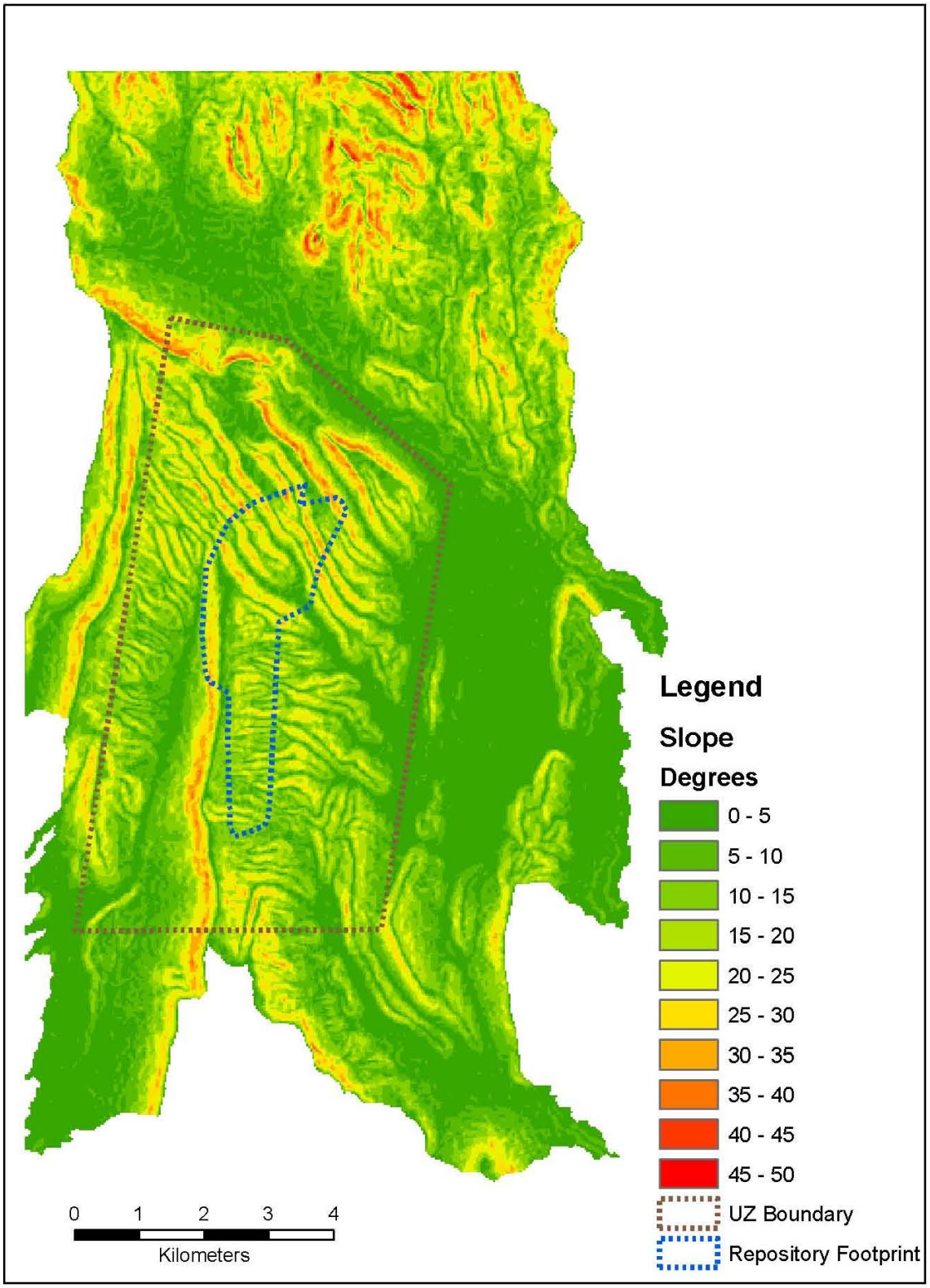

Source: Output DTNs: SN0701SPALAYER.002 and SN0711FTPRNUZB.003.

NOTE: Repository footprint shown for illustrative purposes only.

Figure B-4[a]. Slope across Project Area

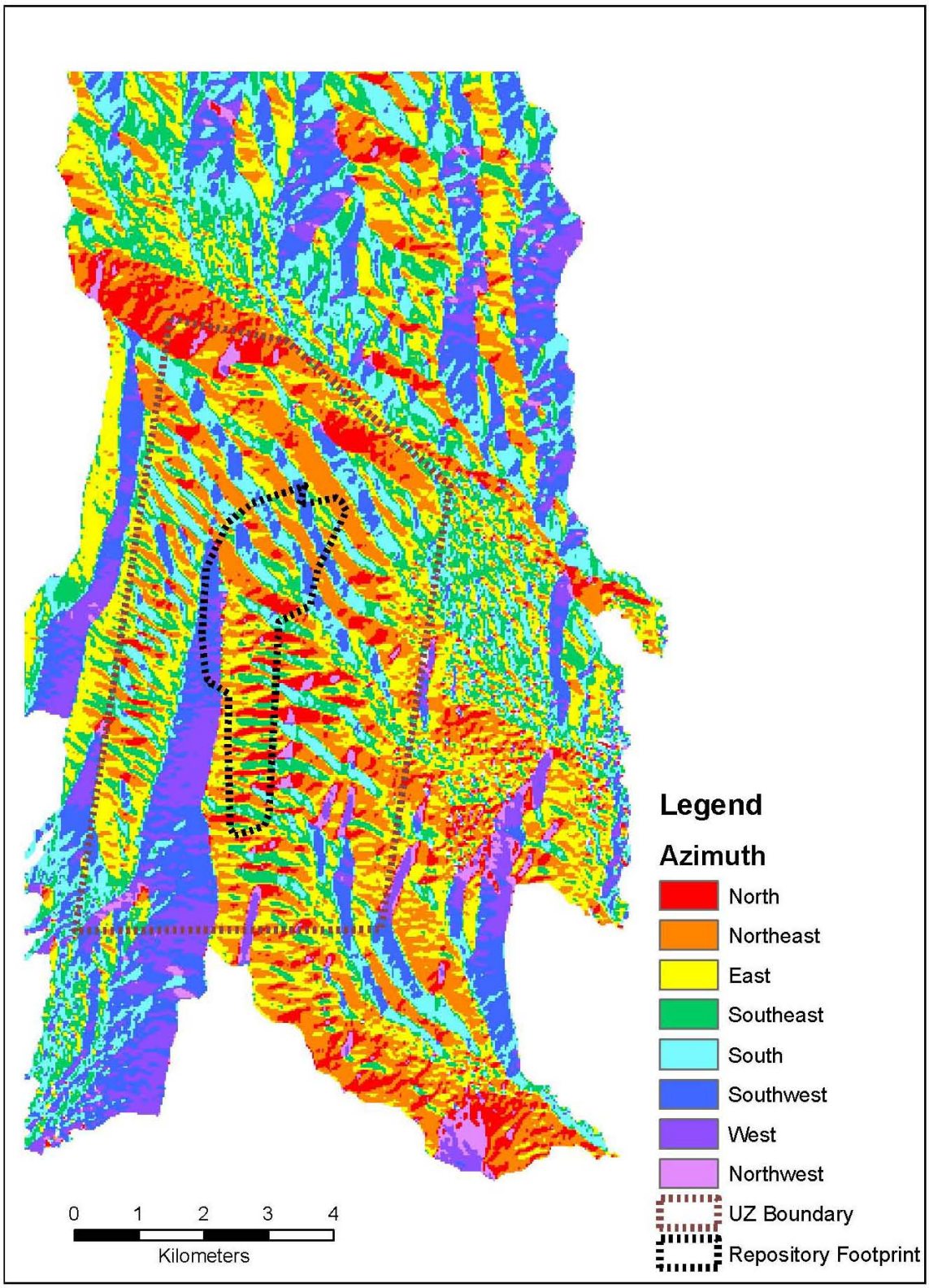
Legend
Azimuth
North
Northeast
East
Southeast
South
Southwest
West
Northwest
UZ Boundary
Repository Footprint
0 1 2 3 4
Kilometers

The *flow direction* function is similar to azimuth, but instead of a compass direction, the function created a numeric code for each cell that represented which neighboring cell water would flow into when leaving the current cell. The resulting layer had values 1, 2, 4, 8, 16, 32, 64, and 128 representing east, southeast, south, southwest, west, northwest, north, and northeast, respectively. This need to determine a direction of flow was why all 'sinks' in the SRTM data set needed to be filled in the previous step. The Full Terrain Processing ArcToolbox used the resultant 'flow direction' data layer to create three additional data sets.

By examination of the flow direction relationships, the *flow accumulation* function calculated the number of upstream pixels for every pixel. The 'flow direction' layer was employed to trace paths of flow with accumulation counts increasing with each new pixel entered or when joining two or more convergent flow paths. A *Flow Accumulation Threshold* was applied to this function to limit the number of drainages represented to only those representing significant accumulation, in this initial case 15,000 upstream grid cells. The resulting 'stream grid' highlighted just these larger streams that possessed a total accumulation of 15,000 upstream cells. The *Stream Link* function assigned unique identifiers to each stream identified as having overcome the flow accumulation threshold.

The last model layer prepared from the topographic data was 'catchment' delineation, the definition of each basin boundary. This delineation process used the concept of pour point, the lowest point along a drainage representing the downslope edge of a drainage basin before it joins another stream from an adjoining basin. Using these pour point locations and the 'flow direction' raster as input, the *Catchment* function mapped all basin boundaries. This function observed where flow direction diverged in opposing directions and assigned that as a basin boundary with all sub-basin boundaries dissolved within the larger basin defined by the pour point at the catchment's outlet.

The resulting catchment raster layer formed seven watersheds. Only three of these watersheds covered a portion of the UZ flow model area and were retained for use in the MASSIF model. This completed the first stage of the project area watershed delineation process. With the Flow Threshold set at 15,000, the resulting basin catchments were all large, but more of the UZ flow model area still fell outside these initial large watersheds. Therefore, the process had to be repeated to generate smaller watersheds to fit into gaps left by the large watersheds. The second and third stages followed the same delineation process using the Full Terrain Processing ArcToolbox, but the flow accumulation value was set to 1,000 and 200 to produce medium and small catchment basins, respectively. The end result of this delineation process was three nearly identical sets of output files, with only the size of the basins in the catchment layer the significant difference, as set by the flow accumulation threshold.

B2.3[a]. FORMATTING THE TERRAIN DATA

During the drainage delineation process, several GIS layers were calculated from the SRTM data. These data files required additional processing to convert them to a format for import into the spatial database. All the GIS layers prepared to this point were raster files, square grid cells with single data values attached. To build a single output file, the data were converted into vector files, a series of rectilinear shapes bounding areas of equal value, whose data values could be combined into multiple-field tables. This process of data formatting is discussed below.

The catchment delineation process used three similar processing streams to produce the necessary outputs. Most of the steps in each delineation produced identical output, except for the catchment size layer, which was dependent on the flow accumulation setting. Therefore, elevation, slope, azimuth and other files were consistent throughout the processing and were not affected by the variable flow accumulation settings between the separate processing streams. With three sets of identical data, only one set needed to be prepared for inclusion in MASSIF. For consistency in description, unless otherwise specified, all terrain data extractions used data prepared during the processing run with flow accumulation set to 200 instead of the identical data sets from the 1,000 and 15,000 flow accumulation model runs.

Four of the raster layers, 'Filldem200', 'Azimuth200', 'Slope200' and 'Flowaccum200' comprised continuous data (floating point grids) that would not transfer into vector format without an additional process. To accomplish this, the decimal range of the values for each raster layer needed to be rounded up or down to create integer values.

The *Raster Calculator* ArcGIS Spatial Analyst performed this with the following formula that analyzes the portion of the continuous value fight of the decimal and rounds up or down accordingly:

```
Int(con([grid1] > 0,con(Abs([grid1] - Int([grid1])) >= 0.5,Ceil([grid1]), Floor([grid1])),con(Abs([grid1]
- Int([grid1])) >= 0.5,Floor([grid1]),Ceil([grid1]))))
```

The delineated catchment files required a different approach to prepare them for the spatial database. The goal of the watershed delineation was to generate as few watersheds as possible that intersect with the UZ flow model area. Experimentation with threshold settings came upon the combination of three settings that would effectively accomplish this goal. Each of the terrain processing stages created a unique catchment file based on the value of flow accumulation threshold (15,000; 1,000; and 200). Each file contained certain watersheds that needed to be included in the final model (those covering a portion of the UZ flow model area and not already covered by a larger watershed) while the others were discarded. The watersheds identified for inclusion were each given a unique sequential number and the remaining watersheds (those that fall completely outside of the UZ flow model area) were set as 'No Data' using the *Reclass* function on each file. The flow accumulation set at 15,000 produced seven basins, three of which were saved. The second stage with a 1,000 flow accumulation produced 105 watersheds. Five of the watersheds covered portions of the UZ flow model area not already covered by the 15,000 flow accumulation settings. Three of the watersheds drain to the same pour point on the edge of the project boundary, so they were combined. Therefore of the five saved watersheds, three were ready to be used in MASSIF. The final stage produced 600 watersheds with the flow accumulation value set at 200. Six of these watersheds covered the last unaccounted for parts of the UZ flow model area. Two of these basins shared a pour point and were combined into a single watershed, thus resulting in five final watersheds. The sets of three, three, and five basins were merged into a final collection of 11 project watersheds. Figure B-6[a] shows this three-stage process and the final 11 drainages. This file was converted to a vector file producing a set of shapes that outlined the project grid cell that belonged in each surface drainage.

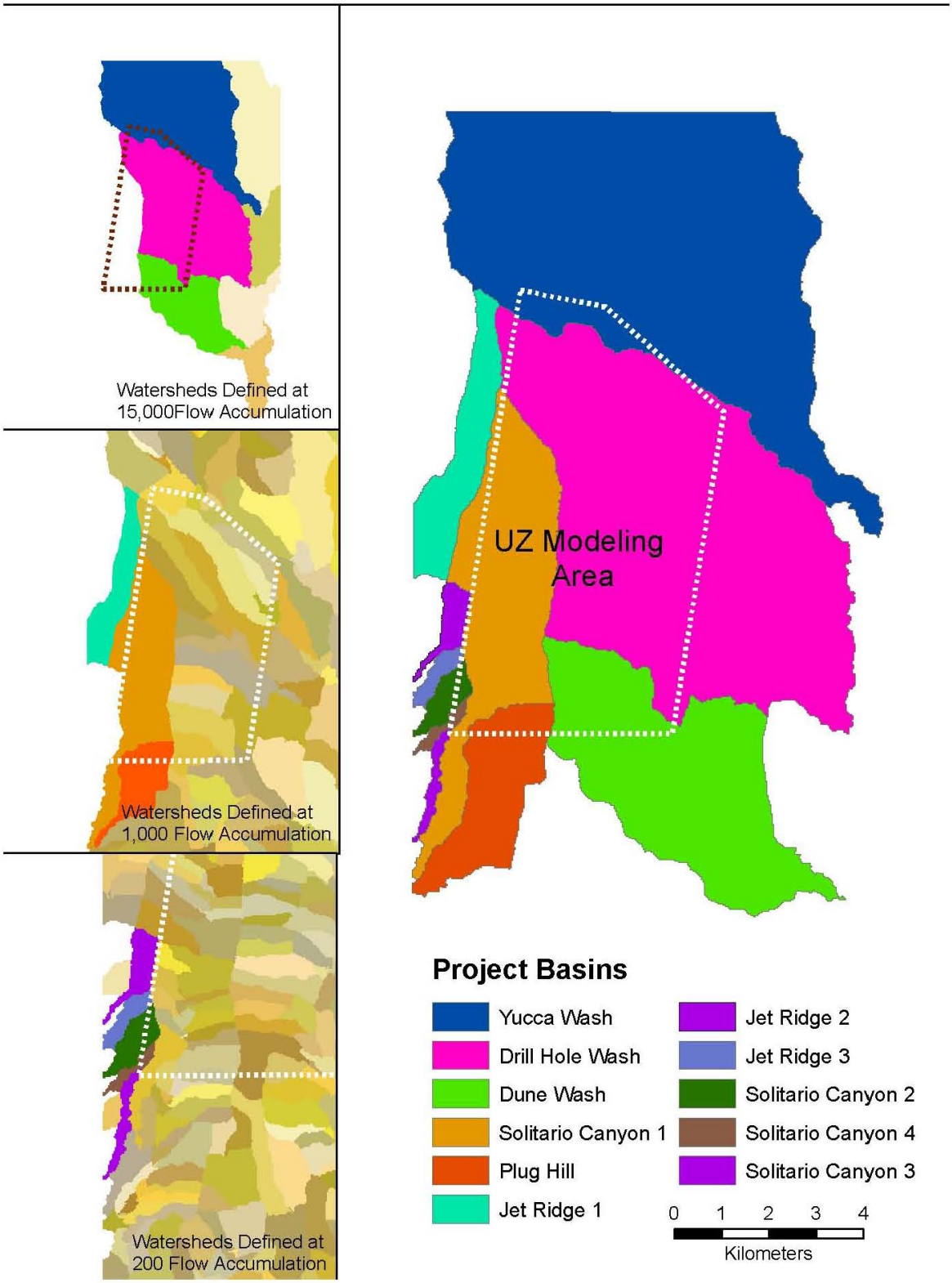

Source: UZ modeling area boundary from Output DTNs: SN0711FTPRNUZB.003, Project basins from SN0701SPALAYER.002, and Watersheds for various flow accumulation values from SN0608DRAINDYM.001.

Figure B-6[a]. Results of Three-Stage Watershed Delineation and Final Basin Combination

B3[a]. ADDITIONAL SPATIAL DATABASE PREPARATION

The final form of the spatial database for the MASSIF infiltration model contained 13 data fields compiled from different data layers. Some layers were created in the steps detailed above and others had been prepared as stand alone data products. Three such products, soil type, soil depth, and bedrock geology, were prepared from geology and soil data outside of the current GIS and were provided in a spatial database for inclusion in MASSIF. The potential vegetative response (PVR) data were created concurrently with the spatial database and imported upon its completion. From the SRTM data and the watershed delineation process, elevation, downstream grid cell identification (ID), slope, azimuth, catchment, and flow accumulation were made available. Two other layers created during the delineation process, catchment and flow accumulation, did not actually go into the final version of the database but were necessary to divide and sort the final data. The grid cell identification number and the spatial coordinates in UTM and latitude and longitude are generic data layers based on the location and dimensions of the YMP area.

B3.1[a]. IMPORTING PREPARED DATA LAYERS

Soil type, soil depth, and bedrock geology were model inputs independently prepared by project specialists. Each input layer was prepared from existing geologic and pedologic data for Yucca Mountain. It was necessary to update each of these three inputs to format them to MASSIF requirements. Details of their preparations and a discussion of the significances of individual classes are in Section 6.5.2. Their DTNs are MO0608SPASDFIM.006 [DIRS 178082] (containing soil type and soil depth) and MO0603SPAGRIDD.003 [DIRS 177121] (containing Bedrock geology), respectively. These data were large ASCII files supplied as tables detailing the data values for each 30-m cell in the MASSIF project boundary. The tables also included latitude, longitude, and UTM coordinates to allow the data to be displayed in a spatial database. All data processing tasks represented in Sections B3.1[a] and B3.2[a] are archived in Output DTN: SN0701SPALAYER.002.

The range of bedrock values and soil depth across the project area from these files are displayed in Figures B-7[a] and B-8[a], respectively. During the course of the project, questions arose about the third downloaded data sets, soil type. A decision, documented in Section 6.5.2.1[a], was made to edit these data prior to entering them into MASSIF due to an unusable data field.

Soil type data required changes from its downloaded form (DTN: MO0608SPASDFIM.006 [DIRS 178082]). The following change was conducted in ArcGIS, and the edited version is preserved in the spatial database (Output DTN: SN0606T0502206.011). Ten values were represented in this layer, but two of the values did not represent an actual soil class. Soil class ‘8’ represented exposed bedrock, and everywhere it is present, it is paired with the accompanying soil depth class ‘5,’ that represents no soil depth. Soil Class ‘10’ had a similar problem as it was originally assigned to areas that had been disturbed by dirt roads or ground clearing. This designation was not consistent across the project area, as most grid cells containing a road were not designated as such. This designation also represented the surface condition and not the actual soil properties, so the accompanying data tables possessed no soil characteristic information for grid cells with this ‘10’ value. Therefore, each ‘10’ value was subjected to a nearest neighbor correction. Cell values of ‘10’ were on-screen edited to the soil

value most prevalent of those surrounding it while taking topographic factors (slope breaks and drainages) into consideration. Figure B-9[a] displays the inconsistent road classification and the 'fix' that was applied. In this figure, seventeen red pixels are overlaying roads and bladed surfaces in the left-hand frame, but are replaced with the model soil classes in the right-hand frame. Nine classes were now present in the final soil class input layer instead of the original ten. This edit occurred in grid cells with surface disturbances across the entire project area and is displayed in Figure B-10[a].

After completing these changes, the soil and bedrock datasets were imported into the spatial database. The soil type layer contained fields for grid cell ID and UTM coordinates, and latitude/longitude coordinates, providing a means of adding this information to the model.

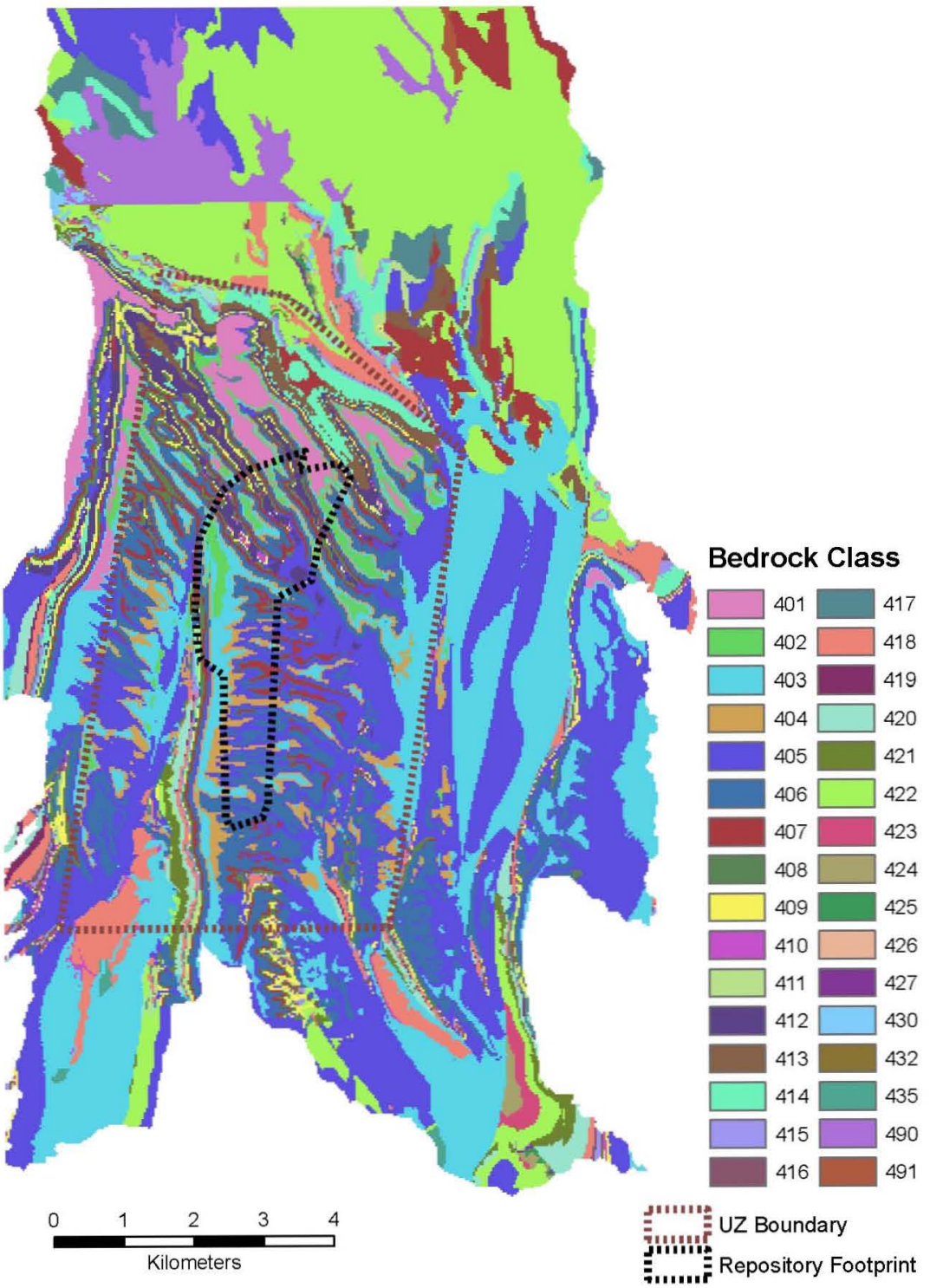

Source: Output DTNs: SN0701SPALAYER.002 and SN0711FTPRNUZB.003. DTN: MO0603SPAGRIDD.003 [DIRS 177121].

NOTE: Repository footprint shown for illustrative purposes only.

Figure B-7[a]. Bedrock Zones across Project Area as described in Section 6.5.2

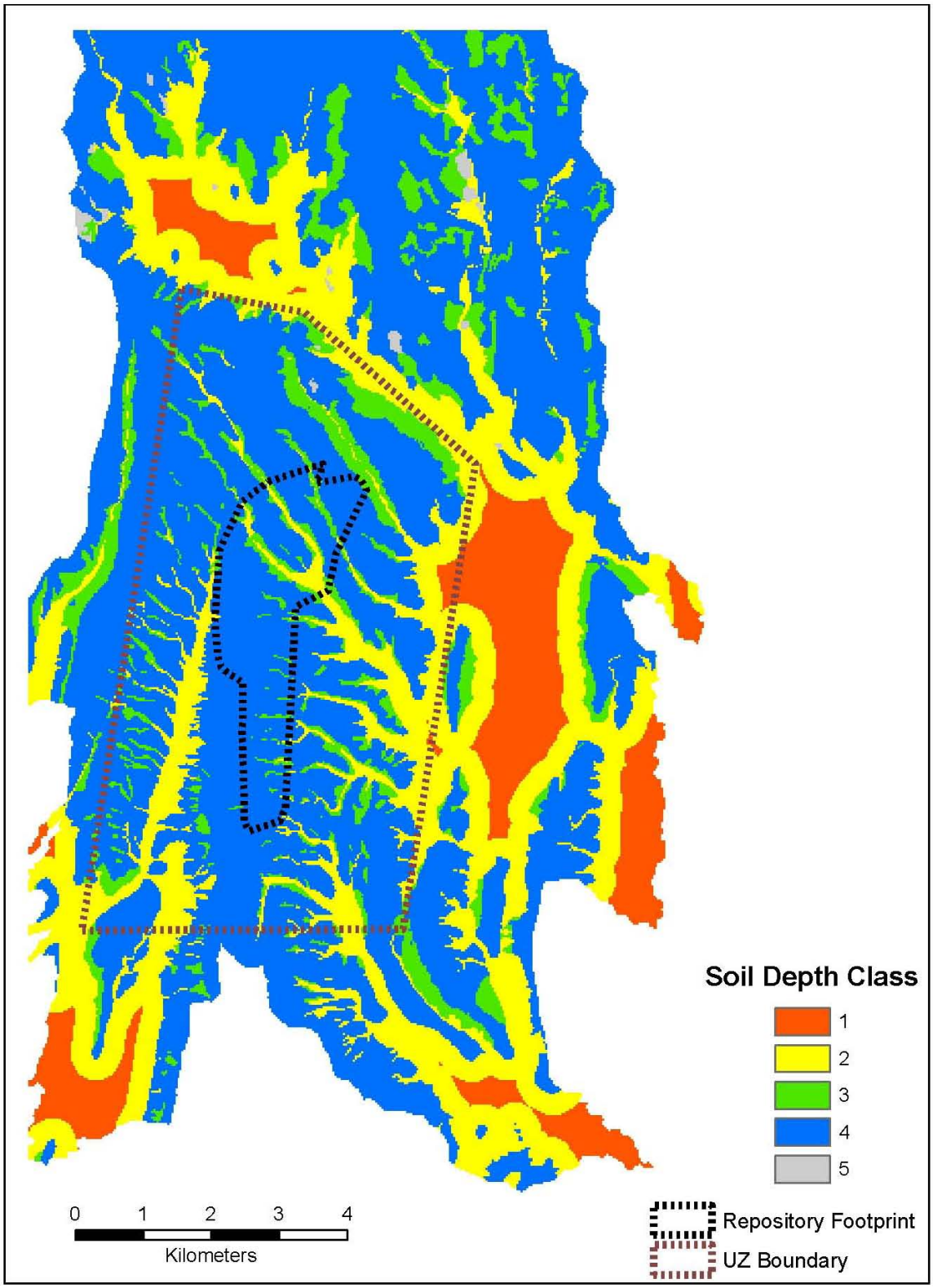

Source: Output DTNs: SN0701SPALAYER.002 and SN0711FTPRNUZB.003.

NOTE: Repository footprint shown for illustrative purposes only.

Figure B-8[a]. Soil Depth Zones across Project Area as described in Section 6.5.2

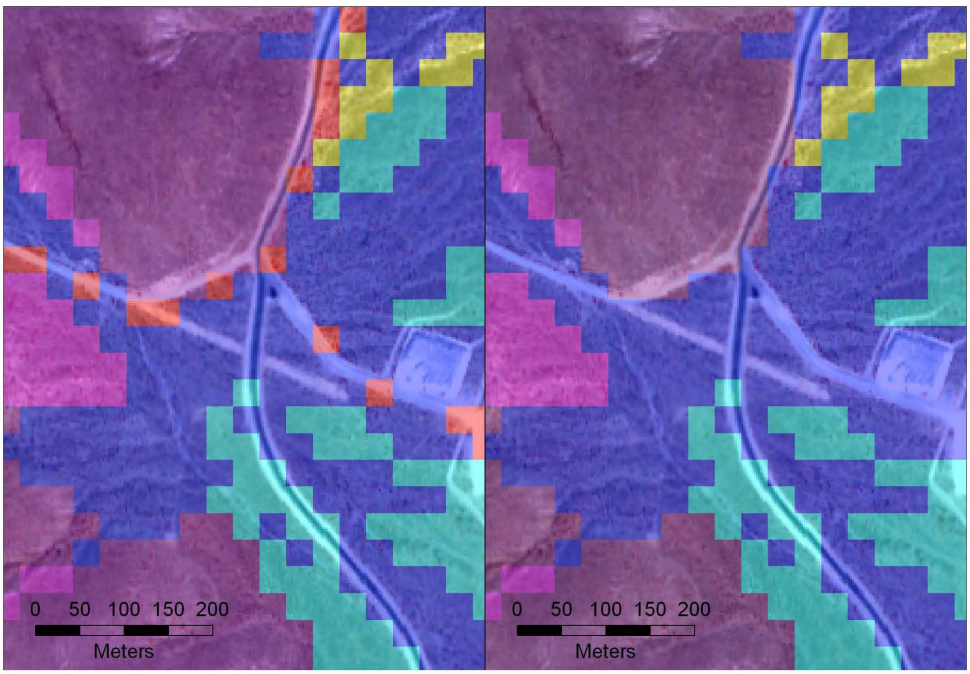

Source: Output DTN: SN0701SPALAYER.002.

Figure B-9[a]. Road Soil Class (Red pixels in left frame) Removed within Project Area and Replaced with Appropriate Soil Class (right frame)

One other data layer was imported from outside the GIS, the PVR, prepared concurrently from Normalized Difference Vegetation Index (NDVI) calculations conducted in ENVI 4.2. Construction of the PVR layer is performed in Output DTN: SN0608PVRATYMT.001 and described in Appendix E with the final result displayed in Figure B-11[a]. The PVR data layer comes out of the image processing ready for inclusion into the spatial database and no further processing was required.

B3.2 DOWNSTREAM CELL CALCULATIONS

The MASSIF model required each model grid cell to know which model cell its surface water flows into. This was important to model correctly the overland flow within the model. ArcGIS did not have a direct means for calculating this value, so additional steps were required to create this data layer. To generate the downstream cell number from each cell, the Flow Direction grid from the Flow200 processing was required. As detailed earlier, Flow Direction provides a grid of eight numbers (1, 2, 4, 8, 16, 32, 64, 132) that represent the downslope direction into the eight surrounding grid cells. Using this information, together with the width of the model boundary grid (367 cells), it was possible to reclassify the flow direction grid into a template for use in Spatial Analyst's Raster Calculator. The Figure B-12[a] diagram below details the spatial relationships involved during the reclassification.

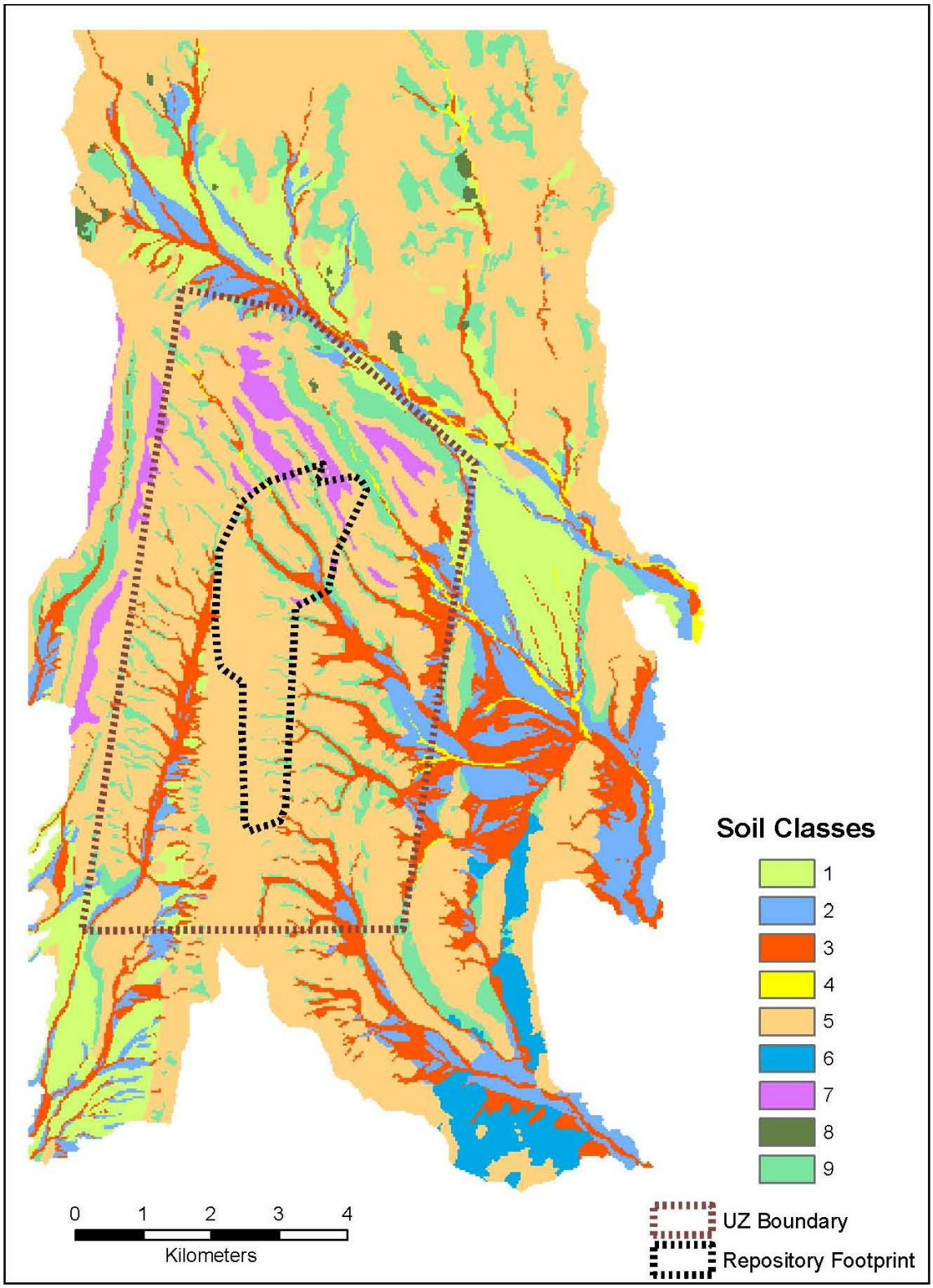

Source: Output DTNs: SN0701SPALAYER.002 and SN0711FTPRNUZB.003.

NOTE: Repository footprint shown for illustrative purposes only.

Figure B-10[a]. Soil Type Zones across Project Area as described in Section 6.5.2

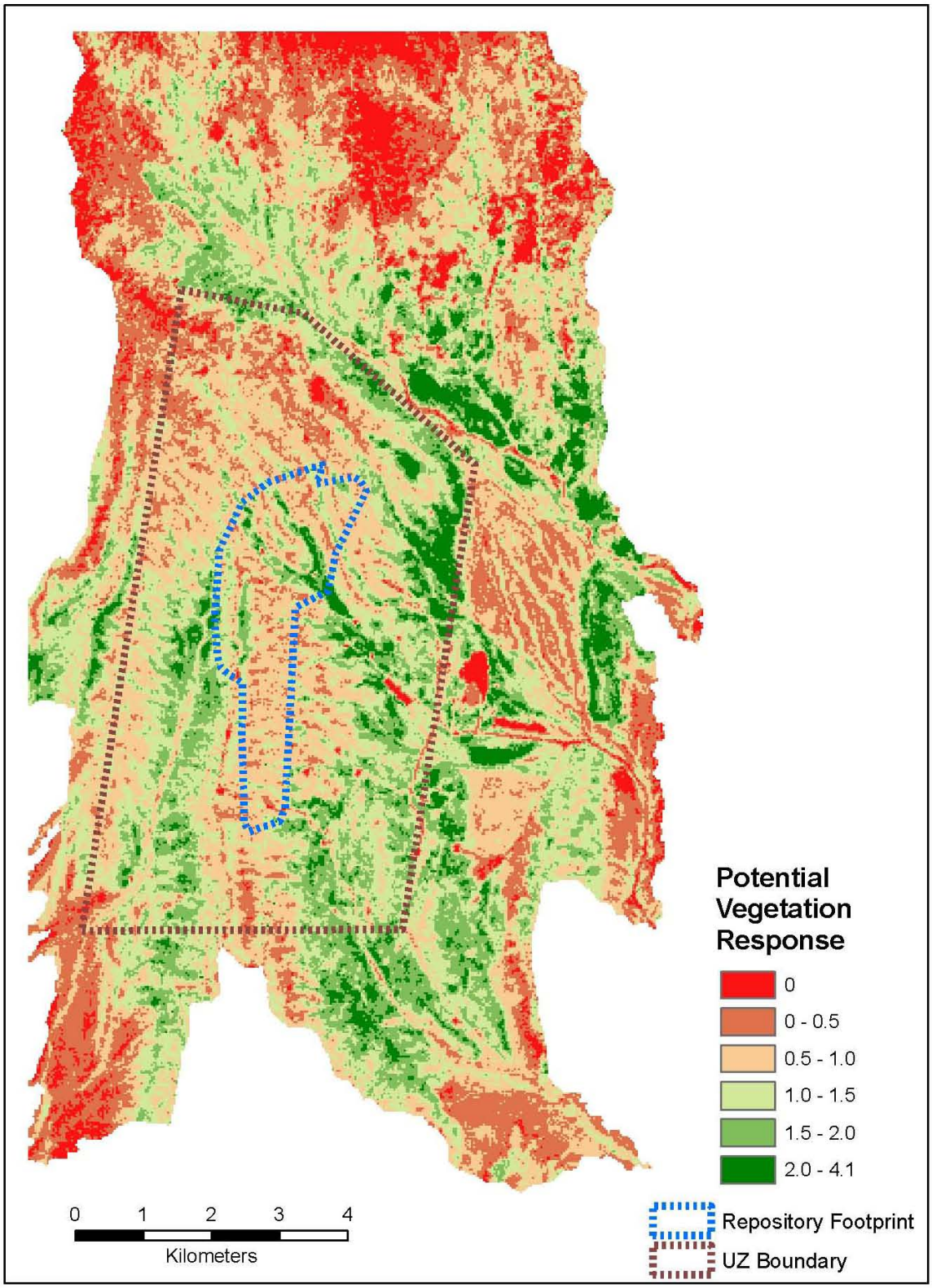
Potential
Vegetation
Response
0
0 - 0.5
0.5 - 1.0
1.0 - 1.5
1.5 - 2.0
2.0 - 4.1
Repository Footprint
UZ Boundary
0
1
2
3
4
Kilometers

Each cell's ID number was added to the downslope reclassified layer (right grid in Figure B-12[a]) to provide the cell ID of the downslope cell. For an example, if the overland flow from cell ID number 1,000 moved into the cell to the southeast, its downslope ID number would be 1,368 (1,000 + 368). The output of this calculation served as the final input layer. With the exception of the downloaded data, all the remaining data layers were extracted from data projected in UTM NAD 83. ArcGIS 9 can integrate data that are in different reference projections, but as a service for future users without this version of ESRI GIS software, each data layer was reprojected to UTM NAD 27 as the last step. All the necessary data now resided in the spatial database, but the spatial relationships among these layers still needed to be developed.

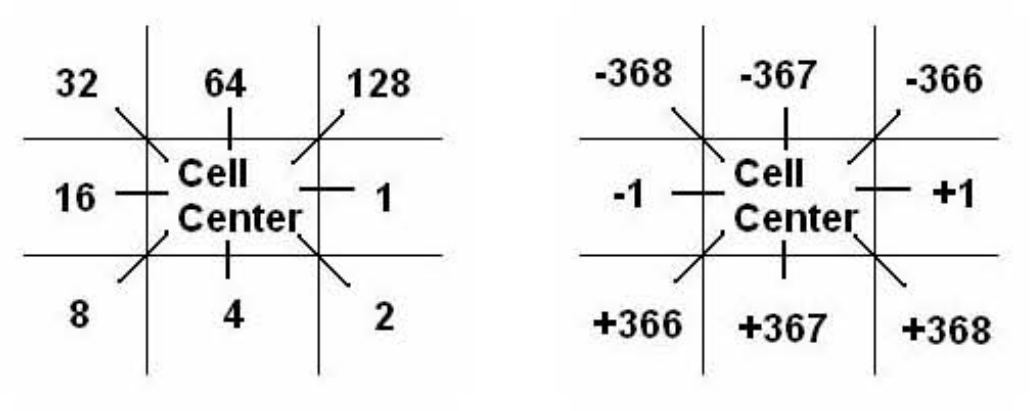

Figure B-12[a]. Downstream Cell ID Adjustment Values

B4[a]. ASSEMBLING THE SPATIAL DATABASE

No change.

B5[a]. DELINEATING GAUGED WATERSHEDS

In addition to the eleven drainage basins that make up the model area, a subset of six drainages were needed to calculate model results that could be compared directly against actual runoff values collected at six surface stream gages located in the project area. This comparison was used to validate the model. Principles similar to those used to create the project area catchments were used to create these gauged watersheds. Previously during the watershed delineation (Section B2.2[a]), the amount of flow accumulation was used to define the project area drainages. In the case of the gauged watersheds, specific locations (stream gages) defined the lower end of each drainage (pour points). All data processing tasks represented in Sections B5.1[a] and B5.2 are archived in Output DTN: SN0608ASSEMBLY.001.

B5.1[a]. IMPORTING THE GAUGE LOCATIONS

The stream gauge locations were provided as sets of coordinates (DTN: MO0601GSCSPINF.000 [DIRS 177236]. These spatial tabular data were input into the GIS to incorporate them into the spatial database. The gauge locations were compared to the created elevation model of the project area.

Due to slight variations in the original elevation data set and the subsequent *Filled* data layer, the model stream network did not always follow actual stream channels. The differences between the two did not overly affect the delineation process, as all that was needed was a slight lateral shift in the pour point location, while the upstream dimensions (number of model grid cells) remained the same (Figure B-13[a]).

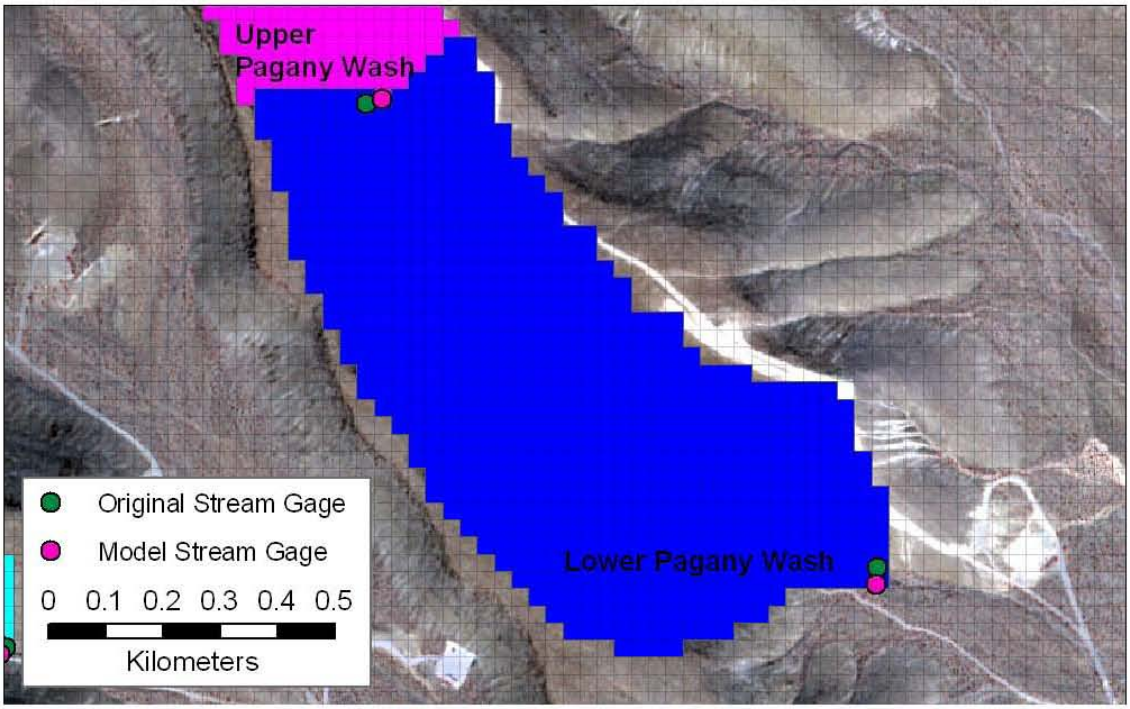

Source: Output DTN: SN0608CWATSHED.001.

Figure B-13[a]. Stream Gauges: Original and Spatial Database Locations

This is a common situation when hydrologic modeling uses cell based elevation data. The elevation data is represented by a sample value that does not always reflect the lowest potential elevation in that cell, which is required for watershed delineation. For the MASSIF model, a single elevation value was being used to represent all variations within a 30-m by 30-m square grid cell, so often a small, narrow drainage was not captured as the dominate trait of that grid cell. However, the general trend of the landscape was incorporated, and the drainage was defined to follow this trend. In steep, narrow valleys, the model easily follows the natural terrain, but in wide, flat valleys with little relief, the model might struggle to follow a small braided stream. In these cases, the model would instead create a representative drainage that followed the general slope and azimuth trend with the understanding that this was the highest probability for the drainage location. The model would follow this slope/azimuth trend until a difference in elevation would once again create a break in the slope to help redefine where the drainage actually has to run.

The *Snap Pour Point* function in ArcGIS hydrology tools was developed to compensate for this drainage discrepancy. *Snap Pour Point* takes point features, such as gauges, and assigns them an exact location on the modeled drainage system so that they can be used for direct future output from the model. The *Snap Pour Point* function is an automated task that is helpful in

manipulating large datasets. For the small number of gauges in this model, the same function was replicated manually with on-screen digitizing with a higher degree of accuracy, as pour point/gauge could be snapped to the drainage to ensure the shift is minimized to as small a lateral shift as possible to maintain the watershed dimension.

As a result of this process, the watershed surface area upstream from a particular model pour point was a close match to actual upstream dimensions from stream gauge. Two of the actual stream gauges fell within a cell designated as a model stream. In three of the six examples, the necessary shift was only into the adjacent cell. Only one example needed a two-pixel shift due to low-elevation variability and filled DEM characteristics associated with the drainage passing through a culvert under an elevated road. The shifts are not that important in construction of the gauged watersheds, as the size of any watershed is based on the topography of the land to provide width and the overall distance of the drainage to provide length. Shifting the pour point perpendicular to the drainage does not change the length of the watershed and has minimal effect on the resulting grid cell count (surface area).

B5.2[a]. DELINEATION AND GAUGED AREA CLIP

No change.

B6[a]. ADDING BOUNDARY IDENTIFIERS TO THE SPATIAL DATA

After the completion of the spatial database for the MASSIF model (Output DTN: SN0606T052206.011), an ancillary database was created that would include model cell identifiers keyed to the location of the repository footprint and the larger area of impact, the UZ flow model area. The knowledge of whether a model grid cell was located within the UZ or repository footprint boundaries was not required to run the MASSIF model properly, but it was useful for explanatory purposes when examining MASSIF results. The file was structured to be easily incorporated into MASSIF model calculations when desired. All data processing tasks represented in Sections B6.1[a] and B6.2[a] are archived in 'Assembly data for geospatial inputs to MASSIF Model of Yucca Mountain' (Output DTN: SN0608ASSEMBLY.001).

B6.1[a] ANCILLARY BOUNDARY FILES CREATION

Boundary coordinates for the repository footprint and the UZ flow model area were both imported from DTN: LB0208HYDSTRAT.001 [DIRS 174491]. *Repository02_Table.xls* contained the 30 vertices of the irregular-shaped footprint. These coordinates were provided in the form of State Plane 27 meters. This was converted to State Plane 27 feet (the traditional unit of measurement for State Plane projections) and saved as *repository_footprint.txt*. This text file was opened in ArcView where the coordinates were displayed as points and saved as an ESRI shapefile. This point shapefile was converted to UTM NAD 27 Zone 11 and saved once again. Using these points as guides, a polygon shapefile was constructed using each vertex in order. This resulted in *Repository_Footprint_update.shp*.

The same steps were used for the UZ boundary coordinates as found *UZ02_Model_Domain.txt*. It was also in the form of State Plane meters, and converted to State Plane feet in *UZ_boundary2.txt*. Once entered into ArcView, the coordinates were displayed as points, saved, and reprojected to UTM NAD 27 Zone 11. This resulting file was saved as

UZ_Boundary_UTM_NAD27.shp. Figure B-15[a] displays these two boundaries and their relationship to the MASSIF model watersheds.

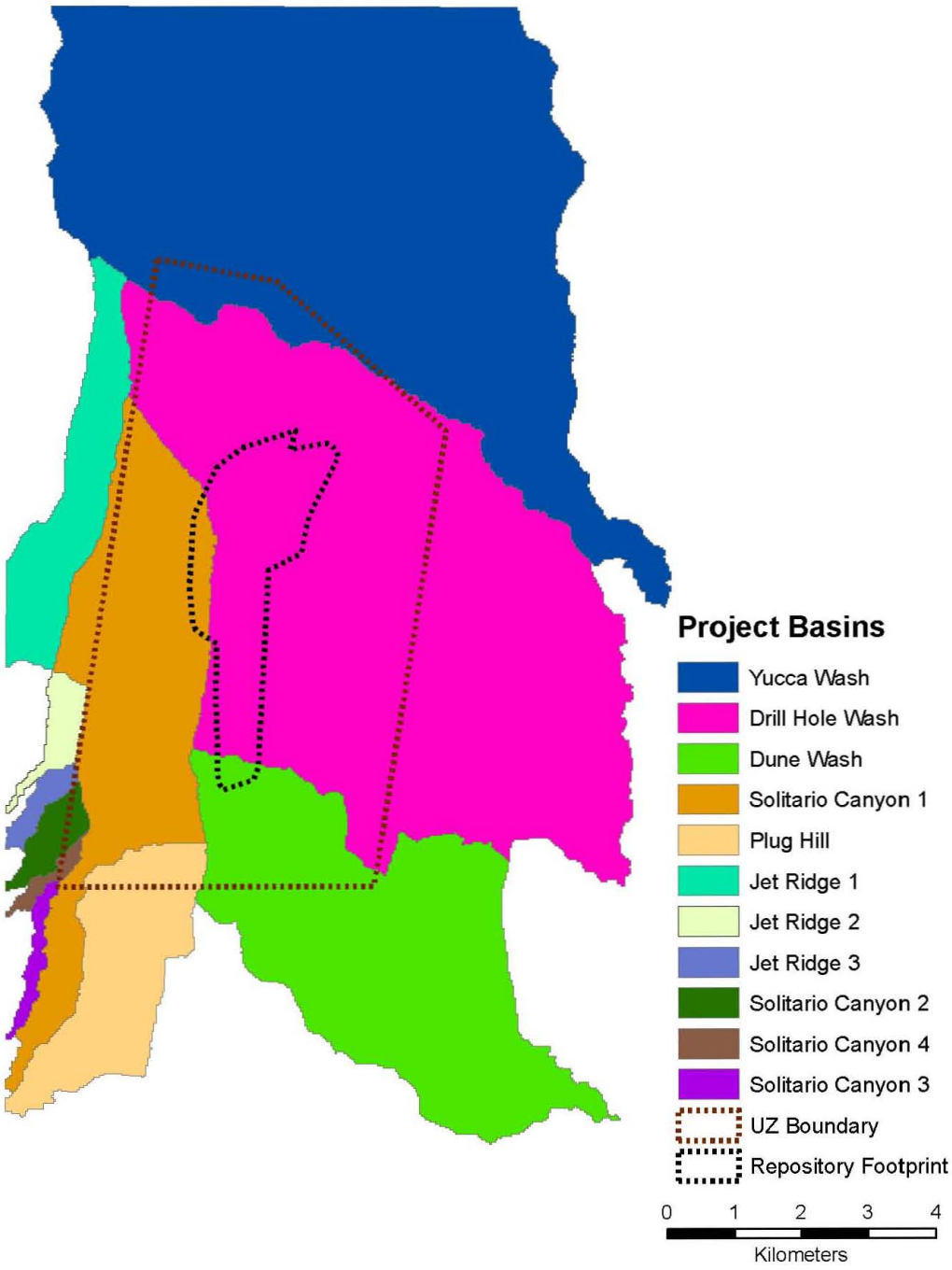

Source: Output DTNs: SN0608DRAINDYM.001 and SN0711FTPRNUZB.003.

NOTE: Repository footprint shown for illustrative purposes only.

Figure B-15[a]. Locations of MASSIF Model Watersheds, UZ Boundary, and the Repository Footprint

In order to make these data compatible to the existing spatial database, it was necessary to modify one of the interim data files that led to the creation of the final spatial database. *All_Layers_Joined_nad27.shp* points file from folder *E2_All_Join* in Output DTN: SN0608ASSEMBLY.001. This file is a point shapefile for the entire project area where each point contains all the MASSIF inputs for a specific model grid cell and is the version of the spatial database prior to the final step of subdivision in the eleven model drainages. Two fields were added to the shapefile's attribute table, one titled 'footprint' and another labeled 'UZ'. A subset of points within *All_Layers_Joined_nad27.shp* was then selected using the UZ boundary file as the selection criterion. All points selected were assigned a '1' value in the attribute table, leaving the unselected points as '0' under the UZ heading. The selection was cleared and second selection of points was conducted using the repository footprint shapefile. These selected points were assigned a '1', leaving the remainder as '0' in the footprint column. The final was saved as *All_Layers_plus_footprint_and_UZ.shp*.

B6.2[a]. BOUNDARY FILES SUBDIVISION

The following preparation methods were nearly identical to the steps taken in Section B4.1 except only three data columns were required and the output was condensed into a single output file, *All_Layers_plus_footprint_and_UZ.shp*. It was then saved into eleven separate shapefiles, once again based on using catchment in the selection process, but this time incorporating the file renaming scheme by size in a single step.

As was the case with the other input files prepared, the MASSIF model required that the data be entered in a particular order. The data needed to be sorted in order from highest elevation to lowest. The renumbering of the final elevation record in each file to a '−3' was not necessary at this step since this column will not be part of the final output.

A few last edits rendered each file ready for input as an ancillary input into the MASSIF model. All columns were deleted with the exception of Cell_ID, Footprint, and UZ and saved as .csv files. The contents in each file were combined into a single file based on order of watershed size that is evident in each file name (order shown in Table B-6[a]). This final combined file is saved as *Updated_UZ_and_Footprint_with MASSIF_ID_Number.csv* and is made available to the MASSIF model as Output DTN: SN0711FTPRNUZB.003.

Table B-6[a]. Boundary Files Watershed Catchments

Catchment ID	Catchment Name
1	01_yucca_wash
2	02_drill_hole_wash
3	03_dune_wash
4	04_solitario_canyon1
5	05_plug_hill
6	06_jet_ridge1
7	08_jet_ridge2
8	09_jet_ridge3
9	07_solitario_canyon2
10	11_solitario_canyon4
11	10_solitario_canyon3

Source: Output DTN: SN0711FTPRNUZB.003.

APPENDIX C[a]
CALCULATION OF ET_0 (REFERENCE EVAPOTRANSPIRATION) AS A FUNCTION OF SLOPE AND AZIMUTH

C1[a]. CALCULATIONS

No change.

C1.1[a]. Initial Calculations

Steps 1 through 18 are calculations required in solar radiation computations or in ET_0 computations. These calculations are general to all grid cells on Yucca Mountain.

INPUTS: Daily maximum and minimum air temperature, $T_{max\ reference}$ and $T_{min\ reference}$ respectively, associated with the reference weather station along with the latitude and elevation of the weather station.

Step 1. Estimate mean daily dew-point temperature, $T_{dew\ general}$ using $T_{min\ reference}$ measured at or simulated for the reference weather station, as described by Allen et al. (2005 [DIRS 176207], Equation E.1):

$$T_{dew\ general} = T_{min\ reference} - K_o \qquad \text{(Eq. C-1[a])}$$

where

K_o is an empirically derived offset. For the southern Nevada climate present-day conditions, K_o was set to 4.5°C, which is an average of 4°C to 5°C recommended by Allen et al.(2005 [DIRS 176207], p. D-29) for spring, summer, and fall periods when the climate is arid to semiarid. K_o was set to 2°C for winter when the climate is somewhat more humid. The values used for K_o will create dew-point temperature–humidity data sets that reflect weather conditions over an ET reference setting of well-watered clipped grass cover that is part of the standard ET_0 calculation definition. It is important, in applying the $ET = K_c ET_0$ approach (where ET is actual ET and K_c is a transpiration or 'crop' coefficient and ET_0 is the reference ET), that the ET_0 calculation represents the reference evapotranspiration that occurs from the standardized reference ET surface. This standardized reference surface, by definition, is an extensive surface of transpiring grass that conditions the atmospheric boundary layer by evaporative cooling and by the addition of water vapor. The conditioning of the boundary layer constitutes an important feedback process to the ET_0 rate and moderates it. The K_c coefficient, which represents the ratio of actual ET to ET_0, and the soil water stress reduction function, which reduces the ET value when soil water content is insufficient to support ET fully, are designed to function in concert with the standardized ET_0 value (Allen et al. 1998 [DIRS 157311], pp. 58, 91, and 161). The ET_0 calculation represents a near upper limit on ET that is experienced under full vegetation cover and adequate soil moisture supply. Under conditions of less than full vegetation cover or less than adequate soil moisture supply, the actual ET rate will be reduced below the standardized ET_0 rate, even though the actual air temperature may increase and humidity may decrease due to the reduced ET (Brutsaert 1982 [DIRS 176615], pp. 224 to 225, and Figure 10.5). Therefore, even though the ambient potential ET rate computed from ambient temperature

and humidity conditions for the dry environment increases under these conditions, by definition, the standardized ET_0 rate remains constant, as it should, due to the adherence to humidity (i.e., dew-point temperature) conditions defined for the reference ET condition. Therefore, it is important that the ET_0 calculation be made using $T_{dew\ general}$ estimated using K_o values that represent the reference ET condition.

The value simulated for $T_{dew\ general}$ will change daily as the value for $T_{min\ reference}$ changes. The $T_{dew\ general}$ from Equation C-1[a] is applied for a single reference weather location, or locations within the study area, with the value derived for $T_{dew\ general}$ used to represent T_{dew} and humidity conditions at all locations within the study area. Section 6.5.4.1 discusses exactly what values of K_o were used and when they were applied for the Mass Accounting System for Soil Infiltration and Flow (MASSIF) analysis of net infiltration. The value K_o = 4.5°C recommended by Allen et al. (2005 [DIRS 176207], p. D-29) for use in a range of climates spanning arid and semiarid is expected to hold for future climate regimes.

Step 2. Calculate actual vapor pressure e_a for use in the FAO Penman-Monteith equation and for estimating precipitable water (W) over the study area (Allen et al. 1998 [DIRS 157311], Equation 14):

$$e_{a\ general} = e^o\left(T_{dew\ general}\right) = 0.6108\ exp\left[\frac{17.27\ T_{dew\ general}}{T_{dew\ general} + 237.3}\right] \qquad \text{(Eq. C-2[a])}$$

where

$e_{a\ general}$ = actual vapor pressure (kPa)
$T_{dew\ general}$ = dew point temperature (°C), from Step 1.

The entire air mass that passes across Yucca Mountain is assumed to have actual vapor pressure as represented by $e_{a\ general}$.

Step 3. Calculate the inverse square relative distance between earth and sun, d_r, for use in the extraterrestrial radiation (R_a) calculation (Allen et al. 1998 [DIRS 157311], Equation 23):

$$d_r = 1 + 0.033\cos\left(\frac{2\ \pi}{365}\ J\right) \qquad \text{(Eq. C-3[a])}$$

where

J = number of the day in the year between 1 (1 January) and 365 or 366 (31 December).

Step 4. Calculate declination of the earth, δ (Allen et al. 1998 [DIRS 157311], Equation 24):

$$\delta = 0.409 \sin\left(\frac{2\pi}{365} J - 1.39\right) \quad \text{(Eq. C-4[a])}$$

Steps 5 through 18 can be computed outside of the grid cell calculation loop when all grid cells are assumed to have the same latitude. This is a valid assumption provided that the entire study area is less than about 40 miles north to south, because extraterrestrial radiation, R_a, varies only slightly with small changes in latitude.

Step 5. Calculate the sunset hour angle, ωs, for a horizontal surface (Allen et al. 1998 [DIRS 157311], Equation 25):

$$\omega_s = \arccos\left[-\tan(\varphi_{reference})\tan(\delta)\right] \quad \text{(Eq. C-5[a])}$$

where

ω_s = sunset hour angle (rad)
$\varphi_{reference}$ = latitude of the reference weather station (rad) (input)
δ = solar declination, from Step 4.

Step 6. Calculate extraterrestrial radiation on a horizontal surface for one 24-hr period, $R_{a\,hor}$ (Allen et al. 1998 [DIRS 157311], Equation 21):

$$R_{a\,hor} = \frac{24(60)}{\pi} G_{sc}\, d_r \left[\omega_s \sin(\varphi_{reference}) \sin(\delta) + \cos(\varphi_{reference}) \cos(\delta) \sin(\omega_s)\right] \quad \text{(Eq. C-6[a])}$$

where

$R_{a\,hor}$ = 24-hr extraterrestrial radiation for a horizontal surface (MJ m^{-2} d^{-1})
G_{sc} = solar constant (0.0820 MJ m^{-2} min^{-1})
d_r = squared inverse relative distance factor for the earth-sun, dimensionless, from Step 3
ω_s = sunset hour angle (radians), from Step 5
$\varphi_{reference}$ = latitude of the reference weather station (rad) (input)
δ = solar declination (radians), from Step 4.

Step 7. Calculate sine of mean solar elevation over 24-hr period, $sin\beta_{24}$, weighted by extraterrestrial radiation (Allen et al. 2005 [DIRS 176207], Equation D.5):

$$sin\beta_{24} = sin\left[0.85 + 0.3\varphi_{reference} sin\left(\frac{2\pi}{365} J - 1.39\right) - 0.42\left(\varphi_{reference}\right)^2\right] \quad \text{(Eq. C-7[a])}$$

where

$sin\beta_{24}$ = sine of the average β (radians) during the daylight period, weighted according to R_a
$\varphi_{reference}$ = latitude of the reference weather station (rad) (input)
J = day of the year.

Values for $sin\beta_{24}$ from Equation C-7[a] should be limited to greater than or equal to 0.01 for numerical stability in Step 10 (Allen et al. 2005 [DIRS 176207], p. D-9).

Step 8. Calculate mean atmospheric pressure for the reference weather station, $P_{reference}$ using the elevation of the reference weather station (Allen et al. 1998 [DIRS 157311], Equation 7):

$$P_{reference} = 101.3\left(\frac{293 - 0.0065\, z_{reference}}{293}\right)^{5.26} \quad \text{(Eq. C-8[a])}$$

where

$P_{reference}$ = atmospheric pressure at the reference weather station (kPa)
$z_{reference}$ = elevation of reference weather station, relative to mean sea level (m).

The 293 parameter in Eq. C-8[a] results from the definition of the standard atmosphere for reference ET_0 calculation where standard air temperature equals 20°C (Allen et al. 1998 [DIRS 157311], p. 31).

Step 9. Calculate precipitable water, W, at the reference weather station (Allen et al. 2005 [DIRS 176207], Equation D.3):

$$W = 0.14\, e_{a\ general}\, P_{reference} + 2.1 \quad \text{(Eq. C-9[a])}$$

where

W = precipitable water in the atmosphere passing over the study area (mm)

$P_{reference}$ = atmospheric pressure at reference weather station (kPa), from Step 8

$e_{a\ general}$ = general, actual vapor pressure of the air, at approximately 2 m (kPa), from Step 2.

Step 10. Calculate 24-hr transmissivity for beam radiation, $K_{Bo\ hor}$ (Allen et al. 2005 [DIRS 176207], Equation D.2):

$$K_{Bo\ hor} = 0.98\, exp\left[\frac{-0.00146\ P_{reference}}{K_{cln}\, sin\beta_{24}} - 0.075\left(\frac{W}{sin\beta_{24}}\right)^{0.4}\right] \quad \text{(Eq. C-10[a])}$$

where

$K_{Bo\ hor}$ = 24-hr transmissivity for clear-sky beam radiation (dimensionless)

K_{cln} = atmospheric cleaness–turbidity coefficient (dimensionless), $0 < K_{cln} \leq 1.0$ where K_{cln} = 1.0 for clean air and $K_{cln} \leq 0.5$ for extremely turbid, dusty or polluted air. K_{cln} = 1.0 was used for Yucca Mountain for present-day conditions, because the air in the area is unpolluted. The K_{cln} = 1.0 was used in determing K_{Rs} in Eq. C-13[a] for estimating $R_{sm\ hor}$ from daily maximum and minimum air temperature and is therefore set to 1.0 here to be congruent with the $R_{sm\ hor}$ estimate.

$P_{reference}$ = atmospheric pressure at reference weather station (kPa), from Step 8

W = precipitable water in the atmosphere (mm), from Step 9

$sin\beta 24$ = sine of average β during the daylight period (radians), from Step 7. Values for $sin\beta 24$ must be limited to greater than or equal to 0.01 for numerical stability (Allen et al. 2005 [DIRS 176207], p. D-8).

Equation C-10[a] was developed by Allen et al. (2005 [DIRS 176207], Equation D.2) for specific application to clear sky conditions.

Step 11. Calculate 24-hr transmissivity for diffuse radiation, $K_{Do\ hor}$ using the ASCE EWRI function (Allen et al. 2005 [DIRS 176207], Equation D.4):

$$K_{Do\,hor} = 0.35 - 0.36\,K_{Bo\,hor} \quad for\ K_{Bo\,hor} \geq 0.15$$
$$K_{Do\,hor} = 0.18 + 0.82\,K_{Bo\,hor} \quad for\ K_{Bo\,hor} < 0.15 \qquad \text{(Eq. C-11[a])}$$

where

$K_{Do\ hor}$ = 24-hr transmissivity for clear-sky diffuse radiation (dimensionless)

$K_{Bo\ hor}$ = 24-hr transmissivity for direct radiation (dimensionless), from Step 10.

Step 12. Calculate clear sky solar radiation over the 24-hr period, $R_{so\ hor}$ (Allen et al. 2005 [DIRS 176207], Equation D.1):

$$R_{so\,hor} = (K_{Bo\ hor} + K_{Do\,hor})\,R_{a\,hor} \qquad \text{(Eq. C-12[a])}$$

where

$R_{so\ hor}$ = clear sky solar radiation over the 24-hr period (MJ m^{-2} d^{-1})

$K_{Do\ hor}$ = transmissivity for clear-sky diffuse radiation (dimensionless), from Step 11

$K_{Bo\ hor}$ = transmissivity for direct radiation (dimensionless), from Step 10

$R_{a\ hor}$ = extraterrestrial radiation, horizontal surface (MJ m^{-2} d^{-1}), from Step 6.

The $R_{so\ hor}$ is calculated using humidity data from the reference station. It applies, however, to the entire study area, because $R_{so\ hor}$ is only weakly sensitive to elevation, changing less than 1% to 2% over the range in elevations experienced in the study area (Appendix C3).

Step 13. Estimate solar radiation on a horizontal surface, $R_{sm\ hor}$, using T_{max} and T_{min} at reference weather station (Allen et al. 1998 [DIRS 157311], Equation 50; Allen 1997 [DIRS 176568], Equation 1):

$$R_{sm\,hor} = K_{Rs} \sqrt{(T_{\max reference} - T_{\min reference})}\, R_{a\,hor} \qquad \text{(Eq. C-13[a])}$$

where

$R_{sm\ hor}$ = estimated solar radiation for horizontal surface (MJ m^{-2} d^{-1})

$R_{a\ hor}$ =extraterrestrial radiation for horizontal surface (MJ m^{-2} d^{-1}), from Step 6

$T_{max\ reference}$ =maximum air temperature measured at the reference weather station (°C)

$T_{min\ reference}$ =minimum air temperature measured at the reference weather station (°C)

K_{Rs} = adjustment coefficient ($°C^{-0.5}$).

The $R_{sm\ hor}$ from Equation C-13[a] must be limited to less than or equal to $R_{so\ hor}$ from Equation C-12[a], since it is theoretically impossible for R_s on a horizontal surface (i.e., the estimate from Equation C-13[a]) to exceed R_s for a horizontal surface under cloud-free conditions (i.e., the estimate from Equation C-12[a]).

The $R_{sm\ hor}$ is calculated for use at all grid cells, provided, a single latitude is used to represent the mountain for purposes of computing extraterrestrial radiation on a horizontal surface in Step 6. For Present-Day (and Future Climate) conditions, K_{Rs} = 0.19 is used for Yucca Mountain, rather than the general value of 0.16 recommended in FAO-56 (Allen et al. 2005 [DIRS 176207]), based on an analysis of diffuse solar radiation measurements from Yucca Mountain (Appendix C3) and on findings by Allen (1997 [DIRS 176568]) for high elevation locations. $R_{sm\ hor}$ is applied to the entire Yucca Mountain study area because clear sky solar radiation,

$R_{so\ hor}$, and consequently $R_{sm\ hor}$, is only weakly sensitive to elevation, changing less than 1% to 2% over the range in elevations experienced in the study area, based on a sensitivity analysis conducted in Appendix C3.

C1.2[a]. Setup for Translation of Horizontal Solar Radiation to any Slope as Represented by Fixed Combinations of Slope and Aspect

No change.

C1.3[a]. Cell-Specific Calculations

No change.

C1.4[a]. ET_0 Calculation

No change.

C2[a]. CREATION OF LOOK-UP TABLE (LUT) FOR PARAMETER R_B

No change.

C3[a]. PARAMETERIZATION OF SOLAR RADIATION EQUATIONS FOR YUCCA MOUNTAIN

No change.

C4[a]. EVALUATION OF DIFFUSE AND TOTAL RADIATION MEASUREMENTS FROM NEAR YUCCA MOUNTAIN

C4.1[a]. INTRODUCTION

No change.

C4.2[a]. COMPARISON OF DIFFUSE COMPONENT TO SIMPLE MODELS FOR AVERAGE DIFFUSE INDICES

No change.

C4.3[a]. SELECTION AND ESTABLISHMENT OF A METHOD TO ESTIMATE THE DIFFUSE INDEX

No change, except for a change in the footer.

INTENTIONALLY LEFT BLANK

APPENDIX D[a]
METHODS FOR DERIVING TRANSPIRATION COEFFICIENTS FOR VEGETATION AT YUCCA MOUNTAIN

D1[a]. INTRODUCTION

No change.

D2[a]. BACKGROUND INFORMATION

No change.

D3[a]. METHODS

D3.1[a]. BASAL TRANSPIRATION COEFFICIENT EQUATIONS

The equations used to develop K_{cb} profiles for desert vegetation are presented in this section.

The FAO-56 K_{cb} profile for agricultural crops reflects transpiration under optimal growth and nonlimiting water conditions. The generalized K_{cb} profile (Figure D-3[a]) includes four growth stages (Allen et al. 1998 [DIRS 157311], pp. 95 and 96): an initial growth stage (planting date to approximately 10% ground cover), a development stage (10% ground cover to effective full cover), a midseason stage (effective full cover to start of maturity), and a late season stage (maturity to harvest or senescence). Effective full cover for agricultural crops is defined as the time when soil shading is nearly complete or 100% covered (Allen et al. 1998 [DIRS 157311], p. 95).

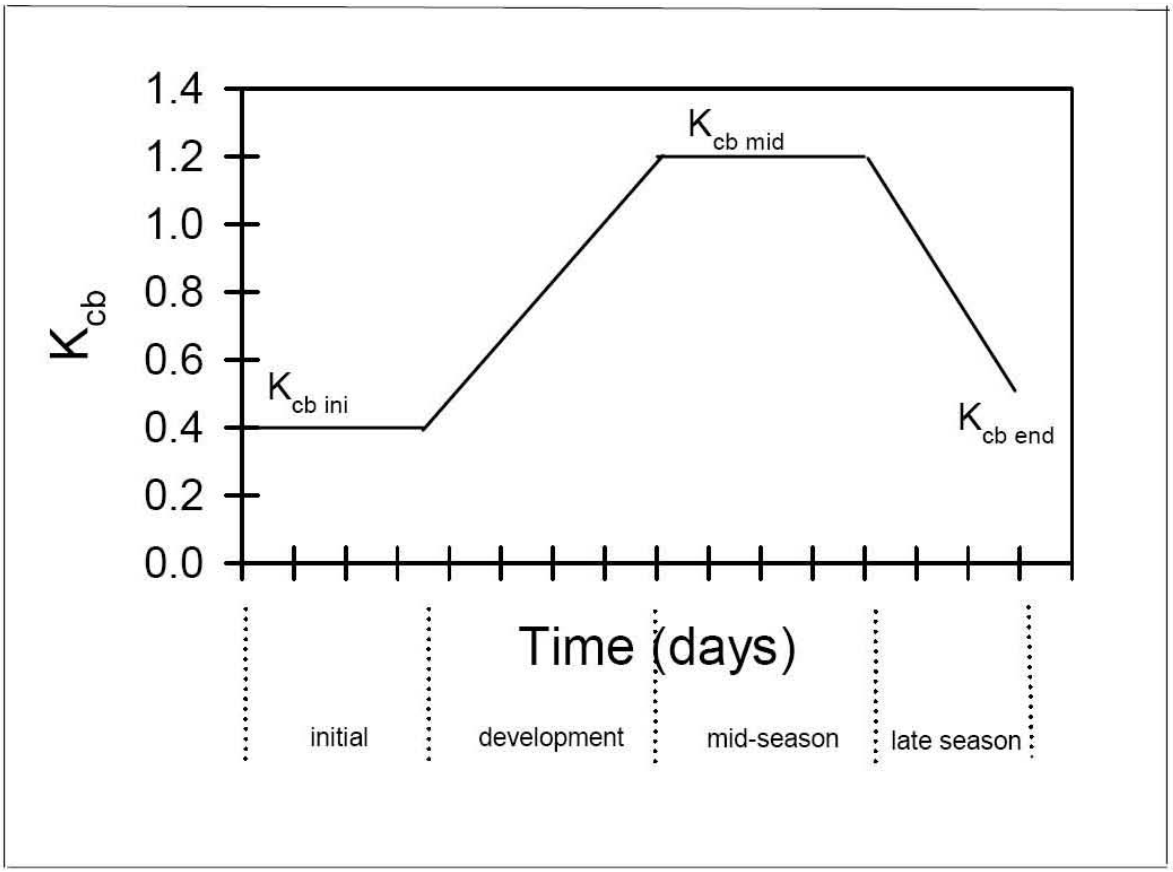

Source: Allen et al. 1998 [DIRS 157311], p. 100, Figure 26.

Figure D-3[a]. Generalized Crop Coefficient Curve

Characteristics of desert vegetation at Yucca Mountain differ from agricultural crops in several ways, including low effective ground cover that rarely exceeds 30% during peak growth periods, little morphological change in mature perennial vegetation across growth stages compared to agricultural crops (e.g., little change in vegetation height and maintenance of a percentage of green canopy throughout the year), and greater degree of stomatal control resulting in lower rates of water loss compared to agricultural crops. Additionally, climatic conditions at Yucca Mountain differ from standard FAO-56 conditions with lower minimum relative humidity (RH_{min}) and higher wind speeds (u_2). To account for these differences, FAO-56 methods for calculating K_{cb} for natural vegetation using effective ground cover, adjustments for stomatal control over water loss, and adjustments for local RH_{min} and u_2 were used Allen et al. (1998 [DIRS 157311], pp. 187 to 193).

Transpiration coefficients for initial ($K_{cb\ ini}$), midseason ($K_{cb\ mid}$), and end of the late season ($K_{cb\ end}$) growth stages were calculated for vegetation types using Equation D-1[a] (Allen et al. 1998 [DIRS 157311], p. 187, Equation 98):

$$K_{cb} = K_{c\min} + (K_{cb\ full} - K_{c\min})\left(\min\left(1,\ 2f_c, (f_{c\ eff})^{\left(\frac{1}{1+h}\right)}\right)\right) \qquad \text{(Eq. D-1[a])}$$

where

K_{cb} = Basal K_{cb} when plant density and/or leaf areas are lower than for full cover conditions
$K_{c\ min}$ = Minimum K_c for bare soil in the presence of vegetation ($K_{c\ min} \approx 0$)
$K_{cb\ full}$ = Estimated basal K_{cb} during the midseason, at peak plant size or height, and full ground cover (Equation D-4[a])
f_c = Observed fraction of soil surface that is covered by vegetation type (0.01 to 1)
$f_{c\ eff}$ = Effective fraction of soil surface covered or shaded by vegetation type (0.01 to 1)
h = Plant height (m).

Equation D-1[a] was recommended for calculating $K_{cb\ mid}$ and $K_{cb\ end}$ (Allen et al. 1998 [DIRS 157311], pp. 187 to 193). Methods for calculating $K_{cb\ ini}$ under standard FAO-56 conditions were suggested for natural, nontypical vegetation (Allen et al. 1998 [DIRS 157311], p. 183). However, those methods were specifically suggested for newly planted annual crops with the magnitude of $K_{cb\ ini}$ primarily determined by soil wetting frequency during irrigation and natural precipitation events. Established perennial vegetation at Yucca Mountain maintains height and some percentage of leaf area during the initial growth stage. Therefore, to account for effects of perennial plant height and cover during the initial growth stage, Equation D-1[a] was used with plant height and reduced cover (compared to that measured at peak growth; Sections D3.2.1 and D3.2.2) to calculate $K_{cb\ ini}$. Because height of annual vegetation varies over the course of the growing season with shorter vegetation during the initial growth stage, both height and cover were reduced (from peak values) to calculated $K_{cb\ ini}$ for annuals using Equation D-1[a]. Daily K_{cb} values for the initial, mid, and end of late season stages were estimated by using daily weather data inputs to calculate $K_{cb\ full}$ (Equation D-6[a]) and the stomatal resistance correction factor (F_r, Equation D-7[a]). According to Allen et al. (2005 [DIRS 176009], p. 4), the equation for $K_{cb\ full}$ can be used for daily estimates when daily measurements of u_2 and RH_{min} are available. To be consistent and to keep the equations on a daily time step, daily weather data inputs were also used for F_r calculations (Equation D-7[a]).

The FAO-56 equation for area- and height-weighting where different fractions of ground are covered by different crops (Allen et al. 2005 [DIRS 176009], p. 199, Equation 104) was not used because of differences in growing season length and stomatal resistance for vegetation types (Section D.3.2). Using Equation 98 to calculate separate profiles for vegetation types and then summing to get one profile for each association (and water year) accounts for this variation, which is important with respect to seasonal *ET*. The vegetation types are independent of one another, with growth stage lengths, cover, and height developed for each type. Because each profile is essentially weighted by cover for the vegetation type, the relative importance of each type is accounted for in the summed profile for each association. Summing the vegetation type profiles resulted in use of total cover that was measured for each association. Setting $K_{c\ min}$ to zero in Equation D-1[a] (as recommended for deserts [see below]) eliminates overestimation of residual evaporation from bare soil in the summed profiles.

Under arid conditions at Yucca Mountain, the upper soil layer dries to very low water content during periods between precipitation events (CRWMS M&O 1999 [DIRS 105031], p. 14, Table 3). Under dry soil conditions and sparse rainfall, Allen et al. (1998 [DIRS 157311], pp. 207 and 209) recommended setting $K_{c\ min}$ to zero to provide for conditions when transpiration is equal to zero. Under these conditions, the soil water balance is controlled by the evaporation term (K_e) of the dual transpiration coefficient. Evaporation following precipitation events is accounted for in the infiltration model by K_e.

In Equation D-1[a], the last term designates use of the minimum of 1, $2f_c$, and $(f_{c\ eff})^{(1/1+h)}$. Cover measurements showed that the total $2f_c$ summed across vegetation types for an association never exceeded a value of 1. Values for $f_{c\ eff}$ were determined for round or spherical-shaped canopies using cover data from Yucca Mountain vegetation associations according to Equation D-2[a] (Allen et al. 1998 [DIRS 157311], p. 188):

$$f_{c\,eff} = \frac{f_c}{\sin(\eta)} \quad \leq 1 \qquad \text{(Eq. D-2[a])}$$

where $\sin(\eta)$ is the sine of the mean angle of the sun, η, above the horizon during midday hours when maximum evapotranspiration is likely to occur. Allen et al. (1998 [DIRS 157311], p. 188) suggest calculating $f_{c\ eff}$ for solar noon using Equation D-3[a] to calculate $\sin(\eta)$:

$$\sin(\eta) = \sin(\psi)\sin(\delta) + \cos(\psi)\cos(\delta) \qquad \text{(Eq. D-3[a])}$$

where

ψ = Latitude (radians)
δ = Solar declination (radians).

Solar declination (δ) is calculated daily (Allen et al. 1998 [DIRS 157311], p. 46, Equation 24):

$$\delta = 0.409 \sin\left(\frac{2\pi}{365} J - 1.39\right) \qquad \text{(Eq. D-4[a])}$$

where

J = Day of year.

To help minimize water loss in arid environments, desert plants are capable of a higher degree of stomatal control than agricultural species (Allen et al. 1998 [DIRS 157311], p. 191). Therefore, it was necessary to apply a stomatal resistance correction factor (F_r, Equation D-7[a]) to Equation D-1[a] when stomatal resistance was estimated to be greater than 100 s m^{-1} (Allen et al. 1998 [DIRS 157311], p. 191). F_r accounts for increases in stomatal resistance during periods of low physiological activity (i.e., initiating or senescing leaves). The F_r does not account for effects of water stress on stomatal resistance. The impact of water stress is implemented by the stress factor (K_s) of the FAO-56 procedure that is used in the daily soil water balance model (Section 6.4).

Transpiration coefficients for development and late growth stages were calculated by linear interpolation between $K_{cb\ ini}$ and $K_{cb\ mid}$ and between $K_{cb\ mid}$ and $K_{cb\ end}$, respectively (Allen et al. 1998 [DIRS 157311], p. 132, Equation 66):

$$K_{cb\ i} = K_{cb\ prev} + \left(\frac{i - \sum L_{prev}}{L_{stage}} \right) \left(K_{cb\ next} - K_{c\ prev} \right) \qquad \text{(Eq. D-5[a])}$$

where

i = Day number within the growing season (1…length of the growing season)

$K_{cb,\ i}$ = Transpiration coefficient on day i

$K_{cb\ prev}$ = K_{cb} at the end of the previous stage

$K_{cb\ next}$ = K_{cb} at the beginning of the next stage

L_{stage} = Length of the stage under consideration (days)

ΣL_{prev} = Sum of the length of all previous stages (days).

The following six steps were used to calculate daily K_{cb}s using Equation D-1[a] and adjusting for stomatal control:

1. Calculate adjustment for the influence of vegetation height for K_{cb} for full cover condition under standard climate ($K_{cb,h}$) (Allen et al. 1998 [DIRS 157311], p. 189, Equation 101):

$$K_{cb,h} = 1.0 + 0.1h \qquad \text{(Eq. D-6[a])}$$

$K_{cb,h}$ is limited to 1.2 for when h >2 (Allen et al. 1998 [DIRS 157311], p. 189).

2. Calculate $K_{cb\ full}$ (Allen et al. 1998 [DIRS 157311], p. 189, Equation 100):

$$K_{cb\ full} = K_{cb,h} + \left[0.04\left(u_2 - 2\right) - 0.004\left(RH_{\min} - 45\right) \right] \left(\frac{h}{3} \right)^{0.3} \qquad \text{(Eq. D-7[a])}$$

where

$K_{cb,\ h}$ = K_{cb} for full cover vegetation under a standard climate (Eq. D-6[a]),
u_2 = Mean wind speed at 2-m height (m s^{-1})
RH_{min} = Minimum daily relative humidity (%)
h = Mean maximum plant height (m).

Equation D-7[a] adjusts for regional climatic differences from the standard climate of FAO-56 ($u_2 = 2$ m s^{-1} and RH_{min} = 45%). This equation can be used for daily estimates when daily measurements of u_2 and RH_{min} are available (Allen et al. 2005 [DIRS 176009], p. 4).

3. Calculate adjustment for stomatal control (Allen et al. 1998 [DIRS 157311], p. 191, Equation 102):

$$F_r \approx \frac{\Delta + \gamma(1 + 0.34u_2)}{\Delta + \gamma\left(1 + 0.34u_2 \frac{r_l}{100}\right)} \qquad \text{(Eq. D-8[a])}$$

where

F_r = stomatal resistance correction factor,
Δ = slope of the saturation vapor pressure curve (kPa $°C^{-1}$),
γ = Psychrometric constant (kPa $°C^{-1}$)
r_l = mean leaf resistance for the vegetation in question (s m^{-1})

4. Determine the minimum of (1, $2f_c$, and $f_{c\,eff}^{(1/1+h)}$)

5. Use values from Steps 1 through 4 in Equation D-1[a] to calculate daily K_{cb}s for each vegetation type per association and water year

6. Adjust daily K_{cb}s (from Step 5) for stomatal control:

$$(K_{cb} \times F_r) \qquad \text{(Eq. D-9[a])}$$

The final step in generating the K_{cb} profiles was to calculate K_{cb} for development and late stages using Equation D-5[[a].

Example calculations using Equations D-1[a] through D-9[a] and K_{cb} profiles are in Section D4[a].

D3.2[a]. Input data

No change.

D4[a]. EXAMPLE CALCULATIONS AND K_{cb} PROFILES

No change.

D5[a]. FUTURE CLIMATE TRANSPIRATION COEFFICIENTS BASED ON AN EXOTIC GRASS MONOCULTURE

No change.

D6[a]. METHODS FOR CALCULATING REFERENCE EVAPOTRANSPIRATION FOR A GENERIC AREA AT YUCCA MOUNTAIN

No change.

D7[a]. NOMENCLATURE FOR EQUATIONS USED IN APPENDIX D

No change.

INTENTIONALLY LEFT BLANK

APPENDIX E[a]
QUANTIFYING AND SIMULATING YUCCA MOUNTAIN VEGETATION RESPONSE

SUMMARY

No change.

E1. GENERAL METHODS AND OVERVIEW FOR THEIR APPLICATION

No change.

E2. DATA PROCESSING AND FUNCTIONAL RELATIONSHIPS

No change.

E2.1 INITIAL PROCESSING STEPS

No change except the sources for Table E-1[a] and Table E-Uncertainty-3[a] shown here.

Table E-1[a]. Landsat TM Data Used for Characterization of Yucca Mountain

WY1998		WY2001		WY2002	
Filename	Sensor	Filename	Sensor	Filename	Sensor
T519971102	TM5	T520001009	TM5	T520011012	TM5
T519980121	TM5	T520010129	TM5	T720011004	TM7
T519980310	TM5	T520010318	TM5	T720011207	TM7
T519980411	TM5	T520010419	TM5	T720020124	TM7
T519980427	TM5	T520010505	TM5	T720020225	TM7
T519981529	TM5	T520010606	TM5	T720020329	TM7
T519980630	TM5	T520010724	TM5	T720020414	TM7
T519980716	TM5	T720001220	TM7	T720020430	TM7
T519980817	TM5	T720010326	TM7	T720020516	TM7
		T720010630	TM7	T720020601	TM7
		T720010817	TM7	T720020617	TM7
				T720020719	TM7
				T720020804	TM7

Source: DTN: SN0712ALANDSAT.002 [DIRS 184297].

NOTE: Filenames list satellite, year, month, and day.

Table E-Uncertainty−3[a]. Reflectance Statistics of Pixel Values within the Model Boundary, Landsat TM5 4/11/1998

Band	Min	Max	Mean	Stdev
Band 3	0.05	0.52	0.16	0.03
Band 4	0.05	0.61	0.24	0.04

Source: DTN: SN0712ALANDSAT.002 [DIRS 184297].

There are no other changes to Appendix E[a].

INTENTIONALLY LEFT BLANK

APPENDIX F[a]
DEVELOPMENT OF STOCHASTIC PRECIPITATION AND OTHER CLIMATE INPUT FILES

This appendix supports Section 6.5.1, Weather Parameters for Anticipated Climate Episodes. Calculation of net infiltration requires an input file containing precipitation, temperature extremes, and mean wind speed on a daily basis. The MASSIF model varies precipitation and temperature with elevation and requires input set to a reference elevation of 1,524 m (5,000 ft), corresponding to the top of Yucca Mountain.

Section F1 is an explanation of the general methods for developing twelve precipitation parameters and twelve temperature parameters that together summarize the precipitation and temperature records at a meteorological station. Section F2 describes the application of these methods to the specific meteorological stations that are representative of each climate. Section F3 explains the development of twelve parameters for wind speed and the selection of 36 parameter uncertainty distributions to capture the range of uncertainty for each climate. Section F4 provides the general method for obtaining a weather input file from a particular set of parameter values.

In addition to the contents of the weather input file, this appendix provides the basis for the precipitation lapse rate. Section 6.5.1 provides the temperature lapse rate, two parameters of precipitation duration, and parameters of snowmelt and sublimation. Section 6.5.4 explains the selection of dew point parameters for each climate.

F1[a]. PARAMETERIZATION OF PRECIPITATION AND TEMPERATURE RECORDS

No change.

F1.1[a]. PARAMETERIZATION OF PRECIPITATION RECORDS

No change.

F1.2[a].PARAMETERIZATION OF TEMPERATURE RECORDS

Output DTN: SN0608T0502206.019 contains MathCAD files for the calculation of parameters to best-fit daily temperature data as a function of day of year, using a least-squares approach. There are four temperature models, one each for minimum temperature on wet days, minimum temperature on dry days, maximum temperature on wet days, and maximum temperature on dry days. Each temperature model is in the form of a sine function described by three parameters, α, β, and γ, representing respectively the magnitude of the first-order term, the phase of the first-order term, and the zero-order term, as follows:

$$Twet_{\min} = \alpha wet_{\min} \sin\left(\frac{x - \beta wet_{\min}}{365/2\pi}\right) + \gamma wet_{\min} \qquad \text{(Eq. F-43[a])}$$

$$Tdry_{\min} = \alpha dry_{\min} \sin\left(\frac{x - \beta dry_{\min}}{365/2\pi}\right) + \gamma dry_{\min} \qquad \text{(Eq. F-44[a])}$$

$$Twet_{\max} = \alpha wet_{\max} \sin\left(\frac{x - \beta wet_{\max}}{365/2\pi}\right) + \gamma wet_{\max} \quad \text{(Eq. F-45[a])}$$

$$Tdry_{\max} = \alpha dry_{\max} \sin\left(\frac{x - \beta dry_{\max}}{365/2\pi}\right) + \gamma dry_{\max} \quad \text{(Eq. F-46[a])}$$

The parameters for this model have the following significance:

- x is the day of year from 1 to 365 (January 1 through December 31; February 29 on leap years is ignored).
- α represents half the annual difference in temperature (minimum or maximum) between summer and winter values, according to the model. It is the amplitude of the sine function and is in units of temperature.
- β represents the calendar day of the year (DOY) when the model temperature is rising and passes through its central value.
- γ is the mean value for the temperature, according to the model.

MathCAD routines were developed to organize the proxy climate site temperature data, including daily minima and maxima. Temperature records were organized by wet days and dry days for each of the proxy sites. For each meteorological station and each temperature model, the DTN includes derivation of values for α, β, and γ to best fit the minimum and maximum temperatures as a function of day of year using a least-squares approach. The three parameters are the result of applying the MathCAD function *minerr* to minimize the sum of the squares of the differences between the measured temperatures and the model temperatures.

As in the precipitation analysis, there are multiple equivalent solutions for the three parameters, with the values for the β parameter separated by half of a year and with the α parameter alternating between positive and negative. However, because all of the proxy sites are in the temperate region of the Northern hemisphere, the functions are very similar, and the initial values could be chosen such that the calculated values of the β parameter would all fall near DOY 115. The initial for α, β, and γ were 20°C, DOY 80, and 30°C, respectively.

Unlike the precipitation analysis, this procedure generates parameters that are not stochastic. In this temperature model, the temperature extremes depend only on the day of the year and whether or not there is precipitation on that day.

There is another aspect in which this analysis differs slightly from that of the precipitation analysis in Section F1.1. That analysis determined each zero-order term as the mean of its data, then the higher-order terms were developed without modifying the lower-order terms. This temperature analysis solves for the zero-order and first-order terms simultaneously. Therefore, although the zero-order term is the mean annual temperature for the model, it may not be exactly the mean of the data. Nevertheless, the MathCAD application estimates the standard uncertainty

for each zero-order term by making the same calculation that would be used for the standard error using the γ parameter in lieu of the mean of the data.

As an example of the results of this analysis, Figure F-1[a] shows the modeled and measured temperature extremes for wet days in the record for Beowawe, Nevada. Modeled versus measured temperatures for recorded dry days are shown in Figure F-2[a]. The modeled temperatures do apply to all days of the year, not just those for which the record has applicable data. Similar figures for each of the proxy sites are contained in Output DTN: SN0608T0502206.019.

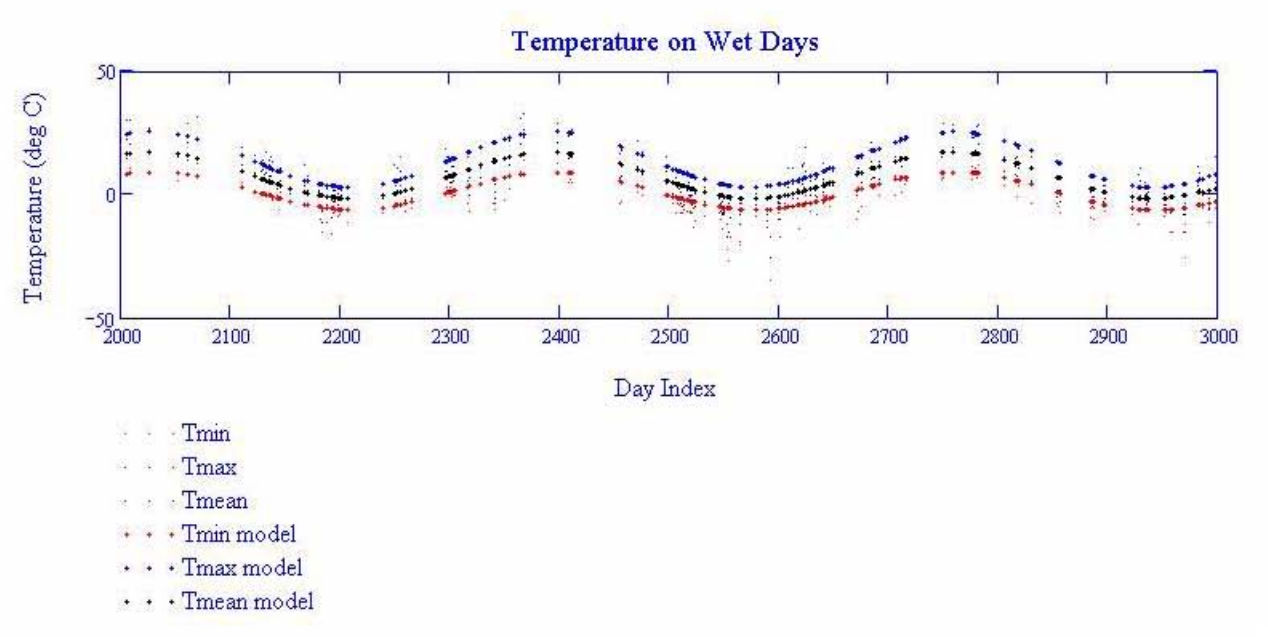

Source: Output DTN: SN0608T0502206.019.

Figure F-1[a]. Model versus Measured Temperatures for Wet Days, Beowawe, Nevada

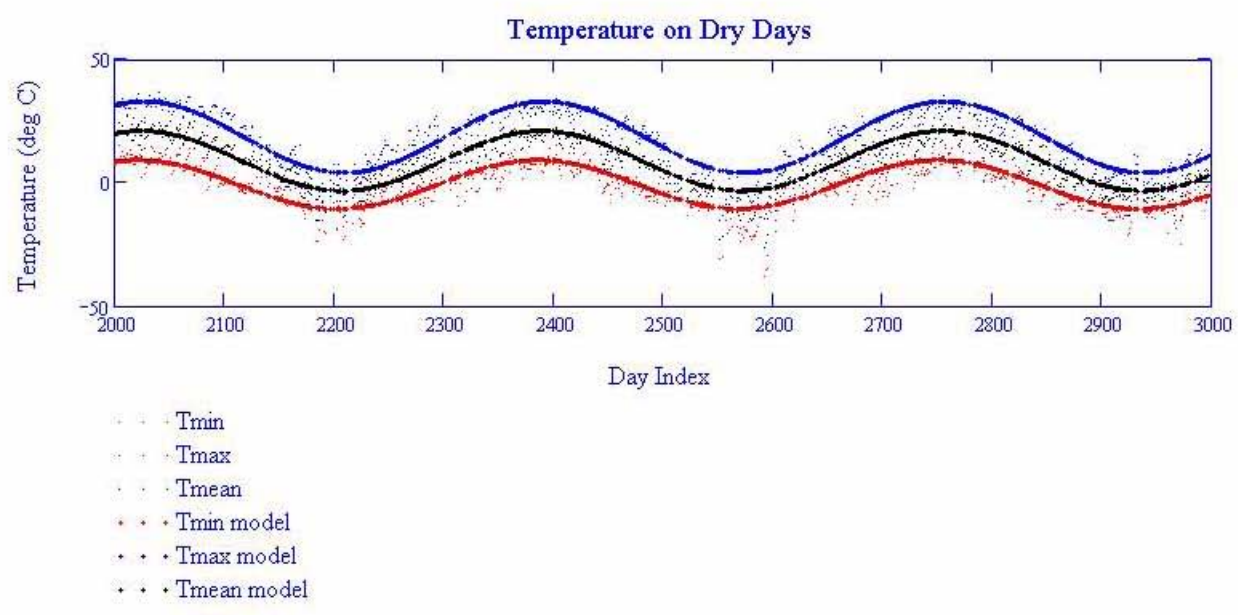

Source: Output DTN: SN0608T0502206.019.

Figure F-2[a]. Model versus Measured Temperatures for Dry Days, Beowawe, Nevada

Applying the approximations of F1.1.4, the mean annual temperature is approximately:

$$MAT = \frac{a_{10}}{1-a_{00}+a_{10}}\cdot\frac{\gamma dry_{\min}+\gamma dry_{\max}}{2} + \frac{1-a_{00}}{1-a_{00}+a_{10}}\cdot\frac{\gamma wet_{\min}+\gamma wet_{\max}}{2} \quad \text{(Eq. F-47[a])}$$

F2[a]. PARAMETERS FOR REPRESENTATIVE METEOROLOGICAL STATIONS

No change.

F2.1[a]. STATIONS REPRESENTING THE PRESENT-DAY CLIMATE

DTNs: SN0601PRECPTMP.002 [DIRS 176122] and SN0608WEATHER1.005 [DIRS 177912] comprise the qualified precipitation records from the ten representative stations. Output DTN: SN0609T0502206.023 contains the Excel workbooks that performed the Fourier analyses of the ten precipitation records. Tables F-1[a] and F-2[a] report results of these analyses. The phase parameters are rounded to one hundredth of a radian (about half a day); the remaining parameters are rounded to a level of precision consistent with the standard error. Although the subsequent analysis omits second-order terms, these two tables provide their magnitudes ($b_{oo,2}$, $b_{1o,2}$, etc.).

Equations F-41 and F-42 provide a method for calculating the approximate MAP implied by the zero-order coefficients. For corroboration of the analyses, Table F-2a[a] compares the MAP implied by the coefficients with the actual MAP at each station. In each case, the MAPs agree to within 10%.

Table F-1[a]. Fourier Parameters for p_{00} and p_{10} at Stations Representing the Present-Day Climate

Station	Station Elevation (m)	a_{00}	a_{00} Standard Error	$b_{00,1}$	$\theta_{00,1}$ (Radians)	$b_{00,2}$	a_{10}	a_{10} Standard Error	$b_{10,1}$	$\theta_{10,1}$ (Radians)	$b_{10,2}$
4JA	1,043	0.939	0.002	0.024	−1.26	0.010	0.621	0.013	0.043	−1.24	0.067
40 MN	1,469	0.929	0.002	0.022	−1.43	0.012	0.514	0.011	0.046	−1.36	0.059
A12	2,283	0.911	0.003	0.025	−1.35	−0.015	0.504	0.011	0.026	−1.54	0.052
Amargosa Farms	747	0.955	0.002	0.023	−1.17	0.016	0.661	0.019	−0.039	+0.53	0.069
Cane Spring	1,219	0.934	0.002	0.028	−1.24	0.013	0.582	0.013	0.052	−1.34	0.072
YM Site 1	1,143	0.937	0.004	0.031	−1.20	−0.009	0.66	0.03	0.09	−1.48	0.09
YM Site 2	1,478	0.941	0.004	0.025	−1.30	0.015	0.60	0.03	0.10	−1.44	0.06
YM Site 3	1,279	0.937	0.004	0.029	−1.39	0.011	0.61	0.02	0.06	−1.42	0.05
YM Site 6	1,315	0.937	0.004	0.030	−1.34	0.017	0.63	0.02	0.06	−1.29	0.06
YM Site 9	838	0.947	0.004	0.031	−1.39	−0.006	0.67	0.03	−0.10	+1.47	−0.06

Source: Output DTN: SN0609T0502206.023.

Table F-2[a]. Fourier Parameters for λ and m at Stations Representing the Present-Day Climate

Station	a_λ (mm)	a_λ Standard Error (mm)	$b_{\lambda,1}$ (mm)	$\theta_{\lambda,1}$ (Radians)	$b_{\lambda,2}$ (mm)	a_m (ln mm)	a_m Standard Error (ln mm)	$b_{m,1}$ (ln mm)	$\theta_{m,1}$ (Radians)	$b_{m,2}$ (ln mm)
4JA	4.42	0.17	−0.75	−0.38	−0.88	0.64	0.04	−0.22	−0.40	−0.16
40 MN	4.68	0.16	−0.54	+0.81	−0.99	0.68	0.03	−0.10	+0.04	−0.16
A12	5.75	0.17	−0.90	−0.64	−1.22	0.92	0.03	−0.19	−0.82	−0.15
Amargosa Farms	5.1	0.3	−0.3	−0.80	−1.1	0.90	0.05	−0.15	−0.84	−0.15
Cane Spring	5.3	0.2	−0.8	−0.36	−1.1	0.82	0.04	−0.17	−0.52	−0.20
YM Site 1	4.9	0.4	−0.8	−0.71	−1.3	0.71	0.08	−0.16	−1.04	−0.20
YM Site 2	5.4	0.4	0.6	+1.46	−1.03	0.85	0.07	−0.10	−1.31	0.20
YM Site 3	5.7	0.4	−0.8	−1.07	−1.49	0.90	0.07	−0.12	−0.91	−0.28
YM Site 6	5.9	0.4	−1.1	−1.27	−1.15	0.95	0.07	−0.10	−0.93	0.26
YM Site 9	3.7	0.3	−0.6	−0.49	−0.62	0.48	0.08	−0.20	−0.36	−0.13

Source: Output DTN: SN0609T0502206.023.

Table F-2a[a]. Mean Annual Precipitation at Site and Regional Stations Compared with Values Implied by Fourier Coefficients

Meteorological Station	Station Elevation (m)	Measured MAP (mm)	MAP Implied by Coefficients (mm)	Years Used for Fourier Analysis (Mar. 1 to Feb. 28)
Amargosa Farms	747	1.1×10^2	1.2×10^2	26 years: 1968, 1969, 1979 to 2000, 2002, 2003
YM Site 9	838	1.1×10^2	1.0×10^2	11 years: 1993 to 2003
4JA	1,043	1.4×10^2	1.4×10^2	45 years: 1959 to 2003
YM Site 1	1,143	1.8×10^2	1.6×10^2	10 years: 1993 to 1998, 2000 to 2003
Cane Spring	1,219	2.0×10^2	2.0×10^2	39 years: 1965 to 2003
YM Site 3	1,279	2.1×10^2	1.9×10^2	11 years: 1993 to 2003

Table F-2a[a]. Mean Annual Precipitation at Site and Regional Stations Compared with Values Implied by Fourier Coefficients (Continued)

YM Site 6	1,315	2.1×10^2	2.0×10^2	11 years: 1993 to 2003
40 MN	1,469	2.1×10^2	2.1×10^2	43 years: 1961 to 2003
YM Site 2	1,478	1.9×10^2	1.8×10^2	11 years: 1993 to 2003
A12	2,283	3.2×10^2	3.1×10^2	41 years: 1960 to 1994, 1998 to 2003

Source: BSC 2006 [DIRS 177081], Table 6.1-4; Section 6.2.5.1 (measured MAPs); from Equations F-41 and F-42, using values from Tables F-1[a] and F-2[a] (implied MAPs); Output DTN: SN0609T0502206.023 (elevations and data years).

Adjustment to an elevation of 1,524 m requires a lapse rate for each first-order precipitation parameter. For each station, Table F-3[a] shows its elevation and each first-order parameter, with parameter lapse rates and uncertainties calculated by the Excel function LINEST.

Generally, the frequency of dry days decreases with elevation and the average wet-day precipitation increases with elevation. However, the MASSIF model makes the approximation that all elevations have wet or dry days when the top of the mountain has a wet or dry day. Therefore, total annual precipitation is adjusted for elevation using an input lapse rate. Table F-3[a] includes the expected MAP for each station, calculated in accordance with Equation F-42, and a precipitation lapse rate and uncertainty calculated by the Excel function LINEST. The table also shows the MAP extrapolated to 1,524 m with the Excel function FORECAST and the precipitation lapse rate expressed as a percentage of the extrapolated value. Thus, the nominal precipitation lapse rate is equal to 134 mm/km divided by 213 mm, which gives 6.3%/100 m. The standard error on this lapse rate is calculated by dividing the standard error on the slope (14 mm/km) by 213 mm, which gives 0.7%/100 m.

Table F-3[a]. Lapse Rates for Parameters of the Present-Day Climate

Station	Station Elevation (m)	a_{00}	a_{10}	a_{λ} (mm)	a_m (ln mm)	Elevation in 100s of Meters	Expected MAP (mm)
4JA	1,043	0.939	0.621	4.42	0.64	10.43	144
40 MN	1,469	0.929	0.514	4.68	0.68	14.69	207
A12	2,283	0.911	0.504	5.75	0.92	22.83	315
Amargosa Farms	747	0.955	0.661	5.1	0.90	7.47	119
Cane Spring	1,219	0.934	0.582	5.3	0.82	12.19	197
YM Site 1	1,143	0.937	0.66	4.9	0.71	11.43	156
YM Site 2	1,478	0.941	0.60	5.4	0.85	14.78	176
YM Site 3	1,279	0.937	0.61	5.7	0.90	12.79	195
YM Site 6	1,315	0.937	0.63	5.9	0.95	13.15	196
YM Site 9	838	0.947	0.67	3.7	0.48	8.38	99
Lapse Rate	—	−0.025 ±0.004 /km	−0.11 ±0.03 /km	0.9 ±0.5 mm/km	0.15 ±0.14 mm/km	—	134 ±14 mm/km
Extrapolated	1,524	—	—	—	—	—	213 mm
Percentage Lapse Rate	—	—	—	—	—	—	6.3 ±0.7 %/100m

NOTE: Data for stations is from Tables F-1[a] and F-2[a], except last column calculated using Equations F-41 and F-42. Lapse rates and their uncertainties are *m* and *se*1, calculated with Excel function LINEST by setting the *known_y's* to the station values and the *known_x's* to station elevations. Extrapolated MAP calculated with Excel function FORECAST by setting *x* to 1,524 m, the *known_y's* to station values of MAP (mm) and the *known_x's* to station elevations. Percentage lapse rate for MAP calculated by dividing lapse rate and uncertainty by extrapolated MAP and dividing by ten to convert from km to 100 m (and multiplying by 100 to get percentage).

To avoid exaggerating the range of uncertainty of each parameter, this section adjusts the values from the various stations to make them comparable. This is particularly necessary for the first-order terms, which have multiple equivalent forms, separated in phase by π. In Tables F-1[a] and F-2[a], some of the coefficients of the first-order terms (b_{00} and b_{10}) are negative. Tables F-4[a] and F-5[a] include adjustment of the first-order terms in accordance with Equation F-37, so that all of the coefficients are positive. In some cases, the phase has been adjusted by 2π to bring it closer to the adjusted phase values at other stations. The phases of the first-order terms correspond to relatively more winter than summer precipitation.

Tables F-4[a] and F-5[a] also include adjustment of the zero-order terms (a_{00} and a_{10}) to the reference elevation of 5,000 ft (1,524 m), using lapse rates from Table F-3[a]. The following equation was used for adjusting values to the reference elevation:

$$adjusted\ value = initial\ value + (ref\ elev - stn\ elev) \times lapse\ rate \quad \text{(Eq. F-48[a])}$$

where *rev elev* is the reference elevation of 5,000 ft (1,524 m), *stn elev* is the elevation for the station where the initial value was based, and *lapse rate* is the value from Table F-3[a].

Almost every summary value in Table F-4[a] or F-5[a] is used in Section F3.1[a], either directly in a parameter uncertainty distribution or indirectly in selecting a distribution. The parameters in the last line of each table are used in Section F3.2[a] to represent the lower bound of the Monsoon climate.

Table F-6[a] provides two additional properties for each station. One is the probability of a wet day, adjusted to the top of the mountain, calculated in accordance with Equation F-39, and rounded to the nearest 1%. The other is the adjusted value for MAP (Equation F-40). After adjustment to the top of the mountain, the range of MAP is about 170 to 250 mm, with only relatively short records falling below 190 mm.

Table F-4[a]. Parameters for p00 and p10 at Stations Representing the Present-Day Climate Adjusted to an Elevation of 1,524 m

Station	Station Elevation (m)	a_{00} [a]	a_{00} Standard Error[b]	$b_{00,1}$ [b]	$\theta_{00,1}$ (Radians)[b]	a_{10} [a]	a_{10} Standard Error[b]	$b_{10,1}$ [b]	$\theta_{10,1}$ (Radians)[b]
4JA	1,043	0.927	0.002	0.024	−1.26	0.568	0.013	0.043	−1.24
40 MN	1,469	0.928	0.002	0.022	−1.43	0.508	0.011	0.046	−1.36
A12	2,283	0.930	0.003	0.025	−1.35	0.587	0.011	0.026	−1.54
Amargosa Farms	747	0.936	0.002	0.023	−1.17	0.576	0.019	0.039[c]	−2.61[c]
Cane Spring	1,219	0.926	0.002	0.028	−1.24	0.548	0.013	0.052	−1.34
YM Site 1	1,143	0.927	0.004	0.031	−1.20	0.62	0.03	0.09	−1.48
YM Site 2	1,478	0.940	0.004	0.025	−1.30	0.60	0.03	0.10	−1.44
YM Site 3	1,279	0.931	0.004	0.029	−1.39	0.58	0.02	0.06	−1.42
YM Site 6	1,315	0.932	0.004	0.030	−1.34	0.61	0.02	0.06	−1.29
YM Site 9	838	0.930	0.004	0.031	−1.39	0.59	0.03	0.10[c]	−1.67[c]
Mean	—	0.931	—	0.027	−1.31	0.58	—	0.06	−1.5
Standard Deviation	—	0.004	—	0.003	0.09	0.03	—	0.03	0.4
Minimum After Subtracting One Standard Error	—	0.924	—	—	—	0.50	—	—	—
Maximum After Adding One Standard Error	—	0.944	—	—	—	0.65	—	—	—
Maximum Plus One Standard Deviation	—	—	—	0.034	—	—	—	0.13	—

Sources: [a] From Table F-1[a], adjusted in accordance with Equation F-48[a].
[b] From Table F-1[a], except as noted.
[c] Sign changed on b, and θ shifted by π.

Table F-5[a]. Parameters for λ and m at Stations Representing the Present-Day Climate Adjusted to an Elevation of 1,524 m

Station	Station Elevation (m)	a_λ (mm)[a]	a_λ Standard Error (mm)[b]	$b_{\lambda,1}$ (mm)[b]	$\theta_{\lambda,1}$ (Radians)[b]	a_m (ln mm)[a]	a_m Standard Error (ln mm)[b]	$b_{m,}$ (ln mm)[b]	$\theta_{m,1}$ (Radians)[b]
4JA	1,043	4.85	0.17	0.75[c]	+2.76[c]	0.71	0.04	0.22[c]	+2.74[c]
40 MN	1,469	4.73	0.16	0.54[c]	+3.95[c]	0.69	0.03	0.10[c]	+3.18[c]
A12	2,283	5.07	0.17	0.90[c]	+2.50[c]	0.80	0.03	0.19[c]	+2.32[c]
Amargosa Farms	747	5.8	0.3	0.3[c]	+2.34[c]	1.02	0.05	0.15[c]	+2.30[c]
Cane Spring	1,219	5.6	0.2	0.8[c]	+2.78[c]	0.87	0.04	0.17[c]	+2.62[c]
YM Site 1	1,143	5.2	0.4	0.8[c]	+2.43[c]	0.77	0.08	0.16[c]	+2.10[c]
YM Site 2	1,478	5.4	0.4	0.6	+1.46	0.86	0.07	0.10[c]	+1.83[c]
YM Site 3	1,279	5.9	0.4	0.8[c]	+2.07[c]	0.94	0.07	0.12[c]	+2.23[c]
YM Site 6	1,315	6.1	0.4	1.1[c]	+1.87[c]	0.98	0.07	0.10[c]	+2.21[c]
YM Site 9	838	4.3	0.3	0.6[c]	+2.65[c]	0.58	0.08	0.20[c]	+2.78[c]
Mean	—	5.3	—	0.7	+2.5	0.82	—	0.15	+2.4
Standard Deviation	—	0.6	—	0.2	0.7	0.14	—	0.04	0.4
Minimum After Subtracting One Standard Error	—	4.0	—	—	—	0.50	—	—	—
Maximum After Adding One Standard Error	—	6.5	—	—	—	1.07	—	—	—
Maximum Plus One Standard Deviation	—	—	—	1.3	—	—	—	0.26	—

Sources: [a] From Table F-2[a], adjusted in accordance with Equation F-48[a].
[b] From Table F-2[a], except as noted.
[c] Sign changed on b, and θ shifted by π.

Table F-6[a]. Wet Day Fraction and Mean Annual Precipitation Implied by Parameters Adjusted to an Elevation of 1,524 m

Meteorological Station	Fraction of Days that are Wet, f_w (%)	Adjusted MAP (mm)	Years Used for Fourier Analysis (Mar. 1 to Feb. 28)
4JA	11	1.9×10^2	45 years: 1959 to 2003
40 MN	12	2.1×10^2	43 years: 1961 to 2003
A12	11	2.0×10^2	41 years: 1960 to 1994, 1998 to 2003
Amargosa Farms	10	2.1×10^2	26 years: 1968, 1969, 1979 to 2000, 2002, 2003
Cane Spring	12	2.5×10^2	39 years: 1965 to 2003
YM Site 1	11	2.1×10^2	10 years: 1993 to 1998, 2000 to 2003
YM Site 2	9	1.8×10^2	11 years: 1993 to 2003
YM Site 3	11	2.4×10^2	11 years: 1993 to 2003
YM Site 6	10	2.2×10^2	11 years: 1993 to 2003
YM Site 9	11	1.7×10^2	11 years: 1993 to 2003

Sources: f_w and MAP from Equations F-41 and F-42, using values from Tables F-4[a] and F-5[a]. Data years from Output DTN: SN0609T0502206.023.

DTN: SN0608WEATHER1.005 [DIRS 177912] contains the qualified temperature records from the Yucca Mountain meteorological stations. Excel files in Output DTN: SN0608T0502206.019 contain temperature records extracted for Yucca Mountain Sites 1, 2, 3, and 6. Output DTN: SN0608T0502206.019 also contains the MathCAD workbooks that analyzed the four temperature records. Tables F-7[a] and F-8[a] report the results of these analyses. The phase parameters are rounded to the nearest day; the remaining parameters are rounded to 0.1°C.

Section F3 uses the ranges of these coefficients as a guide to the uncertainty distributions for the Present-Day climate and for the Monsoon climate. For ease of reference, Tables F-7[a] and F-8[a] show the minimum and maximum values for each of the coefficients of the first-order terms.

Table F-7[a]. Fourier Parameters for Wet Day Temperatures at Stations Representing the Present-Day Climate

Station	γwet_{min} (°C)	γwet_{min} Standard Error (°C)	αwet_{min} (°C)	βwet_{min} (DOY)	γwet_{max} (°C)	γwet_{max} Standard Error (°C)	αwet_{max} (°C)	βwet_{max} (DOY)
YM Site 1	9.2	0.4	9.0	123	18.3	0.5	12.0	118
YM Site 2	8.2	0.4	9.6	124	15.8	0.5	12.4	117
YM Site 3	9.0	0.4	9.0	122	16.9	0.5	12.1	117
YM Site 6	7.9	0.4	8.6	121	16.5	0.5	11.8	116
Minimum	—	—	8.6	121	—	—	11.8	116
Maximum	—	—	9.6	124	—	—	12.4	118

Source: Output DTN: SN0608T0502206.019; folder Present-Day-Temperature; files BSC1_parameters, BSC2_parameters, BSC3_parameters, and BSC6_parameters.

Table F-8[a]. Fourier Parameters for Dry Day Temperatures at Stations Representing the Present-Day Climate

Station	γdry_{min} (°C)	γdry_{min} Standard Error (°C)	αdry_{min} (°C)	βdry_{min} (DOY)	γdry_{max} (°C)	γdry_{max} Standard Error (°C)	αdry_{max} (°C)	βdry_{max} (DOY)
YM Site 1	10.8	0.1	10.0	114	23.3	0.2	12.0	110
YM Site 2	12.2	0.1	10.0	116	21.0	0.2	12.4	109
YM Site 3	11.6	0.1	9.9	114	21.8	0.2	12.0	110
YM Site 6	9.1	0.1	9.4	114	21.6	0.1	11.9	110
Minimum	—	—	9.4	114	—	—	11.9	109
Maximum	—	—	10.0	116	—	—	12.4	110

Source: Output DTN: SN0608T0502206.019; folder Present-Day-Temperature; files BSC1_parameters, BSC2_parameters, BSC3_parameters, and BSC6_parameters.

Before comparing the zero-order coefficients, they are adjusted to an elevation of 1,524 m using a temperature lapse rate of −10°C/km (dry lapse rate from Maidment 1993 [DIRS 125317], p. 3.3), as shown in Table F-9[a]. That table also shows the minimum and maximum of these adjusted zero-order coefficients extended by one standard error in each direction.

Table F-9[a]. Zero-Order Temperature Parameters for Stations Representing the Present-Day Adjusted to an Elevation of 1,524 m

Station	Station Elevation (m)	γwet_{min} (°C)	γwet_{max} (°C)	γdry_{min} (°C)	γdry_{max} (°C)
YM Site 1	1,143	5.4	14.5	7.0	19.5
YM Site 2	1,478	7.7	15.3	11.7	20.5
YM Site 3	1,279	6.6	14.5	9.2	19.4
YM Site 6	1,315	5.8	14.4	7.0	19.5
Minimum Less One Standard Error	—	5.0	13.9	6.9	19.2
Maximum Plus One Standard Error	—	8.1	15.8	11.8	20.7

NOTE: Values from Tables F-7[a] and F-8[a], adjust ed in accordance with Equation F-48[a], using a lapse rate of −10°C/km.

F2.2[a].STATIONS REPRESENTING AN UPPER BOUND FOR THE MONSOON CLIMATE

No change.

F2.3[a]. STATIONS REPRESENTING THE GLACIAL TRANSITION CLIMATE

No change.

F3[a]. SELECTION OF PARAMETER RANGES FOR EACH CLIMATE

No change.

F4[a]. GENERATION OF A WEATHER INPUT FILE FROM A SET OF CLIMATE PARAMETERS

No change.

F5[a]. NOMENCLATURE FOR EQUATIONS USED IN APPENDIX F

No change.

INTENTIONALLY LEFT BLANK

APPENDIX G[a]
DESCRIPTION OF THE MASSIF ROUTINES

No change.

APPENDIX H[a]
SENSITIVITY ANALYSIS OF MEAN ANNUAL INFILTRATION

No change.

APPENDIX I[a]
TREATMENT OF UNCERTAINTIES

No change.

APPENDIX J[a]
SUPPORTING INFORMATION ON VALIDATION OF EVAPOTRANSPIRATION USING SOIL WATER STORAGE MEASUREMENTS IN WEIGHING LYSIMETERS

No change.

APPENDIX K[a]
SUPPORTING INFORMATION ON CORROBORATION OF INFILTRATION USING AN ALTERNATIVE MODEL APPROACH

No change.

APPENDIX L[a]
PRELIMINARY RESULTS AND OUTPUTS

No change except that DTNs: SN0609T0502206.028 [DIRS 178753], SN0609T0502206.024 [DIRS 179063], and SN0609T0502206.029 [DIRS 178862]) are now justified for use in TSPA by SNL (2008 [DIRS 184077]).